FINAL REPORT

RESEARCH AND DEVELOPMENT IN THE FIELD OF PHYSICAL DETERMINATION OF MASS PROPERTIES

(NASA-CR-154071) RESEARCH AND DEVELOPMENT IN THE FIELD OF PHYSICAL DETERMINATION OF MASS PROPERTIES Final Report (Spaco) 588 p

N88-71389

Unclas

00/70 0133300

CONTRACT NAS8-11314

FACILITY FORM 602

~~X66-37407~~ (ACCESSION NUMBER)

(THRU)

660 (PAGES)

2A (CODE)

CR-77471 (NASA CR OR TMX OR AD NUMBER)

23 (CATEGORY)

~~Available to NASA Offices and Research Centers Only~~

Per DAA

AUG 1977
RECEIVED
NASA STI FACILITY
INPUT BRANCH

SPACO, INC.

HUNTSVILLE, ALABAMA

FINAL REPORT

RESEARCH AND DEVELOPMENT IN THE FIELD OF PHYSICAL DETERMINATION OF MASS PROPERTIES

CONTRACT NAS8-11314

BY

SPACO, INC.
MASS METROLOGY LABORATORY
June 15, 1966

~~For Officers and Research Officers Only~~
Per DAA

TABLE OF CONTENTS

Chapter	Title	Page
I	SUMMARY	1
	1.1 SUMMARY OF ACCOMPLISHMENTS OF 1964 - 1965 WORK	1
	1.1.1 Moment of Inertia	1
	1.1.2 Product of Inertia	1
	1.1.3 Principal Axis	1
	1.1.4 Mass Properties of Liquids	2
	1.1.5 Center of Gravity	2
	1.1.6 General Laboratory Improvements	2
	1.2 OBJECTIVES OF 1965 - 1966 WORK	2
	1.2.1 Moment of Inertia	2
	1.2.2 Product of Inertia	3
	1.2.3 Mass Properties of Liquids	3
	1.2.4 Center of Gravity	3
	1.2.5 Mass Measurement	3
	1.3 ACCOMPLISHMENTS OF 1965 - 1966 WORK	4
	1.3.1 Moment of Inertia	4
	1.3.2 Product of Inertia	4
	1.3.3 Mass Properties of Liquids	5
	1.3.4 Center of Gravity	5
	1.3.5 Laboratory Weighing System	6
II	TECHNICAL DISCUSSION	7
	2.1 MOMENT OF INERTIA	7
	2.1.1 Math Model	7
	2.1.1.1 Literature Search	7
	2.1.1.1.1 Introduction	7
	2.1.1.1.2 Classical Moment of Inertia Theory	8
	2.1.1.1.3 Oscillation Theory	10

TABLE OF CONTENTS (Continued)

Chapter	Title	Page
	2.1.1.1.4 Applied Reports	13
	2.1.1.1.5 Conclusions	15
	2.1.1.1.6 References	16
	2.1.1.2 Aerodynamic Drag Tests	22
	2.1.1.2.1 Introduction	22
	2.1.1.2.2 Qualitative Tests	22
	2.1.1.2.2.1 Test Procedure	22
	2.1.1.2.2.2 Test Results and Analysis	23
	2.1.1.2.3 Quantitative Tests	38
	2.1.1.2.3.1 Test Procedure	38
	2.1.1.2.3.2 Test Results and Analysis	41
	2.1.1.2.4 Conclusions	49
	2.1.1.3 Vacuum Chamber Tests	49
	2.1.1.3.1 Introduction	49
	2.1.1.3.2 Experimental Procedure	50
	2.1.1.3.3 Experimental Results	58
	2.1.1.3.4 Conclusions	61
	2.1.1.4 Damping Theory Study	65
	2.1.1.4.1 Introduction	65
	2.1.1.4.2 Analog Computer Simulation	70
	2.1.1.4.3 System Equation and Solution	71
	2.1.1.4.4 Conclusions	77
	2.1.2.1 Improved Period Measuring Device	77
	2.1.2.1.1 General Discussion	77
	2.1.2.1.2 Design Considerations	77
	2.1.2.1.3 Optical System Design	78
	2.1.2.1.3.1 Computations	78
	2.1.2.1.3.2 Construction	78
	2.1.2.1.3.3 Mounting Features	79
	2.1.2.1.4 Test Results	79
	2.1.2.2 Improved Displacement Measuring Device	85
	2.1.2.2.1 Technical Discussion	85
	2.1.2.2.2 Procedure	85
	2.1.2.2.2.1 The System	85
	2.1.2.2.2.2 Prototype Transducer	87
	2.1.2.2.2.3 Signal Conditioner	87
	2.1.2.2.2.4 Counter Conversion	87
	2.1.2.2.2.5 The Present Transducer	90
	2.1.2.2.3 Test Results	90
	2.1.2.2.4 Conclusions	94

TABLE OF CONTENTS (Continued)

Chapter	Title	Page
	2.1.2.2.5 Recommendations	94
	2.1.2.3 Air Bearing Table Improvements	94
	2.1.3 Torsion Rod Investigation	95
	2.1.3.1 Investigate Rod Material	95
	2.1.3.1.1 Introduction	95
	2.1.3.1.2 Basic Elastic Theory	95
	2.1.3.1.3 Torsion Rod Design	99
	2.1.3.1.4 Material Considerations	110
	2.1.3.1.5 Conclusions	112
	2.1.3.2 Design Torsion Rod Tester	116
	2.1.3.3 Fabricate Torsion Rod Tester	116
	2.1.3.4 Torsion Rod Test	116
	2.1.3.4.1 Introduction	116
	2.1.3.4.2 Static Experiments	117
	2.1.3.4.3 Dynamic Experiments	119
	2.1.3.4.4 Torsion Rod Calibration Procedure	131
	2.1.3.4.5 Conclusions	134
	2.1.4 System Analysis	136
	2.1.4.1 Evaluation Tests	136
	2.1.4.2 Results Analysis	136
	2.1.4.2.1 Introduction	136
	2.1.4.2.2 Error Analysis	136
	2.1.4.2.3 Experimental Results	140
	2.1.4.2.4 Conclusions	142
2.2	PRODUCT OF INERTIA PROGRAM	147
	2.2.1 System Improvements	147
	2.2.1.1 Improve Tilt Table	147
	2.2.1.1.1 Introduction	147
	2.2.1.1.2 Objective	147
	2.2.1.1.3 Test Apparatus and Procedure	147
	2.2.1.1.4 Results	149
	2.2.1.1.5 Conclusions and Recommendations	151
	2.2.1.2 Calibrate Standards	151
	2.2.1.2.1 Manufacturing	151
	2.2.1.2.1.1 Machining	151
	2.2.1.2.1.2 Plating	151
	2.2.1.2.1.3 Grinding	160
	2.2.1.2.2 Measurements	160
	2.2.1.2.2.1 Discussion	160

TABLE OF CONTENTS (Continued)

Chapter	Title	Page
	2.2.1.2.2.2 Center of Gravity Location	160
	2.2.1.2.2.3 Product of Inertia Equation	163
	2.2.1.2.2.4 Moment of Inertia Equation	164
	2.2.1.2.2.5 Computer Programs	165
	2.2.1.3 Evaluation Tests	165
	2.2.1.3.1 Technical Discussion	165
	2.2.1.3.2 Procedure	165
	2.2.1.3.3 Test Results	167
	2.2.1.3.4 Conclusions	173
	2.2.1.3.5 Recommendations	173
	2.2.2 System Analysis	173
	2.2.2.1 Evaluation Tests	173
	2.2.2.1.1 Description of Equipment	173
	2.2.2.1.2 Procedure	175
	2.2.2.1.3 Test Results	179
	2.2.2.2. Error Analysis	179
	2.2.2.2.1 Sources of Error	185
	2.2.2.2.1.1 Centrifugal Force	185
	2.2.2.2.1.2 Gyroscopic Effect	185
	2.2.2.2.1.3 Instrumentation Error	185
	2.2.2.2.1.4 Load Cell Tilt	186
	2.2.2.2.1.5 Test Object Tilt	188
	2.2.2.2.1.6 Table Tilt	190
	2.2.2.2.1.7 Aerodynamic Drag	193
	2.2.2.2.2 Mathematical Model	194
	2.2.2.4 Recommendations	195
	2.2.3 Principal Axis	197
2.3	MASS PROPERTIES OF LIQUIDS	199
	2.3.1 Test Program	199
	2.3.1.1 Roll Axis Inertia Tests Using Air Bearing Table	199
	2.3.1.1.1 Introduction	
	2.3.1.1.2 Test Procedure	199
	2.3.1.1.3 Test Results	201
	2.3.1.1.4 Conclusions	206
	2.3.1.2 Displaced Roll Axis Inertia Tests Using Air Bering Table	210
	2.3.1.2.1 Introduction	210
	2.3.1.2.2 Test Objective	210

TABLE OF CONTENTS (Continued)

Chapter	Title	Page
	2.3.1.2.3 Test Procedure	214
	2.3.1.2.4 Test Results	216
	2.3.1.2.5 Conclusions	231
	2.3.1.3 Yaw-Pitch Axis Inertia Tests	232
	2.3.1.4 Yaw-Pitch Axis Inertia Tests Rotating About a Displaced Horizontal Axis	232
	2.3.1.4.1 Introduction	232
	2.3.1.4.2 Yaw-Pitch Axis Tests Using a Torsional Pendulum	233
	2.3.1.4.2.1 Test Procedure	233
	2.3.1.4.3 Displaced Yaw-Pitch Axis Tests Using A Compound Torsional Pendulum System	236
	2.3.1.4.3.1 Test Procedure	236
	2.3.1.4.3.2 Test Results	243
	2.3.1.4.4 Conclusions	245
	2.3.1.5 Ring Baffle Tests Using Government Furnished Plexiglass Tank	245
	2.3.1.5.1 Introduction	245
	2.3.1.5.2 Test Using Plexiglass Tank and Stand	247
	2.3.1.5.2.1 Test Procedure	247
	2.3.1.5.2.2 Test Results	247
	2.3.1.5.3 Tests Using The Air Bearing Table	252
	2.3.1.5.3.1 Test Procedure	252
	2.3.1.5.3.2 Test Results	252
	2.3.1.5.4 Conclusions	261
	2.3.2 Math Model	261
	2.3.2.1 Literature Search	261
	2.3.2.1.1 Introduction	261
	2.3.2.1.2 Interviews	264
	2.3.2.1.3 Literature Searches	265
	2.3.2.1.4 Conclusions	269
	2.3.2.2 Develop Equations for the Moment of Inertia of a Liquid Filled Cylindrical Tank About its Center of Gravity and Displaced Axes	269
	2.3.2.2.1 Introduction	269
	2.3.2.2.2 Moment of Inertia About a Yaw-Pitch Axis	279
	2.3.2.2.3 Moment of Inertia About a Yaw-Pitch Axis	287
	2.3.2.2.4 Moment of Inertia About a Roll Axis	295

TABLE OF CONTENTS (Continued)

Chapter	Title	Page
	2.3.2.2.5 Moment of Inertia About a Displaced Roll Axis	304
	2.3.2.2.6 Conclusions	308
	2.3.2.3 Investigate Analytical Method of Describing the Moment of Inertia of Liquid Filled Tanks With Baffles	314
	2.3.2.3.1 Introduction	314
	2.3.2.3.2 Determination of Approximate Pressure Distribution Across the Ring Baffle	314
	2.3.2.3.3 Influence of Slosh Baffles Upon the Effective Moment of Inertia	325
2.4	CENTER OF GRAVITY	335
	2.4.1 Equipment	335
	2.4.1.1 Spherical Segment Air Bearing Table	335
	2.4.1.1.1 Test Object Support Surface	335
	2.4.1.1.2 Spherical-Segment Air Bearing	337
	2.4.1.1.3 Stabilizing Air Cylinders	337
	2.4.1.1.4 Air Cylinder Control Valve	337
	2.4.1.1.5 Support and Leveling Stand	337
	2.4.1.1.6 Test Object Positioner	338
	2.4.1.2 Moment Detection System (Bytrex)	338
	2.4.1.2.1 Test Object Support Surface	338
	2.4.1.2.2 Support and Leveling Stand	338
	2.4.1.2.3 Overload Protection Supports	340
	2.4.1.2.4 Moment Detector Unit	340
	2.4.1.2.5 Instrumentation and Power Supply Unit	340
	2.4.1.3 Advanced Center of Gravity Locator	341
	2.4.1.4 Optical System	342
	2.4.1.4.1 Modification	344
	2.4.1.5 C. G. Marking System	344
	2.4.1.5.1 Method I	344
	2.4.1.5.2 Method II	345
	2.4.1.5.3 Method III	345
	2.4.2 Test and Evaluations	347
	2.4.2.1 Test Studies - Existing Equipment	347
	2.4.2.2 Comparison of "Null Balance" Method and "Unbalance" Method of C. G. Location Using the Bytrex Unit	351
	2.4.2.3 Systems Evaluation and Comparison Tests	351

TABLE OF CONTENTS (Continued)

Chapter	Title	Page
	2.4.2.3.1 Spherical Segment Air Bearing Table	355
	2.4.2.3.2 "Bytrex" Moment Detection System	355
	2.4.2.3.2.1 System Evaluation Tests	355
	2.4.2.3.3 Modified Bytrex Unit Evaluation	355
	2.4.2.3.3.1 Introduction	358
	2.4.2.3.3.2 Equipment Modification	358
	2.4.2.3.3.3 Evaluation Tests	358
	2.4.2.3.3.4 Test Results	359
	2.4.2.3.3.5 Conclusions	359
	2.4.2.3.3.6 Recommendations	359
	2.5 LABORATORY WEIGHING SYSTEM	361
	2.5.1 Introduction	361
	2.5.2 System Description	361
	2.5.3 Design Considerations	361
	2.5.3.1 Centerpoise	361
	2.5.3.2 Counterweights	364
	2.5.3.3 Flexural Pivots	364
	2.5.4 Calibration	364
	2.6 GENERAL PROJECTS	366
	2.6.1 Low Gravity Test Packages	367
	2.6.1.1 Introduction	367
	2.6.1.2 Procedure	367
	2.6.1.3 Results	372
	2.6.1.4 Conclusions	380
III	PROGRAM MANAGEMENT	388
	3.1 JUNE, 1965 TO DECEMBER, 1965	389
	3.2 DECEMBER, 1965 TO JUNE, 1966	389
	APPENDICES	403
	Appendix A1	407
	Appendix A2	411
	Appendix A3	412
	Appendix A4	413

TABLE OF CONTENTS (Continued)

Chapter	Title	Page
	Appendix A5	417
	Appendix A6	419
	Appendix A7	421
	Appendix A8	423
	Appendix A9	429
	Appendix A10	447
	Appendix A11	461
	Appendix A12	463
	Appendix A13	491
	Appendix B1	495
	Appendix B2	499
	Appendix B3	501
	Appendix B4	503
	Appendix B5	511
	Appendix B6	515
	Appendix B7	519
	Appendix C1	525
	Appendix C2	529
	Appendix C3	531
	Appendix C4	533
	Appendix C5	535
	Appendix C6	537
	Appendix C7	539
	Appendix C8	543
	Appendix C9	551
	Appendix D1	561
	Appendix D2	563
	Appendix E1	567
	Appendix E2	569
	Appendix E3	571
	Appendix E4	573
	Appendix E5	575
	Appendix E6	577
	Appendix E7	579
	Appendix E8	581
	Appendix E9	583
	Appendix E10	585
	Appendix E11	587
	Appendix E12	589
	Appendix E13	591

TABLE OF CONTENTS (Continued)

Chapter	Title	Page
	Appendix E14	593
	Appendix E15	595
	Appendix E16	597
	Appendix E17	599

LIST OF ILLUSTRATIONS

Figure	Title	Page
1	Special Drag Adapters	24
2	Cylindrical Weights	24
3	Theoretical Moment of Inertia Values for Various Drag Configurations	25
4	Test Equipment Arrangement	27
5	Test Results Showing Displacement Versus Number of Cycles	28
6	Test Results Showing ln Displacement Versus Number of Cycles	29
7	Test Results Showing Displacement Versus Number of Cycles	30
8	Test Results Showing ln Displacement Versus Number of Cycles	31
9	Test Results Showing Displacement Versus Number of Cycles	32
10	Test Results Showing ln Displacement Versus Number of Cycles	33
11	Test Results Showing Displacement Versus Number of Cycles	34
12	Test Results Showing ln Displacement Versus Number of Cycles	35
13	Test Results Showing Displacement Versus Number of Cycles	36
14	Test Results Showing ln Displacement Versus Number of Cycles	37
15	Drag Plate Dimensions	39
16	Qualitative Test Equipment Arrangement	40
17	Test Results Showing Displacement Versus Number of Cycles	42
18	Test Results Showing ln Displacement Versus Number of Cycles	43
19	Test Results Showing Period Versus Number of Cycles	44
20	Test Results Showing Displacement Versus Number of Cycles	46
21	Test Results Showing ln Displacement Versus Number of Cycles	47
22	Test Results Showing Period Versus Number of Cycles	48
23	Atcomed Facility	51

LIST OF ILLUSTRATIONS (Continued)

Figure	Title	Page
24	Drag Plate Dimensions	52
25	Dumbbell Assembly	53
26	Pivot Assembly	54
27	Striker Assembly	55
28	Displacement Measuring Device	56
29	Period Measuring Device	57
30	Electronic Equipment	59
31	Log Displacement Versus Number of Cycles	60
32	Period Versus Number of Cycles	62
33	Normalized Period Versus Number of Cycles	63
34	Normalized Period Versus Number of Cycles	64
35	Basic Damped Oscillator Simulation	68
36	Final Computer Program	68
37	Plot of Displacement Versus Time	69
38	Plot of Acceleration Versus Velocity	70
39	Displacement Versus Number of Cycles	73
40	Logarithm of Displacement Versus Number of Cycles	74
41	Period Versus Number of Cycles	75
42	Improved Period Measuring Device	80
43	Mounting Configuration	81
44	Comparison of Old and New Period Measuring Devices With Table Unloaded	82
45	Comparison of Old and New Period Measuring Devices With 60 in-lb-sec^2 Load	83
46	Comparison of Old and New Period Measuring Devices With 90 in-lb-sec^2 Load	84
47	System Block Diagram	86
48	Prototype Displacement Transducer	88
49	Signal Conditioner Schematic	89
50	Counter Conversion Circuit	92
51	Present Displacement Transducer	93
52	Direct Plot of Decaying Pendulum Amplitude From Digital Recorder	96
53	Linear Elastic Stress-Strain Diagram	98
54	Non-Linear Elastic Stress-Strain Diagram	98
55	Torsion in an Elliptical Cross Section	101
56	Torsion in Three Types of Rods	103
57	Torsion in a Thin-Walled Circular Tube	104
58	Magnitude of Stresses in a Circular Rod	107
59	Elemental Segment of a Circular Rod Describing Pure Shear	107

LIST OF ILLUSTRATIONS (Continued)

Figure	Title	Page
60	Static Torsion Rod Test System	118
61	Glass Rod Stress-Strain Curve	120
62	Alumina Rod Stress-Strain Curve	121
63	Mild Steel Stress-Strain Curve	122
64	Carpenter RDS Steel Stress-Strain Curve	123
65	Period Decay Curve for the Air Bearing Table With No Load Using Rod Number 120	126
66	Period Decay Curve for the Air Bearing Table With No Load Using Rod Number 6B	127
67	Dynamic Torsion Rod Test System	130
68	Old Dumbbell Mounting Configuration	132
69	New Dumbbell Mounting Configuration	132
70	Dumbbell Configuration	139
71	Product of Inertia Table	148
72	Static Load Test Arrangement	150
73	Static Test Results – 9.69 lb. Weight	152
74	Measured Versus Calculated Loads 9.69 lb. Weight	153
75	Static Load Test Results – 5.0 lb. Weight	154
76	Measured Versus Calculated Loads 5.0 lb. Weight	155
77	Static Load Test Results – 1.0 lb. Weight	156
78	Measured Versus Calculated Loads 1.0 lb. Weight	157
79	Static Load Test Results – Error	158
80	Measured Versus Calculated Loads 0.48 lb. Weight	159
81	Dimensions of Finish Ground Triangular Standard	161
82	Product of Inertia Standards Terminology	162
83	Center of Gravity Location	163
84	Modified Product of Inertia Table	166
85	Static Test Load Test Arrangement	168
86	Static Load Test Results – -0.48 lb. Weight	169
87	Static Load Test Results – 5.0 lb. Weight	170
88	Static Load Test Results – 9.69 lb. Weight	171
89	Percent Error	172
90	Torque Error	174
91	Product of Inertia System Block Diagram	176
92	System Photograph	177
93	Table Unloaded	178
94	Test Block Number 1	180
95	Test Block Number 2	181
96	Test Block Number 3	182
97	Test Block Number 4	183
98	Zero Offset	184

LIST OF ILLUSTRATION (Continued)

Figure	Title	Page
99	(a) Tilt Table, (b) Structural and Force Triangles	186
100	The Effect of Centrifugal Force Due to Test Object Tilt	188
101	The Effect of Centrifugal Force Due to Table Tilt	191
102	Test Equipment Arrangement	200
103	Ratio of the Moment of Inertia of Water to Solid Versus Aspect Ratio	204
104	Moment of Inertia of Each Tank Versus Aspect Ratio	205
105	Moment of Inertia of Each Tank Versus Pressure Exerted by the Liquid on the Bottom of Each Tank	206
106	Clustered Fuel Tanks	211
107	Various Tank Positions as They Rotate About Axis O	213
108	Test Equipment Arrangement	215
109	Large Tank Dimensions	217
110	Large Tank Positions	218
111	Small Tank Dimensions	219
112	Small Tank Positions	220
113	Moment of Inertia Versus Aspect Ratio for Small Tanks About Their Longitudinal Axes	221
114	Ratio of Moment of Inertia of Water to Solid Versus Ratio of Displacement to Radius for Two Sets of Tanks	228
115	Ratio of Moment of Inertia of Water to Solid Versus Ratio of Displacement to Radius for Different Frequencies	229
116	Vertical Yaw-Pitch Axis Test Set Up	234
117	Horizontal Yaw-Pitch Axis Test Set Up	237
118	I_w/I_s Ratio Versus h/d Ratio	238
119	Displaced Yaw-Pitch Axis Test Set Up	239
120	Equipment Arrangement for Baffle Tests	248
121	Tank Dimensions	249
122	Comparison of Analytical and Experimental Results of I_{eff}/I_{solid}	253
123	Small Tank Dimensions	254
124	I_{eff}/I_{solid} Versus	255
125	Effect of Baffle Spacing on I_{eff}/I_{solid}	256
126	Effect of Displaced Axis on I_{eff}/I_{solid}	263
127	Coordinate System for Pitch Excitations About an Axis Through the Center of Mass of the Liquid	280
128	Ratio of the Moment of Inertia of Liquid to Solid Versus Aspect Ratio for a Completely Filled Cylindrical Tank	286
129	Coordinate System for Pitch-Excitation About Arbitrary Axis	288

LIST OF ILLUSTRATIONS (Continued)

Figure	Title	Page
130	I_{eff}/I_{solid} Versus Aspect Ratio for Various Axis Displacements	294
131	Infinitely Long Roll Oscillating Cylinder	298
132	Analytical Results for I_{eff}/I_{solid} Versus Roll Axis Oscillation Frequencies	306
133	Cylinder Oscillating About a Displaced Axis	307
134	Analytical Results for I_{eff}/I_{solid} Versus Roll Axis Displacement	309
135	Potential Flow About Baffle and Elliptic Coordinates	315
136	Pressure Distribution at the Baffle for Various Baffles	322
137	Distribution of Longitudinal Acceleration $\dot{w}_o$ in Completely Filled Containers	324
138	Pressure Distribution at the Baffle for Various Angles φ	326
139	Container Geometry with Baffles (Reference 4)	331
140	Center of Gravity Locating System Using a Spherical Segment Air Bearing and Optical Telescope	336
141	Moment Detection System for Center of Gravity Determination	339
142	Precision Center of Gravity Locator	343
143	Reduced Grid Pattern	346
144	Ronchi Ruling Grid Pattern	346
145	Telescope Setting for Center of Rotation of Air Bearing Versus Sight Point Elevation	349
146	System C.G. Below Center of Oscillation of Air Bearing Versus Apparent Change in Center of Rotation	350
147	Effect of Table Tilt on C.G. Location Accuracy	354
148	Triangle Standard Axes Position 1-R	357
149	Triangle Standard Axes Position 1-B	357
150	Triangle Standard Axes Position 2-R	357
151	Triangle Standard Axes Position 2-B	357
152	Laboratory Weighing System	362
153	Effect of Centerpoise Weight on Balance Stability	363
154	Moment Detection System for Center of Gravity Location	368
155	Moment of Inertia Measurement of Drop Package	370
156	Drop Package Coordinate Orientation	373
157	Package Tilt Caused by Various Mass Movements	387
158	Program Schedule	390
159	Moment of Inertia Program Schedule	391
160	Moment of Inertia Program Schedule	392
161	Moment of Inertia Program Schedule	393

LIST OF ILLUSTRATIONS (Continued)

Figure	Title	Page
162	Moment of Inertia Program Schedule	394
163	Mass Metrology Laboratory Project Plan	395
164	Mass Metrology Laboratory Overall Program	396
165	Moment of Inertia Program 1.0	397
166	Product of Inertia Program 2.0	398
167	Mass Properties of Liquids Program 3.0	399
168	Center of Gravity Program 4.0	400
169	Mass Measurement Program 5.0	401

LIST OF TABLES

Table	Title	Page
1	Test Results	26
2	Damping Constant Results	65
3	Computer Scaling Factors	71
4	Peak Displacement Measured	91
5	Properties of Non-Circular Torsion Rods	102
6	Properties of Circular Hollow and Solid Rods	109
7	Mechanical Properties of Some Ceramics	113
8	Test Results	124
9	Test Results	125
10	Test Results	129
11	Test Results	129
12	Moment of Inertia Dumbbell Standards	133
13	List of Symbols	133
14	Brackets and Bolts	133
15	Calculated Standard Deviations	135
16	Dimensions of Dumbbell C	141
17	Test Results	143
18	Physical Characteristics of Cylindrical Tanks	202
19	Test Results	203
20	Pressure Exerted by Water on Tank Bottom	203
21	Physical Characteristics of Large Cylindrical Tanks	222
22	Theoretical Moment of Inertia Values For Large Tanks at Various Positions	222
23	Physical Characteristics of Small Cylindrical Tanks	223
24	Theoretical Moment of Inertia Values for Small Tanks at Various Positions	223
25	Test Results for Large Tanks	224
26	Test Results for Small Tanks	225
27	Test Results for Small Tanks	226
28	Test Results for Tank C At Five Displacements Using Rod 28	230
29	Physical Characteristics of Cylindrical Tanks	235
30	Test Results for Suspended Pendulum Tests	240
31	Test Results for Suspended Tank Tests	241
32	Test Results for Supported Tank Tests	242
34	Test Results-Displaced Axis Tests for Tank C	244
35	Test Results - Displaced Axis Tests for Tank D	244
36	Tank Characteristics	250
37	Test Results	251

LIST OF TABLES - Continued

Table	Title	Page
38	Test Results	257
39	Test Results	258
40	Test Results	259
41	Test Results	260
42	Results of I_{eff}/I_{solid} FOR Various Aspect Ratios	285
43	Zeros ϵ_n Of The First Derivative of the Bessel-Function of First Order and First Kind	285
44	Results of I_{eff}/I_{solid} For Vaious Aspect Ratios and Axis Displacements	293
45	Analytical Results for I_{eff}/I_{solid} For The Rod Axis Oscillations	305
46	Analytical Results for I_{eff}/I_{solid} For the Displaced Roll Axis	305
47	Spherical Segment Air Bearing Test Data	348
48	Sight Point Evaluation Test Data	348
49	"Bytrex" Test By the Unbalance Moment Method Using The Bytrex Instrumentation Unit for % Unbalance Readings	352
50	Bytrex Test By the Null-Balance Method Using The Bytrex Instrumentation Unit at Zero Reading	353
51	Accuracy Test - Air Bearing G. G. Locator	356
52	Accuracy Test - Bytrex C. G. Locator	356
53	Results of Modified Bytrex C. G. Locator Sensitivity Test	360
54	Results of Spherical Segment Air Bearing C. G. Locator Sensitivity Test	360
55	Moment of Inertia Measurement of Drop Package	372
56	Effect of Gas Bottle Discharge on Unbalance Moment About X and Y Axes	374
57	Drop Package Tilt Caused By Gas Bottle Discharge	375
58	Effect of Motion Picture Camera Operation on Unbalance Moment	376
59	Drop Package Tilt Caused by Operation Of Motion Picture Camera	377
60	Effect of Liquid Tank Relocation on Unbalance Moment Liquid Level .3" Above Parting Line	378
61	Effect of Liquid Tank Relocation on Unbalance Moment Liquid Level 1.85" Above Parting Line	379
62	Drop Package Tilt Caused by Shift of Liquid Tank One Second After Drop Liquid Level 1.85" Above Parting Line	381

LIST OF TABLES - Continued

Table	Title	Page
63	Drop Package Tilt Caused By Shift of Liquid Tank One Second After Drop Liquid Level 1.85" Above Parting Line	382
64	Drop Package Tilt Caused By Shift Of Liquid Tank Two Seconds After Drop Liquid Level = 1.85" Above Parting Line Acceleration = .032G	383
65	Drop Package Tilt Caused By Shift Of liquid Tank Two Seconds After Drop Liquid Level = 1.85" Above Parting Line Acceleration = .032G	384
66	Drop Package Tilt Caused by Shift of Liquid Tank Three Seconds After Drop Liquid Level = 1.85" Above Parting Line Acceleration = .032G	385
67	Drop Package Tilt Caused By Shift Of Liquid Tank Three Seconds After Drop Liquid Level = 1.85" Above Parting Line Acceleration = .032G	386

I SUMMARY

1.1 SUMMARY OF ACCOMPLISHMENTS OF 1964 - 1965 WORK

1.1.1 Moment of Inertia

1.1.1.1 The "Period Decay Rate" concept was developed to a practical technique which enabled moments of inertia to be determined experimentally to an accuracy of $\pm 0.1\%$.

1.1.1.2 A detailed analysis of analytical curve fitting techniques was made for use in conjunction with the above concept.

1.1.1.3 Specific procedures were established for the experiments performed in the laboratory.

1.1.1.4 The effects of dead weight, air bearing pressure, and external air drag on the damping constant of the system were determined experimentally.

1.1.1.5 The effect of environmental temperature on the accuracy of the moment of inertia measurement system was determined experimentally.

1.1.1.6 The effects of errors in moment of inertia standards and test parameters on system accuracy were determined analytically.

1.1.1.7 A prototype system for measurement of moment of inertia using a capacitive transducer for motion detection was designed, fabricated, and tested.

1.1.1.8 A prototype system was developed for measurement of moment of inertia using an analog computer for real time calculation of the result.

1.1.2 Product of Inertia

1.1.2.1 A prototype machine for measurement of products of inertia was designed, fabricated, and tested. The prototype utilized an instrumented rotating tilt table and an analog computer to solve for the desired results.

1.1.3 Principal Axis

1.1.3.1 A computer program for calculating the location of principal axis from measured moment and products of inertia was tested and proven.

1.1.4 Mass Properties of Liquids

1.1.4.1 A test program to experimentally determine the moment of inertia of a partially filled liquid tank oscillating about its yaw-pitch axis was performed.

1.1.4.2 Progress was made on the derivation of a mathematical expression for the moment of inertia of the above system, although the solution obtained was a poor approximation of the experimental results.

1.1.5 Center of Gravity

1.1.5.1 A precision optical system for center of gravity location was procured, modified, and tested.

1.1.5.2 The government furnished moment detection center of gravity location system was improved and evaluated.

1.1.5.3 The spherical segment air bearing system was refined to a significantly greater accuracy capability than was originally possible.

1.1.6 General Laboratory Improvements

1.1.6.1 A capacitive transducer motion measurement system was designed, fabricated, and evaluated.

1.1.6.2 Numerous improvements to the laboratory capabilities were made by the design and construction of equipment and accessories.

1.2 OBJECTIVES OF 1965 - 1966 WORK

1.2.1 Moment of Inertia

1.2.1.1 The objective of this project is to obtain an exact mathematical expression for the torsional air bearing table system. With this exact expression, only the system experimental errors will have to be considered in order to improve the system accuracy.

1.2.1.2 Improve the accuracy of period and amplitude measurements as required to fulfull the accuracy requirements of the automatic system.

1.2.1.3 The objective of this project is to obtain sufficient information from the material investigation that will allow the best material for use as torsion rods to be selected. The foremost characteristic of the rod is that it must have a very linear stress-strain relationship and have very little mechanical hysteresis.

1.2.1.4 The objective of this project is to analyze the results of various tests and to determine how different factors affect the system. Factors such as load, surface area, temperature, air pressure, and others will be considered.

1.2.2 Product of Inertia

1.2.2.1 Improve the accuracy of the prototype as much as possible, and make modifications as required to improve the overall performance of the system.

1.2.2.2 The object of this project is to perform a thorough analysis of the system for determining products of inertia.

1.2.2.3 The object of this project is to have a computer program that will take the moments and products of inertia about a given point from the present laboratory equipment and calculate the principal axes about that point.

1.2.3 Mass Properties of Liquids

1.2.3.1 The objective of this project is to perform tests to determine the moment of inertia of a liquid filled cylindrical tank about its roll and yaw-pitch axis. Also, some testing to determine the effects of baffles on determining the moment of inertia of a filled tank will be performed.

1.2.3.2 The objective of this program is to derive a mathematical expression either theoretical or empirical that will accurately give the moment of inertia of a liquid filled tank. The model will be relatively simple, so that it can be used in general applications.

1.2.4 Center of Gravity

1.2.4.1 To improve the accuracy of the C.G. location equipment by development of a working system with a resolution compatible with the optical equipment.

1.2.4.2 To develop a center of gravity system that has a large range of capacity and will yield an accuracy of $\pm .001$ inch or better.

1.2.5 Mass Measurement

1.2.5.1 Provide a precision weighing system with a 1,000 lb. capability. The precision should be as high as practical.

1.3 ACCOMPLISHMENTS OF 1965 - 1966

1.3.1 Moment of Inertia

1.3.1.1 A precision system has been developed for rapidly determining mass moments of inertia. This system can handle loads up to 2000 pounds and is accurate to within 0.03 of one percent.

1.3.1.2 Improved period and displacement measuring devices made it possible to measure the period of oscillation at extremely small amplitudes. At these small amplitudes the exact equation of motion can be obtained; therefore, errors produced by aerodynomic drag, object vibration and bearing friction, can be neglected.

1.3.1.3 Other research was performed; however, it did not produce any improvement in the system or its accuracy.

1.3.1.4 A paper on the system entitled, "A Precision System for Determining Mass Moments of Inertia" was presented at the Interdisciplinary Symposium on Apollo Application Programs by the Society of Engineering Science in January, 1966.

1.3.2 Product of Inertia

1.3.2.1 A literature survey was conducted to learn methods of measuring products of inertia and of determining principal axes. The results of this survey are given in Appendix B7.

1.3.2.2 The tilt table assembly was modified and tested. The modification involved mounting the load cell with mono-flexures to eleminate bending moments.

1.3.2.3 Based on the tests mentioned above, the tilt table stability was improved by sacrificing the angular adjustable tilt table in favor of a more rigid one piece table. A stabilizing bar was added to the load cell in an attempt to overcome centrifugal force effects. A test object hold-down fixture was also provided.

1.3.2.4 The product of inertia triangular test standards were manufactured. They were chrome plated and their physical measurements were obtained.

1. 3. 2. 5 A computer program was developed and used with the physical data to compute the center of gravity, products of inertia, moments of inertia, and principal axes of the test standards.

1. 3. 2. 6 A counterweight was provided for counteracting the centrifugal force acting on the load cell. This replaced the stabilizing bar previously tried. Dynamic tests using the test standards showed that the counterweight was effective.

1. 3. 2. 7 A mathematical model for the product of inertia machine was developed.

1. 3. 2. 8 The real time product of inertia computation method, which used the analog computer, was abandoned in favor of the more accurate digital method. This method permits the use of the rate table's speed calibrator which is more accurate than the tachometer method previously used.

1. 3. 3 Mass Properties of Liquids

1. 3. 3. 1 A set of equations have been derived and experimentally verified that will determine the moment of inertia of a liquid filled cylindrical container as it oscillates about various axes. These axes are: roll and yaw-pitch about the center of mass and displaced roll and yaw-pitch.

1. 3. 3. 2 An equation for determining the moment of inertia of a liquid filled tank with various sized ring baffles oscillating about a yaw-pitch axis through the center of mass has been derived and experimentally verified.

1. 3. 3. 3 A paper covering part of this work was presented to the Society of Aeronautical Weight Engineers in May 1966. The paper was entitled, "The Moment of Inertia of Liquid Filled Cylindrical Tanks About Various Axes"

1. 3. 4 Center of Gravity

1. 3. 4. 1 The Bytrex moment detection system was modified and evaluated. The modifications consisted of: (a) Improvements in readout equipment & (b) Mounting the moment detection head on a bearing which allows the rotation & indexing of the object support surface at 90° intervals.

1. 3. 4. 2 The spherical segment air bearing table was tested & evaluated as a center of gravity locating device. An advanced stabilization system was not fabricated because it was decided that the "Bytrex" system was superior.

1. 3. 4. 3 An advanced center of gravity locator was designed.

1.3.4.4 Several systems for marking the center of gravity location on an object were tested & evaluated.

1.3.5 Laboratory Weighing System

1.3.5.1 A compound beam balance was designed, manufactured, assembled and calibrated. The balance provides accurate weights of objects up to 1,000 pounds.

II TECHNICAL DISCUSSION

2.1 MOMENT OF INERTIA

2.1.1 Math Model

2.1.1.1 Literature Search

2.1.1.1.1 Introduction

The accurate knowledge of mass characteristics of launch and space vehicles has been and continues to be a vital factor in the successful performance and operation of space flight. Because the overall missile performance depends on the properties and characteristics of each individual component, the moments of inertia as well as weights, centers of gravity and principal axis of all vehicle components are critical factors in determining precise trajectories and maneuvers. The moments of inertia of vehicle components that have relative motion with respect to the vehicle such as pumps, actuators, controls, gimbals, etc. are vitally important to the vehicle's performance. These values must be known precisely because of the extreme speed at which some of them operate. Movements of these parts during flight could give rise to secondary forces that in turn could effect the overall stability and response of the vehicle. As a result, careful studies and analysis must be made on these dynamic components to assure that no harmful interactions develop to cause resonance and excessive vibration. Another area in which the moment of inertia is a critical factor is that of gravity gradient stablization. Also, other parameters which could critically affect the stability of smaller type space vehicles are the moments of inertia of different human body positions.

The prime objective of the moment of inertia program is to develop a rapid and accurate method of determining moments of inertia of space vehicle components. This program is divided into five separate projects which directly or indirectly add to the prime objective. Each program is further broken down into components which augment the total program.

This report was the result of the Literature Search portion of the Math Model Project. The objective of the Math Model Project was to investigate the theoretical aspect of moment of inertia determining systems presently being used as well as an investigation of older types of systems. Specifically the Literature Search portion was designed to provide a complete understanding of the background and present status of methods of determining

moments of inertia.

The Literature Search was composed of several types of investigations. Primarily the literature search of the Redstone Scientific Information Center yielded the most information. It consisted of a computer search of all reports in the center that had anything to do with moments of inertia. Next, a card index search of text books produced some valuable information on classical moment of inertia theory and oscillation theory. Thirdly, a Defense Documentation Center search of all articles pertaining to moments of inertia provided some more information. Contacts were also made with personnel of the National Bureau of Standards and the Atomic Energy Commission at Los Alamos to obtain any information available on their moment of inertia work. Professional societies such as the American Institute of Astronautics and Aeronautics, Instrument Society of America and the Society of Aeronautical Weight Engineers were contacted to obtain any papers they had published on moments of inertia determination. In summary, every organization that might provide information on the field of moment of inertia determination was contacted.

The report herein has divided into three main sections, classical moment of inertia theory, oscillation theory and applied reports. The first two sections were intended to provide information and new ideas on the method that is presently being used to determine moments of inertia. The classical theory of the torsional pendulum is fairly standard, but the oscillation theory could provide valuable information on the damped oscillating system which is presently used. The last section covers all the reports which describe various methods of determining moments of inertia, both theoretically and experimentally. The total of all reports will provide an insight into the problems and solutions, both past and present, which are to be encountered in determining moments of inertia.

2.1.1.1.2 Classical Moment of Inertia Theory

Moment of inertia theory has been covered in numerous test books of physics and mechanics from high school level to graduate school. An attempt to include all texts that cover moment of inertia theory would be time consuming and fruitless, but a few of the texts which cover the subject are listed in References 1 through 6. References 1 through 4 are very good books on classical mechanics.

In beginning a discussion of the moment of inertia search it will be best to define the quantity. First, to relieve frustrated physics students, the quantity of moment inertia is not an idea which college professors dreamed up to make courses difficult. It is an actual quantity that has a definite use. All objects possess a property called inertia which is implied in Newton's second law. This second law states that all objects will remain at rest if at rest or in motion if in motion, as long as no net force acts on it. The inertia of a body is that property that makes a body at rest or in motion want to continue in its original state unless acted on by an outside force. In translational motion the inertia of an object is called its "mass" and Newton's second law is expressed in Equation 1 where F is the force, m the mass and a the linear

$$F = ma \tag{1}$$

acceleration.

In rotational motion the inertia is called "moment of inertia" a logical term as it suggests. Newton's second law as applied to rotational motion can be derived from Equation 1 and is stated in Equation 2, where T is the torque,

$$T = I\alpha \tag{2}$$

I is the moment of inertia and α is the angular acceleration. From Equation 2 it can be noted that in the motion of rotating systems, the moment of inertia plays a role analogous to that of the mass in translational systems.

The moment of inertia is defined in more detail by Equation 3, where I_{xx} is the moment of inertia about any arbitrary $axis_{xx}$ of a body composed of n particles m_s located at a distance r_s from the axis of rotation. Unlike

$$I_{xx} = \sum_{s=1}^{n} m_s r_s^2 \tag{3}$$

mass, which is constant for a given body the moment of inertia depends on the location and direction of the axis of rotation as well as the way the mass is distributed. Furthermore, for a solid body whose shape can be expressed mathematically the moment with respect to an arbitrary set of axis may be calculated by direct integration as shown in Equation 4, where ρ is the density of the body at position (x, y, z).

$$I_{xx} = \sum_{s=1}^{n} m_s(y_s^2 + z_s^2) = \iiint (y^2 + z^2)\rho \, dxdydz \qquad (4)$$

Likewise the moment of inertia for the other two axis is

$$I_{yy} = \sum_{s=1}^{n} m_s(x_s^2 + z_s^2) = \iiint (x^2 + z^2)\rho \, dxdydz \qquad (5)$$

$$I_{zz} = \sum_{s=1}^{n} m_s(x_s^2 + y_s^2) = \iiint (x^2 + y^2)\rho \, dxdydz \qquad (6)$$

To completely describe the dynamical property of the body, the center of gravity must also be known.

The previous paragraph has described a method of determining moments of inertia theoretically. There are also methods of determining it experimentally. These methods consist of using simple pendulums, compound pendulums, torsional pendulums, filiar pendulums and other types of oscillating systems. The only factors which limit the use of any oscillating system are: the equation of motion of the system contains the moment of inertia explicitly, the equation has a usuable solution and that the pertinent quantities can be obtained from an experimental system. More information on experimental methods will be covered in the applied reports section.

2.1.1.1.3 Oscillation Theory

Since the majority of experimental methods for determining moments of inertia consist of oscillating systems, a major effort will be exerted in investigating oscillatory theory. In particular, the oscillations of a torsional pendulum will be investigated in detail since it is the instrument presently

used for determining moments of inertia.

References 7 through 10 discuss the oscillations of the torsional pendulum in a relatively simple manner. That is, the first and most common assumption is that the system oscillates perfectly and no damping is present. The equation of motion for this system is shown in Equation 7, where I is the

$$I\ddot{\theta} + K\theta = 0 \tag{7}$$

moment of inertia of the oscillating object, $\ddot{\theta}$ is the angular acceleration, K is the spring constant of the rod and θ is the angular displacement. The solution for Equation 7 is easily obtained in terms of I. It is

$$I = KT^2/4\pi^2. \tag{8}$$

As further investigation was made it was realized that the assumption of a perfect system must be abandoned and that damped oscillation must be considered. This damping resulted primarily from the aerodynamic drag of the atmosphere upon the external surface of the object. Other drag forces are present, but they are assumed to be insignificant. The first and simplest damping to consider for this type system is that of viscous damping, a constant damping proportional to the velocity. Equation 9 shows this equation of motion where

$$I\ddot{\theta} + C\dot{\theta} + K\theta = 0 \tag{9}$$

$\dot{\theta}$ is the angular velocity and the other terms are the same as in Equation 7. The solution of Equation 9 in terms of I is

$$\beta = \sqrt{\frac{K}{I} - \frac{C^2}{4I^2}} \tag{10}$$

where β is the frequency of the damped oscillations. If C can be determined then I can be obtained. C/2I can be obtained because it is the slope of the curve of the natural logarithm of displacement versus total time. If C/2I is denoted by α , then Equation 10 can be written as

$$I = \frac{K}{\beta^2 + \alpha^2} \tag{11}$$

Therefore, the solution for the moment of inertia of a constantly damped system is relatively simple. If the damping is very small it can be neglected and Equation 8 will be valid. If the drag is significant the damping term C in Equation 10 will cause β to be smaller than if no drag occurred. Likewise, if β is smaller, I would be larger as shown in Equation 11. This is where the term "additional mass effects" originates, because excess drag causes the moment of inertia to appear larger. The moment of inertia does not actually increase, it just appears thay way. This phenomena is true for all pendulum systems.

These relatively simple systems are the best one to use if possible, because they can be expressed as linear differential equations. Unfortunately, they are not the ones which normally occur in actual practice. In the torsional pendulum system presently used the period of oscillation is not constant; therefore, it cannot be a constantly damped system described by Equation 9. In general the equation can be written as

$$I\ddot{\theta} + f(\dot{\theta}, \theta) + K\theta = 0 \tag{12}$$

where the middle term can represent any function of velocity or displacement. This equation is an example of a non-linear differential equation. The solution of non-linear differential equations is quite difficult and usually results in some approximation method. References 11 through 21 represent a few of the texts on non-linear differential equations. Since one entire component of the Math Model Project is devoted to damping theory, further discussion of non-linear differential equations as applied to the torsional pendulum will be postponed until the damping report. The objective of this damping study will be to determine exactly what type damping the torsional pendulum air bearing table has, then solve the equation which represents this damped system.

2.1.1.1.4 Applied Reports

This section will cover the contents of all the books and reports pertaining to the actual methods used in determining moments of inertia for various objects. The coverage necessarily will have to be in general, but it will provide enough information that the proper report for a particular use can be obtained.

The reports are divided into the following categories:

1. Survey
2. Additional Mass Effects
3. Torsional Pendulums
4. Compound Pendulums
5. Filar Pendulums
6. Component Methods
7. Computer Methods
8. Gravity Gradient Stabilization
9. Human Body Mass Characteristics
10. General Moment of Inertia Reports

These divisions describe the main theme of each report.

The survey reports, References 22 and 23 discuss different methods of determining moments of inertia in a general manner. Reference 22 discusses the pros and cons of various systems such as static methods, torsional system, linear spring system, physical pendulum, filar pendulum and variable center of gravity pendulum. This reference is a very good survey of the different systems mentioned. Reference 23 is similar to Reference 22, but not as detailed.

The next references, 24 through 27, cover aerodynamic drag effects which influence the determination of moment of inertia. This effect is called the "additional mass effect" because aerodynamic drag increases the period of oscillation, thereby effectively increasing the moment of inertia which is dependent on the period. References 24 and 25 are significant contributions to the knowledge of the "additional mass effect". The report presents a resume of test procedures and results of experimental determination of the additional mass effects of flat plates. It compares test data resulting from tests in vacuum and in the atmosphere and also compares its results to those of previous investigations. The report is useful in studying

older methods of testing, but it does not add a great deal to present day techniques. Reference 27 presents formulas for calculating the additional mass corrections for moments of inertia of airplanes. It too is an older report which adds little to the present problem.

The next group of references, 28 through 41, includes reports which cover different methods of determining moments of inertia. References 28 and 29 discuss the torsional pendulum. Reference 28 gives a simple method with limited accuracy for determining moments of inertia of aerospace components. Reference 29 discusses the torsional pendulum and compound pendulum as used in determining the moment of inertia of re-entry bodies. This report gives a very comprehensive coverage of these two methods. References 30 through 33 are mainly concerned with types of compound pendulums and spring retained pendulums. Since a compound pendulum covers anything other than the simple ball and string pendulum, a wide range of systems fall within this category.

The next group covers filar pendulums, any object suspended by two or more supporting elements and allowed to oscillate. It is similar to a torsional pendulum where one rod has been replaced by two or more wires. References 34 through 37 cover tri-filar pendulums. These reports discuss the advantages and disadvantages of filar pendulums as compared to other types. Reference 34 concludes that the tri-filar pendulum is superior in accuracy to the torsional pendulum, while Reference 35 states that the torsional pendulum is the most accurate. Obviously these are the author's opinions and we agree with the latter. Reference 37 covers the use of a bifilar pendulum in determining the moment of inertia of a orbital satellite.

References 38 through 41 include reports of moment of inertia determination by using component parts. The moment of inertia of the various parts is calculated, and transfer formulas are then used to calculate the moment of inertia of the entire body. References 42 and 43 discuss computer methods of determining moments of inertia by using components part anaysis. The computer is a very powerful tool for calculating moments of inertia and other mass characteristics if the components location and characteristics are known very accurately.

The next references cover some special used of moment of inertia determination. References 44 and 45 discuss gravity gradient stablization. This form of stablization depends on the moment of inertia of the satellite and is based on the principal that any satellite will align its long axis, or

axis of minimum moment of inertia, with the local vertical. Gravity gradient stabilization offers a means of significantly improving the reliability of long-life earth satellites and a need for precise moment of inertia determination to avoid excess weight. References 46 through 48 cover the moment of inertia determination of the human body. This is a specialized case for determining moments of inertia but it is very important when precise moment of inertia values must be known. The various moment of inertia values for the human body in different positions could be of vital importance to precision maneuvers of small spacecraft.

The last grouping, References 49 through 72, include reports which pertain to moments of inertia in one form or another. They are not directly related to the present work being performed but they may have some useful information. The last reference requires a special skill for comprehension, since it is written in German. These reports are only a small part of all reports pertaining to moments of inertia but were selected as the most significant to the present work. A search will continue for any old or new reports that might be helpful.

2.1.1.1.5 Conclusions

The literature search for the moment of inertia program has produced much valuable information. In the classical theory section the importance of the quantity of moment of inertia in the dynamical analysis of any type of rotary motion was explained. In particular, torques produced by space vehicle components are directly dependent on the moment of inertia of the rotating object. Although in the past the accuracy of the moment of inertia was not a critical factor that might cause losses of millions of dollars and human lives, today the space age has created a new importance on the accurate determination of moments of inertia.

One significant fact learned is that the Mass Metrology Laboratory has superior methods and accuracies for moment of inertia determination for certain size objects. Therefore, this laboratory represents the present state of the art in moment of inertia determination. For this reason the search could not provide any significant milestone which would greatly aid the present program. The search for old and new works that might be useful will continue.

2.1.1.1.6 References

1. Goldstein, Hebert, Classical Mechanics, Addison - Wesley Publishing Co., Reading, Massachusetts, 1959.

2. MacMillan, William Duncan, Dynamics of Rigid Bodies, Dover Publications, New York, 1936.

3. McCuskey, S. W., An Introduction to Advanced Dynamics, Addison - Wesley Publishing Co., Reading, Massachusetts, 1959.

4. Arnold, Ronald N. and Maunder, Leonard, Gyrodynamics and Its Engineering Application, Academic Press, New York, 1961.

5. Huddleston, John W., Introduction to Engineering Mechanics, Addison - Wesley Publishing Co., Reading, Massachusetts, 1961.

6. Yeh, Hausan and Abrams, Joel I., Mechanics of Solids and Fluids, Volume I, Particles and Rigid Body Mechanics, McGraw - Hill Book Co., New York, 1960.

7. Bauer, H. F., "Mechanical Vibrations, Parts I - III," Dynamic Analysis Branch, Aeroballistic Division, MSFC, Huntsville, Alabama, 1962.

8. Den Hartog, J. P., Mechanical Vibrations, 4th Ed., McGraw - Hill Book Co., New York, 1956.

9. Hansen, H. M. and Chenea, Paul F., Mechanics of Vibrations, John Wiley & Sons, Inc., New York, 1952.

10. Spiegel, Murray R., Applied Differential Equations, Prentice - Hall, Inc., Englewood Cliffs, New Jersey, 1958.

11. Arscott, F. M., Periodic Differential Equations, The MacMillan Co., New York, 1964.

12. Bogoliubov, N. N. and Mitropolsky, Y. A., Asymptotic Methods in the Theory of Non-Linear Oscillations, Hindustan Publishing Corp., Delhi, India, 1961.

13. Denman, Harry H. and Howard, James E., Application of Ultraspherical Polynomials to Non-Linear Oscillations - I. Free Oscillation of the Pendulum, Quarterly of Applied Mathematics, Vol. 22, No. 4, pp 325-330, January, 1965.

14. Denman, Harry H. and Liu, Y. King, Application of Ultraspherical Polynominals to Non-Linear Oscillations II. Free Oscillations, Quarterly of Applied Mathematics, Vol. 22, No. 4, pp 273-292, January, 1965.

15. Koshlyakov, N. S., Smirnov, M. M. and Gliner, E. B., Differential Equations of Mathematical Physics, North - Holland Publishing Co., Amsterdam, Netherlands, 1964.

16. Kryloff, N. M. and Bogoluiboff, N. N., Introduction to Non-Linear Mechanics, Princeton University Press, Princeton, New Jersey, 1947.

17. Lefschetz, S., Editor, Contributions to the Theory of Non-Linear Oscillations, Volumes 1 - 4, Princeton University Press, Princeton, New Jersey, 1950.

18. McLachlan, N. W., Ordinary Non-Linear Differential Equations in Engineering and Physical Sciences, 2nd Ed., Oxford University Press, London, England, 1955.

19. Milne, W. E., Damped Vibrations, University of Oregon Press, Eugene, Oregon, 1923.

20. Minorsky, Nicholas, Non-Linear Oscillations, D. Van Nastrand Co., Inc., Princeton, New Jersey, 1962.

21. Pipes, Louis A., Applied Mathematics for Engineers and Physicists, McGraw - Hill Book Co., Inc., New York, 1958.

22. Harris, E. C., "Selection of Techniques for Measurement of Moment of Inertia", SAWE 503, Douglas Aircraft Co., Long Beach, California, May 19, 1965.

23. Woodward, W. R., "An Arbitrary Axis Inertia Measuring System", SAWE 316, Cosmo Dynamics, Newton Upper Falls, Massachusetts, May 14, 1962.

24. Carpenter, G. T. and Meredith, D. T., "The Derivation of an Efficiency Factor and its Application to a Torsional System for Determining Mass Moments of Inertia", SAWE 296, NASA, Huntsville, Alabama, May 19, 1961.

25. Carpenter, G. T. and Meredith, D. T., "Determining Inertias by Using the Amplitude Decay Rate of a Mechanical Oscillating System", TN D-1114, NASA, Huntsville, Alabama, May, 1962.

26. Gracey, William, "The Additional Mass Effect of Plates as Determined by Experiments", NACA 27th Annual Report, Report No. 707, 1941.

27. Malvestuto, F. S., Jr. and Gale, L. J., "Formulas for Additional Mass Corrections to the Moments of Inertia of Airplanes", Tech. Note 1187, Langley Memorial Aeronautical Laboratory, Langley Field, Virginia, February, 1947.

28. Rogers, N., "Inertia Measurements of Aero Space Equipment", SAWE 448, IBM, Owego, New York, May 21, 1964.

29. Skogh, J., "A Unique Solution to the Moment of Inertia Problem", SAWE 214, Lockheed Missiles and Space Division, Sunnyvale, California, May, 1959.

30. Gracey, W., "The Experimental Determination of the Moments of Inertia of Airplanes by a Simplified Compound-Pendulum Method", TN-1629, Langley Memorial Aeronautical Laboratory, Langley Field, Virginia, June, 1948.

31. Harris, J. B., "Experimental Inertia Tests for Missiles", SAWE 151, Temco Aircraft Corp., Dallas, Texas, May 2, 1957.

32. Kleinhans, R. G., "Experimental Inertia Determination", SAWE 119, Republic Aviation Corp., Farmingdale, New York, May 2, 1955.

33. Robertson, R. L. and Harris, E. C., "A Simplified Technique for Precision Measurement of Moment of Inertia", SAWE 312, Douglas Aircraft Co., Inc., May, 1962.

34. Hughes, G. W., "The Trifilar Pendulum and Its Application to the Experimental Determination of Moments of Inertia", PN 57-SA-51, ASME, Sandia Base, Albuquerque, New Mexico, June 9, 1957.

35. Korr, A. L. and Hyer, P., "A Trifilar Pendulum for the Determination of Moments of Inertia", Report R-1653, Frankford Arsenal, Philadelphia, Pennsylvania, August, 1962.

36. Schueke, R. L., "Trifilar Moment of Inertia Apparatus", SAWE 290, Goodyear Aircraft Corp., Akron, Ohio, May 15, 1961.

37. Dolan, F. J., "Measurement of the Moment of Inertia of the Orbiting Astronomical Observatory", SAWE 380, Grumman Aircraft Engineering, Corp., Beth Page, Long Island, New York, 1963.

38. Denny, L. M. and Durrington, V. L., "Simulation of Mass Properties for Test Vehicles Using the Inertia Component Method", SAWE 304, Boeing Co., Wichita, Kansas, May 14, 1962.

39. Dhanes, L. W., "Moments of Inertia and Centers of Gravity by the Mass Distribution Method", SAWE 637, Douglas Aircraft Co., Inc., Santa Monica, California, May 22, 1958.

40. Marsh, D., "Mass Moment of Inertia Estimation Methods - Manned Aircraft", SAWE 313, Douglas Aircraft Co., Inc., Long Beach, California, May 17, 1962.

41. Welsby, G. R., "A Rapid Inertia Estimating Method", SAWE 499, Martin-Marietta Corp., Denver, Colorado, May 19, 1965.

42. Dudenhoefer, D. E. "The Application of Digital Computers of the Calculation of Moments of Inertia of Aircraft Wings", SAWE 299, North American Aviation, Columbus Division, May, 1959.

43. Spencer, B. C., "Computer Analysis of Dynamic Mass Characteristics", SAWE 502, Douglas Aircraft, Inc., Huntington Beach, California.

44. Schalkowski, S. and Cooley, W. C., "Gravity Gradient Torques on a Sun-Oriented Space Station", TR 001, NASA, Washington, D. C., December 20, 1962.

45. Zanchettin, L. R., "Mass Moment of Inertia Computer Program Used in Optimizing a Gravity Gradient System", SAWE 496, G. E. Co., Philadelphia, Pennsylvania, May 19, 1965.

46. Clauser, C. E., "Moments of Inertia and Centers of Gravity of the Living Human Body", AMRL-TDR-63-36, Wright-Patterson Air Force Base, Ohio, May, 1963.

47. DuBois, J., Santschi, W. R., Walton, D. M., Scott, C. O. and Mazy, F. W., "Moment of Inertia and Center of Gravity of the Living Human Body Encumbered by a Full Pressure Suit", AMRL-TR-64-110, Wright-Patterson Air Force Base, Ohio, November, 1964.

48. Hanavan, E. P., "A Mathematical Model of the Human Body", M.S. Degree Thesis, Aerospace Medical Division, Air Force System Command, Wright-Patterson Air Force Base, Ohio, October, 1964.

49. Alexseev, K. K. and Vosklesenski, V. V., "Increase of Accuracy of Stabilization Systems", ARS Journal, April 9, 1960.

50. Bulgia, J. J., Young, G. R., Timmons, J. D. and Brinkworth, "Analytical Method of Approximating the Motion of a Spinning Vehicle with Variable Mass and Inertia Properties Acted Upon by Several Disturbing Parameters", TR R-110, NASA, Langley Research Center, 1961.

51. Chawla, J. P., "Empirical Formulae for Radii of Gyration of Aircraft", SAWE 78, Hughes Aircraft Co., Culver City, California, May 8, 1952.

52. Colombo, G., "The Motion of Satellite 1958 Epsilon Around its Center of Mass", SR 70, SAO, Cambridge, Massachusetts, July 18, 1961.

53. Dowson, D., "Inertia Effects in Hydrostatic Thrust Bearings", P.N. 60, Journal of Basic Engineering, ASME, June, 1961.

54. Dukes, T. A. and Hargraves, C. R., "Stability Augmentation of Ground Effect Machines", R.N. 601, Princeton University, April, 1962.

55. Ehlers, J. G. and Cowgill, G. R. "Fortran Program for Computing the Principal Moments of Inertia of a Rigid Molecule", TN D-2085, NASA, Lewis Research Center, Cleveland, Ohio, February, 1964.

56. Emery, R. R. and Lewis R. F., "Weight Moment of Inertia Nomographs", SAWE 457, Lockheed Missiles and Space Division, Sunnyvale, California, May 18, 1964.

57. Gerhard, S. L., "Transverse Moments of Inertia by Mechanical Integration", TM 1423, Feltman Research Laboratories, Dover, New Jersey, May, 1964.

58. Glasgow, G. C. and Cronin, J. L., "Cordwise-Bending Effects on Wing-Vibration Modes", Journal Aerospace Science, Vol. 27, pp 962-963, December, 1960.

59. Green, W. E., "The Mominertograph for Determining Axial and Transverse Moments of Inertia of Solids of Revolution", Report R-1708, Frankfort Arsenal, Philadelphia, Pennsylvania, February, 1964.

60. Haggard, C., "The Calculation of the Mass Moments of Inertia of Aircraft", SAWE 148, Hayes Aircraft, Birmingham, Alabama, December 30, 1956.

61. Hering, K. W. and Hufnagle, R. E., "An Internal Sphere System for Complete Attitude Control of Earth Satellites", ARS 1499-60, Perkin-Elmer Corp., Nowalk, Connecticut, December, 1960.

62. Kendall, B. R., "A Graphic Technique for Calculating Time Changing Moments of Inertia", SAWE 386, The Emerson Elec. Mfg. Co., St. Louis, Missouri, May 2, 1963.

63. Koelle, Heinz H., Editor, Handbook of Astronautical Engineering, McGraw - Hill Book Co., New York, 1961.

64. Kopal, Z., "Effects of Thermal Expansion on the Moments of Inertia of the Moon", Icarus, Vol. 4, pp 166-172, Boeing Scientific Research Laboratories, Seattle, Washington, January 19, 1965.

65. Kopal, Z., "Possible Effects of Convection on Lunar Moments of Inertia", Icarus, Vol. 4, pp 173-176, Boeing Scientific Research Laboratories, Seattle, Washington, January 19, 1965.

66. Kurzhals, P. R., "Spin Dynamics of Space Stations Under Transient and Steady-State Excitations and Stabilizing Responses", Thesis for MSAE, VPI, May, 1962.

67. Levinson, C. A., "Moment of Inertia and the Shell Model", Physical Review, Vol. 132, No. 5, December, 1963.

68. McCarron, S. G., "Derivation and General Calculation of Conservative Torques Exerted at the Paddle-Arm Axis of a Laboratory Model Satellite and the Determination of the Moment of Inertia about the Paddle-Arm Axis of a Rectangular Solar Paddle with Variable Pitch", TMX-54604, NASA, Goddard Space Flight Center, Greenbelt, Maryland, September, 1963.

69. Rucorn, S. K., "Changes in the Earth's Moment of Inertia", Nature, Vol. 204, p. 823-825, November 28, 1964.

70. Yarov-yarovoi, M. S., "On the Computation of Higher Partial Derivitives of a Composite Function", N64-16191, NASA, March 17, 1959.

71. Worley, W. J., and Wang, H., "Geometrical and Inertial Properties of a Class of Thin Shells of Revolution", University of Illinois.

72. Wowries, W. E., "Determination of Inertia Moments from Pendulum Tests", (In German), VDI Zeitshrift, Vol. 106, June, 1964.

2.1.1.2 Aerodynamic Drag Tests

2.1.1.2.1 Introduction

The prime objective of the moment of inertia program was to develop a rapid and accurate method of determining moments of inertia of space vehicle components. This program was divided into five separate projects which directly or indirectly added to the prime objective. Each project was further broken down into components which augment the total program. This report was the result of the Aerodynamic Drag Test portion of the Math Model Project. The objective of the Math Model Project was to investigate the theoretical aspect of the moment of inertia determining system and to develop the exact mathematical expression for the torsional air bearing table system. With this exact expression only the system's experimental errors will have to be considered in order to improve the system's accuracy. Specifically the Aerodynamic Drag portion was designed to provide experimental data from which the theoretical expressions could be derived.

The Aerodynamic drag tests were divided into two categories; qualitative and quantitative. The first tests were performed using five drag configurations at three different frequencies. The test objects used here had a large variation in drag, but their physical size limited an accurate determination of their moment of inertia. Therefore, the results of these fifteen tests were compared to each other to show the effect of object surface area and oscillating frequency on the damping of the system. The later tests were designed to show the exact effect of damping on the determination of moments of inertia. In these tests two precision drag objects with different surface areas but identical masses and moments of inertia were used to show the exact effect on moment of inertia determination.

2.1.1.2.2 Qualitative Tests

2.1.1.2.2.1 Test Procedure

The test equipment used for these tests consisted of the torsional pendulum air bearing table and the period and displacement measuring devices. The period measuring device consisted of a photocell and light source with a knife edge mounted to the table top for breaking the light beam. A Hewlett-Packard 524D frequency counter and 560A digital recorder was used for measuring periods and giving an automatic printout. The displacements were measured manually by using a radian scale, light source, and mirror arrangement. A mild steel torsion rod was used for producing forced oscillations. A special cylindrical drag adapter with four drag plates was used to provide different drags. The cylindrical drag adapter or air shield was used to provide a constant table drag independent of the load or drag configuration. The frequency of oscillation of the table was reduced by placing 100 pound cylindrical weights

on the table top at a specific location. The dimensions and characteristics of the drag configurations and the cylindrical weights are shown in Figures 1 and 2 respectively. The moments of inertia of these various arrangements of weights and drag plates are shown in Figure 3.

The test equipment was arranged as shown in Figure 4. The air bearing table was first leveled on the isolated platform. Next, the air pressure was regulated to 30 psi then the appropriate test objects were mounted on the table. Finally, the torsion rod was inserted into the table to avoid any compressive forces from being placed on the rod. The period timing device and the displacement measuring apparatus were aligned to give a zero reading for zero displacement. The electronic equipment was allowed to warm up at least 30 minutes before testing began. A ten period average was recorded automatically every 20th cycle and the corresponding displacement was recorded manually.

The tests were performed by displacing the table top to a maximum displacement of 0.05 radians. The table top was then allowed to decay to a maximum displacement of 0.035 radians. The data was recorded between a displacement of 0.035 and 0.001 radians. The information obtained from each test was: test number, date, personnel, temperature, humidity, drag plate, number of weights, and the 10 period average and displacement every 20th cycle starting at a maximum displacement of 0.0035. Each test was repeated at least three times to provide good repeatable data. The test procedure for these tests are shown in Appendix A 1.

2.1.1.2.2.2 Test Results and Analysis

The results of these tests are shown in Table 1 and Figures 5 through 14. Table 1 shows the moment of inertia calculations for the various configurations. The period was obtained by averaging all the periods between displacement of 0.002 and 0.001 radians. The moment of inertia was then calculated by using.

$$I = \frac{KT^2}{4\pi^2} \tag{13}$$

where K is the rod spring constant. The theoretical moments of inertia were calculated in Figure 3. The percentage difference in the experimental and theoretical values is shown in the last column of Table 1. The percentage difference increases for a given weight as the drag plate size increases and for a given drag plate as the weight increases. This error was caused by the

FIGURE 1

SPECIAL DRAG ADAPTERS

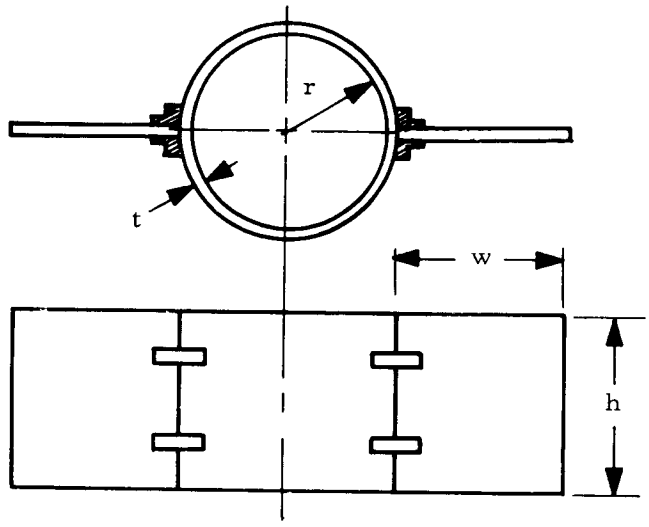

Cylindrical Adapter

r = 11.62 in.
t = 0.094 in.
h = 26.02 in.
w = 20.41 lbs.

Drag Plates	W	h	w
A	1.89 lbs.	26.02 in.	6.0 in.
B	3.79	26.02	12.0
C	5.66	26.02	18.0
D	7.58	25.02	24.0

FIGURE 2

CYLINDRICAL WEIGHTS

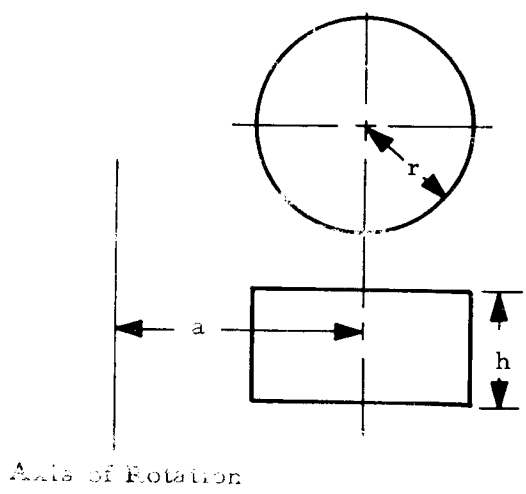

r = 5.0 in.
h = 4.45 in.
a = 6.5 in.
W = 98.92 lbs.
M = .257 lb-sec^2/in.

FIGURE 3

Theoretical Moment of Inertia Values For Various Drag Configurations

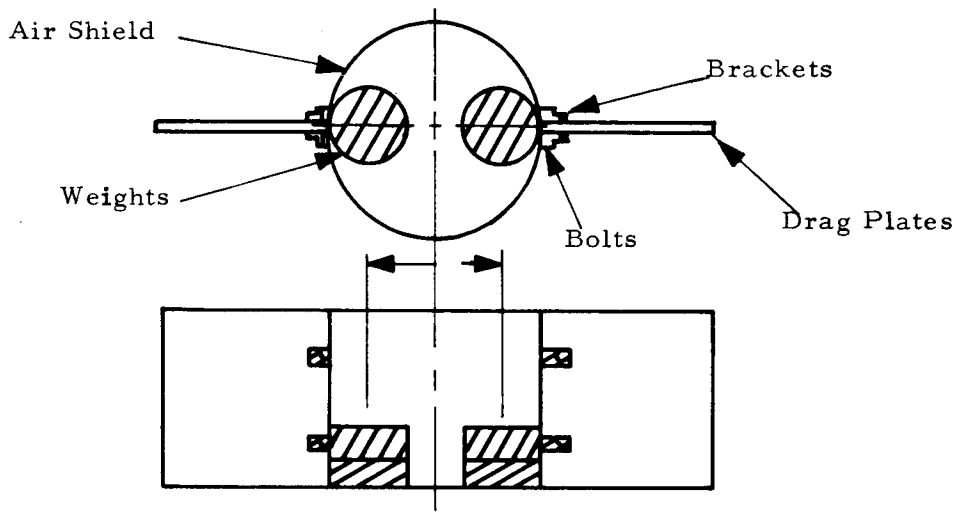

Object	Moment of Inertia
Table Top	9.93 in-lb-sec^2
Air Shield	6.43
Brackets and Bolts	0.69
Drag Plate A	2.12
Drag Plate B	6.32
Drag Plate C	13.24
Drag Plate D	23.75
Weights	14.01

Combined Moment of Inertias

Weight / Drag Plate	0 lbs.	200 lbs.	400 lbs.
None	16.36	44.38	72.40
A	19.17	47.19	75.21
B	23.37	51.39	79.41
C	30.29	58.31	86.33
D	40.80	68.32	96.84

TABLE 1

TEST RESULTS

Drag Plate	Weight	Period	I_{exp}	I_{theo}	% Difference
None	0 lbs.	0.49254	16.38	16.36	0.12
"	200	0.81040	44.36	44.38	0.05
"	400	1.03548	72.43	72.40	0.04
A	0	0.53395	19.26	19.17	0.47
"	200	0.83442	47.03	47.19	0.34
"	400	1.05229	74.79	75.21	0.56
B	0	0.59244	23.70	23.37	1.41
"	200	0.87514	51.73	51.39	0.66
"	400	1.08269	79.18	79.41	0.29
C	0	0.68043	31.27	30.29	3.24
"	200	0.93537	59.10	58.31	1.35
"	400	1.12520	85.57	86.33	0.88
D	0	0.80046	43.28	40.80	6.08
"	200	1.02184	70.53	68.82	2.48
"	400	1.19883	97.07	96.84	0.24

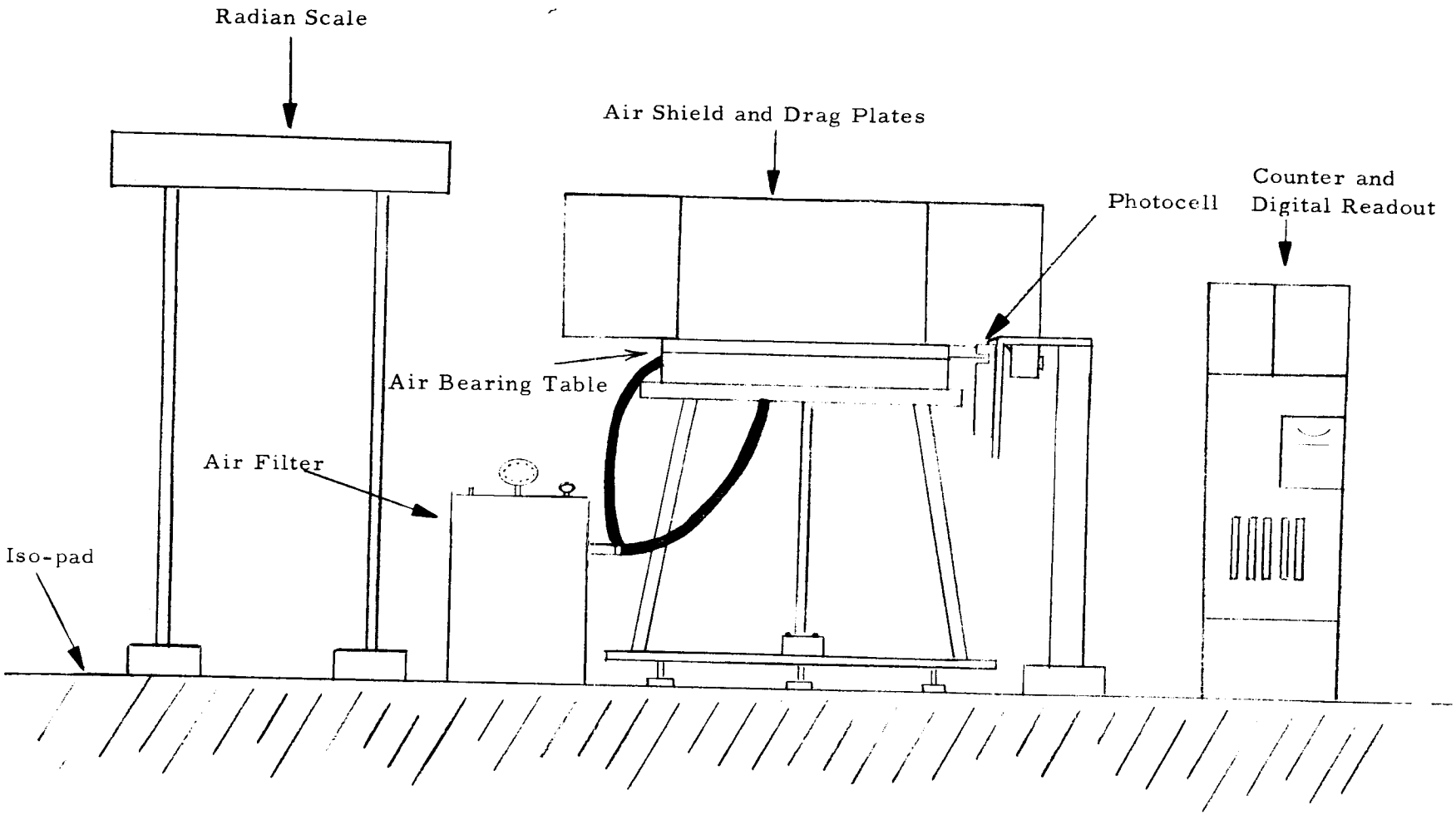

FIGURE 4

TEST EQUIPMENT ARRANGEMENT

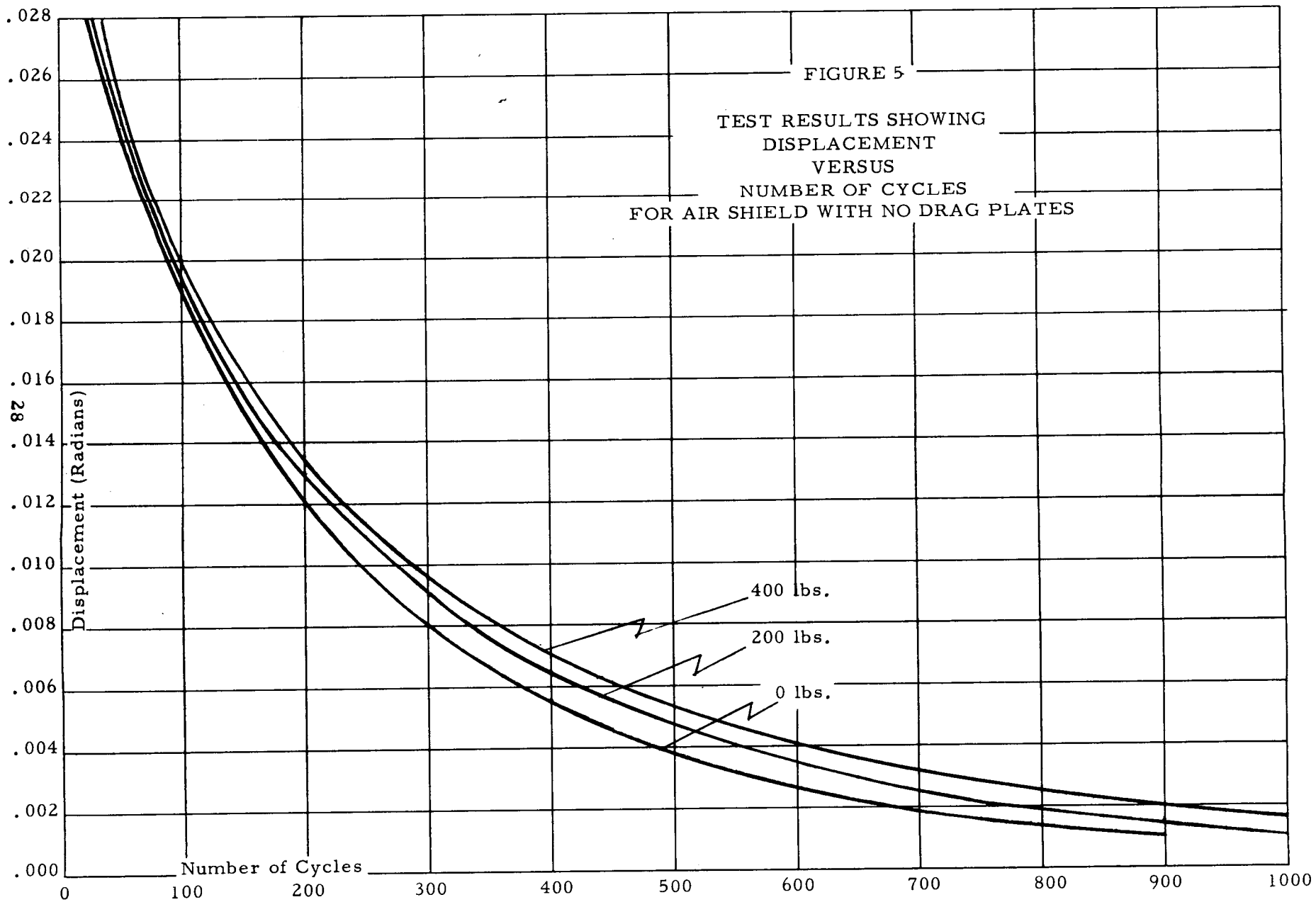

FIGURE 5

TEST RESULTS SHOWING
DISPLACEMENT
VERSUS
NUMBER OF CYCLES
FOR AIR SHIELD WITH NO DRAG PLATES

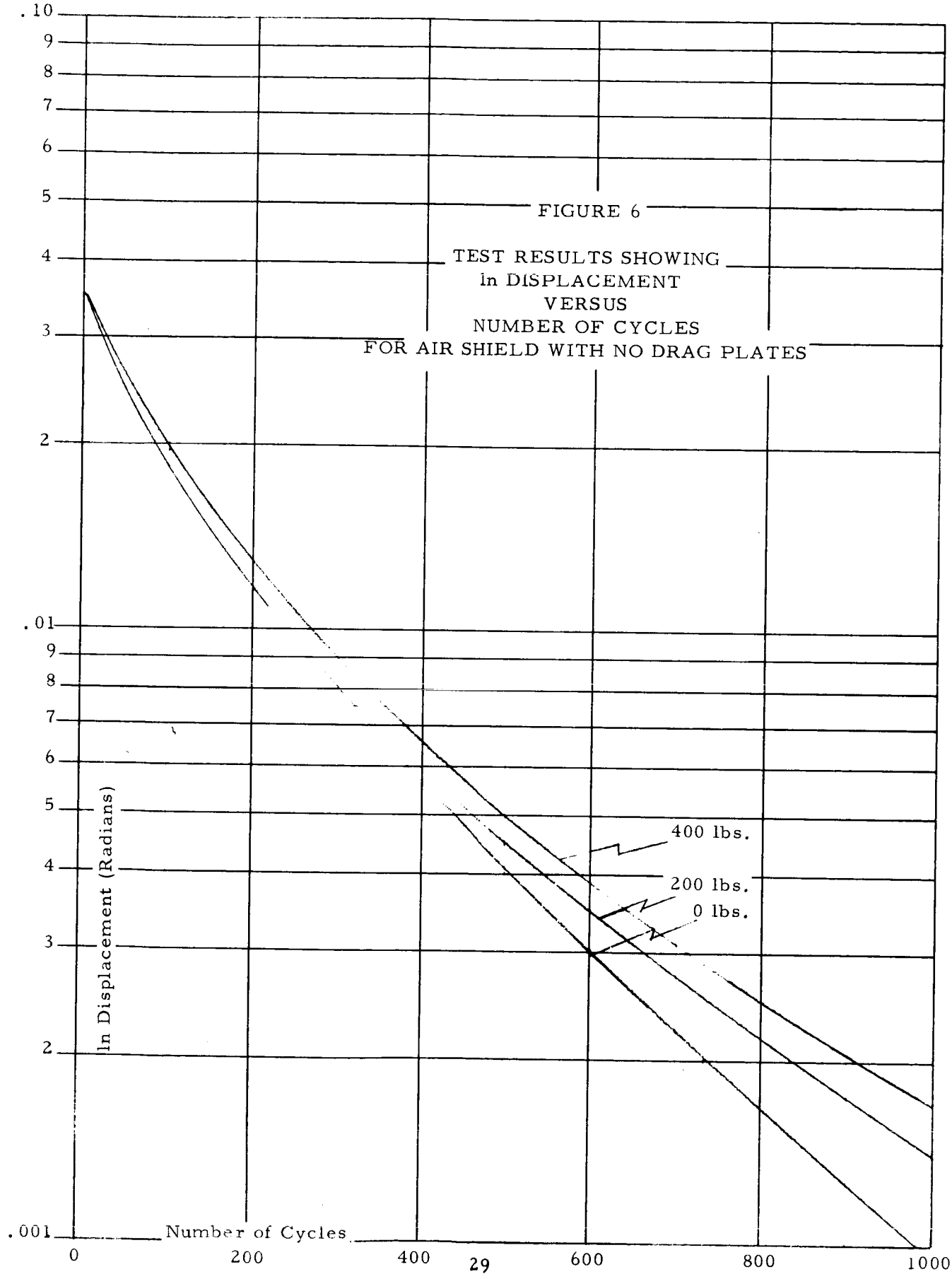

FIGURE 6

TEST RESULTS SHOWING
ln DISPLACEMENT
VERSUS
NUMBER OF CYCLES
FOR AIR SHIELD WITH NO DRAG PLATES

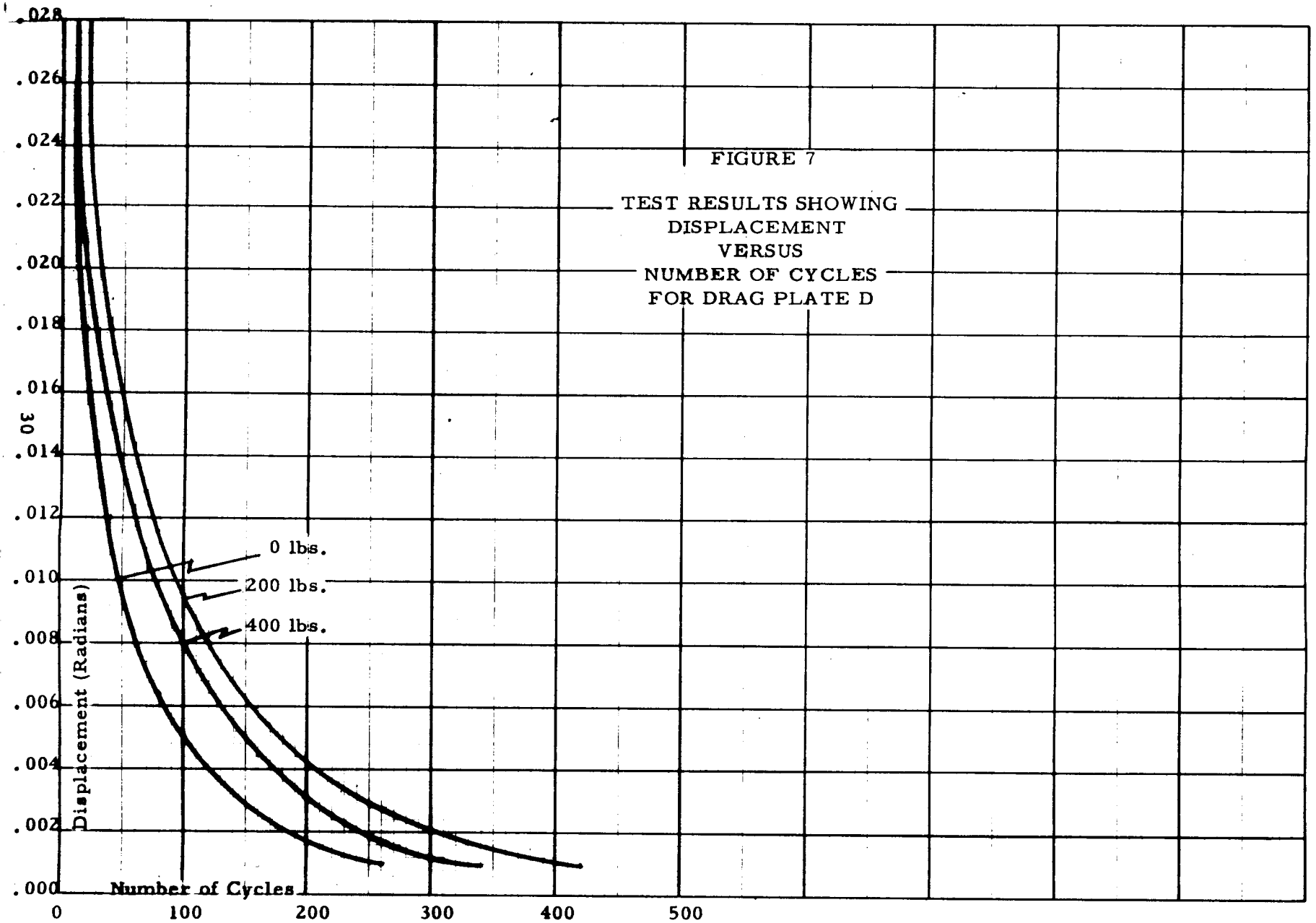

FIGURE 7

TEST RESULTS SHOWING DISPLACEMENT VERSUS NUMBER OF CYCLES FOR DRAG PLATE D

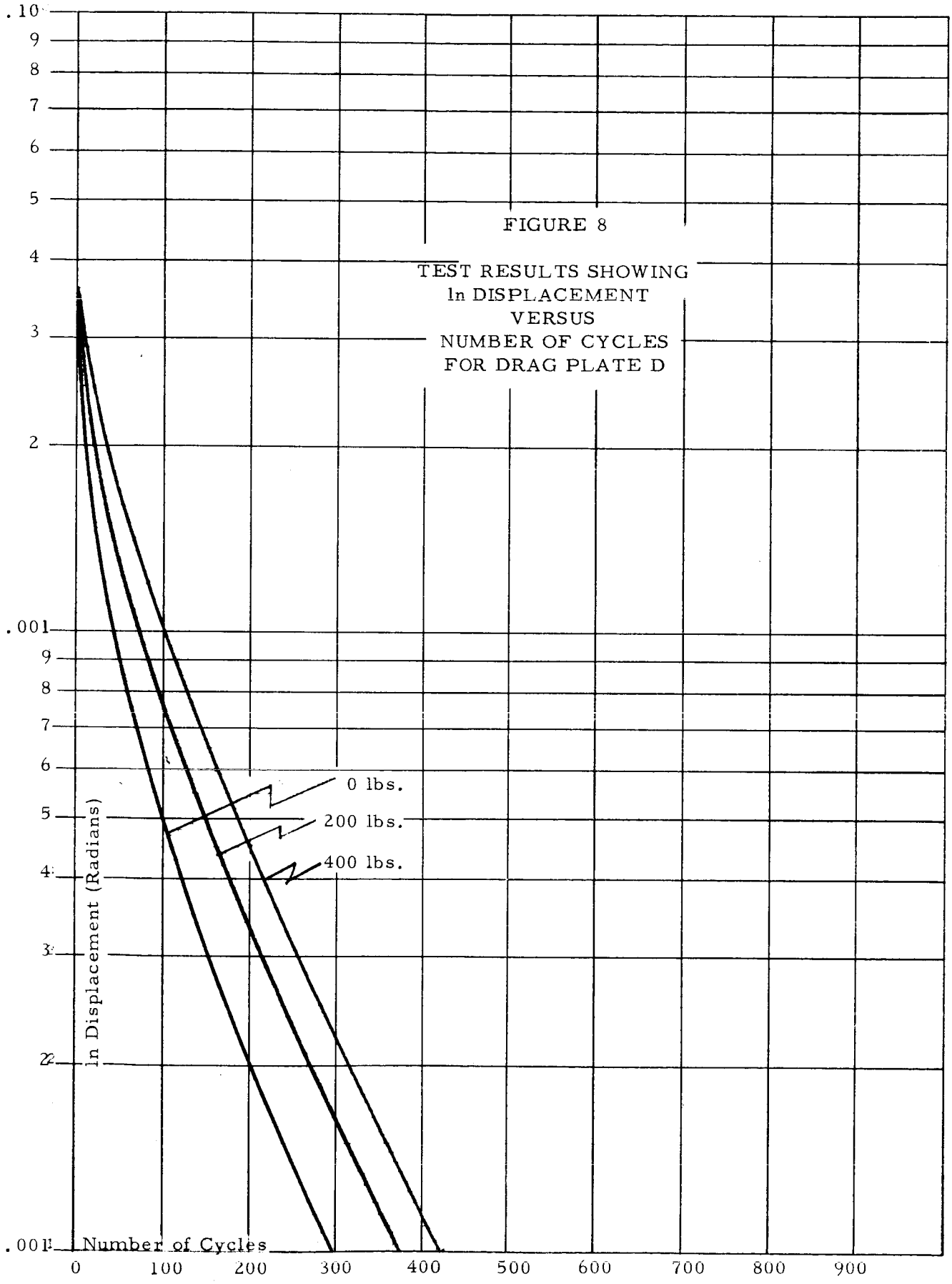

FIGURE 8

TEST RESULTS SHOWING
ln DISPLACEMENT
VERSUS
NUMBER OF CYCLES
FOR DRAG PLATE D

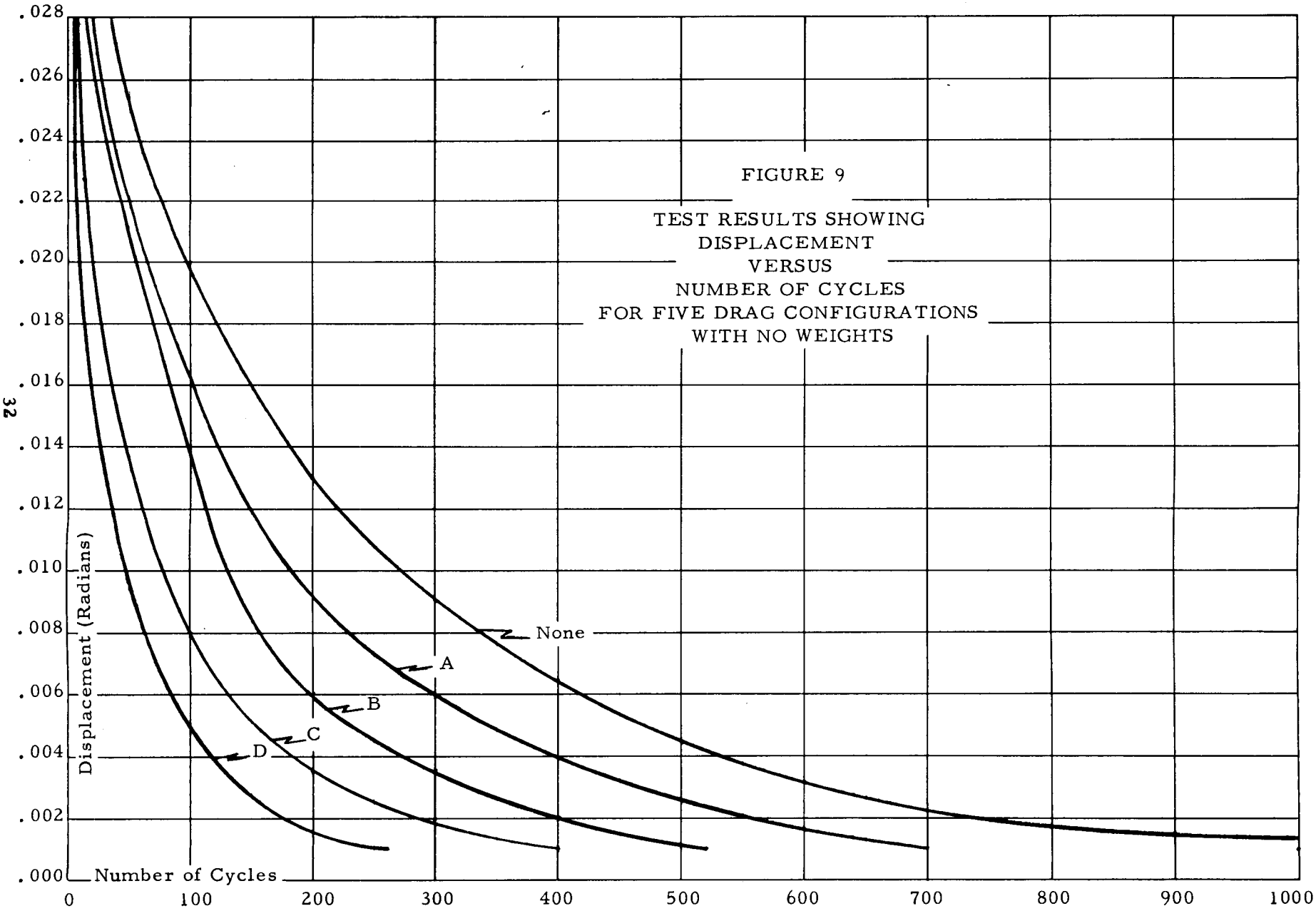

FIGURE 9

TEST RESULTS SHOWING
DISPLACEMENT
VERSUS
NUMBER OF CYCLES
FOR FIVE DRAG CONFIGURATIONS
WITH NO WEIGHTS

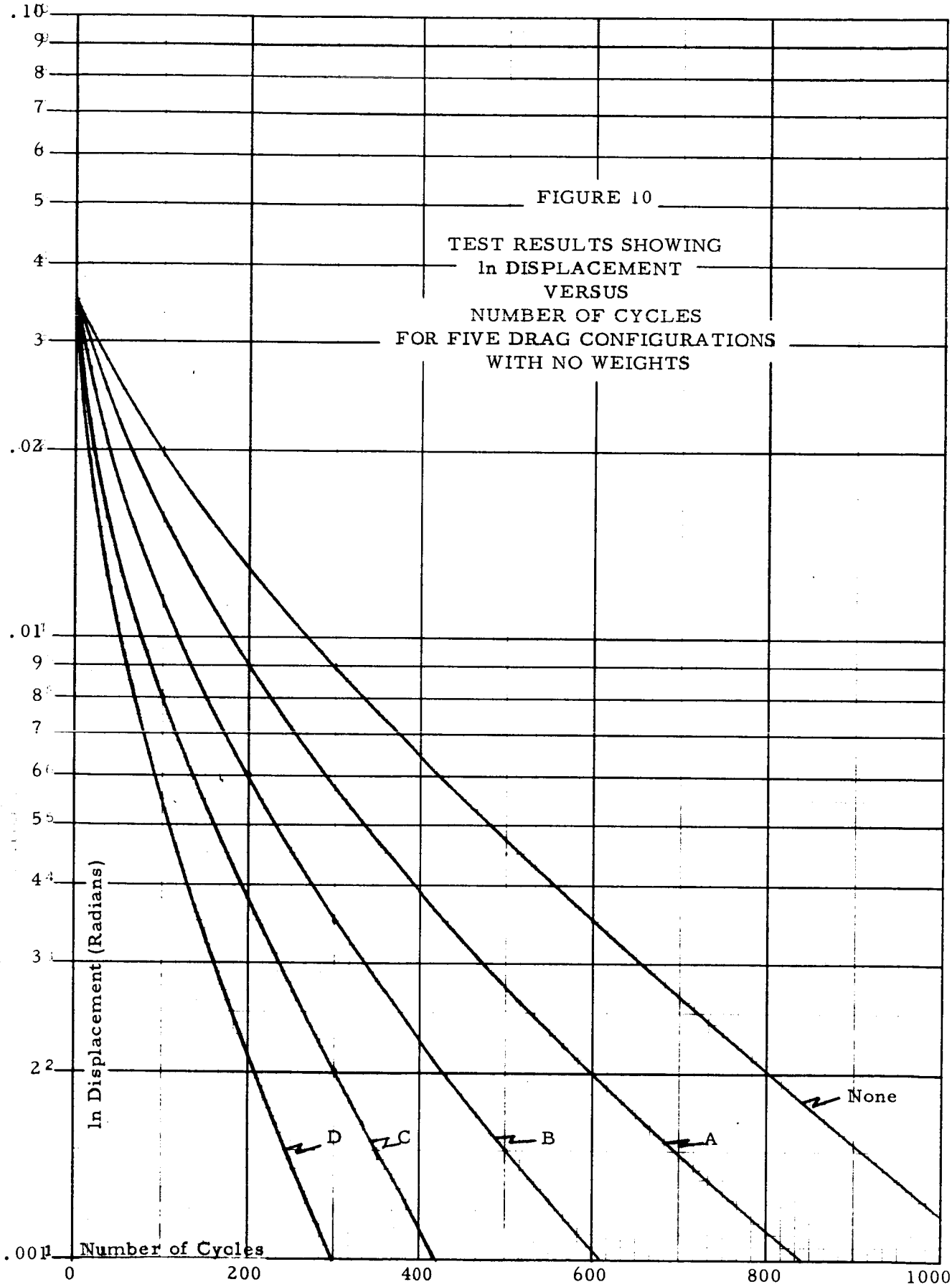
FIGURE 10
TEST RESULTS SHOWING
ln DISPLACEMENT
VERSUS
NUMBER OF CYCLES
FOR FIVE DRAG CONFIGURATIONS
WITH NO WEIGHTS
ln Displacement (Radians)
Number of Cycles
.10
.02
.01
.001
0
200
400
600
800
1000
None
A
B
C
D

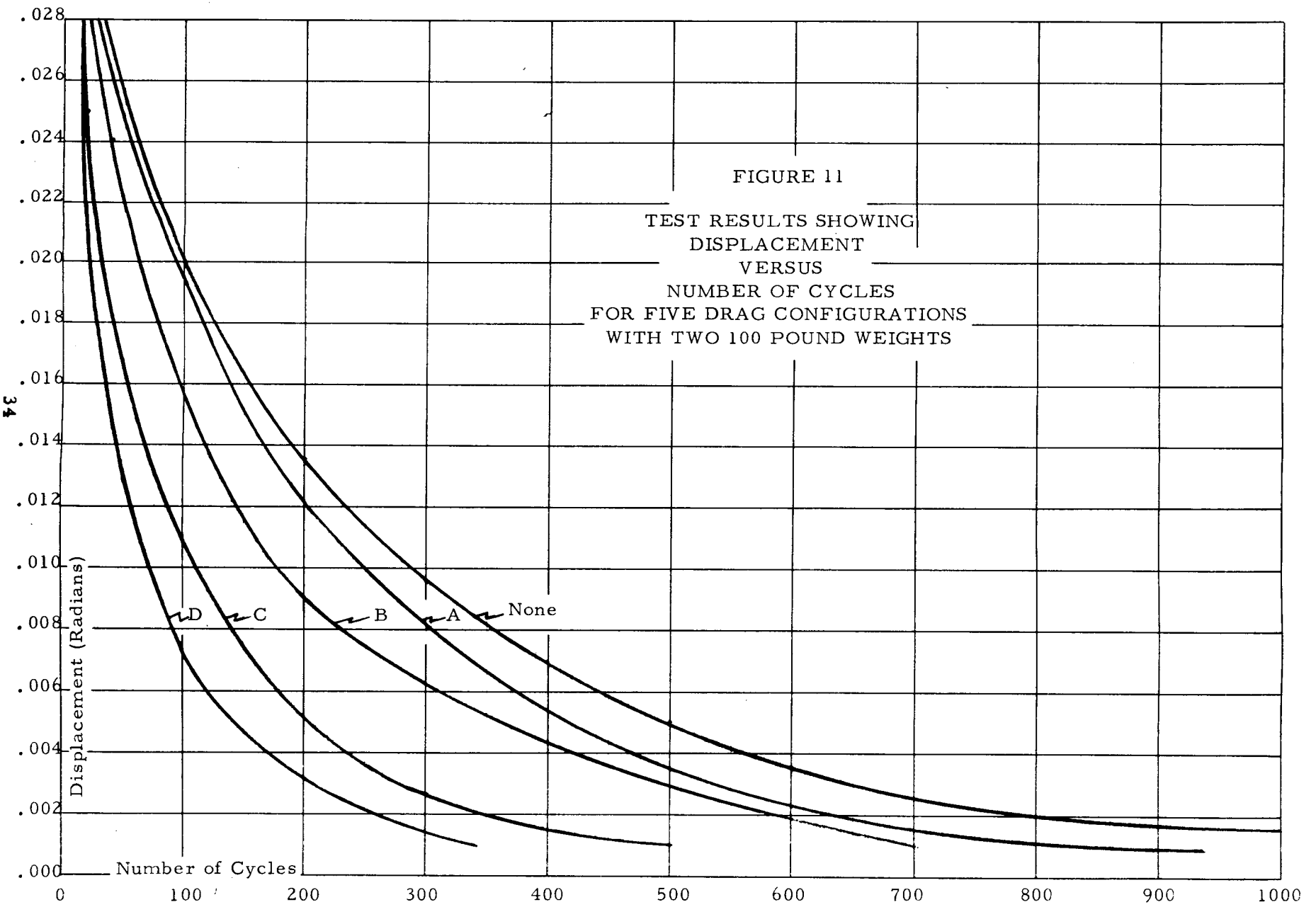

FIGURE 11

TEST RESULTS SHOWING
DISPLACEMENT
VERSUS
NUMBER OF CYCLES
FOR FIVE DRAG CONFIGURATIONS
WITH TWO 100 POUND WEIGHTS

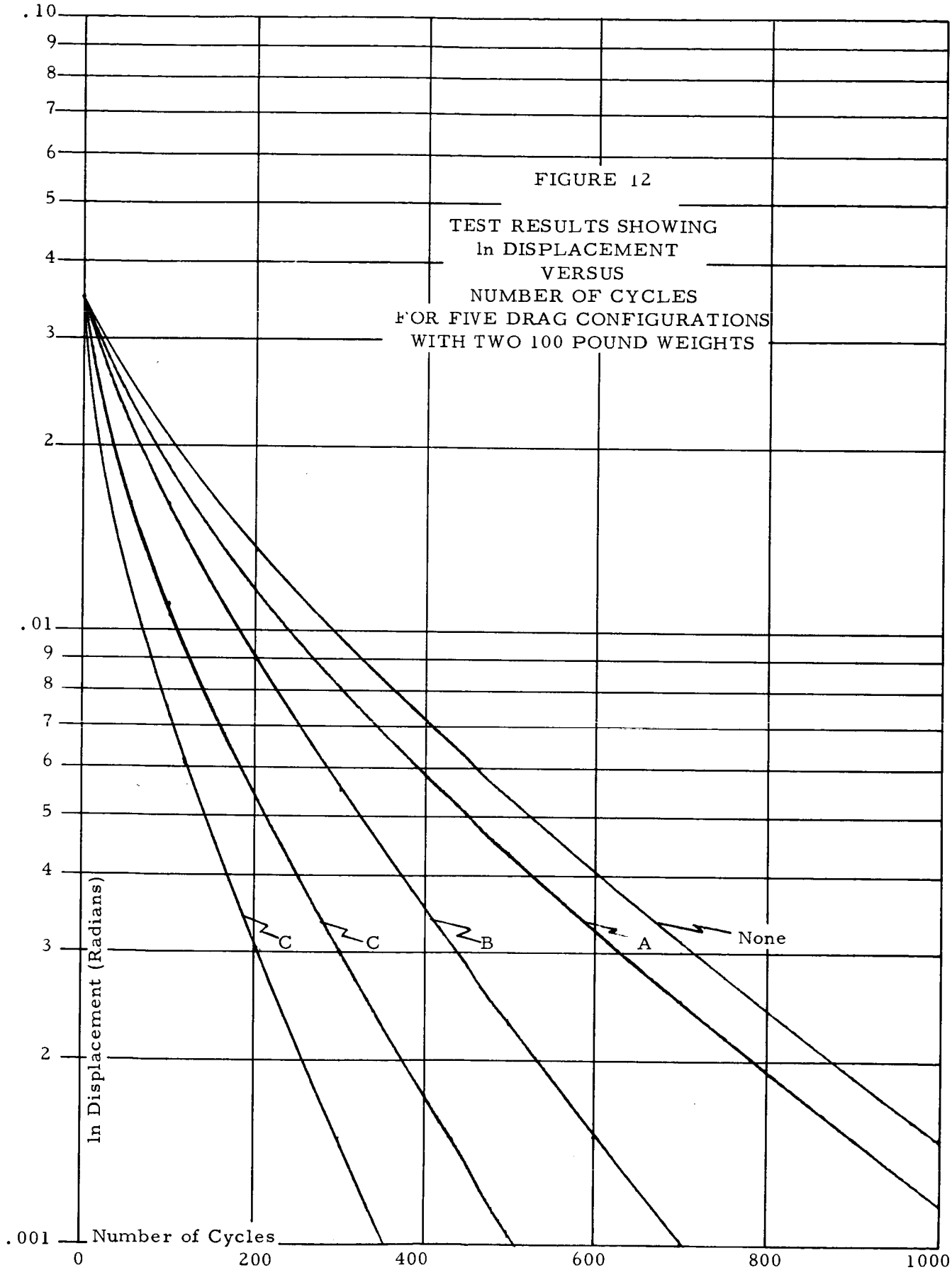

FIGURE 12

TEST RESULTS SHOWING
ln DISPLACEMENT
VERSUS
NUMBER OF CYCLES
FOR FIVE DRAG CONFIGURATIONS
WITH TWO 100 POUND WEIGHTS

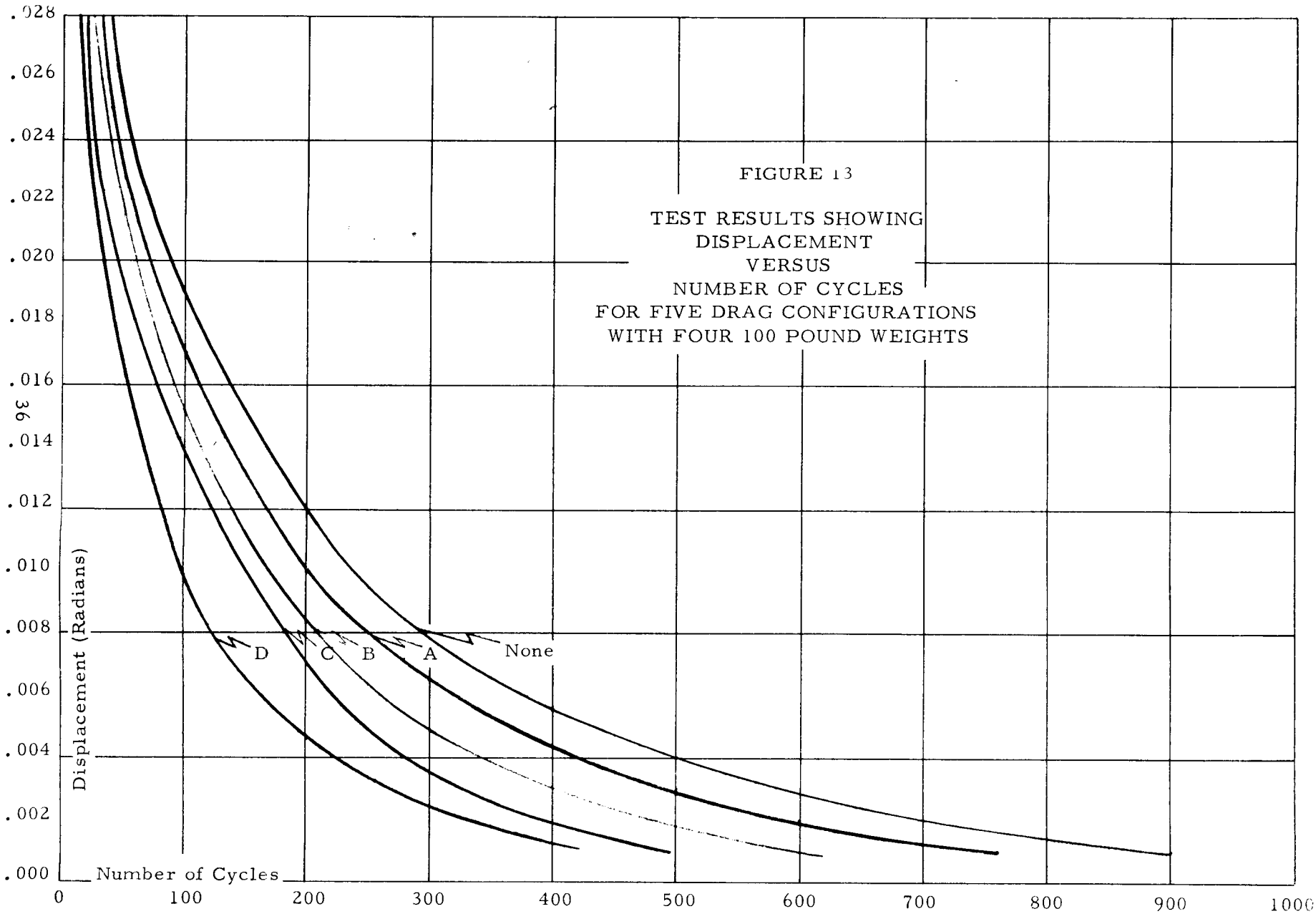

FIGURE 13

TEST RESULTS SHOWING DISPLACEMENT VERSUS NUMBER OF CYCLES FOR FIVE DRAG CONFIGURATIONS WITH FOUR 100 POUND WEIGHTS

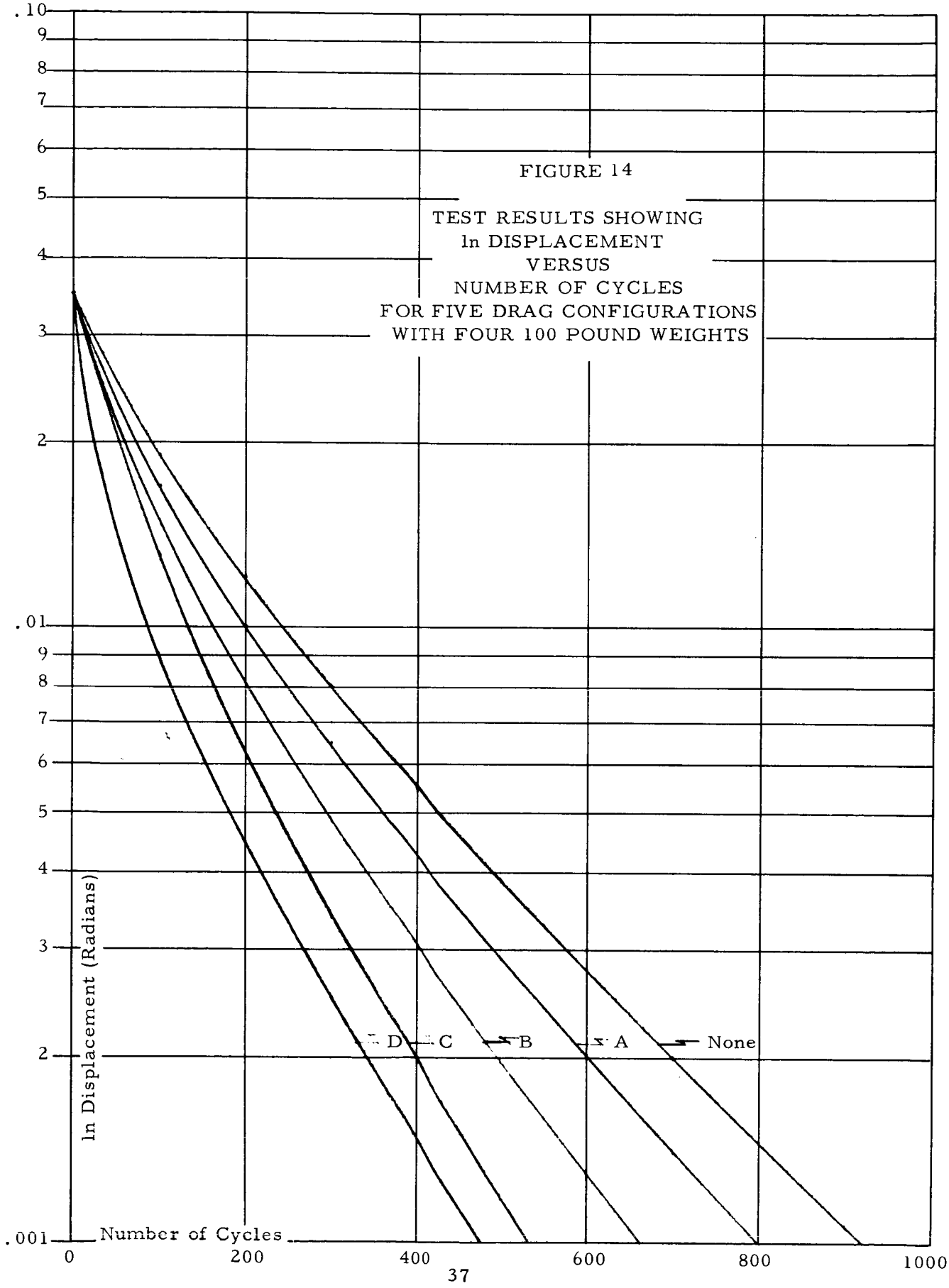

FIGURE 14

TEST RESULTS SHOWING
ln DISPLACEMENT
VERSUS
NUMBER OF CYCLES
FOR FIVE DRAG CONFIGURATIONS
WITH FOUR 100 POUND WEIGHTS

instability of the drag plates at higher frequencies. This assumption was verified by mounting braces to the drag plates and rerunning the tests. The percentage difference was greatly reduced by stiffening the drag plates.

Figures 5 through 14 graphically show the effect of various drags on the oscillating system. Figure 5 shows the rate of decay for the air shield with three different weights. This configuration represents the minimum drag and the figure shows that the frequency of oscillation, which is inversely related to the load, has little effect. However, the higher frequencies do dampen out somewhat faster. The data used in Figure 6 is the same as in Figure 5. This plot is used because the slope of the curve in this plot is proportional to the damping constant of the system. This plot readily shows which configuration has the largest damping. Figures 7 and 8 show the same type data as in Figures 5 and 6, where drag plate D has been used. Drag plate D represents the maximum drag configuration. By observing Figures 5 through 8 it is noted that the damping for drag plate D is much greater than that for no drag plate and that the drag increases with frequency of oscillation. Figures 9 through 14 show the results of all the tests in a different manner. Again these tests show that the drag increases as the size of the drag plate increases and as the frequency of oscillation increases. The logarithmic plots verify the above conclusions and they also proved that the damping for all these systems is relatively small at low amplitudes. The quantitative tests will show these results in more detail where stiff drag plates have been used to eliminate all mechanical vibration.

2.1.1.2.3 Quantitative Tests

2.1.1.2.3.1 Test Procedure

The quantitative tests also used the air bearing table and the period measuring device mentioned before. Two displacement measuring devices were used to cover large and small amplitudes. One device was the one previously described and the new device is described in Section 2.1.2.2. This new device was much more precise and has a resolution of 17 microradians. A mild steel rod was used for the forcing element. The drag plates used in these tests were precisely made plates with special adapters for mounting the plates to dumbbell standard C. These plates were designed to have the same mass and moment of inertia but different surface areas. The plate dimensions are given in Figure 15. The frequency of oscillation was varied by using different torsion rods.

The test equipment was arranged as shown in Figure 16 and the set up was identical to that already described. The output of the displacement measuring device was fed into a Hewlett-Packard 524D frequency counter and a 560A

FIGURE 15

DRAG PLATE DIMENSIONS

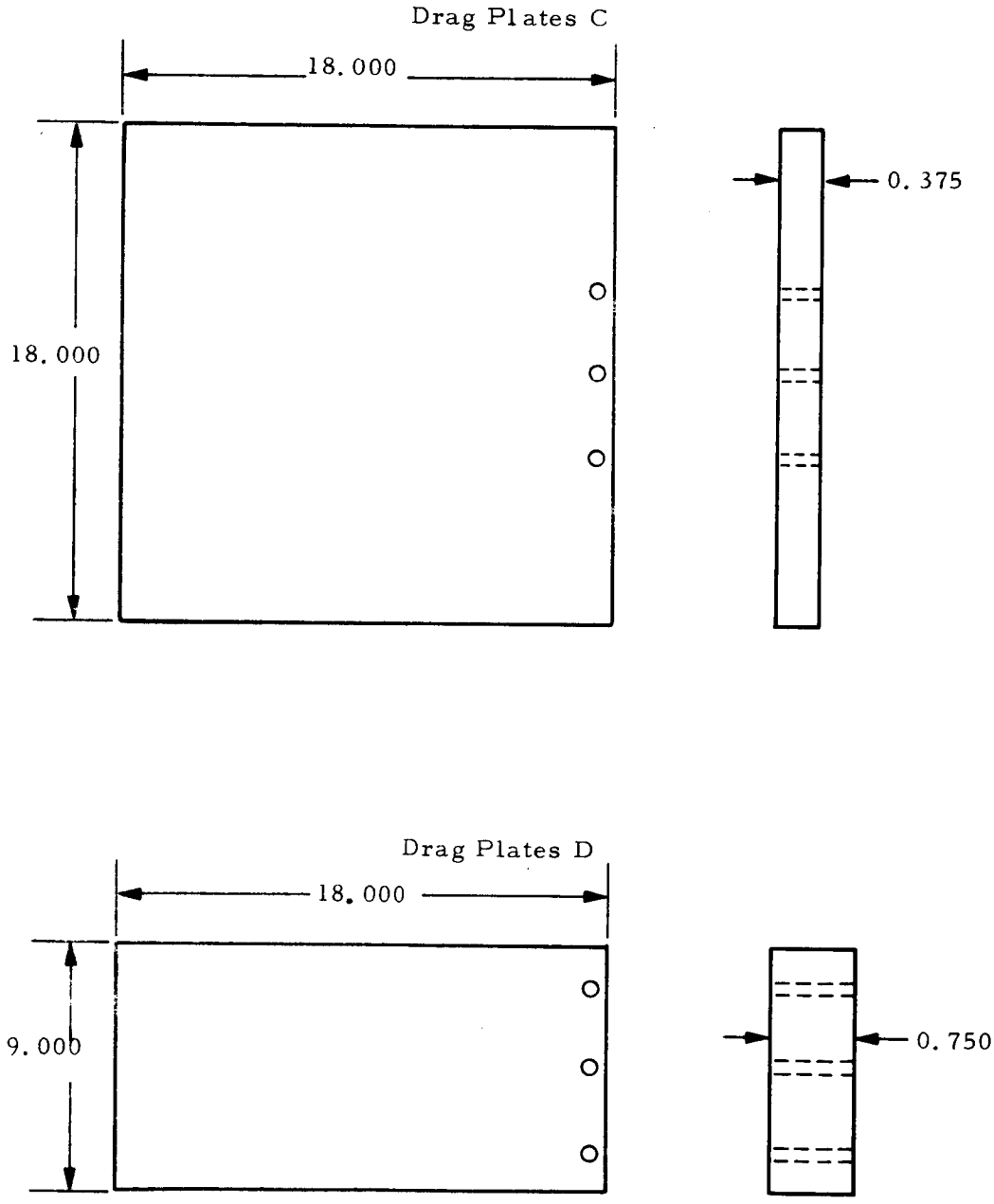

FIGURE 6

QUALITATIVE TEST EQUIPMENT ARRANGEMENT

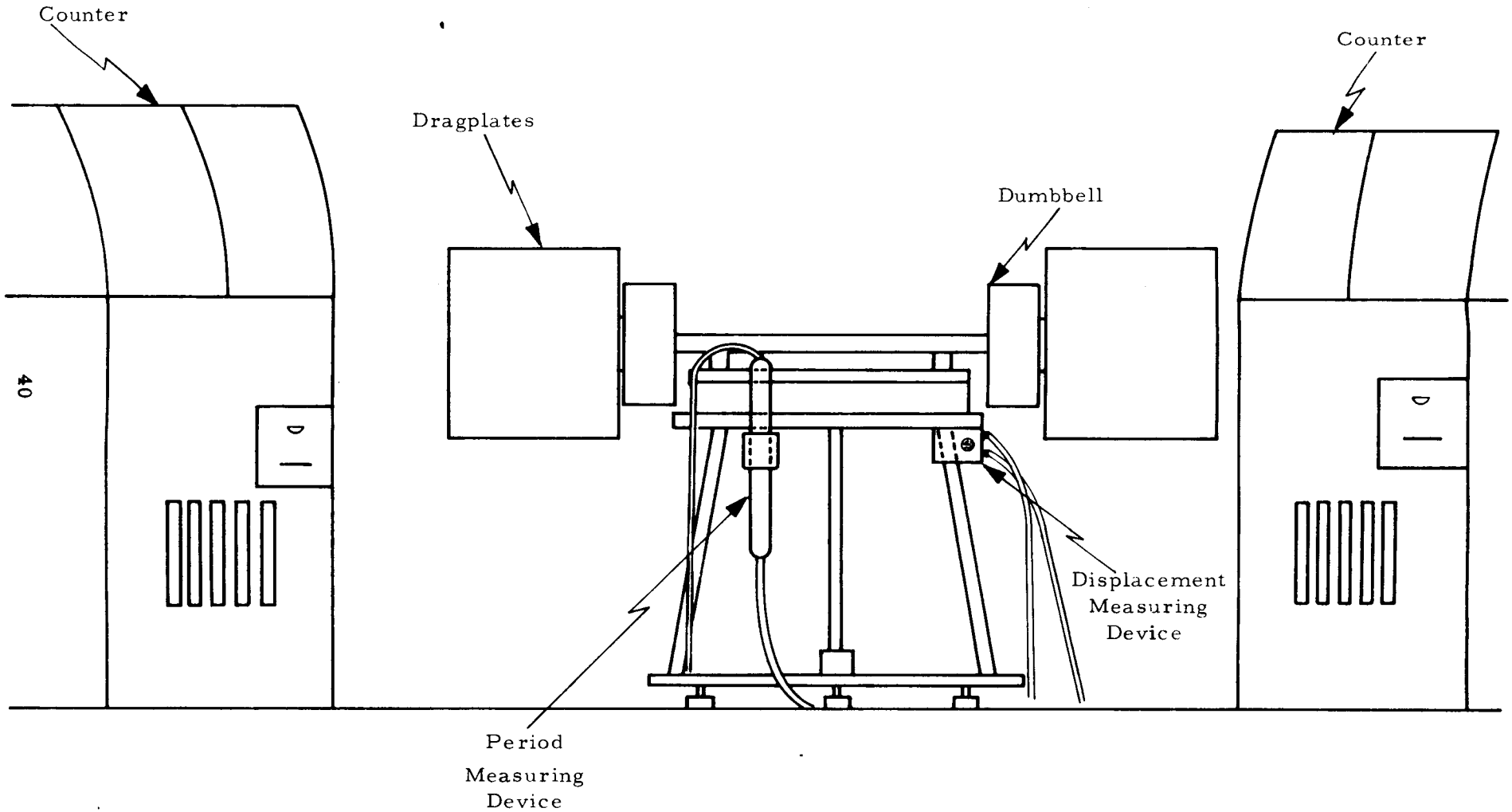

digital recorder. This provided an automatic readout of both period and displacement which simplified the test procedure. Single as well as 10 period averages were used with the displacement being recorded every other cycle. The starting and stopping displacements were varied depending on the data required. The test procedure for these tests is shown in Appendix A2.

2.1.1.2.3.2 Test Results and Analysis

The tests were composed of the following:

1. Rod 120, Drag Plate C, Dumbbell C
2. Rod 120, Drag Plate D, Dumbbell C
3. Rod 28, Drag Plate C, Dumbbell C
4. Rod 28, Drag Plate D, Dumbbell C

Plots of the results of the tests are shown in Figures 17 through 22. The first obvious conclusions which can be made from these figures is that a large drag plate and higher frequencies of oscillation cause more damping as previously shown. This conculsion will be examined in more detail.

The test results will be compared to that of a constantly damped system which has been used before. The equation of motion of this system is

$$I\ddot{\theta} + C\dot{\theta} + K\theta = 0 \tag{14}$$

The solution of this equation gives for the moment of inertia

$$I = \frac{K}{4\pi^2/T^2 + C^2/4I^2} \tag{15}$$

where K is the rod constant, T the period of oscillation, C is the damping constant, and I is the moment of inertia. The term C/2I is the slope of the curve of log of maximum displacement plotted against time; therefore, it is extremely important in determining the damping. Figure 18 is the plot of $\mathrm{Ln}\,\theta$ versus the number of cycles, which can be converted to time easily by multiplying the period by the number of cycles. The slope of the curve decreases as the amplitude decays and approaches a straight line. The damping constant

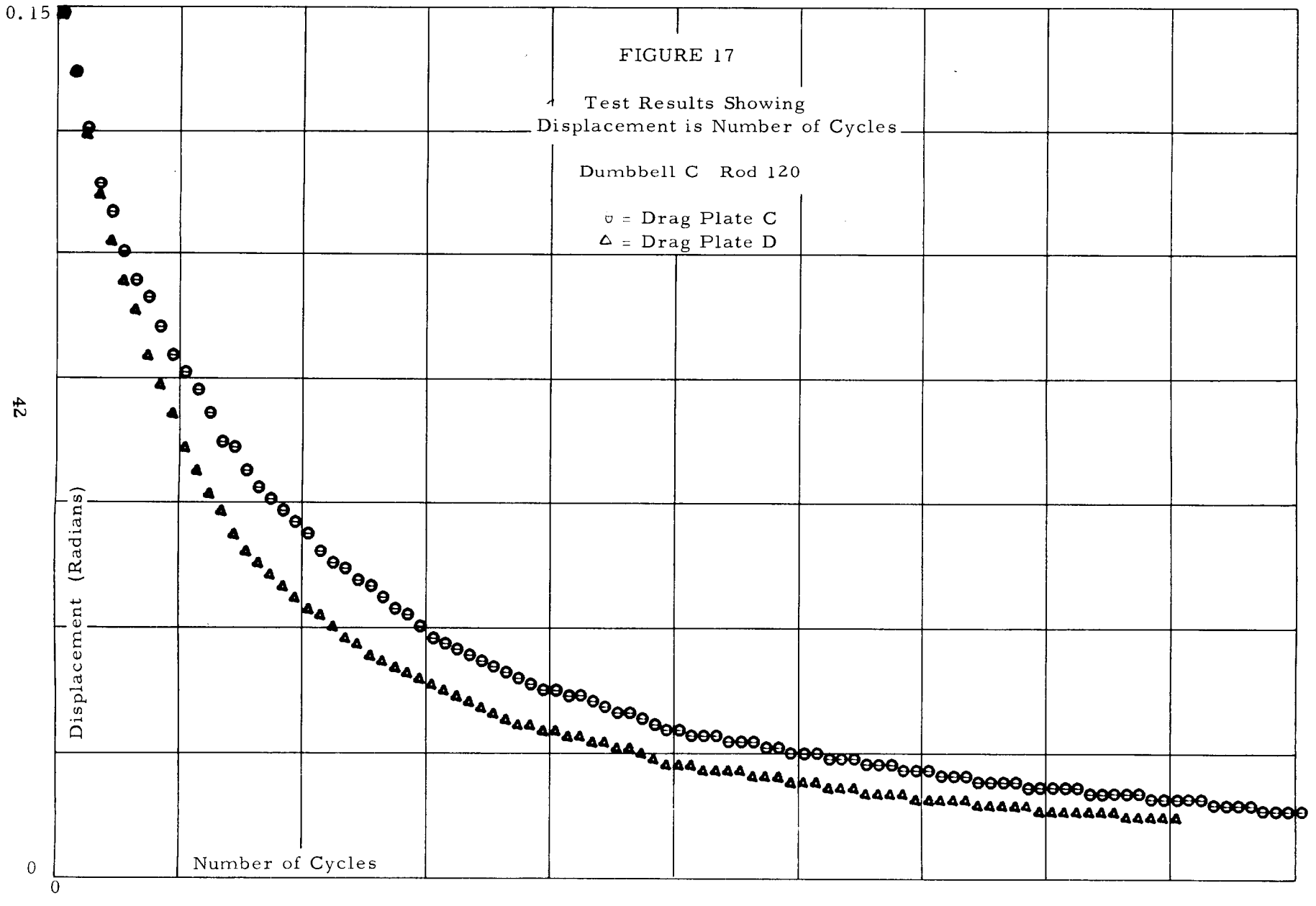

FIGURE 17

Test Results Showing
Displacement is Number of Cycles

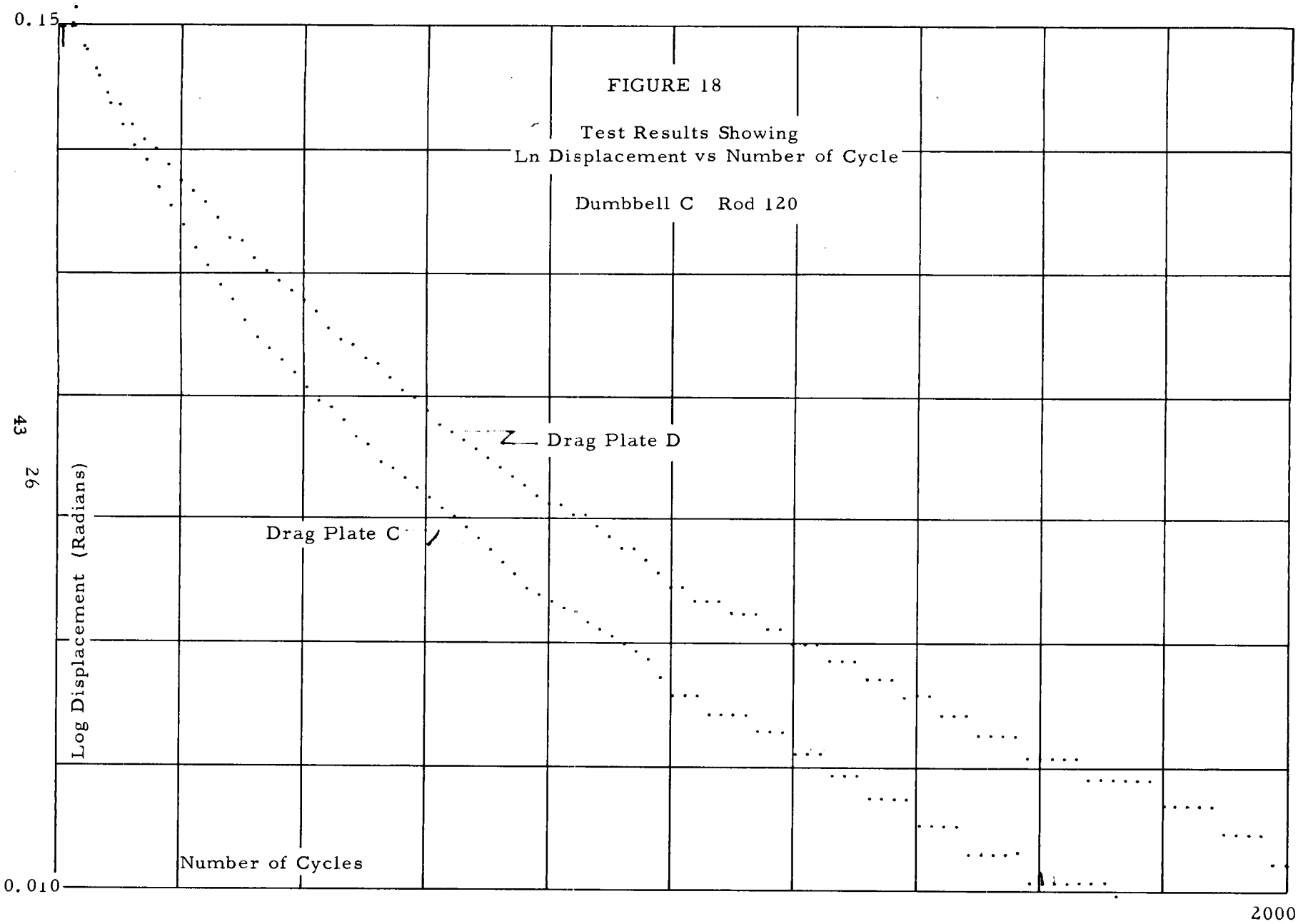

FIGURE 18

Test Results Showing
Ln Displacement vs Number of Cycle

Dumbbell C Rod 120

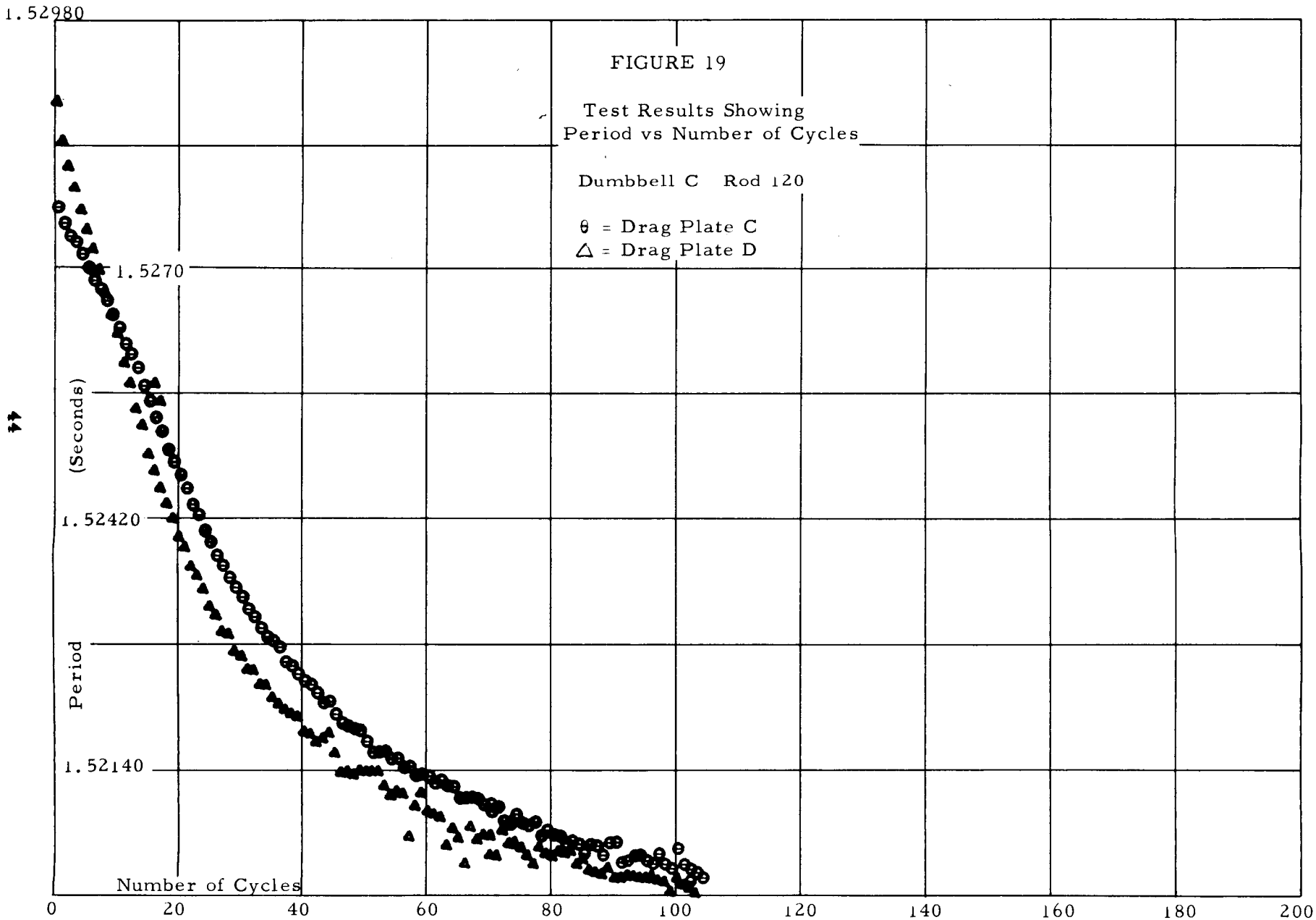

FIGURE 19

Test Results Showing
Period vs Number of Cycles

Dumbbell C Rod 120

C as determined from the slope of the curve at two different ranges is shown below:

Displacement	Damping Constant - C	
	Drag Plate C	Drag Plate D
0.15 - 0.10	0.52	0.69
0.013 - 0.010	0.17	0.18

This result shows that at large amplitudes the damping is larger for the large drag plate but as the amplitude decays the damping decreases and the values for both plates approach a constant value. It should be noted that the term C/2I, or the slope of the curve is approximately 5×10^{-4}. If this is applied to Equation 15, where $4\pi^2/T^2$ is of the order of magnitude of 20 and $C^2/4I^2$ is approximately 20×10^{-8} we can see that the damping term is insignificant and Equation 15 becomes

$$I = KT^2/4\pi^2 \tag{16}$$

This damping relationship in further verified be examining the curve of period versus number of cycles in Figure 19. The period decay for the large plate is greater that that of the small plate at large amplitudes, but at smaller amplitudes the periods approach each other. Therefore, the moment of inertia value becomes the same, independent of the object surface area.

Now examine the data using the same set-up with a different torsion rod which produces larger periods. This data is shown in Figures 20 through 22. The damping constant C for these tests are shown below:

Displacement	Damping Constant - C	
	Drag Plate C	Drag Plate D
0.015 - 0.10	0.034	0.065
0.013 - 0.010	0.019	0.034

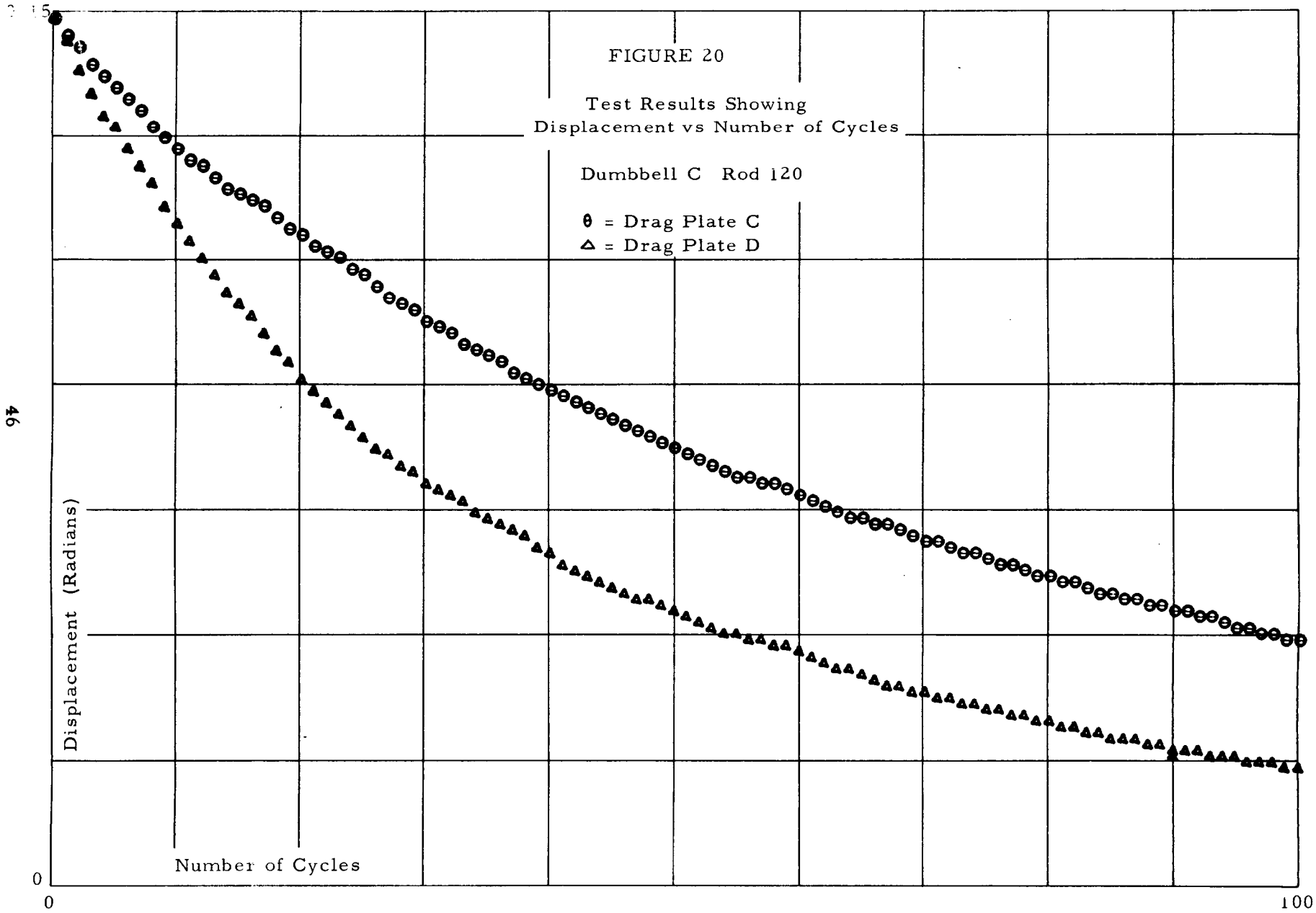
FIGURE 20
Test Results Showing
Displacement vs Number of Cycles
Dumbbell C Rod 120
θ = Drag Plate C
△ = Drag Plate D
Displacement (Radians)
Number of Cycles
0
0
100

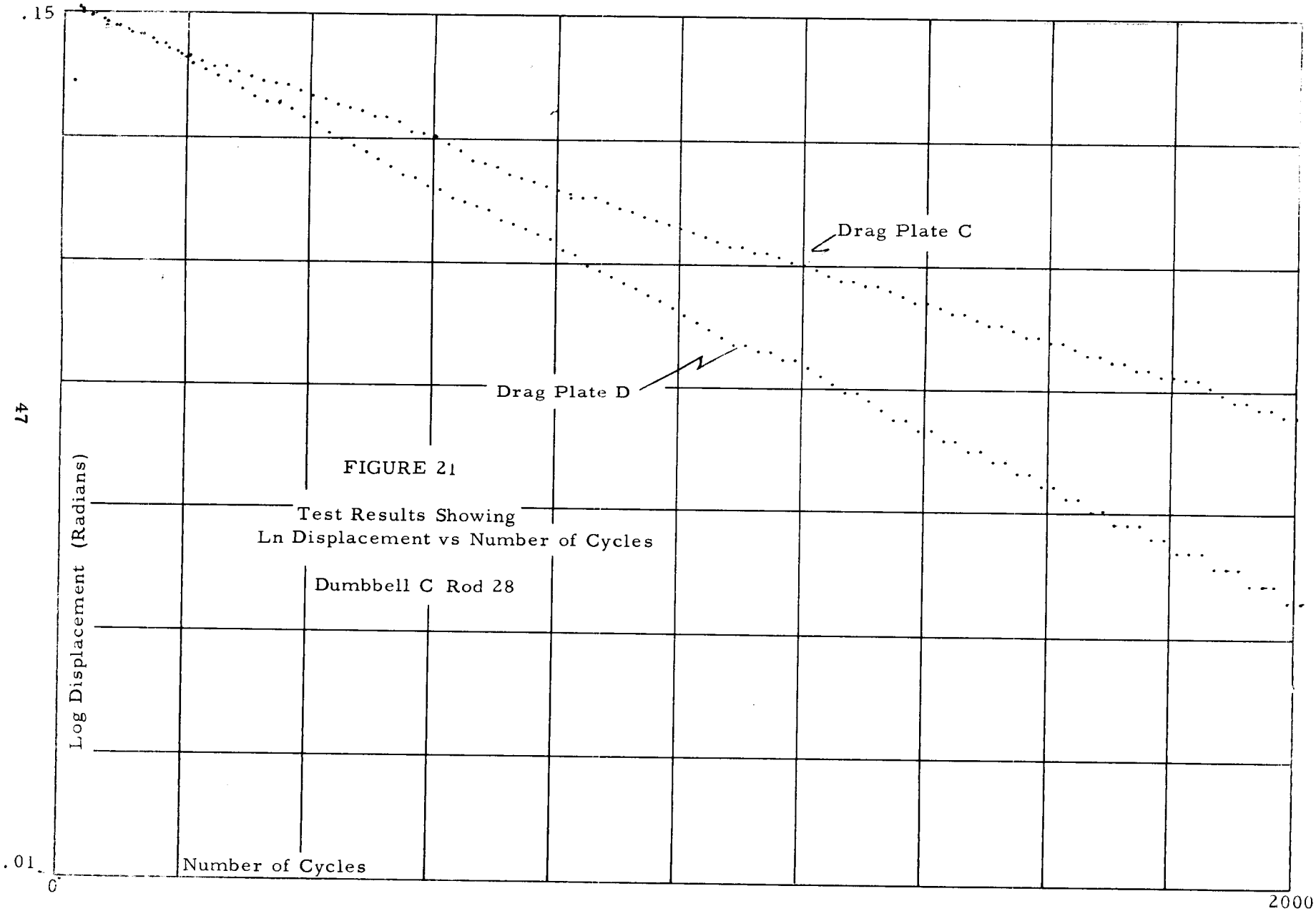

FIGURE 21

Test Results Showing
Ln Displacement vs Number of Cycles

Dumbbell C Rod 28

FIGURE 22

Test Results Showing
Period vs Number of Cycles

Dumbbell C Rod 28

θ = Drag Plate C
= Drag Plate D

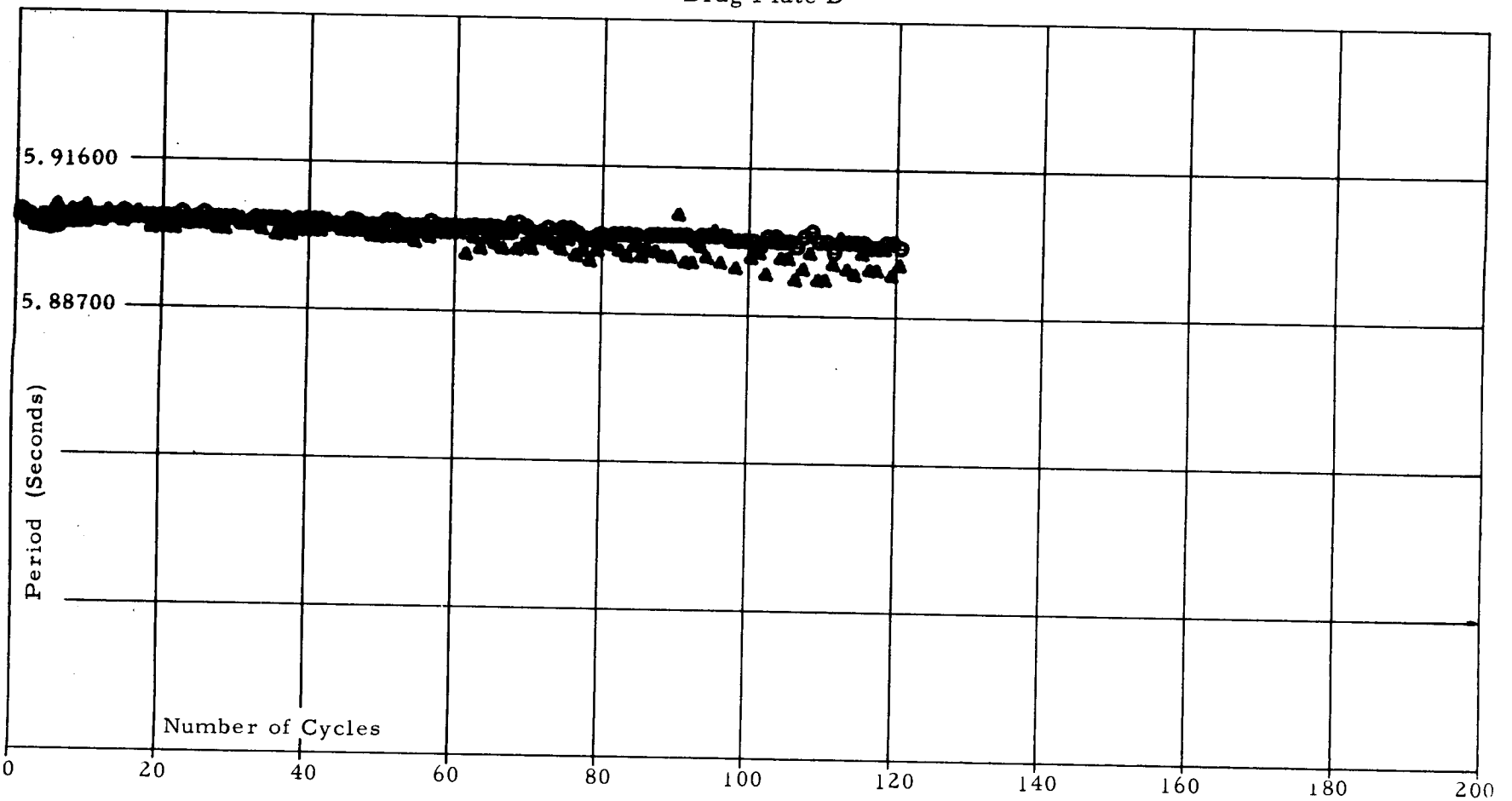

Again we have the same type results as discussed before except the damping constants at the low displacements are not as close. This does not present any problem because the damping constant is so small. This is further verified by Figure 22 which shows that the period of oscillation remains very constant for these small damping factors: that is, the damping is very constant. Therefore, the frequency of oscillation does effect the damping as compared to the other data, but at small amplitudes this effect is small.

2.1.1.2.4 Conclusions

The results of this experimental program has proven that even though the frequency of oscillation and the objects surface area does effect the amount of damping, this damping is negligible at extremely small amplitudes. The equation of motion for this system at these low amplitudes is that of a constantly damped oscillator where the damping is proportional to the first power of the velocity. At larger amplitudes the damping term is more complicated and must be analyzed in more detail to determine the exact equation of motion.

Moments of inertia can be determined precisely by using the results of this program; that is, $I = KT^2/4\pi^2$ at a displacement range of 0.5 to 0.1 milliradians. Further analysis of the damping at larger amplitudes will be conducted in the damping theory study project component. The data from this report along with the vacuum chamber test results will be used in this analysis. The results of this analysis will give a better understanding of the damping for any amplitude.

2.1.1.3 Vacuum Chamber Tests

2.1.1.3.1 Introduction

The effect of drag on an object moving through any medium has always presented problems. The size of the object, as well as its velocity and surrounding medium, have a large effect on the amount of drag produced. Since the drag is a direct force which tends to decelerate the moving object, it causes an energy loss in the system.

The energy losses produced by aerodynamic drag directly effects the experimental determination of moments of inertia because as oscillating system is always used. Some of these systems are: torsional pendulum, filiar pendulum, and compound pendulum. The moment of inertia determination in each system is directly related to the square of the period of oscillation. Since drag causes the period of oscillation to increase, the effect of drag in a moment of inertia determining system is normally referred to as the "additional mass effect". This effect is shown better in Equations 17 and 18.

$$I = f(m) \qquad \text{theoretically} \qquad (17)$$

$$I = f(T^2) \qquad \text{experimentally} \qquad (18)$$

These two equations show that the mass and period are directly related; therefore, a period increase causes an apparent mass increase.

This effective mass increase is detrimental to moment of inertia measurement because it produces a variable value for the moment of inertia which is larger than the true value. This value depends on the object's size, oscillation frequency, amplitude of oscillation, and surrounding medium. The first three variables have been investigated experimentally. (Reference Paragraph 2.1.1.2). The results showed that an increase in any of these variables produced an increase in the moment of inertia. However, at extremely small amplitudes, .001 radians or less, there were no appreciable losses regardless of object's size or frequency of oscillation. From these conclusions, it is obvious that a reduction of pressure in the surrounding medium would not affect the moment of inertia measurements at small amplitudes. However, by reducing the pressure a better understanding of aerodynamic drag can be obtained.

2.1.1.3.2 Experimental Procedure

The ATCOMED facility of the Quality and Reliability Assurance Laboratory at Marshall Space Flight Center, shown in Figure 23, was used to provide the various vacuum levels. The vacuum chamber is a 16 foot long by 12 foot diameter cylindrical capable of operating at 5×10^{-6} mm Hg (Torr). The testing in the vacuum chamber can be controlled by either the manual or automatic test station.

A torsional pendulum system was used for producing the oscillations in the vacuum chamber. The torsion rod was mounted to a machined plate in the top of the chamber, and a dumbbell with drag plates as shown in Figure 24, was attached to the other end as shown in Figure 25. The dumbbell has a pivot bearing plate attached as shown in Figure 26. The pivot solenoid was aligned under the dumbbell in such a manner that the pivot point was in line with the torsion rod axis.

The striker assembly was mounted on the base plate as shown in Figure 27. The striker arm was adjusted so that the distance between the striker arm and dumbbell was one-half the maximum travel of the striker. The displacement measuring device was mounted as shown in Figure 28, and the period measuring device as shown in Figure 29.

FIGURE 23

ATCOMED FACILITY

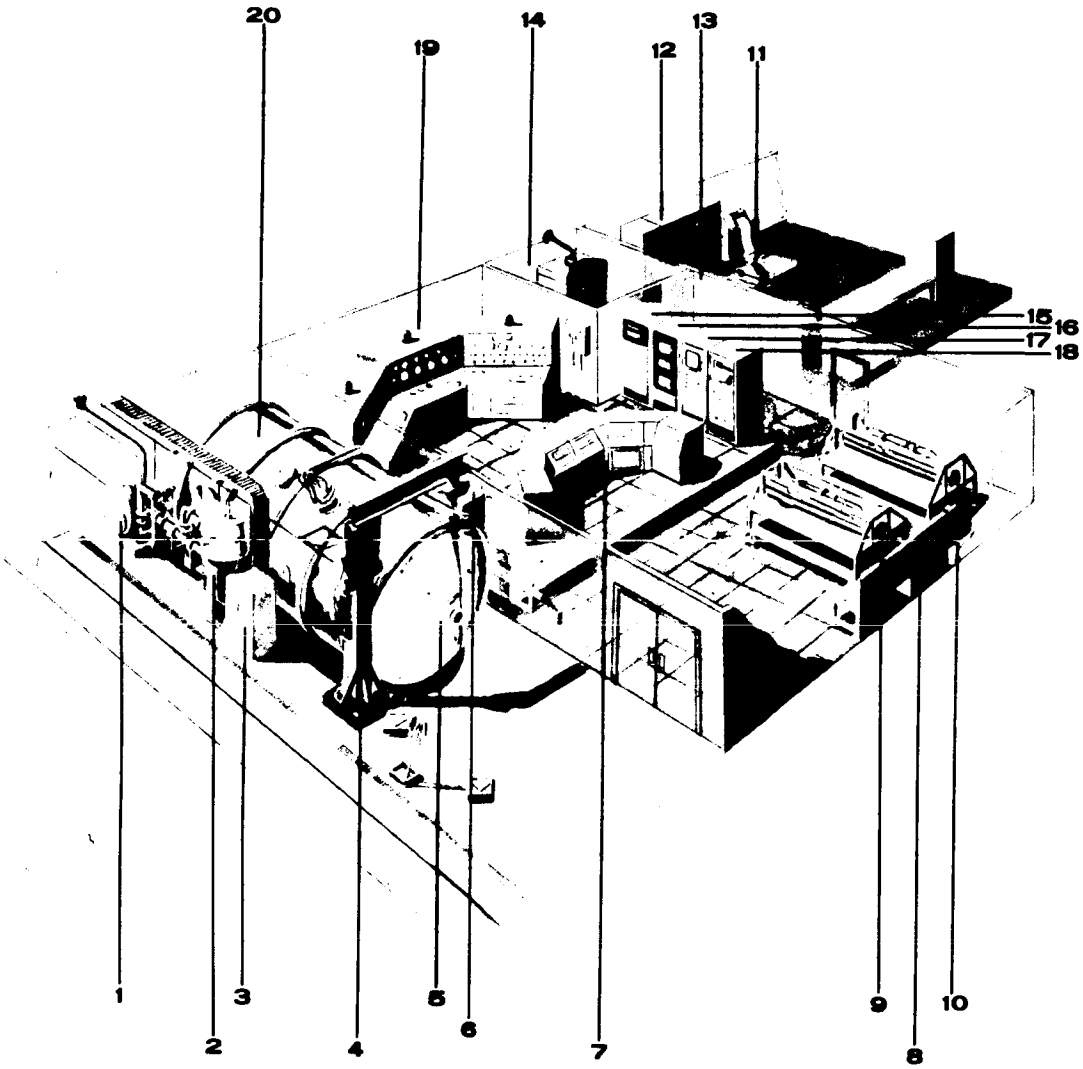

1·MECHANICAL PUMP
2·DIFFUSION PUMP
3·VACUUM SYSTEM CONTROL
4·VACUUM CHAMBER ACCESS DOOR HOIST
5·VACUUM CHAMBER ACCESS DOOR
6·TEST DISTRIBUTOR RACK
7·CONTROL CONSOLE
8·COMPONENTS TEST BENCH
9·LOX SYSTEM CART
10·CONTROL SYSTEM CART
11·COMPUTER CONTROL DESK
12·COMPUTER
13·AUTOMATIC TEST STATION
14·RADIOTRACER ROOM
15·TEMPERATURE RECORDER
16·EVENTS RECORDER
17·AUXILIARY ANALOG RECORDER
18·MAIN ANALOG RECORDER
19·PNEUMATIC CONTROL CONSOLES
20·VACUUM CHAMBER

FIGURE 24

DRAG PLATE DIMENSIONS

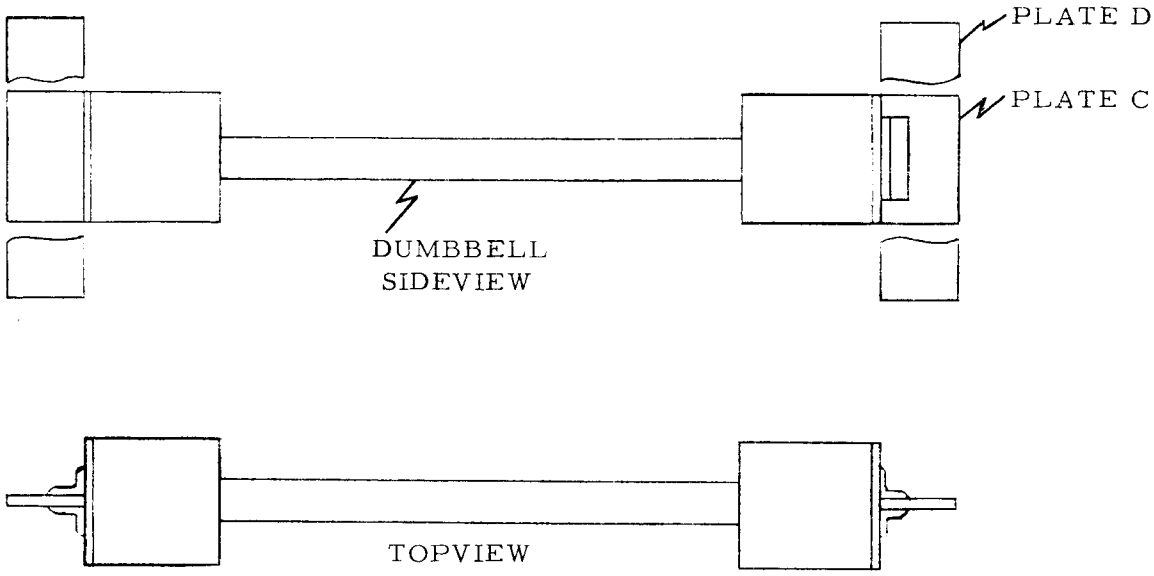

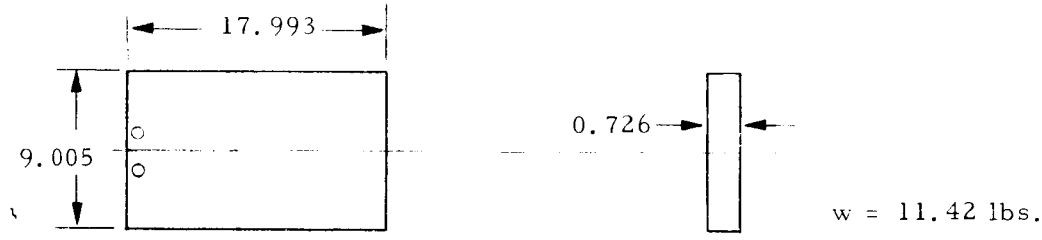

DRAG PLATE C

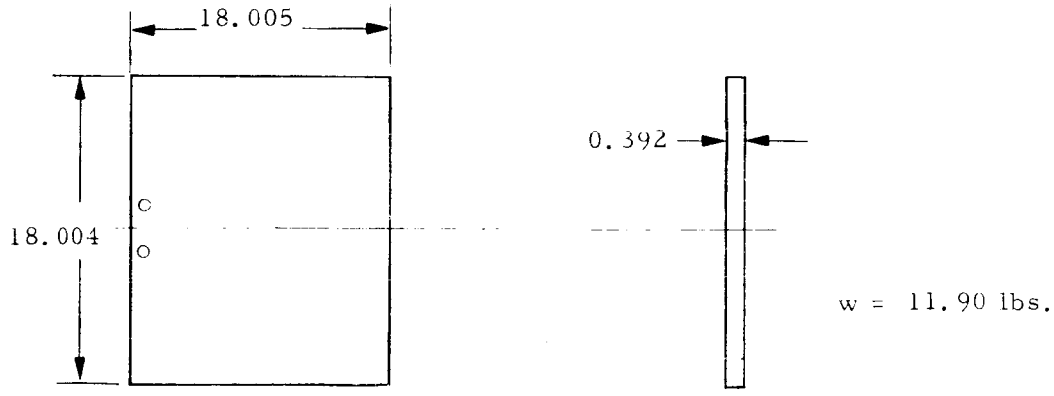

DRAG PLATE D

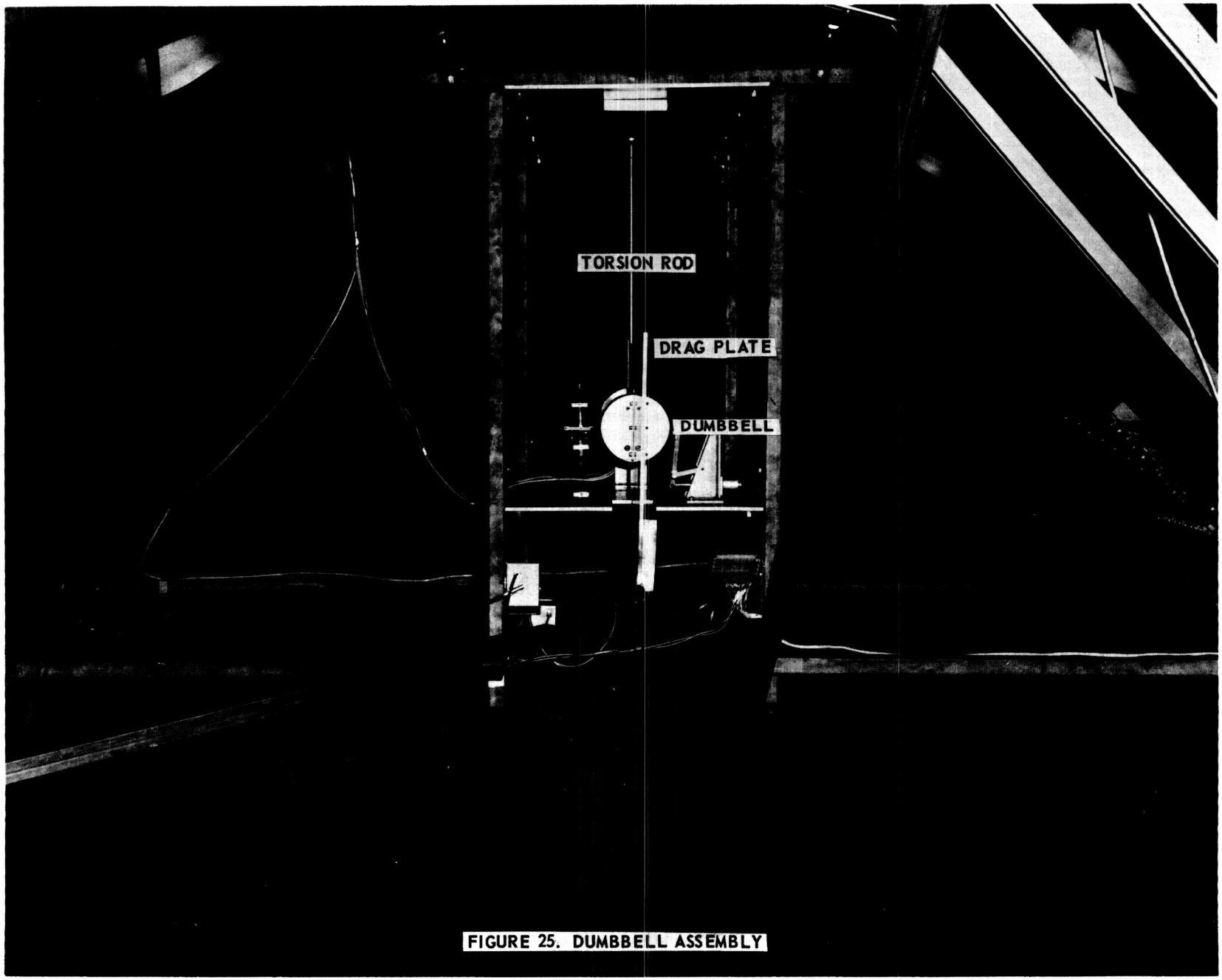

FIGURE 25. DUMBBELL ASSEMBLY

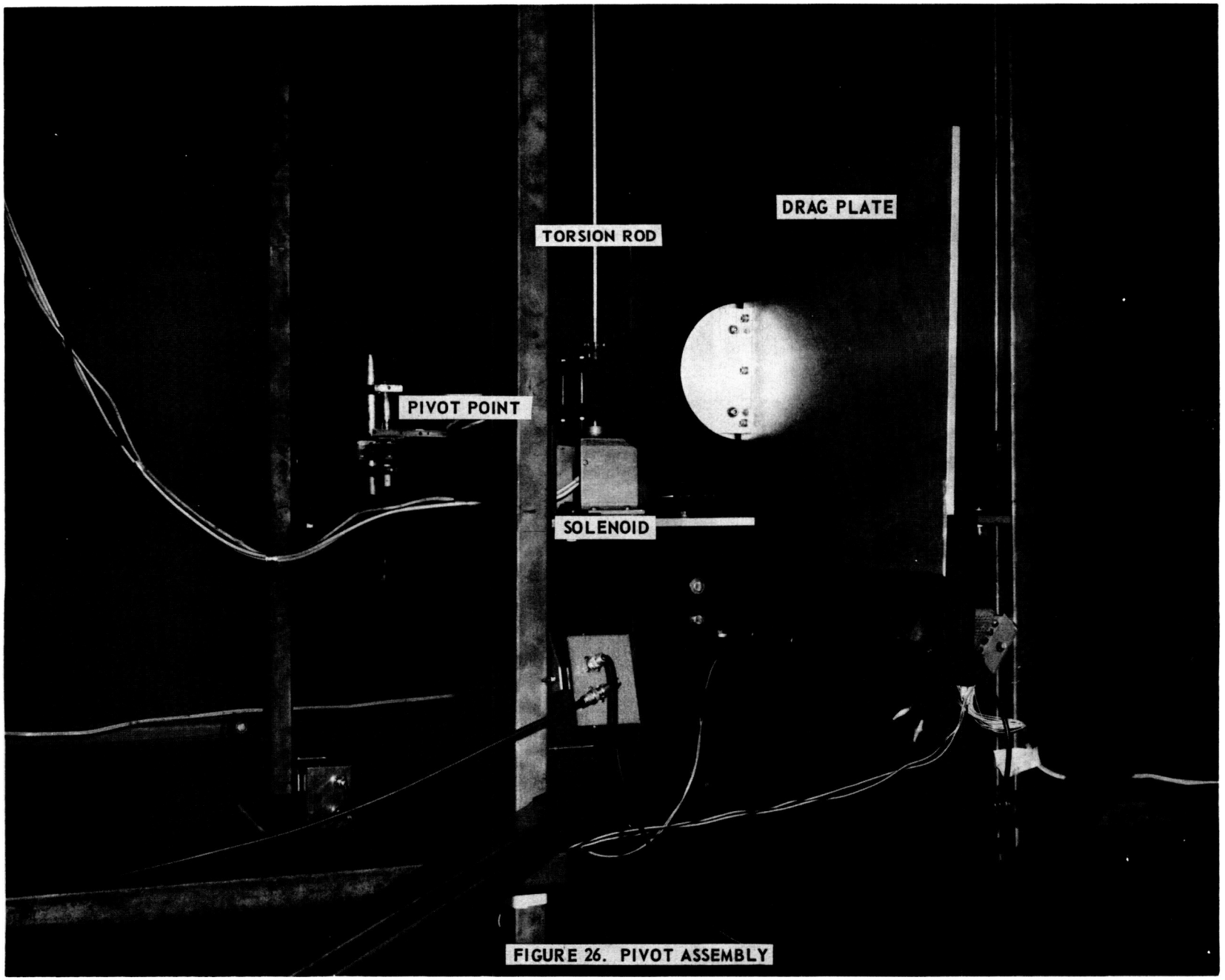

FIGURE 26. PIVOT ASSEMBLY

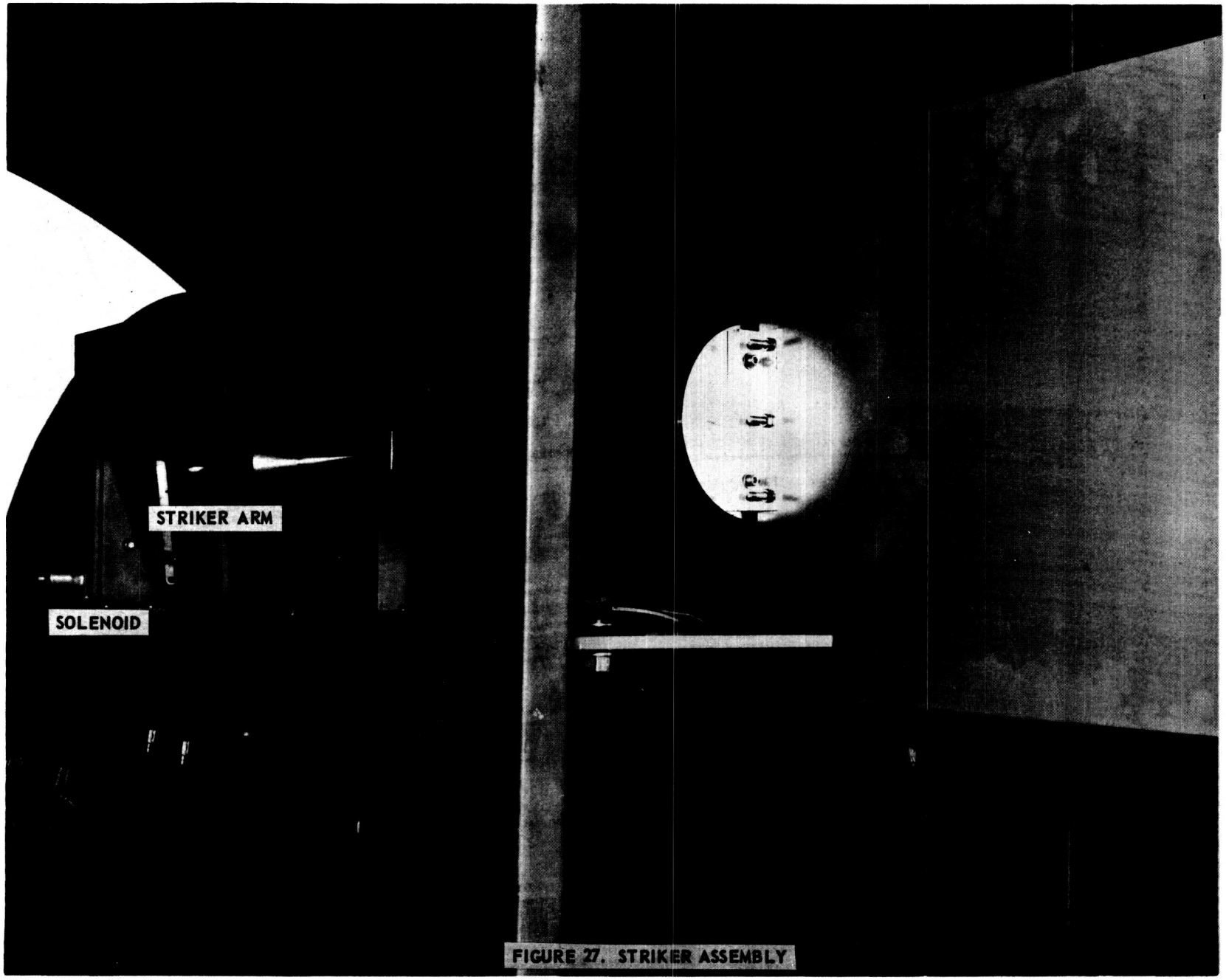

FIGURE 27. STRIKER ASSEMBLY

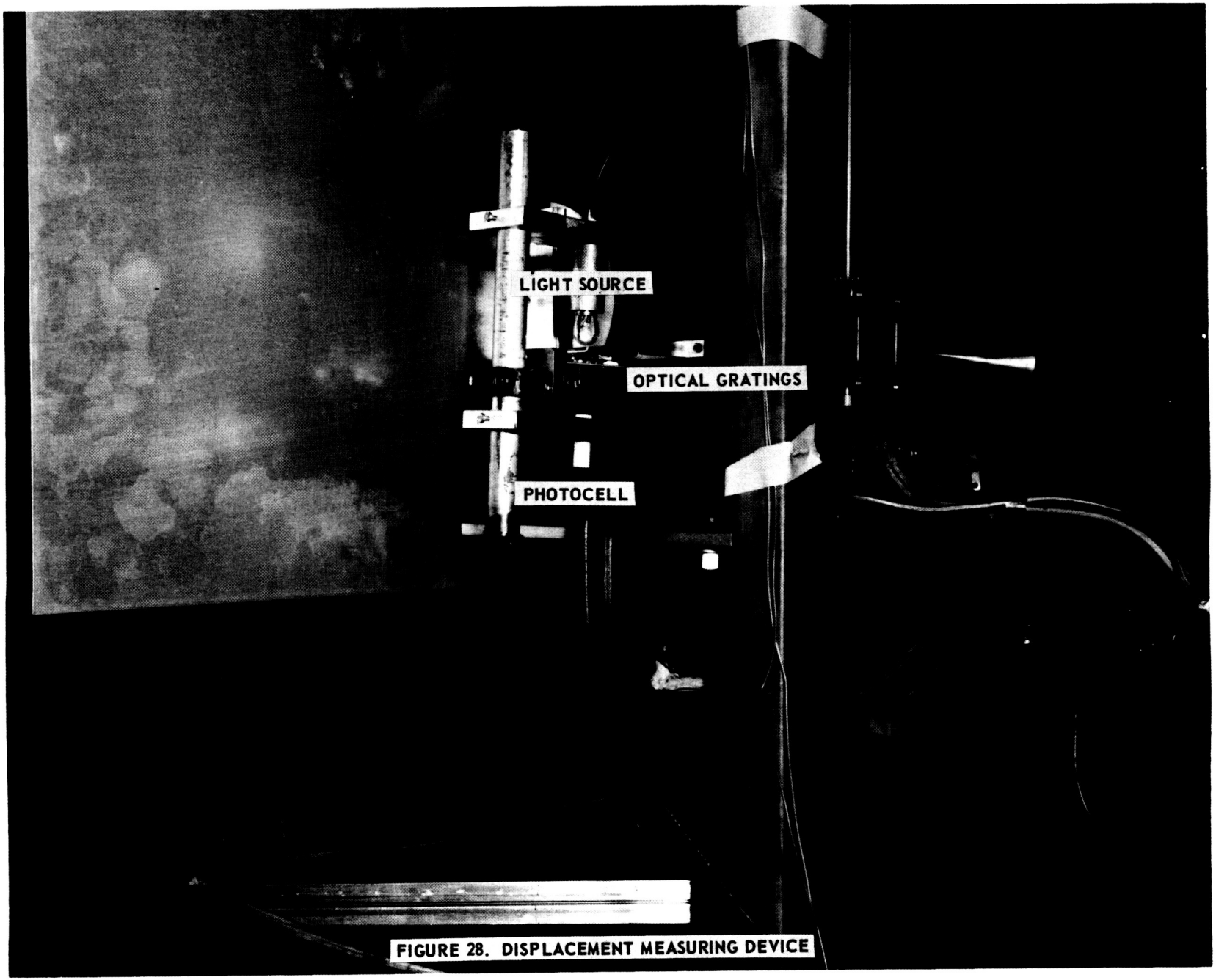

FIGURE 28. DISPLACEMENT MEASURING DEVICE

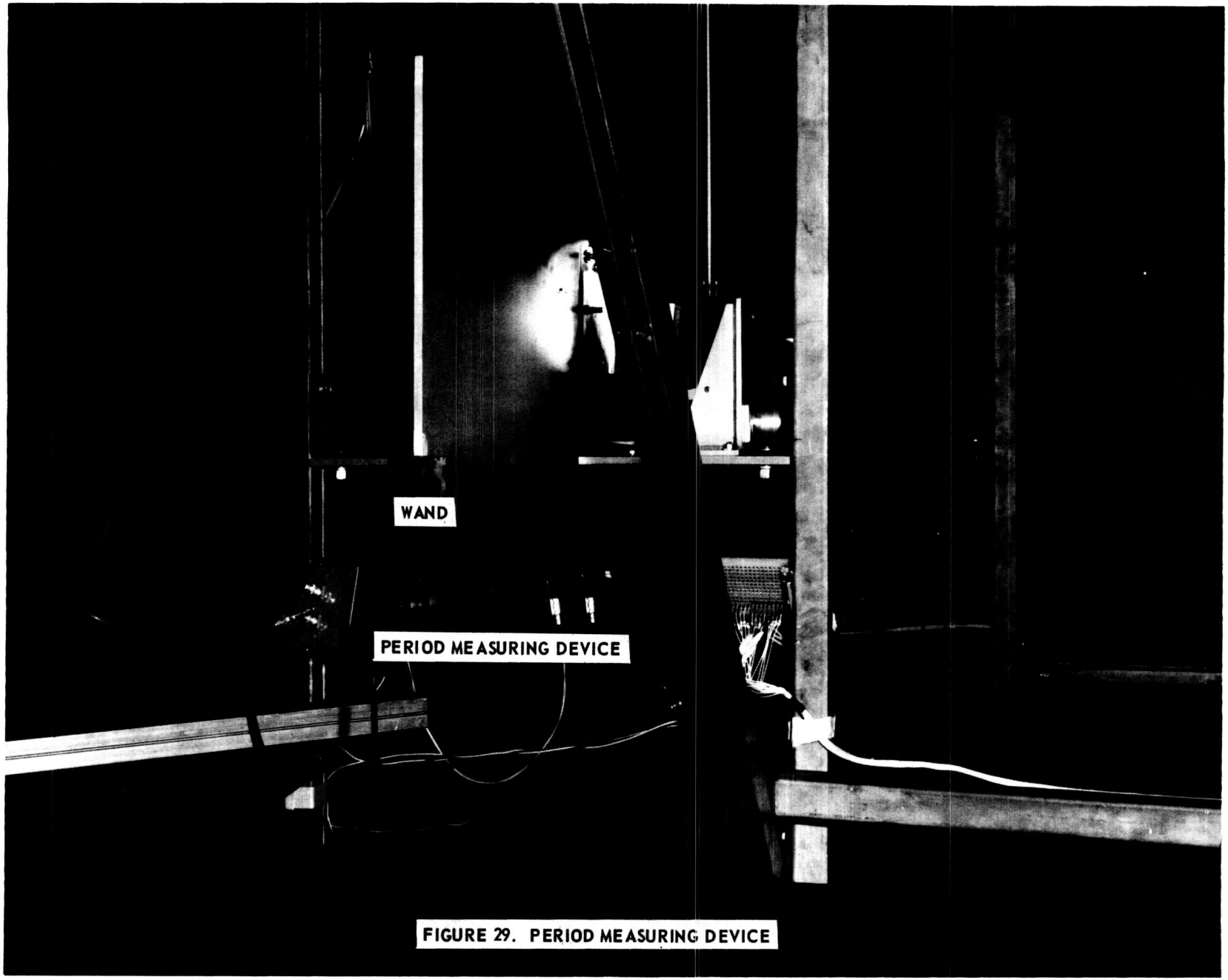

FIGURE 29. PERIOD MEASURING DEVICE

The wiring for both devices and the solenoids were connected through the electrical system of the vacuum chamber into the control room. Inside the control room the displacement device output was connected to a Hewlett-Packard 524D counter, then to a 560A digital printer. The output of the period measuring device was connected to a Beckman preset counter, then into a Beckman 7360 counter and printer. The power wires for the solenoids were connected to a relay operated control board in the control room where they could be operated separately. Figure 30 shows the electronic equipment in the control room. A closed circuit T.V. was used to monitor the oscillations of the dumbbell.

With this test set up the experiments could be controlled entirely from the control room. The dumbbell, drag plates, and torsion rod required for a specific test were mounted in the chamber. The chamber door was closed and the require vacuum was obtained. From the control panel the pivot solenoid was engaged to stabalize the dumbbell. The striker was actuated to start the dumbbell oscillating. When the proper amplitude was reached, the period and displacement devices were energized and data was obtained. This procedure was repeated to obtain the data for each set of variables. An operating test procedure is shown in Appendix A3.

2.1.1.3.3 Experimental Results

The results were obtained by using dumbbell C, rod 120, drag plates C and D at pressures of 760, 1.0, 10^{-2}, and 10^{-4} torr. The data obtained was the displacement between 300 and 20 on the counter, (each unit is equal to 5.55×10^{-5} radians) and the period for this displacement range. To save space, only the plots of these data are presented herein. Each curve represents the average of at least three tests.

Figure 31 shows the plot of log displacement versus number of cycles. This curve is used because its slope is directly related to the viscous damping of the oscillating system. The equation of motion of the system is assumed to be

$$I\ddot{\theta} + C\dot{\theta} + K\theta = 0. \tag{19}$$

Its solution is

$$\theta = Ae^{-\frac{Ct}{2I}} \sin(\beta t + \varphi) \tag{20}$$

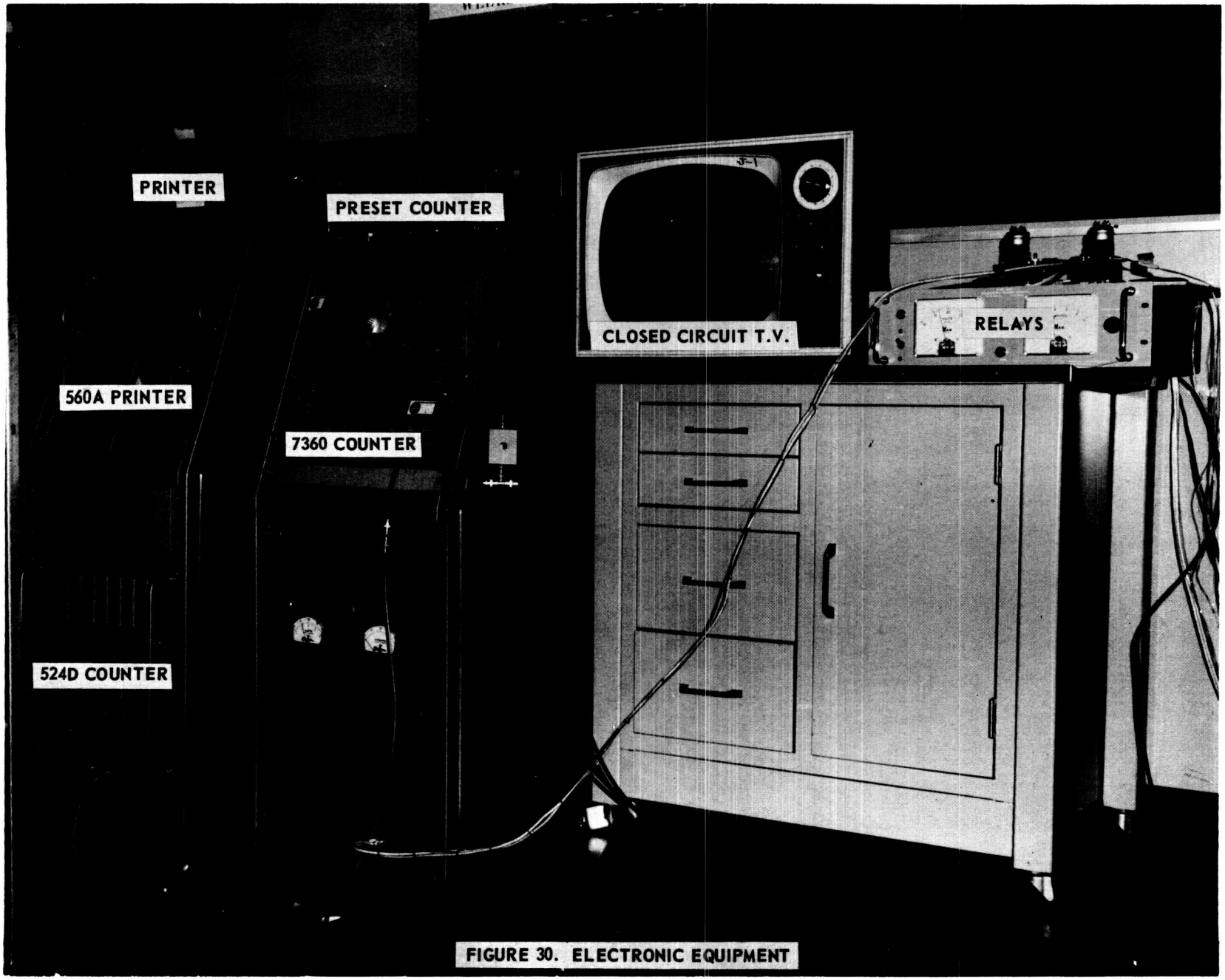

FIGURE 30. ELECTRONIC EQUIPMENT

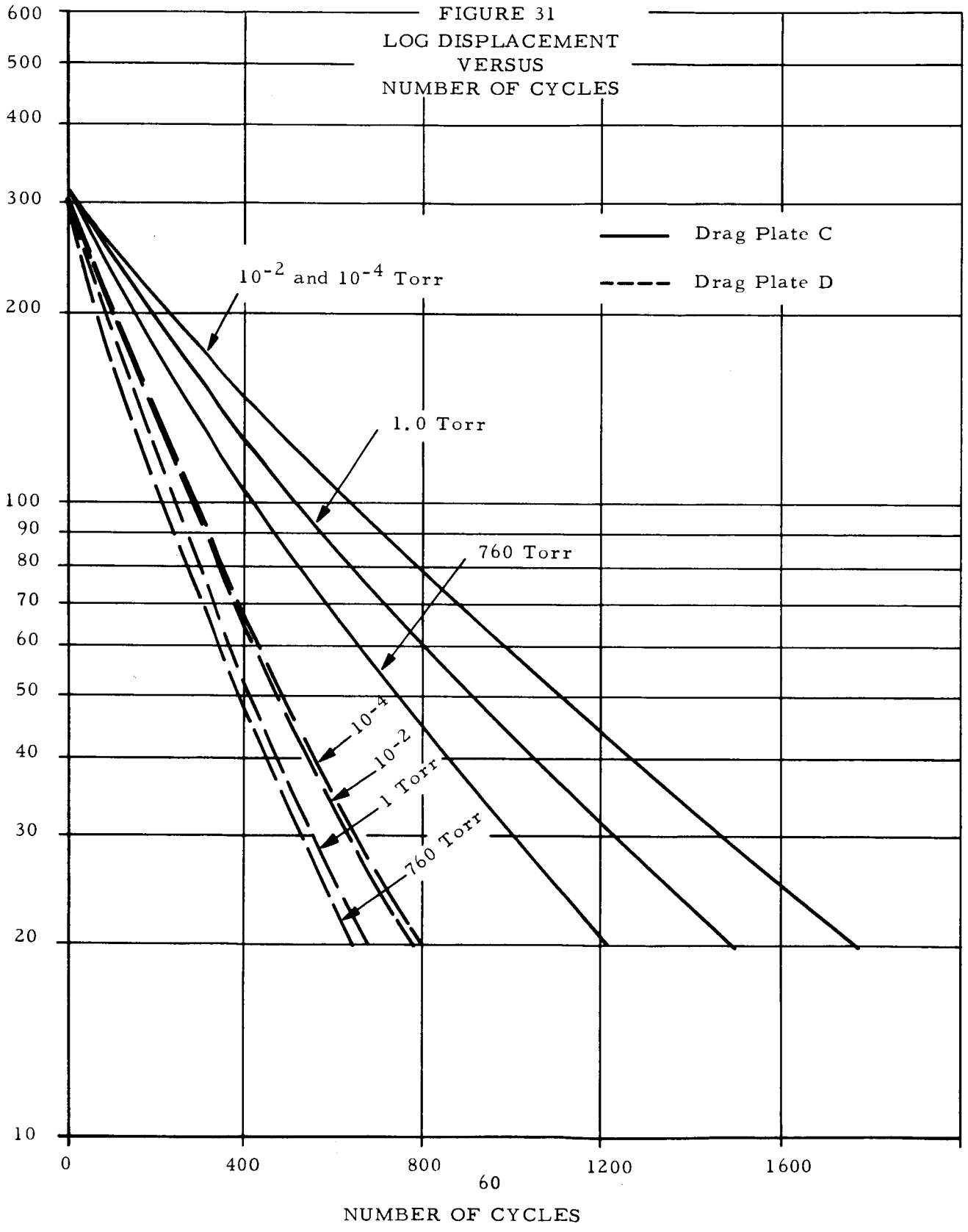
FIGURE 31
LOG DISPLACEMENT
VERSUS
NUMBER OF CYCLES
600
500
400
300
200
100
90
80
70
60
50
40
30
20
10
0
400
800
1200
1600
Drag Plate C
Drag Plate D
10^{-2} and 10^{-4} Torr
1.0 Torr
760 Torr
10^{-4}
10^{-2}
1 Torr
760 Torr
NUMBER OF CYCLES

where β is the oscillating frequency. Equation 20 can be written as

$$\ln\theta = \ln A - (C/2I)t$$

if maximum amplitudes are considered. Therefore, the slope of the curve of $\ln\theta$ plotted against t (total time) will give C/2I. This solution has been used to calculate the damping term for these tests and the results are shown in Table 2.

From Table 2 and Figure 31, it can be seen that the damping does decrease as the pressure decreases and as the surface area of the oscillating object decreases. When the pressure reaches 10^{-2} to 10^{-4} torr, the damping appears to approach a constant value for each separate drag plate.

The period data for drag plate C is shown in plotted form in Figure 32. There is no obvious correlation between the period curves and the pressure. The shift in the period curves is attributed to the temperature variations. From prior tests, it has been determined that one degree change in temperature changes the period of oscillation by 0.00012 seconds, for this specific set up. The variation in periods in Figure 10 is approximately 0.0004 seconds. However, the temperature variation was at least 10°F during the testing. Therefore, this period variation is well within the expected limits.

The results shown in Figure 32 have been normalized in Figure 33. That is, the constant periods at the low amplitudes have been set equal to each other. There is still no correlation between the period and pressure. Figure 34 shows the data for drag plate D.

2.1.1.3.4 Conclusions

The results obtained from the vacuum chamber tests did not produce the necessary data for completely analysing the effect of varying pressures on the damping rate. Even though the reduction in pressure did reduce the drag, an appreciable amount of drag was still remaining at very low pressures. This drag was probably caused by the effects of vibrations of the chamber and its surroundings. Also, there could be noticeable nonlinearities in the torsion rod which was not expected. This latter effect will be examined in the dynamic torsion rod tests.

The results obtained from the period data was very disappointing. It was hoped that the period decay rate would yield some useful information; however, the data was so scattered because of the uncontrollable variables that is was unusable.

FIGURE 32

PERIOD VERSUS NUMBER OF CYCLES
FOR DRAG PLATE C

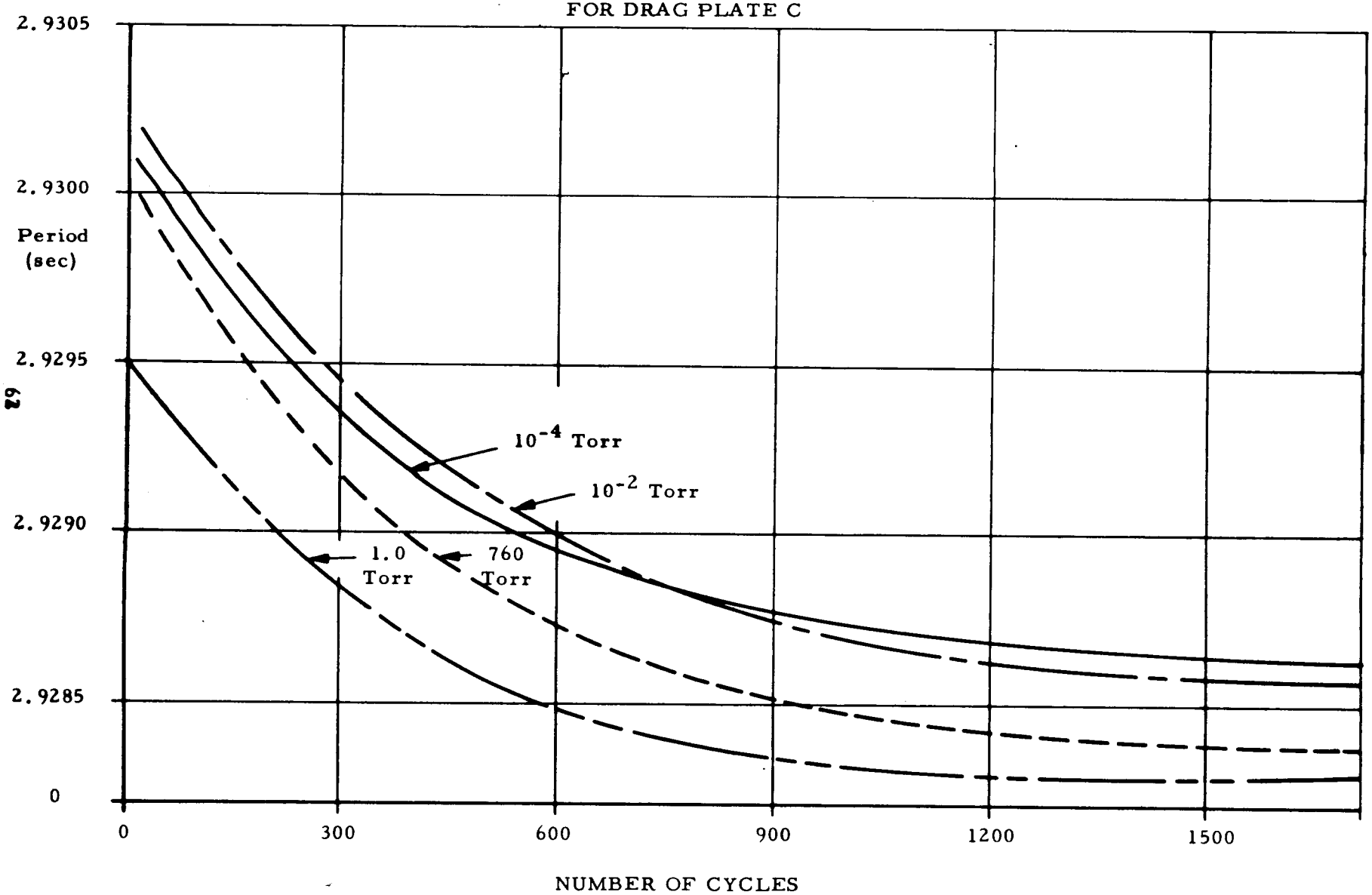

FIGURE 33

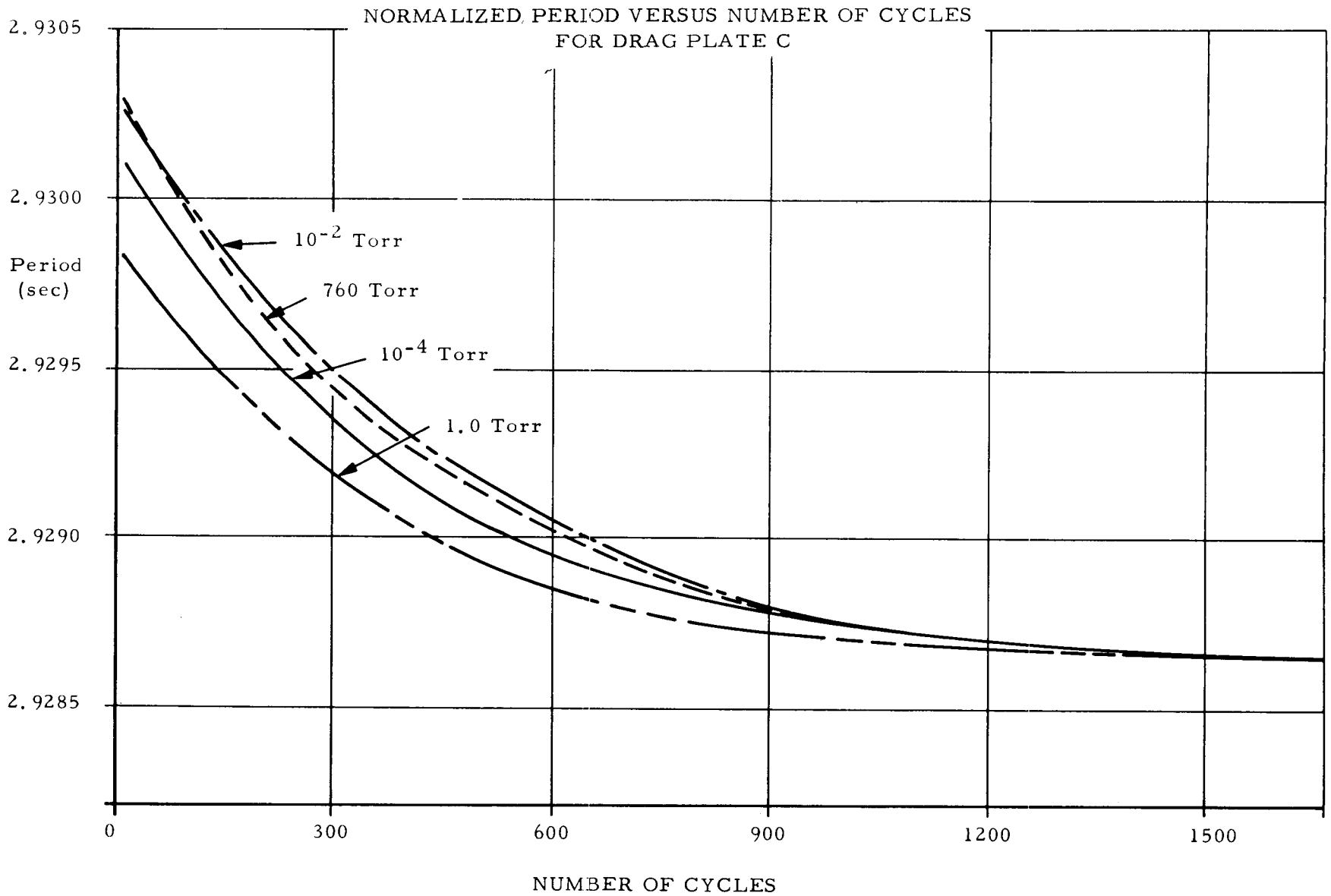
NORMALIZED PERIOD VERSUS NUMBER OF CYCLES
FOR DRAG PLATE C
2.9305
2.9300
2.9295
2.9290
2.9285
Period
(sec)
10^{-2} Torr
760 Torr
10^{-4} Torr
1.0 Torr
0
300
600
900
1200
1500
NUMBER OF CYCLES

FIGURE 34

NORMALIZED PERIOD VERSUS NUMBER OF CYCLES
FOR DRAG PLATE D

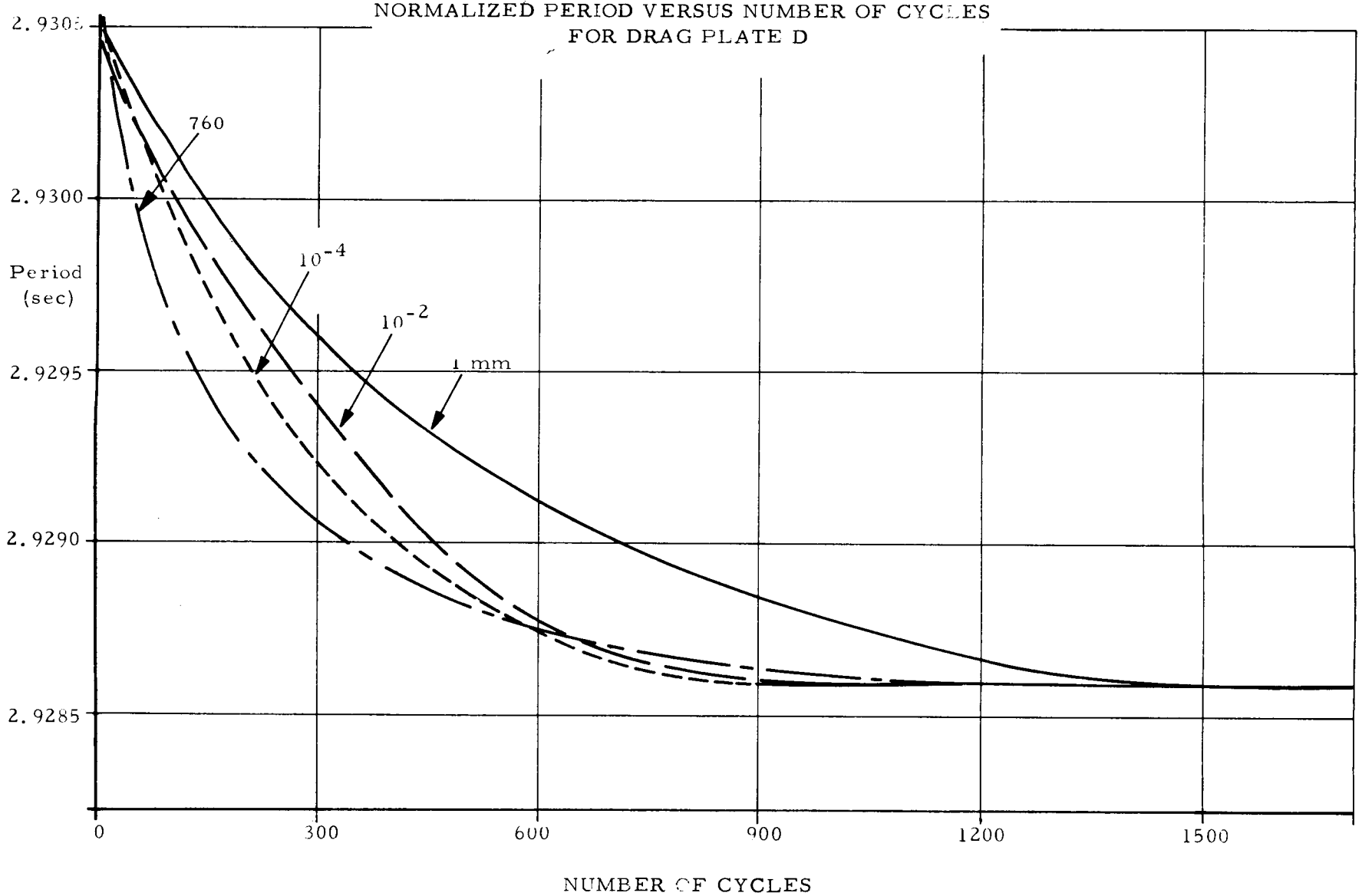

TABLE 2
DAMPING CONSTANT RESULTS

Pressure	Drag Plate C	Drag Plate D
760 torr	0.88 in-lb-sec	1.67 in-lb-sec
1.0	0.72	1.58
10^{-2}	0.60	1.37
10^{-4}	0.60	1.34

One interesting effect was encountered which was not completely explained. There was a definite shift for the large drag plates as the pressure decreased from 760 to 50 torr. Several tests were performed to try to determine the cause of this effect. The conclusions drawn from these tests were that the natural frequency of the vacuum chamber was close to that of the oscillating dumbbell. A change in pressure produced a physical change in the chamber; thereby, causing the frequency of oscillation of the dumbbell to change. This effect was not noticed with either the small plates or with no plates; therefore, it was assumed to be a specific characteristic of the large plates. An investigation of this effect was not pursued in detail, because it would not be helpful to the total moment of inertia program.

The primary conclusion drawn from the vacuum chamber tests is that all variables must be closely controlled before useful data can be obtained. The adverse effects caused by random vibrations and temperature changes completely overshadowed the vacuum effects which were of interest. Further testing may provide more useful data; however, a better controlled system must be used.

2.1.1.4 Damping Theory Study

2.1.1.4.1 Introduction

A study to determine the exact equation of motion of the oscillating torsional pendulum has been conducted. The purpose of this study was to obtain an equation whose solution would give the moment of inertia of the oscillating object regardless of the amplitude of oscillation. If this were possible, the equation would account for aerodynamic drag losses, torsion rod non-linearities, system friction, and any other losses which hinder precision moment of inertia determination.

Three experimental programs were conducted to help determine the causes of the system's losses. These tests examined the effects of: (1) aerodynamic drag, (2) external pressure, and (3) torsion rod effects. None of these tests provided data which could be used to analytically evaluate the system; however, some information was gained from these tests and is discussed in each respective report.

The first assumption for the equation of motion of the system was,

$$I\ddot{\theta} + f(\dot{\theta}) + K\theta = 0 \tag{21}$$

where the damping was directly related to the velocity. After further tests and analyses, it was learned that the equation was much more involved. In general it resembles

$$I(\alpha)\ddot{\theta} + C(\alpha) + K(\alpha) = 0 \tag{22}$$

where $\alpha = \ddot{\theta}, \dot{\theta}, \theta.$

This equation shows that the moment of inertia of the object is dependent upon the angular displacement, velocity, and acceleration of the system. This is caused by the instability of the object which varies with it's construction. The damping term is also dependent on the same variable because of the aerodynamic drag and air bearing losses in the system. The non-linearities in the torsion rod are produced by the same variables. This is a general equation for the system which indicates that all these factors may not have to be considered; however, it does show the complexity of the equation.

An attempt was made to simulate the damped equation of motion of the oscillating pendulum on an analog computor. Mr. Hugh Zeanah of the N.A.S.A. Computation Laboratory used the best hybrid analog computer available at the laboratory in trying to simulate the equation. The results were unsatisfactory because the computer could not be scaled down accurately to simulate the small displacements and period changes.

A through theoretical analysis was not attempted, because of the time required to thoroughly investigate the system to find the exact equation of motion. This decision did not affect the moment of inertia determination program because an exact equation for a given displacement range is available. This equation has been used before and it is

$$I\ddot{\theta} + C\dot{\theta} + K\theta = 0. \tag{23}$$

This equation was simulated on the PACE TR-48 analog computer available in the Mass Metrology Laboratory. This result will be discussed later. Also the report will discuss Equation 21 in detail and show how it is applied to the moment of inertia determining system to obtain precise data.

2.1.1.4.2 Analog Computer Simulation

The classical damped oscillator represented by Equation 23 was simulated on the PACE TR-48 analog computor so that it could be analyzed. A brief statement of the problem simulated and the method of programming the computer demonstrated the usefulness of the computer. The equation simulated was:

$$I\ddot{\theta} + C\dot{\theta} + K\theta = 0 \tag{24}$$

where:

I	=	moment of inertia
C	=	damping constant
K	=	rod spring constant
θ	=	angular displacement
$\dot{\theta}$	=	angular velocity
$\ddot{\theta}$	=	angular acceleration

The basic computer diagram is shown in Figure 35. The computer must now be amplitude scaled so that the actual problem can be simulated without overloading the computer. Data obtained from the air bearing table tests were used as a representative example. Table 3 shows the factors used for amplitude scaling the computer. The computer equation now becomes,

$$\left[I\ddot{\theta}\right] = \frac{-C}{50I}\left[50\dot{\theta}\right]\frac{-K}{200I}\left[200\theta\right] \tag{25}$$

The problem data is,

I	=	60 in-lb-sec^2
K	=	3,000 in-lb/rad
C	=	.30 in-lb/sec
θ_o	=	.05 rad

The final computer diagram is shown in Figure 36. The results of this problem simulation is best illustrated in Figures 37 and 38. Figure 37 shows the output of the x - y plotter where angular displacement has been plotted against elapsed time. This figure depicts the familiar damped oscillating system. Figure 38 shows the plot of angular acceleration versus angular velocity for the same problem.

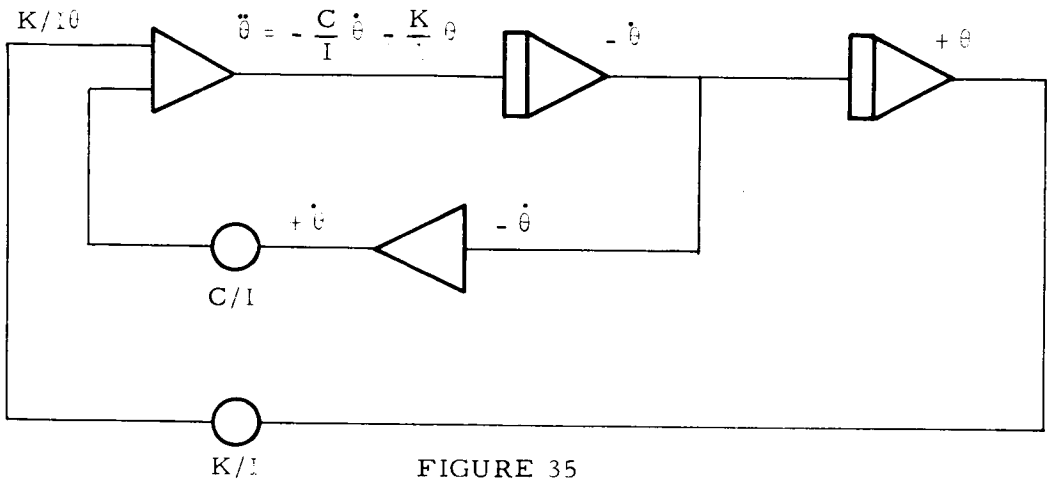

FIGURE 35

BASIC DAMPED OSCILLATOR SIMULATION

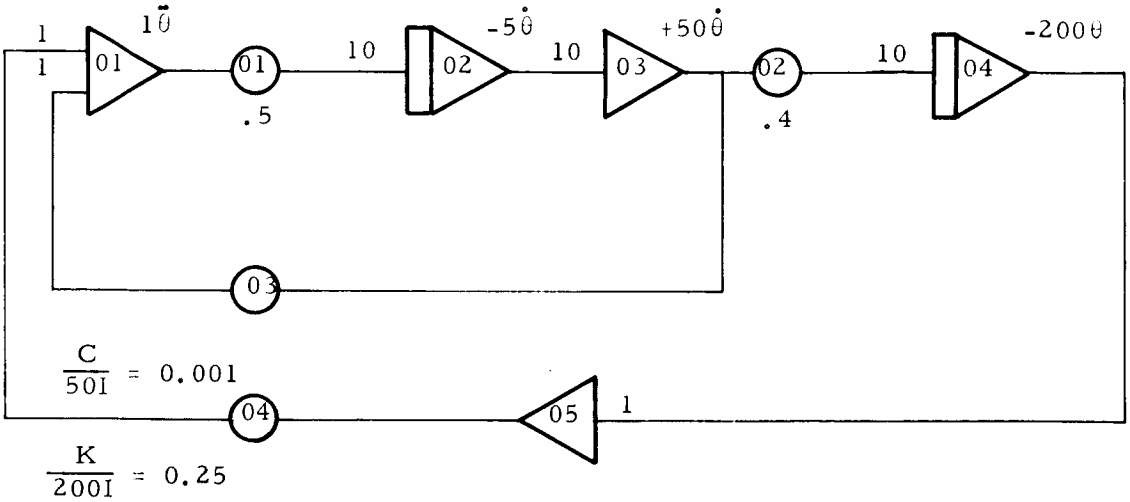

FIGURE 36

FINAL COMPUTER PROGRAM

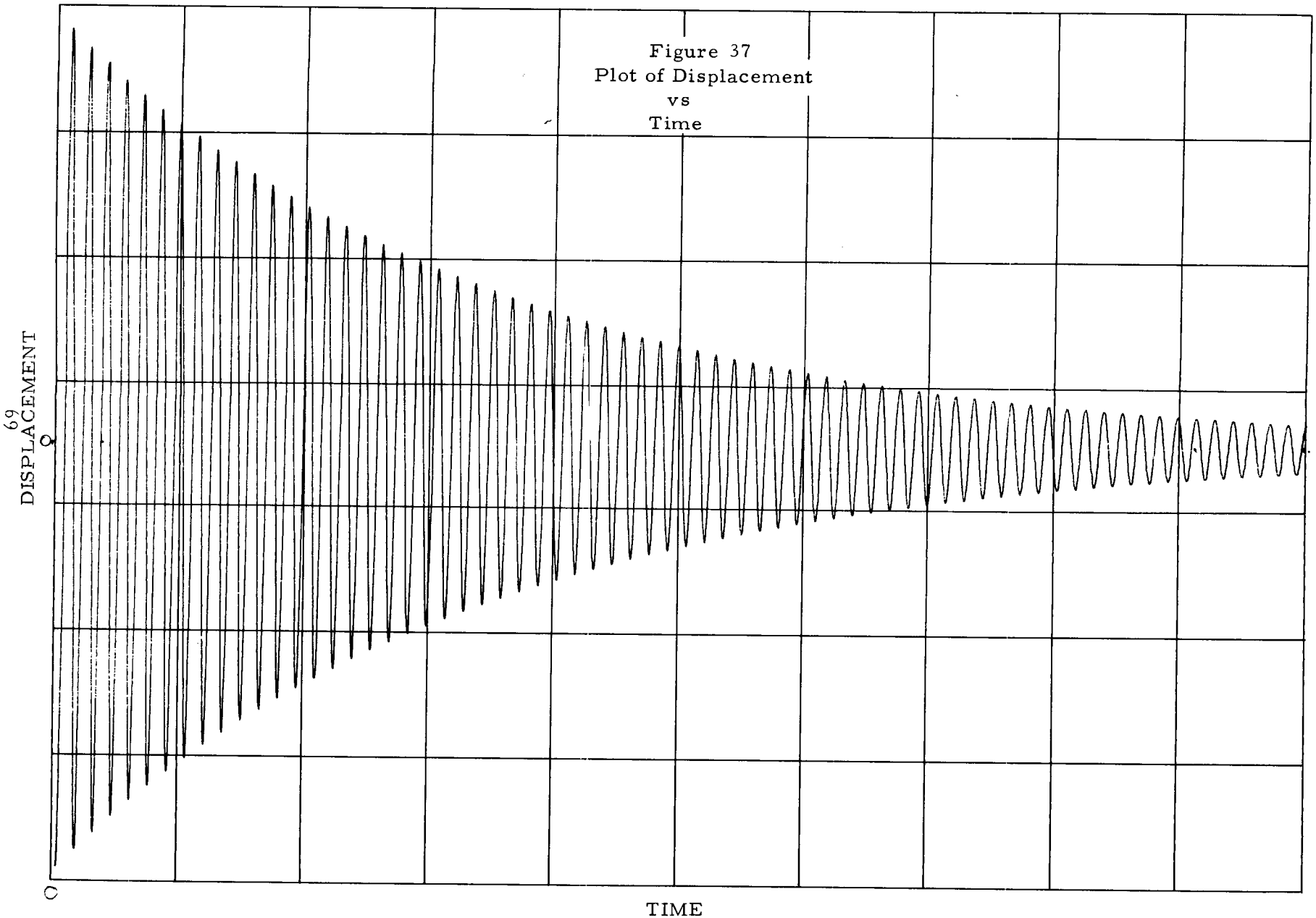

Figure 37
Plot of Displacement
vs
Time

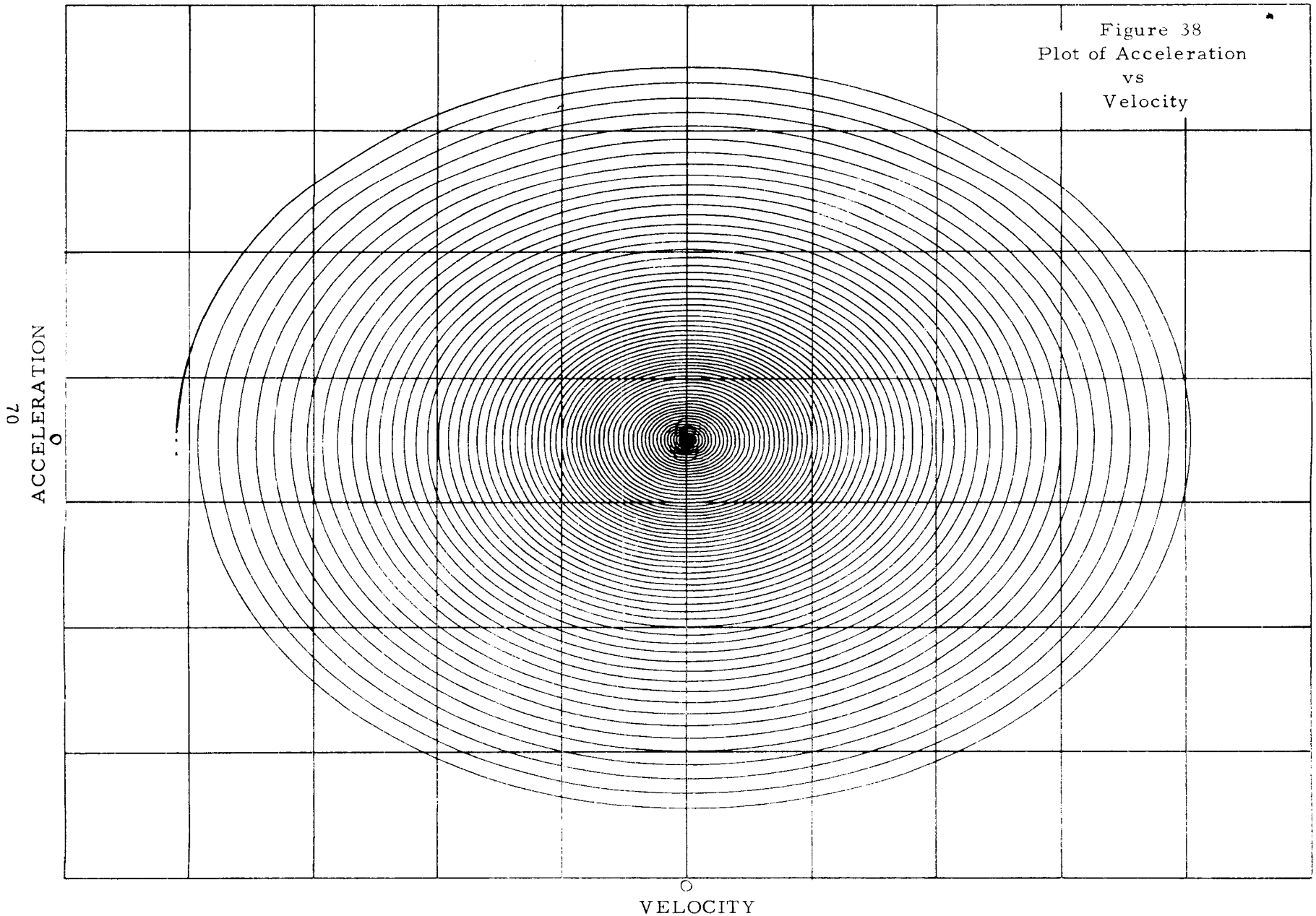

Figure 38
Plot of Acceleration
vs
Velocity

TABLE 3
COMPUTER SCALING FACTORS

Problem Variable	Maximum Voltage Available	Maximum Problem Variables	Scale Factor	Machine Variable
θ	10 volts	.05 radians	10/.05 = 200	[200 θ]
$\dot{\theta}$	10 volts	.02 radians/sec	10/.2 = 50	[50 θ]
$\ddot{\theta}$	10 volts	8.00 radians/sec^2	10/8 = 1.25	[1 θ]

The computer simulation of the damped oscillating torsional pendulum appears to be very satisfactory. The next step in using the computer would be to substitute a varying damping function for C in Equation 21 that will actually simulate the motion of the torsional pendulum air bearing table. This simulation was not possible; therefore the exact mathematical model of the damped system could not be obtained.

2.1.1.4.3 System Equation and Solution

A discussion of the damping theory was given in the 1964 - 1965 Annual Report; however, refinement in the equipment has made some changes in that analysis. The solution to Equation 23 is,

$$\theta = Ae^{-\frac{Ct}{2I}} \sin(\beta t + \varphi) \tag{26}$$

where

$$\beta^2 = K/I - C^2/4I^2 \tag{27}$$

β is the frequency of oscillation of the system and it is related to the period by, $\beta = 2\pi/T$. Equation 27 can be rewritten as,

$$I = \frac{K}{\beta^2 + \alpha^2} \tag{28}$$

where

$$\alpha = C/2I.$$

The equation is written in this manner because the value of α can be obtained. If only the maximum amplitude of oscillation are considered then Equation 26 becomes,

$$\theta = Ae^{-\frac{Ct}{2I}} \tag{29}$$

which is equivalent to,

$$\ln\theta = \ln A - (C/2I)t. \qquad (30$$

If $\ln\theta$ is plotted against t, then the slope of the straight line which results will be equal to - C/2I. Now Equation 28 can be solved for I.

This approach will be applied to typical data obtained from the air bearing system. This data is shown in plotted form in Figures 39 through 41. Figure 39 shows the typical decay rate of an oscillating system. Figure 40 shows the log plot of displacement versus number of cycles. This plot is used to solve Equation 30. Since most log plots are to the base 10, a conversion of Equation 30,

$$\ln\theta = 2.303 \log_{10}\theta, \qquad (31)$$

must be made. Also, the number of cycles in the figure must be converted to t. This is done by letting

$$t = N \times T, \qquad (32)$$

where N is the number of cycle and T is the average period of oscillation at small amplitudes. From this data α or C/2I can be determined.

The plot of period versus number of cycles is shown in Figure 41. There the period decays gradually at first then it approaches a constant value. The period scatter also increases but it remains random which does not affect the period average. This curve, along with the one in Figure 40, proves that the system can be expressed by Equation 23 for a range of approximately 0.001 radians to zero.

The results in this particular test, shown in Figures 39 through 41, will be used to show how the moment of inertia is calculated. The displacement

FIGURE 39

DISPLACEMENT VERSUS NUMBER OF CYCLES

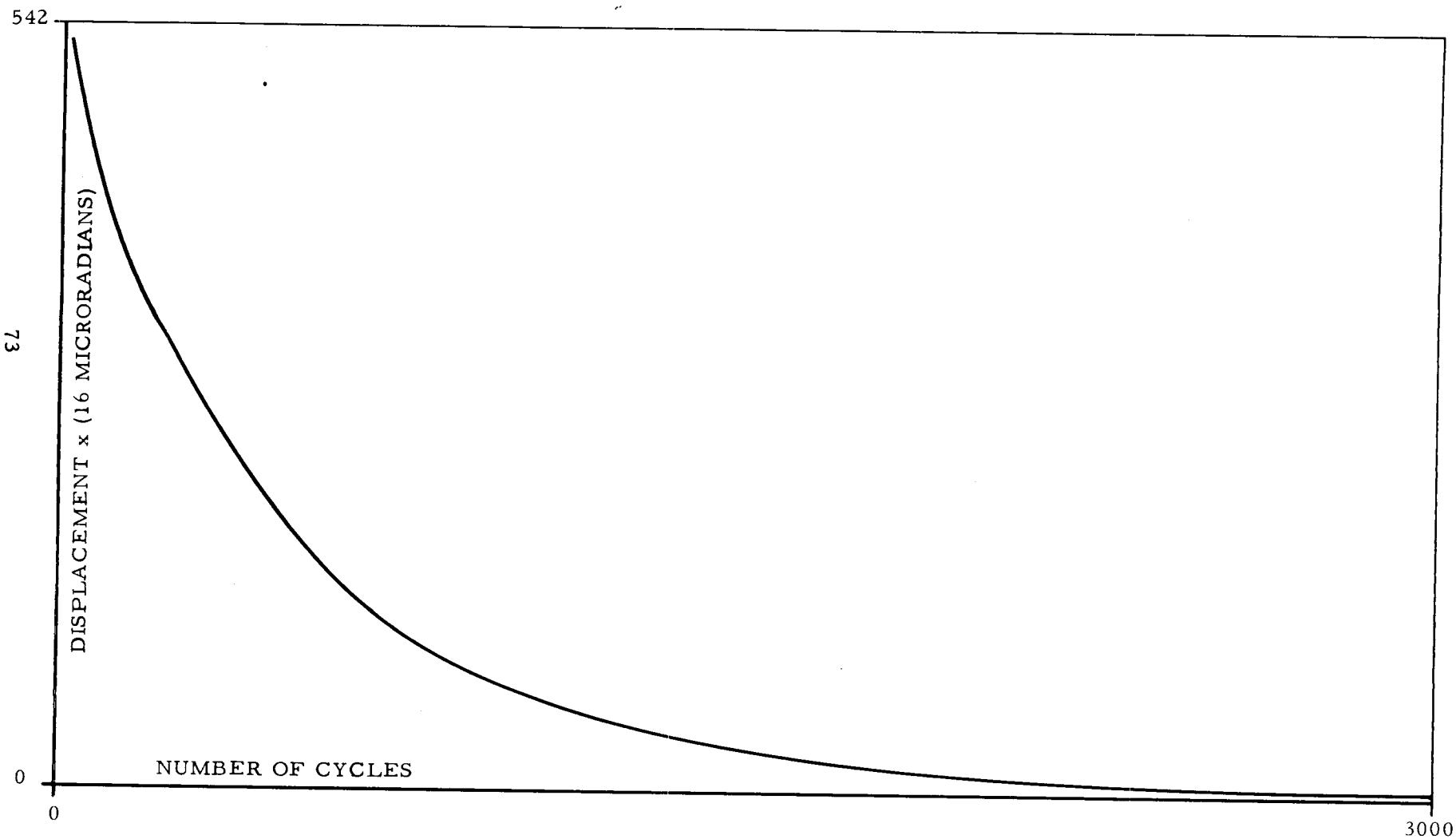

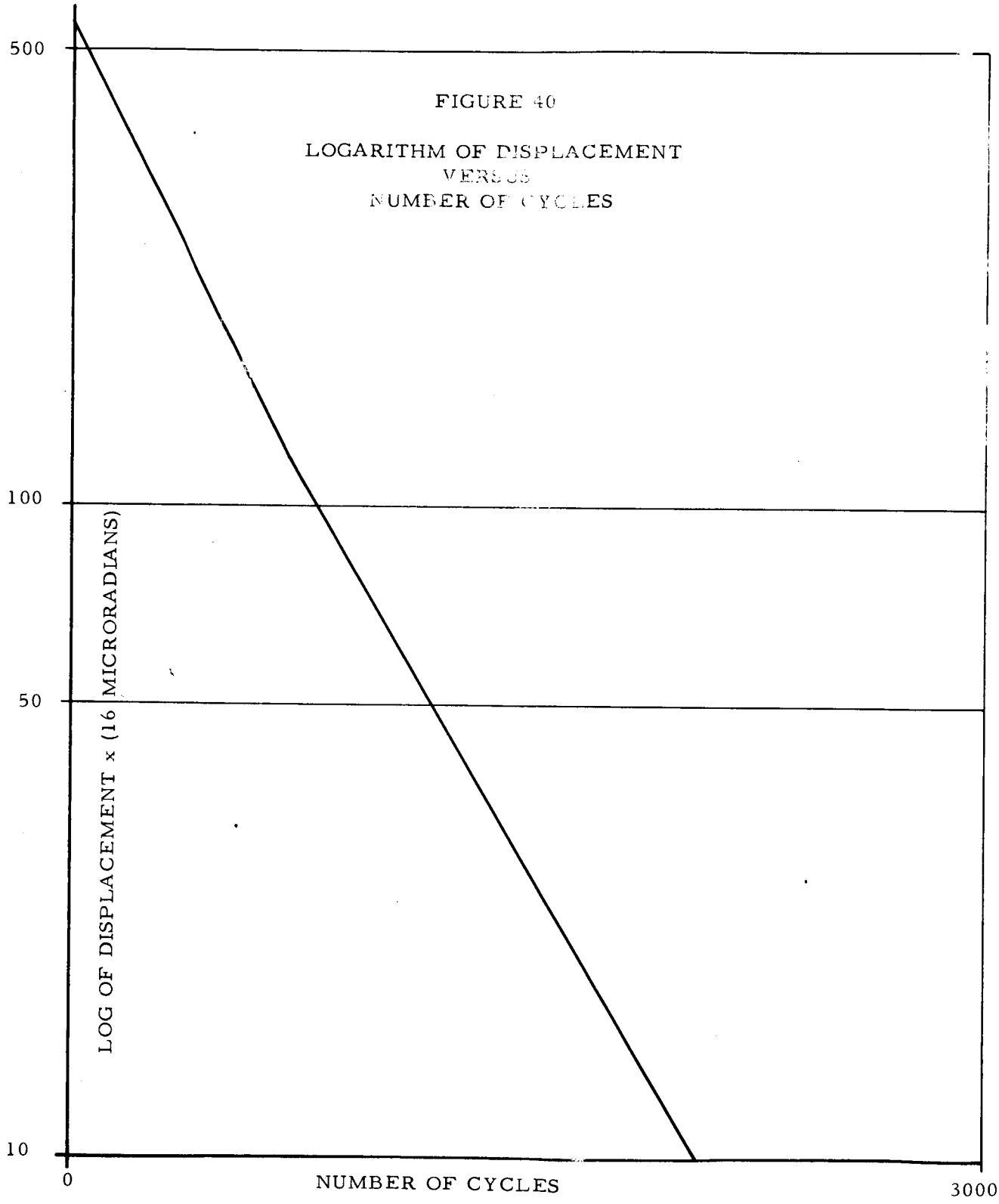

FIGURE 40

LOGARITHM OF DISPLACEMENT
VERSUS
NUMBER OF CYCLES

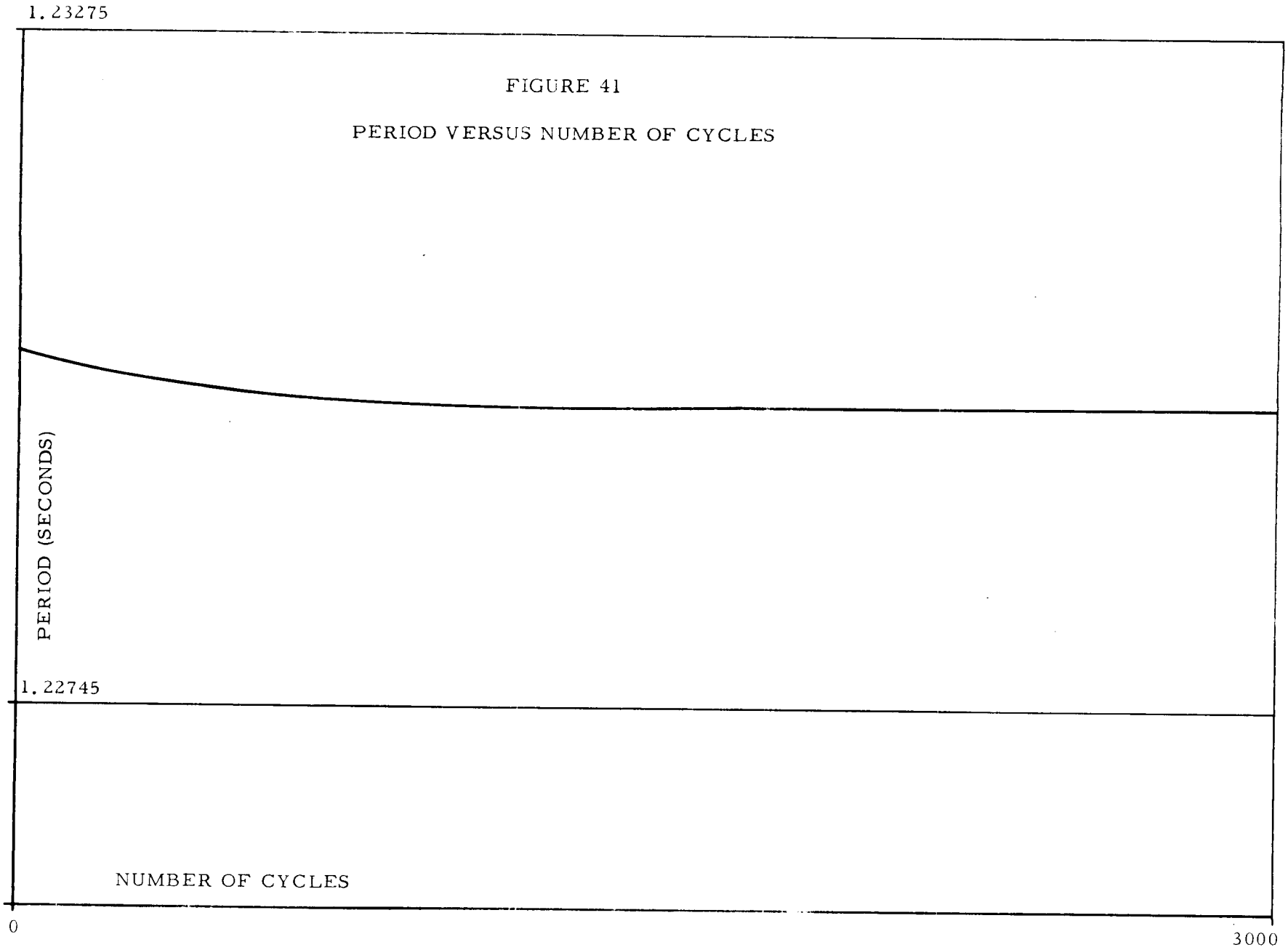

FIGURE 41

PERIOD VERSUS NUMBER OF CYCLES

range used is 0.001 radians down to 0.0004 radians for a total of 500 cycles. The average period in this range was 1.22908 sec. The value for the rod constant was 2662.873 in-lbs and the moment of inertia of the table top and dumbbell was 101.894 in-lb-sec^2. First calculate α and β .

$$\alpha = \frac{\ln\theta_1 - \ln\theta_2}{t_1 - t_2} \tag{33}$$

$$\alpha = \frac{2.303(\log_{10}0.001 - \log_{10}0.0004)}{1.22908(500)} = 0.00148$$

$$\beta = 2\pi/T = 5.11210 \tag{34}$$

Now Equation 28 can be solved for I. This gives

$$I = \frac{2662.873}{26.134 + 2.19 \times 10^{-6}} = 101.894 \text{ in-lb-sec}^2 \tag{35}$$

Here we see that the term for α is extremely small in comparison to that of β . If we solve Equation 28 with and without α we obtain

$$I_{\beta + \alpha} = 101.894758 \text{ in-lb-sec}^2$$

and

$$I_{\beta} = 101.894767 \text{ in-lb-sec}^2$$

or

$$I_\beta - I_{\beta + \alpha} = 0.000009 \text{ in-lb-sec}^2$$

This represents an error in moment of inertia determination of approximately $8 \times 10^{-6}\%$. This result proves that for a typical object the moment of inertia can be determined by measuring the period of oscillation in the range of 0.001 radians or less and using it in

$$I = KT^2/4\pi^2. \tag{36}$$

All other losses and errors normally encountered can be neglected.

2.1.1.4.4 Conclusions

A method of obtaining precise values for the moment of inertia of an oscillating object has eliminated the need for a thorough damping theory study. The results of this report proved that for a given range of amplitudes the equation, $I = KT^2/4\pi^2$, will exactly represent the equation of motion of the system. For the sake of pure analytical research further work in this area may produce some very interesting results.

2.1.2 System Improvements

2.1.2.1 Improved Period Measuring Device

2.1.2.1.1. General Discussion

The purpose in building an improved period measuring device is two-fold. First, a higher resolution in period measurements is needed in order to realize the full potential of the air bearing table as an instrument for measuring moments of inertia. Secondly, the displacement measuring device has been improved to the point where its usefulness is limited by the resolution of the device for measuring period. In order to meet both of these objectives, a new period measuring device was designed, built and evaluated.

2.1.2.1.2 Design Considerations

Since the resolution of the previous displacement measuring system was 1/300th inch, it was decided that the new period measuring device's resolution should be 1/600th inch or better. It was felt that this value could easily be achieved using the system concept of the original period measuring

device if a better optical system was provided and if the wand type of interrupter was replaced with a knife edge type.

Investigation revealed that the required resolution of 1/600th inch could be achieved in the optical system alone using readily available components. The gain of the amplifier would improve this appreciably.

2.1.2.1.3 Optical System Design

2.1.2.1.3.1 Computations - A No. 1003 lamp was chosen for an exciter because of its illumination and small filament diameter (1/64th inch). If it is assumed that the filament sag is no greater than half the filament diameter, the required image reduction becomes:

$$R = \frac{S}{I} = \frac{1.5\ (1/64'')}{1/600''} = 14 \qquad (37)$$

where: R = linear reduction
S = source size
I = image size

The tube length was chosen such as to make the lamp to lens distance 13 inches. Using this value, the maximum distance of the image from the lens becomes 0.93 inch as follows:

$$Di = \frac{Ds}{R} = \frac{13\text{ in.}}{14} = 0.93\text{ in.} \qquad (38)$$

where: Di = distance from lens to image
Ds = distance from source to lens

A symmetrical telescopic eyepiece having an equivalent focal length of 0.75 inch was chosen as a candidate for the reducing lens because of its good optical properties and availability. Checking to see if its image reduction is large enough for use in the system:

$$Di = \frac{f\ Ds}{Ds-f} = \frac{0.75\text{ in. x } 13\text{ in.}}{13\text{ in. } - 0.75\text{ in.}} = 0.80\text{ in.} \qquad (39)$$

where: f = equivalent focal length of the eyepiece

Since the actual Di (0.80 in.) is less than the maximum value (0.93 in.) the image reduction is large enough.

2.1.2.1.3.2 Construction

1. Housing - The optical components consist of a reducing lens, an exciter lamp assemble, a photo-electric detector with mounting, and three light stops. These components are housed in a 19-inch long metal tube as shown in Figure 42. The inside diameter of this tube is 1 1/4-inches to accomodate the reducing lens. The components are held in the housing with set screws. A section is cut out of the housing between the reducing lens and photo-electric detector to allow a knife edge to move between them and interrupt the light beam. The inside of the housing is painted dull black.

2. Reducing Lens - A symmetrical telescopic eyepiece (Edmunds Catalog No. 30, 316) is used for the reducing lens. This eyepiece has coated lens elements and an equivalent focal length of 0.75 inch.

3. Exciter Lamp Assembly - The exciter lamp is a No. 1003 automotive lamp. Its socket is attached to its mount with three screws and compression springs. This arrangement allows for easy alignment of the exciter lamp. The mount is a cap which slips into one end of the housing. The power cord leads out through a hole in the center of the mount.

4. Light Stops - Three light stops are placed between the exciter lamp and the reducing lens to reduce the amount of scattered light reaching the lens, thereby improving resolution. They consist of thin diaphragms having openings just large enough to admit the desired light, and are painted dull black to minimize light scatter.

5. Photo-electric Detector and Mount - The photo-electric detector is a Texas Instruments No. H-38. It is held in its mount by a set screw which grips the signal cable. The mount slips into one end of the housing and can be adjusted in and out.

2.1.2.1.3.3 Mounting Features - The optical system is mounted to the air bearing table on a dove tail cross slide mechanism having micrometer screw adjustments. This arrangement (see Figure 43) provides controllable vertical and lateral adjustments for precise alignment.

2.1.2.1.4 Test Results

Figures 44, 45, and 46 compare the data obtained with the original and improved versions of the period measuring device. It was expected that the scatter (noise) would be reduced, and it was—in some cases, e.g. in Figure 45. Figures 44 and 46, however, show very little difference either way. This data was taken at displacements near 0.001 radian, which is not far from the cut-off point for the original device. The improved model will detect oscillations at displacements less than 0.0001 radian. This is low enough to permit readout of the oscillation period as it becomes asymptotic.

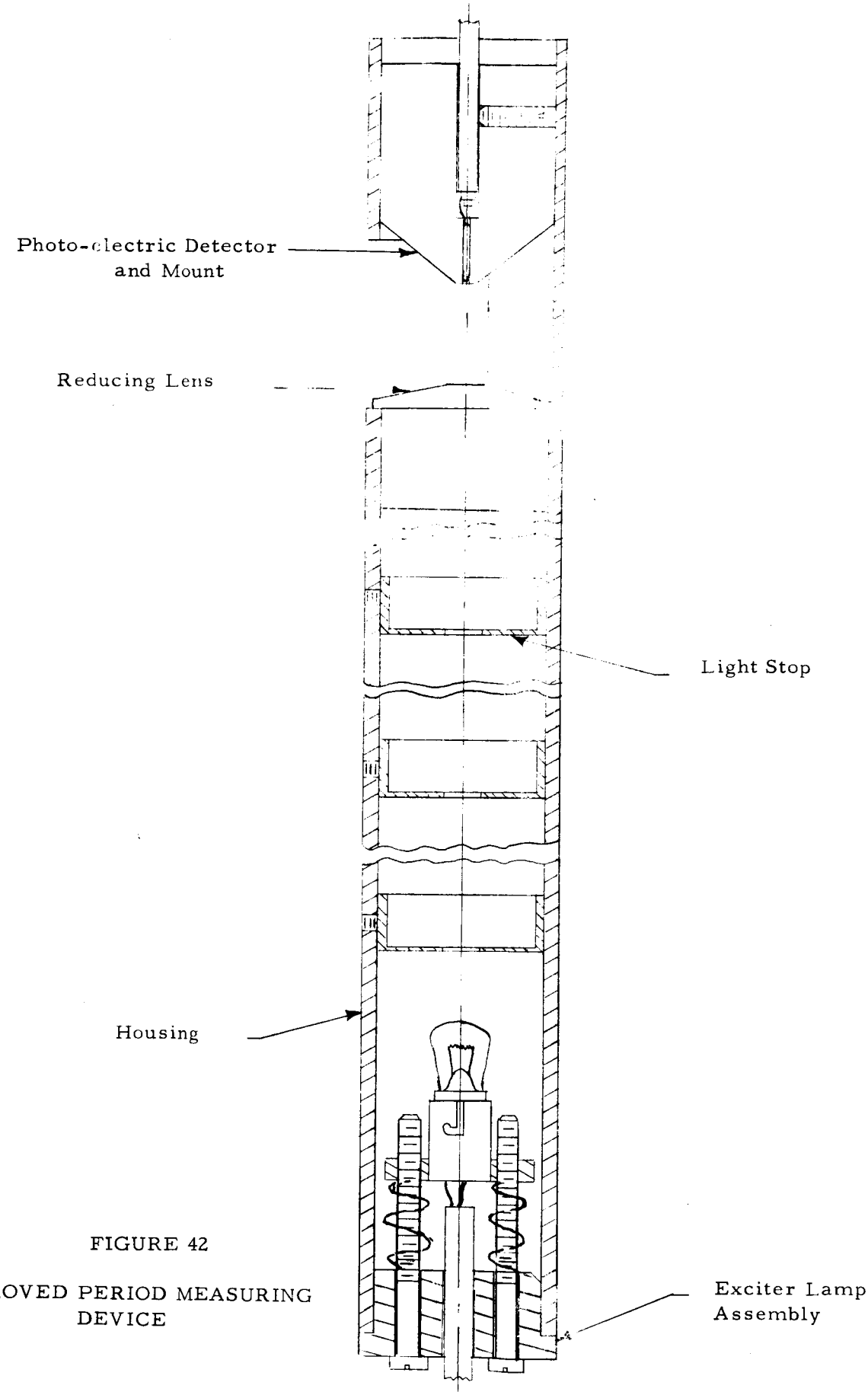

FIGURE 42

IMPROVED PERIOD MEASURING DEVICE

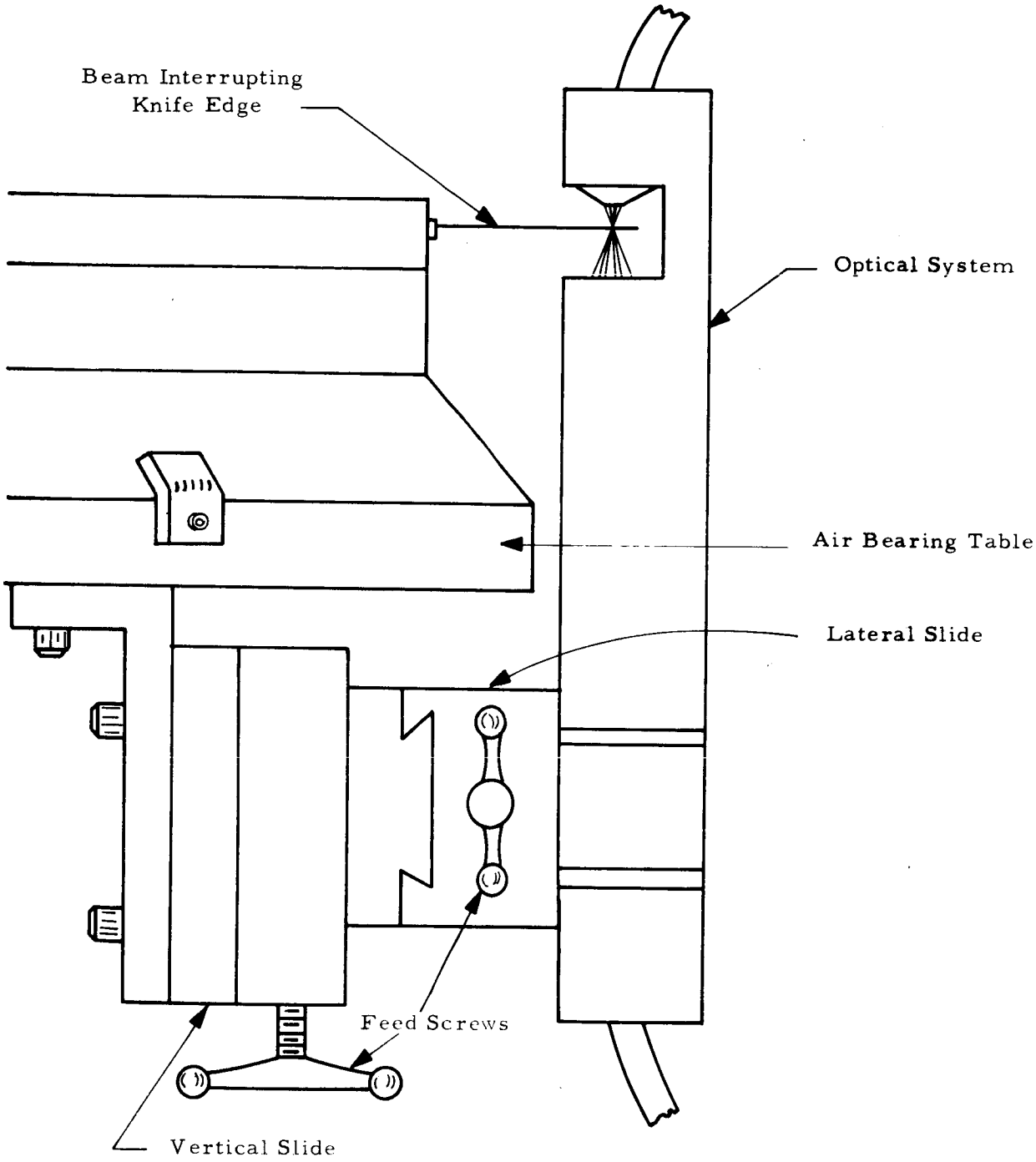

FIGURE 43

MOUNTING CONFIGURATION

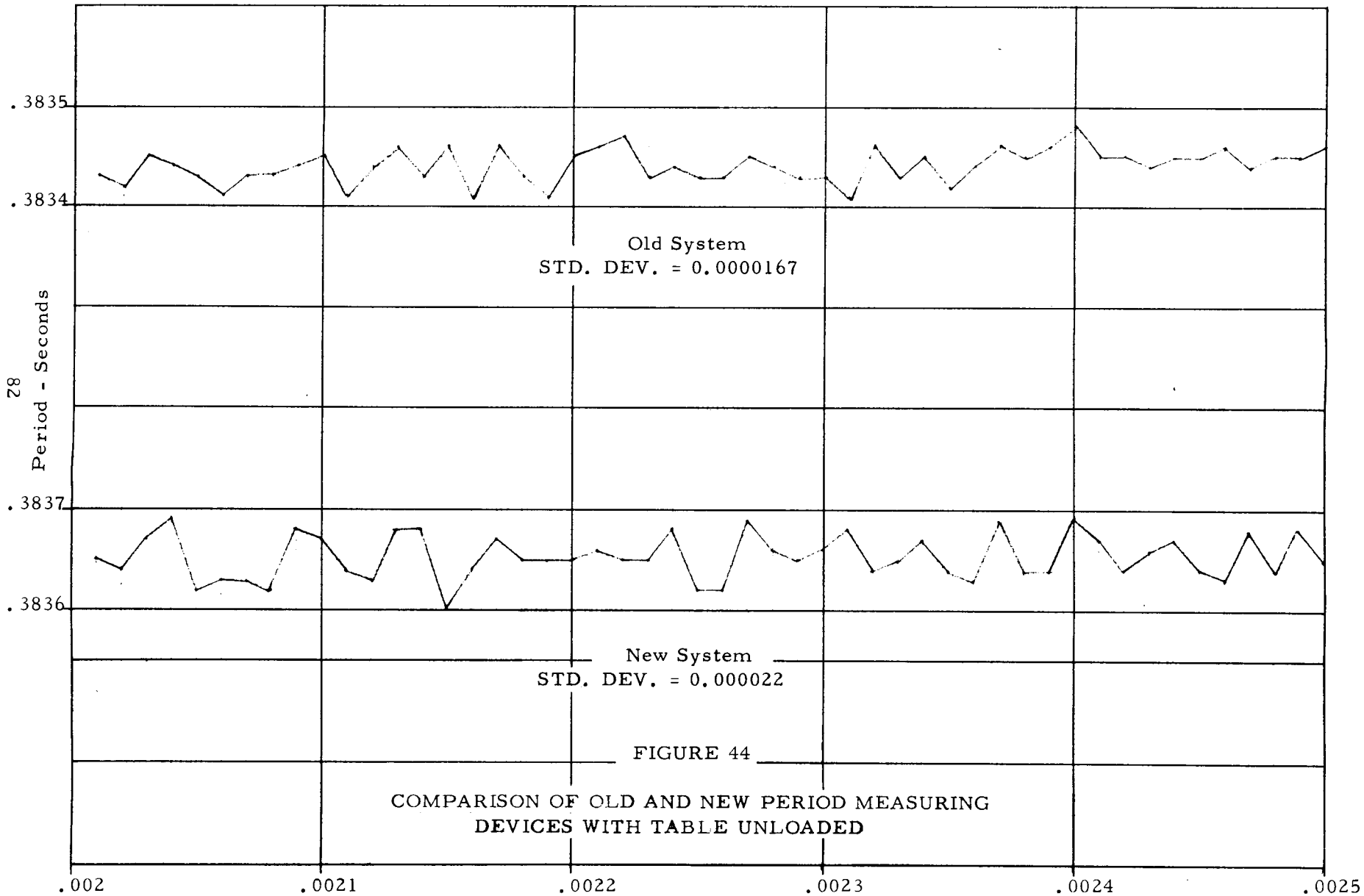

FIGURE 44

COMPARISON OF OLD AND NEW PERIOD MEASURING DEVICES WITH TABLE UNLOADED

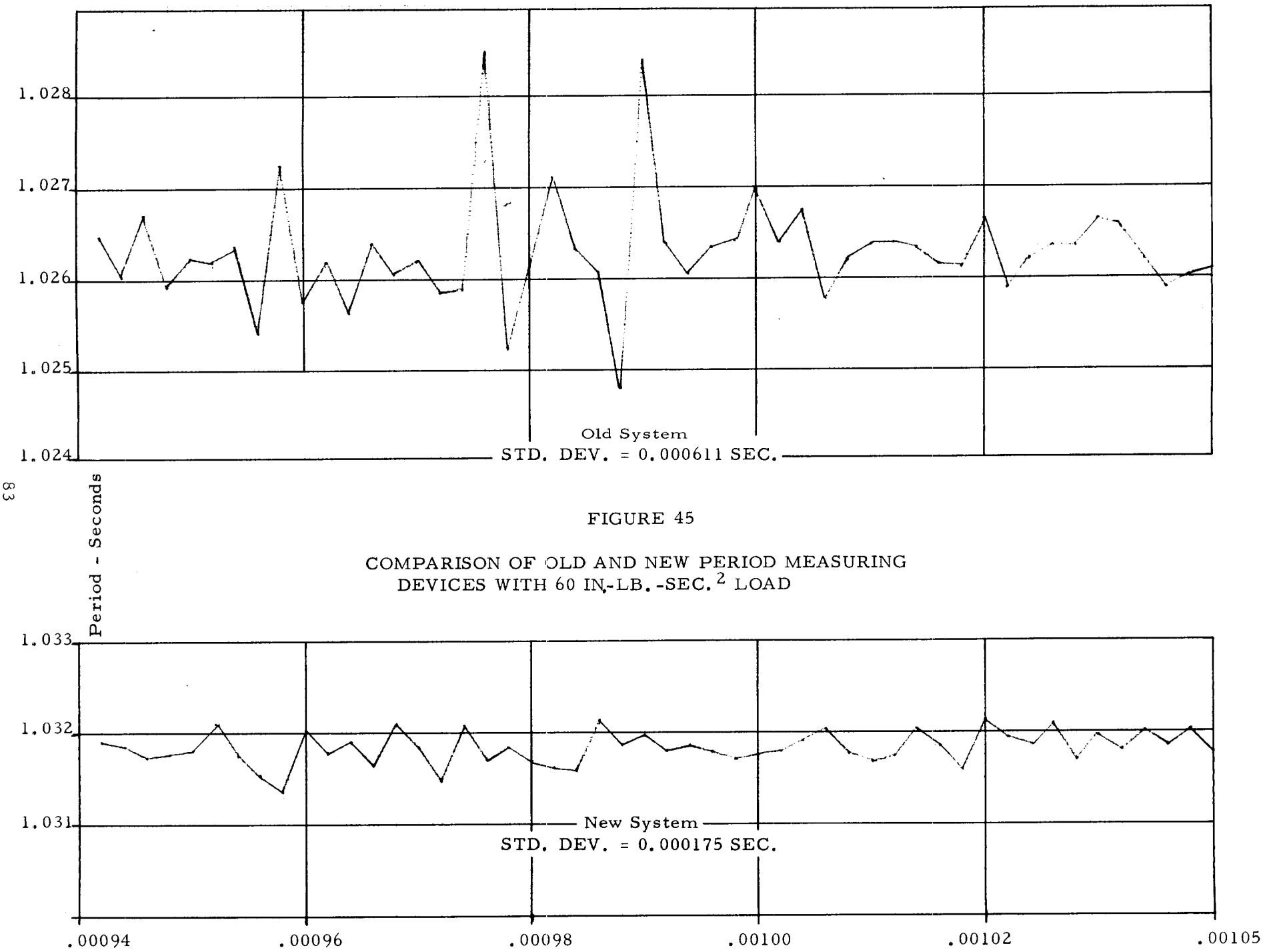

FIGURE 45

COMPARISON OF OLD AND NEW PERIOD MEASURING DEVICES WITH 60 IN.-LB.-SEC.^{2} LOAD

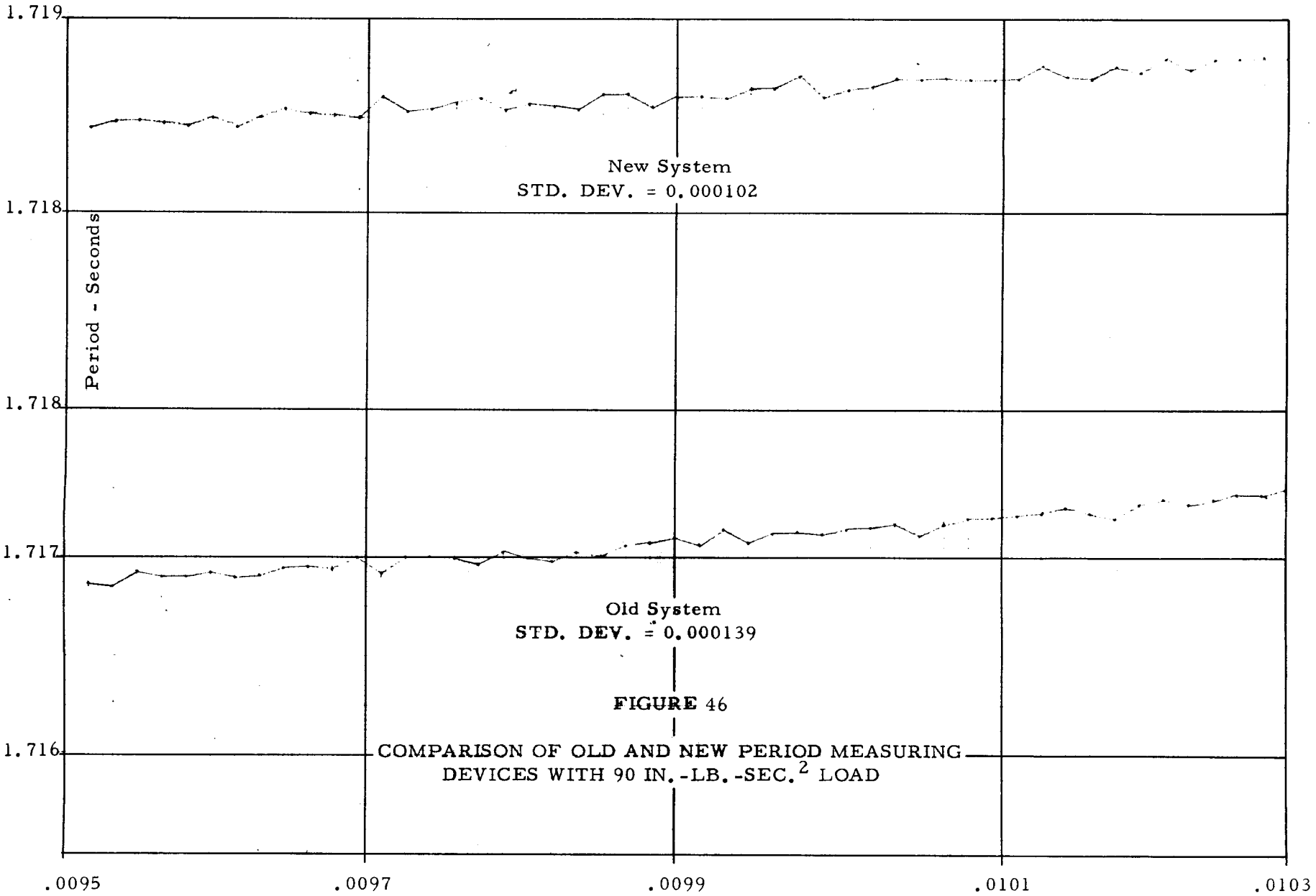

FIGURE 46

COMPARISON OF OLD AND NEW PERIOD MEASURING DEVICES WITH 90 IN.-LB.-SEC.^{2} LOAD

2.1.2.2 Improved Displacement Measuring Device

2.1.2.2.1 Technical Discussion

In making measurements on any system involving mechanical motion, it is desirable to be able to accurately measure the magnitude of that motion. When using the torsional pendulum to determine the moment of inertia, it is the period of oscillation that is of primary interest, but it is also desirable to know the angular displacement of the oscillating mass.

Early efforts at measuring the angular displacement involved reflecting a beam of light from a small plane mirror that was mounted on the oscillating mass. The reflected light beam would sweep across a radian sector as the pendulum oscillated, and the angular displacement could be determined by observation. This method, being somewhat cumbersome, afforded measurements of peak displacement down only to about one milliradian. Thus, its use involved the following:

1. Poor resolution.
2. Human interpretation.
3. A darkened test area.
4. Considerable set-up time.
5. Considerable floor space.

In order to improve on this situation, a displacement measuring system based on the Ronchi ruling was developed.

2.1.2.2.2 Procedure

2.1.2.2.2.1 The System

In the displacement transducer used with this system, a pair of identical Ronchi rulings is used to modulate a beam of light as the torsional pendulum oscillates. The light fluctuations are picked up by a photoelectric detector. Then they are amplified, converted to rectangular pulses, and counted by an electronic counter as shown in the system block diagram, Figure 47. Each of these counts represents a definite small angle through which the pendulum has turned. By accumulating these counts, the counter registers the total angle through which the pendulum has turned. Another photoelectric unit (the period measuring device which is discussed elsewhere) detects the motion of a vane attached to the edge of the pendulum and provides a voltage gate to the electronic counter to establish its counting period. The period of the gate is equal to the pendulum's period of oscillation.

The voltage gate thus provides a time base for the counter and allows it to accuumulate displacement pulses for one oscillation period. The number

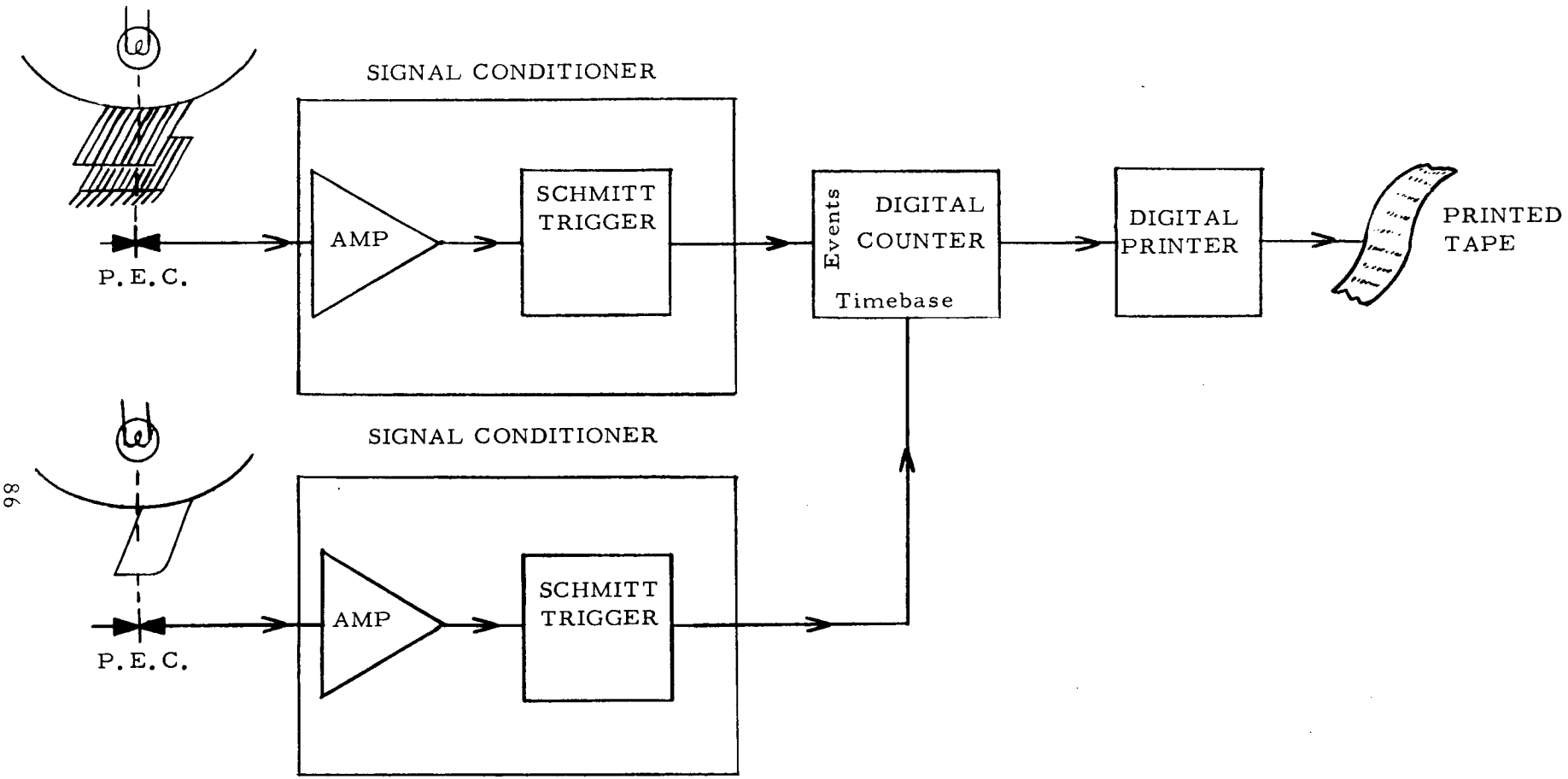

FIGURE 47

SYSTEM BLOCK DIAGRAM

registered by the counter thus represents twice the peak-to-peak angular displacement of the pendulum. This number is printed on paper tape by the numerical printer.

2.1.2.2.2.2 Prototype Transducer

A sketch of the prototype transducer is shown in Figure 48. In this transducer a pair of one inch square Ronchi rulings are mounted such that there is a small space between them. One of the rulings is movable, being mounted on a small bracket which is attached to the edge of the torsional pendulum. The other is fixed and is mounted on an adjustable support. The adjustments are for alignment purposes and allow for adjustment of the spacing between the two rulings as will as for the orientation of the fixed ruling. The rulings are oriented so that their lines are parallel to their own centerlines which intersect the rotational axis of the pendulum at right angles. Light from the exciter lamp mounted a few inches above the rulings passes through them, illuminating the photoelectric detector mounted beneath. The interference pattern produced by the light passing through the two rulings sweeps across the detector as the pendulum oscillates, causing its output to be modulated.

The rulings consist of equally spaced opaque lines on one side of a piece of clear flat glass. The width of the spaces between the lines is the same as that of the lines. The resolution obtained with the transducer depends on the number of lines per inch. One thousand lines per inch rulings are presently being used. Since the transducer is located at a 15 inch radius pendulum can be measured to an accuracy of 17 microradians.

2.1.2.2.2.3 Signal Conditioner

The fluctuations in the output of the photoelectric detector are amplified and converted to rectangular pulses in the signal conditioner. A schematic diagram of this unit is shown in Figure 49. An input emitter follower provides a high impedance load for the photoelectric detector, a Texas Instrument type H-38 photoduodiode. Following this is one stage voltage amplification. The amplifier drives an emitter follower which provides a low impedance source for operating the Schmitt trigger following it. The Schmitt trigger provides rectangular pulses at the output jack of the signal conditioner.

2.1.2.2.2.4 Counter Conversion

In order to use the voltage gate from the period measuring divice to provide a time base in the electronic counter (a Hewlett-Packard model 524D) a slight modification to the counter was required. In the counter a decade divider (a plug-in unit) is ordinarily used. This unit divides down the internal clock frequency to provide a lower frequency to be used for the

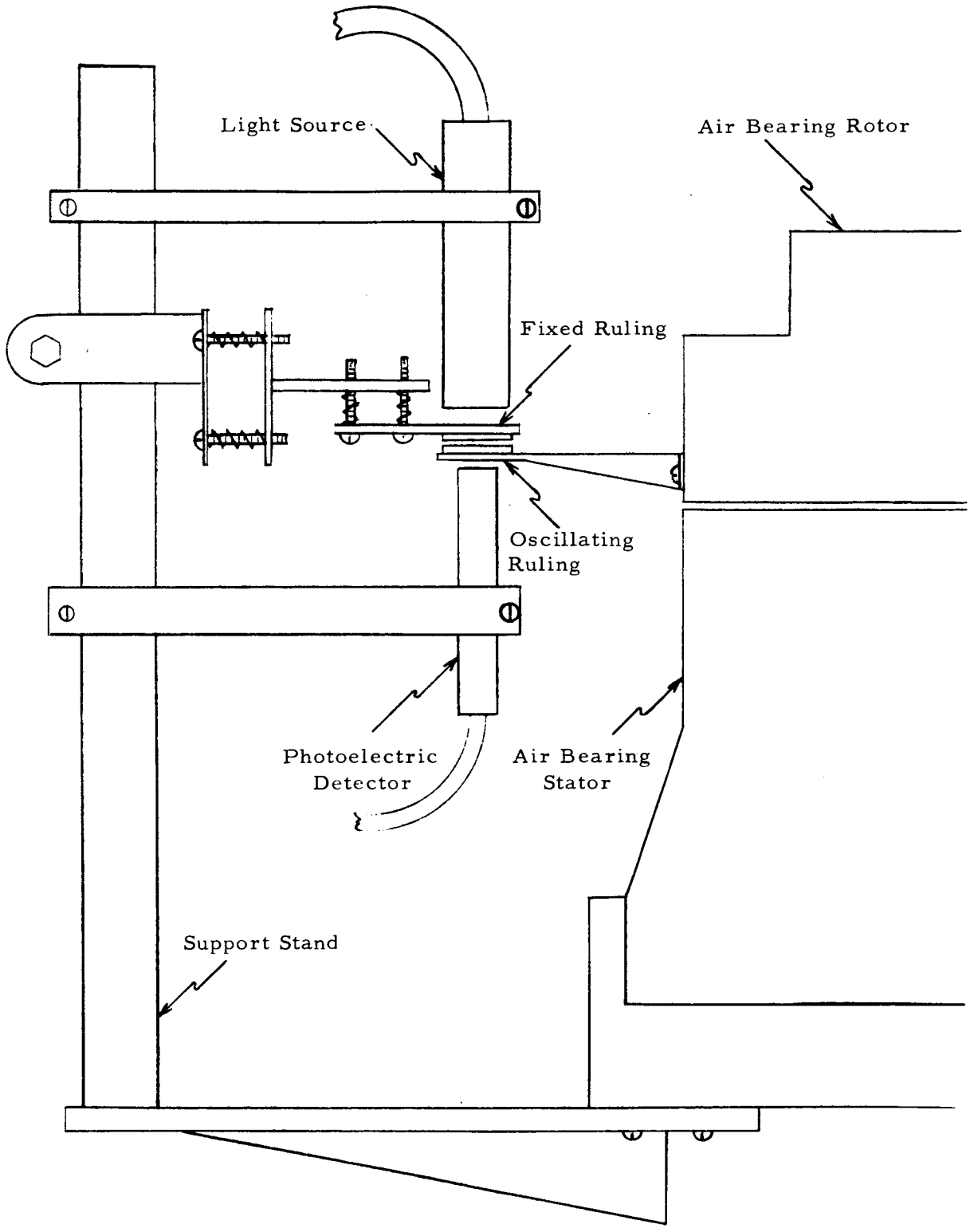

FIGURE 48

PROTOTYPE DISPLACEMENT TRANSDUCER

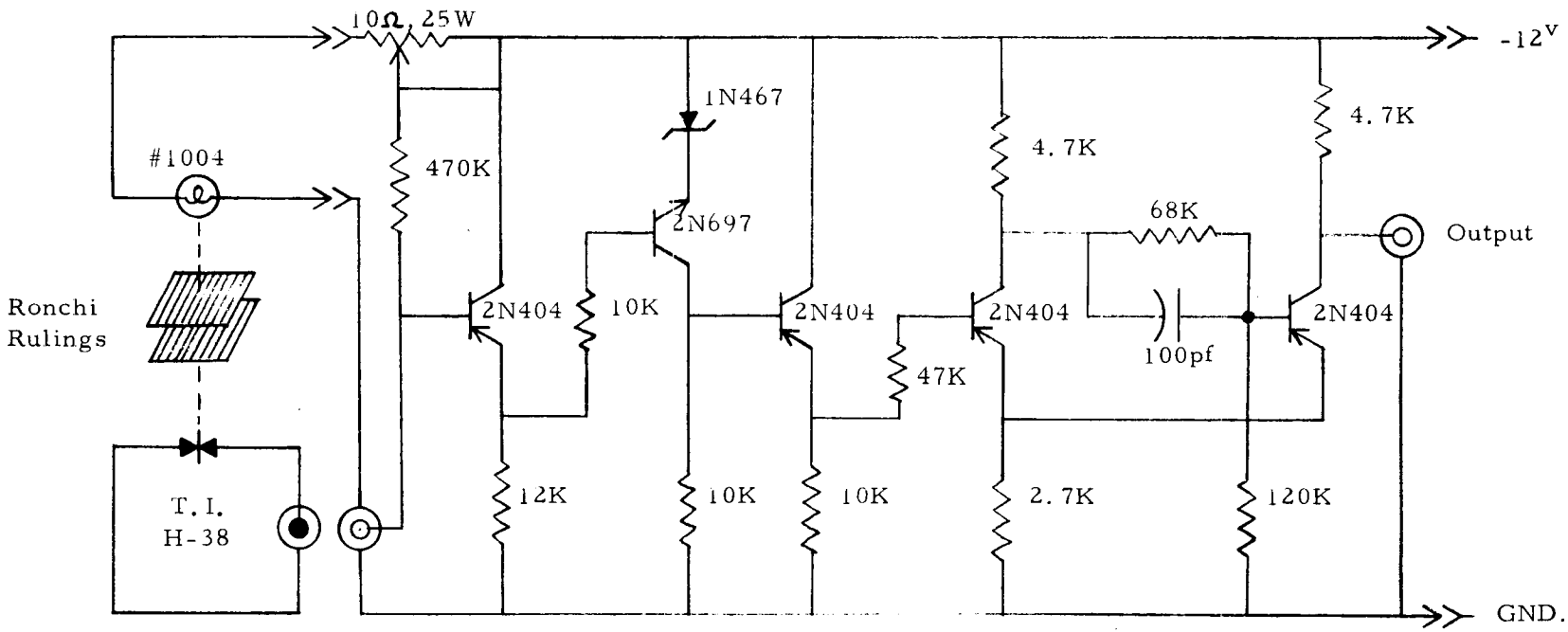

FIGURE 49

SIGNAL CONDITIONER SCHEMATIC

time base. In order to convert the counter for measuring displacement, the decade divider was replaced with another plug-in unit, which uses the voltage gate mentioned above to provide the time base. A schematic of this unit, which is a Schmitt trigger, is shown in Figure 50.

2.1.2.2.2.5 The Present Transducer

Based on the experience acquired in using the prototype transducer, and operational model was designed and built. Although the new transducer is basically the same as the prototype, several changes were incorporated into its design. The major drawbacks to the prototype were sensitivity to vibrations and difficulty of adjustment. These drawbacks have been virtually eliminated in the new transducer, shown in Figure 51. It is very rigidly built. The rulings are mounted in cells which can be rotated in their holders for angular alignment. A table extension is sometimes used on the pendulum. In order to provide clearance for it the photoelectric detector, rather than the exciter lamp, is mounted above the rulings and movable ruling's holder is offset. The spacing between the two rulings is adjusted by raising or lowering the exciter lamp housing. Two large knurled nuts are provided for making this adjustment. The lower of these serves as a lock after making the adjustment. The distance from the exciter lamp to the rulings can be varied by sliding the lamp holder up or down. This may also be rotated to orient the lamp's filament with the rulings. The detector can be raised or lowered in its holder to adjust the detector to ruling distance. All adjustments are locked by set screws unless other locking means are provided. The main assembly mount has slotted holes for attaching to the torsional pendulum's air bearing stater. These allow for radial alignment of the main assembly. Circular mounting slots in the exciter lamp housing guide allow for an additional angular adjustment of the fixed ruling. All the machined parts are of black anodized aluminum. The operating radius of the new transducer has been increased to 15.5 inches.

2.1.2.2.3 Test Results

The accuracy and linearity of the transducer was checked by comparison with a Tuckerman autocollimator. Testing was done in accordance with the test procedure given in Appendix A3.

The test results are tabulated in Table 4. It is seen that the angular values as measured by the displacement transducer are slightly larger than those obtained with the autocollimator and that the difference in the values obtained with the two methods is essentially constant. This indicates a zero offset in the autocollimator. This is understandable since its scale can probably be read no closer than 2%. Thus it appears that the displacement transducer is both accurate and linear within the experimental accuracy.

TABLE 4

PEAK DISPLACEMENT MEASURED			
Run No.	By Autocollimator	By Displacement Transducer	
		Counts	Angle
1	0.012 radian	751	0.01211 radian
2	0.012 radian	751	0.01211 radian
3	0.012 radian	752	0.01213 radian
4	0.006 radian	382	0.00616 radian
5	0.006 radian	382	0.00616 radian
6	0.006 radian	380	0.00613 radian

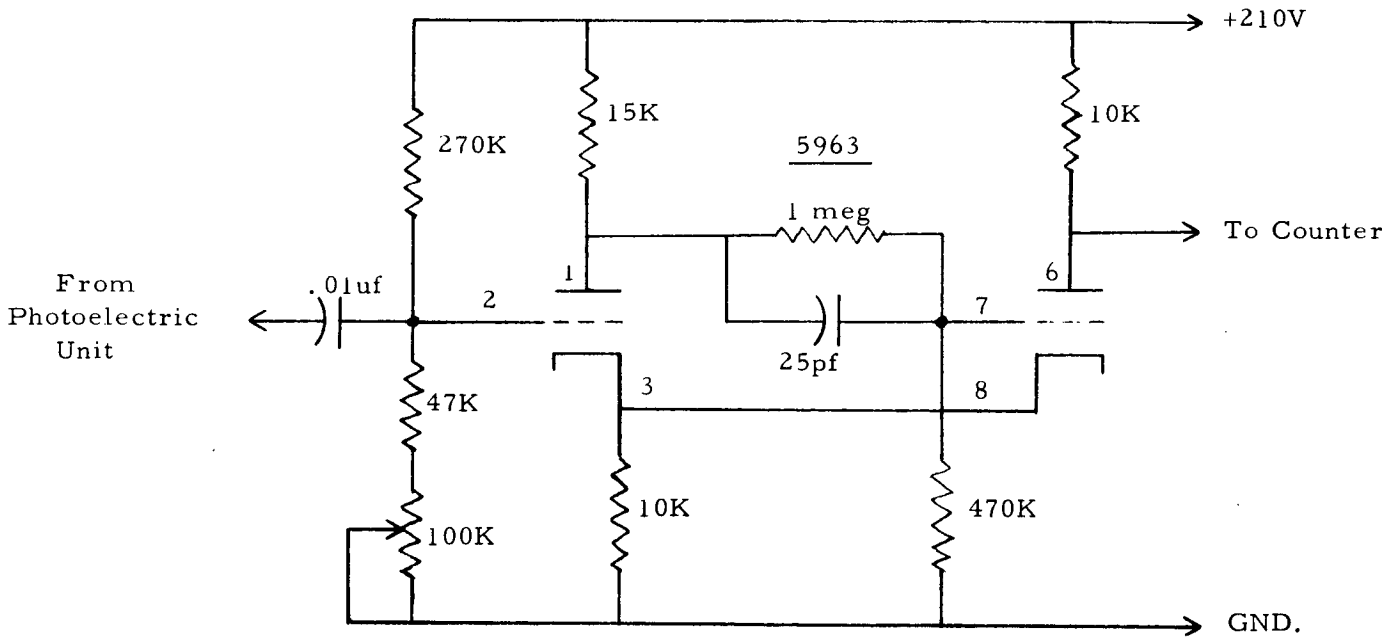

FIGURE 50

COUNTER CONVERSION CIRCUIT
(Plug-in Unit)

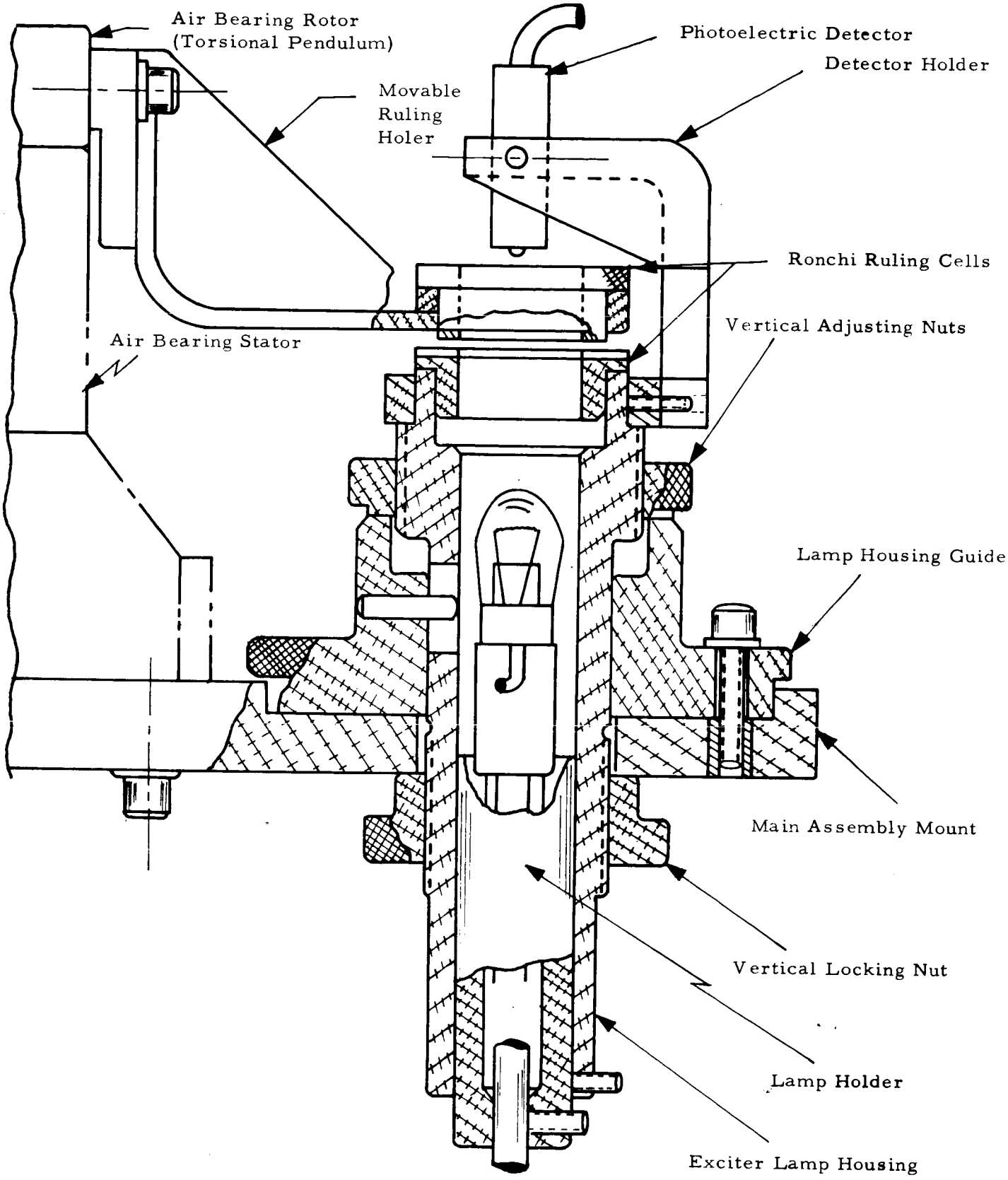

FIGURE 51
PRESENT DISPLACEMENT TRANSDUCER

2.1.2.2.4 Conclusions

Based on the tests it can be said that the displacement transducer accuracy depends on the resolution (lines per inch) of the rulings used with the reading is accurate within two counts. The peak displacement error obtained with 1000 lines per inch rulings at a 15.5 inch radius is therefore well within one count or 16 microradians. Imperfections in the rulings are averaged over the number of lines seen by the detector. The rulings mentioned above can be used reliably to about 12 milliradians peak displacement. This limitation is due to loss of contrast caused by reduced parallelism between the two rulings at the larger angular displacements. However, it is of no concern at the small angles presently of interest.

An error is introduced by using rulings having parallel lines rather than radial lines. Within the displacement limitation described above this error, amounting to only .0025%, is insignificant. The use of rulings having radial lines would remove this error source and the displacement limitation.

2.1.2.2.5 Recommendations

In order to improve the resolution of the present displacement transducer, the use of rulings with more lines per inch would be indicated. It is believed however, that the present 1000 lines per inch is approaching the limiting value for a system which requires that the pair of rulings not be in contact. It is also believed that optical diffraction effects would reduce contrast with higher resolution rulings.

Since the system has been developed about as far as practical in its present form, any substantial improvement would have to come about through an electronic innovation or some other system.

2.1.2.3 Air Bearing Table Improvements

The air bearing table improvement section was included to take care of any modifications which might be necessary to improve the operation of the system. Fortunately no major changes were necessary. Minor changes such as tension and bracket modification and air filter rearrangement were accomplished; however, this did not affect the operation of the system.

One adaptation which aided the collection of data was a direct plot of displacement and period data.

The analog output on the Hewlett-Packard 560 digital recorders was used for the first time with an X-Y recorder. Experiments were made with the set-up for direct plotting for moment of inertia tests. Using the equipment on hand with such an arrangement, it was possible to plot directly the period-time relationship, log period-time, period displacement, log period-displacement, period-long displacement, displacement-time, and log-displacement-

time. The voltage appearing at the analog output of the recorder was proportional to any three consecutive digits of the last number printed, making possible any amount of scale magnification.

Figure 52 is a sample plot with the equipment showing the peak displacement of a damped torsional pendulum with respect to time. The irregularities in the curve are believed to be the result of dirty contacts in the digital recorder.

2.1.3 Torsion Rod Investingation

2.1.3.1 Investigate Rod Material

2.1.3.1.1 Introduction

The rod material investigation portion of the torsion rod project is designed to determine what material and rod design will provide maximum accuracy for the torsional pendulum moment of inertia determing system. The selection of the torsional pendulum method of determing moments of inertia over other pendulum methods is dependent on a very accurate torsion rod spring constant. The rod constant's accuracy in turn depends on the linearity of the material used in the rod. For this reason a very linear material must be obtained. Theoretically, a perfect elastic material would be ideal for the torsion rod. Since a perfect elastic material does not exist in nature, a search had to be made that would produce the best elastic material that could be fabricated into the proper shape. Another factor to consider is that of the cost of the material and its fabrication, which can become rather expensive for some materials.

At the present time there appears to be a limited need for materials that have nearly perfect elastic characteristics. This was concluded after a survery of various steel, glass and ceramic manufacturers revealed that detailed information on stress-strain relations was not available. Therefore, a material search and test program will have to be conducted by the Mass Metrology Laboratory to evaluate the elastic properties of various materials for use as a torsion rod.

2.1.3.1.2 Basic Elastic Theory

Elasticity is the property of a material that allows it to be loaded, which causes a deformation, then when it is unloaded it returns to its original shape. This property of elasticity is expressed by Hooke's law shown in Equation 40. Hooke's law states that the modulus of elasticity is equal to the ration of stress to strain, where stress is the load per unit area and strain is the elongation per unit length. Another relationship which expresses

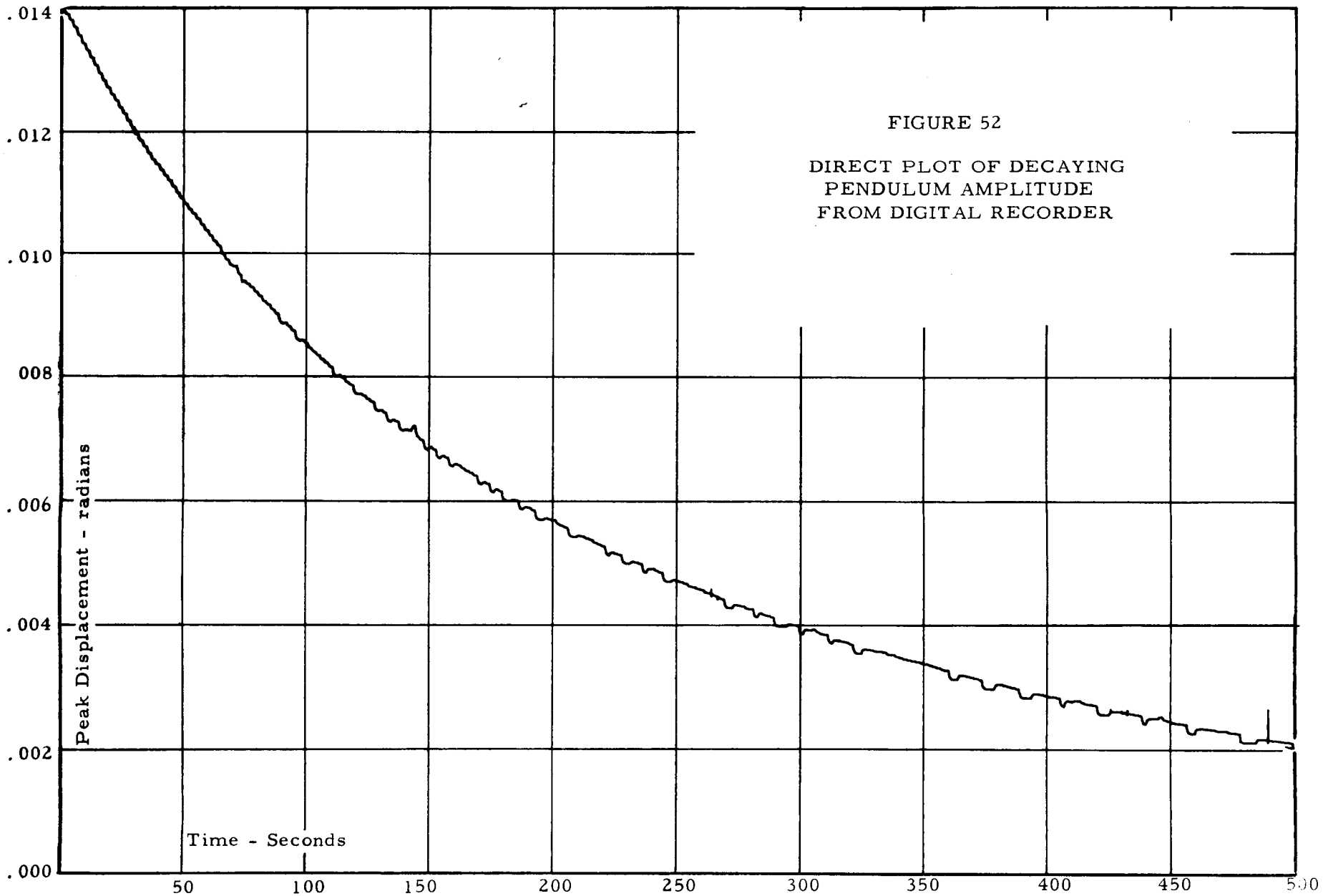

FIGURE 52

DIRECT PLOT OF DECAYING PENDULUM AMPLITUDE FROM DIGITAL RECORDER

$$E = \partial / \epsilon \tag{40}$$

the property of elasticity is Poisson's ratio. This ratio relates the lateral strain to the longitudinal strain as shown in Equation 41. Both the modulus

$$u = \epsilon_y / \epsilon_x \tag{41}$$

of elasticity and Poisson's ratio are a measure of the stiffness of a material.

Theoretically, Hooke's law expresses a linear relationship between stress and strain as shown in Figure 53. In this figure the elongation is exactly proportional to the load, both upon loading and unloading. In actual practice no materials exhibit a perfect linear relationship but rather a non-linear characteristic as shown in Figure 54. This figure shows that as the material is loaded, the stress-strain relationship is not exactly linear; likewise, upon unloading the curve is nonlinear again and does not trace the original curve. The non-linearity of the curve depends upon the material used and its properties such as stiffness, elastic strength and resilience. The term elastic resilience is the ability of a material to absorb energy elastically; that is, as long as the deformation is both elastic and linear, the energy stored in the material is recoverable in the form of strain energy. An example of an elastic material which is nonlinear is shown in Figure 54. The area between the two curves represents the energy lost during the elastic action. This energy loss is in the form of internal friction and represents a good example of mechanical hysteresis. The three terms resilience, internal friction and mechanical hysteresis are all good terms for defining the non-linearity of an elastic material. For example a linear material has a high resilience, low internal friction and a small hysteresis loop.

Another loss which exhibits a nonlinear effect is elastic aftereffect or delayed elasticity, a transient variation of strain with time. If a rod of any material is stressed by applying a load, the elongation does not immediately assume its final value. Instead, an instantaneous strain is followed by a further elongation, which grows slowly and at a disinishing rate until it comes to rest. The same is true when the load is removed. This phenomenan is referred to as the aftereffect and does not include plastic deformations, which do not recover when the load is removed. These aftereffects include thermoelastic action, atomic diffusion, magnetoelastic effect, the uncoiling of long-chain molecules in polymers, heterogenity and others. Most elastic aftereffects are quite small since the area of a single hysteresis loop is almost insignificant compared with the total strain energy. When mechanical vibrations are involved, the energy lost may be larger. Elastic aftereffect is a form of internal friction. It varies from material to material, and for a given material it varies depending on frequency, temperature and previous treatment of the material. For an oscillating system this form of internal friction acts as a damping agent.

FIGURE 53

Linear Elastic Stress-Strain Diagram

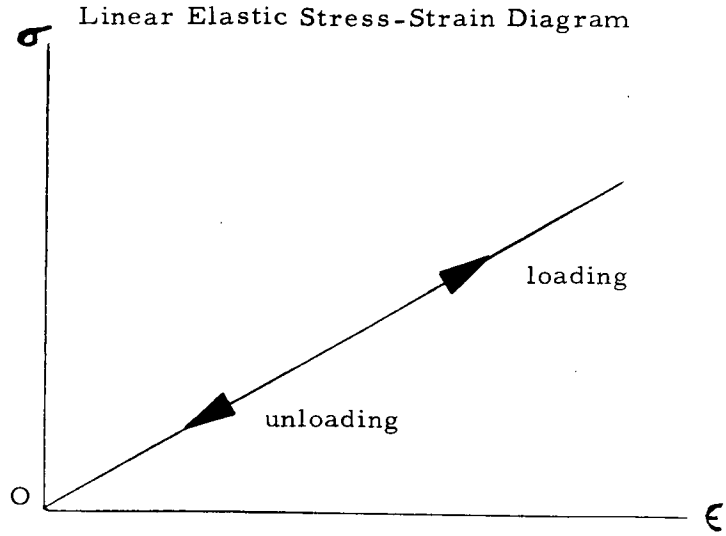

FIGURE 54

Non-Linear Elastic Stress-Strain Diagram

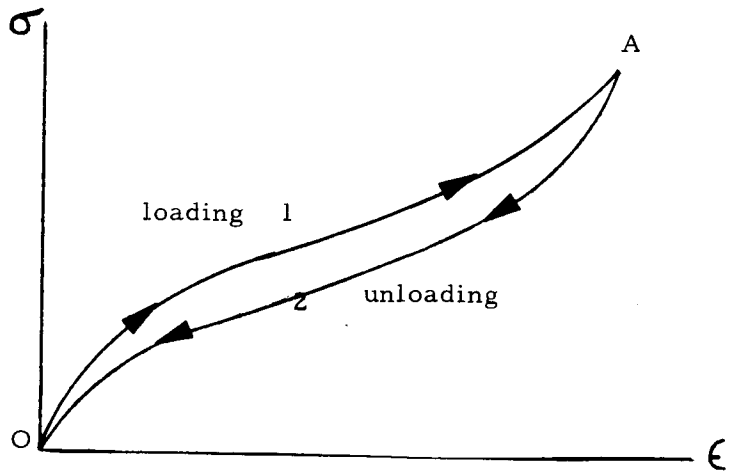

One method of measuring internal friction is $\Delta \omega / \omega$ where $\Delta \omega$ is the energy dissipated per cycle, given by the area within the hysteresis loop, and ω is the total strain energy per unit volume. To give an idea of the order of magnitude of internal friction for some materials, a chart is shown below. Impurities in metals have a pronounced effect on internal friction and in some

Material	Internal Friction $\Delta \omega / \omega$
Rubber	0.6
Metal	0.05 - 0.0001
Glass	0.000002

cases may increase the internal friction by a factor of 1000 or more. From the theoretical consideration of material properties, it is easy to choose the properties which will give an exactly linear, elastic effect, but in practice an actual material with these properties is hard to find.

2.1.3.1.3 Torsion Rod Design

The next consideration in selecting a rod material is the shape or design of the material that will best utilize the properties of the material. In using a torsional pendulum, the basic shape is fairly well defined; that is, some type of bar or rod must be used. The design of the bar, either circular, square, rectangular, solid or hollow will have to be such that the optimum linearity properties in torsion are obtained.

In determing the shape of the rod, one main factor to be considered is that of the forces applied to the rod. This consideration is greatly simplified by using the air bearing table. The air bearing table is designed in such a manner that only shearing forces are produced in the rod. Tensile and compressive load are eliminated by loading the table before the rod is inserted. Since circular rods exhibit pure shear while in torsion, their use would be the first and obvious selection, but other shapes must be considered to make the investigation complete.

A solid bar of non-circular cross section will be considered first. As early as 1853, St. Venant showed that a plane transverse section of a bar of non-circular cross section before twisting does not remain a plane section after twisting. The plane becomes a warped surface, and the warping is accompanied by an increase of shearing stress in some parts of the section and a decrease in others as compared to stresses that would occur if the section did not warp, as in a circular cross section. As an example the elliptical rod shown in Figure 55 will be considered. The rod's cross section is ABA'B', and it is twisted

about its longitudinal axis OO'. At any points A, B, A' or B' the stresses produced by torsion on the rod are parallel to the surface, whereas at points C and C', the stresses have components inwards and outwards. Consider a small volume Δ v within the rod. The top of the element has an inward stress while the outside of the element has a downward stress to maintain the shape of the volume element. Similar action applies to the other sides. It is up and down vertical forces which cause the planes of any cross section to buckle when strained. The elliptical rod in Figure 55 has maximum shearing stresses at points B and B', the minor axis. If the plane section had remained plane so that the shearing stresses were proportional to the distance from the axis, the stresses would be minimum at the minor axis. Similarly, for a rectangular rod the maximum shearing stress is at the points nearest the axis and a zero stress at the corners. Figure 56 shows the contours for three shapes of rods. The surfaces C and c are convex and concave respectively, representing the direction of warping. The arrow shows the direction of twist.

Another factor which affects the torsional stiffness and strength of a bar of non-circular cross section is the polar moment of inertia. This property is often referred to as St. Venant's paradox. It states that if two rods of the same elastic material have non-circular cross sections, the rod with the smaller polar moment of inertia has the greater torsional stiffness and strength. provided the areas are everywhere convex.

Since rods of non-circular cross section present so many complications and no real advantages, the choice of circular rods is simple. The non-circular rods could be used, but non-uniform stresses and warping as compared to pure shear of a circular rod would only introduce problems. For general information the properties of four non-circular rods are given in Table 5. These rods do have applications where design limitations restrict the use of circular rods.

Next a circular rod which represents pure shear when in torsion will be considered. A thin-walled tube is one of the simplest examples of complex stress distribution; therefore, its use for torsion rod investigations will be ideal. Also, a solid shaft can be considered as a set of concentric thin-walled tubes; therefore, its study will just be an extension of the thin-wall case.

To begin the investigation of a thin-walled circular tube consider Figure 57. The force exerted around the circumference of the tube for one cross section is denoted by P_s. The shearing stress for the cross-sectional area A is $\tau = P_s/A$; likewise, for an element of the cross section $\tau = P_s/A$. The torque about the center of the shaft is ΔP_s xr or $T = \tau r \Delta A$, where r is the radius of the tube. (It is assumed that the thin-walled means a tube whose walls are small compared with the tube radius.) The total torque is

$$T = \Sigma r \; P_s = \Sigma \tau r \; A = \tau r A \qquad (42)$$

FIGURE 55

Torsion in an Elliptical Cross Section

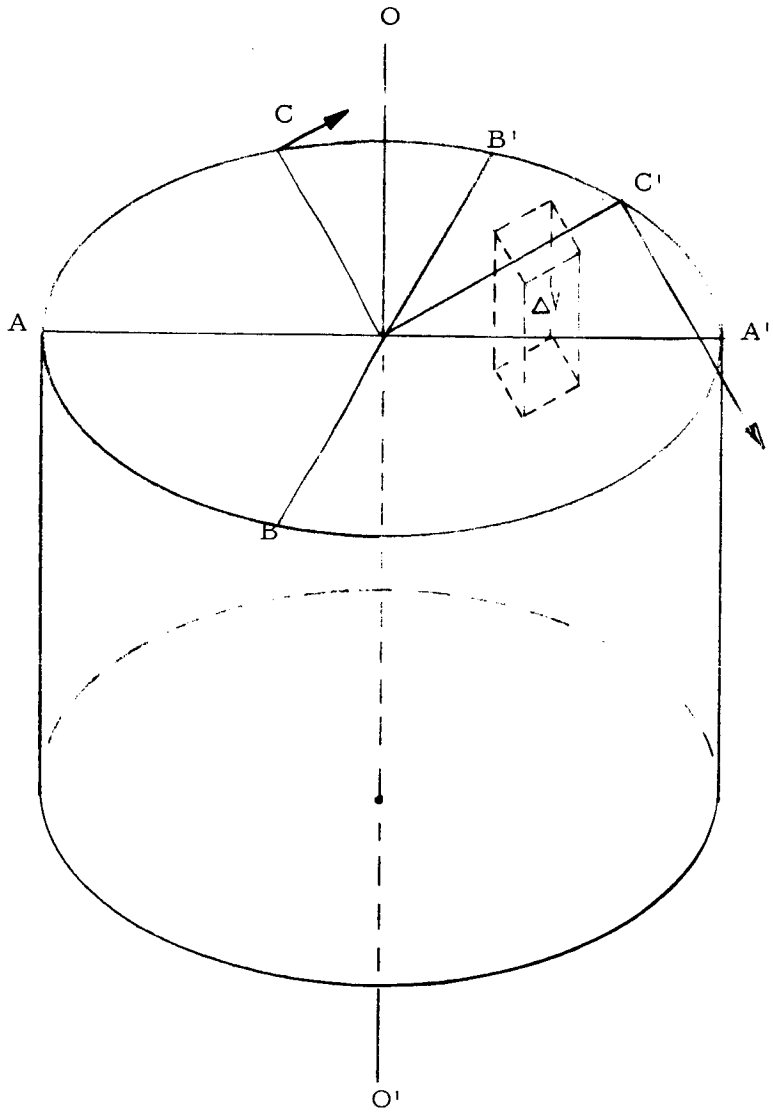

TABLE 5

Properties of Non-Circular Torsion Rods

Cross Section	Dimensions	Polar Moment of Inertia	Torsional Rigidity	Relationship Between Angle of Twist per Unit Length & the Twisting Moment	Relationship Between Shearing Stress & Twisting Moment
Elliptical	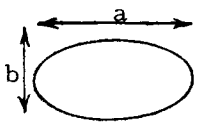	$J = \frac{\pi a^3 b^3}{16(a^2+b^2)}$	$K = \frac{G\pi a^3 b^3}{16L(a^2+b^2)}$	$\phi = \frac{16T(a^2+b^2)}{\pi a^3 b^3 G}$	$\tau = \frac{16T}{\pi a^2 b}$
Prismatic (Equilateral Triangle Section)	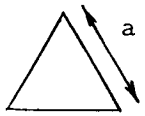	$J = \frac{\sqrt{3}}{80} a^4$	$K = \frac{GD^4}{46.2L}$	$\phi = \frac{T}{GJ}$	$\tau = \frac{20T}{a^3}$
Rectangle	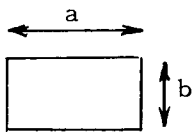	$J = K_1\left(\frac{a^3b^3}{a^2+b^2}\right)$ $K = \frac{1}{3.645-0.06a/b}$	$K = \frac{K_1 a^3 b^3 G}{(a^2+b^2)L}$	$\phi = \frac{T}{GK_1(a^3b^3)/(a^2+b^2)}$	$\tau = \frac{T}{K_2 ab^2}$ $K_2 = \frac{1}{3(1.0+0.6a/b)}$
Square	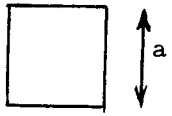	$J = 0.1406a^4$	$K = \frac{0.1406a^4G}{L}$	$\phi = \frac{T}{0.1406a^2G}$	$\tau = \frac{T}{0.2082a^3}$

FIGURE 56

Torsion in Three Types of Rods

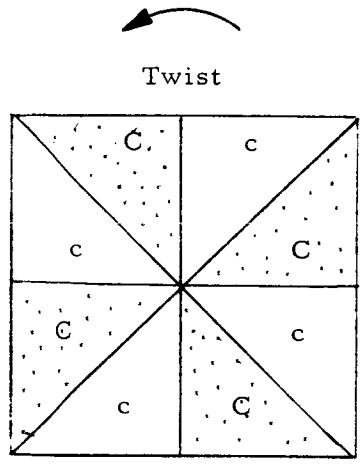

Square

C is convex warping and c is concave.

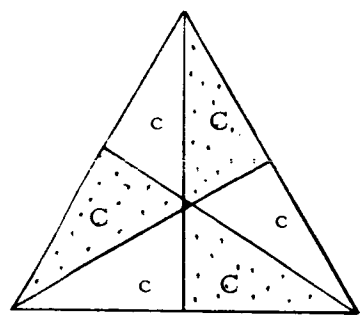

Prismatic

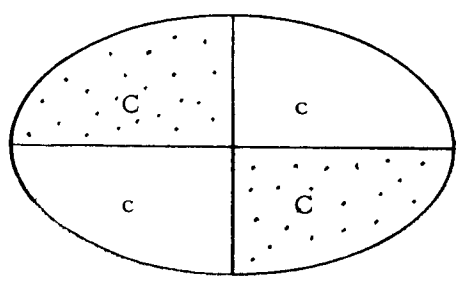

Elliptical

FIGURE 57

Torsion In a Thin-Walled Circular Tube

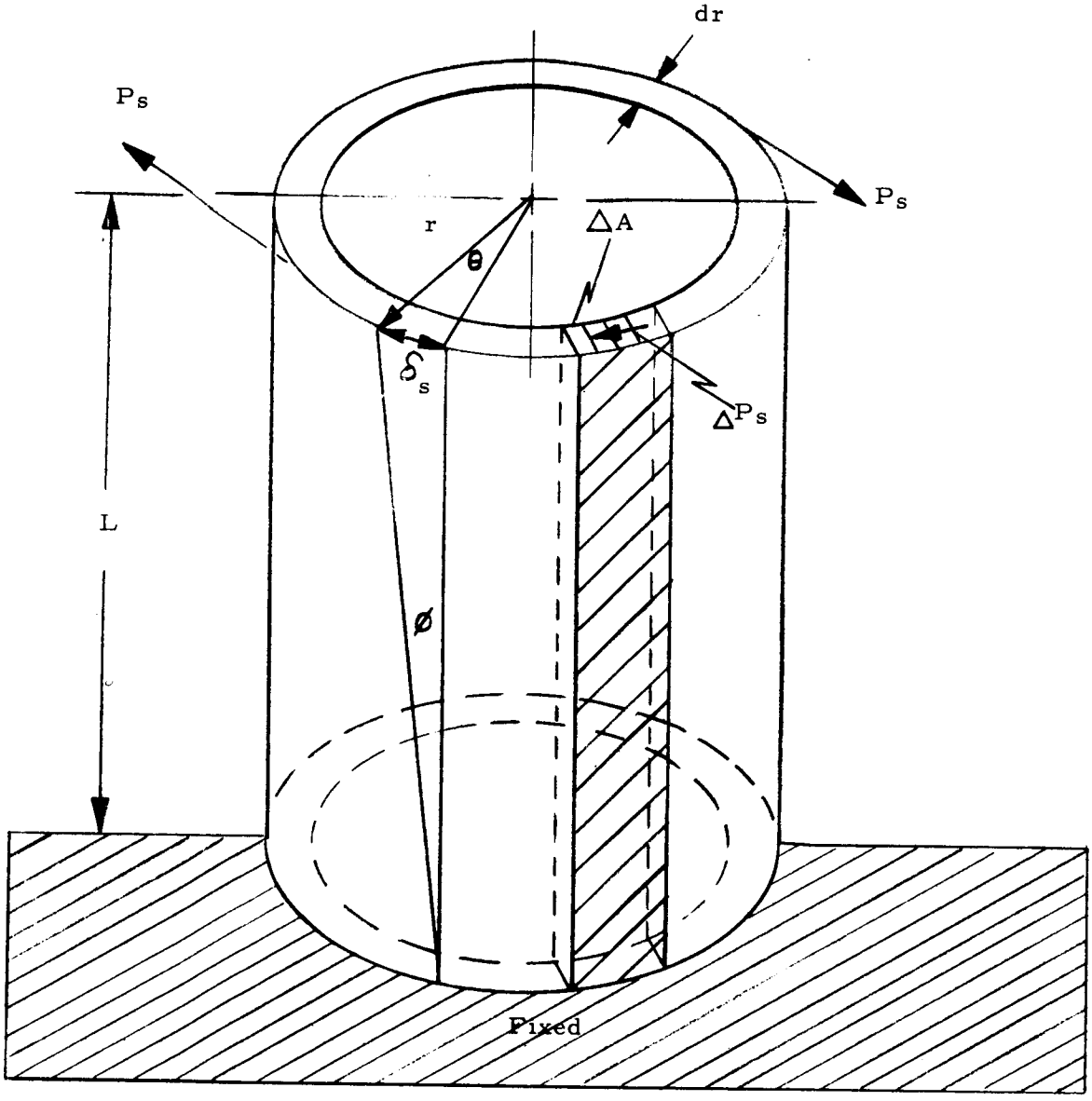

since all A's are at a constant radius. Likewise,

$$\tau = T/Ar \tag{43}$$

and

$$\tau = T/2\pi r^2 dr \tag{44}$$

where dr is the wall thickness.

The distortion produced by the shearing stress is also represented in Figure 57. The shearing displacement δ_s is the displacement of the top of the shaft with respect to the fixed bottom. The shearing strain, ν , is the unit shearing displacement, δ_s, divided by the rod length, given in Equation 45.

$$\nu = \delta_s/L. \tag{45}$$

Also, from Figure 57

$$\gamma = \sin\phi = \delta_s/L \tag{46}$$

and

$$\sin\theta = \delta_s/r. \tag{47}$$

From Equations 46 and 47

$$r\sin\theta = L\sin\phi \tag{48}$$

but for small angles Equation 48 becomes

$$r\theta = L\phi. \tag{49}$$

The shearing displacement of one end of this unit length relative to its fixed end is $\delta_s = r\theta$, Equation 47, where θ is the angle of the twist per unit length,

$$\theta = \phi/L. \tag{50}$$

From Equation 45

$$\nu = \delta_s/L = r\theta/L \tag{51}$$

for a unit length.

If the behavior of the material is studied by applying various torques to the rod, provided they do not exceed the elastic limit, a linear relation will result that follows Hooke's law,

$$G = \tau/\nu. \tag{52}$$

G is the modulus of rigidity or sometimes called the modulus of elasticity in shear. The equation for G varies with rod shape, but it can easily be calculated from the equations already given. Since materials that follow Hooke's law in tension usually do in shear also, an expression that relates E and G can be derived. This expression is

$$G = E/2(1 + u) \tag{53}$$

where u is Poisson's ratio. The derivation of Equation 53 can be obtained in most mechanics books.

In considering a solid shaft, there are no changes in dimensions radially, tangentially or axially; therefore, there will be no normal stresses in these directions. Also, the material at the outer surface will be stressed to the limit assigned as the working stress and inner material will be stressed in a decreasing manner from the outside as shown in Figure 58. Figure 59 shows the action of pure shear in a solid rod. The only significant difference between a hollow and solid shaft is the weight involved. A hollow shaft can give a much higher value of strength per pound than a solid shaft.

In further investigating the properties of a circular solid rod Equation 44 for the torque of a hollow rod will be considered.

$$T = \tau 2\pi r^2 dr \tag{54}$$

In Equation 54 replace τ with $G\nu$ from Equation 52 and substitute $r\theta/L$ for ν from Equation 49. Now Equation 54 becomes

$$T = (Gr\theta/L)2\pi r^2 dr = 2\pi G\theta r^3 dr/L. \tag{55}$$

If Equation 55 is integrated from 0 to R for a solid shaft, it becomes

$$T = \frac{\pi \theta G R^4}{2L} \tag{56}$$

FIGURE 58

Magnitude of Stresses in a Circular Rod

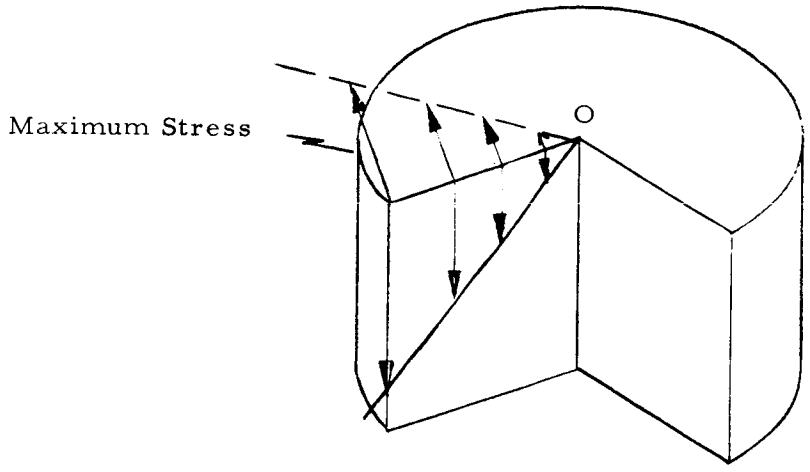

FIGURE 59

Elemental Segment of a Circular Rod Describing Pure Shear

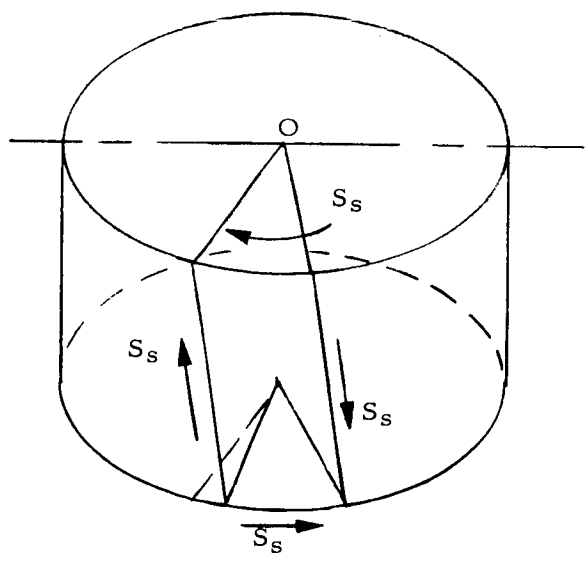

By definition

$$J = \pi R^4/2 = \pi D^4/32 \tag{57}$$

where J is called the polar moment of inertia or the torsional moment of inertia. Now Equation 56 becomes

$$T = \frac{\theta GJ}{L}, \tag{58}$$

or

$$T = K\theta \tag{59}$$

where

$$K = \frac{GJ}{L}, \tag{60}$$

K is defined as the ratio of the applied torque to the angular displacement produced. It is called the moment of torsion of the rod, spring rate, rod constant and others. The moment of torsion is a constant, for a perfectly linear elastic material, depending only on the specimen's shape, whereas the rigidity modulus depends only on the material used.

The spring rate for a hollow shaft is

$$K = \frac{\pi (D^4 - d^4)G}{32L} \tag{61}$$

where D is the outside diameter and d the inside diameter. This is similar to the solid shaft since it is just the difference between K for a solid rod and that of a void. Table 6 lists the other properties of hollow and solid circular rods.

Another factor which must be considered is the method of fastening the rod to the table. Previously, circular end plates were precisely mounted at a 90-degree angle with respect to the rod and silver soldered. The silver solder has enough strength so that there is no slipage between the end plate and the rod. The end plates so that the rod can be aligned vertically to eliminate any side loads. With this arrangement the rod is in pure torsion between the two end plates.

The use of silver solder has been very satisfactory for steel rods and end plates, but it cannot be used for glass and ceramics. Hopefully, one of the new high strength epoxies can be used in the same manner as the silver solder; therefore, a search for a suitable epoxy has begun.

TABLE 6

Properties of Circular Hollow and Solid Rods

Cross Section	Dimensions	Polar Moment of Inertia	Torsional Rigidity	Relationship Between Angle of Twist per Unit Length & the Twisting Moment	Relationship Between Shearing Stress & Twisting Moment
Hollow Circular Section	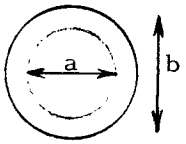	$J = \frac{\pi(a^4-b^4)}{32}$	$K = \frac{\pi(a^4-b^4)\,G}{32L}$	$\phi = \frac{T}{JG}$	$\tau = \frac{16T}{\pi(a^4-b^4)/a}$
Solid Circular Section	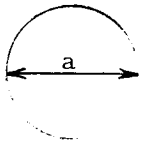	$J = \frac{\pi a^4}{32}$	$K = \frac{GJ}{L}$	$\phi = \frac{T}{JG}$	$\tau = \frac{16T}{\pi a^3}$

2.1.3.1.4 Material Considerations

The most important consideration of selecting a torsion rod is the material from which it will be made. In Par. 2.1.3.1.1 the theoretical properties of the ideal material were thoroughly outlined. Now the material that most closely resembles this theoretical model must be selected. Since the torsional rigidity is of prime importance, the mechanical properties of the material will be the most important characteristics. Thermal properties could present some problem, but this is not anticipated.

Fundamentally, the properties of a material depend on the nature of the particular material alone. To understand the properties of the material in detail, a thorough understanding of atomic structure must be realized. Since it is not an objective of this report to study atomic structure, the reader is referred to texts on the subject. References 3 and 4 in the Bibliography are good sources for this information. With an understanding of atomic structure, the initial material selection is made easier. Even when properties can be derived theoretically, experiments must provide the necessary data for actual use.

The materials to be considered for use as torsion rods will be broken down into two classes, metals and ceramics. Other materials could be considered, but past experience has proven that these two classes more nearly exhibit the necessary properties.

The study of metals could be endless. Metallurgical knowledge had its beginning in the stone age and will continue to be explored as long as a civilization exists. In modern times the progress in the field of metallurgy has been tremendous; therefore, a study of all new metals as they are fabricated would be an endless task. In order to limit the investigation of rod materials, only steels will be considered. Since much more research and progress has been made with steels in the area of high strength and linear elastic properties other metals will not be considered.

Alloy steel will be considered primarily because it has superior strength properties to ordinary carbon steel. By definition an alloy steel is one which the maximum specified content of elements exceeds one or more of the following limits or in which a definite range or a definite minimum quantity of any

Manganese	-	1.65%
Silicon	-	0.60%
Copper	-	0.60%

of any of the following elements is specified or required within the limits of the commercial field of alloy steels: aluminum, chromium up to 3.99%,

cobalt, columbium, molybdenum, nickel, titanium, tungsten, vanadium, zirconium, or any other element added to obtain a desired alloying effect. To further improve the properties of alloy steel, special heat treatment is usually necessary. Five forms of heat treatment are available:

(1) Quenching and Tempering
(2) Normalizing
(3) Annealing
(4) Spheroidize-Annealing
(5) Stress-Relieving

depending on what properties are needed from the steel.

In general the mechanical properties of an alloy steel will depend on the alloying elements and the heat treatment method. For this reason many alloy steels are available; therefore, a list of alloy steels and their mechanical properties available from all steel companies will be obtained. After these lists are obtained, a selection of the best linear material will be made, and samples will be tested to determine their suitability as rods for the air bearing table.

The other materials to be considered are those classified as ceramics. This traditional title primarily refers to clay products, cement and silicate glass, but in recent years new ceramics have gained in importance. One area of new development is that of pure oxide ceramics. These oxides have been developed to a high state of uniformity and exhibit outstanding properties. Some of the more common oxides are alumina (Al_2O_3), beryllia (BeO), forsterite (Mg_2SiO_4), magnesia (MgO), spinel ($MgAl_2O_4$), thoria (ThO_2), and zirconia (ZrO_2). In the area of ceramics, silica glass and ceramic oxides exhibit the best strength properties; therefore, they will be discussed in more detail.

First, silicon glass will be discussed. The terminology "Fused Quartz" and "Fused Silica" will be used interchangeably since from a strict terminology standpoint, they are the same. By common practice "Fused Quartz" has come to be associated with the transparent variety while "Fused Silica" is associated with the translucent type. Fused quartz or fused silica is made by heating high purity, naturally occurring quartz crystals to a sufficiently high temperature to produce an amporphous condition. The clear varieties can have a purity of 99.97 to 99.98% SiO_2 with alumina Al_2O_3 as the major impurity. Many other types of glasses are available by including different oxides.

Glass in general, like all ceramics, is a brittle material, thus, it does not plastically deform before failure, and it fractures from tensile stresses. The stress-strain curve for glass is a straight line up to the breaking point. For ordinary purposes it can be assummed that glass is perfectly elastic up to the point of fracture, and it has the lowest known internal friction of any material. Glass also has a very low coefficient of thermal expansion which will help eleviate any temperature problem with the rod. In general, the mechanical properties of fused quartz are:

Tensile Strength	-	7,000 psi.
Modulus of Elasticity	-	10×10^6 psi.
Modulus of Rigidity	-	4.5×10^6 psi.
Poisson's Ratio	-	0.18 - 0.22

Dr. J. S. McCartney of the Physical Properties Research Department of Corning Glass has highly recommended fused quartz as the best material possible for our use. For best results the fused quartz must be pure with a precision finish. Other manufacturers of fused quartz have been contacted to obtain information on their highest quality fused quartz. The following companies also offer precision fused quartz: Thermal American Fused Quartz, General Electric and Ruska Instrument Company.

The last materials to be considered are those of ceramic oxides. Since these materials are in the same class as fused quartz, they exhibit similar properties. These oxides like fused quartz are brittle, have a linear stress-strain relationship and a low thermal coefficient of expansion. The actual physical properties vary for different oxides, and Table 7 shows the strength properties of greatest interest for the most common oxides. From Table 7 it can be seen that the purer the material the greater the strength and naturally the cost will be greater. Likewise, as in the case of alloy steels and fused quartz, manufacturers will have to be contacted to obtain the latest data on ceramic properties; then test specimens will be ordered and tested. Several companies contacted to date that offer high grade ceramics are: Coors Porcelain Co., Saxonburg Ceramics Inc., McDaniel Refractory Porcelain Co., Diamonite, Carborundum Co. and Corning Glass Works.

2.1.3.1.5 Conclusions

The material investigation project has been qualitative in nature. The material to be used and rod design have been derived from previous works of others. Since explicit data is not availalable on torsional properties of all materials, a test program must be performed by the Mass Metrology Laboratory to obtain the best material. The design of the rods will be a solid circular shaft. A circular rod is best for torsional shear forces and is relatively easy to fabricate and grind. A hollow shaft would be just as suitable except for the higher cost. The materials to be tested are alloy steels, ceramics, and fused quartz. The specific alloys and ceramics will depend on data available from manufacturers and their prices. To obtain the optimum properties, a high purity and smooth finish quartz rod must be used. Again, cost will be a factor in selecting the fused quartz to be used.

The next step in obtaining the proper material is that of design and fibrication of a torsion rod testing machine. The air bearing table along with standard weights and a precision displacement measuring device will be used as basic instruments for testing the linearity of various materials. After the

TABLE 7

Mechanical Properties of Some Ceramics

	Modulus of Elasticity	Modulus of Rigidity	Possion's Ratio
Alumina (Al_2O_3)			
85 % Pure	33×10^6 psi	13×10^6 psi	0.22
94 %	41	17	0.21
96 %	44	18	0.21
98 %	49	20	0.22
99 %	50	21	0.21
99 % Cast	46	19	0.21
99.5 %	52	22	0.21
99.9 % (TM Coram)	57.1	--	0.235
Beryllia (BeO)			
96 % Pure	44	17	0.30
98 %	45	17	0.30
99.5 %	51	20	0.26
Steatite	14	--	--
Mullite	10	--	--
Silicon Carbide	56	--	--
Magnesia (MgO)	30.5	--	--

LIST OF SYMBOLS

SYMBOL	DEFINITION
E	Tensile Modulus of Elasticity or Young's Modulus; Units - lbs/in^2
σ	Normal Stress; Units - lbs/in^2
ϵ	Strain; Unitless
ω	Internal Friction
v	Volume; Units - in^3
τ	Shearing Stress
P_s	Force on Rod Circumference; Units - lbs
A	Cross Sectional Area; Units - in^2
r	Rod Radius; Units - inches
dr	Tube Thickness
T	Torque; Units - in-lbs
δ_s	Shearing Displacement
γ	Shearing Strain
ϕ	Longitudinal Angle of Twist of a Rod
θ	Axial Angle of Twist of a Rod
L	Rod Length
G	Shearing Modulus of Elasticity or Modulus of Rigidity; Units - lbs/in^2
u	Poisson's Ratio; Unitless
J	Polar Moment of Inertia or Torsional Moment of Inertia; Units - in^4
K	Rod Constant or Spring Constant; Units - in-lbs/radian
D	Outside Rod Diameter
d	Inside Rod Diameter

REFERENCES

1. Burke, J. E., Progress in Ceramic Science, Pergamon Press, New York, 1961.

2. Chironis, Nicholas P., Editor, Spring Design and Application, McGraw-Hill Book Co., Inc., New York, 1961.

3. Keyser, Carl A., Basic Engineering Metallurgy, Prentice-Hall Inc., Englewood Cliffs, New Jersey, 1959.

4. Kingery, W. D., Introduction to Ceramics, John Wiley & Sons, New York, 1960.

5. Landau, L. D., and Lifshitz, E. M., Theory of Elasticity, Addison-Wesley Publishing Co., Inc., Reading, Massachusetts, 1959.

6. McMillan, P. W., Glass-Ceramics, Academic Press, New York, 1964.

7. Morey, George W., The Properties of Glass, 2nd Ed., Reinhold Publishing Corp., New York, 1954.

8. Phillips, C. J., Glass, the Miracle Worker, 2nd Ed., Pitman Publishing Corp., New York, 1948.

9. Quick Facts about Alloy Steel, 8th Ed., Bethlehem Steel, Bethlehem, Pennsylvania, 1964.

10. Richards, Cedric W., Engineering Material Science, Wadsworth Publishing Co., Inc., Belmont, California, 1961.

11. Seely, Fred B., and Smith, James O., Advanced Mechanics of Materials, 2nd Ed., John Wiley & Sons, Inc., New York, 1952.

12. Sisco, Frank T., Editor, Engineering Metallurgy, Pitman Publishing Corp., New York, 1957.

13. Spotts, M. F., Design of Machine Elements, 3rd. Ed., Prentice-Hall Inc., Englewood Cliffs, New Jersey, 1961.

14. Stevels, J. M., Progress in the Theory of the Physical Properties of Glass, Elsevier Publishing Co., Inc., New York, 1948.

15. Timoshenko, S., and MacCullough, G. H., Elements of Strength of Materials, McGraw-Hill Book Co., Inc., New York, 1949.

16. Zener, Clarence, Elasticity and Anelasticity of Metals, University of Chicago Press, Chicago, Illinois, 1948.

17. Zwikker, C., Physical Properties of Solid Materials, Pergamon Press, New York, 1954.

materials to be tested are obtained, they will be fabricated into usable torsion rods and tested. Finally, a report of the torsion rod tests will be prepared from which the best torsion rod material will be selected.

2.1.3.2 Design Torsion Rod Tester

Several designs based on the classical method of measuring the modulus of rigidity were considered. Each design contained gas lubricated bearings, calibrated weights and an optical angular measuring device. Since all the designs that were considered produced approximately the same degree of accuracy, the most non-expensive system was selected. This system consisted of the 24 inch air bearing table, a small pulley air bearing and the Davidson Auto-Collimator. All this equipment was available; therefore, only special collets, brackets and weight pans had to be fabricated. The torsion rods were ordered in the correct diameter; therefore, no grinding was necessary. Only the Carpenter RDS steel had to be heat treated to the proper hardness. The other rods were used as were obtained. The end plates were orginally connected to the torsion rods with Armstrong epoxy. This arrangement worked for several rods, but in general the alignment between the end plates and torsion rods was not accurate enough to keep the ceramic rods form breaking. This epoxy method was replaced with special collets with brass bushing inserts. This design proved to be suitable for the static as well as dynamic tests. The operation of this system is discussed in Paragraph 2.1.3.4.

2.1.3.3 Fabricate Torsion Rod Tester

Since the main components of the system were already available, only a few parts had to be fabricated. The parts were: two special collets, brackets and weight pans. All parts were fabricated at Spaco. The system was assembled after all parts were available and tests were performed as discussed in Paragraph 2.1.3.4, which follows.

2.1.3.4 Torsion Rod Test

2.1.3.4.1 Introduction

The Torsion Rod Project of the Moment of the Moment of Inertia Program was designed to produce sufficient information about rod materials so that the best material could be selected for use as torsion rods. The project was divided into two main areas. First a literature search was conducted to find information on various materials and designs for torsion rods. The results of this search are covered in Section 2.1.3.1. This report gives a theoretical analysis of the rod design and shows that the most ideal rod must have a very linear stress-strain relationship, low mechanical hysteresis and small energy losses. Section 2.1.3.1 also discusses the various materials which were considered for use as torsion rods. The four materials which were selected as possibilities for torsion rods because of their physical characteristics as well as their availability and cost were:

1. Fused Quartz (Glass)
2. Alumina (99% pure)
3. Mild Steel (B 1113)
4. Carpenter RDS Steel

The second portion of this project which is reported herein is the testing of the torsion rods and the results that were obtained. Two separate types of experiments were designed for testing the torsion rods in order to obtain better results. These tests are designated static and dynamic because of the method of loading the torsion rods. For the static experiments, a special system was designed and fabricated as described in Sections 2.1.3.2 and 2.1.3.3 respectively. The dynamic experiments used the basic air bearing table system with a few minor modifications. The report herein discusses these experiments and their results. Also a torsion rod calibration procedure is discussed.

2.1.3.4.2 Static Experiments

The static torsion rod tests were based on the classical method of testing. That is, a known torque was applied to the rod and the angular displacement was recorded. The main difference between these tests and the classical ones is that the equipment was much more sophisticated than the classical physics laboratory set-up. The test procedure for these tests are shown in Appendix A4. From Figure 60 it can be seen that the three main pieces of equipment are the 24 inch air bearing table, a small pulley bearing which supports the applied load, and an auto-collimator for measuring the angular displacements. The operation of the 24 inch air bearing table needs no explanation because it has been discussed in other reports in much detail. The pulley air bearing is used to redirect the horizontal force applied for torquing the torsion rod. The air bearing has very little friction; therefore, the losses attributed to the bearing can be neglected. Two weight pans are used for applying the loads because a counter weight is needed for obtaining a true zero load.

The Davidson Auto-Collimator is designed to monitor the reflecting surface of an external mirror either in a horizontal or a vertical axis, detect any angular variations with respect of the optical axis, and convert the angular information into three separate readouts. It has an accuracy of ± 0.1 seconds of arc for 10 seconds or less, and ± 1 second of arc for angles approximately 100 seconds. For more information on its principles of operations and instructions for operation, the reader is referred to the Operation and Instruction Manual.

The problem of mounting the ceramic torsion rod to steel brackets was first solved by using epoxy to attach the steel end plates to the ceramic rods. The steel rods could be easily attached by using silver solder.

FIGURE 60

STATIC TORSION ROD TEST SYSTEM

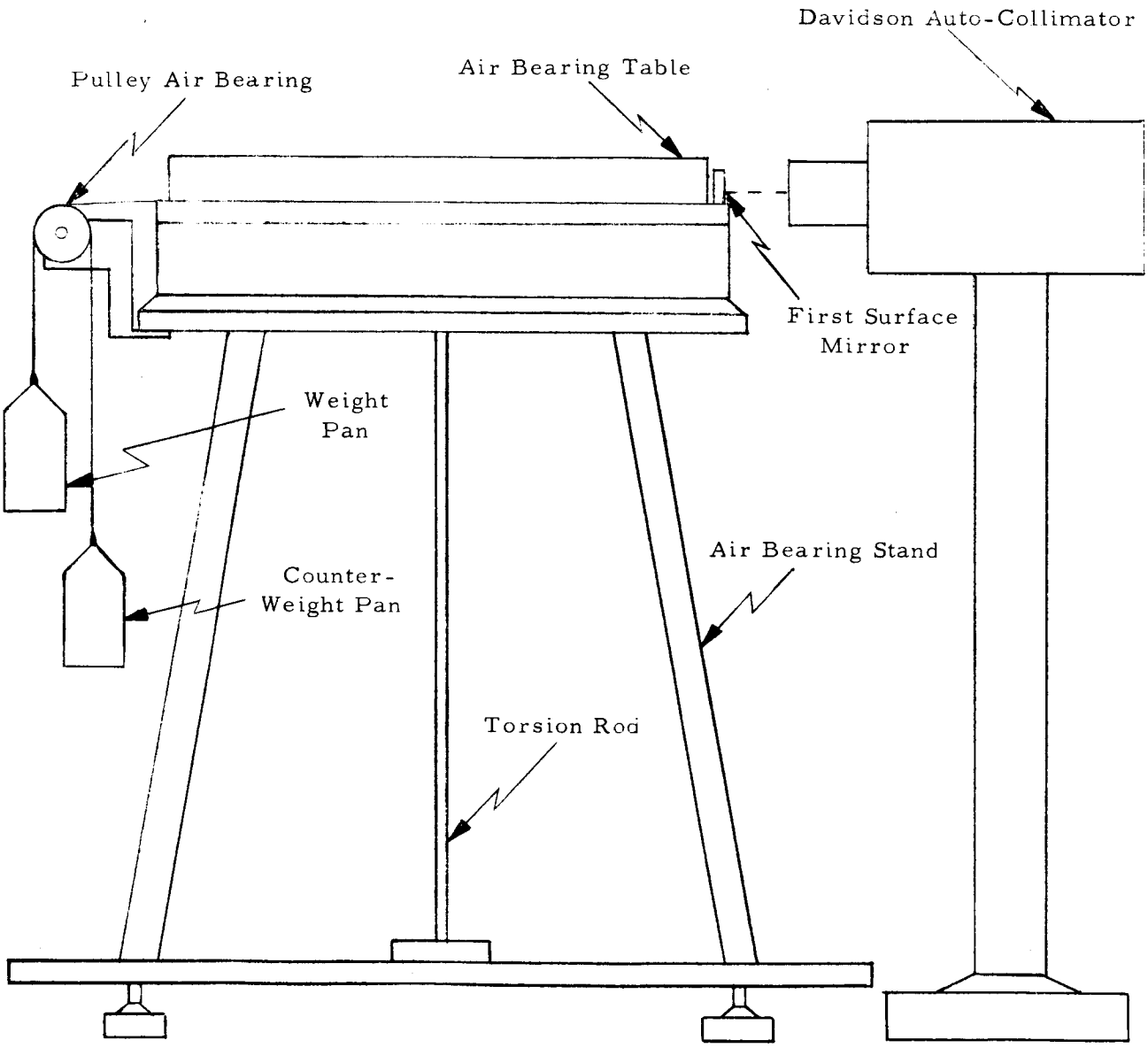

Several tests were performed using this type bracket arrangement and these tests will be discussed in the dynamic section. However, problems were encountered with the epoxy method because a perfect alignment of the rods and end plate could not be obtained. This error caused the ceramic rods to break when they were mounted in the table. Therefore, two special collets with brass bushing inserts were designed and fabricated to hold the ceramic rods. These collets were sufficient for the test program, but a new design would be necessary if a permanent mount in the air bearing table is required. The epoxy method may work if perfect alignment could be obtained; however, this is very expensive.

The static tests were performed by mounting the desired torsion rod in the special collet in the air bearing table, aligning the optical equipment and obtaining the displacements for a given load. The test results for the four rods are given in Tables 8 and 9 and in plotted form in Figures 61 through 64. The conclusions drawn from these tests are; that all four rods have linear stress-strain characteristics for the range of displacements covered and for the capability of the experimental system. At low amplitudes, the points are scattered, but this is caused by the stray vibrations which the sensitive system can detect. The static test was not conclusive in determining whether one rod was better than another.

2.1.3.4.3 Dynamic Experiments

Since there was no known method of dynamically determining the linearity of the torsion rods, a method of comparison was used to evaluate their dynamic characteristics. The four torsions rods were subjected to the same conditions and a comparison of the number of cycles which each oscillated was made. Since the number of cycles is directly related to the linearity of the stress-strain curve and the mechanical hysteresis. First a rough preliminary test was performed to test the epoxy end plates and to determine if there was a difference in the characteristics of the fused silica rod and the mild steel rod. Figure 65 shows the results of the mild steel rod, number 120. In the chart below the curve the first line shows the displacement range of the curve where the vertical line represents the beginning of that displacement shown. The second horizontal line shows the average period for that displacement range and the third and fourth lines show the standard deviation of the period and the total number of cycles respectively for the same displacement range. The last three rows were only completed for a displacement of .0009 radians and below because the decay rate of the larger amplitudes would make the data meaningless. Figure 66 shows the same type data for the fused silica rod, numbered 6B.

In comparing the results exhibited in Figures 65 and 66, it is first noted that the decay rate is greater for the fused silica rod than the steel rod down to amplitudes of approximately .0009 radians. This was probably attributed to the fact that the epoxy holding the end plates was not completely hardened or that the epoxy was not strong enough for the larger displacements. This

F. L. MOSELEY COMPANY

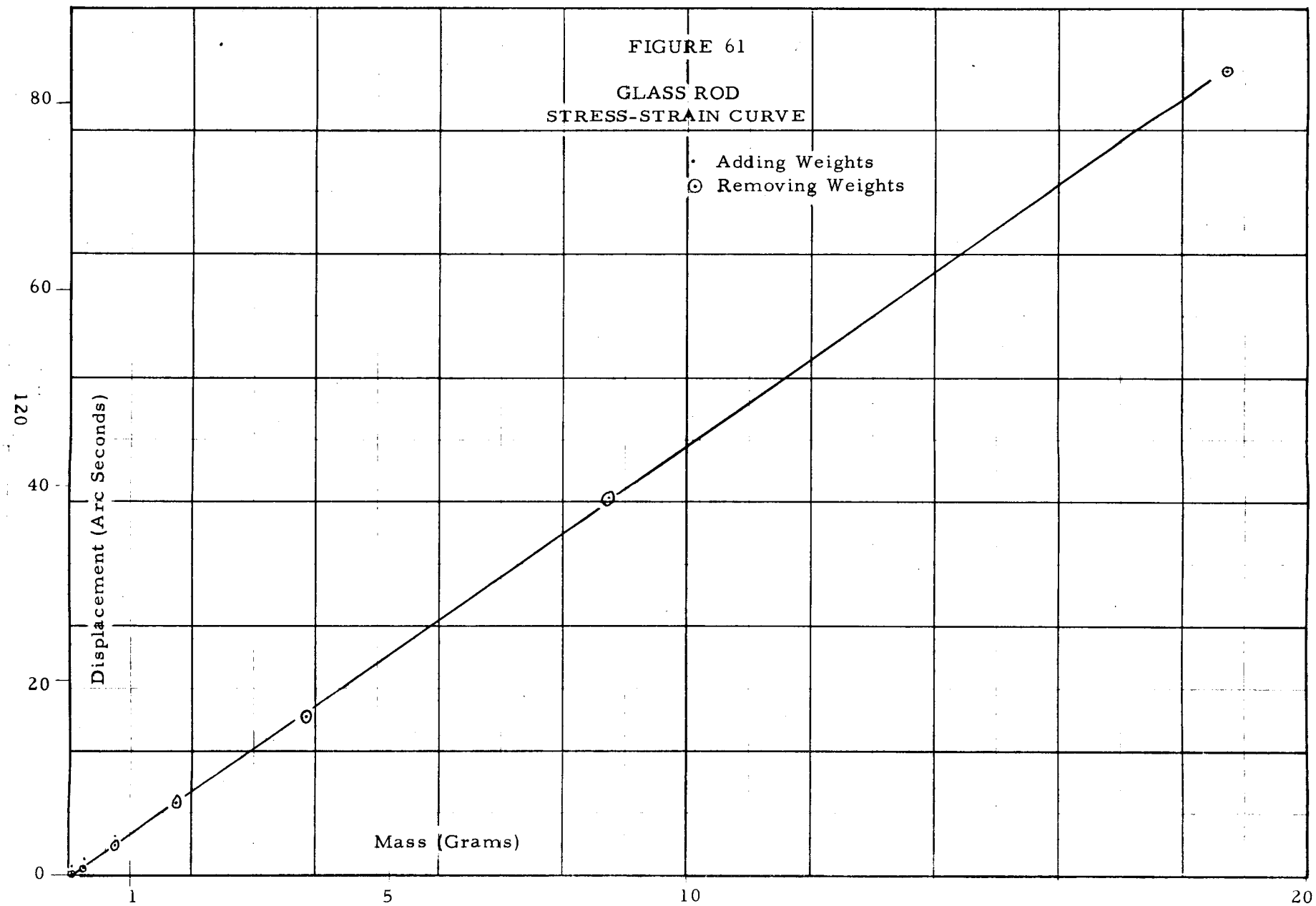

FIGURE 61

GLASS ROD
STRESS-STRAIN CURVE

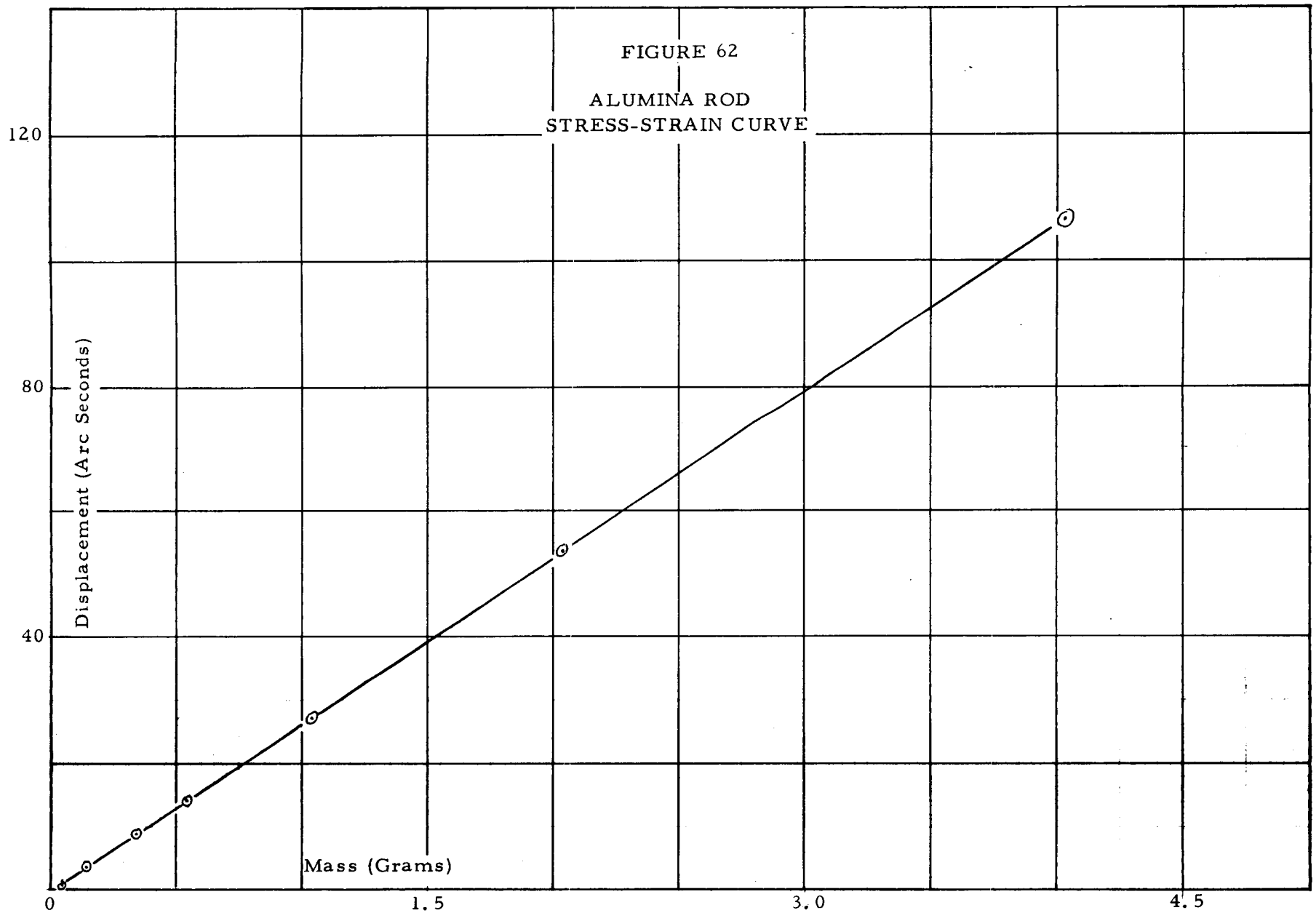

FIGURE 62

ALUMINA ROD
STRESS-STRAIN CURVE

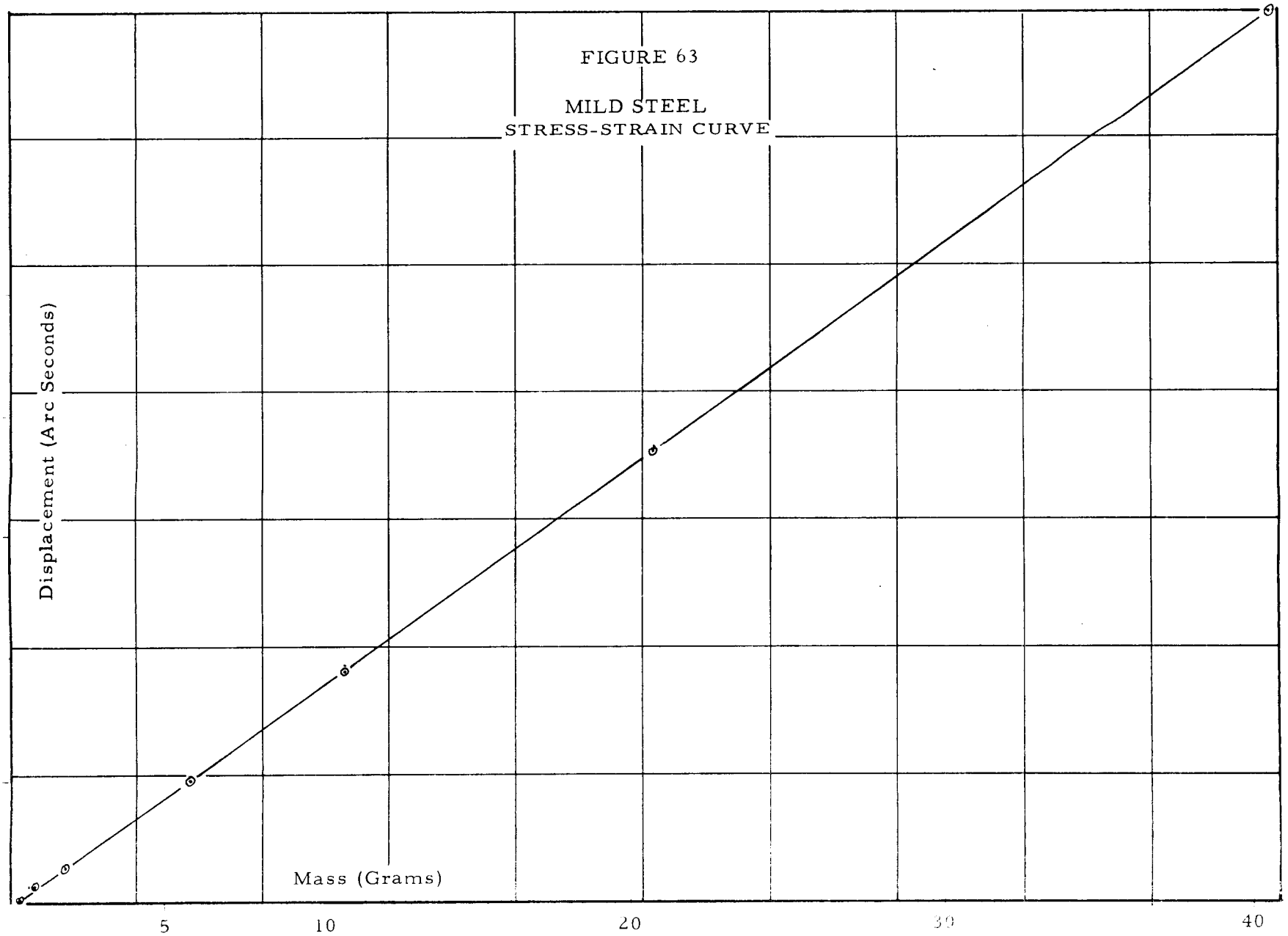

FIGURE 63

MILD STEEL
STRESS-STRAIN CURVE

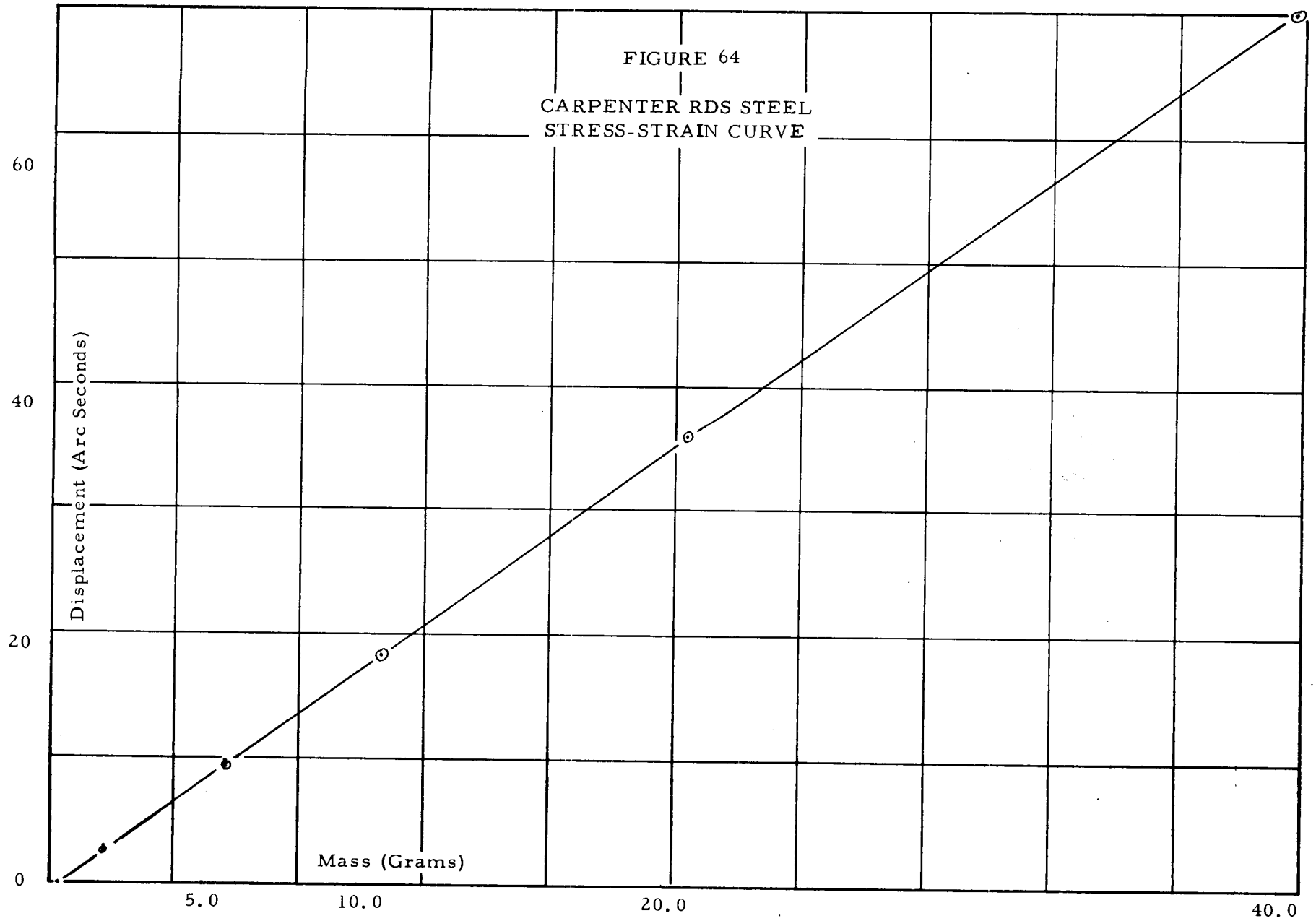

FIGURE 64

CARPENTER RDS STEEL
STRESS-STRAIN CURVE

TABLE 8

TEST RESULTS

Fused Quartz

Mass (Grams)	Displacement (Arc Seconds) Mass Added	Mass Removed
0.150	0.53	0.73
0.350	1.37	1.47
0.850	3.90	4.07
1.850	8.66	8.70
5.850	27.96	28.20
10.850	101.76	101.73

Alumina

Mass (Grams)	Displacement (Arc Seconds) Mass Added	Mass Removed
0.500	1.43	1.00
1.500	3.83	3.53
3.500	8.97	8.77
5.500	14.17	14.03
10.500	27.30	27.17
20.500	53.50	53.50
40.500	106.43	106.43

TABLE 9

TEST RESULTS

Mild Steel

Mass (Grams)	Displacement (Arc Seconds) Mass Added	Mass Removed
0.300	0.57	0.37
0.800	1.40	1.53
1.800	2.97	2.97
5.800	10.23	10.37
20.800	37.57	37.53
40.800	74.03	74.03

Carpenter RDS Steel

Mass (Grams)	Displacement (Arc Seconds) Mass Added	Mass Removed
0.300	0.37	-0.03
0.800	1.27	0.90
1.800	3.07	2.73
5.800	10.27	9.93
10.800	19.27	19.27
20.800	37.37	37.63
40.800	73.80	73.80

FIGURE 65

PERIOD DECAY CURVE FOR THE AIR BEARING TABLE WITH NO LOAD USING MILD STEEL ROD NO. 120

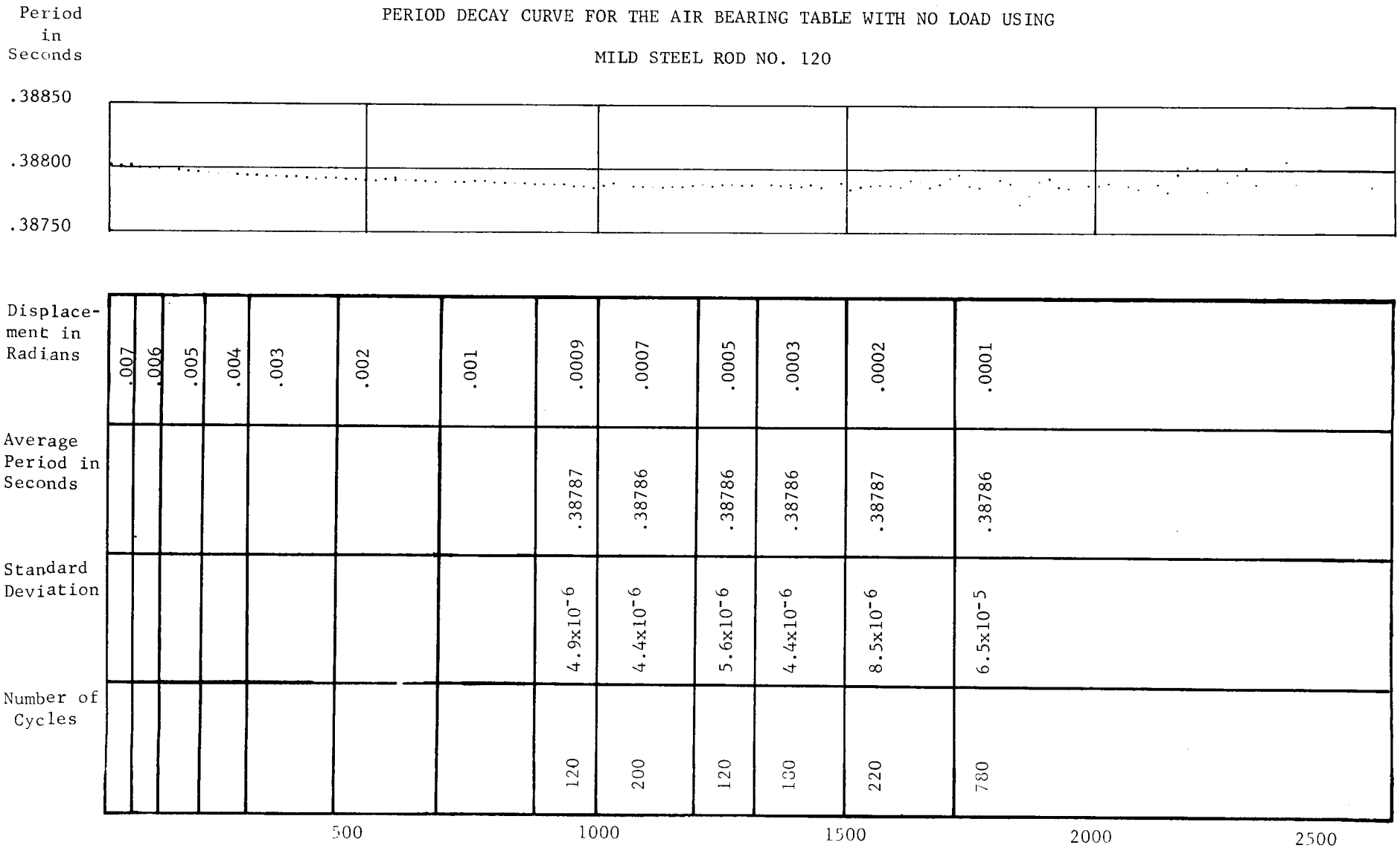

Displacement in Radians	Average Period in Seconds	Standard Deviation	Number of Cycles
.007			
.006			
.005			
.004			
.003			
.002			
.001			
.0009	.38787	4.9×10^{-6}	120
.0007	.38786	4.4×10^{-6}	200
.0005	.38786	5.6×10^{-6}	120
.0003	.38786	4.4×10^{-6}	130
.0002	.38787	8.5×10^{-6}	220
.0001	.38786	6.5×10^{-5}	780

FIGURE 66

PERIOD DECAY CURVE FOR THE AIR BEARING TABLE WITH NO LOAD USING FUSED SILICA ROD NO. 6B

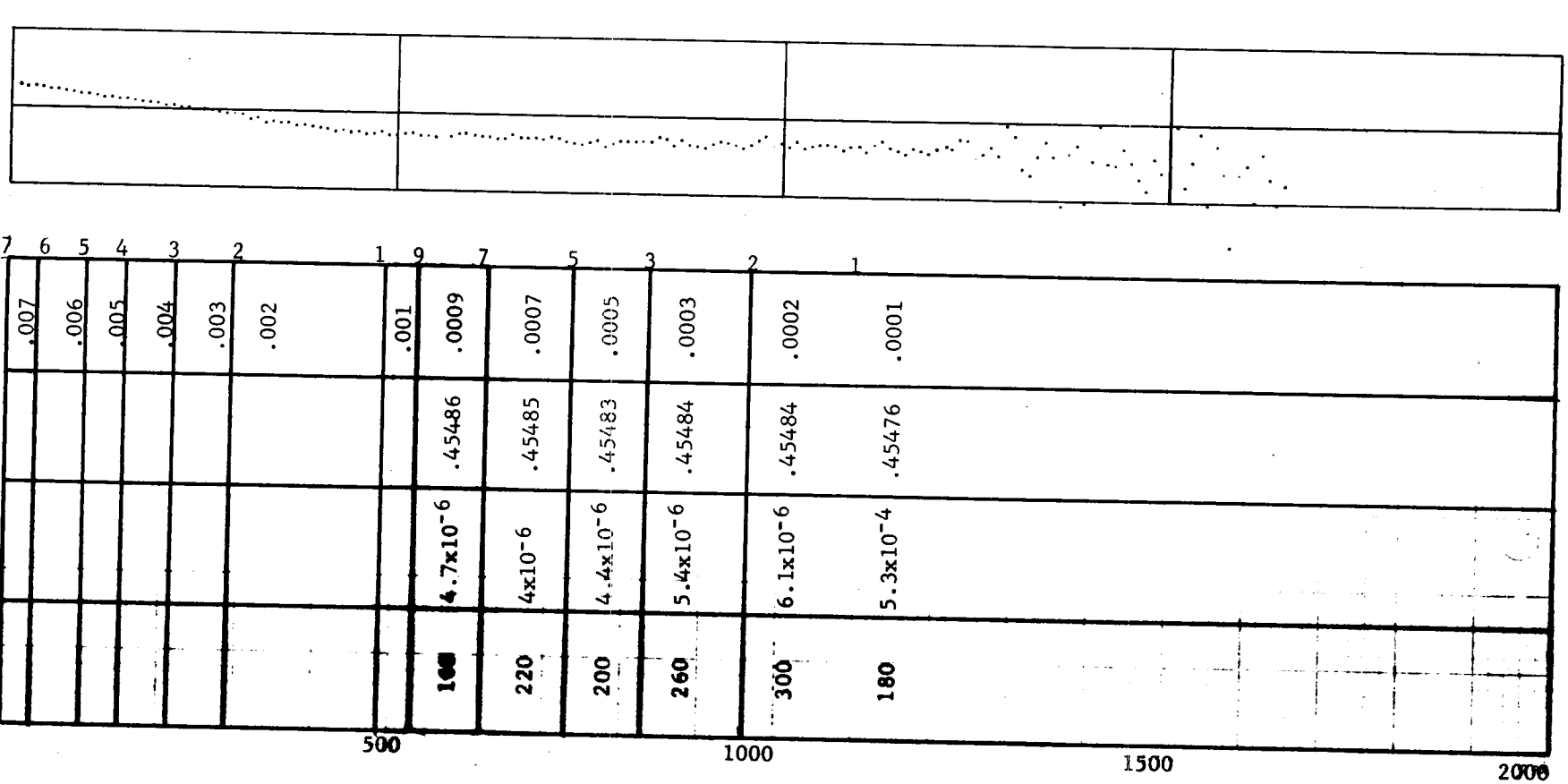

	7	6	5	4	3	2	1	9	7	5	3	2	1	
Displacement in Radians	.007	.006	.005	.004	.003	.002	.001	.0009	.0007	.0005	.0003	.0002	.0001	
Average Period in Seconds								.45486	.45485	.45483	.45484	.45484	.45476	
Standard Deviation								4.7×10^{-6}	4×10^{-6}	4.4×10^{-6}	5.4×10^{-6}	6.1×10^{-6}	5.3×10^{-4}	
Number of Cycles								**160**	**220**	**200**	**260**	**300**	**180**	

characteristic did not appear at lower amplitudes. The periods were not identical because the rods had different spring constants.

The periods for the steel rod were constant from .0007 radians down through .0001 radians. For the glass rod, the consistency from .0007 to .0001 radians was not as good. A maximum deviation of 2×10^{-5} appeared down to .0002 radians and a deviation of 8×10^{-5} appeared at .0001. The standard deviation of both rods was approximately constant at 5×10^{-6} down to .0001 radians. At this point the glass rod showed the largest deviation again. The glass rod changed by a factor of 100 while the steel rod varied only by a factor of 10. The last category was the only place where the glass rod was obviously better. The glass rod oscillated more cycles at each displacement than the steel rod.

The only definite conclusions which could be drawn from this result was that the mechanical hysteresis of the fused silica rod was less than that of the steel rod because it oscillated longer. Also, it appears from both of these tests that the period scatter was caused by external mechanical vibrations at .0001 radians. The reason the fused silica rod had greater scatter than the steel rod was because the larger number of cycles at these low amplitudes. Since the period was essentially constant before it reached this displacement, these adverse effects will not harm the moment of inertia determination of the air bearing table. The next set of tests were more precise in order to determine the exact difference in the rod's mechanical characteristics. The special collet had to be used because of the alignment problem with the fused quartz and alumina rods. This problem had not been encountered on the previous tests. The tests were performed by using the air bearing system in its normal method of measuring moments of inertia. Figure 67 shows the test set-up with the two drag adapters used for adjusting the period of oscillation. These adapters were rigidly mounted to the table top so that a constant aerodynamic drag would be present during all the tests. Weights were added to or removed from the cylindrical drag adapters so that the period of oscillation would be constant for all four rods. The only variable in the tests was that of the stress level in each rod because the modules of rigidity and rod diameter were not equal. However, the stress levels were very close to each other; therefore, they did not produce any adverse effect. The tests were performed by displacing the table top and counting the number of cycles between the maximum displacements of 1000×10^{-6} and 100×10^{-6} radians. The specific test procedure is shown in Appendix A5.

The test results are shown in Tables 10 and 11. Each rod was tested at least eight times and the average number of cycles and average period for each rod is shown in the Tables. From these results it is obvious that the fused quartz (glass) rod has the least mechanical losses of the four.

TABLE 10

TEST RESULTS

Fused Quartz		Alumina	
Average Period	Number of Cycles (between 1000-100 x 10^{-6} rad)	Average Period	Number of Cycles (between 1000-100 x 10^{-6} rad)
0.6136	1176	0.6135	798
0.6136	1226	0.6135	808
0.6136	1282	0.6132	882
0.6136	1236	0.6132	826
0.6136	1252	0.6132	970
0.6136	1182	0.6133	1014
0.6136	1272	0.6133	1008
		0.6133	968
		0.6133	976
		0.6134	
Average - 0.6136	Average - 1233		Average - 908

TABLE 11

TEST RESULTS

Mild Steel		Carpenter RDS Steel	
Average Period	Number of Cycles (between 1000-100 x 10^{-6} rad)	Average Period	Number of Cycles (between 1000-100 x 10^{-6} rad)
0.6137	694	0.6136	470
0.6136	718	0.6135	474
0.6136	702	0.6135	464
0.6135	696	0.6135	474
0.6135	708	0.6135	476
0.6135	676	0.6135	478
0.6135	680	0.6135	470
0.6135	660	0.6135	478
0.6135	666	0.6135	476
Average - 0.6136	Average - 689	Average - 0.6135	Average - 473

FIGURE 67

DYNAMIC TORSION ROD TEST SYSTEM

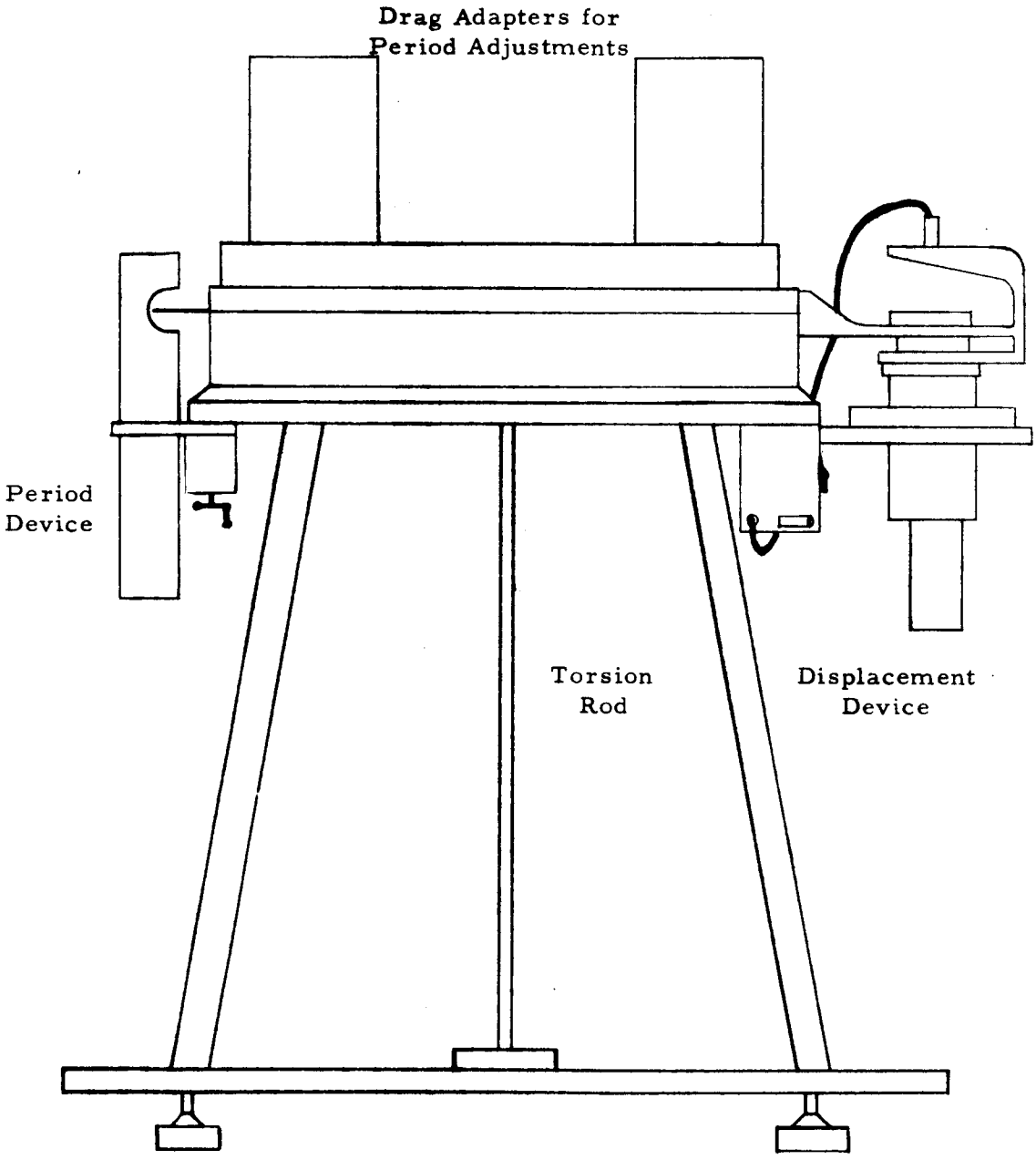

2.1.3.4.4 Torsion Rod Calibration Procedure

A series of tests were conducted to demonstrate a method of calibration torsion rods. This particular test series was for a steel rod; however, it is applicable to any type rod.

Before the tests could be performed a modification had to be made to the dumbbells and the air bearing table to eliminate unwanted dumbbell motions. The previous dumbbell arrangement is shown in Figure 68. The one center bracket for mounting the dumbbell to the air beaiing table, as shown in Figure 68, was not rigid enough to keep the dumbbell from oscillating with respect to the table top. This previous compound oscillating system produced errors in the moment of inertia determination by causing erroneous period measurements. These unwanted oscillations were alleviated by mounting the dumbbell to the air bearing table with two brackets as shown in Figure 69. The design and location of these brackets is such that the oscillations of the dumbbell with respect to the table top is negligible.

The weight and moment of inertia of the dumbbells had to be recalculated because of the modification stated above. The new weight and moment of inertia of each dumbbell is given in Table 12.

The tests were performed in accordance with the test procedure shown in Appendix A6.

The test procedure is self-explanatory except for possibly the period measurement range. The period was measured between .002 and .001 radians as a result of previous experiments and theoretical work. By using the theory of the period decay rate of an oscillating system, the optimum period for de termining the moment of inertia is at the minimum amplitudes. This is true because the damping decreases as the amplitude decreases. The displacement of .002 to .001 radians was used because it was the minimum displacement that could be obtained with the equipment at that time.

Six separate tests were performed to determine the spring constant by using four dumbbells. Two tests were performed to determine the moment of inertia of the table top and bracket combinations.

Table 13 shows the notations used in the calculations. Table 14 shows which brackets and bolts were used with each dumbbell and the calculated moment of inertia of each set of bolts with respect to the axis of rotation. The moment of inertia of the bolts had to be calculated because they could not be determined experimentally.

The rod spring constant is determined by using Equation 62 where the appropriate dumbbell, brackets, and bolts are used. The moment of inertia of the dumbbells and bolts is used as a standard for calculating the rod spring

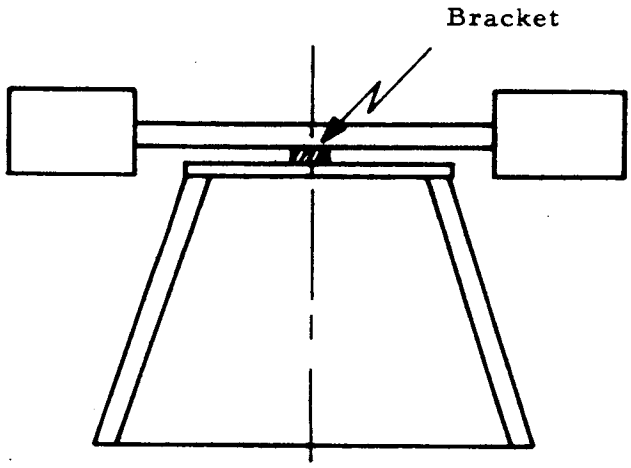

FIGURE 68
OLD DUMBBELL MOUNTING CONFIGURATION

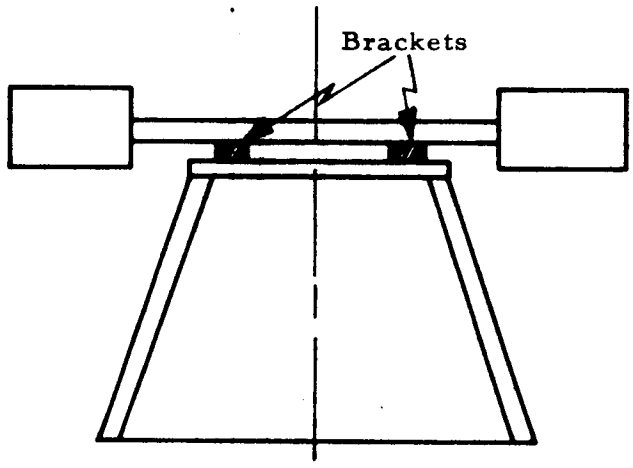

FIGURE 69
NEW DUMMBBELL MOUNTING CONFIGURATION

TABLE 12
MOMENT OF INERTIA DUMBBELL STANDARDS

Dumbbell	A	B	C	D	E
Weight (lbs)	74.963	112.856	182.802	198.731	290.947
Moment of Inertia (in-lb-sec^2)	27.504	60.934	92.516	124.108	188.059

TABLE 13
LIST OF SYMBOLS

BKA	=	Brackets A
BKB	=	Brackets B
BOA	=	Bolts A
BOC	=	Bolts B
T	=	Table Top
DBB	=	Dumbbell B
DBC	=	Dumbbell C
DBD	=	Dumbbell D
DBE	=	Dumbbell E

TABLE 14
BRACKETS AND BOLTS

Dumbbell	Brackets	Bolts	Bolts
A	B	B	.032 in-lb-sec^2
B	A	A	.034 in-lb-sec^2
C	B	C	.037 in-lb-sec^2
D	A	A	.034 in-lb-sec^2
E	A	A	.034 in-lb-sec^2

$$K = \frac{4\pi^2(I_{DB} + I_{BO})}{T^2_{DB + BK + BO + T} - T^2_{BK + T}} \tag{62}$$

constants. Equation 62 is derived from Equations 63 through 65.

$$I_{BK + T} = \frac{KT^2_{BK + T}}{4\pi^2} \tag{63}$$

$$I_{DB + BK + BO + T} = \frac{KT^2_{DB + BK + BO + T}}{4\pi^2} \tag{64}$$

$$I_{DB} = I_{BO} = \frac{K}{4\pi^2}(T^2_{DB + BK + BO + T} - T^2_{BK + T}) \tag{65}$$

Table 15 shows the test results along with the standard deviation of the periods for each tests. The spring constant calculated from four dumbbells is also given along with the average spring constant and its standard deviation.

The results from these tests are very good. The percentage difference of the standard deviation of the spring constant value from its mean value is approaching the accuracy of .01% which is the goal for moment of inertia determinations. The standard deviation for each test is also very good. As an example, the standard deviation for DBC + BKB + BOC +T is .000042 seconds. This represents an error of .007% in the moment of inertia of the object, assuming the rod constant is a constant value. This percentage error is not typical of all tests but with further experimentation and research an error less than .01% can be maintained.

2.1.3.4.5 Conclusions

This test program has produced enough information to verify that fused quartz is the best material to use for torsion rod material. This is a general statement concluded from the results of these tests. For a specific percentage inprovement of fused quartz over other materials, a detailed series of tests must be completed. The disadvantages in mounting ceramic rods are much greater than those for steel rods and for general torsion rod applications the glass rods would not be feasible. Even for use in the air bearing table, the fused quartz rods present problems in mounting. Since the moment of inertia of objects can presently be determined to an accuracy of approximately 0.03 percent with steel rods, the need for using fused quartz rods is not imperative. However, when greater accuracies are needed the fused quartz torsion rod should be used.

TABLE 15
CALCULATED STANDARD DEVIATIONS

Test Object	Average Period	Standard Deviation	Spring Constant
BKA + T	0.401323 sec.	0.000097	-
BKB + T	0.406423 sec.	0.000089	-
DBB + BKA + BOA + T	1.031813 sec.	0.000070	2663.023
DBC + BKB + BKC + T	1.239780 sec.	0.000042	2662.937
DBD + BKA + BOA + T	1.414829 sec.	0.000032	2662.134
DBE + BKA + BOA + T	1.717203 sec.	0.000075	2663.398
		Average	2662.873 in-lb
		Standard Deviation	.532
		Percentage Difference	.02%

The use of the air bearing system as a material tester probably has great possibilities. A large number of other tests could be performed on the torsion rods; however, there is not a specific need for this work at present.

2.1.4 System Analysis

2.1.4.1 Evaluation Tests

The evaluation tests section was designed to provide test data in order to determine the optimum capabilities of the system. The tests were performed and are discussed in the Results Analysis Section.

2.1.4.2 Results Analysis

2.1.4.2.1 Introduction

The System Analysis Project of the Moment of Inertia Program was designed to determine the accuracy to which moments of inertia could be obtained using the air bearing system. This analysis was performed after all improvements and modifications had been made on the system. The results herein give the capabilities of the system and the accuracy which should normally be obtained from future moment of inertia determinations.

The equation of motion to be used in calculating the moment of inertia has been discussed in several previous reports and in detail in Par. 2.1.1.4. In this report it was shown that for a given amplitude range, the equation

$$I = KT^2/4\pi^2 \tag{66}$$

will accurately represent the moment of inertia of the object. The error analysis is performed on Equation 66 where the variables are the rod constant K and the period of oscillation T. Other related variables such as temperature, humidity, and table air pressure, were eliminated by performing the test under the same set of conditions. The effects of the earth's rotation on the system were investigated and these results are entered in Appendix A7. This procedure would be applicable to an actual test because the torsion rod would be calibrated immediately before making a moment of inertia measurement.

2.1.4.2.2 Error Analysis

The error analysis used here is the same as that included in last years annual report. Equation 66 is the basic equation to be used. The variation in the moment of inertia dI, is determined by examining the variables dK and dT as shown below.

$$dI = \left(\frac{\partial I}{\partial K}\right)dK + \left(\frac{\partial I}{\partial T}\right)dT \tag{67}$$

Equation 67 is obtained by taking the total derivative of Equation 66. Since $I = f(K, T)$

$$\frac{\partial I}{\partial K} = \frac{T^2}{4\pi^2} \tag{68}$$

and

$$\frac{\partial I}{\partial T} = \frac{KT}{2\pi^2} \tag{69}$$

The variable dK is obtained from

$$K = 4\pi^2 T^2 / I' \tag{70}$$

where I' is now a standard value with a given variation dI', determined from its dimensional accuracy. dK is defined as

$$dK = \left(\frac{\partial K}{\partial I'}\right)dI' + \left(\frac{\partial K}{\partial T}\right)dT \tag{71}$$

where

$$\frac{\partial K}{\partial I'} = \frac{4\pi^2}{T^2} \tag{72}$$

and

$$\frac{\partial K}{\partial T} = \frac{8\pi^2 I'}{T^3} \tag{73}$$

The variable dI' is determined by examining the variation of the objects demensions and weight. For a dumbbell standard, the moment of inertia is

$$I' = \left(\frac{M_t}{2D^2h + Dc^2hc}\right)\left(2D^2h\left[\frac{D^2}{16} + \frac{h^2}{12}\right] + R^2 + D_c{}^2h_c\left[\frac{D_c{}^2}{16} + \frac{h_c{}^2}{12}\right]\right) \tag{74}$$

where the nomenclature is shown in Figure 70. The variation, dI' is

$$dI' = \left(\frac{\partial I'}{\partial M_t}\right)dM_t + \left(\frac{\partial I'}{\partial D}\right)dD + \left(\frac{\partial I'}{\partial h}\right)dh + \left(\frac{\partial I'}{\partial h_c}\right)dh_c + \left(\frac{\partial I'}{\partial D_c}\right)dD_c + \left(\frac{\partial I'}{\partial R}\right)dR \tag{75}$$

The variables in the parentheses are given in last years annual report and will not be repeated. The variation dT is obtained from the experimental results in a statistical manner. If Equations 67, 68, 69, 71, 72, 73, and 75 are combined we obtain

$$dI = \left(\frac{T^2}{4\pi^2}\right)\left[\left(\frac{4\pi^2}{T^2}\right)\left\{\frac{\partial I'}{\partial M_t}dM_t + \frac{\partial I'}{\partial D}dD + \frac{\partial I'}{\partial h}dh + \frac{\partial I'}{\partial h_c}dh_c + \frac{\partial I'}{\partial D_c}dD_c + \frac{\partial I'}{\partial R}dR\right\} + \frac{8\pi I'}{T^3}(dT)\right] + \left(\frac{KT}{2\pi^2}\right)dT \tag{76}$$

or

$$dI = \left(\frac{\partial I'}{\partial M_t}\right)dM_t + \left(\frac{\partial I'}{\partial D}\right)dD + \left(\frac{\partial I'}{\partial h}\right)dh + \left(\frac{\partial I'}{\partial h_c}\right)dD_c + \left(\frac{\partial I'}{\partial R}\right)\partial R + \frac{2I'dT}{\pi T} + \frac{KTdT}{2\pi^2} \tag{77}$$

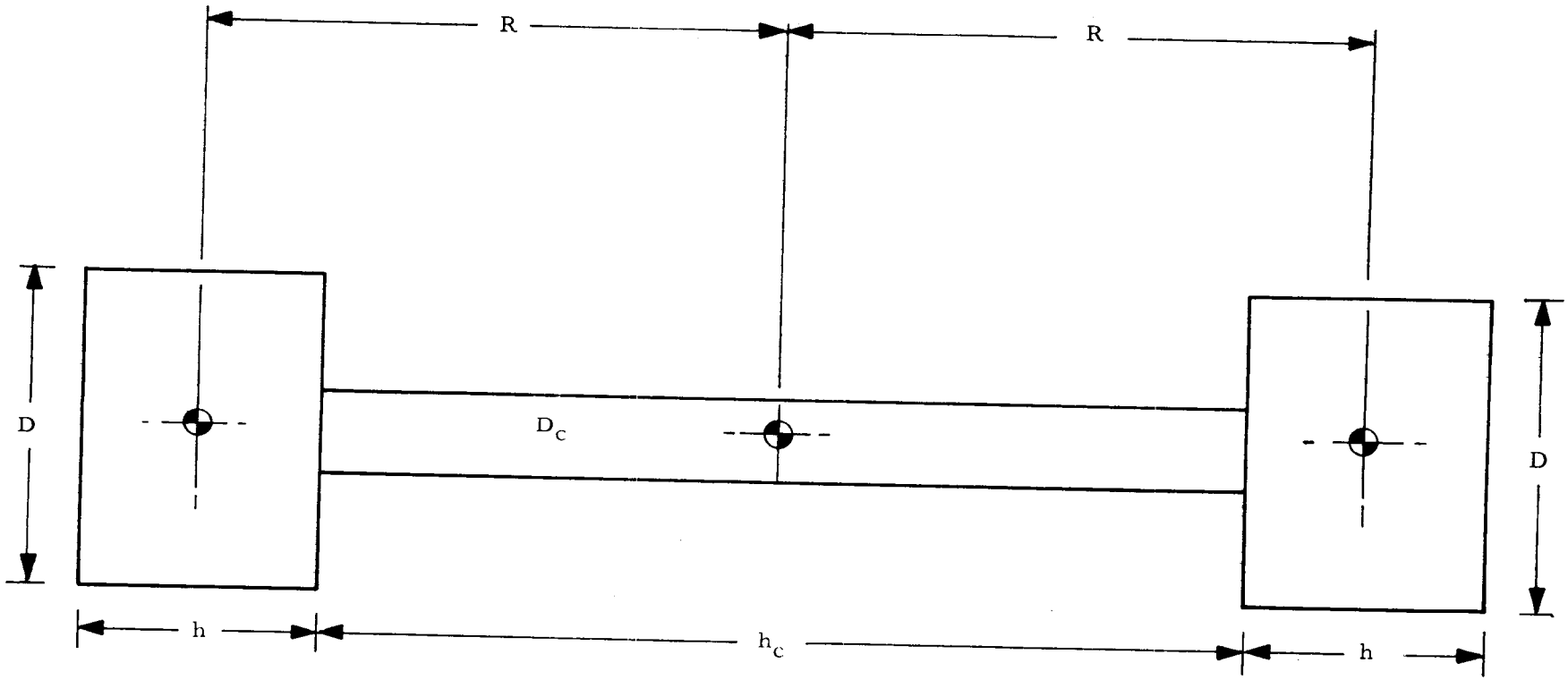

FIGURE 70

DUMBBELL CONFIGURATION

Equation 77 will yield the variation in the value for the moment of inertia where the variables are the standard deviations of several measurements. The value of dI can then be used in

$$\frac{dI}{I} \times 100\% = \%\ \text{error} \tag{78}$$

to determine the error in the moment of inertia measurement.

2.1.4.2.3 Experimental Results

Dumbbell C was used in a series of tests to obtain data for the error analysis. The dimensions of dumbbell C are shown in Table 16. The weight of the dumbbell was obtained by personnel at the Army Calibration Laboratory. A report on the work the Calibration Laboratory performed is included in Appendix A8. The data for dumbbell C is as follows,

$$w = 182.821 \qquad M_t = 0.474 \qquad dM_t = 10.37 \times 10^{-6}.$$

This data was obtained from Appendix A9 which discusses the computer program for calculating the dumbbell moments of inertia. This discussion also includes an error analysis of the misaligment of the dumbbell's center of moss on the table top. The terms in parenthesis are calculated by using the equations shown in last years annual report. These equations yield,

$$\begin{aligned}
\partial I/\partial M_t &= 0.50598 \\
\partial I/\partial D &= 33.14892 \\
\partial I/\partial h &= 22.09400 \\
\partial I/\partial h_c &= 0.67539 \\
\partial I/\partial D_c &= 10.76278 \\
\partial I/\partial R &= 12.69358
\end{aligned}$$

The period data was obtained from a series of 100 tests. Each test was performed in an identical manner as shown in the test procedure in Appendix A10. The table top was displaced to 0.001 radians where a 10 period average was obtained for every 20 cycles up to 500 cycles. Each data point was then punched on a computer card so the mean and standard deviation could be obtained for each test. The statistical analysis computer program was compiled by J. Johnston and is entered in Appendix A11. Appendix A12 shows a sample print out of one test analysis. The only results used were

TABLE 16

DIMENSIONS OF DUMBBELL C

D	h	D_c	h_c	R
6.6270 in.	8.422 in.	1.949 in.	20.056 in.	14.250 in.
6.6270	8.442	1.949	20.058	14.250
6.6270	8.442	1.949	20.057	14.2495
6.6270	8.442	1.949	20.058	14.250
6.6265	8.442	1.948		
6.6270	8.442	1.947		
6.6265	8.442	1.947		
6.6265	8.442	1.949		
6.6270		1.948		
6.6270		1.950		
6.6265		1.950		
6.6265		1.950		
6.6270		1.950		
6.6265		1.949		
6.6265		1.950		
6.6265		1.950		
		1.950		
		1.949		
		1.949		

	D	h	D_c	h_c	R
Mean	6.6268	8.4220	1.9491	20.0578	14.2499

	dD	dh	dD_c	dh_c	dR
Standard Deviation	0.0003	0.0001	0.0009	0.0005	0.0002

the arithmetic mean and standard deviation. The other results are available for future analysis. The test results are shown in Table 17. The tests are grouped because of the temperature variations which could not be controlled for all tests. It is very obvious from these results that the temperature can greatly affect the moment of inertia value obtained from the system. However, the standard deviation for all tests was only 178×10^{-6} seconds. For the calculations here the period average and standard deviation for tests 1826 through 1835 will be used because the temperature was very constant during these tests. The data used was,

mean period = 1.229836 sec.
standard deviation = 8.18535×10^{-6} sec.

Using all the previous data, Equation 77 yields

$$dI = 0.02747$$

and

$$\frac{dI}{I} \times 100\% = 0.027\%$$

This error represents the approximate accuracy which moments of inertia can be determined by using the air bearing system.

2.1.4.2.4 Conclusions

The accuracy with which the moment of inertia of an unknown object weighing between 20 and 2000 pounds can be determined is in the order of 0.03%. This accuracy can be easily obtained for any unknown object as long as the variables are held constant. Greater accuracies probably could be obtained if other conditions were required; however, this is not necessary at this time.

The results of this project have verified that this moment of inertia system represents the state of the art and that the accuracy is sufficient for the present need in moment of inertia determination of space vehicle components.

TABLE 17

TEST RESULTS

Test No.	Date	Temp	Mean Period	Std. Dev.
1826	3-31	70°F	1.229828 sec.	26×10^{-6} sec.
1827	3-31	70°F	1.229838	41
1828	3-31	70°F	1.229832	26
1829	3-31	70°F	1.229854	
1830	3-31	70°F	1.229836	43×10^{-6}
1831	3-31	70°F	1.229842	33
1832	3-31	70°F	1.229836	42
1833	3-31	70°F	1.229837	24
1834	3-31	70°F	1.229836	35
1835	3-31	70°F	1.229832	53
			1.229836	8×10^{-6}
1836	3-31	70°F	1.229774 sec.	31×10^{-6} sec.
1837	3-31	70°F	1.229792	32
1838	3-31	70°F	1.229771	38
1839	3-31	70°F	1.229788	38
1840	3-31	69°F	1.229789	45
1841	3-31	69°F	1.229789	38
1842	3-31	69°F	1.229808	28
1843	3-31	69°F	1.229806	34
1844	3-31	69°F	1.229804	25
1845	3-31	69°F	1.229818	43
			1.2297937	15×10^{-6}
1846	3-31	69°F	1.229766 sec.	30×10^{-6} sec.
1847	3-31	69°F	1.229775	42
1848	3-31	69°F	1.229772	40
1849	3-31	69°F	1.229780	27
1850	3-31	69°F	1.229778	32
1851	3-31	69°F	1.229779	38
1852	3-31	69°F	1.229775	38
1853	3-31	69°F	1.229765	34
1854	3-31	69°F	1.229787	33
1855	3-31	69°F	1.229794	27
			1.229777	8×10^{-6}

TABLE 17 (CONT'D)

Test No.	Date	Temp	Mean Period	Std. Dev.
1856	3-31	70°F	1.229905 sec.	36 x 10^{-6} sec.
1857	3-31	70°F	1.229908	38
1858	3-31	70°F	1.229887	23
1859	3-31	70°F	1.2298775	38
1860	3-31	70°F	1.229884	26
1861	3-31	70°F	1.2298633	32
1862	3-31	70°F	1.229857	34
1863	3-31	70°F	1.229853	40
1864	3-31	70°F	1.229831	22
1865	3-31	70°F	1.229818	24
			1.22992288	64 x 10^{-6}
1866	3-31	70°F	1.230023 sec.	23 x 10^{-6} sec.
1867	3-31	70°F	1.230029	39
1868	3-31	70°F	1.230021	38
1869	3-31	70°F	1.229971	35
1870	3-31	70°F	1.229968	23
1871	3-31	70°F	1.229957	30
1872	3-31	71°F	1.229949	30
1873	3-31	72°F	1.229952	25
1874	3-31	72°F	1.229947	34
1875	3-31	72°F	1.229959	29
1876	3-31	72°F	1.230139	31
1877	4-4	72°F	1.230131	24
1878	4-4	72°F	1.230125	20
1879	4-4	72°F	1.230115	20
1880	4-4	72°F	1.230111	22
1881	4-4	72°F	1.230104	32
1882	4-4	73°F	1.230097	25
1883	4-4	73°F	1.230086	35
1884	4-4	73°F	1.230079	29
1885	4-4	73°F	1.230067	26
			1.230105	23 x 10^{-6}
1886	4-5	68°F	1.229723 sec.	26 x 10^{-6} sec.
1887	4-5	68°F	1.229708	21
1888	4-5	68°F	1.229682	35
1889	4-5	68°F	1.229674	35
1890	4-5	68°F	1.229637	22
1891	4-5	69°F	1.229617	26
1892	4-5	69°F	1.229599	34

TABLE 17 (CONT'D)

Test No.	Date	Temp	Mean Period	Std. Dev.
1893	4-5	70°F	1.229587 sec.	30 x 10^{-6} sec.
1894	4-5	70°F	1.229567	34
1895	4-5	70°F	1.229557	32
			1.229635	59 x 10^{-6}
1896	4-5	70°F	1.230019 sec.	22 x 10^{-6} sec.
1897	4-5	70°F	1.230011	35
1898	4-5	70°F	1.229998	25
1899	4-5	70°F	1.229892	34
1900	4-5	70°F	1.229836	23
1901	4-5	70°F	1.229830	35
1902	4-5	70°F	1.229812	32
1903	4-5	72°F	1.229794	29
1904	4-5	72°F	1.229773	21
1905	4-5	72°F	1.229752	29
			1.229872	59 x 10^{-6}
1906	4-5	72°F	1.229836 sec.	25 x 10^{-6} sec.
1907	4-5	72°F	1.229830	24
1908	4-5	72°F	1.230119	24
1909	4-5	73°F	1.230119	38
1910	4-5	73°F	1.230110	21
1911	4-5	73°F	1.230091	21
1912	4-5	73°F	1.230077	27
1913	4-5	73°F	1.230057	32
1914	4-5	73°F	1.230058	25
1915	4-5	73°F	1.230035	28
			1.230092	33 x 10^{-6}
1916	4-6	74°F	1.230212 sec.	27 x 10^{-6} sec.
1917	4-6	75°F	1.230207	42
1918	4-6	74°F	1.2302238	31
1919	4-6	74°F	1.230220	19
1920	4-6	73°F	1.230237	37
1921	4-6	73°F	1.230235	25
1922	4-6	73°F	1.230246	27
1923	4-6	73°F	1.230244	19
1924	4-6	73°F	1.230257	22
1925	4-6	73°F	1.230264	32
			1.230234	19 x 10^{-6}

2.2 PRODUCT OF INERTIA PROGRAM

2.2.1 System Improvements

2.2.1.1 Improve Tilt Table

2.2.1.1.1 Introduction

The product of inertia machine developed by SPACO for MSFC is used for determining the product of inertia of various flight hardware. This will then be used with the moment of inertia data to locate the principal axes of the objects. In use, the machine rotates the test object about its center of gravity. The unbalanced dynamic force tends to tilt the support plate upon which the test object is secured. This tilting force, or torque, is measured by a load cell which restrains the support plate. The load cell output voltage is amplified and then read by a digital voltmeter. The angular velocity is determined by measuring the period between timing pulses which are generated photoelectrically by the rotation of the machine. An electronic counter is used to measure the period. Knowing the torque and angular velocity, the product of inertia can be computed from the basic equation:

$$\text{Product of Inertia} = \frac{\text{Torque}}{(\text{Angular Velocity})^2} \tag{79}$$

A precision rate table supplies the rotational motion. The support plate is arranged so that it can tilt about an axis which is perpendicular to the rotational axis. The load cell is located a fixed distance from the tilt axis so that its output represents torque.

2.2.1.1.2 Objective

The purpose of the test was to determine if the inherent accuracy and repeatability of the tilt table design is adequate for the overall accuracy requirements of the product of inertia measurement system. This was done by measuring the load cell signal response to known static loads applied to the object support surface. Since it is anticipated that this portion will be the weakest link of the system, the results of this test are vital to the system development.

2.2.1.1.3 Test Apparatus and Procedure

Figure 71 shows the Inland Controls Model 712 rate table with a Revere universal load cell mounted under one side of the support plate. The support

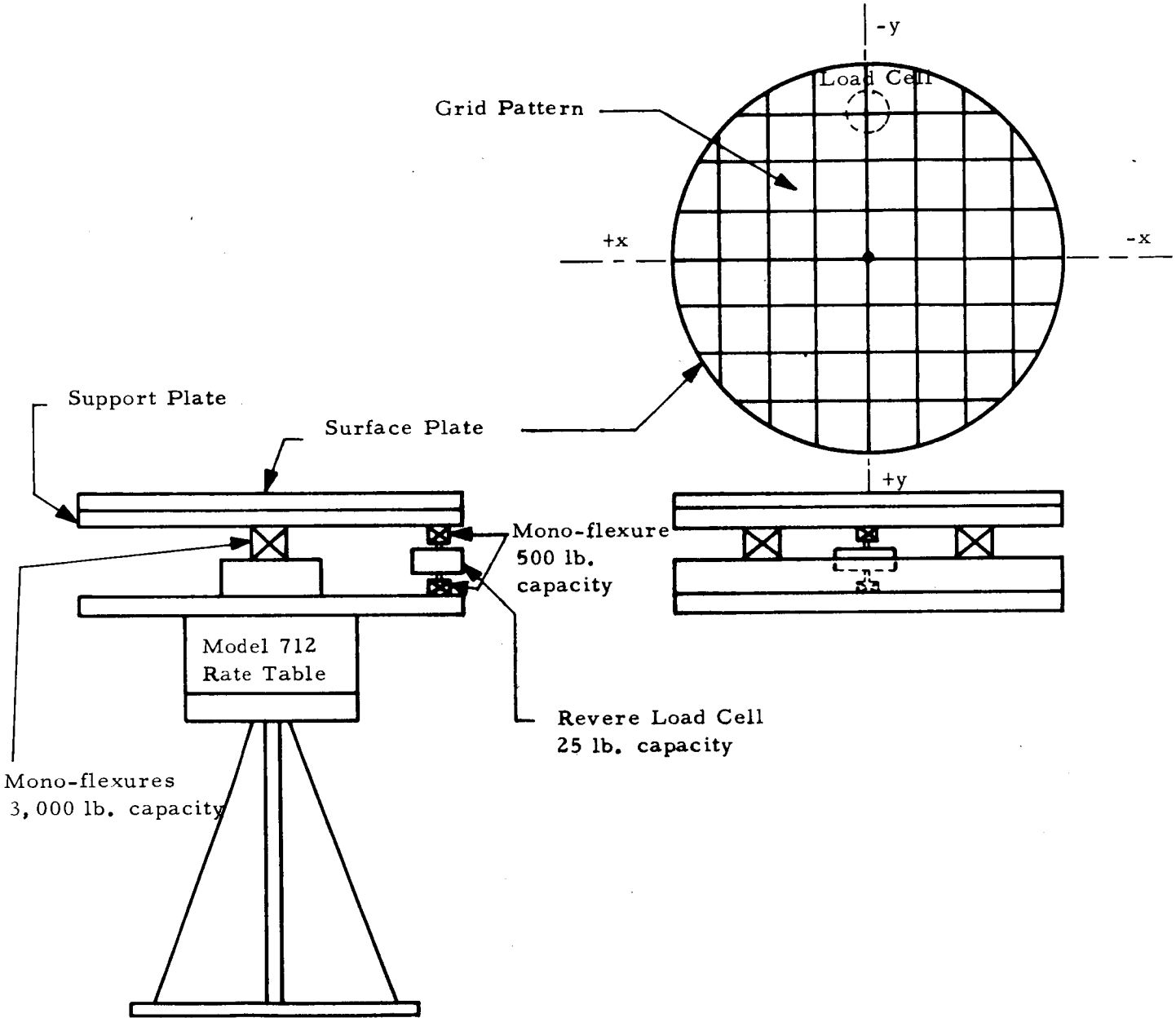

FIGURE 71

PRODUCT OF INERTIA TABLE

plate is supported in the center by two mono-flexures which have a rated capacity of 3,000 lbs. each. The Revere load cell is suspended between two mono-flexures which have a rated capacity of 500 lbs. each. The flexures were used on the load cell to help eliminate any side loading which may result when the surface plate is deflected. The load cell is a precision cell with a rated capacity of 25 lbs., and can withstand an overload of 150% of its rated capacity.

The load cell is connected through slip rings in the rate table to an EAI Model TR-48 analog computer which is used to solve Equation 79 and display the product of inertia on a digital voltmeter. In this test the computer was used merely to amplify the load cell output voltage and to supply the regulated power source for the cell. The computer output was read on a Hewlett-Packard Model 3460A digital voltmeter. Before the test was started the surface plate was machined for flatness and roundness to insure static balance, and a 3-inch grid pattern was engraved on the plate such that various weights could be removed from the surface and relocated each time in exactly the same loctation. The four different standard weights ranging from 9.69 to 0.48 lbs. were each run through three complete cycles. Each cycle consisted of locating a single weight at each of the approximately 37 to 45 different grid positions and recording the output of the load cell. To minimize misleading data due to slowly changing test conditions, the order of testing was randomized. Two random charts were utilized, one to determine the order of the various grid positions and the other to determine the weight to be cycled. In placing the standard weights on the surface plate it was noted carefully which weight axis was parallel to the center flexure axis, so that each time the weight was relocated on the plate it had the same orientation relative to the flexure axis (See Figure 72). This helped to minimize any errors resulting from mislocation of the centers of gravity of the weights. The gain of the amplifiers was calibrated for an output level of 0.100 volt/in-lb torque. Each time a different standard weight was used the system was recalibrated using the weight of the standard multiplied by the known distance from the flexure axis to give a particular output from the computer. (Example: 9.69 lbs. x 9 in. x .100 volt/in-lb = 8.721 volts.) The test procedure is included as Appendix B5.

The test results for each of the cycles were recorded on grid sheets so that each position reading could be referred to clearly and accurately. The three readings for each grid position were then averaged and placed on a new grid sheet. These average readings were plotted on a graph vs calculated values.

2.2.1.1.4 Results

The results indicated that the accuracy of the load measurement was inferior when the weights were located on the side of the table opposite from the load cell. The average error on the load cell side was .186% compared

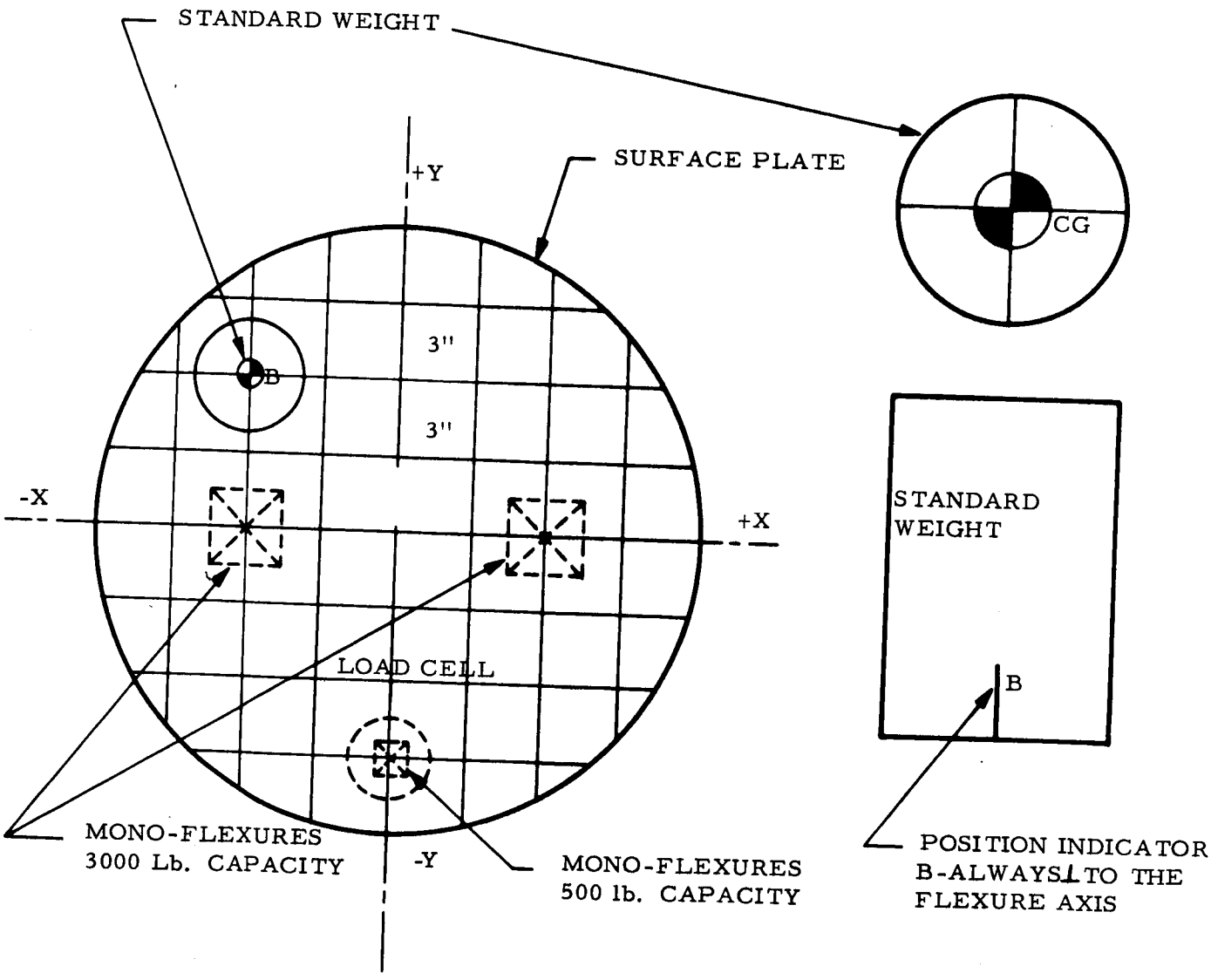

FIGURE 72

STATIC LOAD TEST ARRANGEMENT

with .288% on the other side. There was also a tendency toward greater per cent errors nearer the flexure axis, but this is probably a result of the lower force on the load cell. No significant correlation between weight and error could be observed. All of the readings on a particular grid line parallel to the axis were averaged, and this value was used along with the calculated value to determine the per cent error. The results are shown in Figures 73 through 80. Along the flexure axis, where per cent error figures cannot be defined, the error in volts is given.

2.2.1.1.5 Conclusions and Recommendations

From the test results it is apparent that the best accuracy that can be expected from the tilt table load measuring system is in the order of 0.2%. Considering all of the components involved, this is a very respectable accuracy, although it is not adequate for the system requirements. Further testing will be necessary to determine specific causes of the measured inaccuracies. Typical causes would be: mechanical misalignment, load cell non-linearity and non-repeatability, amplifier drift, mislocation of the standard weights, etc. There is test data to substantiate the belief that the object support plate may have moved on the lower support plate during part of the test. This movement of the surface plate could have been enough to induce some of the error measured in the system. Before any real sound conclusion can be derived, a new test must be designed using only one securely fastened plate. The use of only one plate would eliminate one serious problem and help to narrow the field of possible sources of error.

2.2.1.2 Calibrate Standards

2.2.1.2.1 Manufacturing

2.2.1.2.1.1 Machining

The product of inertia test standards were machined from "Meehanite", a brand of cast iron selected for its homogeneous crystaline structure. As originally made the standards were in the form of a right prism having a right triangular cross section. Trouble was experienced with fracturing of the acute angular edges, so they were later ground off truncated.

2.2.1.2.1.2 Plating

The standards were chrome plated using a two step method. The electrodes were relocated for the second step to avoid the bare spots where the electrodes were originally attached. The plating process left the surface of the standards uneven. This was because the second plating did not build up evenly.

FIGURE 73
STATIC TEST RESULTS -
9.69 lb WEIGHT

Average for all Three Tests

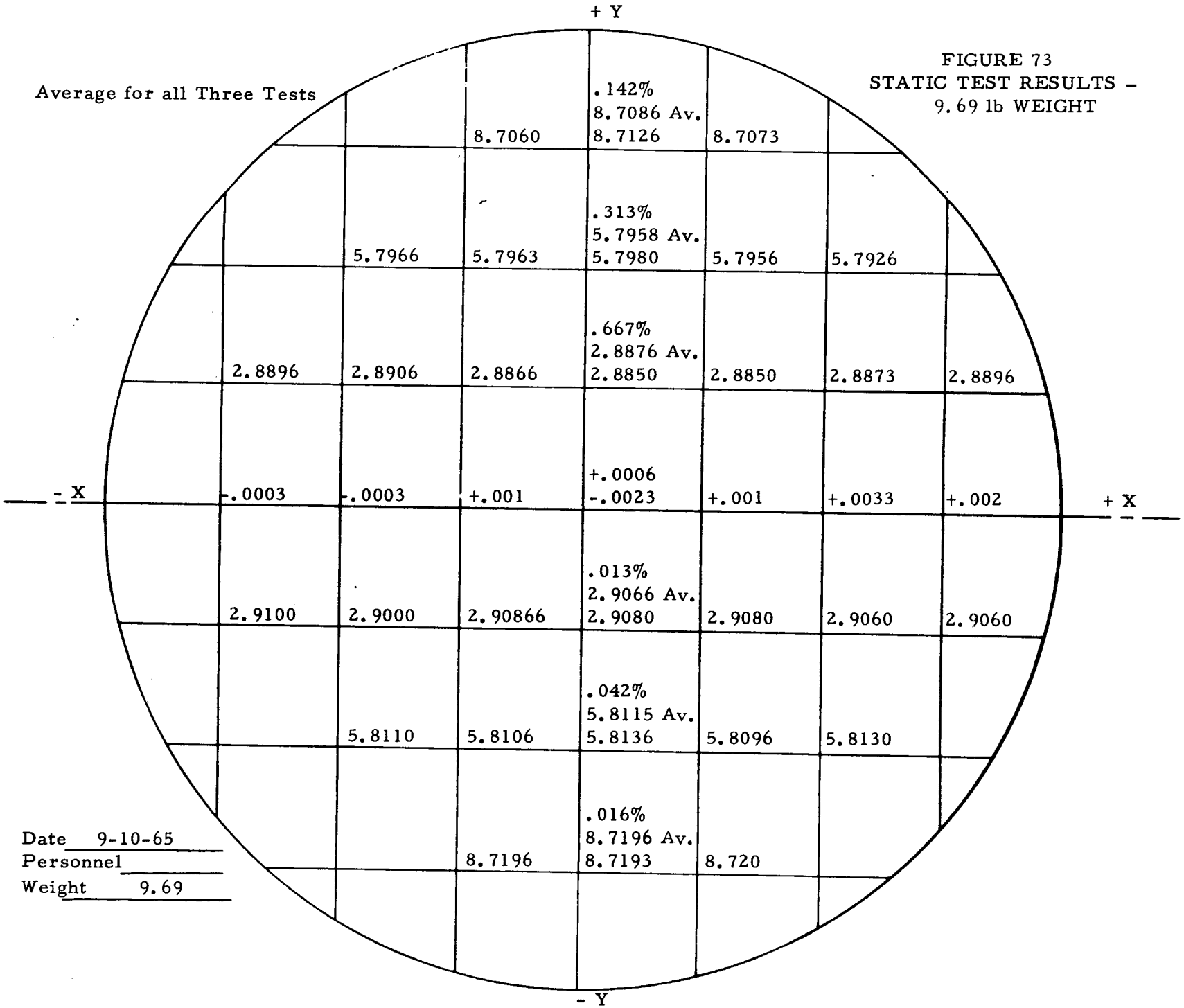

Date 9-10-65
Personnel
Weight 9.69

FIGURE 74

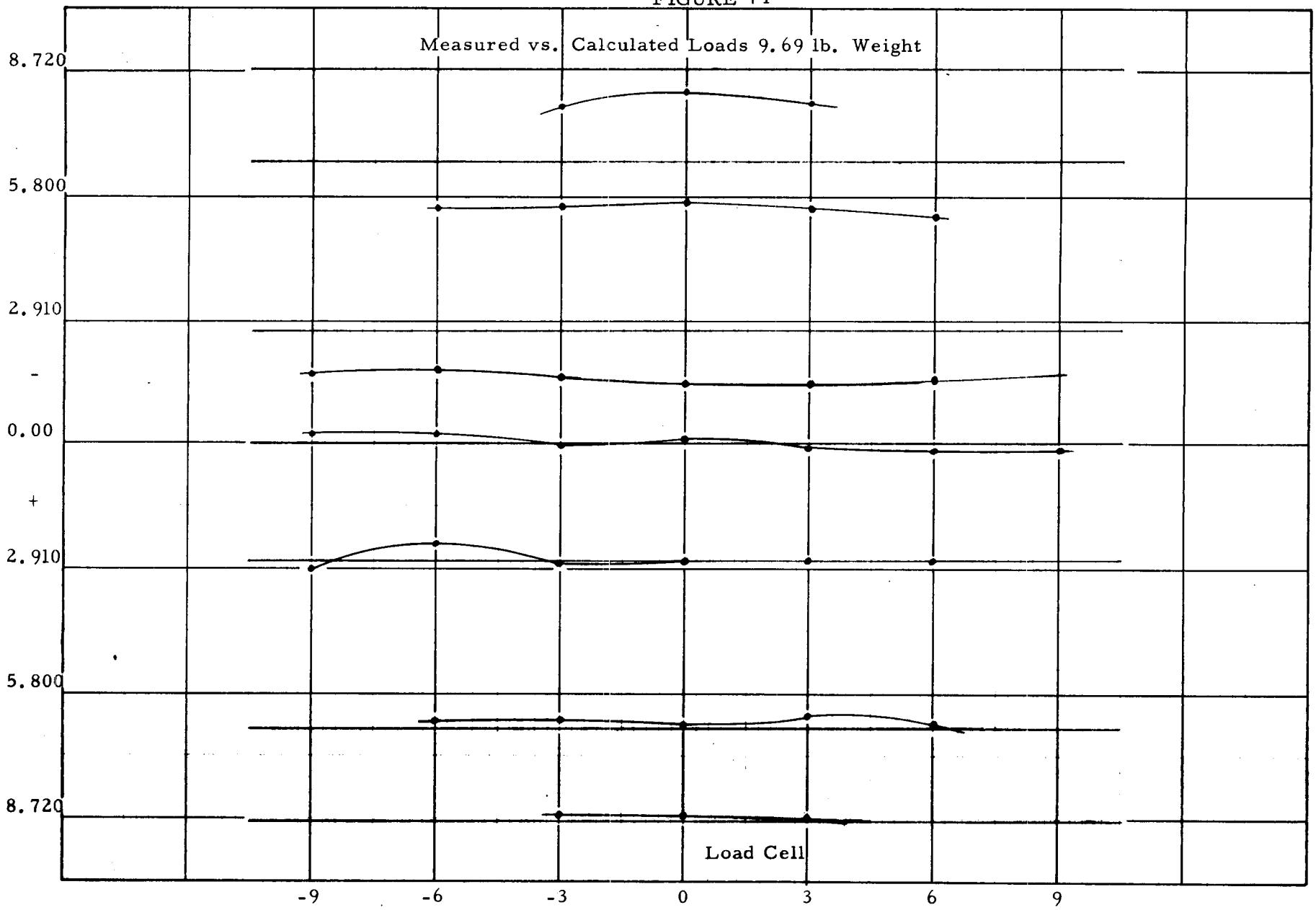
Measured vs. Calculated Loads 9.69 lb. Weight
8.720
5.800
2.910
-
0.00
+
2.910
5.800
8.720
Load Cell
-9
-6
-3
0
3
6
9

FIGURE 75
STATIC LOAD TEST RESULTS -
5.0 lb. WEIGHT

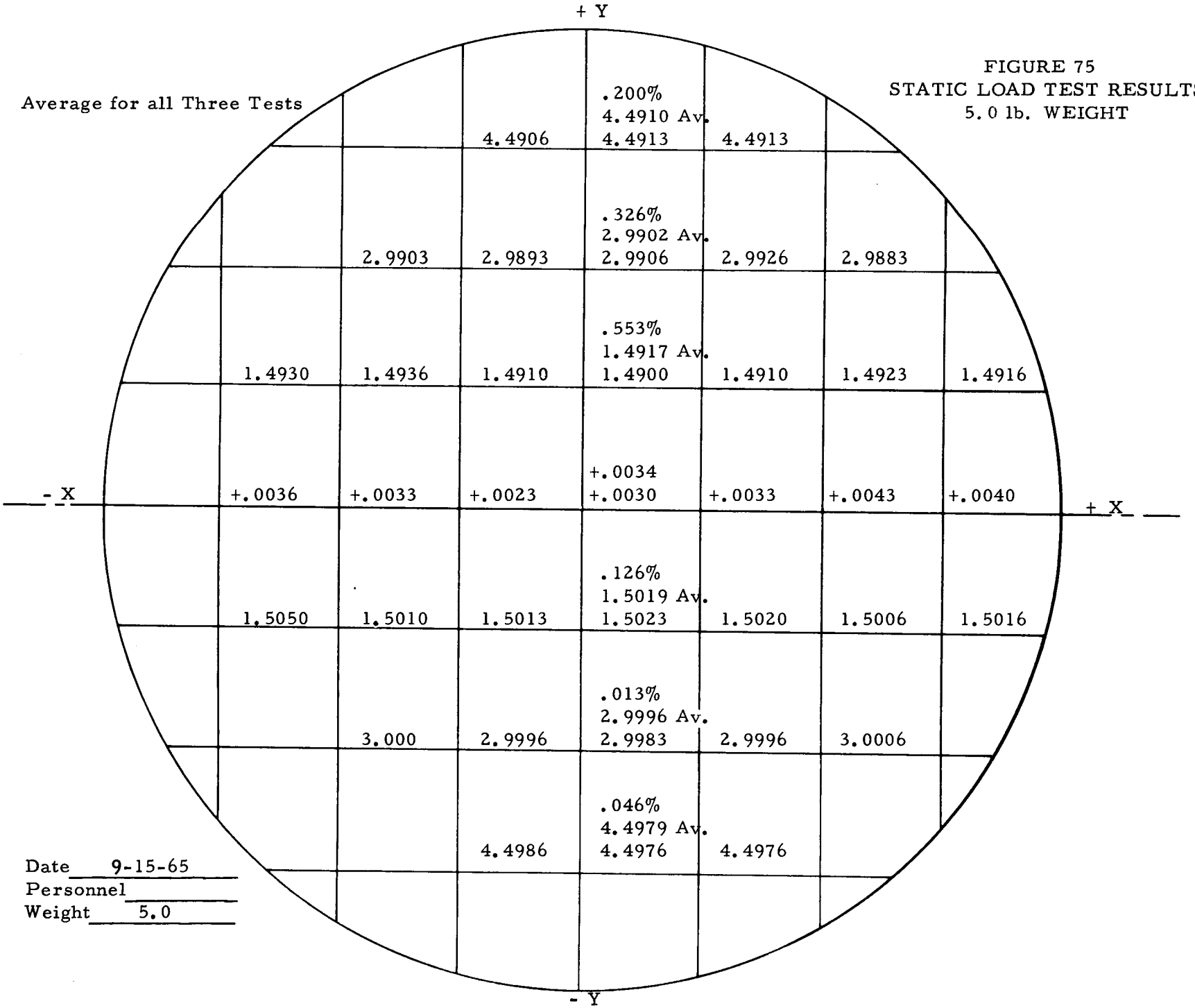

Date 9-15-65
Personnel
Weight 5.0

FIGURE 76

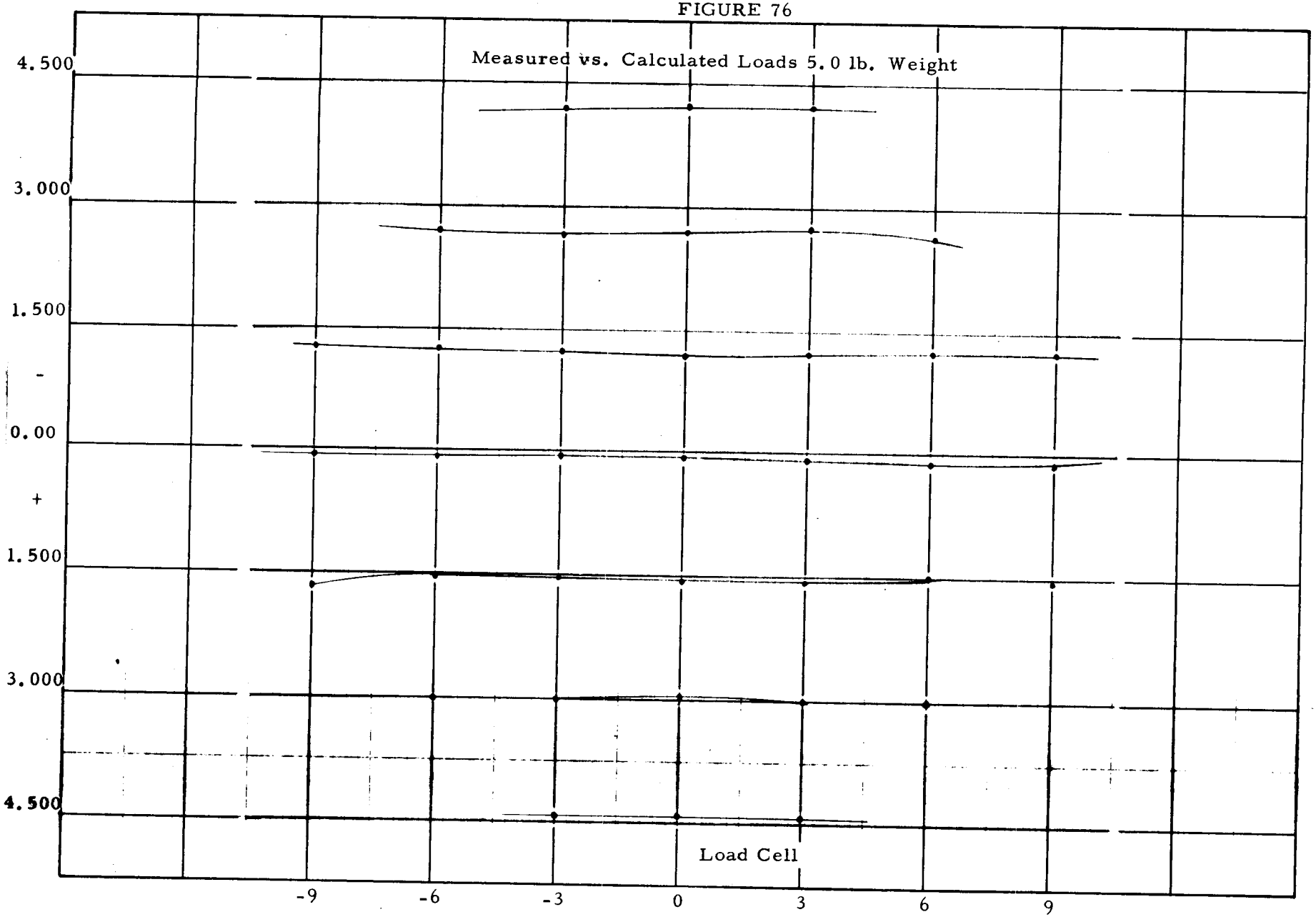
Measured vs. Calculated Loads 5.0 lb. Weight
4.500
3.000
1.500
-
0.00
+
1.500
3.000
4.500
Load Cell
-9
-6
-3
0
3
6
9

FIGURE 77
STATIC LOAD TEST RESULTS -
1.0 lb. WEIGHT

Average for all Three Tests

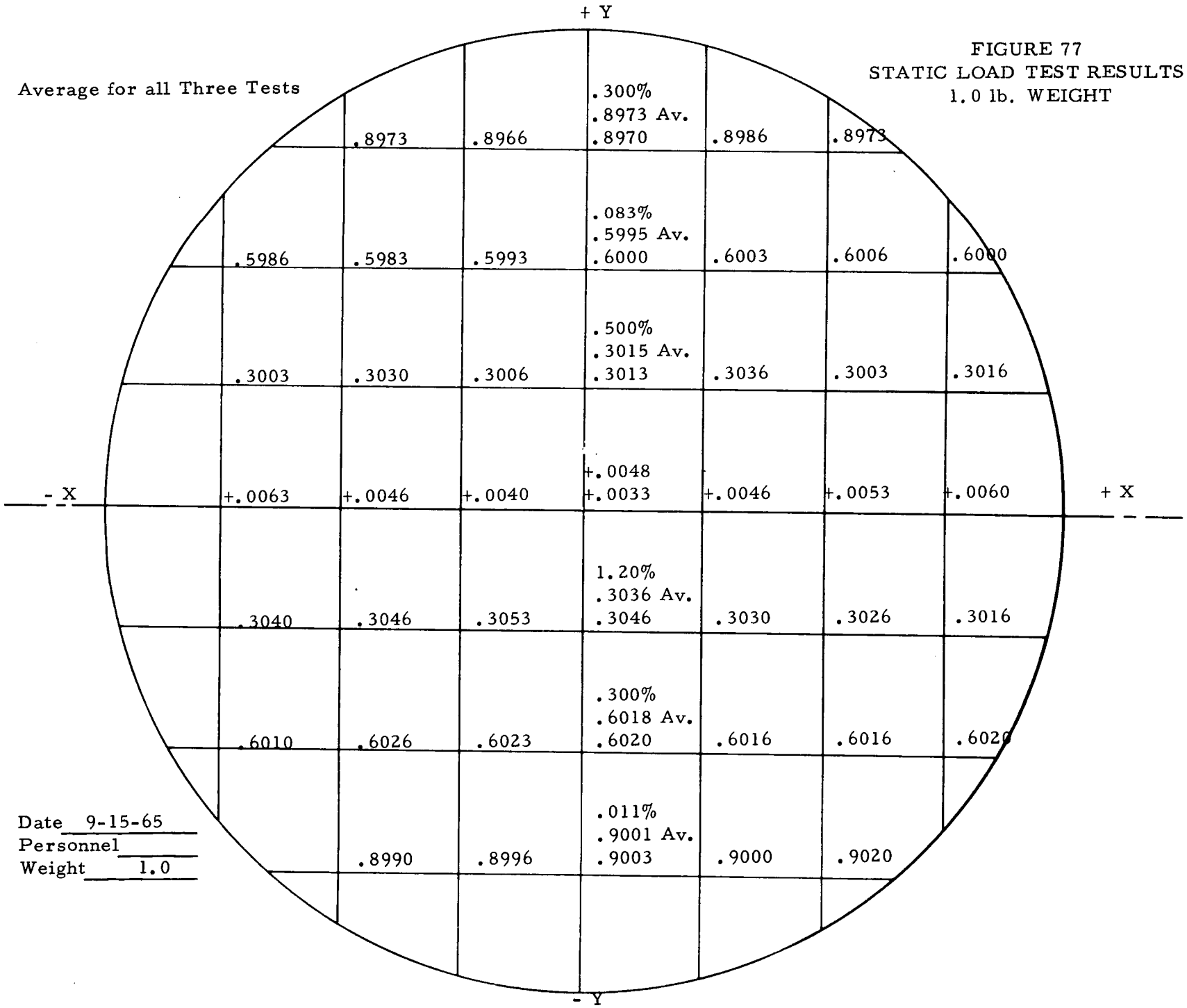

Date 9-15-65
Personnel
Weight 1.0

FIGURE 78

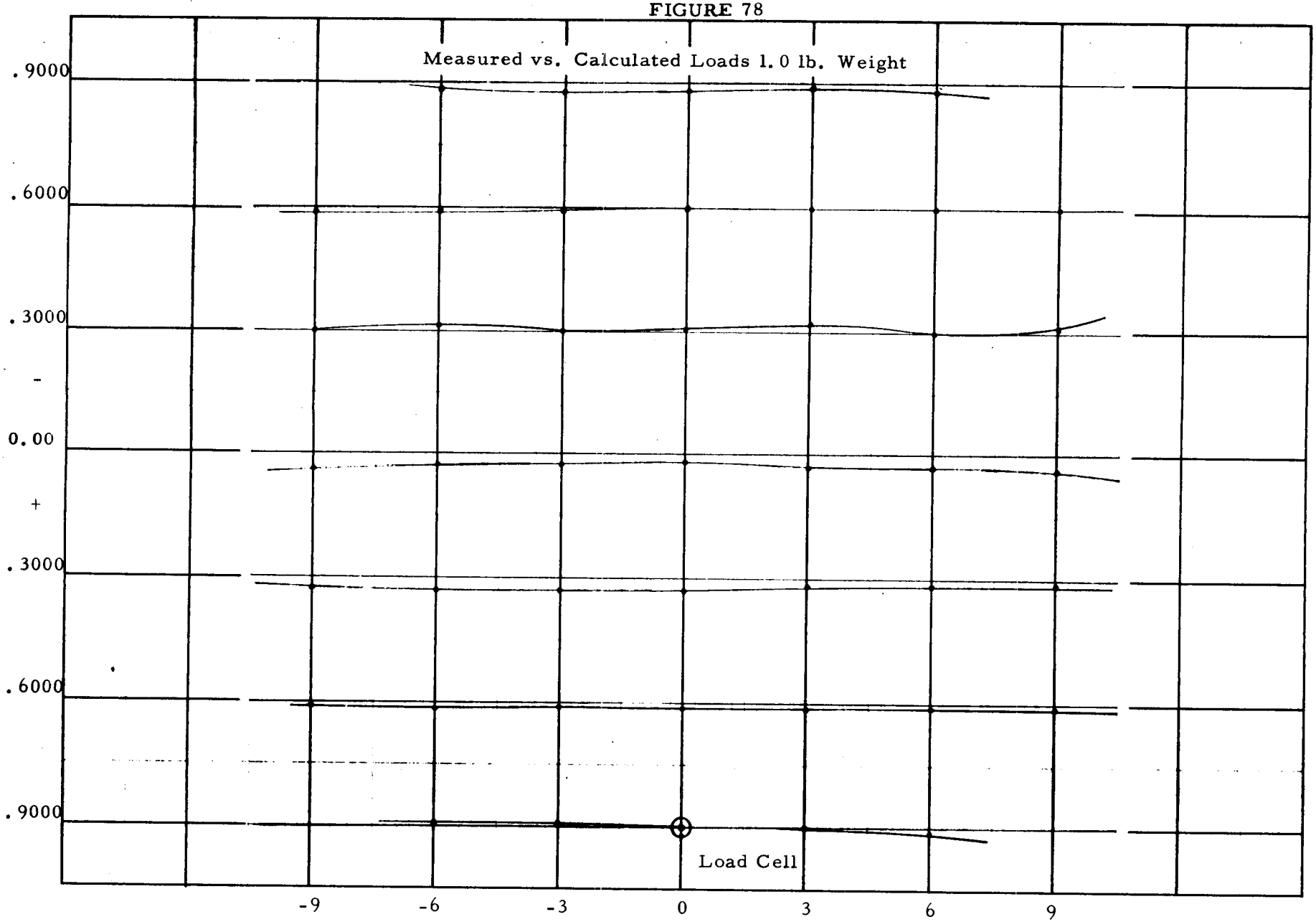
Measured vs. Calculated Loads 1.0 lb. Weight
.9000
.6000
.3000
-
0.00
+
.3000
.6000
.9000
Load Cell
-9
-6
-3
0
3
6
9

FIGURE 79
STATIC LOAD TEST RESULTS - ERROR

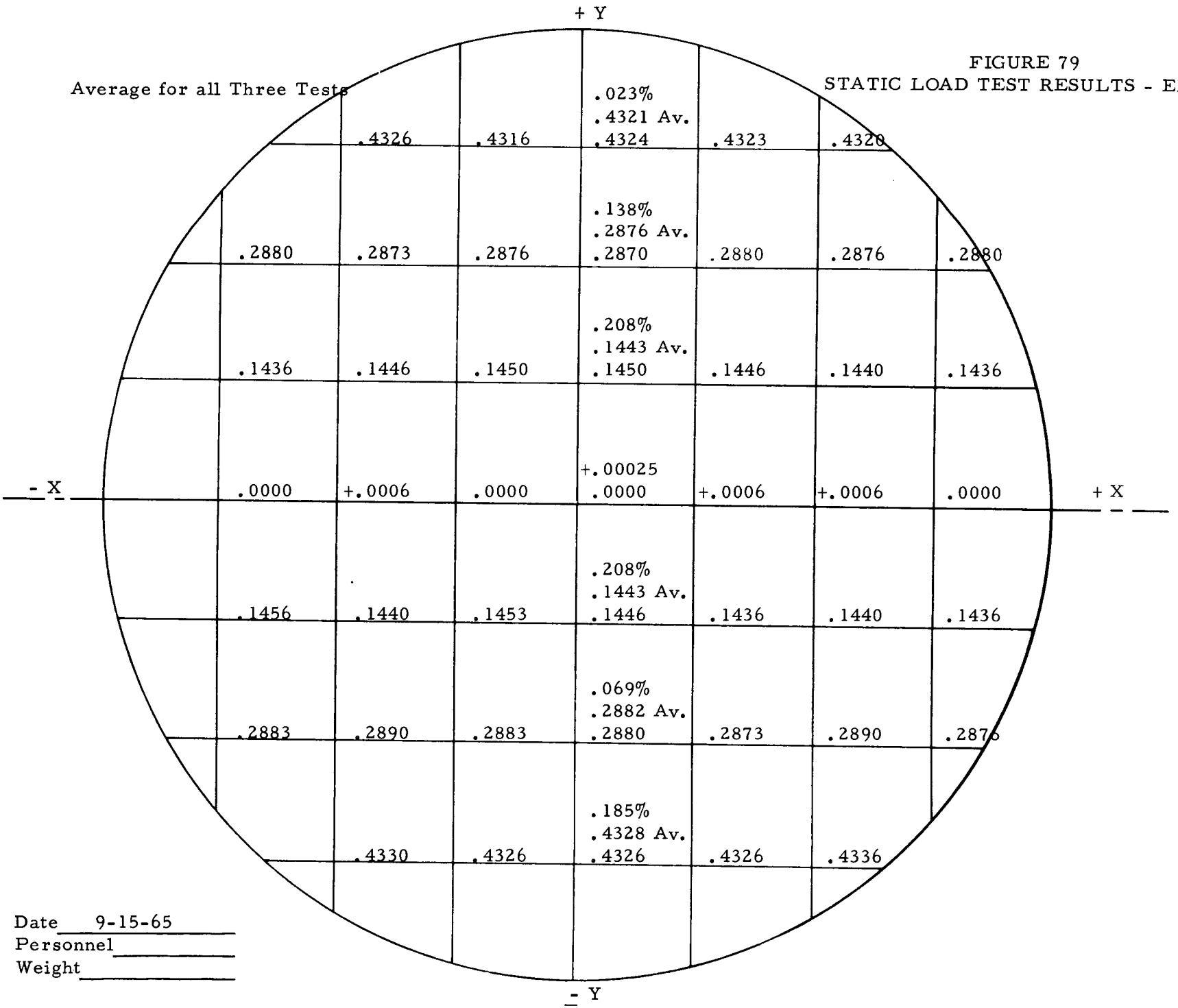

Date 9-15-65
Personnel
Weight

FIGURE 80

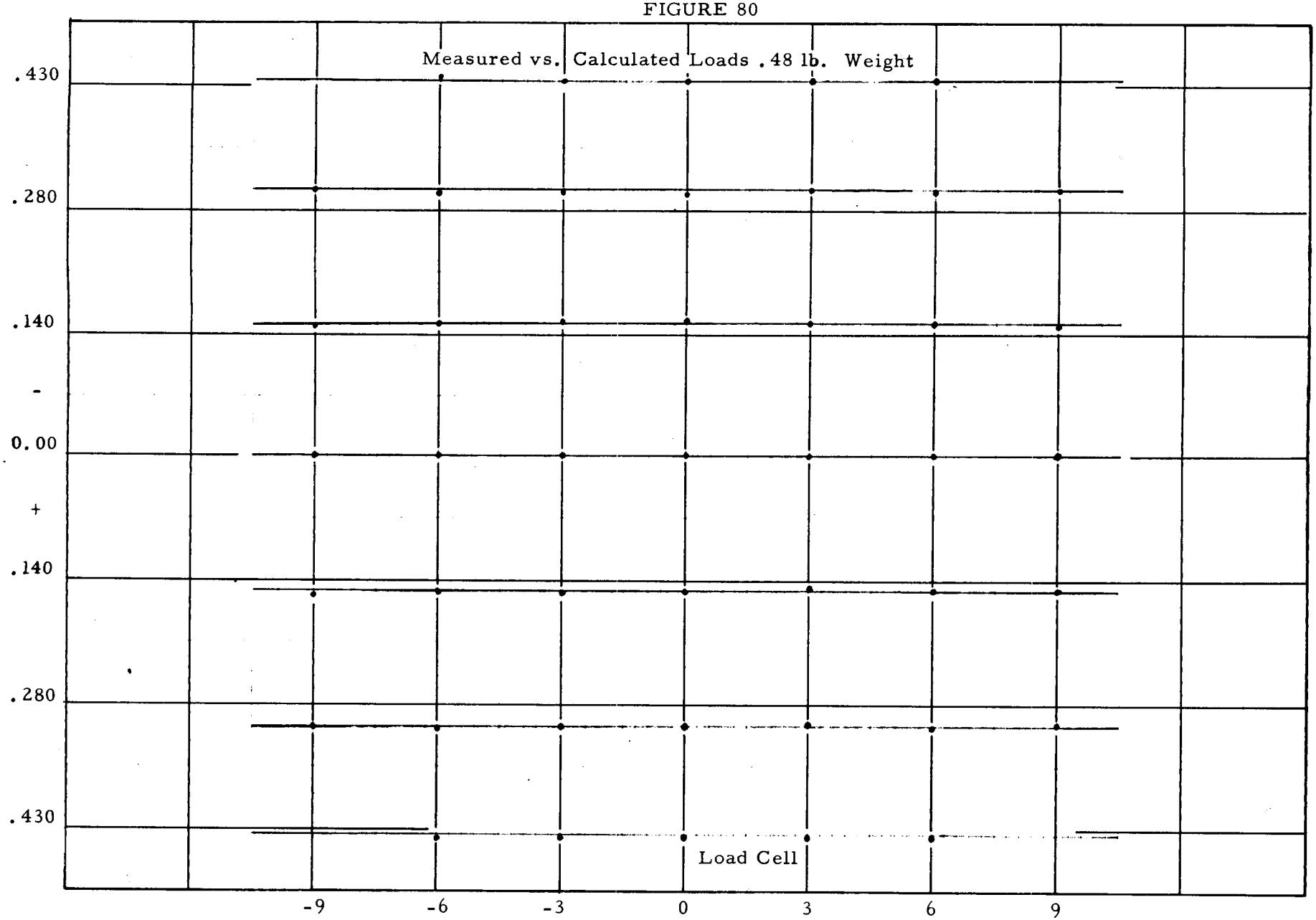
Measured vs. Calculated Loads .48 lb. Weight
.430
.280
.140
-
0.00
+
.140
.280
.430
Load Cell
-9
-6
-3
0
3
6
9

2.2.1.2.1.3 Grinding

One of the test blocks was ground after plating in order to give it a smooth surface. The plating was penetrated in one area during grinding, so this standard will have to be kept oiled to prevent rusting.

Based on the experience with this test standard, it was decided to use the others without the final grinding.

2.2.1.2.2 Measurements

2.2.1.2.2.1 Discussion

The test standards were weighed and their dimensions measured. Figure 81 is a sample of the data sheets used for recording the dimensions. Each of the basic dimensions were taken in several places and then averaged to get the average basic dimensions shown in Figure 82, e.g. dimensions J, K, and L in Figure 81 were averaged to obtain dimension D in Figure 82. The following equations and computer programs for center of gravity, products of inertia, and moments of inertia refer to the average dimensions as indicated in Figure 82.

2.2.1.2.2.2 Center of Gravity Location

The equation for calculating one coordinate, X, of the center of gravity is given by:

$$X = A - \frac{A^3(2B + C) - 3A^2CD + D^2(C - B)(3A - D)}{3A^2(B + C) + 3D^2(C - B) - 6ACD} \qquad (80)$$

The location of dimensions A, B, C, and D are given in Figure 83. A, B, C, and D are the average dimensions as discussed above. The other coordinate, Y, in Figure 83 is found from the same equation by interchanging A and B along with C and D.

2.2.1.2.2.3 Product of Inertia Equation

The product of inertia of the triangular test standards can be computed from the equation given below. The last three terms of the equation correct for the missing acute angular edges. The dimensional quantities are those shown in Figure 82. The product of inertia equation is:

$$I_{xz} = X_a Y_a X_{ma}/36 - X_{ba} Y_{ba} X_{ma} + X_{bb} Y_{bb} X_{mb} + X_{bc} Y_{bc} X_{mc} \qquad (81)$$

FIGURE 81

DIMENSION OF FINISH
GROUND TRIANGULAR STANDARD

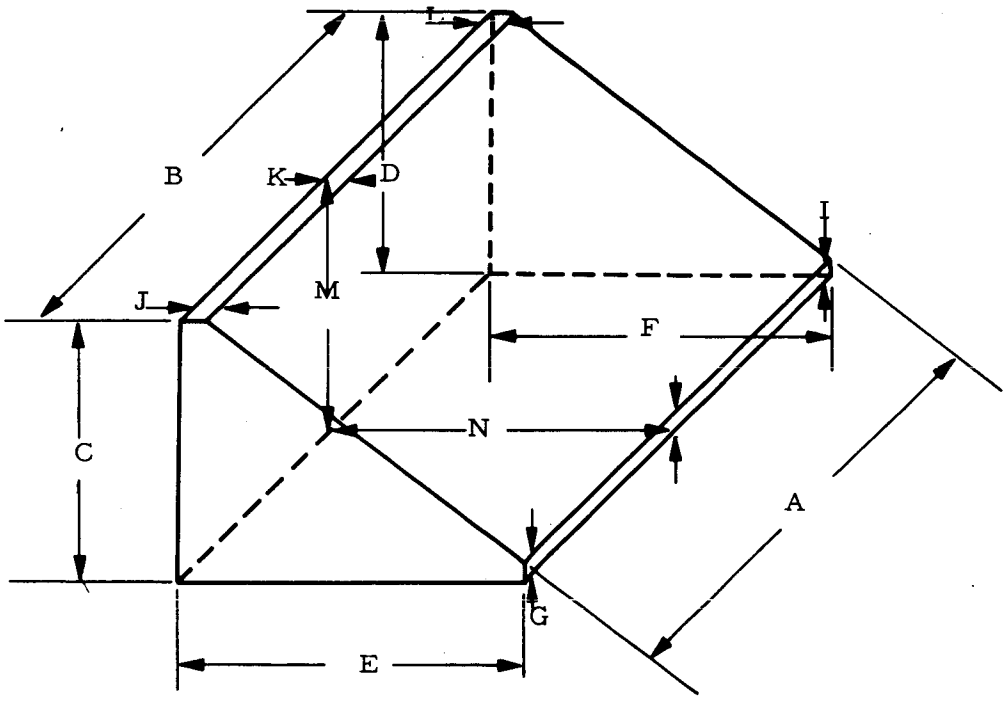

NO.	DISTANCE	NO	DISTANCE
A	5.3218	J	.1345
B	5.3217 - 5.3220	K	.135
C	5.2218	L	.135
D	5.2219	M	5.2218
E	5.8481	N	5.8480
F	5.8480	REMARKS:	
G	.1245		
H	.1255		
I	.126		

FIGURE 82

PRODUCT OF INERTIA STANDARDS
TERMINOLOGY

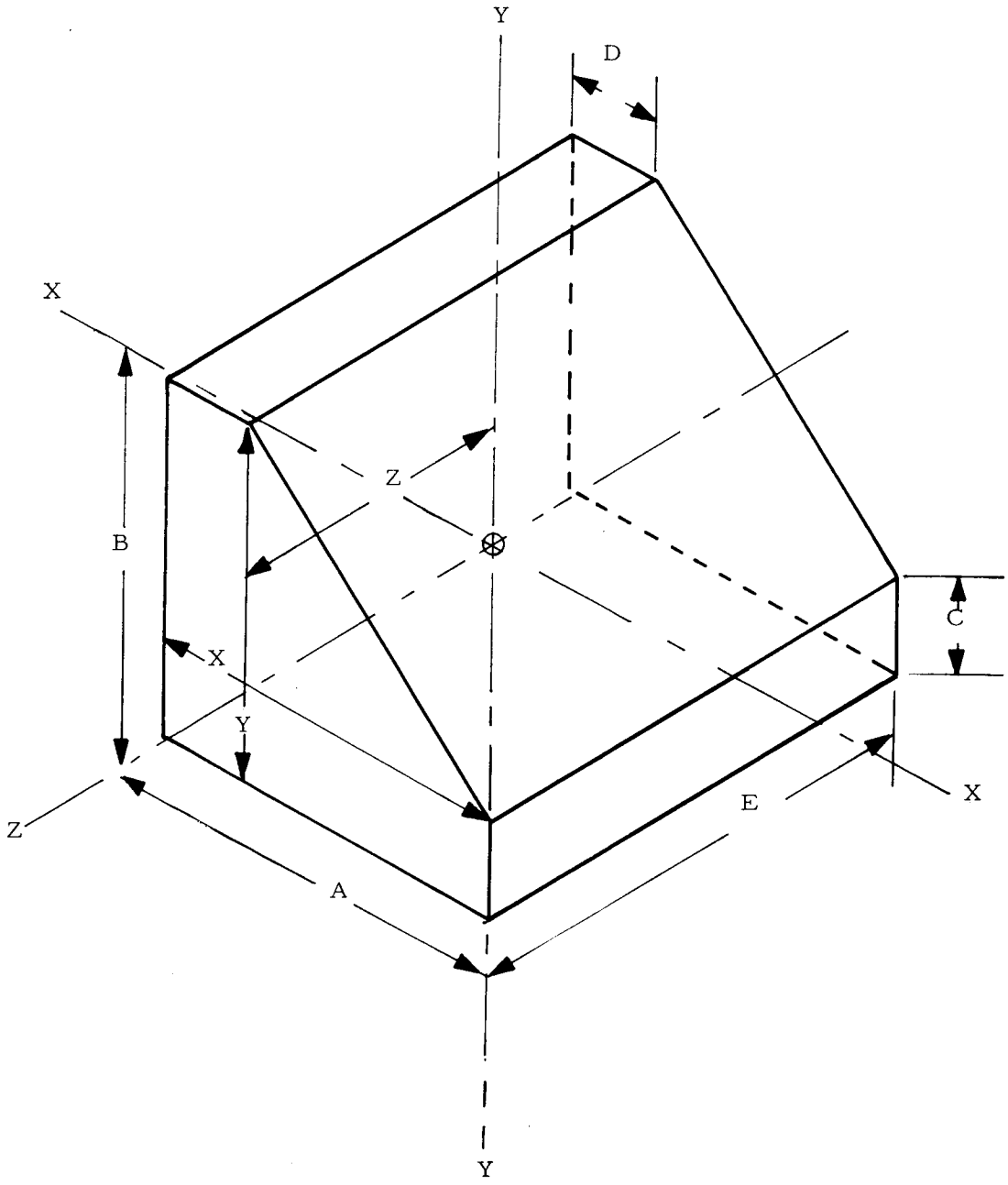

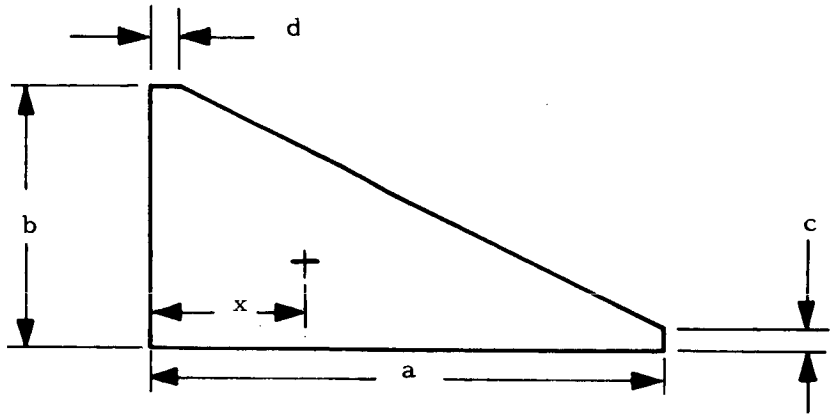

Figure 83. Center of Gravity Location

where: A, B, C, D, and E are linear dimensions.

W	=	weight	
G	=	acceleration due to gravity	
X_a	=	$A - D$	(82)
Y_a	=	$B - C$	(83)
X_{ma}	=	$A_a P$	(84)
A_a	=	$X_a Y_a / 2$	(85)
P	=	X_{mt} / A_t	(86)
X_{mt}	=	W / G	(87)
A_t	=	$A_a + A_b + A_c$	(88)
A_b	=	$D Y_a$	(89)
A_c	=	AC	(90)
X_{ba}	=	$A - X - 2X_a / 3$	(91)
X	=	$A - X_n / X_d$	(92)
X_n	=	$A^3(2B + C) - 3A^2CD + D^2(C - B)(3A - D)$	(93)
X_d	=	$3A^2(B + C) + 3D^2(C - B) - 6ACD$	(94)
Y_{ba}	=	$B - Y - 2Y_a / 3$	(95)
Y	=	$B - Y_n / Y_d$	(96)
Y_n	=	$B^3(2A + D) - 3B^2CD + C^2(D - A)(3B - C)$	(97)
Y_d	=	$3B^2(A + D) + 3C^2(D - A) - 6BCD$	(98)
X_{bb}	=	$X - D/2$	(99)
Y_{bb}	=	$(B + C)/Z - Y$	(100)
X_{mb}	=	$A_b P$	(101)
X_{bc}	=	$A/2 - X$	(102)
Y_{bc}	=	$Y - C/2$	(103)
X_{mc}	=	$A_c P$	(104)

It is worth noting that the above equation also gives the value of I_{yz}, since I_{yz} is equal to I_{xz}. Because of the symmetry of the objects about the X-Y plane, I_{xy} is zero.

2.2.1.2.2.4 Moment of Inertia Equation

The moment of inertia equations for the triangular test standards are given below. The dimensional quantitites in these equations also refer to those shown in Figure 82. The moment of inertia equations are:

$$I_{xx} = \frac{M_o}{36}\left[2(B+Q)^2 + 3E^2\right] + M_o\left(\frac{B+Q}{3} - Y\right)^2 - \frac{M_s}{36}(2Q^2+3E^2) -$$

$$M_s\left(B+\frac{Q}{3} - Y\right)^2 - \frac{M_v}{36}(2C^2+3E^2) - M_v\left(Y - \frac{C}{3}\right)^2 \qquad (105)$$

$$I_{yy} = \frac{M_o}{36}\left[2(A+R)^2 + 3E^2\right] + M_o\left(\frac{A+R}{3} - X\right)^2 - \frac{M_s}{36}(2D^2+3E^2) -$$

$$M_s\left(X - \frac{D}{3}\right)^2 - \frac{M_v}{36}(2R^2+3E^2) - M_v\left(A+\frac{R}{3} - X\right)^2 \qquad (106)$$

$$I_{zz} = \frac{M_o}{18}\left[(A+R)^2 + (B+Q)^2\right] + M_o\left[\left(\frac{B+Q}{3} - Y\right)^2 + \left(\frac{A+R}{3} - X\right)^2\right] -$$

$$M_s\left[\frac{D^2+Q^2}{18} + \left(X - \frac{D}{3}\right)^2 + \left(B+\frac{Q}{3} - Y\right)^2\right] - M_v\left[\frac{R^2+C^2}{18} +\right.$$

$$\left.\left(A+\frac{R}{3} - X\right)^2 + \left(Y - \frac{C}{3}\right)^2\right] \qquad (107)$$

where: A, B, C, D, and E are linear dimensions.

W	=	weight	
G	=	acceleration due to gravity	
M_o	=	$M_t + M_s + M_v$	(108)
M_t	=	W/G	(109)
M_s	=	$M_t QD/D_{iv}$	(110)
M_v	=	$M_t CR/D_{iv}$	(111)
R	=	$C(D-A)/(C-B)$	(112)
D_{iv}	=	$AB + AC + BD - CD$	(113)
Q	=	$D(C-B)/(D-A)$	(114)

$$X = A - \frac{A^3(2B+C) - 3A^2CD + D^2(C-B)(3A-D)}{3A^2(B+C) + 3D^2(C-B) - 6ACD} \qquad (115)$$

$$Y = B - \frac{B^3(2A+D) - 3B^2CD + C^2(D-A)(3B-C)}{3B^2(A+D) + 3C^2(D-A) - 6BCD} \qquad (116)$$

2.2.1.2.2.5 Computer Programs

The computer program for computing the center of mass, products of inertia, and moments of inertia of the triangular test standards is given in Appendix B2. This is in "Fortran II" language.

Appendix B3 is a subroutine program for the program described above. It is used to compute the principal axes and direction cosines of the triangular test standards.

The program and subroutine program mentioned above were used to compute the various inertial properties of the seven triangular test standards. The printout of this data is given in Appendix B4.

2.2.1.3 Evaluation Tests

2.2.1.3.1 Technical Discussion

The results obtained in tests with the new load cell arrangement indicated the need for some additional modifications. It was felt that the stability of the tilt table could be significantly improved by replacing the angular adjustable two-piece table with a single plate. Also, the need for a load cell stabilizing system to offset centrifugal force effects was apparent. These modifications were made and the evaluation tests were run.

2.2.1.3.2 Procedure

The revised machine is shown in Figure 84. The 24 inch diameter support plate is supported at its center by two mono-flexures having a rated capacity of 3,000 lbs. each. These flexures are mounted to a support bar which is attached to the Inland Controls precision rate table. The support plate has an engraved three inch grid pattern to provide a reference for placing weights thereon.

The Revere load cell is mounted between two mono-flexures having a rated capacity of 500 lbs. These flexures remove bending moment tendencies (due to surface plate tilt) from the load cell. The load cell is of the super precision class and has a rated capacity of 25 lbs. with a 150% overload tolerance. Electrical connections are made to the load cell through slip rings in the rate table.

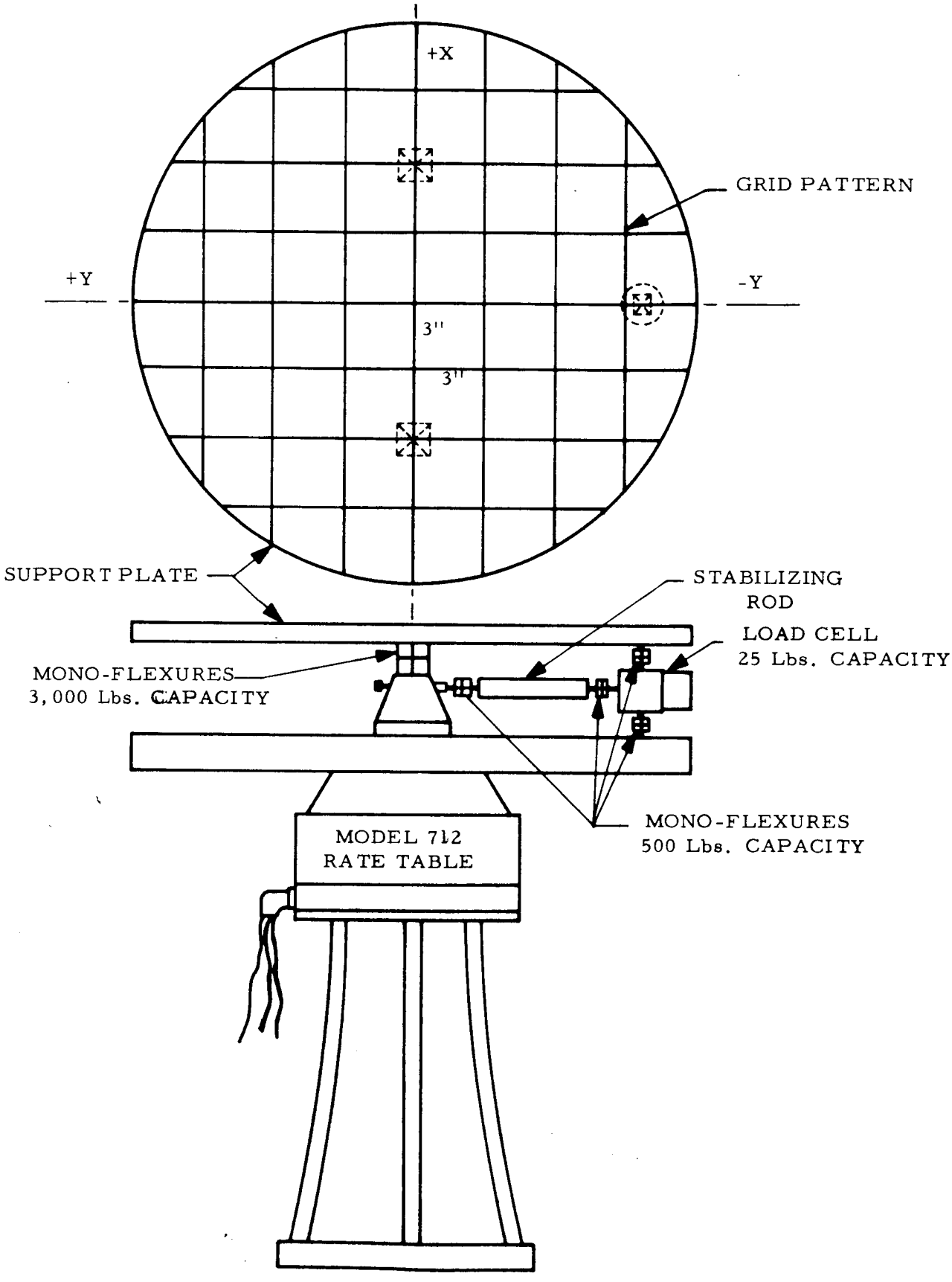

FIGURE 84
MODIFIED PRODUCT OF INERTIA TABLE

A stabilizing rod is used in the new design to offset the effect of centrifugal force on the load cell. This rod ties the load cell body to the support bar. Two 500 lb. mono-flexures remove bending moment tendencies from this source. In use, a small amount of compression pre-load is placed in the rod. The amount of pre-load, 0.22 lb.-in. equivalency, was determined empirically by dynamic testing.

In order to determine the linearity of the torque readout, static tests were made. Operational amplifiers on the E.A.I. Model TR-48 analog computer were used to amplify the load cell output voltage to drive a Hewlett-Packard Model 3460A digital voltmeter. A gain pot was used so that the output could be standardized. A known weight was used to standardize the output to 0.1 volt per lb.-in. of torque. The computer's regulated power supply was used to excite the load cell.

Three standard weights ranging from 0.48 to 9.69 lbs. were used for the tests. Each weight was run through two complete cycles. The weights were placed on each of the 45 grid positions and the DVM readings were recorded on a grid data sheet. The weights were kept oriented as shown in Figure 85 throughout the tests. Reference marks on the weights were used to accurately position the weights on the grid positions. The order of testing was randomized to compensate for slowly changing test conditions. Two random charts were used—one to determine the test weight sequence, the other to determine the grid position sequence for each weight.

2.2.1.3.3 Test Results

Testing was performed in accordance with the test procedure in Appendix B1. The values obtained for each pair of tests were averaged for each grid position and the averages were recorded on a new grid sheet. These grid sheets are given in Figures 86, 87, and 88. The values on this sheet were then averaged along each line parallel to the tilt axis and these values were used to calculate the average percent deviation from the best straight line passing through the origin. These errors are portrayed in graphical form in Figure 89. B-1

It is noted that the error curves have the same general shape for positive torque, i.e. when the load cell is in tension. This is also true for the two lighter weights in the case of negative torque. This indicates that the load cell response is very linear. The "S" shaped characteristics could be attributed to errors in the engraved line spacing. The error was generally larger for negative torque. As would be expected, the largest percent error was experienced for the 0.48 lb. weight. The amount of this error is 0.83% of the test weight, but only .016% of the load cell full scale. Although the results obtained for the two larger weights are somewhat improved over the previous

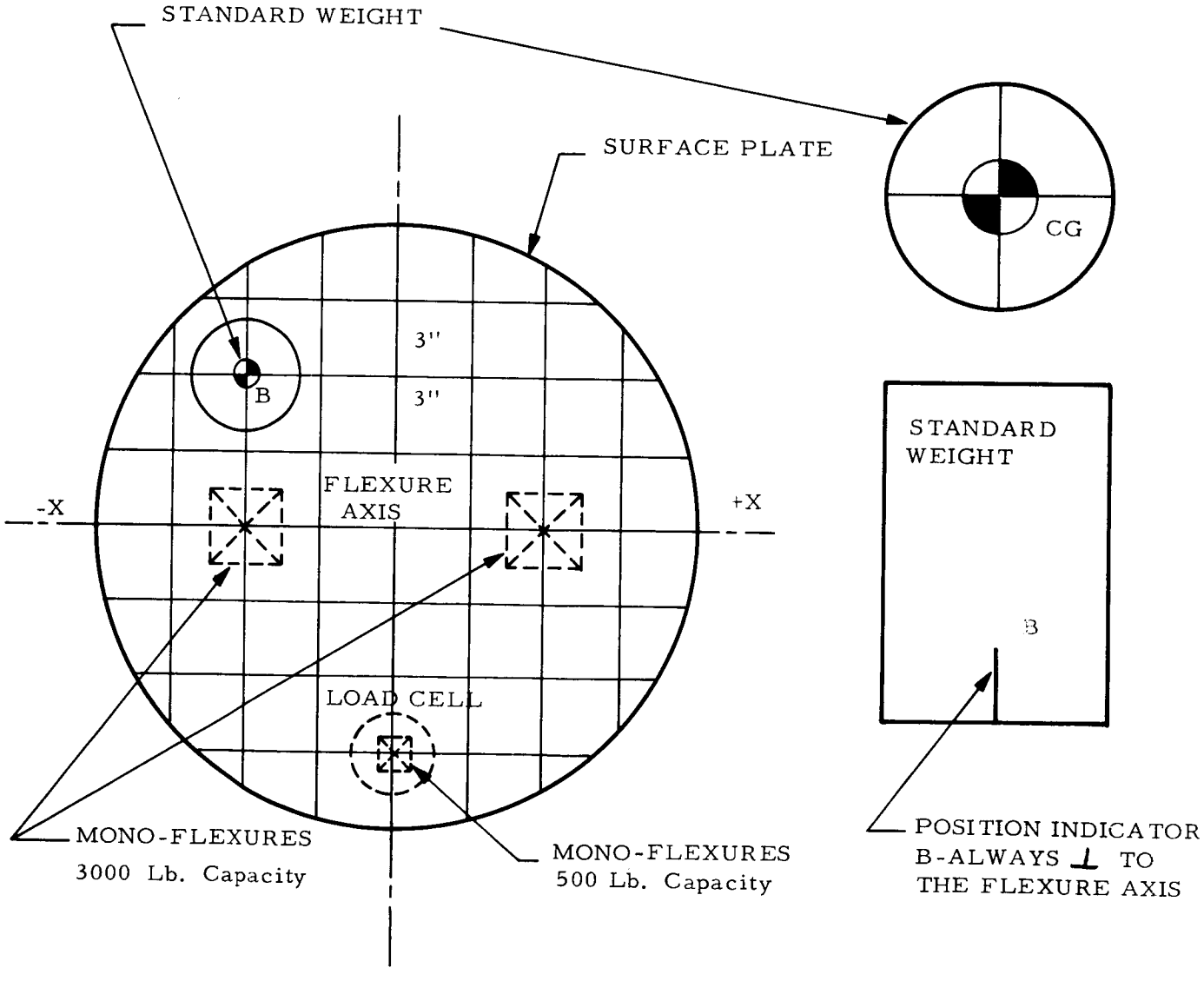

FIGURE 85

STATIC TEST LOAD TEST ARRANGEMENT

FIGURE 86
STATIC LOAD TEST RESULTS -
-0.48 lb. WEIGHT

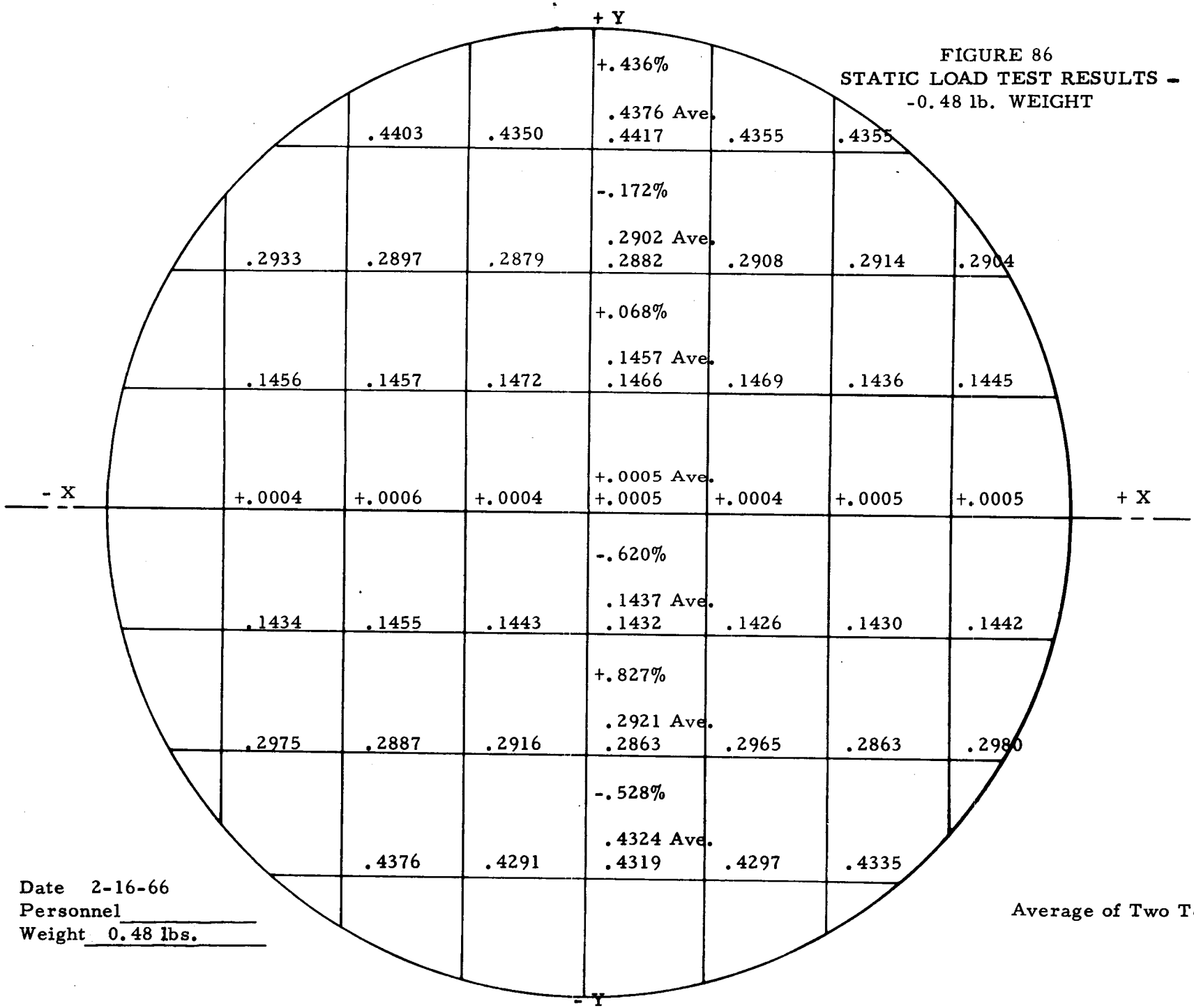

Date 2-16-66
Personnel
Weight 0.48 lbs.

Average of Two Tests

FIGURE 87
STATIC LOAD TEST RESULTS -
5.0 lb WEIGHT

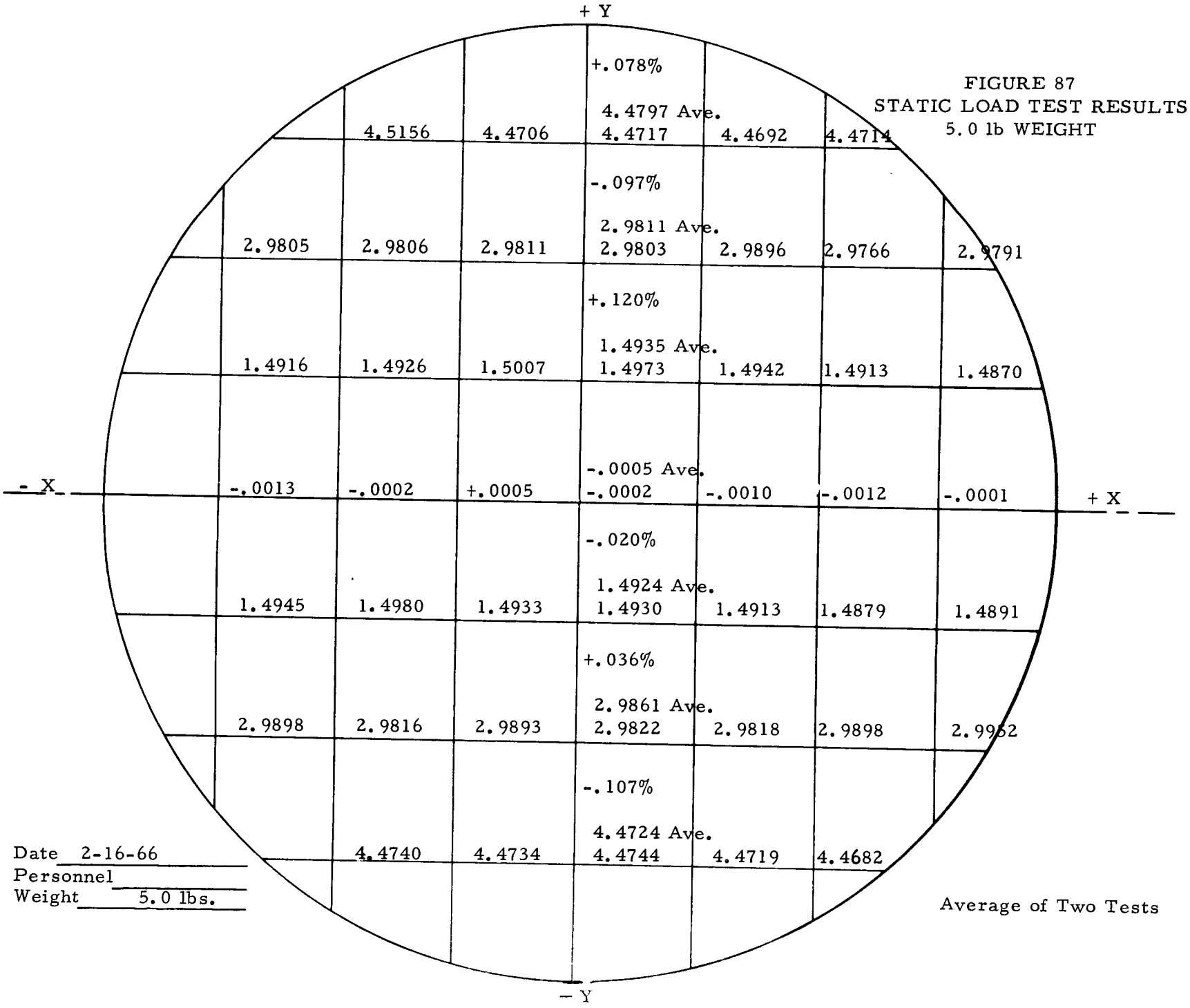

Date 2-16-66
Personnel
Weight 5.0 lbs.

Average of Two Tests

FIGURE 88
STATIC LOAD TEST RESULTS -
9.69 lb. WEIGHT

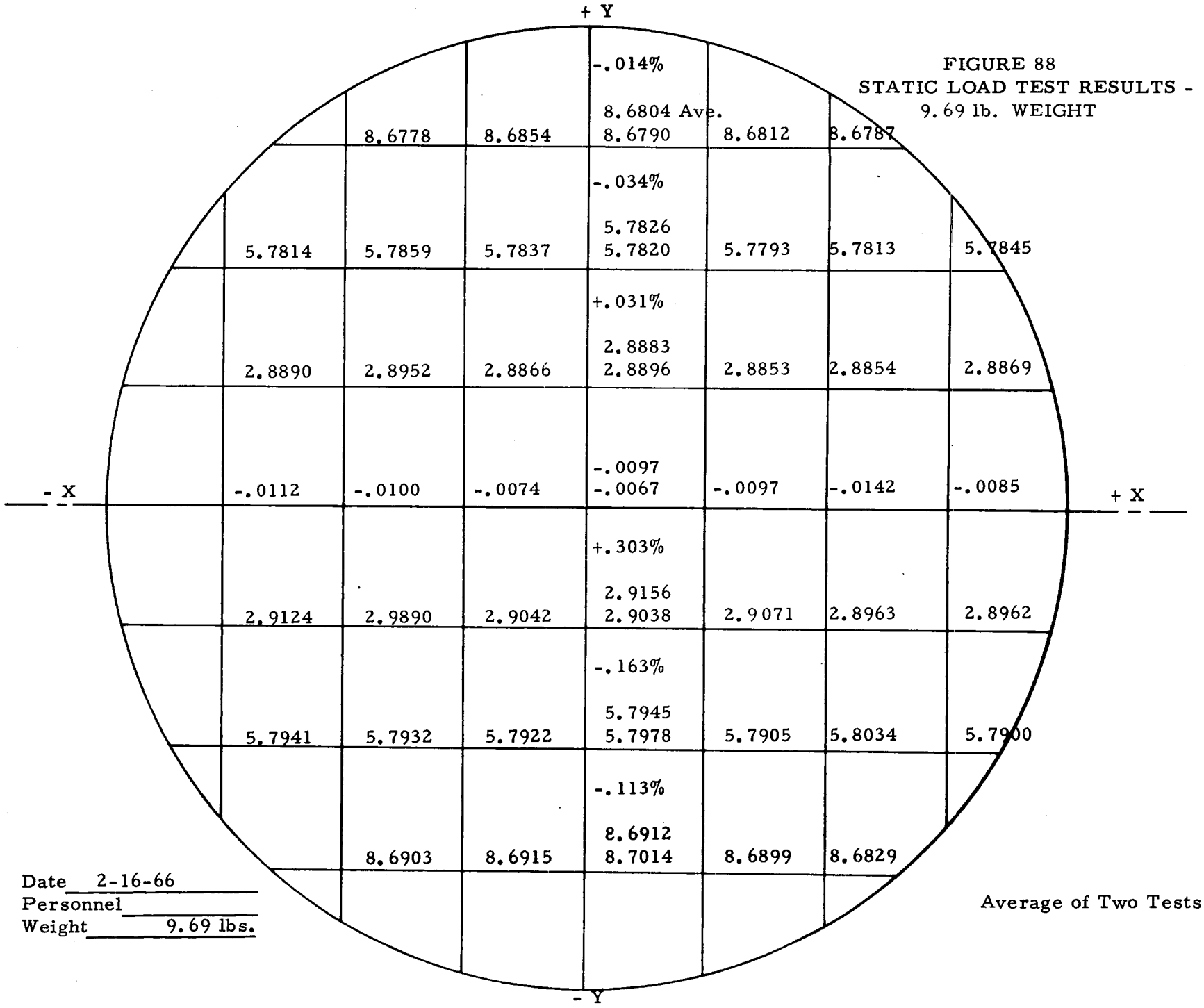

Date 2-16-66
Personnel
Weight 9.69 lbs.

Average of Two Tests

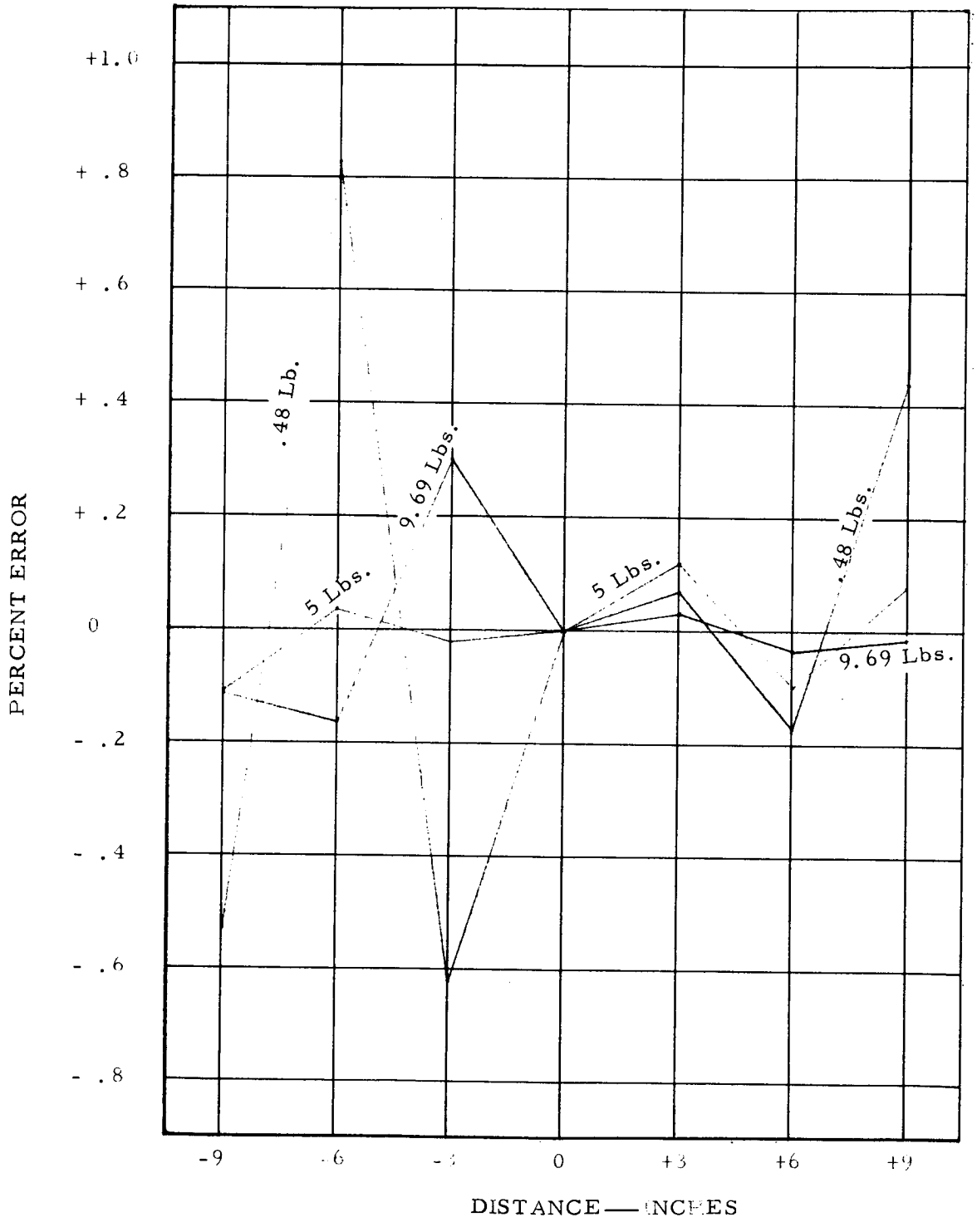

Figure 89

PERCENT ERROR

design, they were not as good for the 0.48 lb. weight. This is believed due to a considerable amount of amplifier instability experienced during the tests. This instability would naturally have a larger effect on the lower output levels.

Figure 90 is a plot of the actual torque error for each of the weights. It can be seen that whereas the percent error was larger for the 0.48 lb. weight, the torque error is larger for the 9.69 lb. weight. This is due to the large ratio of the two weights. Except for one reading with the 9.69 lb. weight, all errors were well within the normal accuracy rating of the load cell.

2.2.1.3.4 Conclusions

It can be concluded that the product of inertia machine should be operated with the load cell in tension for best results. The static error should be less than 0.5% for unbalanced loads of more than one-half pound under this condition. Errors in the grid line engraving will not show up in product of inertia measurements since test objects will be located on the support plate in the position that gives a null on the output meter. The center of gravity is then directly over the flexure axis.

2.2.1.3.5 Recommendations

To improve the measurement accuracy it is recommended that high stability instrumentation be used. Better results could also be obtained with the test object orientated so as to place the load cell in tension when the machine is running.

2.2.2 System Analysis

2.2.2.1 Evaluation Tests

2.2.2.1.1 Description of Equipment

In order to determine the principal axes of an object, it is necessary to know the product of inertia of the object. This can be measured with the product of inertia machine developed by SPACO, INC. for MSFC. The machine rotates the test object about its center of gravity. If the product of inertia about the rotational axis is not zero, a torque will be developed by the unbalanced dynamic force. This force will tend to tilt the table upon which the test object is secured. The tilting force, or torque, is measured by a load cell which supplies the restraining force. The load cell output is amplified and measured by a digital voltmeter. The angular velocity is determined by measuring the rotational period. Timing pulses generated photoelectrically by the machine's rotation are presented to an electronic counter which

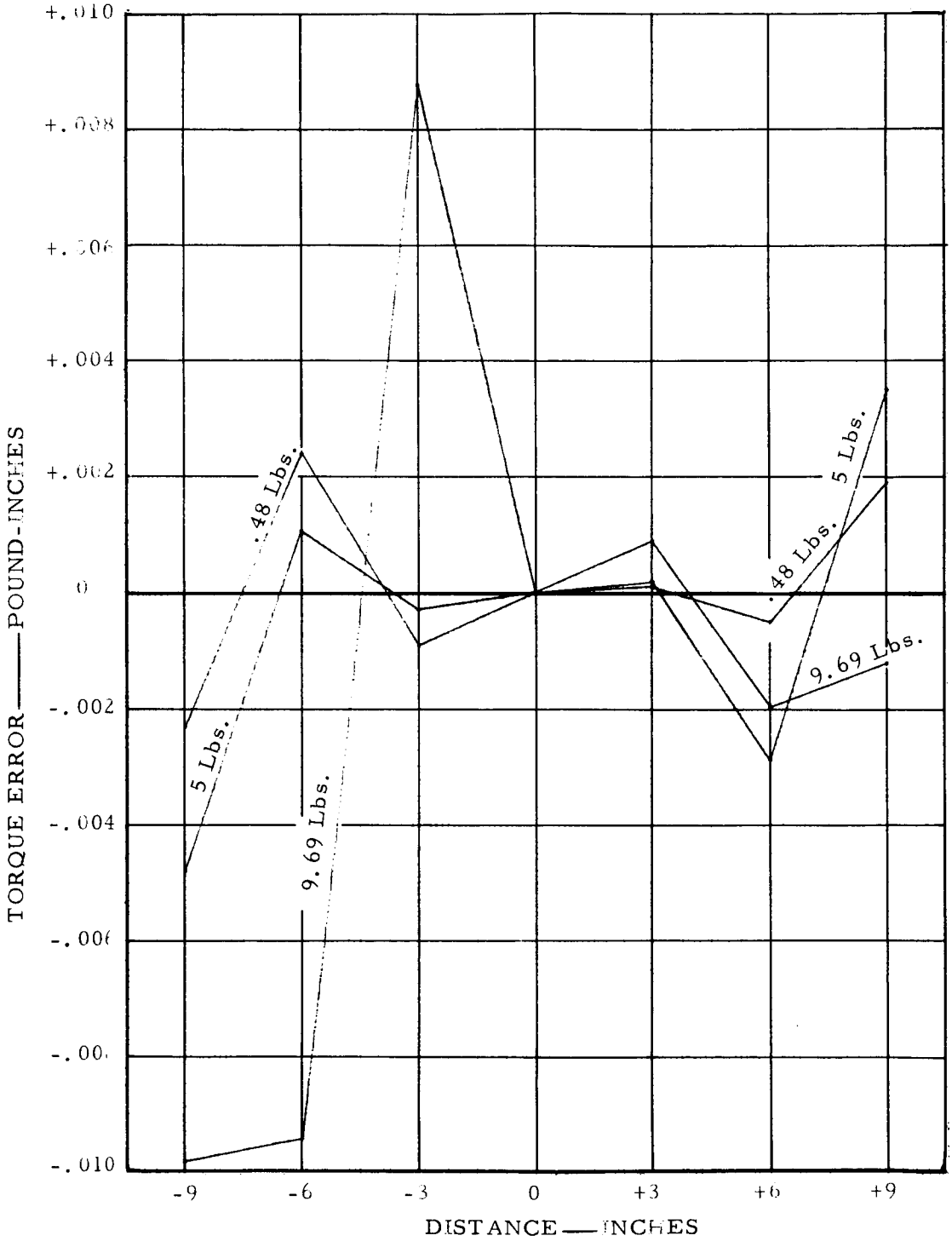

FIGURE 90

TORQUE ERROR

operates in the period measurement mode. Knowing the torque and angular velocity, the product of inertia is computed from the classical equation:

$$\text{Product of Inertia} = \frac{\text{Torque}}{(\text{Angular Velocity})^2} \tag{117}$$

Operational amplifiers on the E.A.I. Model TR-48 analog computer were used to amplify the load cell output voltage and drive a Hewlett-Packard Model 3460A digital voltmeter. A gain potentiometer was used to standardize the output. A zeroing potentiometer was also incorporated. The computer's regulated power supply was used to excite the load cell.

The rate table's rotational speed controls and speed calibrator was furnished with the rate table. Any speed up to 1500 degress per second (26.18 radians per second) is available from the unit. The speed calibrator provides timing pulses to drive an electronic counter. The pulses are derived from a photo-electric transducer mounted on the rate table. A C.M.C. Model 226A electronic counter was used to measure the period of the timing pulses. The period and torque was used in the following modified equation to obtain the product of inertia:

$$\text{Product of Inertia} = \frac{\text{Torque x Period}}{4\pi^2} \tag{118}$$

2.2.2.1.2 Procedure

When the static tests were run to determine the tilt table accuracy, a stabilizing rod was used to tie the load cell to the tilt table support bar. It was expected that this measure would offset the effect of centrifugal force on the load cell during dynamic tests. Preliminary tests revealed that the stabilizing rod was unsatisfactory, so another method of compensation was tried. This involves the use of the counterweight as previously described. The counterweight weighs 1.5 lbs. which is equal to the weight of the load cell. The position of the counterweight on the rod was adjusted to make the centrifugal force acting on it equal to that acting on the load cell. This compensates for all speeds and removes the centrifugal force influence from all parts of the load cell except the sensitive element itself, which cannot be compensated mechanically. The sensitive element has a low mass, however, and does not appear to be influenced adversely. The effectiveness of the counterweight and its bearing plate can be seen in Figure 93 which shows the dynamic test results with the tilt table unloaded. Curve 2, in Figure 93, shows the product of inertia

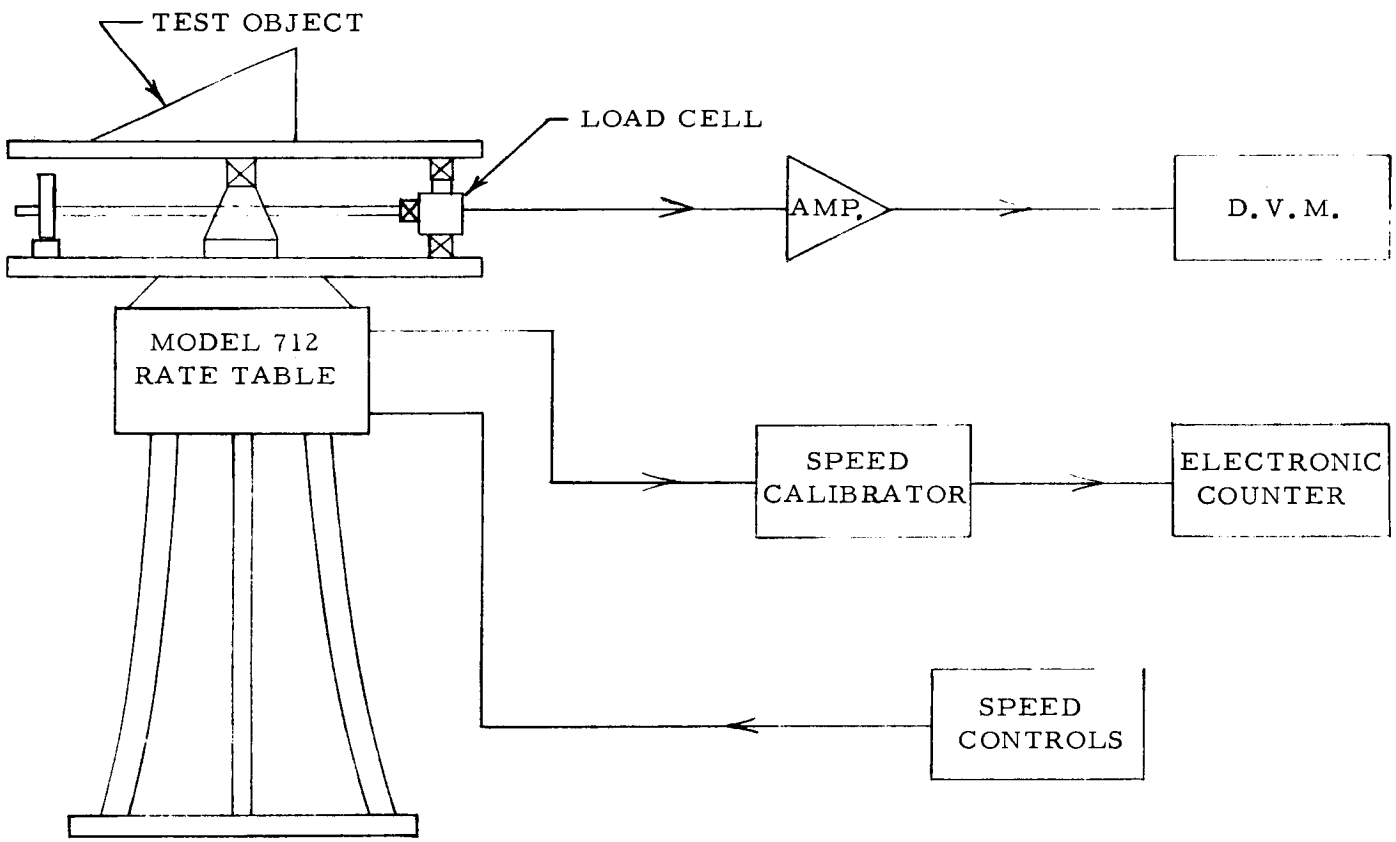

FIGURE 91

PRODUCT OF INERTIA
SYSTEM BLOCK DIAGRAM

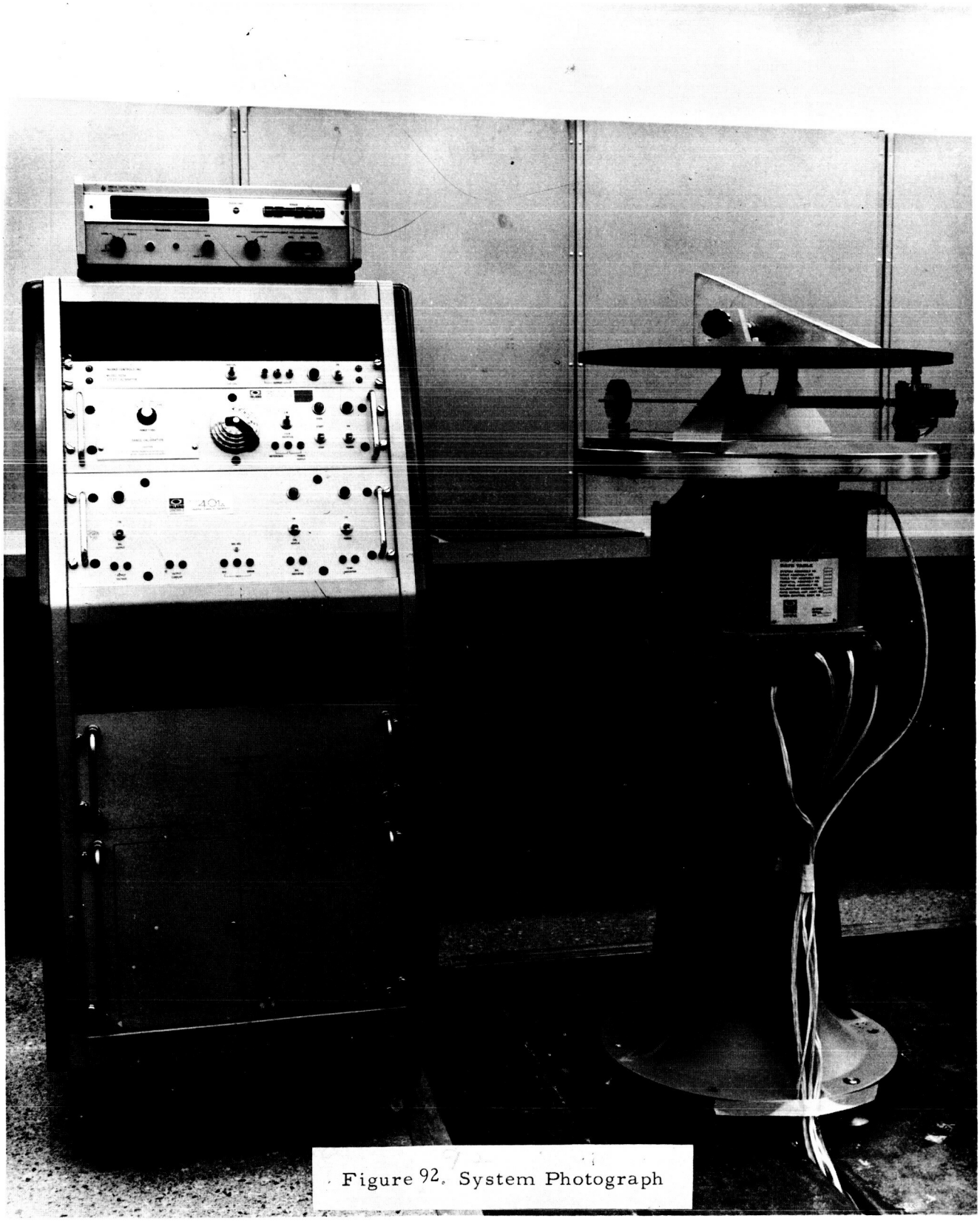

Figure 92. System Photograph

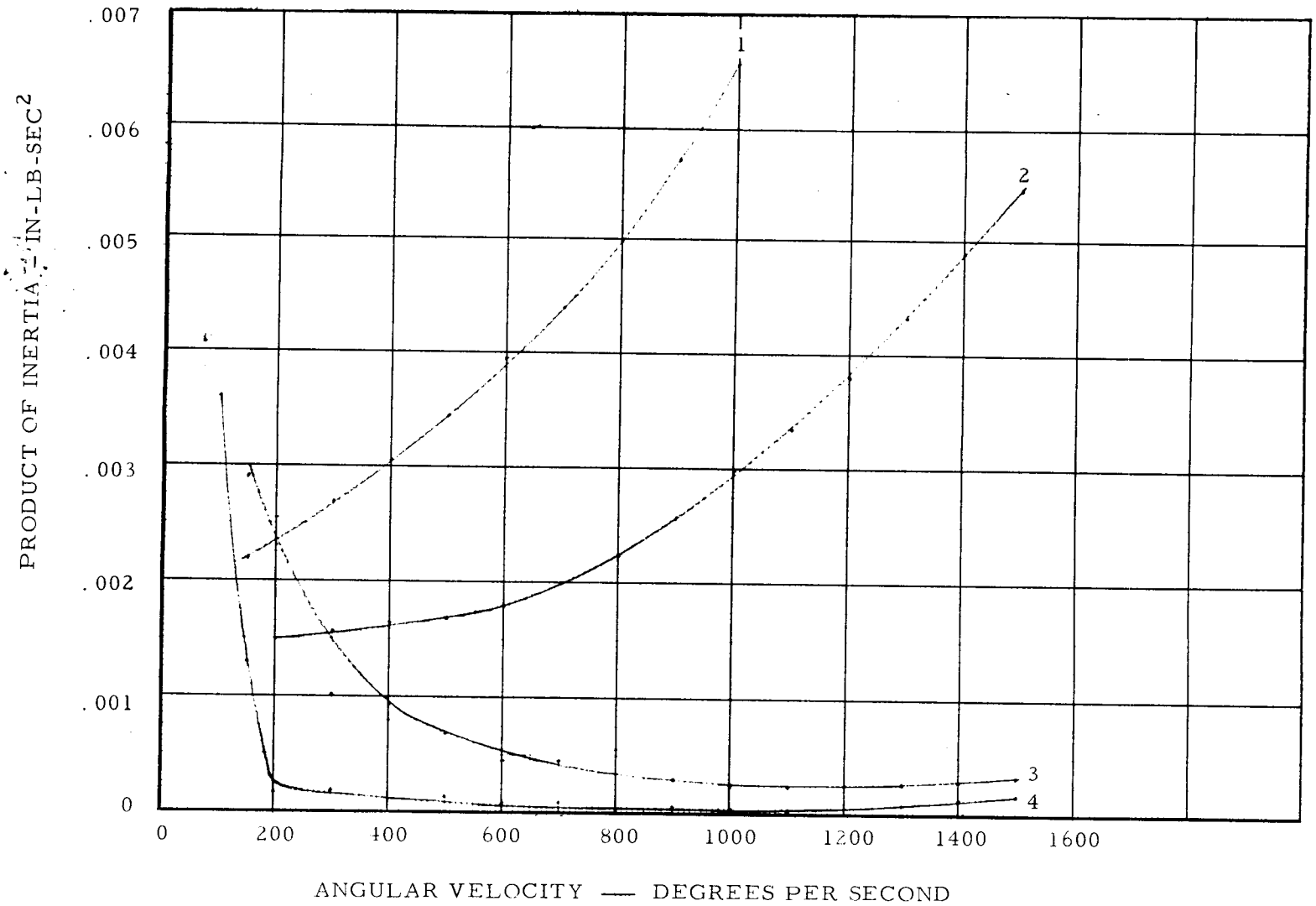

FIGURE 93
TABLE UNLOADED

measured without the counterweight. Curve 1 shows the effect of attaching a one-half pound weight to the load cell. This clearly shows the effect of centrifugal force. Curve 3 was measured with the counterweight added to the system, but without the bearing plate. Curve 4 was measured with the bearing plate added to remove bending moment from the connecting rod. This bending moment is a result of the g force acting on the counterweight. The slight upturn in Curve 4 at high speeds could be due to a slight missmatch between the load-cell and counterweight; or, it could be due to the centrifugal force, which acts on the sensitive element of the load cell, coming into play. The test procedure is included as Appendix B5.

2.2.2.1.3 Test Results

Tests were run on four representative triangular standard test blocks. The results are shown in Figures 94, 95, 96, and 97. The tests were run first without the load cell counterweight. Then they were repeated with the counterweight installed. In each figure, the curve legend is as follows:

Curve 1 - Load cell in tension; w/o counterweight.
Curve 2 - Load cell in compression; w/o counterweight.
Curve 3 - Load cell in tension; w/counterweight.
Curve 4 - Load cell in compression; w/counterweight.
Dashed Curve - Computed product of inertia based on weight and dimensions.

Examination of the curves shows that the uncompensated tests have a divergent tendency with increasing speed that is more prominent for the test blocks having the lower product of inertia. This is to be expected since the load cell centrifugal force would have a greater influence on lower product of inertia test blocks. In all cases after the counterweight was installed, the curves have a convergent tendency.

It is interesting to note that all of the curves which extend below 300 degrees per second either turn up or down at very low speeds. In order to investigate this effect for Curve 3 in Figure 96, a typical curve, the torquing force was plotted versus ω^2 for low speeds. The result is the curve in Figure 98 which shows a slight zero offset force of 0.008 lbs. When this correction was applied, Curve 5 in Figure 96 resulted. Although this curve is much flatter than Curve 3, the flaring tendency is still observed, but at a lower speed. It is now apparent that this flare effect is due to measurement inaccuracies at low speeds which is the same as saying we are approaching the indeterminate form of zero divided by zero.

2.2.2.2 Error Analysis

There are seven (7) possible sources of errors in the product of inertia machine, they are as follows:

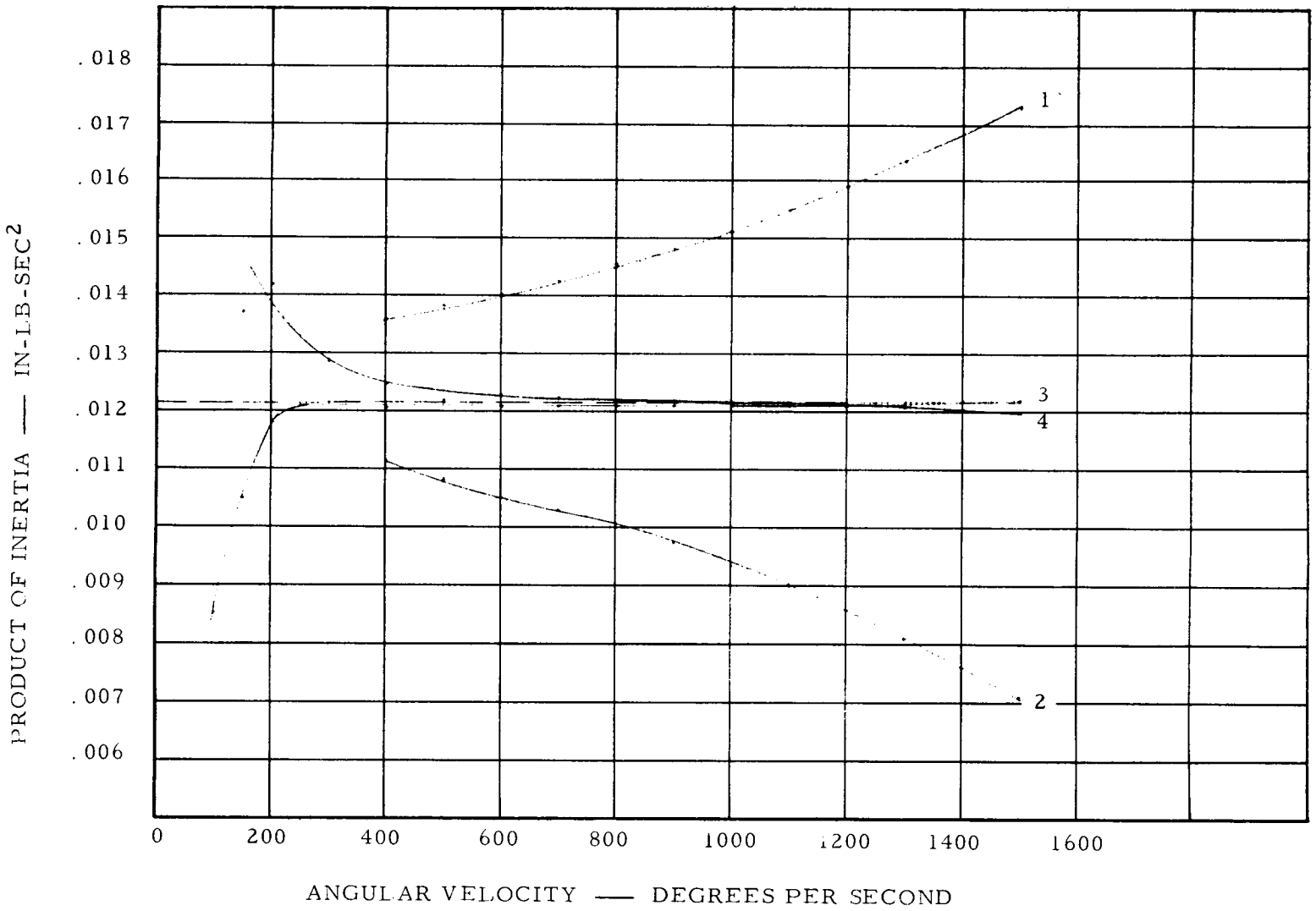

Figure 94
TEST BLOCK NO. 1

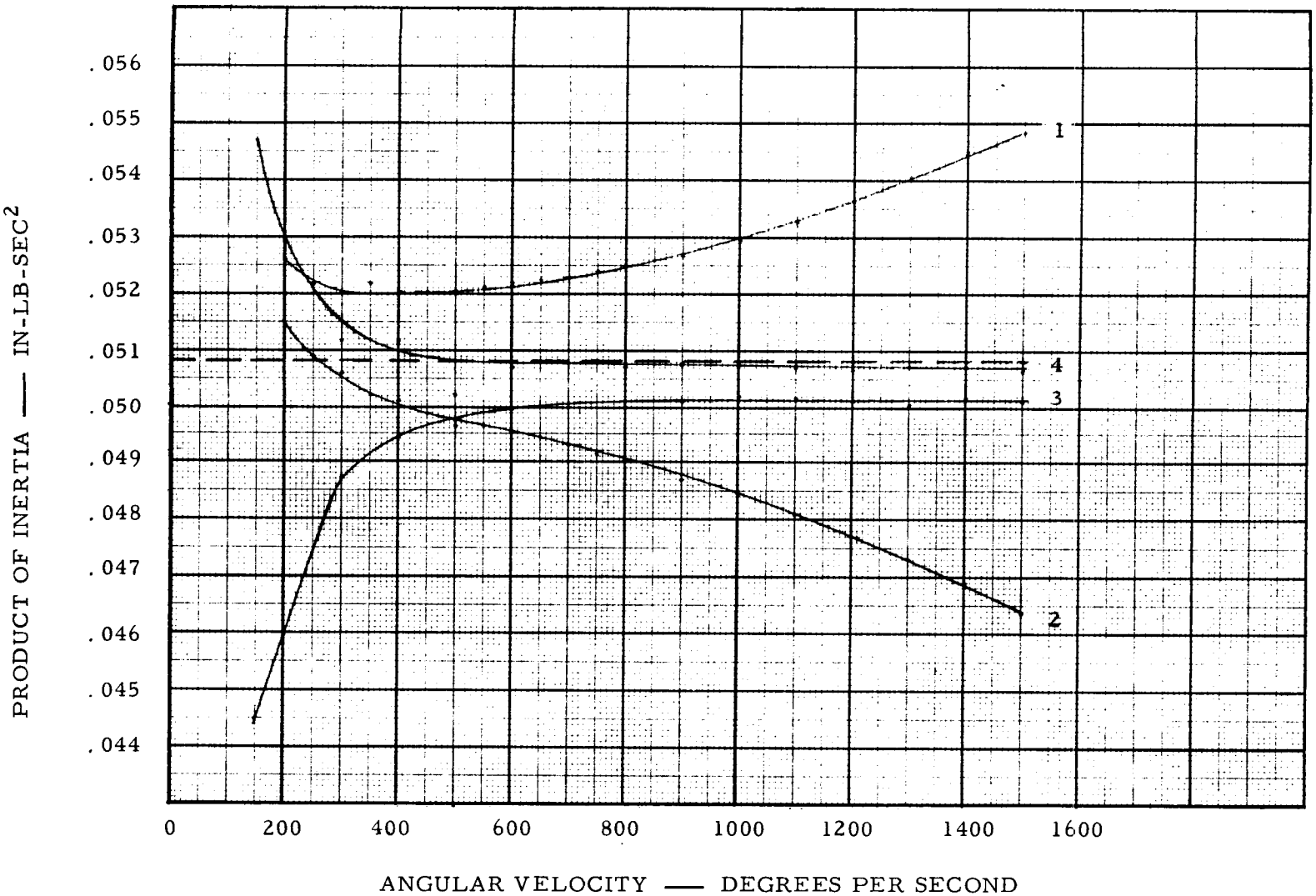

FIGURE 95
TEST BLOCK NO. 2

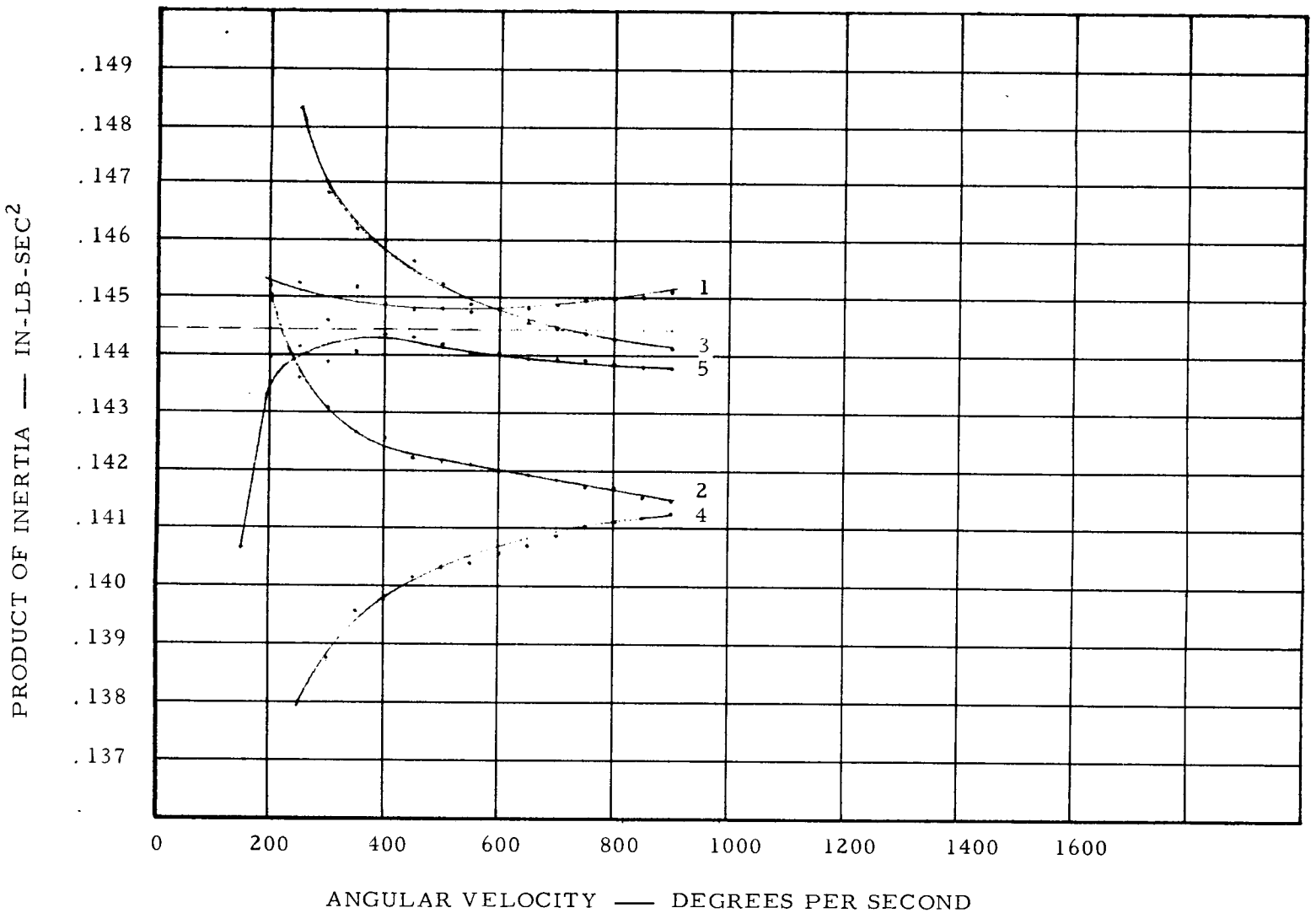

FIGURE 96
TEST BLOCK NO. 3

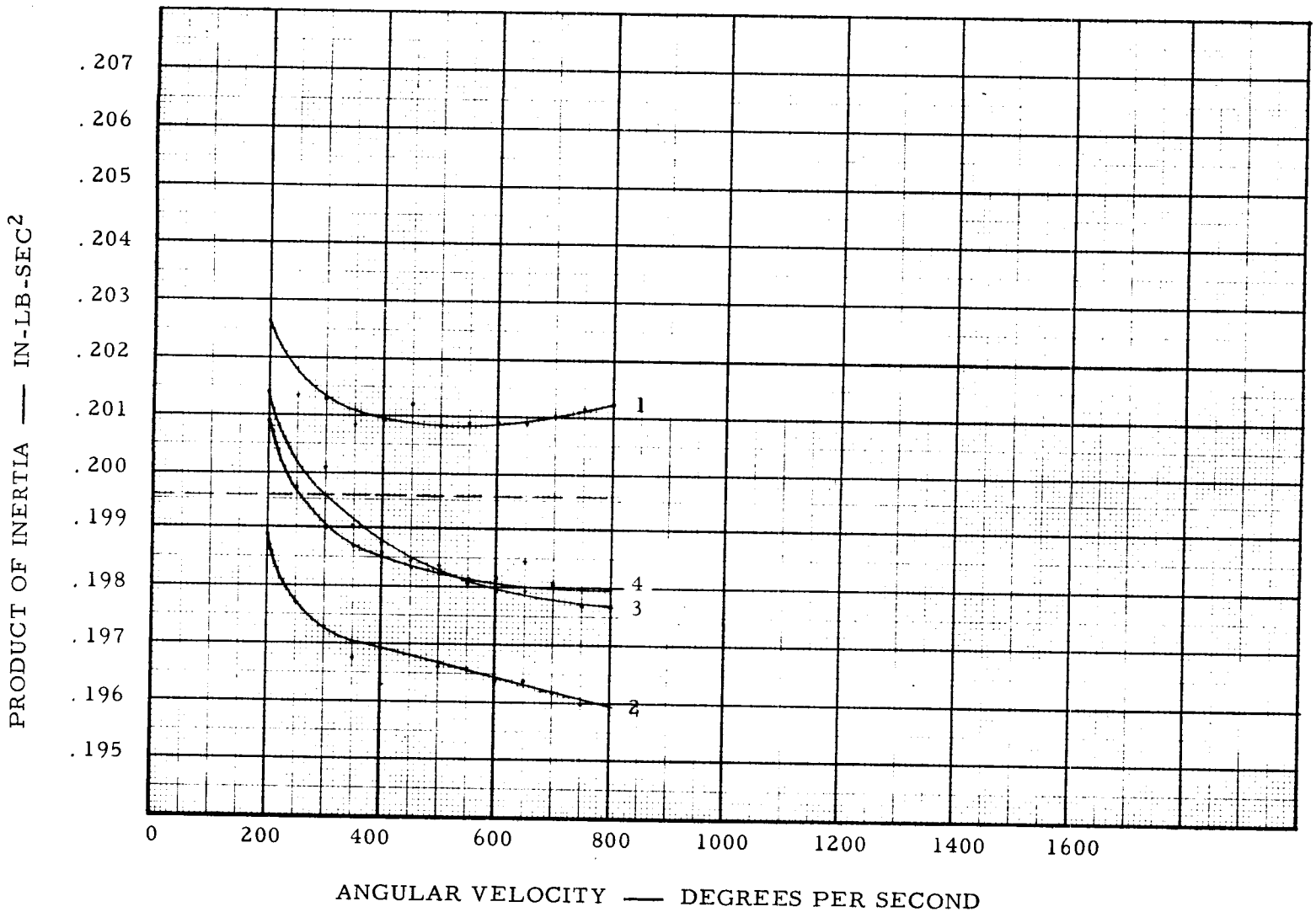

FIGURE 97
TEST BLOCK NO. 4

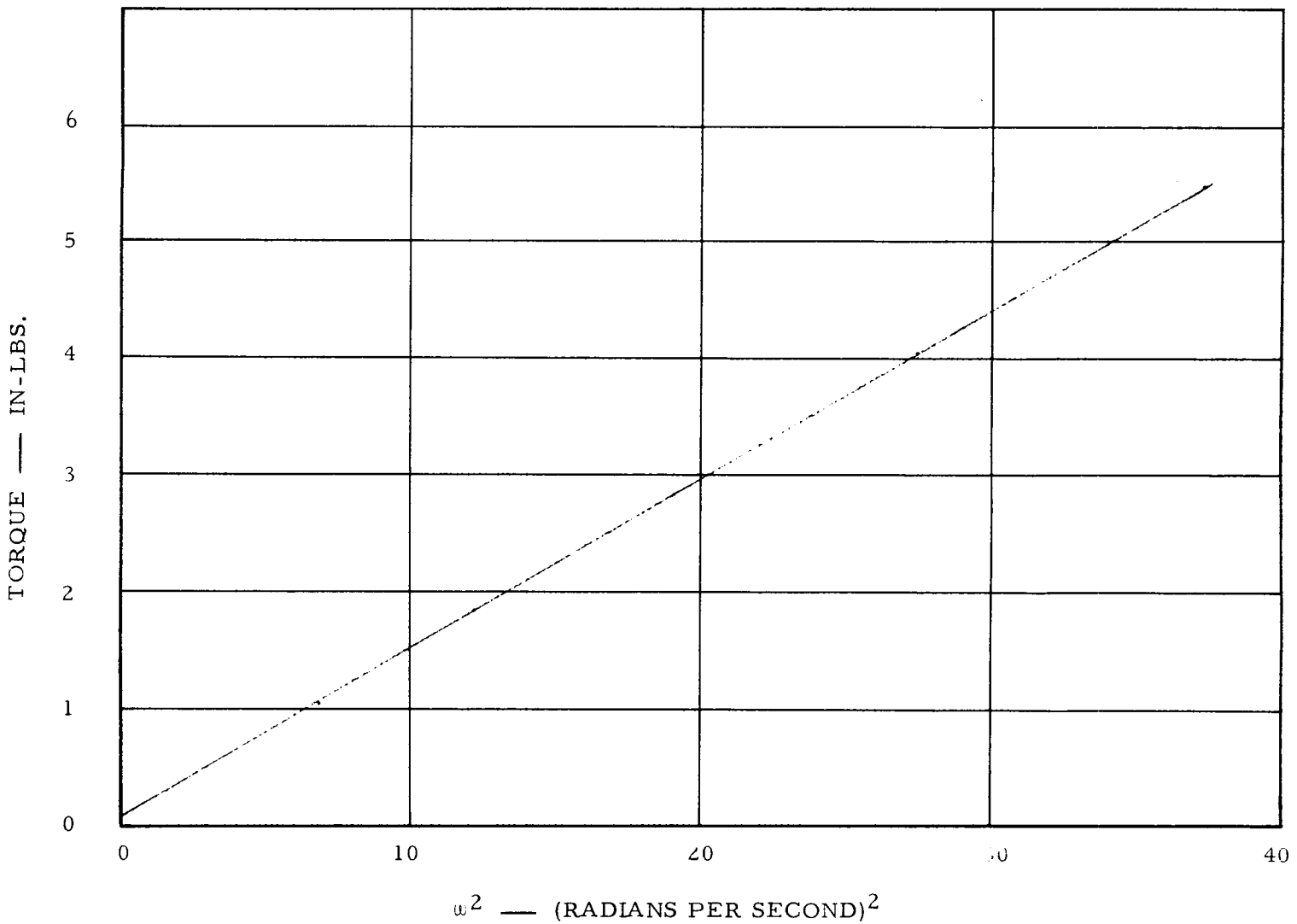

FIGURE 98
ZERO OFFSET

1. Centrifugal force on load cell
2. Gyroscopic effects
3. Instrumentation error
4. Load cell tilt
5. Test object tilt
6. Table tilt
7. Aerodynamic effects

These error sources listed above cause the system to depart from the ideal case which is given by the classical equation:

$$I_{xy} = \frac{f_T s_1}{\omega^2} \tag{119}$$

where:

I = Product of Inertia
f_T = Torquing Force
s_1 = Distance between table tilt axis and upper load cell flexure point.
ω = Angular Velocity

We will examine them in the order in which they appear in the list.

2.2.2.2.1 Sources of Error

2.2.2.2.1.1 Centrifugal Force

The centrifugal force effect has been discussed previously. It can be almost completely neutralized with the counterweight arrangement, at least within the speed capabilities of the present machine.

2.2.2.2.1.2 Gyroscopic Effect

The gyroscopic effect, caused by the combination of the machine and earth rotations, produces a torque on the machine. This torque tends to tilt the machine towards one of the earth's poles (depending on the direction of rotation of the machine). The result of this torque is to cause an oscillating torque on the tilt table whose period is the same as the machine's rotational period. This results in a small ripple in the load cell output. Although the amplitude of this ripple increases with speed, so does its frequency. Therefore, it is easily removed by filtering and presents no problem.

2.2.2.2.1.3 Instrumentation Error

The instrumentation error is limited primarily to load cell and amplifier errors. The R.M.S. error of the load cell is approximately 0.07%. Some

drift was noticed in the operational amplifiers used in the test set-up. A high quality load cell amplifier should make this error source negligible. The high resolution digital voltmeter used in the tests did not contribute to the instrumentation error.

2.2.2.2.1.4 Load Cell Tilt

When the table tilts from its normal position, the load cell axis is no longer normal to the tilt table. This means that the load cell output no longer represents the true torque.

Figure 99 (a) shows the tilt table with the three flexural points. The structural triangle connecting these flexural points is given along with a force triangle in Figure 99 (b).

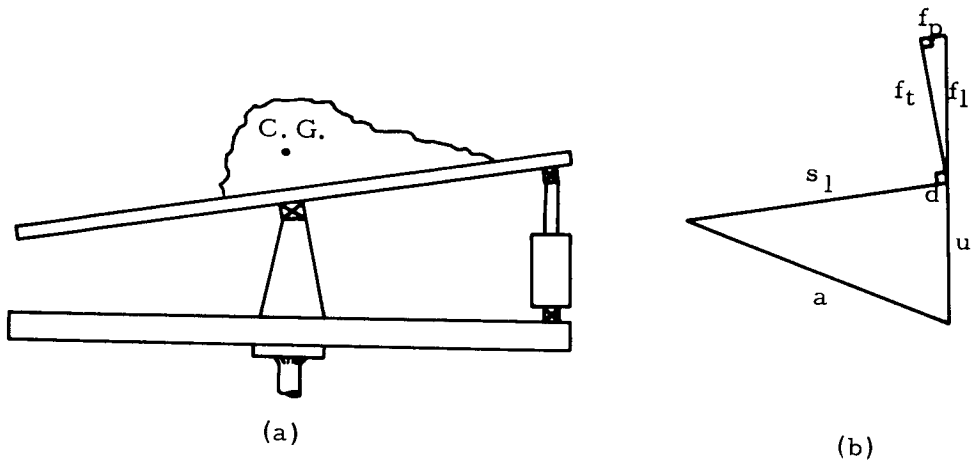

Figure 99. (a) Tilt Table, (b) Structural and Force Triangles

Examining the two triangles reveals that β in the force triangle equals α in the structural triangle. This is true because f_P is parallel to s_l and f_L is parallel to u. It therefore follows that:

$$f_T = f_L \sin \beta = f_L \sin \alpha \tag{120}$$

where:

f_T = the torquing force which is normal to the tilt table surface and applied through the upper load cell flexural point.

f_L = the axial force acting on the load cell (along u).

α = the angle between the tilt table surface and the load cell axis (the table surface is parellel to s_1).

β = the angle between f_L and f_P.

Applying the law of cosines to the structural triangle gives:

$$\cos \alpha = \frac{s_1^2 - a^2 + u^2}{2 s_1 u} \tag{121}$$

where:

a = the distance between the tilt table flexural axis and the upper load cell flexural point.

u = the distance between the upper and lower load cell flexural points.

Since the variable u is a function of the axial force on the load cell it can be replaced with that function. Thus:

$$u = f(f_L) = k_1 + k_2 f_L \tag{122}$$

where:

k_1 = the unloaded length between the load cell's flexural points.

k_2 = the load cell's spring rate (rated deflection/ rated load).

f_L = the axial force on the load cell*

Replacing u with $f(f_L)$ in Equation 121 we get:

$$\cos \alpha = \frac{s_1^2 - a^2 + (k_1 + k_2 f_L)^2}{2 s_1 (k_1 + k_2 f_L)} \tag{123}$$

Substituting α from Equation 123 into Equation 120 we get:

*By definition the load cell force, f_L, is taken as positive when the load cell is in tension.

$$f_T = f_L \sin \cos^{-1} \frac{s_1^2 - a^2 + (k_1 + k_2 f_L)^2}{2s_1(k_1 + k_2 f_L)} \tag{124}$$

Equation 124 corrects the load cell force for load cell tilt.

2.2.2.2.1.5 Test Object Tilt

The table is shown tilted in Figure 100. This causes the center of gravity, C.G., of the test object to be displaced from the rotational axis thereby producing a centrifugal force f_{C1}. The force f_1, which is a component of f_{C1}, will cause a new torque, $f_1 s_2$, which will aid that due to the product of inertia. Thus, we must subtract this new torque from $f_T s_1$ in order to neutralize it.

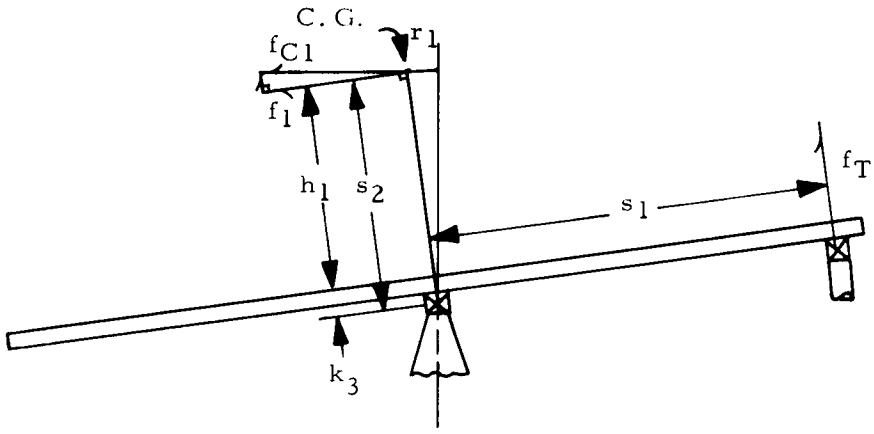

Figure 100. The effect of centrifugal force due to test object tilt.

Thus:

$$I_{xy} = \frac{f_T s_1 - f_1 s_2}{\omega^2} \tag{125}$$

The following derivation is based on these four assumptions:

1. $f_1 \approx f_{C1}$
2. $r_1 \approx$ the arc through which the test object C.G. point rotates due to tilt.
3. The angle of tilt is proportional to f_T.
4. $f_T \approx f_L$

These assumptions are valid because the angle of tilt is very small (approximately 2 minutes of arc). The centrifugal force acting at the center of gravity of the test object is given by:

$$f_{C1} = \frac{W_o}{g} r\omega^2 \tag{126}$$

where:

f_{C1}	=	the centrifugal force
W_o	=	the test object's weight
g	=	the acceleration due to gravity
r_1	=	the radius of gyration

From Assumption 1:

$$f_1 \approx f_{C1} \tag{127}$$

Therefore:

$$f_1 \approx \frac{W_o}{g} r_1 \omega^2 \tag{128}$$

Since the C. G. point moves through the same angle as the table tilts, and based on Assumption 2:

$$r_1 \approx \frac{s_2}{s_1} k_2 f_L \tag{129}$$

where: s_2 = the height of the C. G. point above the tilt table flexural axis.

Substituting Equation 129 into Equation 128, we get:

$$f_1 \approx \frac{W_o}{g} \left(\frac{s_2}{s_1}\right) k_2 f_L \omega^2 \tag{130}$$

Multiplying both sides by s_2:

$$f_1 s_2 \approx \frac{W_o s_2^2 k_2 f_L \omega^2}{g s_1} \tag{131}$$

Since:

$$s_2 = h_1 + k_3 \tag{132}$$

where:

h_1 = the normal distance from the C. G. point to the tilt table surface.

k_3 = the distance between the tilt table surface and the table's flexural point.

Substituting Equation 132 into the right hand side of Equation 131 and rearranging we get:

$$f_1 s_2 \approx \frac{k_2 (h_1 + k_3)^2 W_o f_L \omega^2}{g s_1} \tag{133}$$

Equation 133 is the torque which must be subtracted from the torque $f_T s_1$ to correct for test object tilt.

2.2.2.2.1.6 Table Tilt

When the table tilts, the centrifugal force acting on the table causes a torque, $f_2 h_2$, which tends to prevent the table from tilting.

Figure 101 shows the centrifugal force, f_{C2}, acting on the centroid, C, of each half of the table. The derivation of the torque $f_2 h_2$ is based on the following assumptions:

1. The displacement of the table's center from the rotational axis is negligible.
2. $r_2 \approx s_3$

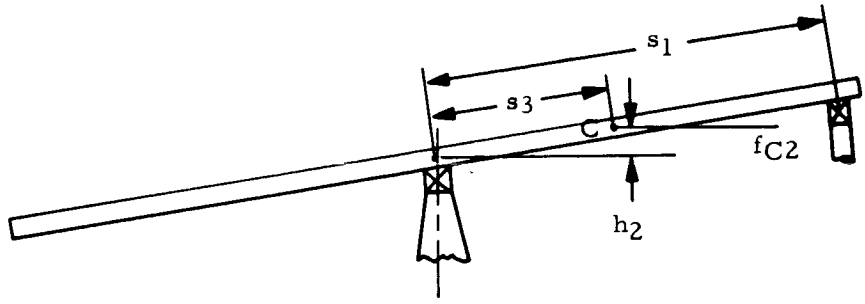

Figure 101. The effect of centrifugal force due to table tilt.

These assumptions are valid because the angle of tilt is very small (approximately 2 minutes of angle). The centrifugal force acting on each half of the table is given by:

$$f_{C2} = \frac{W_T/2}{g} r_2 \omega_2 \tag{134}$$

where:

f_{C2}	=	the centrifugal force acting on each half of the table.
W_T	=	the weight of the table.
r_2	=	the radius of gyration.

Since f_{C2} is one-half the force producing the torque, f_2h_2:

$$f_2h_2 = 2f_{C2}h_2 \tag{135}$$

where:

f_2	=	the force tending to prevent the table from tilting.
h_2	=	the moment arm of f_2 (and f_{C2}).

Substituting Equation 134 into Equation 135, we get:

$$f_2h_2 = \frac{W_T}{g} r_2 \omega^2 h_2 \tag{136}$$

From Assumption 4:

$$r_2 \approx s_3 \tag{137}$$

where: s_3 = the distance from the table's center to the centroid, C.

Therefore:

$$f_2 h_2 \approx \frac{W_T}{g} s_3 \omega^2 h_2 \tag{138}$$

Based on the location of the centroid of a semicircle:

$$s_3 = 0.4244 r_T \tag{139}$$

where: r_T = the table's radius

The table's weight is computed as follows:

$$W_T = \pi r_T^2 t_T d_T \tag{140}$$

where: t_T = the table thickness.
d_T = the density of the table.

The moment arm is computed as follows:

$$h_2 \approx \frac{s_3}{s_1} k_2 f_L \tag{141}$$

Substituting Equation 139, Equation 140, and Equation 141 into the right hand side of Equation 138, we get:

$$f_2 h_2 \approx \frac{\pi r_T^2 t_T d_T}{g} \cdot \frac{(0.4244 r_T)^2 \omega^2}{s_1} k_2 f_L \tag{142}$$

Equation 142 is the torque which must be added to the torque $f_T s_1$ to correct for table tilt.

2.2.2.2.1.7 Aerodynamic Drag

The calssical aerodynamic drag equation is given as:

$$D = C_D(\rho/2)V^2A \tag{143}$$

where:

D	=	the drag force in pounds.
C_D	=	the drag coefficient.
ρ	=	the air density in slugs per cubic feet.
V	=	the air velocity in feet per second.
A	=	the projected frontal area in feet^2.

The air velocity, V, in Equation 143 depends on the distance of the centroid of the projected frontal area from the table's rotational axis.
is found as follows:

$$V = \omega R \tag{144}$$

where:

R	=	the distance of the centroid of the projected frontal area from the table's rotational axis.

Substituting Equation 144 into Equation 143, we get:

$$D = C_D(\rho/2)(\omega R)^2A \tag{145}$$

The drag force moment arm, s_4, is found from:

$$s_4 = h_3 + k_3 \tag{146}$$

where:

s_4	=	the height of the centroid of the projected frontal area, A, above the tilt table flexural axis.
h_3	=	the height of the centroid of the projected frontal area, A, above the table surface.

Multiplying Equation 145 by Equation 146 we get the torque due to air drag:

$$Ds_4 = C_D(\rho/2)(\omega R)^2 A(h_3 + k_3) \tag{147}$$

Equation 147 is the torque which must be added to or, depending on the test object configuration, subtracted from the torque $f_T s_1$ to correct for aerodynamic drag.

2.2.2.2.2 Mathematical Model

The product of inertia equation which corrects for load cell tilt, test object tilt, table tilt, and aerodynamic drag will be of the form:

$$I_{xy} \approx \frac{f_T s_1 - f_1 s_2 + f_2 h_2 \pm Ds_3}{\omega^2} \tag{148}$$

Substituting Equation 124, Equation 133, Equation 142, and Equation 147 into Equation 148 we obtain the corrected product of inertia equation:

$$I_{xy} \approx \frac{f_L s_1 \sin \cos^{-1} \dfrac{s_1^2 - a^2 + (k_1 + k_2 f_L)^2}{2s_1(k_1 + k_2 f_L)} - \dfrac{k_2(h_1 + k_3) W_o f_L \omega^2}{g s_1} + \dfrac{\pi r_T^2 t_T d_T}{g} \cdot \dfrac{(0.4244 r_T)^2 \omega^2}{s_1} k_2 f_L \pm}{\omega^2}$$

$$\frac{C_D(\rho/2)(\omega R)^2 A(h_3 + k_3)}{\omega^2} \tag{149}$$

Simplifying Equation 149 we get:

$$I_{xy} \approx \frac{f_L s_1}{\omega^2} \sin \cos^{-1} \frac{s_1^2 - a^2 + (k_1 + k_2 f_L)^2}{2 s_1 (k_1 + k_2 f_L)} -$$

$$\frac{k_2 (h_1 + k_3) W_o f_L}{g s_1} + \frac{\pi r_T^2 t_T d_T (0.4244 r_T)^2}{g s_1} k_2 f_L \pm C_D (\rho/2) \cdot$$

$$R^2 A (h_3 + k_3) \qquad (150)$$

Equation 150 is very close to the exact product of inertia equation.

2.2.2.3 Conclusions

So that the system equation (equation 150 above) may be applied to a typical test made with the existing system, the system and test block no. 2 parameters, along with the test conditions, are given as follows:

System Parameters –

a	=	10.788 in.
d_T	=	0.098 lbs./in.^{3}
k_1	=	4.047 in.
k_2	=	0.00024 in./lb.
k_3	=	1.094 in.
s_1	=	10.000 in.
r_t	=	12.00 in.
t_T	=	0.594 in.

Test Block No. 2 Parameters –

A	=	17.367 in.^{2}
C_D	=	1.28 in.
h_1	=	1.7799 in.
h_3	=	1.800 in.
R	=	2.2172 in.
W_o	=	22.212 lbs.

Test Conditions –

f_L = 3.4220 lbs.
g = 385.7 in./sec^2
ω = 26.1799 rad./sec.
ρ = 0.1146×10^{-6} lb. sec.^{2}/in.^{4}

Using these parameters, the following values for each term of Equation 150 were computed to be:

Load cell tilt correction:		+ .050107 in. lb. sec.^{2}
Test object tilt correction:		- .00001359 in. lb. sec.^{2}
Table tilt correction:		+ .00000036 in. lb. sec.^{2}
Air drag correction:		+ .0000181 in. lb. sec.^{2}
	Total	+ .050112 in. lb. sec.^{2}

Rounding the total off to five significant figures, we get 0.050112 in. lb. sec.^{2} for the corrected product of inertia. The value obtained by using Equation 119, the basic equation, is 0.050107 in. lb. sec.^{2}. Comparing this to the corrected value we get an error of -0.01%.

This is negligible when compared to the R.M.S. load cell error which can amount to 0.07%. Although the load cell force in the above example was only 3.4220 lbs. (compared to the rated value of 25 lbs.), it was approaching the maximum recommended force of 3.5 lbs. The machine becomes unstable around 3.8 lbs.

Examining the corrections shown above, it can be seen that load cell tilt can be neglected since the sin cos^{-1} factor is virtually unity. The table tilt correction is also seen to be negligible. Thus, the test object tilt, aerodynamic effects, and load cell error are the only significant factors.

When the corrected product of inertia, as obtained in the example above, is compared to the calculated value based on the dimensions and weight of the test block, an error of 1.39% is obtained. This relatively large error is believed to be due to a slight amount of slippage of the test block along the tilt table surface with increasing speed. The hold-down fixture design could conceivably permit this. Some amplifier drift was also experienced.

2.2.2.4 Recommendations

It might prove desirable to replace the present load cell with one having a lower load rating, say 5 lbs. This would provide better torque resolution. The use of a high quality load cell amplifier would also afford an improvement, An improved counterweight suspension should be provided. The use of flexures,

for this purpose, should be investigated. Better still would be a tilt system design that would have the load cell at the rotational axis. Aerodynamic effects could be eliminated by providing a symmetrical cover for the tilt table. This cover would enclose the test object and tilt table, being attached to the rate table proper.

2.2.3 Principal Axis

A general computer program was developed for calculating the principal axes and direction cosines of an object. This is the same program as was developed under the 1964-65 phase of the work except that it has been re-written in Fortran IV language for use with the IBM 360 computer.

With this program, the principal axes and direction cosines of an object can be determined if the three moments of inertia and three products of inertia about the same point are known. This program is included in Appendix B6.

2.3 MASS PROPERTIES OF LIQUIDS

2.3.1 Test Program

2.3.1.1 Roll Axis Inertia Tests Using Air Bearing Table

2.3.1.1.1 Introduction

This project is one of five in the mass properties of liquids program which was designed to investigate the moments of inertia of liquids in filled cylindrical tanks. In particular this project was designed to determine experimentally the moment of inertia of a liquid filled cylindrical tank about its roll axis. Previous investigations, References 1 through 3, have assumed that the moment of inertia about the roll axis of a liquid filled cylindrical tank was zero. This assumption is valid for certain degrees of accuracy because a cylindrical tank rotating about its roll axis places very little constraint on the liquid. The only restraining force produced between the liquid and the tank is that caused by the liquid's viscous friction exerted on the tank walls, bottom and top. Since most liquids used as fuels have a relatively low viscosity, the liquid acts as a free body within the tank; thereby, producing a very small effective moment of inertia.

As advanced space flight requires precise knowledge of vehicle mass characteristics, a more accurate determination of liquid moments of inertia must be known.

For this reason this project was undertaken; to experimentally determine the exact moment of inertia about the roll axis of a cylindrical tank.

2.3.1.1.2 Test Procedure

The test procedure for determining the moment of inertia of the cylindrical tanks was greatly simplified by using the air bearing table. The basic equipment consisted of the 24-inch air bearing table, the photocell timing device, the displacement measuring device, the torsion rod and cylindrical tanks. Associated equipment such as period counters and digital recorders were used to automate the data collection.

The equipment was arranged as shown in Figure 102. The air bearing table was first leveled on the iso-pad; then the appropriate tank was placed on the table and the air pressure was regulated for the given tank. Lastly, torsion rod number 120 was inserted into the table to avoid any compressive forces from being placed on the rod. The period timing device and the displacement measuring apparatus were aligned to give a zero reading for zero displacement. The periods were recorded automatically and the displacements were determined manually.

The testing consisted of displacing the table top to a given displacement and recording the data as the oscillations decayed. The displacement used was obtained from previous experiments. Initially, the table top was

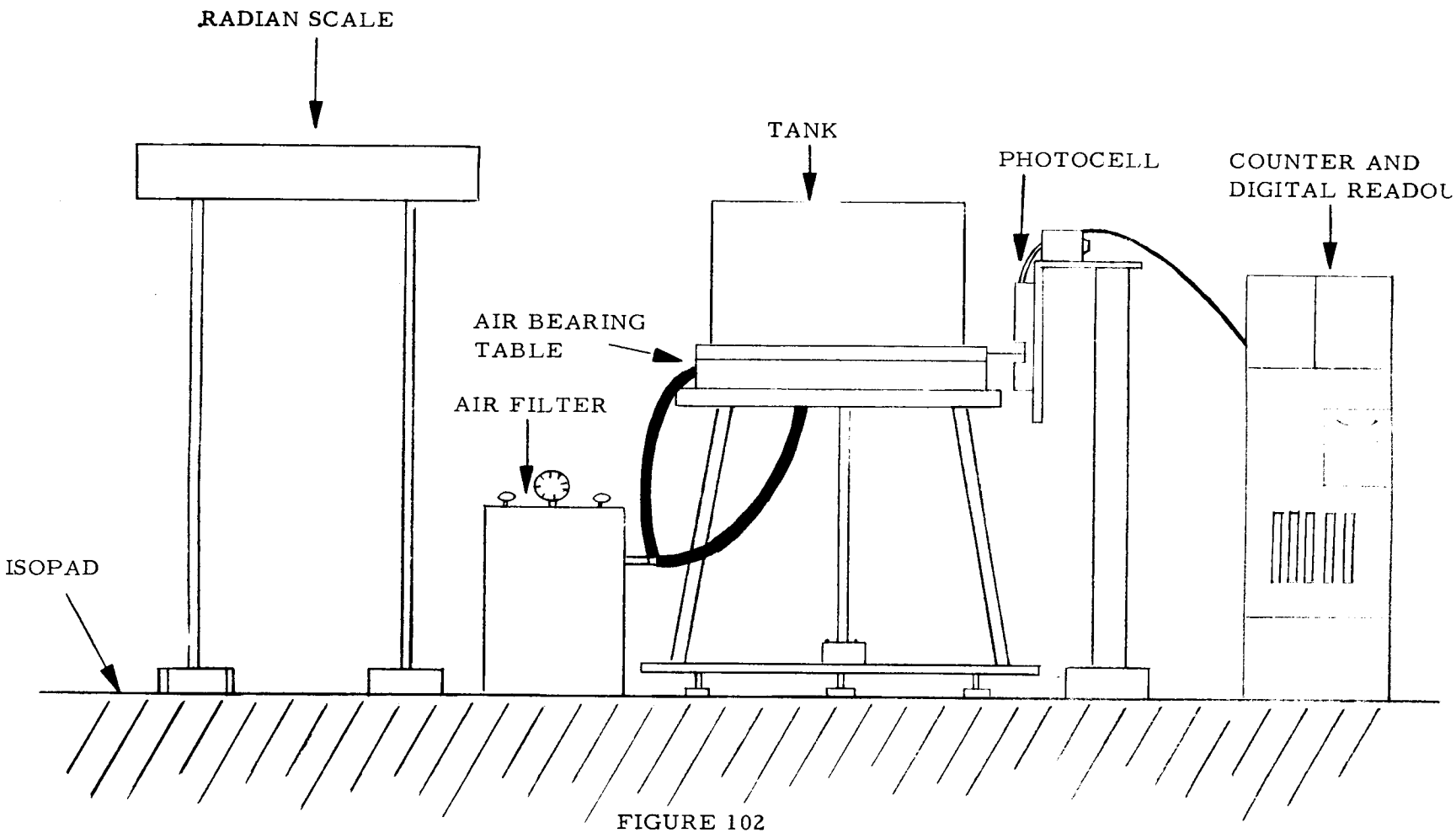

FIGURE 102

TEST EQUIPMENT ARRANGEMENT

displaced until the maximum displacement was .006 radians. From here it was released. When the maximum displacement reaced .004 radians, the time was recorded until the maximum amplitude decayed to .003 radians. This displacement was used because aerodynamic drag can be ignored at these amplitudes for the accuracies needed. Also, a preliminary test was performed to be sure that the moment of inertia was not dependent on the amplitude of oscillation. The average period was then obtained by dividing the total time by the number of cycles. This average period was then used in Equation 151 .

$$I = \frac{KT^2}{4\pi^2} \tag{151}$$

to calculate the moment of inertia of the table with the unknown object. Each test was repeated at least five times to be sure repeatable data was obtained. A sample test procedure is shown in Appendix C1.

The five circular cylindrical tanks have the properties shown in Table 18. Each tank was tested empty and full so that any aerodynamic drag or other losses would cancel out, and the moment of inertia of the liquid only remains. This procedure eliminated calculating the moment of inertia of the empty tanks which could have produced additional errors.

2.3.1.1.3 Test Results

The results of the tests shown in Table 19 prove that the moment of inertia about the roll axis of a filled cylindrical tank is quite small but not zero. The ratio of the moment of inertia of the water to the moment of inertia of water in a solid state is approximately 0.5% for all aspect ratios. Figure 103 shows a plot of the aspect ratio versus the water to solid ratio, where a straight line has been projected along the mean of the four values.

An error analysis has been performed on the air bearing table system to determine its accuracy. Under present conditions it can obtain accuracies of .05% where calibrated dumbbells have been used. Therefore, accuracies of at least 0.1% can easily be assumed for the tank tests being performed. This lesser accuracy is used because of the rough tank dimensions which introduce some errors in aligning the tanks on the center axis of the table.

Figure 104 shows another plot of the test results. The moment of inertia of each tank is plotted against the aspect ratio. A straight line with a slope of minus 0.326 has been projected through the data points. Limited data has resulted in a straight line assumption because it represents the most

TABLE 18

PHYSICAL CHARACTERISTICS OF CYLINDRICAL TANKS

Tank	W_e	W_f	h	d	t
A	30.27 lbs.	128.0 lbs.	6.5 in.	24.25 in.	.25 in.
B	36.23	231.0	12.5	24.25	.25
C	72.77	381.0	20.0	24.50	.375
D	103.00	684.0	36.75	24.50	.375

Water in Tank	W_w	m_w	h_w	d_w	h_w/d_w	I_t
A	97.73 lbs.	.253 lb-sec^2/in	6.0 in.	23.75 in.	.253	17.84 in-lb-sec^2
B	194.77	.505	12.0	23.75	.505	35.61
C	308.23	.799	19.25	23.75	.811	56.34
D	581.00	1.506	36.0	23.75	1.515	106.18

TABLE 19

TEST RESULTS

Tank	T_e	T_f	I_e	I_f	I_w	I_w/I_t
A	.50952 sec.	.51098 sec.	17.51 in-lb-sec^2	17.61 in-lb-sec^2	0.10 in-lb-sec^2	.56%
B	.53753	.53993	19.49	19.66	0.17	.48
C	.68076	.68313	31.26	31.48	0.22	.39
D	.80746	.81227	43.98	44.50	0.52	.49

TABLE 20

PRESSURE EXERTED BY WATER ON TANK BOTTOM

Tank	h_w/d_w	F	A	P
A	.253	97.73 lbs.	443.01 in^2	0.221 lb/in^2
B	.505	194.77	443.01	0.440
C	.811	308.23	443.01	0.696
D	1.515	581.00	443.01	1.311

FIGURE 103

RATIO OF THE MOMENT OF INERTIA OF
WATER TO SOLID
VERSUS
ASPECT RATIO

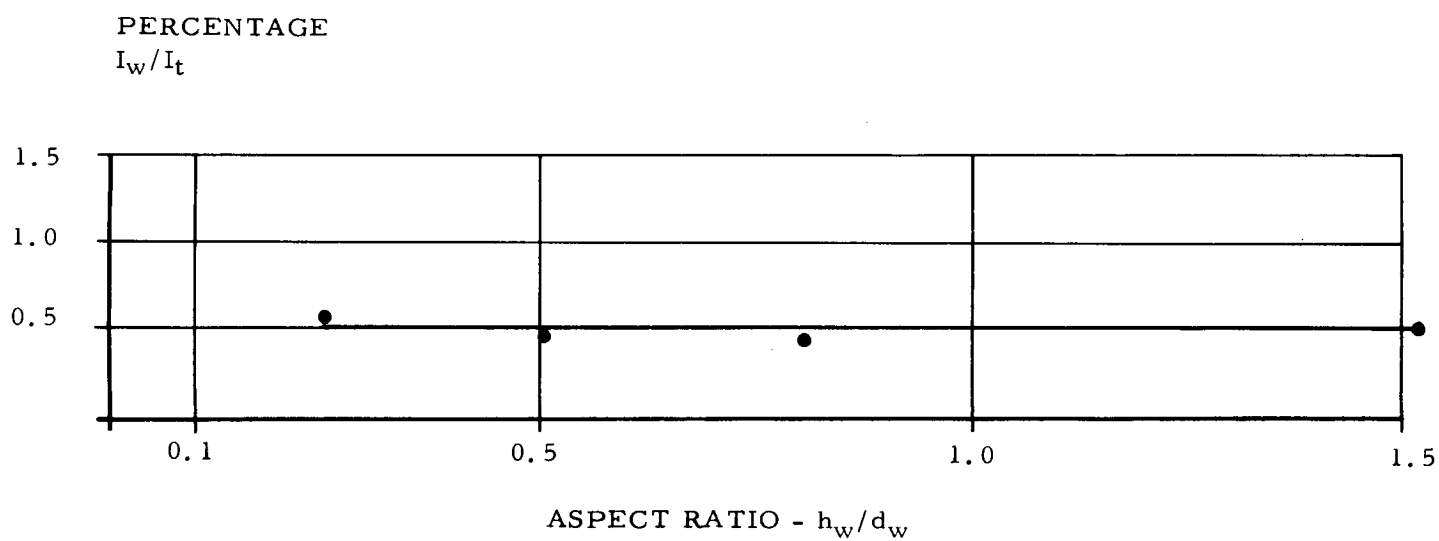

FIGURE 104

MOMENT OF INERTIA OF EACH TANK
VERSUS
ASPECT RATIO

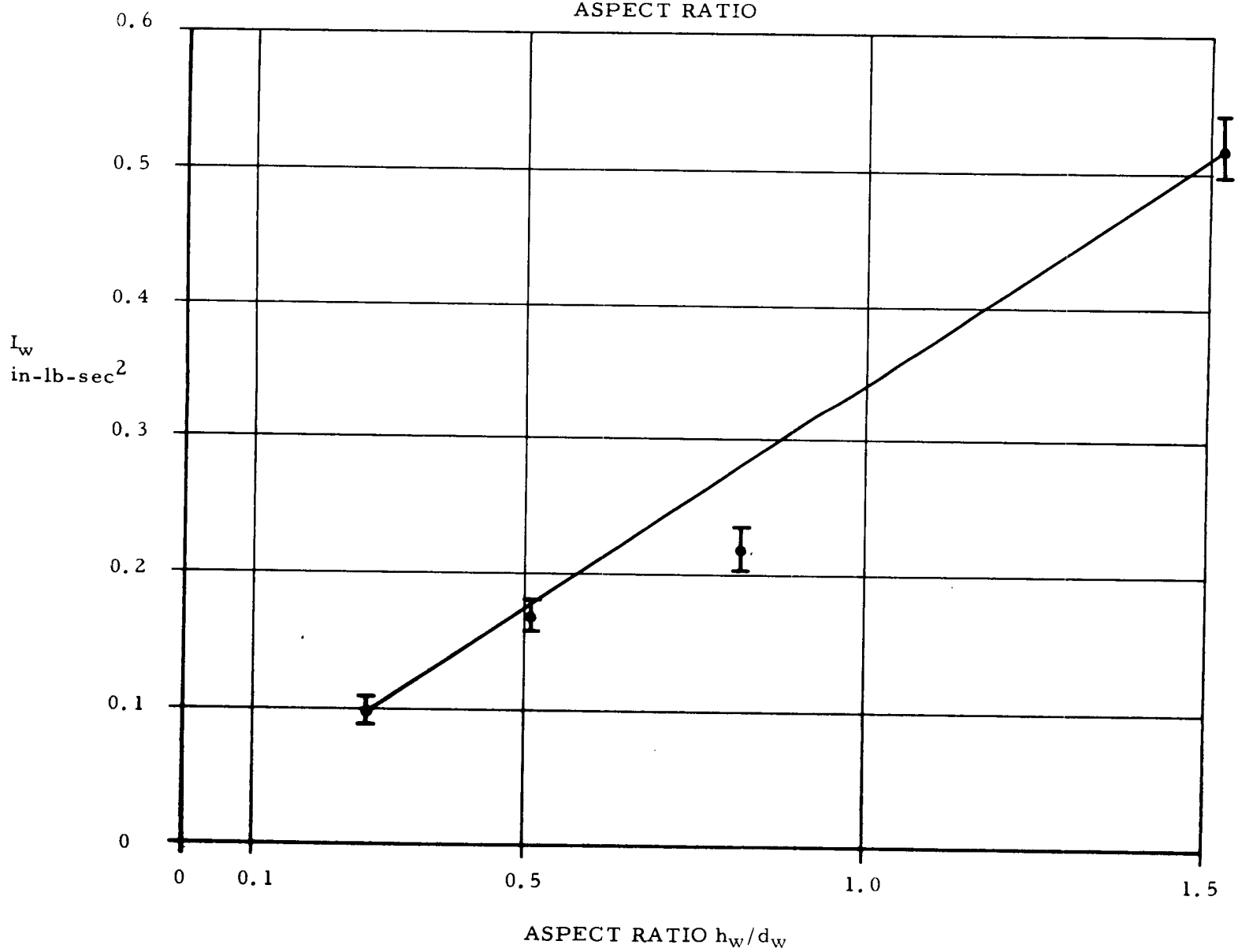

logical approach, considering the linear relationship of the tank size and moment of inertia. One experimental point resulting from tank C is removed from the straight line, but this can be attributed to experimental error. The other three points fall very near the straight line. The lines on Figure 104 represent the range that .1% error will cover for each tank results.

In hopes of finding some physical relationship of the tank and its moment of inertia, the pressure exerted by the water on the bottom of each tank was calculated and is shown in Table 20. Figure 105 is a plot of the moment of inertia versus the pressure. A straight line is obtained with a slope of 0.385. Tank C again exhibits the maximum deviation from the straight line which is attributed to experimental error.

2.3.1.1.4 Conclusions

The assumption that the moment of inertia about the roll axis of a cylindrical filled tank is zero for accuracies of 0.5% or less, has been proven to be valid. For accuracies better than 0.5% it appears from the results of Figure 104 and 105 that the moment of inertia of a cylindrical tank about its roll axis is proportional to the aspect ratio and the pressure exerted on the bottom of the tank. The aspect ratio and the pressure are related to each other in the physical size of the tank. But the pressure is also dependent on the liquid density and the acceleration forces placed on the liquid. This latter force can be extremely large during launch and re-entry of space vehicles. The data from this test program gives accurate data for determining the roll moment of inertia of a cylindrical tank filled with water in a gravity field of one "g". This emperical data is applicable to any cylindrical tank containing water or a similar liquid in a one "g" field. It would also yield very good results for a partially filled tank because the top surface friction of a filled tank adds very little to the moment of inertia.

Another factor which affects the moment of inertia of a liquid is its viscosity. The viscosity of a liquid will introduce friction between the liquid and the tank walls, bottom and top. This in turn will cause the liquid to have a greater adhesion to the tank; thereby, causing the liquid to follow more closely the tank motions. As more liquid mass follows the tank's motion, the moment of inertia of the liquid increases. For a liquid with low viscosity, the tank and liquid act as a separate body, producing a relatively lower effective moment of inertia.

Future testing of roll axis moments of inertia should include more of the same type tests performed here to verify the assumption that tank C gave bad experimental data and that a straight line is valid for the moment of inertia versus aspect ratio plot. Other tests should include detail studies of various liquid viscosities. Also, the frequency of oscillation of the

LIST OF SYMBOLS

SYMBOL	DEFINITION
W_e	Weight of Empty Tank in Pounds
W_f	Weight of Tank Filled with Water in Pounds
W_w	Weight of Water in Pounds
g	Acceleration of Gravity = 385.684 in/sec^2
m_w	Mass of Water = W_w/g lb-sec^2/in
h	Tank Height in Inches
h_w	Water Height
d	Tank Diameter
d_w	Water Diameter
t	Tank Wall Thickness
h_w/d_w	Aspect Ratio of Water
T_e	Period of Oscillation for Empty Tank in Seconds
T_f	Period of Oscillation for Full Tank
K	Rod Spring Constant = 2662.873 in-lb for Rod Number 120
I_e	Moment of Inertia for Empty Tank and Table Top = $KT_e^2/4\pi^2$ in-lb-sec^2
I_f	Moment of Inertia for Full Tank and Table Top = $KT_f^2/4\pi^2$ in-lb-sec^2
I_w	Moment of Inertia of Water = $I_f - I_e$
I_t	Moment of Inertia of Water if it were a Solid = $m_w d_w^2/8$ in-lb-sec^2
I_w/I_t	Ratio of the Moment of Inertia of Water to that of Water as a Solid
F	Force Exerted by Water on Tank Bottom
A	Area of Tank Bottom
P	Pressure Exerted by Water on Tank Bottom

REFERENCES

1. Bauer, H. F. "Fluid Oscillations in a Circular Cylindrical Tank", Report No. DA-TR-1-58, ABMA, April, 1958.

2. Bauer, H. F. "The Effective Moment of Inertia in Roll of Propellant and Roll Damping", Report No. DA-TM-67-59, ABMA, May, 1959.

3. Gleghorn, G. J., "Motion of Fluid in a Cylindrical Tank", Memorandum, The Ramo-Wooldridge Corporation, Los Angeles, California, February, 1956.

FIGURE 105

MOMENT OF INERTIA OF EACH TANK
VERSUS
PRESSURE EXERTED BY THE LIQUID ON THE BOTTOM OF EACH TANK

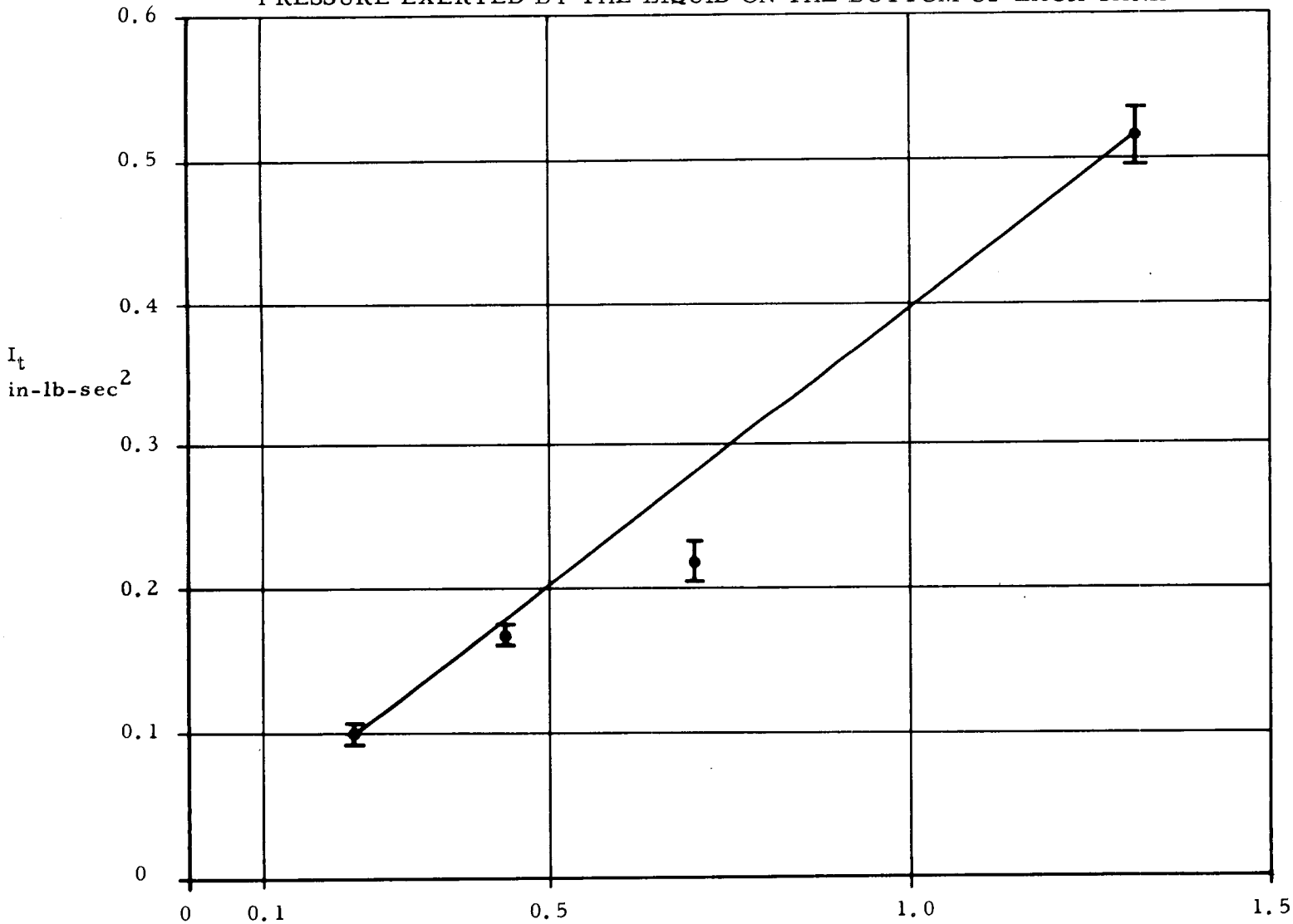

tanks should be investigated to determine this effect on the moment of inertia. If future tests are conducted, more aspect ratios should be included to give more detailed data.

2.3.1.2 Displaced Roll Axis Inertia Tests Using Air Bearing Table

2.3.1.2.1 Introduction

This project component is a continuation of the test project for the Mass Properties of Liquids Program. This report is one of a series for experimentally determining the moment of inertia of filled cylindrical tanks about various axes. It discusses the results of experimentation to determine the moment of inertia of a filled cylindrical tank about a displaced roll axis. The objective of this report, as well as the others, is to provide useful information for the determination of liquid moments of inertia.

A specific application for the displaced roll axis moment of inertia results is in the clustered fuel tanks as shown in Figure 106. Here the outside tanks add a considerable amount to the moment of inertia of the total vehicle as compared to the centrally located fuel tank. The results of this study could be used for any type of liquid tank displaced from the longitudinal axis.

The Mass Metrology Laboratory at SPACO, INC. has the capability of performing precise moment of inertia measurements with the torsional pendulum air bearing table; thereby providing an accurate method of studying liquid moments of inertia. Some authors have assumed that the moment of inertia transfer formula is valid for liquids. This may be true for some accuracies but precision testing will be necessary before definite conclusions can be made. This portion of the test project was designed to provide such information.

2.3.1.2.2 Test Objective

The primary objective of this experiment was to determine the effect of translating the axis of rotation of a water filled cylindrical tank on the water's moment of inertia. As a part of this objective the correlation between the aspect ratio and the moment of inertia of the translated tank was investigated. Also, the relationship between the displacement of the tank from the axis of rotation and its moment of inertia was analyzed.

In previous reports, References 1 and 2, the moment of inertia transfer formula was assumed to apply for liquids. In Equation 152, I is

$$I = I_o + mL^2 \tag{152}$$

FIGURE 106

CLUSTERED FUEL TANKS

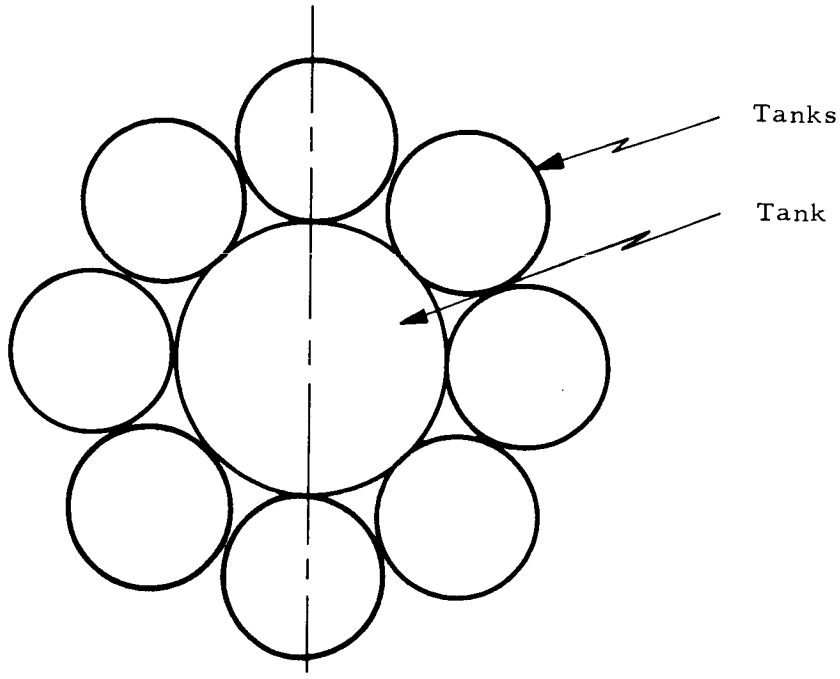

Top View

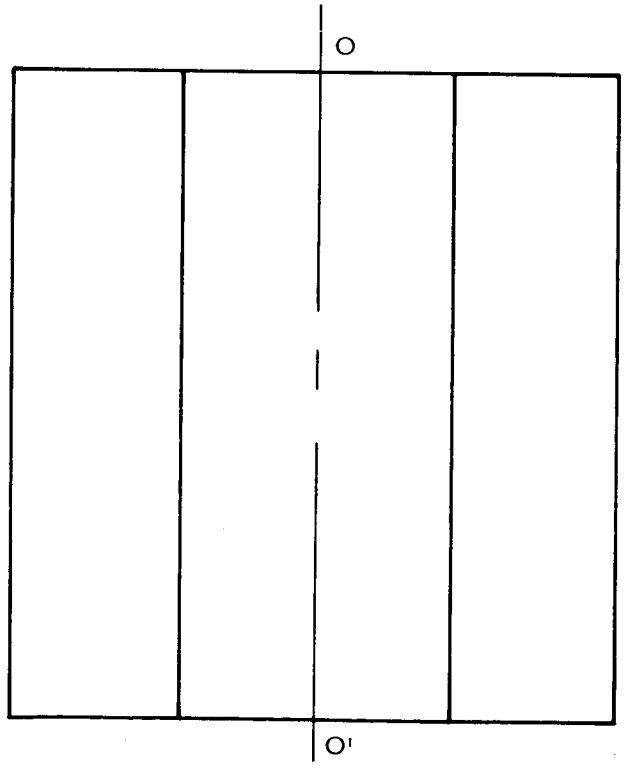

Side View

the moment of inertia of the object about its displaced axis, I_o is the moment of inertia of the object about its own center of gravity, m is the mass of the object and L is the distance between the center of gravity and the axis of rotation. Since liquids do not conform to all the rules which apply to solids as noted in previous reports, there is no reason to assume that they do, in this case. The only reason a liquid obeys any mechanical laws of solids is because of the boundary conditions they are subjected to. As an example, in a cylindrical tank which rotates about its central axis, the liquid is not bounded at all; therefore, it acts independently of the tank. The viscosity of the liquid which causes it to adhere to itself and the tank walls is the only factor which makes the liquid partially obey the solid laws.

For a cylindrical tank rotating about a displaced axis, the boundary conditions must again be considered. Figure 107 shows several tank positions with respect to the axis of rotation. The tank's center of gravity is denoted by x and the axis of rotation is denoted by O. The shaded area shows the part of the liquid which is not bounded by the tank. In part A of the figure the liquid is not bounded by the tank at all; therefore, theoretically a perfect liquid would remain fixed as the tank rotated about it. This is not exactly true for an actual liquid as shown in Section 2.3.1.1, but a small percentage of the liquid does rotate with the tank. In part B the unbounded liquid is less than that in part A because the tank has been displaced by a distance L from the axis of rotation. The radius arm r circumscribes the unbounded area as the tank rotates about the displaced axis O. In part C the same effect applies with still less unbounded liquid. In part D the axis of rotation is on the edge of the tank and the liquid is completely bounded as the tank rotates about O. The same is true in part E as the tank is moved further from the axis of rotation.

If all liquids were perfect, this theoretical analysis of the boundary conditions would solve all problems in calculating moments of inertia. But no liquids are perfect; therefore, they must obey certain other laws. One such law is derived from the velocity potential theory. This theory treats the the liquid as individual particles and accounts for the action of each particle. The viscosity of liquids is one of the main properties which affects the behaviour behavior of the liquid. Also, the motion of the liquid has a large effect on the manner in which it acts.

In experimentally investigating a liquid only the effective moment of inertia can be observed. This is true because the liquid must be oscillated in order to determine its period of oscillation from which the moment of inertia is determined. This period of oscillation for a liquid is not the same as that of a solid because the liquid has internal motions within the tank. Therefore, this moment of inertia of the liquid is called the effective moment of inertia because the period of oscillation represents

FIGURE 107

VARIOUS TANK POSITIONS AS
THEY ROTATE ABOUT AXIS O

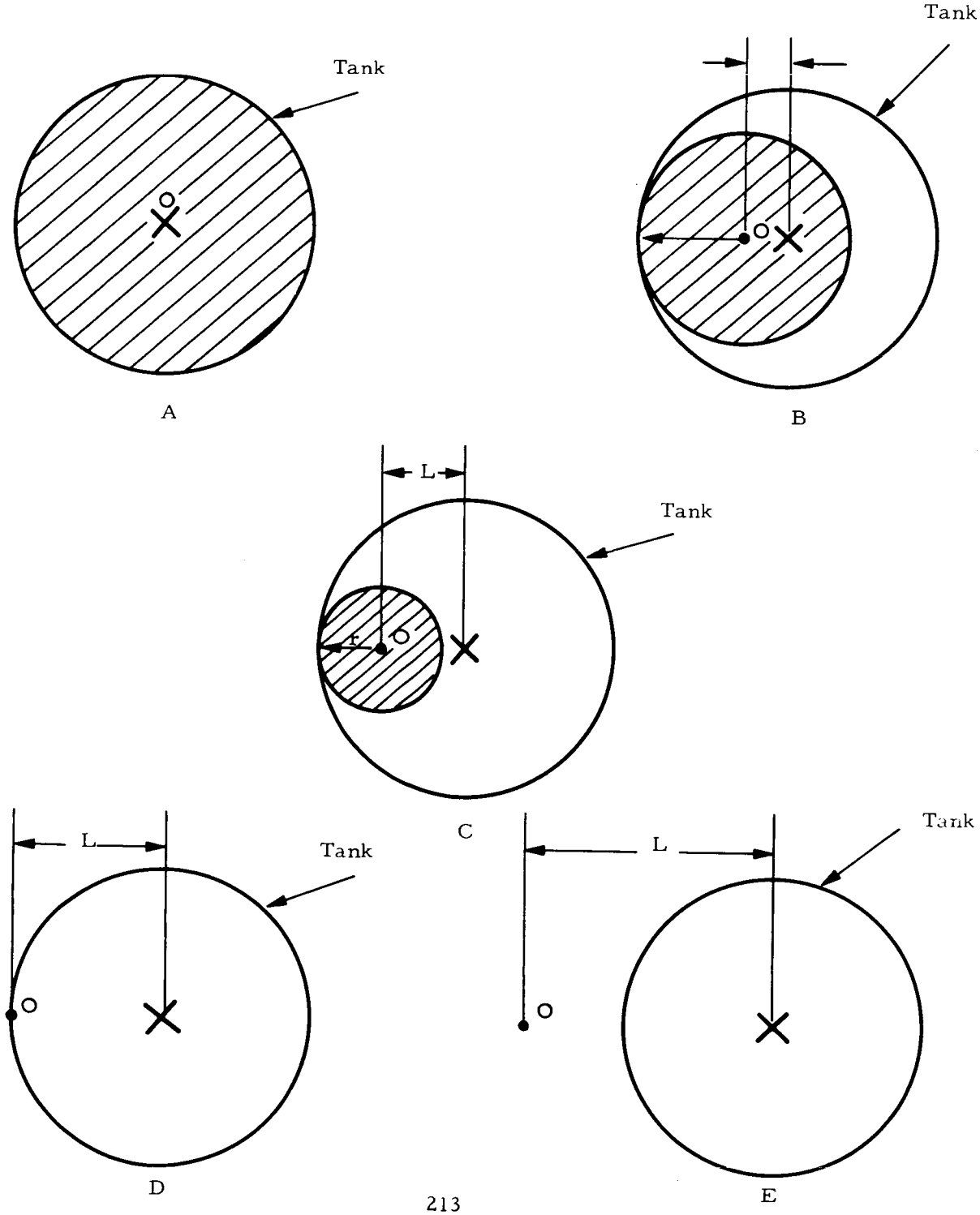

an equivalent solid moment of inertia. In determining the moment of inertia of any liquid, the results will be dependent on tank shape, axis of rotation and the frequency of oscillation. This project component will investigate the specific case of the moment of inertia of a cylindrical tank about a displaced roll axis for several frequencies.

2.3.1.2.3 Test Procedure

The test procedure for determining the moment of inertia of the cylindrical tanks was similar to that used in Section 2.3.1.1 with the addition of automatic recording of displacement data. The basic equipment consisted of the 24-inch air bearing table, an extension ring, the photocell timing device, the displacement measuring device, the torsion rod and cylindrical tanks. Associated equipment such as period counters and digital recorders was used to automate the data collection.

The equipment was arranged as shown in Figure 108. The air bearing table was first leveled on the iso-pad; then the appropriate tank was placed on the table and the air pressure was regulated for the given tank. Finally, the torsion rod was inserted into the table to avoid any compressive forces from being placed on the rod. The period timing device and the displacement measuring apparatus were aligned to give a zero reading for zero displacement. The periods and displacements were recorded automatically.

The testing consisted of displacing the table top to a given displacement and recording the data as the oscillations decayed. The displacement used was obtained from previous experiments. Initially, the table top was displaced until the maximum displacement was .006 radians. At .006 radians it was released. When the maximum displacement reached .005 radians, the period was recorded in 10 period averages every 20th cycle until the maximum amplitude decayed to .004 radians. This displacement was used because aerodynamic drag can be ignored at these amplitudes for the accuracies needed. Also, a preliminary test was performed to be sure that the moment of inertia was not dependent on the amplitude of oscillation. An average of the 10 period averages was obtained to use in Equation 153 in calculating the moment of inertia of the table with the unknown object. Each

$$I = KT^2/4\pi^2 \tag{153}$$

tank was tested empty and full so that any aerodynamic drag or other losses would cancel out, and only the moment of inertia of the liquid would remain. This procedure eliminated calculating the moment of inertia of the empty

FIGURE 108

TEST EQUIPMENT ARRANGEMENT

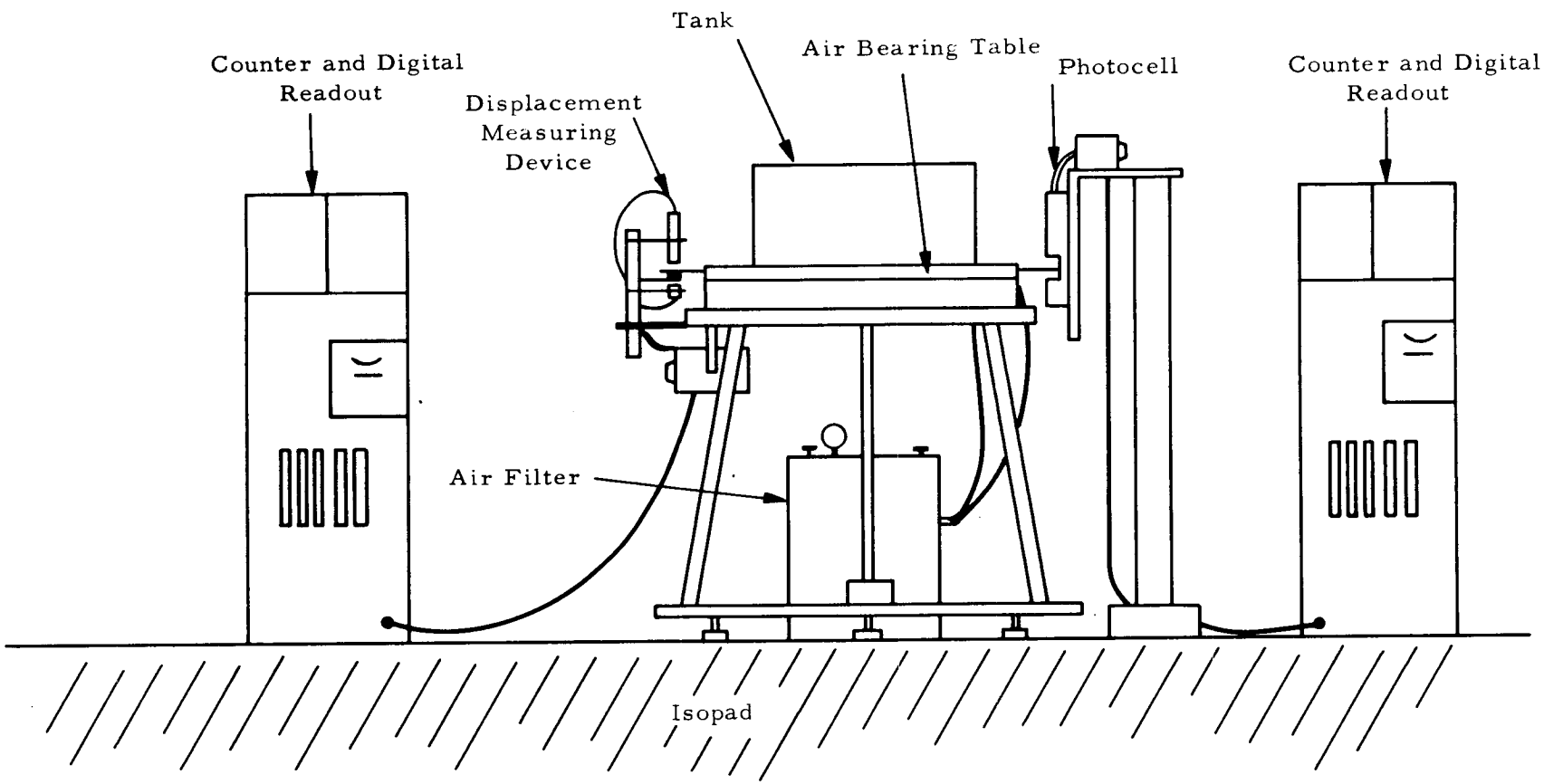

tanks which could have produced additional errors. Each test was repeated at least three (3) times to be sure that repeatable data was being obtained. A sample test procedure is shown in Appendix C2.

Two sets of tanks had to be used in performing the tests because the original tanks were too heavy for the air bearing table when they were displaced from the center axis of the table. The original set of tanks was designated the large tanks and have the dimensions shown in Figure 109. Table 21 shows the physical characteristics of the large tanks and Table 22 shows the theoretical values for the moment of inertia of the water within the tanks if it were a solid at various locations on the air bearing table. Figure 110 shows the various locations of the large tanks. The extension ring had to be used for all the large tanks due to their size.

The second set of tanks was designated the small tanks as seen by their dimensions in Figure 111. Table 23 gives the physical characteristics of the small tanks and Table 24 gives the theoretical moment of inertia of the water if it were a solid at various tank positions. Figure 112 shows the various locations for the small tanks.

2.3.1.2.4 Test Results

The test results for all the experiments are listed in Tables 25 through 28. In Table 25 for $L_1 = 0$, the test results are the same as that in Section 2.3.1.1. This data is presented again for comparison to the data for the small tanks at $L_1 = 0$ shown in Table 26. In comparing these two sets of data it was noted that the percentage of I_w/I_t for each set of tanks was different. The large tanks have a relatively constant value of 0.5 percent, while the small tanks have a decreasing I_w/I_t ratio of 2.3 to 1.4 percent for increasing aspect ratios. The difference between these two sets of data was attributed to the variation in tank sizes and possibly the tank construction. The large tanks were bulky and not as precisely made as the small tanks. Also, a small experimental error would have greatly affected these results.

Another reason for presenting this data again is to verify the assumption that the moment of inertia plotted against the aspect ratio produces a straight line. In Section 2.3.1.1 the selection of a straight line for the same type plot was not exactly evident because of a bad data point. Figure 113 shows the results of this test. The slope of the curve is not the same as that for the large tank, but this follows from the other changes already mentioned. In order to analyze this difference more closely further tests will have to be performed at a later time.

The remaining data in Table 26 and that in Table 27 was obtained to show the relationship between the moment of inertia, the tank aspect ratios

FIGURE 109

LARGE TANK DIMENSIONS

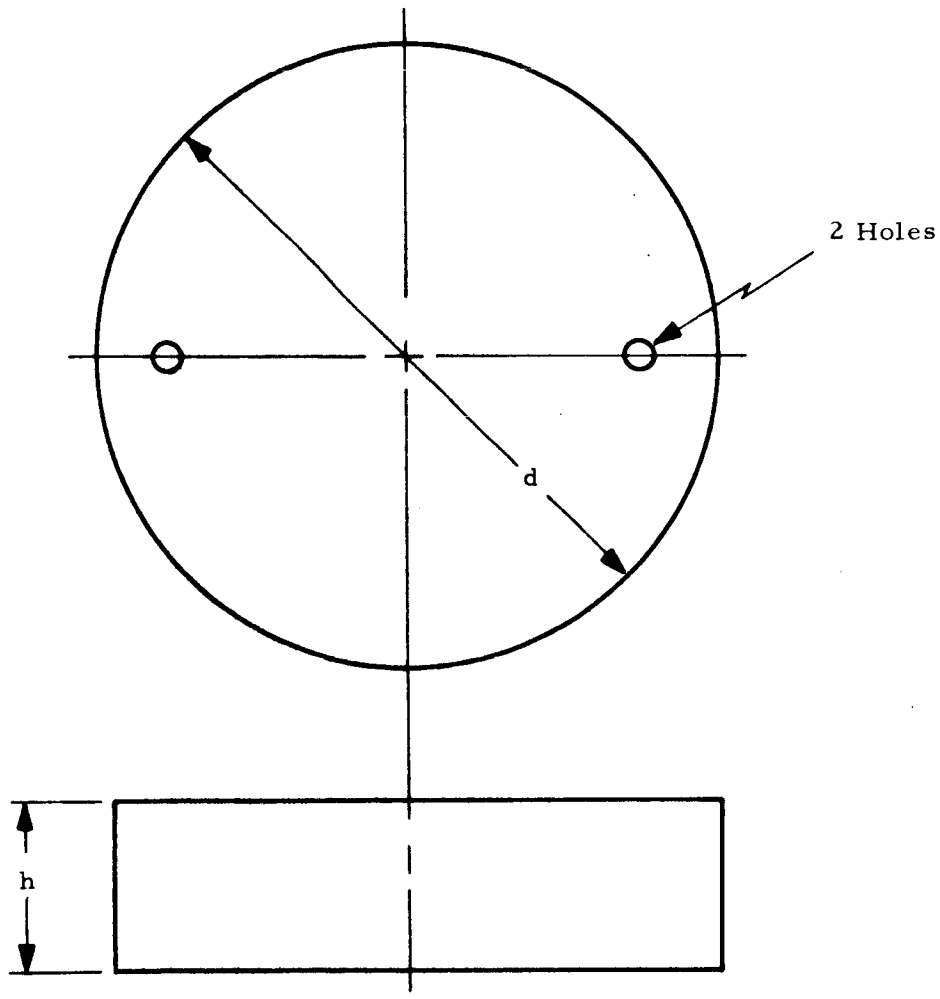

	Tank A	Tank B	Tank C	Tank D
d	23.75	23.75	23.75	23.75
h	6.0	12.0	19.25	36.0
h/d	0.253	0.505	0.811	1.515

FIGURE 110

LARGE TANK POSITIONS

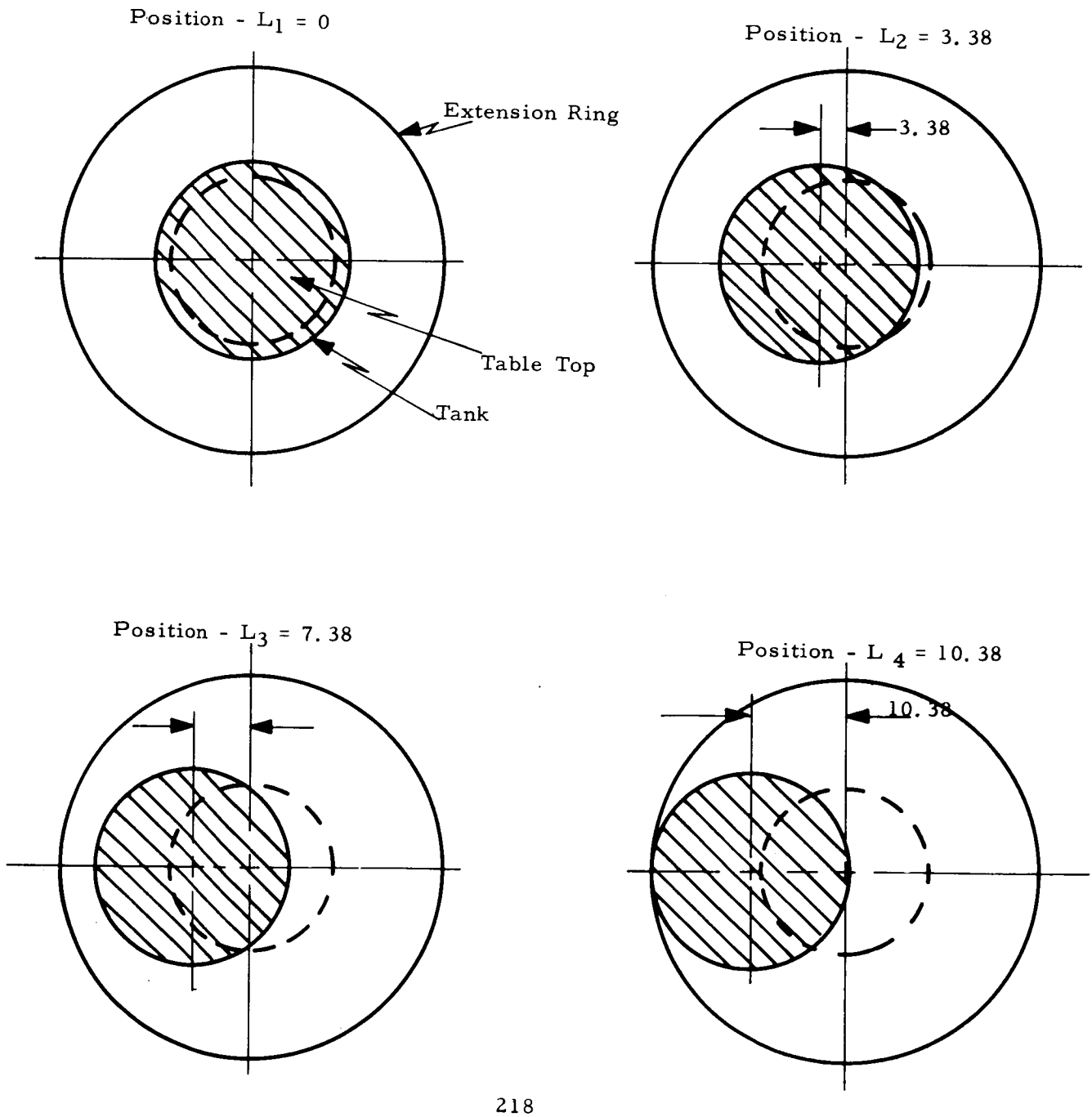

FIGURE 111

SMALL TANK DIMENSIONS

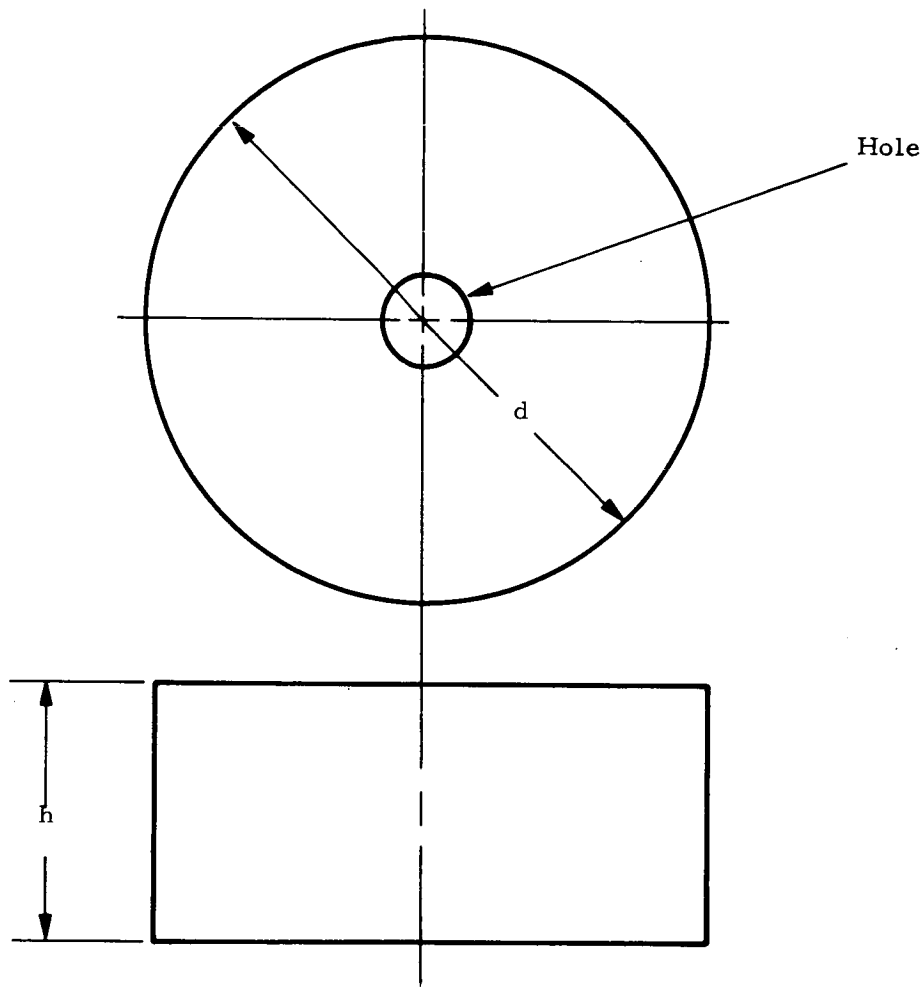

	Tank A	Tank B	Tank C	Tank D	Tank E
d	7.50	7.50	7.50	7.50	7.50
h	1.93	3.80	5.65	7.53	11.35
h/d	.257	.507	.753	1.004	1.513

FIGURE 112

SMALL TANK POSITIONS

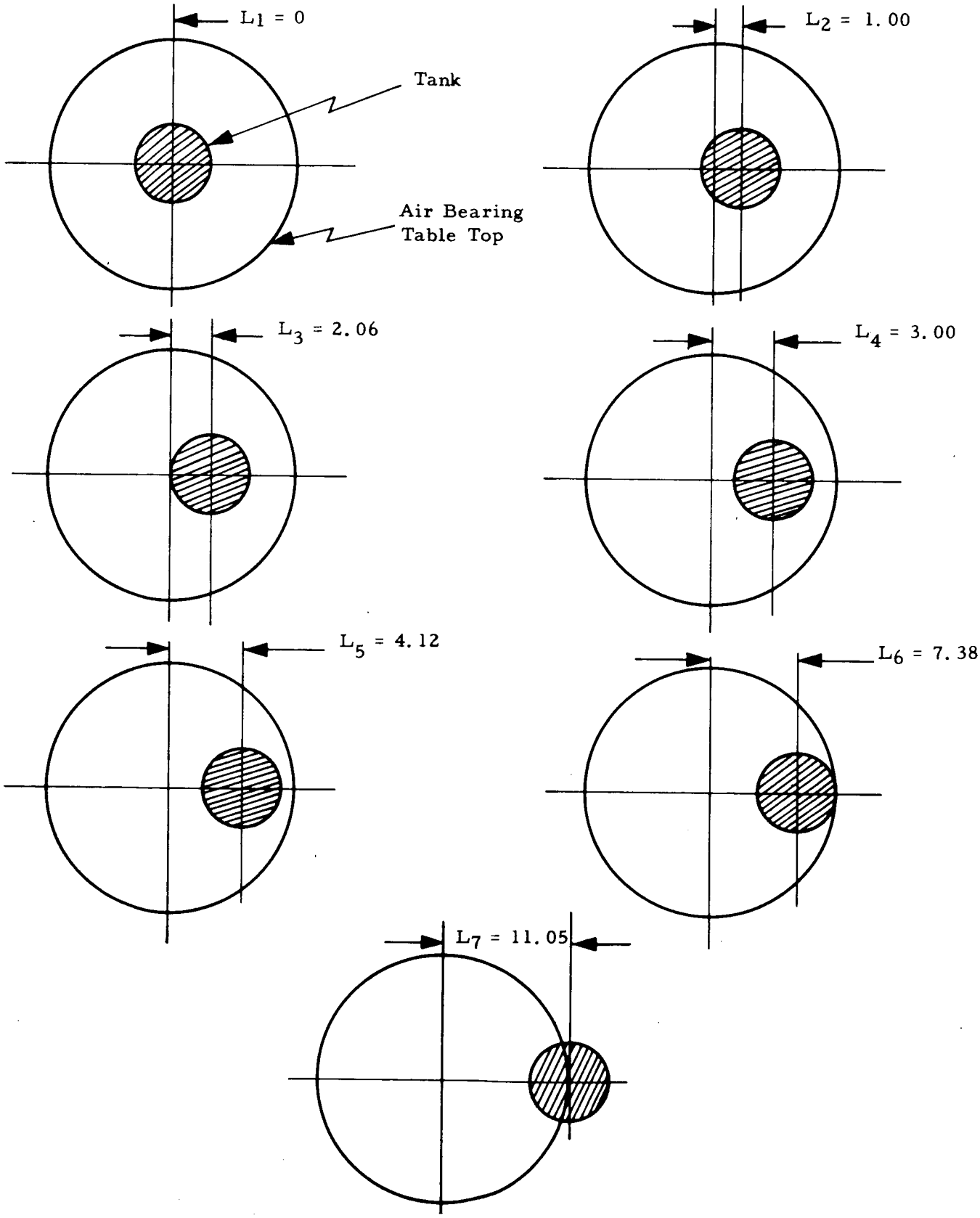

FIGURE 113

MOMENT OF INERTIA
VERSUS
ASPECT RATIO
FOR SMALL TANKS ABOUT THEIR LONGITUDINAL AXES

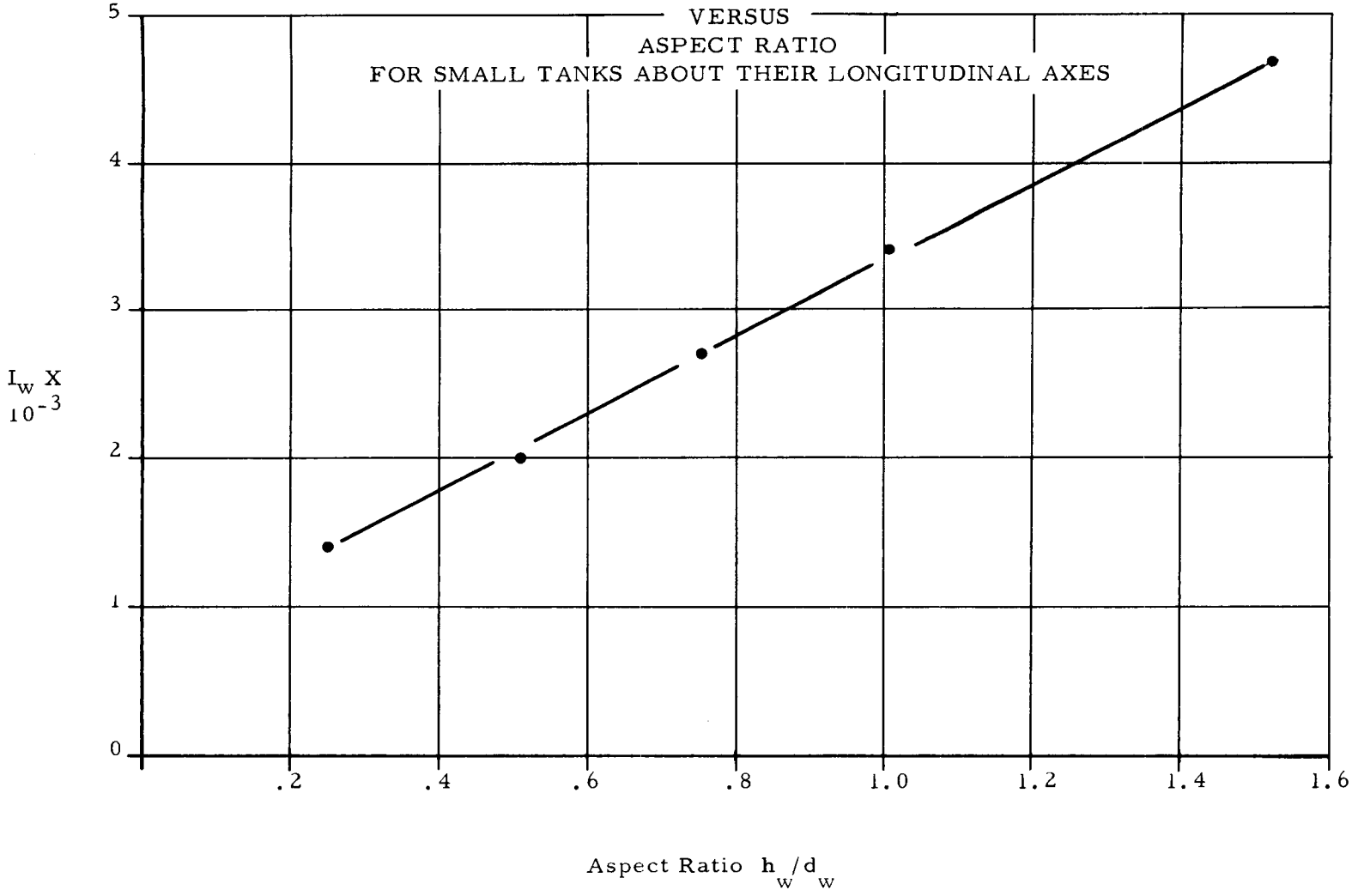

TABLE 21

PHYSICAL CHARACTERISTICS OF LARGE CYLINDRICAL TANKS

Tank	W_e	W_f	h	d	t
A	30.27 lbs.	128.0 lbs.	6.5 in.	24.25 in.	0.25 in.
B	36.23	231.0	12.5	24.25	0.25
C	72.77	381.0	20.0	24.50	0.375
D	103.00	684.0	36.75	24.50	0.375

Water in Tank	W_w	m_w	h_w	d_w	h_w/d_w
A	97.73 lbs.	0.253 lb-sec^2/in	6.0 in.	23.75 in.	0.253
B	194.77	0.505	12.0	23.75	0.505
C	308.23	0.799	19.25	23.75	0.811
D	581.00	1.506	36.0	23.75	1.515

TABLE 22

THEORETICAL MOMENT OF INERTIA VALUES
FOR LARGE TANKS AT VARIOUS POSITIONS

Tank	I_t $L_1 = 0$	I_t $L_2 = 3.38$	I_t $L_3 = 7.38$	I_t $L_4 = 10.38$
A	17.84 in-lb-sec^2	20.74 in-lb-sec^2	31.62 in-lb-sec^2	45.10 in-lb-sec^2
B	35.61	41.38	63.11	90.02
C	56.34	65.47	99.86	142.4[illegible]
D	106.18	123.39	188.20	268.44

TABLE 23

PHYSICAL CHARACTERISTICS OF SMALL CYLINDRICAL TANKS

Tank	h	d	h/d	W_e	W_f	W_w	M_w
A'	1.93 in.	7.50 in.	.257	3.20 lbs.	6.45 lbs.	3.25 lbs.	.0084
B'	3.80	7.50	.507	3.78	10.18	6.40	.0166
C'	5.65	7.50	.753	4.35	13.89	9.45	.0245
D'	7.53	7.50	1.004	4.93	17.62	12.69	.0329
E'	11.35	7.50	1.513	6.13	25.30	19.17	.0497

TABLE 24

THEORETICAL MOMENT OF INERTIA VALUES FOR

SMALL TANKS AT VARIOUS POSITIONS

Tank	I_t $L_1 = 0$	I_t $L_2=1.00$	I_t $L_3=2.06$	I_t $L_4=3.00$	I_t $L_5=4.12$	I_t $L_6=7.38$	I_t $L_7=11.05$
A'	0.0592	0.068	0.095	0.135	0.202	0.518	1.085
B'	0.1166	0.133	0.187	0.265	0.398	1.020	2.144
C'	0.1723	0.197	0.276	0.393	0.588	1.507	3.164
D'	0.2313	0.264	0.371	0.527	0.790	1.937	4.248
E'	0.3495	0.399	0.560	0.797	1.193	3.056	6.418

TABLE 25

TEST RESULTS FOR LARGE TANKS

Tank	T_e seconds	T_f seconds	I_e in-lb-sec^2	I_f in-lb-sec^2	I_w in-lb-sec^2	I_w/I_t percentage
Tank Position - $L_1 = 0$						
A	0.50952	0.51098	17.51	17.61	0.10	0.56
B	0.53753	0.53993	19.49	19.66	0.17	0.48
C	0.68076	0.68313	31.26	31.48	0.22	0.39
D	0.80746	0.81227	43.98	44.50	0.52	0.49
					Avg.	0.48
Tank Position - $L_2 = 3.38$						
A	0.97296	0.99545	63.85	66.84	2.99	14.42
B	0.99080	1.03555	66.22	72.33	6.12	14.79
C	1.08340	1.15233	79.17	89.57	10.39	15.87
					Avg.	15.03
Tank Position - $L_3 = 7.38$						
A	0.99483	1.09348	66.76	80.65	13.90	43.96
B	1.01618	1.20608	69.65	98.12	28.47	45.11
					Avg.	44.54
Tank Position - $L_4 = 10.38$						
A	1.02287	1.20733	70.57	98.32	27.75	61.53
B	1.04869	1.38569	74.18	129.52	55.34	61.48
					Avg.	61.51

TABLE 26

TEST RESULTS FOR SMALL TANKS

Tank	T_e seconds	T_f seconds	I_e in-lb-sec^2	I_f in-lb-sec^2	I_w in-lb-sec^2	I_w/I_t percentage
Tank Position - $L_1 = 0$						
A'	0.38548	0.38550	10.0226	10.0240	0.0014	2.28%
B'	0.385896	0.38593	10.0442	10.0462	0.0020	1.74
C'	0.38634	0.38639	10.0671	10.0698	0.0027	1.56
D'	0.38675	0.38682	10.0887	10.0921	0.0034	1.46
E'	0.38770	0.38779	10.1386	10.1434	0.0047	1.35
					Avg.	1.68
Tank Position - $L_2 = 1.00$						
B'	0.38609	0.38644	10.054	10.072	0.018	13.68
D'	0.38702	0.38771	10.103	10.139	0.036	13.53
					Avg.	13.61
Tank Position - $L_3 = 2.06$						
C'	0.38725	0.38921	10.12	10.22	0.10	36.23
E'	0.389-8	0.39317	10.21	10.43	0.22	39.29
					Avg.	37.76
Tank Position - $L_4 = 3.00$						
C'	0.38762	0.39044	10.13	10.28	0.15	55.98
E'	0.38897	0.39450	10.21	10.50	0.29	55.32
					Avg.	55.65

TABLE 27

TEST RESULTS FOR SMALL TANKS

Tank	T_e seconds	T_f seconds	I_e in-lb-sec^2	I_f in-lb-sec^2	I_w in-lb-sec^2	I_w/I_t percentage
Tank Position - L_5 = 4.12						
A'	0.38823	0.39094	10.17	10.31	0.14	70.42
B'	0.38919	0.39461	10.22	10.50	0.28	71.99
C'	0.39001	0.39816	10.26	10.69	0.43	73.75
D'	0.39086	0.40147	10.30	10.87	0.57	71.73
E'	0.39269	0.40842	10.40	11.25	0.85	71.23
					Avg.	71.82
Tank Position - L_6 = 7.38						
A'	0.39407	0.40258	10.47	10.93	0.46	88.88
B'	0.39600	0.41250	10.58	11.48	0.90	88.20
C'	0.39797	0.42229	10.68	12.02	1.34	89.27
D'	0.39992	0.43188	10.79	12.58	1.79	92.58
E'	0.40356	0.45054	10.99	13.69	2.70	88.54
					Avg.	89.49
Tank Position - L_7 = 11.05						
A'	0.40449	0.42299	11.04	12.07	1.03	95.27
B'	0.40822	0.44413	11.24	13.30	2.06	96.46
C'	0.41203	0.46375	11.45	14.51	3.06	96.66
D'	0.41565	0.48243	11.65	15.70	4.05	95.29
E'	0.42288	0.51949	12.06	18.20	6.14	95.76
					Avg.	95.89

and the tank displacements from the axis of rotation. The ratio of the moment of inertia of water to that of a theoretical solid is used in all comparisons because it gives a constant value which could be used for any size tank. The relationship between the aspect ratio and the I_w/I_t ratio appears to be const ant for each tank position for both large and small tanks. The small variations which do appear are well within the experimental error of the system. For further investigations the ratio of I_w/I_t for a given displacement will be the average of the results for all the aspect ratios as shown in Tables 25 through 27.

The next consideration is that of the relationship between the ratio of I_w/I_t to the distance the tank is displaced from its axis of rotation. This displacement is always referred to as a parallel axis through the center of gravity of the tank. Another term which will be used to relate the displacement is L/R, where L is the perpendicular distance between the tank center of gravity and the axis of rotation and R is the tank radius. The purpose of this term is twofold; it applies to any size tank and R represents the displacement at which the liquid is completely bounded if it rotates about that point. Figure 114 shows the relationship between I_w/I_t and L/R for both sets of tanks. For most purposes the relationship could be assumed linear up to a displacement of L/R equal 100 percent. The results for both tanks appear to agree with a slope of 0.7. Above this L/R point the data for the small tank appears to approach 100 percent I_w/I_t asymptotically. This curve was analyzed to see if it was an exponential, but it was not. Data for the large tanks tanks could not be obtained in this region because they were too heavy for the air bearing table at these distances. Even at smaller distances the larger tanks had to be eliminated.

The results of the last series of tests is shown in Table 28. Here the effect of frequency change on the I_w/I_t ratio for a given displacement was analyzed. The test procedure was the same except for a change from rod 120 to rod 28 to reduce the frequency of oscillation. Since the frequency is the reciprocal of the period, the period has been used to represent the frequency change because the period is used in all the calculations. Only one small tank was used because the aspect ratios did not affect the I_w/I_t ratios. Figure 115 shows the I_w/I_t plotted against L/R for two different frequencies. Since the frequencies did not remain constant for each tank, the average of the frequencies is taken as a good representative value. The results of these tests show that for the frequency range covered there is little change in I_w/I_t for a given displacement. A small change in I_w/I_t for the displacements of 50 and 100 percent of L/R could be attributed to experimental error because the difference is so small. For a large frequency variation a change in I_w/I_t would be expected.

FIGURE 114

RATIO OF MOMENT OF INERTIA OF WATER TO SOLID
VERSUS
RATIO OF DISPLACEMENT TO RADIUS FOR
TWO SETS OF TANKS

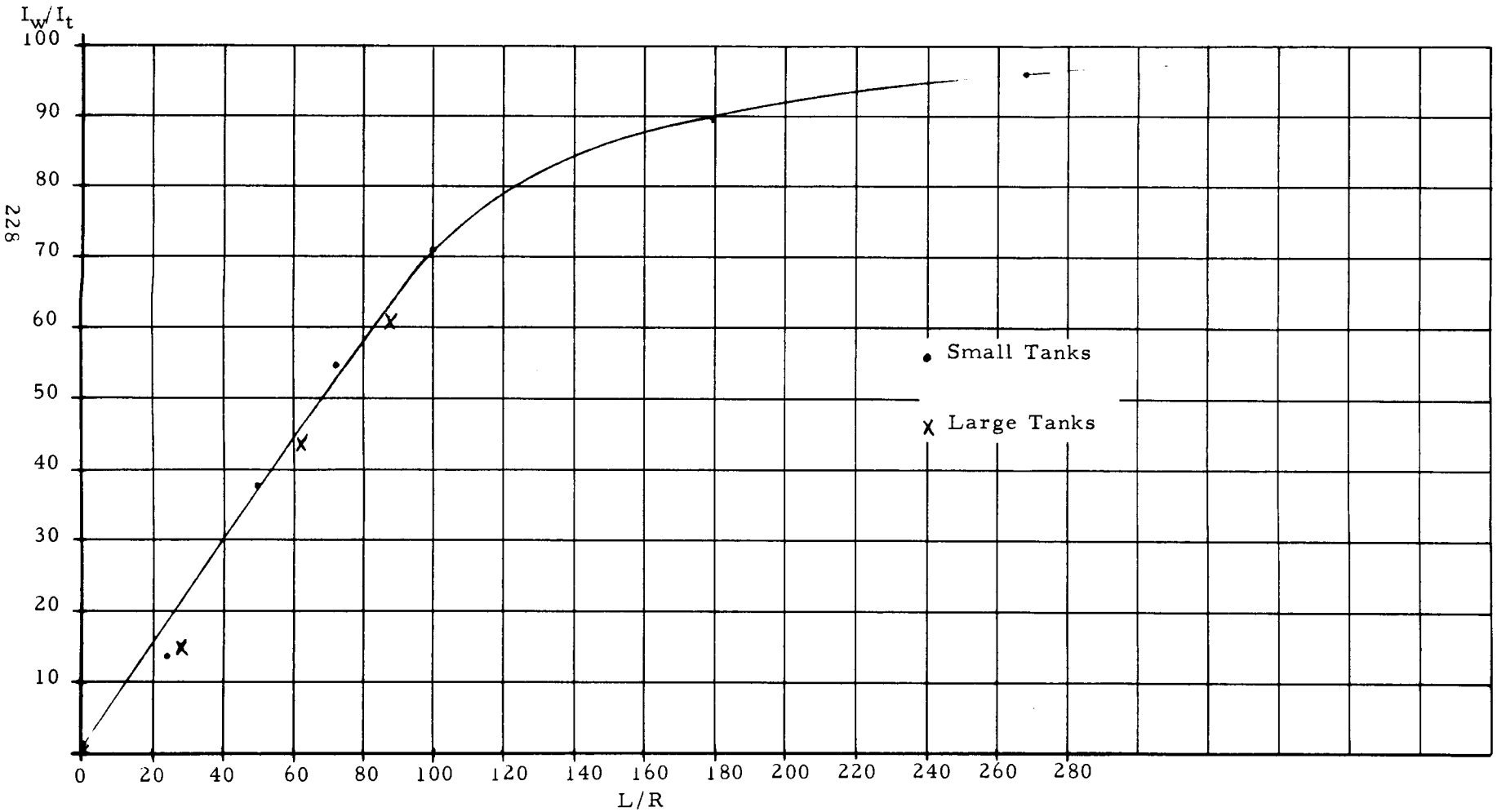

FIGURE 115

RATIO OF MOMENT OF INERTIA OF WATER TO SOLID
VERSUS
RATIO OF DISPLACEMENT TO RADIUS
FOR DIFFERENT FREQUENCIES

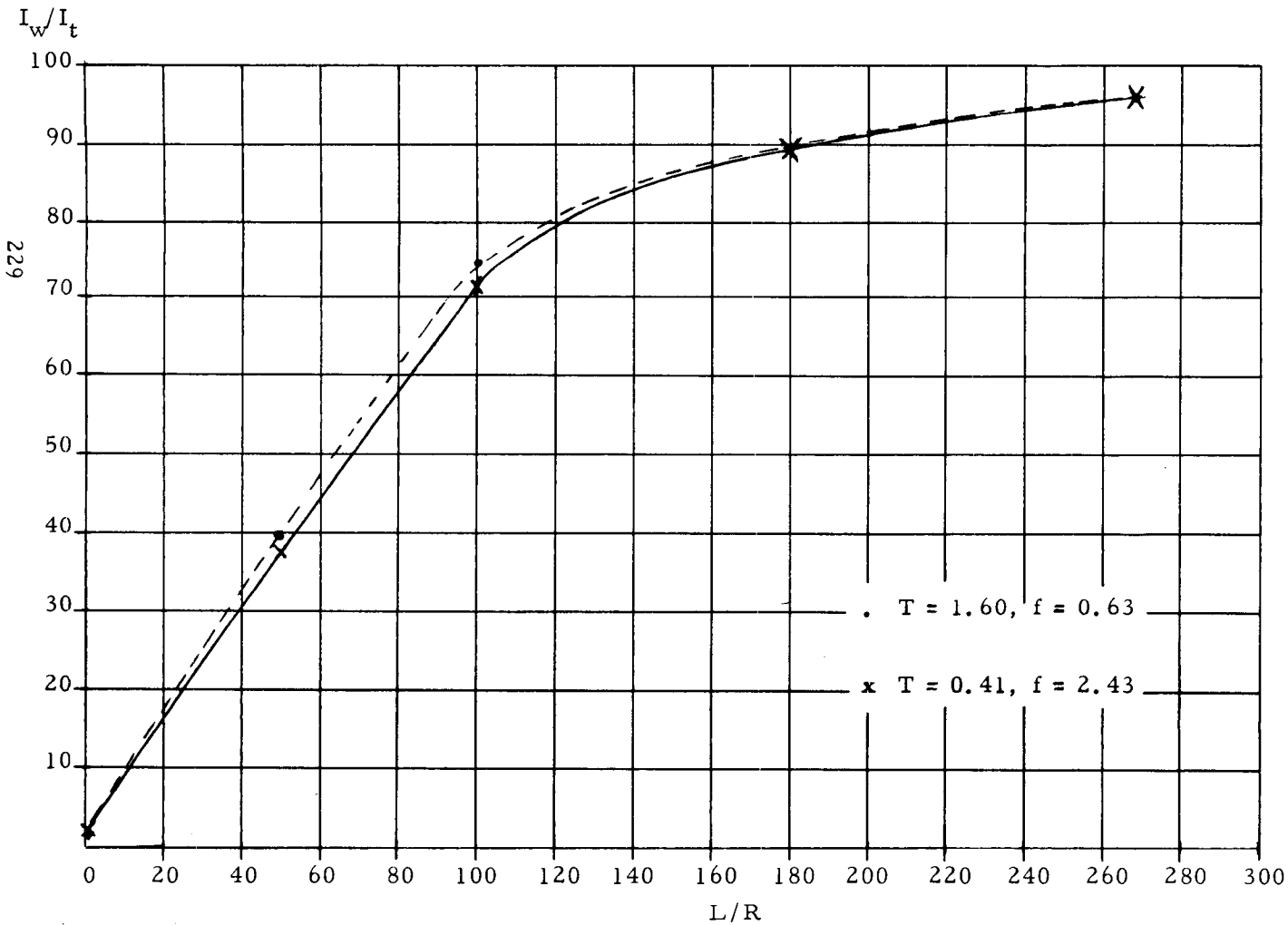

TABLE 28

TEST RESULTS FOR TANK C' AT FIVE DISPLACEMENTS

USING ROD 28

Displacement inches	T_e seconds	T_f seconds	I_e in-lb-sec^2	I_f in-lb-sec^2	I_w in-lb-sec^2	I_w/I_t percentage
$L_1 = 0$	1.49846	1.49864	10.014	10.016	0.002	1.40
$L_3 = 2.06$	1.50249	1.51062	10.068	10.177	0.109	39.57
$L_5 = 4.12$	1.51334	1.54557	10.214	10.653	0.440	74.78
$L_6 = 7.38$	1.54457	1.63912	10.640	11.982	1.342	89.08
$L_7 = 11.05$	1.59971	1.79962	11.413	14.443	3.031	95.91

The accuracies of the test results herein are the same as in the previous experiment, 0.1 percent. This is true because the air bearing table has a relatively constant error which depends somewhat on the object's size. The only other error which could have been introduced in this test program is that of aligning the tanks accurately on the table. The rough finish on the tanks and the bulkiness of the large tanks made this alignment difficult. The maximum error introduced by this misalignment could have not been greater than 0.5 percent.

2.3.1.2.5 Conclusions

The results of these tests have proven that the moment of inertia of a liquid rotating about a displaced axis does not obey the laws of solids for all cases. As a verification of Section 2.3.1.1 the first portion of the tests showed that the moment of inertia about the roll axis of a cylindrical tank was very small. For the 24-inch diameter tanks, approximately a 0.5 percentage I_w/I_t resulted for all aspect ratios while for the 8-inch diameter tanks a percentage of approximately 2.0 I_w/I_t resulted for the minimum aspect ratio and decreased as the aspect ratio increased. This variation was attributed to the difference in tank sizes. A linear relationship for the moment of inertia of the water and the aspect ratio was obtained as in Section 2.3.1.1 but the slope of the curves for the large and small tanks was different as would be expected. Further testing will be necessary if accuracies less than 2.0 percent are to be obtained for all size tanks.

The second series of tests produced valuable information pertaining to displaced axis liquid moments of inertia. The first results were that the aspect ratio did not affect the ratio I_w/I_t for a given displacement. Secondly the relationship between I_w/I_t and L/R was linear within experimental error for both sets of tanks up to an L/R ratio of 100 percent. The slope of the curve for this plot was approximately 0.7 for both tanks. The conclusions from these results were that the relationship of I_w/I_t to L/R was linear for a displacement of L= R and that this relationship was approximately

$$0.70(L/R) = I_w/I_t. \tag{154}$$

For a displacement of L > R the ratio of I_w/I_t appeared to approach 100 percent asymptotically as L/R increased. For example, at L/R of 200 percent I_w/I_t was 92 percent and at L/R of 300 percent, I_w/I_t was 97 percent. Therefore, depending on the accuracy desired, the ratio of L/R varied for the assumption I_w equal I_t. For practical purposes at L equals 4R, the I_w equals I_t.

The last tests were performed to determine the frequency effects on the moment of inertia. The effect of frequency on the moment of inertia was insignificant in these tests. This was true because of the limited frequency range available from the test equipment. For a larger frequency spread, a difference in moments of inertia would be expected, since liquid motion is frequency dependent.

The results of this test program were satisfactory and will be very useful in the theoretical equation correlation.

2.3.1.3 Yaw-Pitch Axis Inertia Tests

A series of tests were performed to determine the moment of inertia of a filled cylindrical tank as it oscillates about its yaw-pitch axis. The axis of oscillation was through the center of gravity and the tanks were oriented both in a horizontal and vertical direction. The results of this test program are reported in Section 2.3.1.4 which follows.

2.3.1.4 Yaw-Pitch Axis Inertia Tests Rotating About a Displaced Horizontal Axis

2.3.1.4.1 Introduction

This project component completes the testing which was performed in order to determine the moment of inertia of filled cylindrical tanks about various axes, and covers the yaw-pitch and displaced yaw-pitch axis tests. The results of these tests will be used to verify the accuracy of analytical expressions which have been derived.

The yaw-pitch axis tests were performed in two different ways to determine the effect of the tanks orientation on the liquid moment of inertia. First, the tanks were suspended from a torsion rod from the ceiling with their longitudinal axis parallel to the surface of the earth. Secondly, they were mounted in a stand with their longitudinal axis perpendicular to the earth. The later case also used a torsion rod to produce the oscillations. Five tanks, two feet in diameter, but with different aspect ratios were used with tap water as the liquid. Also, four different frequencies of oscillation were used on each tank to determine if the moment of inertia was frequency dependent.

The displaced yaw-pitch axis tests were performed using two of the previous mentioned tanks and the later procedure described above. The rotation axis of the tanks was displaced from the center of mass of the tank at various displacements and was oscillated as a compound pendulum. Also, torsion rods were added to change the frequency of oscillation. These tests provide

very good results for the moment of inertia of a liquid filled tank about any yaw-pitch axis.

2.3.1.4.2 Yaw-Pitch Axis Tests Using a Torsional Pendulum

2.3.1.4.2.1 Test Procedure

The first tests performed were those with the tank oscillating about a vertical axis perpendicular to the tank's longitudinal axis. Figure 116 shows this test set-up. An I-beam permanently mounted in the ceiling was used as the supporting element. This beam was equipped with leveling plates so that the rod could be aligned vertically on the plate. The tank was then mounted to the other end of the rod. Five tanks were used in the experiments, each with a diameter of approximately two feet but with different lengths. The exact tank dimensions are given in Table 29 where the tank designation, A through E, will be used in the remainder of the report.

The other equipment was used to determine the maximum amplitudes and periods of oscillations of the tank. The maximum amplitudes were measured by using a light source, mirror, and a calibrated radian scale located at exactly 140 inches from the axis of rotation. The light was reflected off of a mirror mounted on the torsion rod onto the radian scale where the maximum displacement was obtained by reading the scale directly. The period measuring system consisted of a light source, photocell, knife edge, electronic circuitry, and a counter. The knife edge was mounted on the tank and the photo detector was aligned so that the knife edge broke the light beam as the tank oscillated. The output from the detector was fed via appropriate electronic circuitry into a digital counter which determined the period of oscillation. A digital printer was also available for recording the data output.

The tests were performed by displacing the tank and taking a period average of the first 50 cycles as the amplitues decayed from 0.03 radians. To stabilize the oscillations a teflon bearing was placed against the torsion rod. The tank was initially displaced to 0.05 radians and when it decayed to 0.03 radians the bearing was removed. The period was then used in

$$I = KT^2/4\pi^2 \tag{155}$$

where K is the rod constant, to determine the moment of inertia of the tank.

FIGURE 116

VERTICAL YAW-PITCH AXIS TEST SET UP

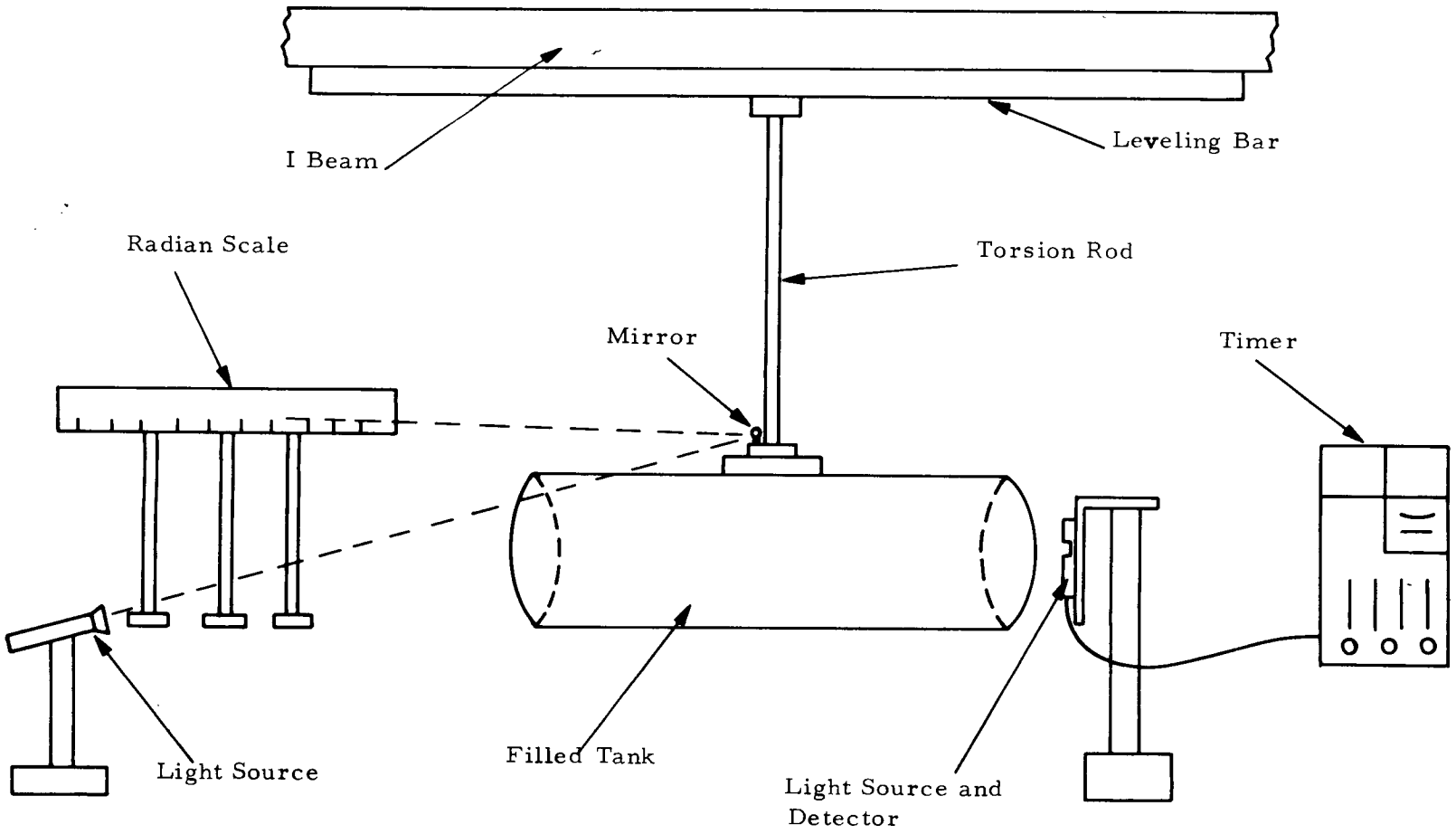

TABLE 29

Physical Characteristics of Cylindrical Tanks

Tank	W_e	W_f	h	d	t
A	30.27 lbs.	128.0 lbs.	6.5 in.	24.25 in.	.25 in.
B	36.23	231.0	12.5	24.25	.25
C	72.77	381.0	20.0	24.50	.375
D	103.00	684.0	36.75	24.50	.375
E	130.00	906.0	48.75	24.50	.375

Water in Tank	W_w	m_w	h_w	d_w	h_w/d_w	I_s
A	97.73 lbs.	.253 lb-sec^2/in	6.0 in.	23.75 in.	.253	9.68 in-lb-sec^2
B	194.77	.505	12.0	23.75	.505	23.86
C	308.23	.799	19.25	23.75	.811	52.84
D	581.00	1.506	36.0	23.75	1.515	215.74
E	776.00	2.012	48.0	23.75	2.021	457.23

Since amplitude does not affect the moment of inertia, small displacements were used to prevent aerodynamic losses. Each test was performed three times for repeatability. The test procedure is shown in Appendix C3.

Each tank was tested empty and full with four different torsion rods. The difference between the moment of inertia of the empty and full tank was that of the water for a given frequency. This value was then compared to the theoretical value for that of a solid. The results of these tests are shown in Tables 30 and 31 wherethe symbols are defined in the List of Symbols.

Next the yaw-pitch axis tests were performed with the axis of rotation in a horizontal plane but still perpendicular to the tank longitudinal axis. Figure 117 shows this test set-up. The test procedure for this set-up is the same as that previously described with the exception of the displacement measuring equipment. In this tests a calibrated scale was mounted under the tank and a wand attached to the tank was used to read the maximum displacements. The tank was supported by special brackets and oscillated in ball bearings. Four different torsion rods were used again to produce different frequencies of oscillation. The test procedure for these tests are shown in Appendix C4. These test results are shown in Tables 32 and 33.

2.3.1.4.2.2 Test Results

The first obvious conclusion which can be made from these tests is that the orientation of the axis of rotation does not affect the value of the moment of inertia of a filled cylindrical tank. This would be expected because the orientation does not affect the liquid. The results of these two separate tests gave very good results. Next, the frequency of oscillation did not affect the moment of inertia for the frequency range covered. Extremely high or low frequencies would probably have an effect on the moment of inertia just as higher or lower viscosity liquids would. The effect of varing aspect ratios can best be shown in Figure 118 where I_w/I_s is plotted against h/d. The shape of this curve agrees with the results of other investigators. These results will be compared to the analytical expression derived in Section 2.3.2.2 to verify the accuracy of the analytical expressions.

2.3.1.4.3 Displaced Yaw-Pitch Axis Tests Using A Compound Torsional Pendulum System

2.3.1.4.3.1 Test Procedure

The test procedure for the displaced axis was identical to that previously discussed with the exception of the axis of rotation being displaced various amounts as shown in Figure 119. The moment of inertia of this

FIGURE 117

HORIZONTAL YAW-PITCH AXIS TEST SET UP

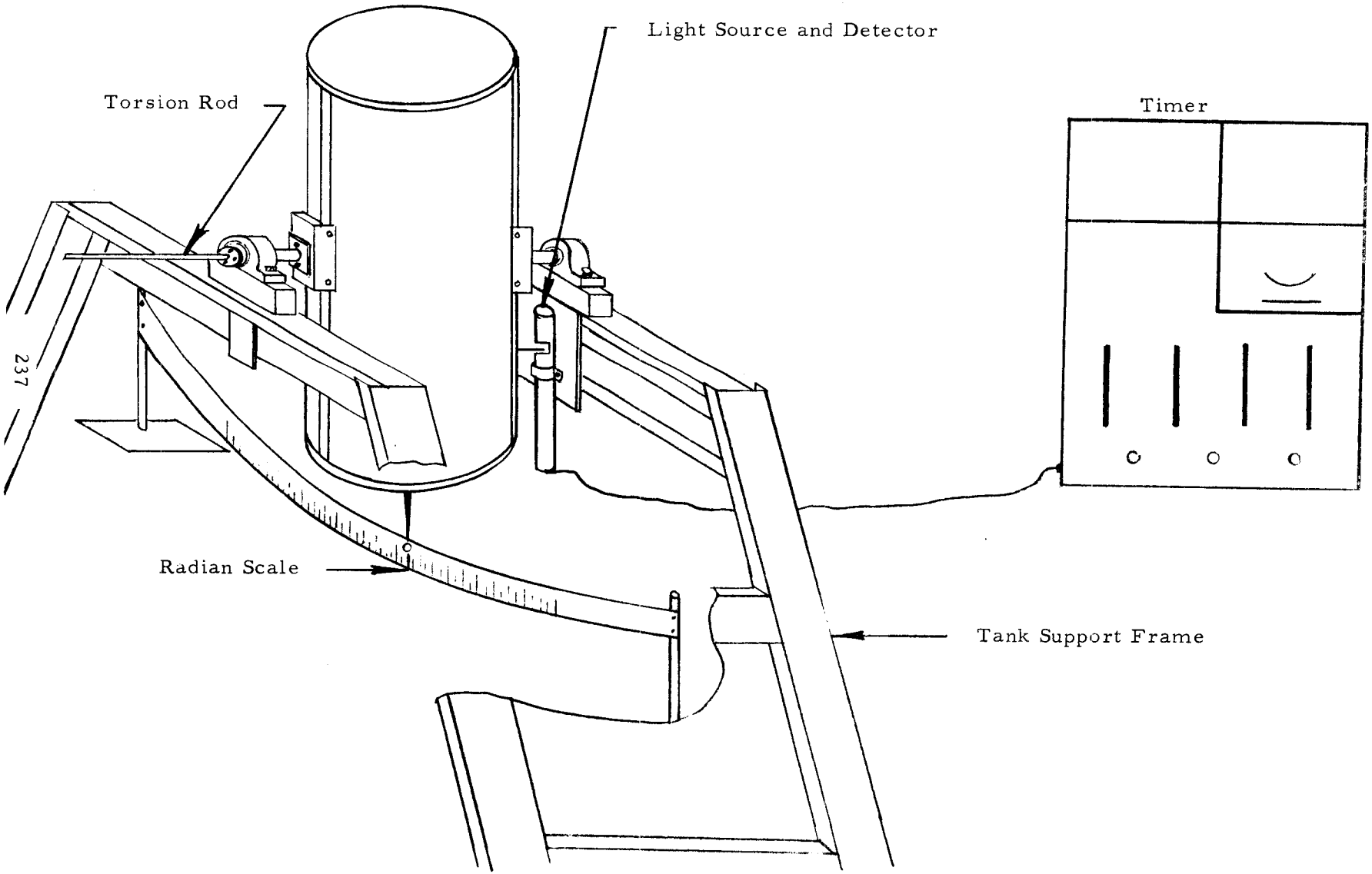

FIGURE 118

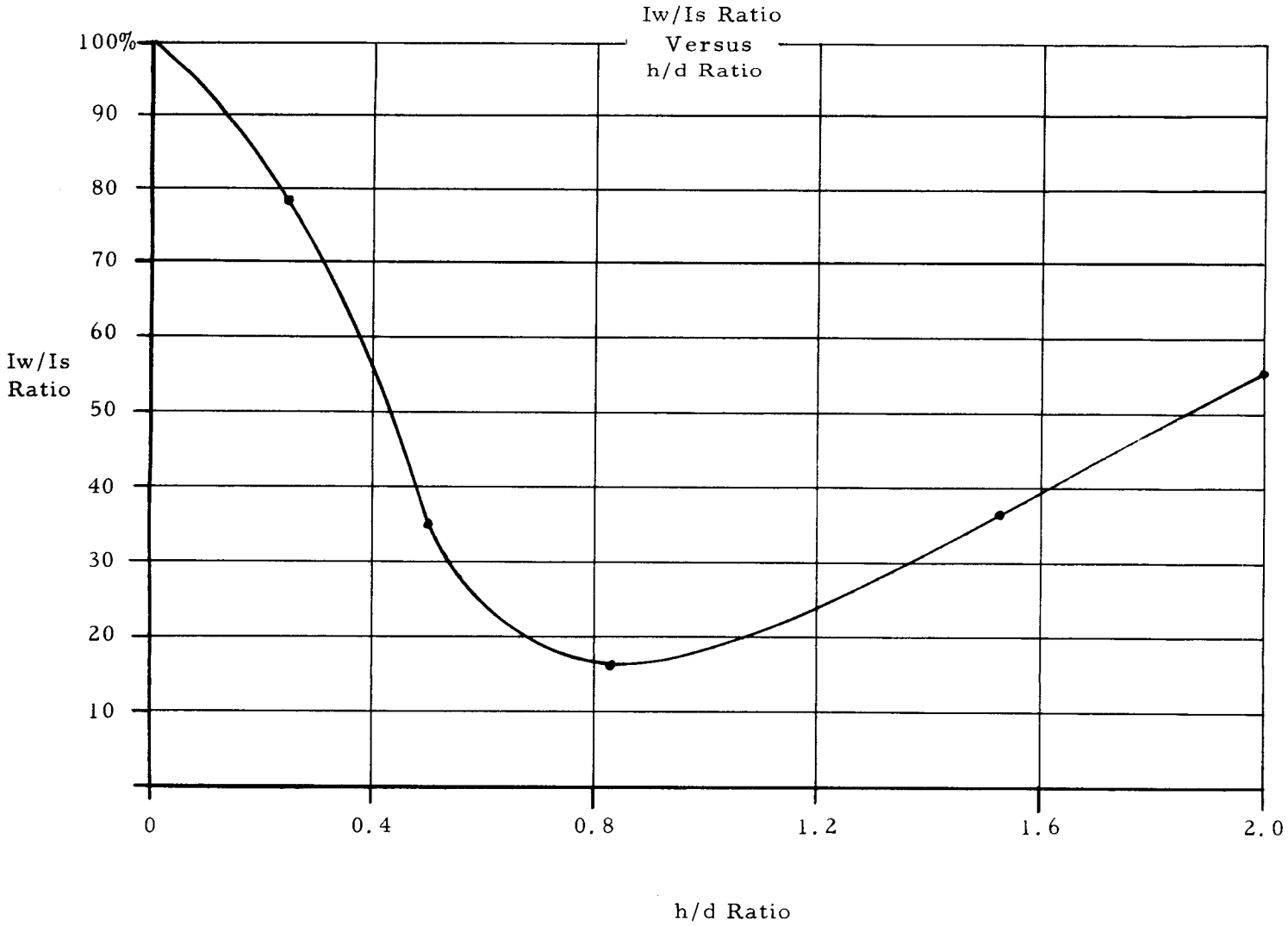
Iw/Is Ratio
Versus
h/d Ratio
100%
90
80
70
60
50
40
30
20
10
Iw/Is
Ratio
0
0.4
0.8
1.2
1.6
2.0
h/d Ratio

FIGURE 119

DISPLACED YAW-PITCH AXIS TEST SET UP

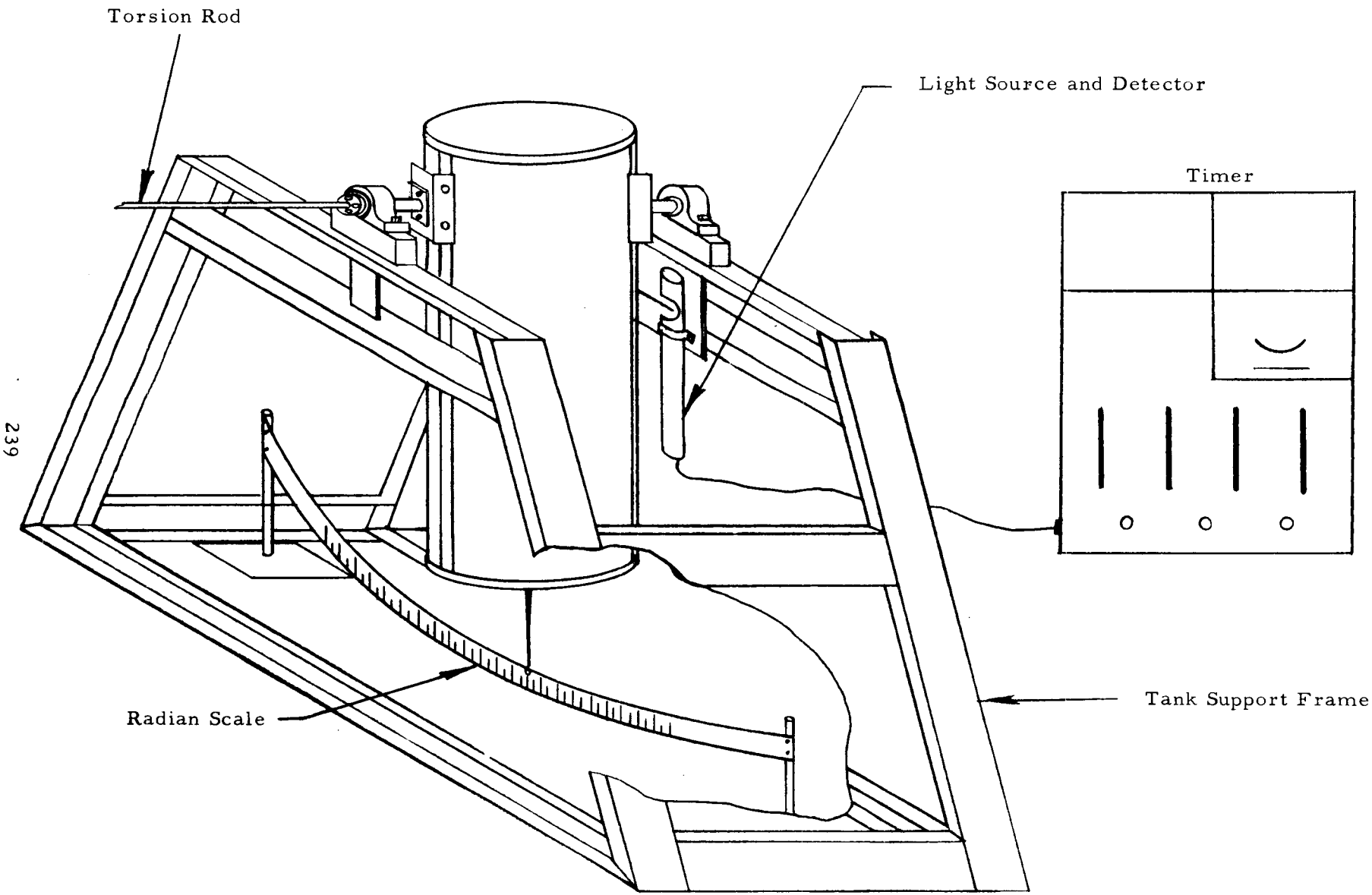

TABLE 30

Test Results For Suspended Pendulum Tests

Tank	h/d	Rod	Rod Constant	T_e sec.	T_f sec.	f cycles/sec
	.253	3	68.87	1.48450	2.53857	.39392
A	"	104	482.11	.56523	.96594	1.03526
	"	101	1,540.68	.31454	.53697	1.86230
	"	103	3,007.54	.22217	.38040	2.62881
	.505	3	68.87	1.97480	2.96949	.33676
B	"	104	482.11	.74604	1.12347	.89010
	"	102	2,058.52	.36201	.54170	1.84604
	"	108	5,008.31	.23177	.34732	2.87918
	.811	3	68.87	3.52671	4.16086	.24033
C	"	101	1,540.68	.74759	.87942	1.137110
	"	107	7,503.23	.33763	.39532	2.52960
	"	122	15,559.47	.23431	.27438	3.64458
	1.515	3	68.87	6.07029	9.03067	.11073
D	"	109	3,752.66	.82211	1.22213	.81824
	"	122	15,559.47	.40281	.59586	1.67824
	"	123	49,177.49	.227216	.340698	2.93515

TABLE 31

Test Results For Suspended Tank Tests

Tank	f cycles/sec	I_e in-lb-sec^2	I_f in-lb-sec^2	I_w in-lb-sec^2	I_w/I_s	I_w/I_s Average
	.39392	3.84	11.24	7.40	76.4%	
A	1.02966	3.90	11.39	7.49	77.4	76.7%
	1.86230	3.86	11.25	7.39	76.3	
	2.62881	3.85	11.28	7.43	76.8	
	.33676	6.80	15.38	8.58	36.0%	
B	.89010	6.80	15.41	8.62	35.2	35.9%
	1.84604	6.83	15.30	8.47	35.5	
	2.87919	6.81	15.30	8.49	35.7	
	.24033	21.70	30.21	8.50	16.1%	
C	1.13711	21.81	30.18	8.37	15.8	15.6%
	2.52960	21.66	29.70	8.04	15.2	
	3.64458	21.64	29.67	8.03	15.2	
	.11073	64.28	142.27	77.99	46.3%	
D	.81824	64.24	141.98	77.74	46.1	36.2%
	1.68127	63.95	139.93	75.98	45.1	
	2.93515	64.31	144.60	80.28	47.6	

TABLE 32

Test Results For Supported Tank Tests

Tank	h/d	Rod	Rod Constant	T_e sec.	T_f sec.	f cycles/sec.
	.811	106	975.68	1.18480	1.31760	.75895
C	"	103	3,077.54	.66605	.74341	1.34515
	"	107	7,503.23	.43115	.47795	2.09226
	"	122	15,559.47	.30160	.33420	2.99222
	1.515	106	975.68	1.78660	2.51403	.39776
D	"	103	3,077.54	1.00586	1.41520	.70661
	"	107	7,503.23	.64032	.90402	1.10617
	"	122	15,559.47	.44553	.63501	1.57477
	2.021	106	975.68	2.31049	3.93631	.25404
E	"	103	3,077.54	1.30521	2.21738	.45098
	"	107	7,503.23	.84472	1.43039	.69911
	"	122	15,559.47	.57872	.98612	1.01407

TABLE 33

Test Results For Supported Tank Tests

Tank	f cycles/sec.	I_e in-lb-sec^2	I_f in-lb-sec^2	I_w in-lb-sec^2	I_w/I_s	I_w/I_s Average
	.75895	34.69	42.91	8.22	15.6%	
C	1.34515	34.58	43.08	8.50	16.1	15.625
	2.09226	35.33	43.42	8.09	15.3	
	2.99222	35.85	44.03	8.18	15.5	
	.39776	78.89	156.20	77.31	35.8%	
D	.70661	78.87	156.13	77.26	35.8	36.225
	1.10617	77.92	155.33	77.41	35.9	
	1.57477	78.23	158.92	80.69	37.4	
	.25404	131.93	382.94	251.00	54.9%	
E	.45098	132.80	383.29	250.49	54.8	55.05
	.69911	135.62	388.86	253.24	55.4	
	1.01407	132.56	384.34	251.78	55.1	

system is determined by using:

$$I = (WL + K)T^2/4\pi^2 \tag{156}$$

This equation is obtained from the equation of motion of the system which is:

$$I\ddot{\theta} + WL\sin\theta + K\theta - Mf = 0 \tag{157}$$

where:

W	=	weight of the system
L	=	distance between the pivot point and center of mass of the system
K	=	rod constant
Mf	=	losses (air drag, bearing friction, etc.)

For small angles of displacement we can let,

$$\sin\theta = \theta$$

and neglect Mf which is relatively small. The moment of inertia of the water was determined by subtracting I_f from I_e for a given rod constant and axis displacement. The test procedure is shown in Appendix C5. The results of these tests are shown in Tables 34 and 35 where tank C and D have been used.

2. 3. 1. 4. 3. 2 Test Results

The frequency of oscillation in these tests did not affect the moment of inertia. The variation in the values of the moment of inertia was attributed to experimental error. As the axis displacement increased so did the moment of inertia, as was expected. Also, the ratio of I_w/I_s increased as the aspect ratio increased. The term ν shown in the test results is defined as:

$$\nu = 1/2 + L/h \tag{158}$$

where:

L	=	distance between pivot point and center of mass of the tank
h	=	tank height

TABLE 34

Test Results
Displaced Axis Tests For Tank C
Aspect Ratio—0.811

Rod Number	Rod Constant	Moment of Inertias (in-lb-sec^2)				
		L_1 = 2.0"	L_2 = 5.0"	L_3 = 8.0"	L_4 = 11.0"	L_s = 21.0"
None	------	-----	-----	-----	105.28	364.30
106	975.68	10.96	31.02	62.64	109.35	373.57
103	3077.54	11.34	35.06	63.76	114.64	373.57
107	7503.23	-----	32.19	65.38	112.05	------
Averages-I_w		11.15	32.76	63.93	110.33	370.48
Theoretical-I_s		56.04	72.82	103.98	149.52	404.41
I_w/I_s		0.20	0.45	0.615	0.735	0.92
ν		0.60	0.76	0.92	1.07	1.60

TABLE 35

Test Results
Displaced Axis Tests For Tank D
Aspect Ratio—1.506

Rod Number	Rod Constant	Moment of Inertias (in-lb-sec^2)			
		L_1 = 4.0"	L_2 = 10.0"	L_3 = 16.0"	L_4 = 21.0"
None	-------	96.16	222.80	458.73	738.45
106	975.68	102.22	227.75	463.15	744.54
103	3077.54	103.86	230.25	469.38	750.12
Average-I_w		100.75	226.93	463.75	744.37
Theoretical-I_s		239.84	366.34	601.28	879.89
I_w/I_s		0.42	0.62	0.77	0.85
ν		0.61	0.78	0.94	1.08

This will be used in comparing the experimental results to the analytical results in Section 2. 3. 2. 2.

2. 3. 1. 4. 4 Conclusions

The results of these tests did not present anything new or unexpected. The main purpose of testing was to verify the analytical expressions which are derived in Section 2. 3. 2. 2 so that the moment of inertia can be obtained for any size cylindrical tank under various conditions. Section 2. 3. 2. 2 will discuss these results in more detail.

2. 3. 1. 5 Ring Baffle Tests Using Government Furnished Plexiglass Tank

2. 3. 1. 5. 1 Introduction

The studies covering the moment of inertia of a filled cylindrical tank with smooth walls has been investigated in detail in prior projects of the mass properties of liquids program. In continuing the program, this project will investigate the effect of various ring baffles; that is, different baffle widths and spacings, on the liquid moment of inertia of a filled cylindrical tank as it oscillates about a yaw-pitch axis.

Baffles are mainly used as liquid slosh suppressors in launch vehicle fuel tanks. Slosh is defined as liquid surface motion in a partially filled tank as compared to the internal rotational motion in a filled tank. This slosh can be very detrimental to the stability of the vehicle if the slosh frequency approaches that of the control frequency of the space vehicle. Therefore, baffles are used to prevent the slosh from reaching such frequencies and magnitudes which could impair the flight, if not completely destroy the vehicle.

Since baffles are used in most fuel tanks, it is necessary to determine the effect of baffles on the liquid moment of inertia. The motion of liquid within a container is determined by its boundary conditions and the tanks motion. The boundary conditions are also dependent on the tanks shape and objects, such as baffles, within the tank. An analytical solution for such a system is extremely difficult to solve if not impossible; therefore, experimental studies of the problem are necessary.

The test program presented here is similiar to the other liquid programs with the exception of the use of baffles. The government furnished plexiglass tanks with baffles was used in a support stand for one set of tests and a segment of the plexiglass tank was used on the air bearing table for another set of tests. Better data was obtained in the latter method.

LIST OF SYMBOLS

SYMBOL	DEFINITION
W_e	Weight of Empty Tank in Pounds
W_f	Weight of Tank Filled with Water in Pounds
W_w	Weight of Water in Pounds
g	Acceleration of Gravity - 385.684 in/sec^2
m_w	Mass of Water = W_w/g lb-sec^2/in
h	Tank Height in Inches
h_w	Water Height
d	Tank Diameter
d_w	Water Diameter
t	Tank Wall Thickness
h_w/d_w	Aspect Ratio of Water
T_e	Period of Oscillation for Empty Tank in Seconds
T_f	Period of Oscillation for Full Tank
f	Frequency of Oscillation of Full Tank
K	Rod Spring Constant
I_e	Moment of Inertia for Empty Tank and Table Top
I_f	Moment of Inertia for Full Tank and Table Top
I_s	Moment of Inertia of Water = $I_f - I_e$
I_s	Moment of Inertia of Water if it were a Solid
I_w/I_s	Ratio of the Moment of Inertia of Water so that of Water as a Solid
L	Distance Between Pivot Point and Center of Mass

The results of this program will be used to help derive analytical expressions for tanks with ring baffles.

2.3.1.5.2 Test Using Plexiglass Tank and Stand

2.3.1.5.2.1 Test Procedure

Figure 120 shows the equipment arrangement for these tests and Figure 121 shows the tank and baffle dimensions. Table 36 gives the tank characteristics. The center of mass of the empty tank was measured on the Bytrex System and that of the full tank was calculated using the known dimensions. This latter position was verified after the tank was mounted in the stand. All tests were performed about the center of mass of the full system and the results for the empty system were transferred to the center of mass of the empty system. The period of oscillation was measured by using a photo detector and counter which was equipped with a digital printer. The period of oscillation was varied by using different torsion rods. The maximum displacements were measured with a calibrated scale mounted under the tank. Small displacements were used so that aerodynamic drag losses would be small. The moment of inertia of the system was determined by using:

$$I = KT^2/4\pi^2 \tag{159}$$

where K is the rod constant of the rod being used and T is the period of oscillation. A detailed test procedure is shown in Appendix C6.

2.3.1.5.2.2 Test Results

The test results are shown in Table 37. I_e, the moment of inertia of the empty system has been determined by using Equation 159. Because the empty system is oscillated about a displaced axis we must use:

$$I = (WL + K)T^2/4\pi^2 \tag{160}$$

to determine $I_{c.m.}$. This is accomplished by subtracting $WLT^2/4$ from I in Equation 160 to obtain $I_{e\ c.m.}$. $I_{f\ c.m.}$ is determined by using Equation 159 where the full tank is oscillated about its center of mass. I_{eff} is determined by subtracting $I_{e\ c.m.}$ which eliminates the tank. I_{eff}/I_{solid} is then determined where I_{solid} is calculated in Table 37. The results without baffles are the same as above, except $I_{e\ c.m.}$ was determined by subtracting $I_{baffles}$ from the $I_{e\ c.m.}$ with baffles.

The bottom of the tank is a hemisphere, but it was analytically converted to an equivalent flat bottom. Reference 1, for comparison to other

FIGURE 120

EQUIPMENT ARRANGEMENT FOR BAFFLE TESTS

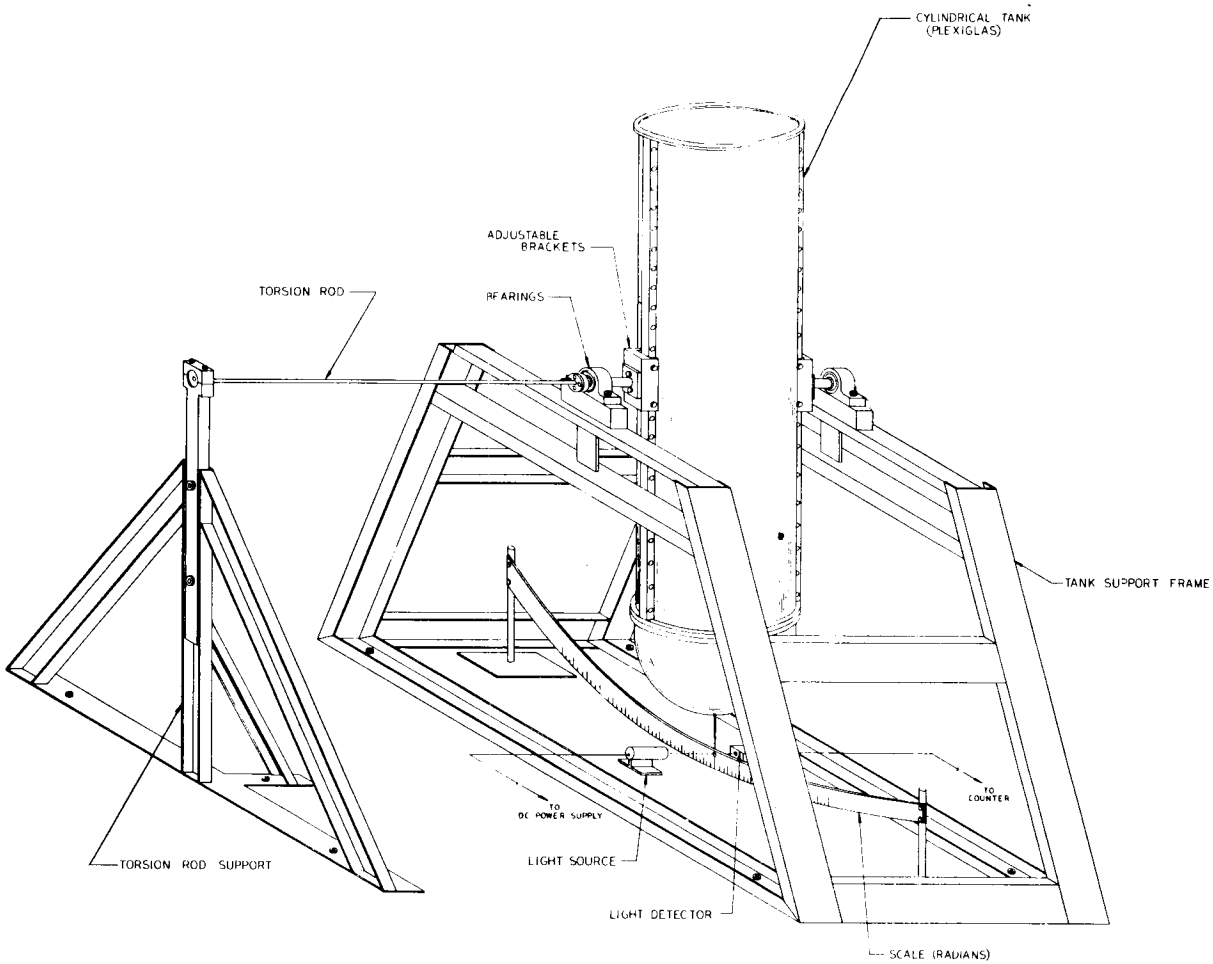

FIGURE 121

TANK DIMENSIONS

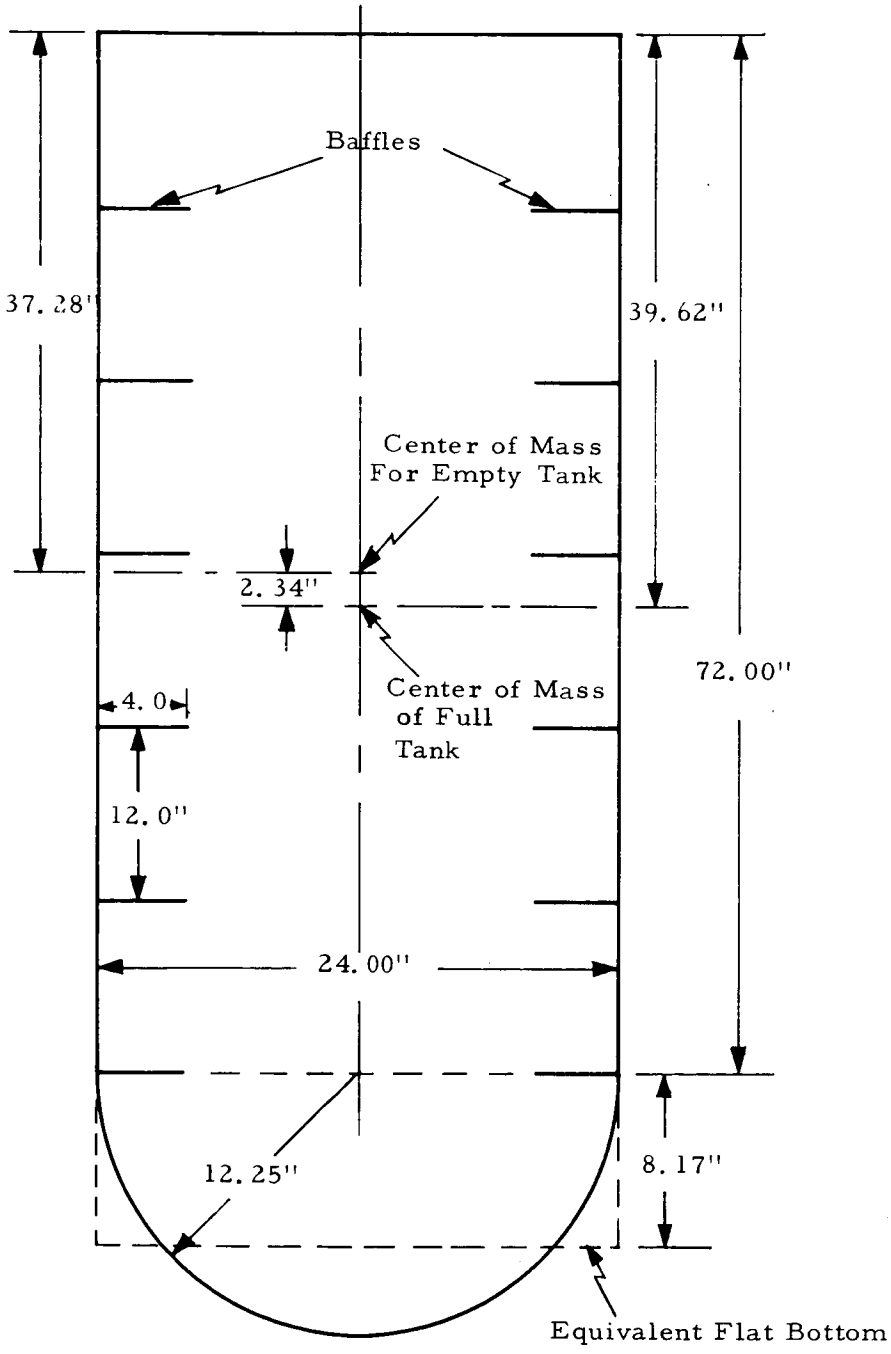

TABLE 36

TANK CHARACTERISTICS

h	$= 80.17''$	g	$= 385.684\ in/sec^2$
d	$= 24.0''$	ρ_{water}	$= 0.036\ lb/in^3$
a	$= 12.0''$	$W_{empty\ tank}$	$= 207.0$ lbs.
b	$= 12.0''$	$W_{baffles}$	$= 14.0$ lbs.
w	$= 3.0''$	$I_{baffles}$	$= 16.99\ in\text{-}lb\text{-}sec^2$
h/a	$= 6.68''$		

A. Hemisphere of Water

$V = 2\pi a^3/3 = 3850.0\ in^3 \quad W = V\rho = 138.75$ lbs. $\quad M = 0.36\ \frac{lbs.\text{-}sec^2}{in}$

$I_{c.m.} = 0.26\ Ma^2 = 14.05\ in\text{-}lb\text{-}sec^2$

$I_{c.m.\ full\ tank} = I_{c.m.} + ML^2_{hemi} = 506.20\ in\text{-}lb\text{-}sec^2$

B. Cylinder of Water

$V = \pi a^2 h = 32,572.0\ in^3 \quad W = V\rho = 1173.9$ lbs. $\quad M = 3.044\ \frac{lb\text{-}sec^2}{in}$

$I_{c.m.} = M(d^2/16 + h^2/12) = 1424.57\ in\text{-}lb\text{-}sec^2$

$I_{c.m.\ full\ tank} = I_{c.m.} + ML^2_{cyl} = 1464.48\ in\text{-}lb\text{-}sec^2$

C. System of Water

$I_{solid} = I_{c.m.\ hemisphere} + I_{c.m.\ cylinder} = 1970.68\ in\text{-}lb\text{-}sec^2$

D. Equivalent Flat Bottom

$h' = 3850/\pi(12.25)^2 = 8.17''$

TABLE 37

TEST RESULTS

Plexiglass Tank with 4.0" Baffles Spaced 12.0"

Rod	103	107	122
K	3077.54	7503.23	15,559.47
T_e	2.3100	1.4220	0.9843
I_e	415.98	384.32	381.85
$I_{e\ c.m.}$	350.51	359.51	369.96
T_f	5.0497	3.2428	2.2670
$I_{f\ c.m.}$	1987.81	1998.62	2025.53
$I_{eff} = I_{f\ c.m.} - I_{e\ c.m.}$	1637.31	1639.11	1655.57
I_{eff}/I_{solid}	0.83	0.83	0.84

Average I_{eff}/I_{solid} = 0.83

Plexiglass Tank with No Baffles

$I_{e\ c.m.}$	333.52	342.52	352.97
T_f	4.840	3.1601	2.2446
$I_{f\ c.m.}$	1826.15	1897.98	1983.93
$I_{eff} = I_{f\ c.m.} - I_{e\ c.m.}$	1492.63	1555.46	1630.96
I_{eff}/I_{solid}	0.76	0.79	0.82

Average I_{eff}/I_{solid} = 0.79

data. This is accomplished by equating the volume of a hemisphere to that of a cylinder and calculating the height. This has been accomplished in Table 37.

The results of these tests are compared to the analytical curve for a smooth walled cylinder in Figure 122. The results are very good for the no-baffle case and the increase of I_{eff}/I_{solid} for the baffle case is as expected.

The limited amount of data obtained from this test set-up is attributed to several causes. The main cause is the tank size. Only one aspect ratio can be tested and this ratio is too large to produce worthwhile data. The effect of baffles at this ratio is relatively small, compared to that at a smaller ratio. The large size of the tank also presents problems in testing. Small torsion rods cannot be used because they cannot drive the large tank. When larger rods are used the stationary mount holding the end of the rods defects under the large forces. This is evident in the test results presented in Table 36 where the moment of inertia increases with the rod constant. This occurs because the effective K becomes less; therefore, T increases and I increases. All these problems have led to the design of a smaller tank which can be mounted on the air bearing table. These tests produced better results.

2.3.1.5.3 Tests Using The Air Bearing Table

2.3.1.5.3.1 Test Procedure

In order to save money and time, a two foot segment of the government furnished plexiglass tank was used for the air bearing table test. Since baffles and spacers were already provided for the plexiglass tank, the only modifications required were those of sealing one end of the tank and fabricating brackets for mounting the tank to the air bearing table. Figure 123 shows the tank dimensions, baffle width, and spacings used in the tests. The detailed operation of the moment of inertia determining system is covered in Reference 2; therefore, it will not be repeated here. The actual test procedure used is shown in Appendix C7.

2.3.1.5.3.2 Test Results

The test results for the 4.0 and 1.2 inch baffles are shown in Tables 38 and 39 respectively and plotted in Figure 124. The results show that wider baffles and a larger number of baffles produce a larger effective moment of inertia, as was expected. Tables 40 and 41 show the test results for the 1.2 inch baffles with 3 inch spacer. The only difference in each test is the number of baffles and their locations, as shown in the tables. Figure 125 shows these results in plotted form. The baffles have more effect if they

FIGURE 122

COMPARISON OF ANALYTICAL AND EXPERIMENTAL RESULTS OF I_{eff}/I_{solid}

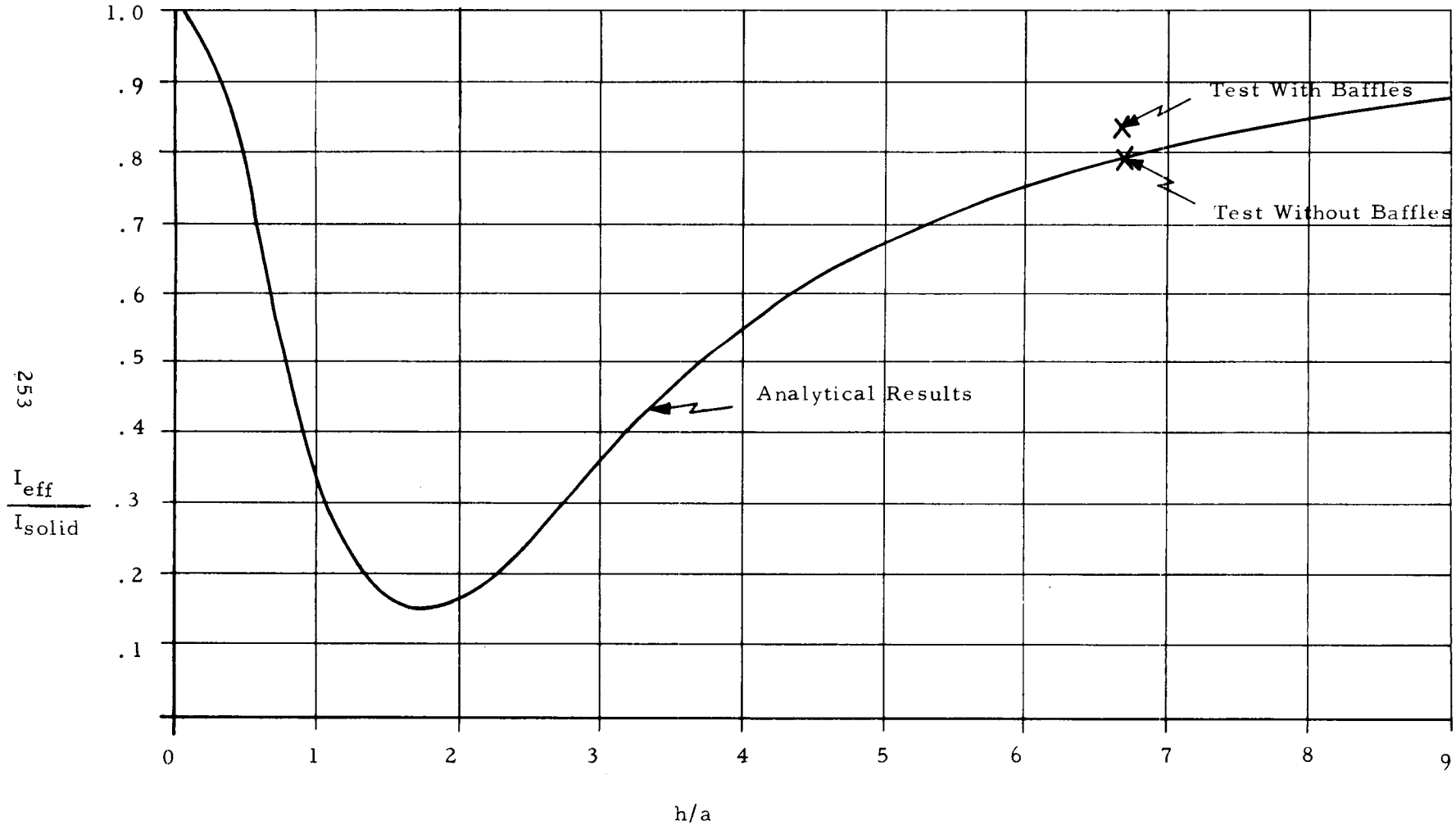

FIGURE 123

SMALL TANK DIMENSIONS

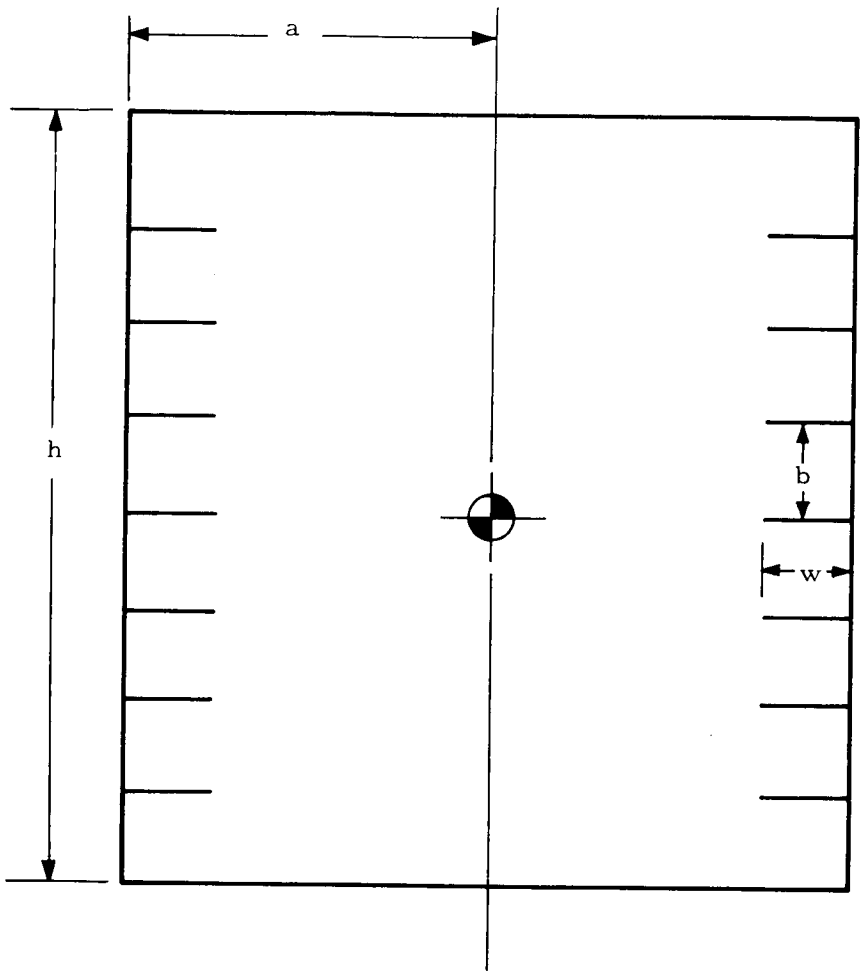

h = 24.0"	a = 12.0"	h/a = 2.0"
w = 4.0", 1.2"		w/a = 0.33, 0.10
b = 3.0", 4.0", 6.0"		b/a = 0.25, 0.33, 0.50
W_e = 73.0 lbs.	W_f = 468.0 lbs.	W_w = 395.0 lbs.

FIGURE 124

I_{eff}/I_{solid} VERSUS NUMBER OF BAFFLES

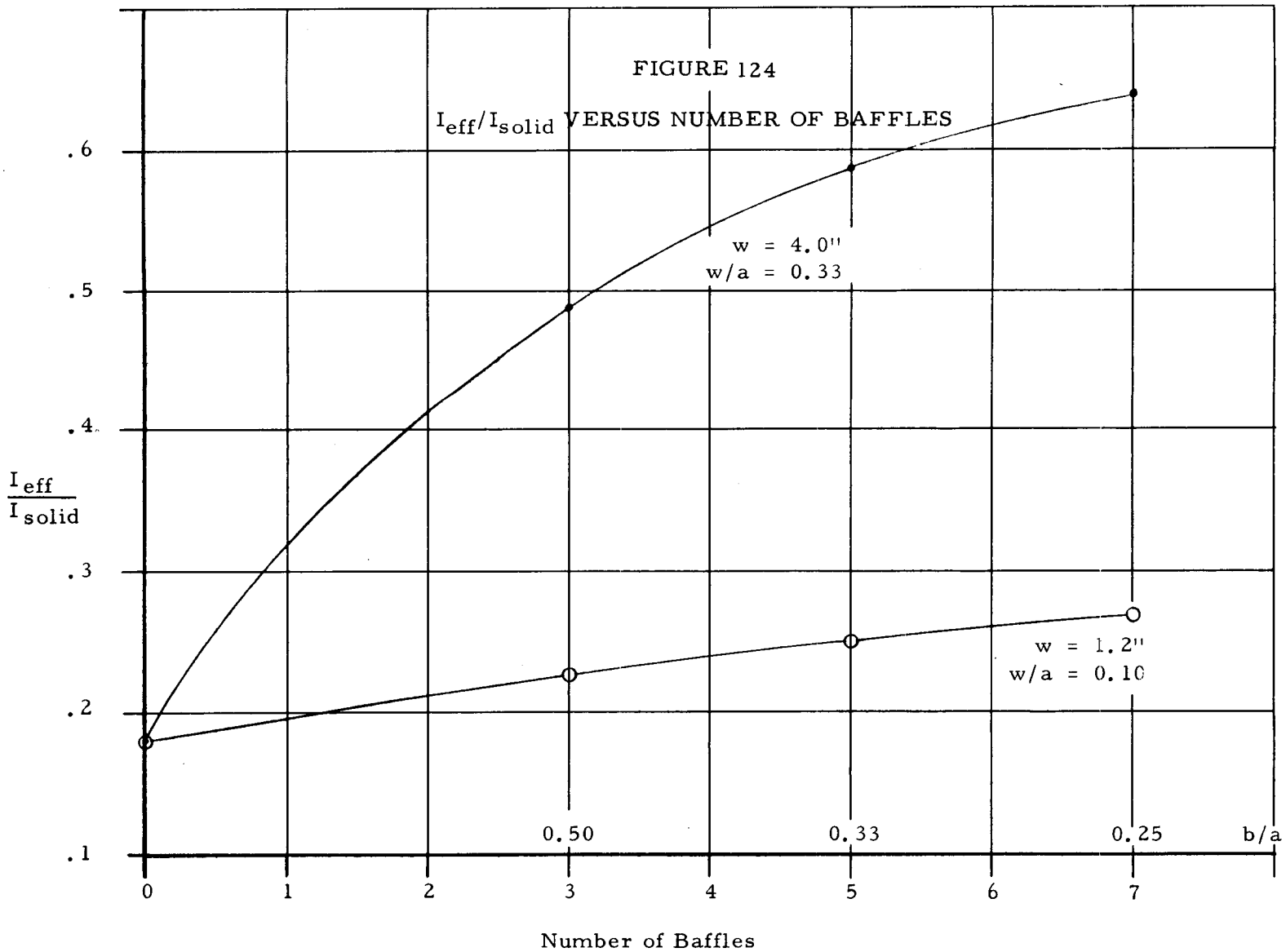

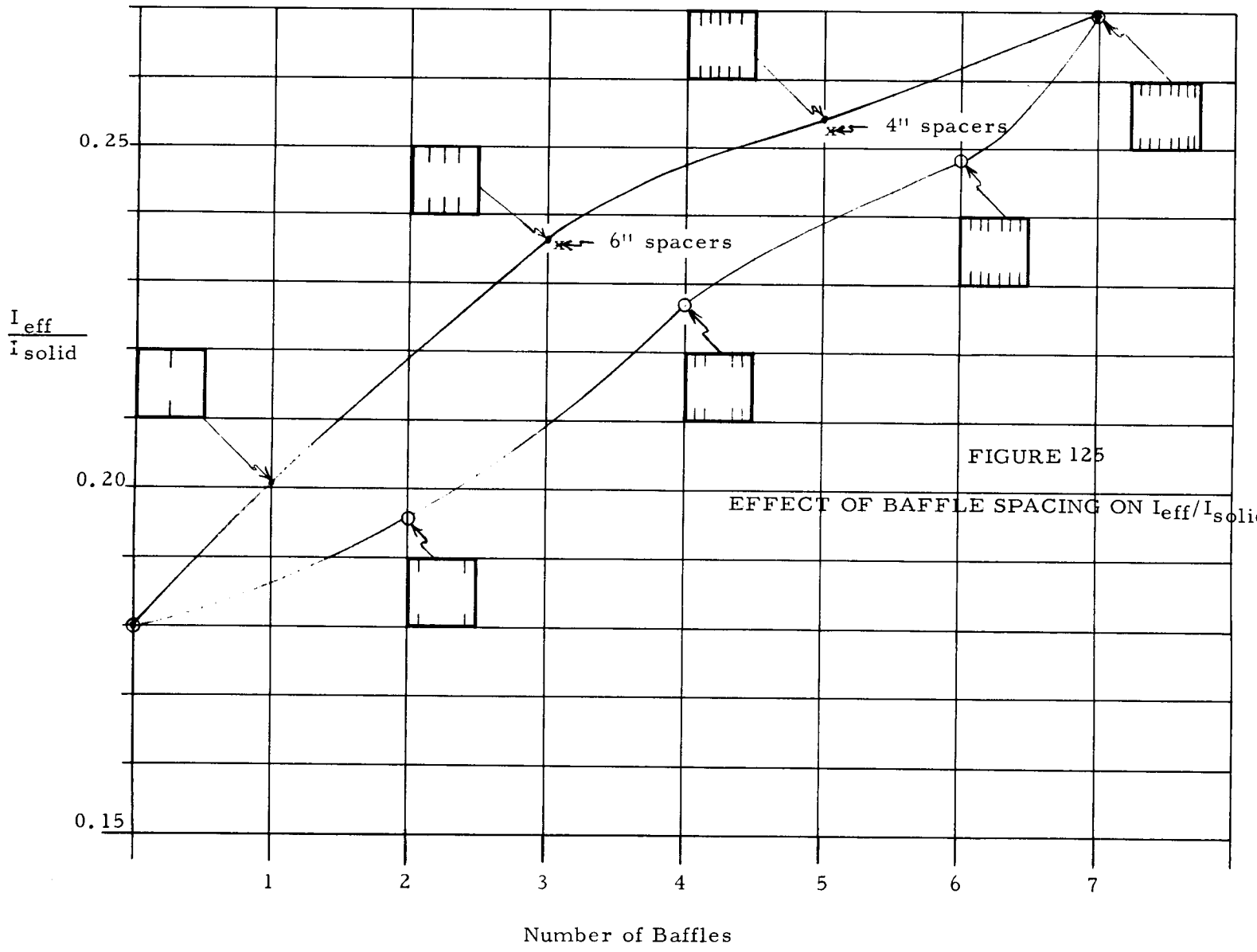

FIGURE 125

EFFECT OF BAFFLE SPACING ON I_{eff}/I_{solid}

TABLE 38

TEST RESULTS

w = 4.0" w/a = 0.33

Number of Baffles	None	3	5	7
	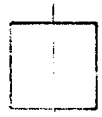	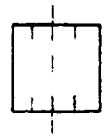	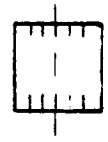	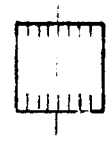
Baffle Location				
b	------	6.0 "	4.0 "	3.0 "
b/a	------	0.50	0.33	0.25
T_e	0.4901	0.4979	0.5022	0.5089
T_f	0.5732	0.6978	0.7331	0.7547
I_e	41.54	42.70	43.63	44.61
I_f	56.82	83.98	92.96	98.24
I_{eff}	15.28	41.27	49.34	53.63
I_{solid}	86.03	84.94	84.29	83.42
I_{eff}/I_{solid}	0.18	0.49	0.59	0.64

$I = KT^2/4\pi^2$ K = 6828.0 in-lbs.

$I_{eff} = I_f - I_e$

$I_{solid} = (W_{liq} - W_B)(d^2/16 + h^2/12)/g$

W_{liq} = 395.0 lbs.

W_{3B} = 5.0 lbs.

W_{5B} = 8.0 lbs.

W_{7B} = 12.0 lbs.

TABLE 39

TEST RESULTS

w = 1.2" w/a = 0.10"

Number of Baffles	None	3	5	7
		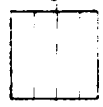		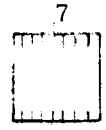
Baffle Location				
b	------	6.0 "	4.0 "	3.0 "
b/a	------	0.50	0.33	0.25
T_e	0.4902	0.4947	0.497	0.498
T_f	0.573	0.598	0.607	0.616
I_e	41.55	42.32	42.64	42.93
I_f	56.76	61.80	63.73	65.57
I_{eff}	15.21	19.48	21.09	22.63
I_{solid}	86.03	85.59	85.38	85.16
I_{eff}/I_{solid}	0.18	0.23	0.25	0.27

$I = KT^2/4\pi^2$ K = 6828.0 in-lbs.

$I_{eff} = I_f - I_e$

$I_{solid} = (W_{liq} - W_B)(d^2/16 + h^2/12)/g$

W_{liq} = 395.0 lbs.
W_{3B} = 2.0 lbs.
W_{5B} = 3.0 lbs.
W_{7B} = 4.0 lbs.

TABLE 40

TEST RESULTS

w = 1.2" w/a = 0.10" b = 3.0" b/a = 0.25"

Number of Baffles	1	3	5
Baffle Location	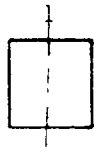	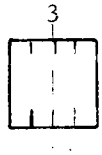	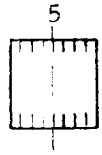
T_e	0.4927	0.4943	0.4956
T_f	0.5853	0.6025	0.6092
I_e	42.02	42.27	42.48
I_f	59.26	62.58	64.19
I_{eff}	17.25	20.30	21.71
I_{solid}	85.81	85.59	85.38
I_{eff}/I_{solid}	0.20	0.24	0.25

$I = KT^2/4\pi^2$ K = 6828.0 in-lbs.

$I_{eff} = I_f - I_e$

$I_{solid} = (W_{liq} - W_B)(d^2/16 + h^2/12)/g$

W_{liq} = 395.0 lbs.

W_{1B} = 1.0 lbs.

W_{3B} = 2.0 lbs.

W_{5B} = 3.0 lbs.

TABLE 41

TEST RESULTS

w = 1.2" w/a = 0.10" b = 3.0" b/a = 0.25"

Number of Baffles	2	4	6
Baffle Location	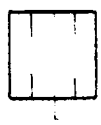	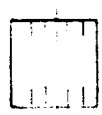	
T_e	0.4940	0.4952	0.4971
T_f	0.5844	0.5984	0.6084
I_e	42.22	42.42	42.75
I_f	59.07	61.95	64.03
I_{eff}	16.85	19.52	21.29
I_{solid}	85.81	85.59	85.38
I_{eff}/I_{solid}	0.20	0.23	0.25

$I = KT^2/4\pi^2$ K = 6828.0 in-lbs.

$I_{eff} = I_f - I_e$

$I_{solid} = (W_{liq} - W_B)(d^2/16 + h^2/12)/g$

W_{liq} = 395.0 lbs.

W_{2B} = 1.0 lbs.

W_{4B} = 2.0 lbs.

W_{6B} = 3.0 lbs.

are located near the axis of rotation. This is further verified by the previous results for 4 inch baffles where 6 and 4 inch spacers were used. These are shown by the x's on the graph.

The location of the baffles produces a much more pronounced effect if the results in Reference 3 are used. Figure 126 shows the results for baffles with 3 inch spacings and the results of Reference 3. The curves are of different magnitude because of the different 2/a ration, but the slopes of the curves vary because of the axis of oscillation of the tanks. The small sketches in Figure 126 show the axis of oscillations for both tests. The exact location of the axis of oscillation is not given for the tests in Reference 3, but for the other tests it is in the center of the tank. We see for this latter case that the effective moment of inertia increases more rapidly for the baffles in the center of the tank, than for those at the outer limits. For the other tank the effective moment of inertia increases rapidly for the center baffle, then the change decreases for the three baffles and again a rapid increase for five baffles. This latter result is obtained because the added baffles approach the axis of oscillation of the tank. Therefore, not only is the baffle width and spacing important, but also the baffle location with respect to the axis of rotation.

2.3.1.5.4 Conclusions

Baffles increase the effective moment of inertia of a liquid because they create new boundary conditons on the liquid which causes more liquid to follow the motion of the tank. Therefore, wider and closer spaced baffles produce a greater moment of inertia. Also the location of the baffles has a large effect on the change in moment of inertia.

The results of these tests will be used to verify the analytical expressions derived in Section 2.3.2.3. The results of this program will produce equations which can be used to determine the moment of inertia of cylindrical tanks with ring baffles.

2.3.2 Math Model

2.3.2.1 Literature Search

2.3.2.1.1 Introduction

A complete understanding of the background and present status of the problems and associated solutions for liquid dynamics as they are related to space flight, is the prime object of this search. For many years, the instability problems produced by fuel carried aboard space craft have been investigated. Many of the original problems present in older missiles have

LIST OF SYMBOLS

Symbol	Definition
I	Moment of Inertia (in-lb-sec^2)
I_{eff}	Effective moment of inertia of liquid
I_{solid}	Moment of Inertia of liquid in solidified state
K	Torsion rod constant (in-lb)
T	Period of oscillation (sec)
L	Distance between pivot point and center of mass (in)
W	Weight (lbs)
M	Mass (lb-sec^2/in)
e	Empty tank
f	Full tank
c.m.	Center of mass
h	Tank height (in)
a	Tank radius (in)
d	Tank diameter (in)
b	Baffle spacing (in)
w	Baffle width (in)
g	Acceleration of gravity (in/sec^2)
B	Baffles
liq	Denotes the water

FIGURE 126

EFFECT OF DISPLACED AXIS ON I_{eff}/I_{solid}

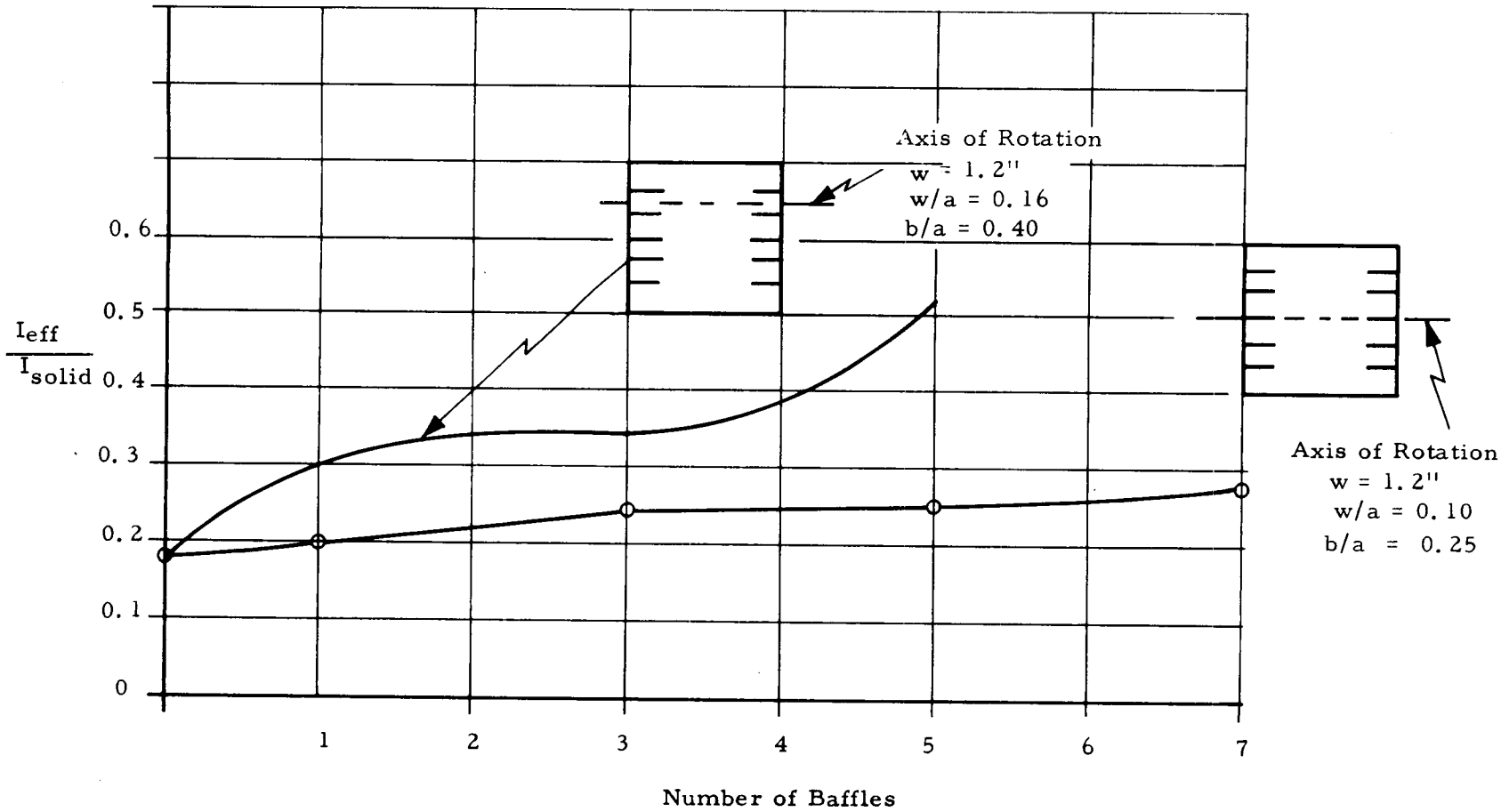

been sufficiently corrected so that fuel slosh is not detrimental to stable missile flight. As launch vehicles become larger and space flights extend to greater distances, mass properties of liquids will present greater problems. At launch, some vehicles today are ninety percent fuel by weight; also, extended flights such as the lunar missions will require a better understanding of fuel dynamics to enable precise trajectories. Another area that might present problems is that of low-gravity conditions for both filled and partially filled fuel tanks.

The major emphasis of this search was placed on the moment of inertia of filled tanks. Even though most fuel tanks are usually in the partially filled state, a study of filled tanks is beneficial for several reasons. First, this study will reveal the internal behavior of liquid as it rotates about a given axis. This will give a better insight into the correlation between the moment of inertia theory for liquids and solids of the same shape. Secondly, since liquid sloshing represents only a small percentage of the behavior of liquid in a large tank, the filled tank solutions will be very nearly the same as those of the partially filled tank. Also, the filled tank experiments are easier to analyze than those of partially filled tanks.

The search consisted of interviews with several people experienced in liquid tank dynamics as well as literature surveys. The latter of the two produced much more information but the interviews were helpful also.

2.3.2.1.2 Interviews

An interview with Dr. Werner R. Eulitz, Aero-Space Engineer(Propulsion and Power, AST Liquid Propulsion System), of the Propulsion and Vehicle Engineering Laboratory at MSFC, who has been working in the field of fuel sloshing since the early days of the Redstone, revealed that the Redstone had some serious slosh problems at its infancy. These were soon corrected; however, by using the so-called "beer can" anti-slosh device which was replaced by baffles in the latter missiles. Dr. Eulitz stated that fuel sloshing is not a major problem at present, but the effect of bending tank walls as tanks get larger may present problems.

The next interview was conducted with Mr. Robert S. Ryan, Supervisory Aero-Space Engineer of the Aero-Astrodynamics Laboratory. Mr. Ryan referred us to the works of Dr. Helmut F. Bauer, a noted authority on fuel dynamic problems in space vehicles, to obtain information on the moments of inertia of liquids. Several of Bauer's reports are included herein and will be discussed later in detail. Mr. Ryan stated that the basic fuel problems had been solved. Mr. H. Norman Abramson of the southwest Research Institute in San Antonio, Texas, has done much of Mr. Ryan's work for approximately seven years. Twenty-three reports by Mr. Abramson

or his associates are included in this report. A complete list of reports on liquid dynamics in rocket propellant tanks published by the Southwest Research Institute has been obtained, and efforts are being made to obtain copies of all these reports. At the present time, Mr. Abramson is doing some work for Mr. Ryan on some specific problems related to fuel sloshing. Mr. Ryan also has several contractors working on zero gravity liquid problems. These are research programs to determine what effects low and zero gravity have on liquid dynamics.

A conversation with Mr. B. C. Spencer of the Douglas Missile and Space Division at the SAWE Convention in Denver, Colorado, revealed that the moment of inertia of actual fuel tanks presented very few problems. He stated that rough estimates were used in determining moments of inertia of liquids and that these estimates were well within the tolerances allowed for the overall space craft's moment of inertia. Mr. Spencer stated that they are not involved in performing research on liquid moments of inertia but they are interested in finding out the results of other researchers so that they can use this information in their determinations.

2. 3. 2. 1. 3 Literature Searches

The literature search portion of this survey consisted of a thorough search of both the Redstone Scientific Information Center and the Defense Documentation Center. Three different searches were conducted by the personnel at the Redstone Scientific Information Center to obtain all possible information on liquid behavior in tanks. The searches are computerized and they serached every document in the Center for the key words; Sloshing, Liquid Sloshing and Baffles. The search of the Defense Documentation Center was similar except only one subject was used-Liquid Sloshing. The Defense Documentation Center contains all documents prepared by the government and its contractors. The International Aerospace Abstracts were also searched for pertinent material. Likewise, the Society of Aeronautical Weight Engineers publications were thoroughly investigated. Lastly, a review of many texts was undertaken to find applicable basic hydrodynamic theory.

As a result of these various searches, a list of all books and reports available in the Mass Metrology Laboratory at SPACO, INC. is given in the references. This reference includes all books and reports from the previous yearly effort as well as the ones produced from the latest searches. An asterisk marks the books and reports not included in the June, 1965 annual report. The groupings are divided into the following main subjects:

1. Basic Hydrodynamic Theory
2. Liquid Moments of Inertia
3. Liquid Baffling

4. Sloshing in General
5. Effects of Sloshing on Missile Stability
6. Zero Gravity Liquid Studies
7. Other Reports Related to Liquids

A summary of each grouping will be given along with more detailed information on certain reports.

The first group of books and reports (Ref. 1 through Ref. 18) are concerned with basic hydrodynamic theory. A further sub-division of this grouping classifies (Ref. 1 through Ref. 5) as text books on classical hydrodynamics. (Ref. 2) is by far the most notable text on basic classical hydrodynamics and has been used for many years as the authority on hydrodynamics (Ref. 6) is also a classic on potential theory. It is very valuable in the study of velocity potential theory which is the basis of hydrodynamic theory.

(Ref. 7 through Ref. 15) are reports on basic hydrodynamic theory. (Ref. 7) gives the linearized fluid dynamic equations for a liquid with a free fluid surface in a circular cylindrical tank, performing harmonic translation and rotation around the center of gravity of the undisturbed fluid. These equations were solved for an ideal fluid (incompressible and non-viscous). The general solutions of the velocity potential are derived for the free oscillations and for two forced oscillations (translation and rotation). The wave form of the free fluid surface, the pressure distribution and the fluid force on the tank walls, the moment of the fluid around the center of gravity of the undisturbed fluid, the velocity distribution and the center of force are given. The effect of the fluid for different frequencies and fluid height to tank diameter ratio are shown on the various curves. This reference is invaluable for the study of basic hydrodynamics for a circular cylindrical tank. (Ref. 8) gives the solution for damped fluid oscillations by introducing imaginary terms in the resonance terms. Physical limit considerations for ideal fluid and for infinite damping lead to transformation of the original formulae in (Ref. 7). Measurements with different damping devices were performed and the approximate damping factors were determined from different measurements such as, free fluid surface, fluid force, pressure difference and their phases. The experimental values were taken into theoretical curve sets with different damping factors and the approximate damping factor was determined at resonance. An iteration method also gave the approximate damping factor from the experimental results. This reference gives a more practical approach to liquid problems since it includes damping which cannot be neglected in actual experiments.

(Ref. 9 through Ref. 15) are similar to (Ref. 7). They take a slightly different approach and do not go into as much detail, but they are still

basically the same. (Ref. 16 through Ref. 18) are also basic but are more applied to the effect of fuel motion in airplane tanks. These reports are some of the first presented which describe the adverse effect of fuel slosh on aircraft stability.

The next grouping (Ref. 19 through Ref. 25) includes reports pertaining to liquid moments of inertia. (Ref. 19) uses the results of (Ref. 7 and Ref. 8) to determine the moment of inertia of an ideal fluid in a completely filled circular cylindrical tank. In previous calculation the moment of inertia of a liquid in a circular cylindrical tank was treated as a mass-point or solid cylindrical body. Since the moment of inertia of a fluid is considerably different, this investigation was carried out. The moment of inertia of the ideal fluid was compared with the moment of inertia of the same fluid in a frozen state. Due to the complexity of the case with friction, no damping could be incorporated. But, it can be seen that the value of the moment of inertia (1 fluid to 1 solid) with damping are located between the ratio of the ideal fluid case and unity. The moment of inertia of a fluid in a partially filled tank is strongly frequency dependent. It has been obtained for translational and rotational motion of the tank from the results of (Ref. 7 and Ref. 8). This report is extemely helpful in our liquid moment of inertia study. Some of the results of this report were used in our last year's project.

(Ref. 20) determines the moment of inertia and an approximate damping factor in roll oscillation for a propellant system of a clustered missile. The main portion of the moment of inertia is contributed by the outer tanks. Also it was found that the moment of inertia is frequency dependent. (Ref. 21) is very similar to (Ref. 20) containing the same subject matter.

In (Ref. 22) a method is presented for calculation of the mass and mass moment of inertia of a liquid in a circular cylindrical tank. The tank is assumed to be similar to that of a vertically rising ballistic missile. That is, the acceleration is assumed to be parallel to the tank's longitudinal axis. A solution is found which greatly simplifies the efforts of the weights and dynamics groups, while giving proper consideration to the physical effects involved.

(Ref. 23) experimentally investigates the moment of inertia and the damping of a liquid in a completely filled, closed cylindrical tank, with and without baffles. The results are compared to Bauer's mechanical model, and it is shown that a simpler model, which, however, is not conceptually correct for extememly large damping, is sufficient for cases where only small damping is expected. An approximate method of computing the liquid moment of inertia in a baffled tank is given. This report published by the Southwest Research Institute contains some very useful information for our study of moments of inertia.

(Ref. 24) presents a correlation of experimental measurement and analytical prediction of free, planar oscillations of tank of mercury hung on a pendulum. The reports describe a test set-up very similar to ours. It goes into more detail than just the moment of inertia but it is useful in comparing our procedures and results to their tests. The purpose of (Ref. 25) is to verify the results in (Ref. 10) for the effective rotary inertia of fluid in a circular cylindrical tank about an axis perpendicular to the longitudinal axis of the cylinder. The experimental results agreed fairly well with the theoretical results of (Ref. 10).

(Ref. 26) is an older report which contains studies of the fluid dynamics of some different-shaped fuel tanks in a horizontal flight attitude and undergoing pitching oscillations of a few degrees. The moment of inertia of the fluid was determined for the various tanks over a range of tank fullness from empty to full. For the tank-full case, comparisons of the experimental moment of inertia of the fluid with some theoretical solutions for the moment of inertia of fluid in tanks having elliptic and rectangular sections indicate that the theoretical solutions predict the experimental values for the elliptic and rectangular tanks and offer engineering approximations of the fluid moment of inertia for some tanks of other shapes. It was found that the ratio of the fluid inertia to the solid inertia for a given tank fullness increased as the tank fineness ratio increased. However, for a given tank the ratio of the fluid inertia to the solid inertia for the same fullness was essentially constant over a large range of tank fullnesses and had approximately the value indicated for the tank-full condition.

The third group (Ref. 27 through Ref. 38) includes reports on liquid baffles and baffling. Different types of baffles are discussed as well as different types of tanks. These reports will be helpful in our baffling tests using the government furnished plexiglass tank. (Ref. 39 through Ref. 93) include reports which pertain to liquid sloshing in some form or another. They cover many different aspects of slosh over a wide range of applications. These reports can be referred to when a specific problem arises. For example, (Ref. 39) is helpful in converting liquid behavior in a hemipherical bottom tank to a flat bottom tank. This report has been helpful for calculation on our plexiglass tank. (Ref. 84 through Ref. 92) cover slosh in spherical tanks. The properties of slosh in toroids are discussed in (Ref. 93).

The fifth group (Ref. 95 through 108) contains reports which cover the effect of fuel behavior on the stability of missile flight. Some of the reports go into much more detail than just fuel problems but they are useful in studying the many adverse effects produced by missile flight.

(Ref. 109 through 113) contain the sixth grouping covering zero gravity liquid problem. Presently we are not working in this field but it should be

considered since new problems will result from weightlessness. It appears that zero gravity may present major problems to the behavior of liquid in extended space flights.

The last group (Ref. 114 to Ref. 125) includes all reports that do not fall within the previous groups. These reports pertain to liquid properties in one form or another and may be useful for some specific problems.

2. 3. 2. 1. 4 Conclusions

The literature survey of the mass properties of liquids program has produced many valuable books and reports. The search has not produced all the reports pertaining to liquid slosh but it does include a good many of the better known reports. These reports have been very useful in the past and will continue to be useful in the future for the mass properties of liquids program. The search for reports pertaining to liquid problems will continue so that complete and up to date information on the latest technologies in this field will be available.

2. 3. 2. 2 Develop Equations for the Moment of Inertia of a Liquid Filled Clyindrical Tank about its Center of Gravity and Displaced Axes

2. 3. 2. 2. 1 Introduction

As launch vehicles get larger and, consequently, the liquid fuel carried aboard increases, the dynamic behavior of the vehicle will depend strongly on the fuel mass in the vehicle. In order to predict the motion of the vehicle as it rotates during launch, the moment of inertia of the liquid about various axes must be known. The objective of the Math Model Project of the Mass Properties of Liquids Program was to derive mathematical expressions, either theoretical or empirical, that would accurately determine the moment of inertia of a filled cylindrical tank. The results of this project were to be correlated with the Test Project to verify the accuracy of the equations that were derived. The final results were to be a set of equations, tables and/or graphs which could easily be used to provide accurate values for the moment of inertia of a filled cylindrical tank.

The Math Model Project is divided into three phases. The first is a Literature Search which has been completed and is covered in Section 2. 3. 2. 1. This search provided background information for the present program. The second phase which this report covers was established to develop equations for the moment of inertia of a liquid filled cylindrical tank as it oscillates about various roll and yaw-pitch axes. The last phase was designed to study the effect of various baffle configurations on the moment of inertia of cylindrical tanks.

REFERENCES

1. Binder, R. C., Advanced Fluid Dynamic and Fluid Machinery, Prentice-Hall, Inc., Englewood, New Jersey, 1951.

2. Lamb, H., Hydrodynamics, 6th Edition, Dover Publications, New York, 1932.

3. Rayleigh, B., The Theory of Sound, 2nd Edition, Dover Publications, New York, 1945.

4. Rouse, Hunter, Advanced Mechanics of Fluids, Prentice-Hall, Inc., Englewood, New Jersey, 1959.

5. Streeter, V. L., Fluid Dynamics, McGraw-Hill Book Company, Inc., New York, 1948.

6. Kellogg, O. D., Foundations of Potential Theory, Dover Publications, New York, 1929.

7. Bauer, H. F., "Fuel Oscillations in a Circular Cylindrical Tank", DA-TR-1-58, April 18, 1958.

8. Bauer, H. F. "Fluid Oscillations in a Cylindrical Tank with Damping", DA-TR-4-58, ABMA, April 23, 1958.

9. Brooks, J. E., "Dynamics of Fluids in Moving Containers", GM 04.4-26, TRW Space Tech. Labs., February, 1959.

10. Gleghorn, G. J., "Motion of Fluid in a Cylindrical Tank", Ramo-Wooldridge Corp., Memo, February 7, 1956.

11. Kachigan, K., "Forced Oscillations of a Fluid in a Cylindrical Tank," ZU-7-046, Convair, October, 1955.

12. Lorell, Jack, "Forces Produced by Fuel Oscillations", Progress Report No. 20-149, Jet Propulsion Lab., October, 1951.

13. Schmitt, A. F., "Forced Oscillation of a Fluid in a Cylindrical Tank Undergoing Both Translation and Rotation," ZU-7-069, Convair, October, 1956.

14. Schmitt, A. F. "Forced Oscillations of a Fluid in a Cylindrical Tank Oscillating in a Carried Acceleration Field - A Correction", ZU-7-074, Convair, February, 1957.

15. Trembath, N. W., "Fluid Sloshing in Tanks of Arbitrary Shape", G.M. 45 3-378, Ramo-Wooldridge Corp., August 28, 1957.

16. Graham, E. W. & Rodriquez, A. M., "The Characteristics of Fuel Motion which Affect Airplane Dynamics," Jour. App. Mech., September, 1952.

17. Luskin, H. & Lapin, E., "An Analytical Approach to the Fuel Sloshing and Buffeting Problems of Aircraft", Jour. Aero. Sc. Vol. 19 No. 4, April, 1952.

18. Schy, A. A. "Theoretical Analysis of the Effects of Fuel Motion on Airplanes Dynamics", Report 1080, NACA, Langley Field, Nov. 21, 1950.

19. Bauer, H. F., "The Moment of Inertia of a Liquid in a Circular Cylindrical Tank", DA-TR-5-58, ABMA, April, 1958.

20. Bauer, H. F., "The Effective Moment of Inertia in Roll of Propellant and Roll Damping", DA-TM-67-59, ABMA, May 26, 1959.

21. Bauer, H. F., "Propellant Oscillations in the Containers of a Roll Oscillating Space Vehicle and Moment of Inertia of Liquid", AIAA Publication CP-8, Structures and Materials Conference, April, 1960.

22. Harvey, T. J., "Moment of Inertia of Liquids in Cylindrical Tanks", SAWE Tech. Paper No. 184, LMSD-56263, Lockheed Missile System Division, May 19, 1958.

23. Dodge, F. T. and Kana, D. D., "Moment of Inertia and Damping of Liquids in Baffled Cylindrical Tanks", TR No. 4, Project No. 02-1072, SWRI, June, 1965.

24. Warner, R. W. and Caldwell, J. T., "Experimental Evaluation of Analytical Models for the Inertias and Natural Frequencies of Fuel Sloshing in Circular Cylindrical Tanks", TN D-856, NASA, Moffett Field, 1961.

25. Chobotov, V. & Fowler, J..R., "Experimental Investigations of the Moment of Inertia in a Cylindrical Tank", Ramo-Wooldridge Corp., February, 1957.

26. Widmayer, E., & Reese, J. R., "Moment of Inertia and Damping of Fluid in Tanks Undergoing Pitching Oscillations", RM L5 3E01a, NACA, Langley Field, June, 1953.

27. Abramson, H. N. & Garza, L. R., "Some Measurements of the Effects of Ring Baffles in Cylindrical Tanks", Jour. of Spacecraft and Rockets, 1964.

28. Abramson, H. N. & Ransleben, G. E., "A Note on the Effectiveness of Two Types of Slosh Suppression Devices", Project 43-768-2, Report No. 6, SWRI, June, 1959.

29. Baer, H. W., "An approximate Approach to the Prevention of Sloshing of an Incompressible Fluid by Introduction of Mechanical Damping", Report No. GM-TM-83, Ramo-Wooldridge Corp., May, 1956.

30. Bauer, H. F., "An Approximate Effect of Ring Stiffener on the Pressure Districution in an Oscillating Cylindrical Tank Partly Filled with Liquid", DA-M-114, ABMA, September, 1957.

31. Bauer, H. F., "The Damping Factor Provided by Flat Annular Ring Baffles for Free Fluid Surface Oscillations", MTP-Aero-62-81, NASA, Nov., 1962.

32. Cole, H. A. & Gambucc, B. J., "Measured Two-Dimentional Damping Effectiveness of Fuel-Sloshing Baffles Applied to Ring Baffles in Cylindrical Tanks", TN D-694, NASA, Ames Research Center, Moffett Field, California, February, 1961.

33. Eulitz, W. R., "Theoretical Discussion of the Sloshing Phenomena and Proposed Method for Depressing of Sloshing in Fuel Containers of Missiles", ORDAB DSM-45, ABMA, January, 1957.

34. Garza, L. R., "A Brief Comparison of Ring and Asymmetrical Baffle Characteristics", TR-6, NAS8-1535, SWRI, April, 1963.

35. Garza, T. R. & Abramson, H. N., "Measurements of Liquids Damping Provided by Ring Baffles in Cylindrical Tanks", TR No. 5, Project No. 6-1072-2, SWRI, April, 1963.

36. Langer, C. G., "A Preliminary Analysis of Optimum Design of Ring & Pantition Antislosh Bubbles", TR No. 4, Project No. 6-1072-2, SWRI, 1963.

37. Silveira, M. A., Stephens, D. G. & Leonard, H. W., "An Experimental Investigation of the Damping of Liquid Oscillations in Cylindrical Tanks with Various Baffles", TN D-715, NASA, Langley Field, Va., May, 1961.

38. Stephens, D. G., Leonard, H. W. & Silveira, M. A., "An Experimental Investigation of the Damping of Liquid Oscillations in an Oblate Spheroidal Tank With and Without Baffles", TN D-808, NASA, Langley Field, June, 1961.

39. Abramson, H. N. & Ransleben, G. E., "Some Comparison of Sloshing Behavior in Cylindrical Tanks with Flat and Conical Bottoms", Report No. 4, Project 43-768-2, SWRI, May, 1959.

40. Abramson, H. N. & Ransleben, G. E., "A Note on Wall Pressure Distributions During Sloshing on Rigid Tanks", SWRI TR No. 5, SWRI Project 43-768-2, June, 1959.

41. Abramson, H. N. & Ransleben, G. E., "A Theoretical & Experimental Study of Fuel Sloshing", 1251-QPR-7, SWRI, February 1, 1960.

42. Abramson, H. N. & Ransleben, G. E., Chu, Wen-Hwa, & Squire, W., "A Theoretical & Experimental Study of Fuel Sloshing", 1251-QPR-8, SWRI, May, 1960.

43. Abramson, H. N. & Ransleben, G. E., "Simulation of Fuel Sloshing Characteristics in Missile Tanks by Use of Small Models", ARS Journal, July,1960.

44. Abramson, H. N., Garza, L. R. & Kana, D. D., "Liquid Sloshing in Compartmented Cylindrical Tanks", ARS Journal, June, 1962.

45. Abramson, H. N. "Dynamic Behavior of Liquid in Moving Containers", Applied Mechanics Reviews, Vol. 16, No. 7, July, 1963.

46. Baron, M. L. & Bleich, H. H., "The Dynamics Analysis of Empty and Partially Full Cylindrical Tanks, Part I. Frequencies and Modes of Free Vibration and Transient Response by Modes Analysis", DASA No. 1123A, Paul Weidlinger, Consulting Engineer, New York, New York, May, 1959.

47. Baron, M. L. & Skalak, R., "Free Virbrations of Fluid-Filled Cylindrical Shells", Jour. Eng. Mech. Div., June, 1962.

48. Bauer, H. F., "The Effect of Propellant Sloshing on the Stability of an Accelerometer Controlled Rigid Space Vehicle", TN-D-1831, NASA, Oct., 1963.

49. Bauer, H. F. "Fluid Oscillations of a Circular Cylindrical Tank Performing Lissajous-Oscillations", DA-TR-2-58, ABMA, April, 1958.

50. Bauer, H. F., "Fluid Oscillations in a Circular Cylindrical Tank Due to Bending of Tank Wall", TR-3-58, ABMA, April 18, 1958.

51. Bauer, H. F., "Fluid Oscillations in the Containers of a Space Vehicle and Their Influence Upon Stability", TR R-187, NASA, MSFC, Feb., 1964.

52. Bauer, H. F., "Liquid Sloshing in a Cylindrical Quarter Tank", MTP-Aero-63-72, NASA, Huntsville, Alabama, October, 1963.

53. Bauer, H. F., "Liquid Sloshing in a Cylindrical Quarter Tank", AIAA Jour. Vol. 1, No. 11, November, 1963.

54. Bauer, H. F. "Mechanical Analogy of Fluid Oscillations in Cylindrical Tanks with Circular and Annular Cross Section", MTP-Aero-61-1, MSFC, Jan. 12, 1961.

55. Bauer, H. F., "Mechanical Analogy of Fluid Oscillations in Cylindrical Tanks with Circular and Annular Cross Section", MTP Aero 61-4, NASA, Jan., 1961.

56. Bauer, H. F., "Theory of the Fluid Oscillations in a Circular Cylindrical Ring Tank Partially Filled with Liquid", TN D-557, NASA, December, 1960.

57. Bauer, H. F. "Theory of Liquid Sloshing in Compartmented Cylindrical Tanks Due to Bending Excitation", MTP-Aero-62-61, NASA, July, 1962.

58. Bauer, H. F., "Theory of Liquid Sloshing in Compartmented Cylindrical Tanks Due to Bending Excitation", AIAA Jour. Vol. 1 No. 7, July, 1963.

59. Bhuta, P. G. & Koval, L. R., "Coupled Oscillatinns of a Liquid with Free Surface in a Tank Having a Flexible Bottom, ZAMP, Vol. 15, 1964.

60. Brown, K. M., "Laboratory Test of Fuel Sloshing", Report No. Dev-783, Douglas Testing Division, March, 1954.

61. Chu, Wen-Hwa, "Sloshing of Liquids in Cylindrical Tanks of Elliptic Cross Section", ARS Journal, SWRI, April, 1960.

62. Cooper, R. M., "Dynamics of Liquids in Moving Containers", Space Technology Laboratories, ARS Journal.

63. Dodge, F. T., Kana, D. D. & Abramson, H. N., "Liquid Surface Oscillations in Longitudinally Excited Rigid Cylindrical Containers", TR-2, NAS-11045, SWRI, April, 1964.

64. Eulitz, W. R., "Discrpeancies with Δ p Sensors for Monitoring Liquid Propellant Sloshing Driving Rocket Flight", MTP-P&VE-P-62-6, NASA, MSFC.

65. Eulitz, W. R., "The Sloshing Phenomenon and the Mechanism of a Liquid in Motion in an Oscillating Missile Container", DS-R-31, ABMA, Oct., 30, 1957.

66. Hieatt, J. J. & Riley, J. D., "Digital Program for Fluid Sloshing in Tanks with Axial Symmetry", TM-59-0000-00 389, Space Tech. Lab., September 30, 1959.

67. Karpov, B. G., "Experimental Observations of the Dynamic Behavior of Liquid Filled Shell", Report No. 1171, Ballistic Research Labs, Maryland, August, 1962.

68. Knopp, M., "Centrifugal Sloshing", PA-2297-0212, TRW Space Tech. Labs., June, 1959.

69. Lawrence, H. R., Wang, C. J. & Reddy, R. B., "Variational Solution of Fuel Sloshing Modes", Ramo-Wooldridge Corp., November, 1958.

70. Miles, J. W., "Free Surface Oscillations in a Rotating Liquid", Vol. 2 No. 3, The Physics of Fluids, May-June, 1959.

71. Miles, J. W., "On the Sloshing of Liquid in a Flexible Tank," Jour. of Applied Mechanics, June, 1958.

72. Miles, J. W., "Ring Damping of Free Surface Oscillations in a Circular Tank", Journal of Applied Mechanics, June, 1958.

73. O'Neill, J. R., "Final Report on an Experimental Investigation of Sloshing", STL/TR-59-0000-09960, Space Tech. Labs, March 4, 1960.

74. Reissner, E., "Complementary Energy Procedure for Vibrations of Liquid Filled Circular Cylindrical Tanks", GM-TR-203, Ramo-Wooldridge Corp., June 19, 1957.

75. Reissner, E., "Notes on Forced and Free Vibrations of Pressurized Cylindrical Shells which Contain a Heavy Liquid with Free Surface", GM-TR-87, Ramo-Wooldridge Corp., November, 1956.

76. Sewall, J. L., "An Experimental and Theoretical Study of the Effect of Fuel on Pitching Translation Flutter", TN-4166, NACA, December, 1957.

77. Sloane, M. N., "The Dynamics of the Sloshing Phenomen", GM-60-5111-2, Space Tech. Labs., (C).

78. Smith, C. C., "The Effects of Fuel Sloshing on the Laterial Stability of a Free-Flying Airplane Model", RM No. L8C16, NACA, June, 1948.

79. Stephens, D. G. & Leonard, H. W., "The Coupled Dynamic Response of a Tank Partially Filled with a Liquid and Undergoing Free and Forced Planar Oscillations", TN-D-1945, NASA, Langley Field, August, 1963.

80. Sweitzer, D., "Sloshing of Liquid Propellants", Report No. 67, Jet Propulsion Labs, 1959, (C).

81. Townsend, A. A., "The Development of Turbulent Boundary Layers with Negligible Wall Stress", Fluid Mech., 1959.

82. Troesch, B. A., "Some New Exact Sloshing Solutions", STL NN-132, TRW-Space Tch. Labs, March, 1959.

83. Troesch, B. A., "Free Oscillasions of a Fluid in a Container", Boundary Problems in Differential Equations, Pages 279-299, Editor, Langer, R. E., University of Wisconsin Press, 1960.

84. Abramson, H. N., Chu, Wen-Hwa & Garza, L. R., "Liquid Sloshing in Spherical Tanks", AIAA Journal, Vol. 1, No. 2, Pages 384-389, February, 1963.

85. Bauer, H. F., "Determination of Approximate First Natural Frequencies of a Fluid in a Spherical Tank", DA-TN-75-58, October, 1958.

86. Budiansky, B., "Sloshing of Liquids in Circular Canals and Spherical Tanks", Jour. Aero/Space Sciences, Vol. 27, No. 3, March, 1960.

87. Chu, Wen-Hwa, "Liquid Sloshing in a Spherical Tank Filled to an Arbitrary Depth", Report No. 4, SWRI, December, 1962.

88. Gray, S. P., "Properties of Spheres, Spheroids & Elliptical Lenses Used as Propellant Tanks", MTP-P&VE-F-61-16, December 5, 1961.

89. McCarty, J. L. & Stephens, D. G., "Investigation of the Natural Frequencies of Fluids in Spherical and Cylindrical Tanks", TN-D-252, NASA, Langley Field, May, 1960.

90. Stofan, A. J. and Armstead, A. L., "Analytical & Experimental Investigation of Forces & Frequencies Resulting from Liquid Sloshing in a Spherical Tank", TN D-1281, NASA, Lewis Research Center, 1962.

91. Stofan, A. J., and Pauli, A. J., "Experimental Damping of Liquid Oscillations in a Spherical Tank by Positive-Expulsion Bags & Diaphrams", TN D 1311, NASA, Lewis Research Center, July, 1962.

92. Summer, I. E., & Stofan, A. J., "An Experimental Investigation of the Viscous Damping of Liquid Sloshing in Spherical Tanks", TN D-1991, NASA, Washington, December, 1963.

93. Gray, S.P. & Burns, R. E., "Properties of Toroids with Circular Cross Sections Used as Propellant Tanks", MTP-P&VE-F-62-9, August 1, 1962.

94. Abramson, H. N., Lindholsn, W. S., Kana, D. D. and Chu, Wen-Hwa, "Research on Liquid Dynamics in Missile Fuel Tanks", TR No. 6, Project No. 4-961-2, SWRI, 1961.

95. Armstrong, G. L. and Kachigan, K., "Propellant Sloshing", Sections 14.14115, Handbook Astronautical Engineering, Editor H. H. Koelle, McGraw-Hill Book Co., New York, 1961.

96. Bauer, H. F., "Parametric Study of the Influence of Propellant Sloshing on the Stability of Space Craft", Jour. Aerospace Sc., October, 1961.

97. Bauer, H. F. "Propellant Behavior in the Tanks of Large Space Vehicles", MTP-AERO-61-81, NASA, MSFC, 1961.

98. Brooks, J. A., "Generalized Missile Dynamic Analysis, VII Programming", GM-TR-0165-00431, Space Tech. Labs, April, 1958.

99. Clark, C. D., "Effect of Propellant Oscillation on Saturn Roll Moment of Inertia", DA-TN-87-59, ABMA, (C).

100. Hays, P. J., "Stability Analysis of Saturn Block II, S-IV Stage Flight", MTP-Aero-63-27, NASA, MSFC, April, 1963.

101. Hays, P. J., & Sumrall, J. P., "Stability Analysis of Saturn SA-5 with Live S-IV Stage", TM X053017, NASA, MSFC, March, 1964.

102. Heist, E. K., "Equations of Motion of Missile with Sloshing", GM-TM-148, Ramo-Wooldridge Corp., February 8, 1956.

103. Martin, D. G., "Control System Equations", Report No. EM 8-14, Space Tech. Labs, April, 1958.

104. McKenna, K. J., Palmer, J. L. & Wakamiya, Y., "Final Report of Saturn V Control Systems Sudies", TRW for NASA, MSFC under NAS8-2635, Feb., 1964.

105. Miles, J. W. & Young, D., "Generalized Missile Dynamics Analysis, IV Sloshing", GM TR-0165-00361, Space Tech. Labs, April, 1958.

106. Sandoff, P. E., "Principles of Design of Dynamically Similar Models for Large Propellant Tanks", TN-D-99, NASA, Washington, January, 1960.

107. Townsend, D. "Saturn V Wind Response Studies", MTP AERO 63-63, Sept. 1963.

108. Young, D. "Generalized Missile Dynamic Analysis II - Equations of Motion", GM-TR-0165-00359, Space Tech. Labs, April, 1958.

109. Benedikt, E. F., "Scale of Separation Phenomena in Liquids Under Conditions of Nearly Free Fall", ARS Jour., February, 1959.

110. Kribetsky, Bauer, W. H., Locus, Padlog, Robinson & Walters, "Final Report-Report on Zero-Gravity Expulsion Techniques", Report 7129-9333003, NASA r-44, Bell Aerosystems, March, 1962.

111. Petrash, D. A., Nelson, T. M. & Otto, E. W. "Effect of Surface Energy on the Liquid-Vapor Interface Configuration During Weightlessness", Lewis Research Center, TN-D-1582, NASA, January, 1963.

112. Reynolds, W. C., "Behavior of Liquids in Free Fall", Jour. of the Aero/Space Sciences, December, 1959.

113. "Proceeding of the Zero-Gravity Fluid Behavior", NASA Headquarters, Washington, D. C. October, 1963.

The following reports were presented at the proceeding:

A. Smithson, J. C., "Some Zero-Gravity Problems of Manned Space Flight", Manned Spacecraft Center.

B. Wood, C. C., Platt, G. K., "Definition of Potential Zero and Low "g" Problems Related to Space Vehicle Design", MSFC.

C. Otto, E. W., "LRC Zero-Gravity Research Program and Facilities", Lewis Research Center.

D. Crabs, C. C., "LRC Aircraft Zero-Gravity Test Facilities", Lewis Research Center.

E. Nussle, R. C., "Liquid-Vapor Interface Configuration and Time Response", Lewis Research Center.

F. Masica, W. J., "Effect of Outflow and Acceleration Disturbances on the Liquid-Vapor Interface", Lewis Research Center.

G. Petrash, D. A., "The Design of Propellant Tankage Suitable for Use During Weightlessness", Lewis Research Center.

H. Meng, C. R. & Ball, C. L., "Pumping Considerations for Zero-Gravity Applications", Lewis Research Center.

I. Siegel, R. & Keshock, E. Q., "Nucleate Boiling Bubble Dynamics in Saturated Water Under Reduced Gravity Conditions", Lewis Research Center.

J. Aydelott, J. C., "The Effect of Weightlessness on Pressure Rise Characteristics of a Hydrogen Dewar".

K. Papell, S. S., "Introduction of Magnetic Colloids into Propellants for Liquid Orientation and Venting Control in Zero Gravity by means of Magnetic Body Forces", Lewis Research Center.

L. Papell, S. S., Graham, R. W., and Benser, W. A., "Forced Convective Boiling and Super Critical Heat Transfer in a Flow Under a Varying Body Force Including Zero Gravity", Lewis Research Center.

M. Otto, E. W., "Centaur Propellant Interface Control in Coast Flight", Lewis Research Center.

N. Papell, S. S., "Zero and Reduced Gravity Simulation on a Pool-Boiling System (Including Burnout) Using Magnetic Body Forces on a Colloidal Magnetic Fluid", Lewis Research Center.

O. Saari, M. J. "Project MECA", Lewis Research Center.

P. McArdle, J. G., "Project MECA Rocket Experiment and WASP Sounding Rocket".

Q. Watt, J. J., Nime, E. J., "The Effects of Zero Gravity and Low Gravity on the Start-up of the Nuclear Rocket", Lewis Research Center.

R. Wood, C. C. & Swalley, F. E. "Research in Support of Zero and Reduced Gravity Fluid Mechanics and Heat Transfer", MSFC.

S. Lucas, J. W., "Free Fall Capsule Feasibility and Capillary-Pump Test Requirements", Jet Propulsion Laboratory.

T. Hennigan, T. J., "Operation of Electrochemical Cells in Low-Gravity Environments", Goddard Space Flight Center.

U. Del Duca, M. G., "Life Support Zero-G Experiments", NASA Headquarters.

V. Thomas, L. P., "The X-15 as a Zero-Gravity Test Facility", Flight Research Center.

W. Beam, R. M., "On the Stability of Liquid Lays Spread Over Simple Curved Bodies", Ames Research Center.

X. Blackshear, W. T., "An Investigation of the Liquid Equilibrium Free Surface in an Area of Low Gravity Forcesand Small Rates of Rotation", Langley Research Center.

Y. Eide, D. G., "Analysis of the Variation of the Pitch Motion of a Vehicle Due to Fuel Sloshing in a Space Environment", Langley Research Center.

Z. Platt, R. J., Jr., "Two Condenser Projects for Space Power", Langley Research Center.

114. Abramson, H. N., Chu, Wen-Hwa, Garza, L. R. and Ransleben, G. E., "Some Studies of Liquid Rotation and Vortexing in Rocket Propellant Tanks", TN-D-1212, NASA, Washington, January, 1962.

115. Berlot, R. R., "Production of Rotation in a Confined Liquid Through Translational Motion of the Boundaries", Jour. App. Mech., Dec. 1959.

116. Dodge, F. T., "A Review of Research Studies on Bubbles Motion in Liquids Contained in Vertically Vibrating Tanks", TR No. 1, Proj. No. 1-1391-2, SWRI, December, 1963.

117. Harlow, F. H. and Fromm, J. E., "Computer Experiments in Fluid Dynamics", Scientific American, March, 1965.

118. Kana, D. D., "A Resistive Wheatstone Bridge Liquid Wave Height Transducer", NAS8-11045, SWRI-TR-3, May, 1964.

119. Kana, D. D. and Dodge, F. T., "Bubble Behavior in Liquids Contained in Vertically Vibrated Tanks", TR No. 4, Proj. No. 02-1391, SWRI, 1964.

120. Lees, L. & Reeves, B. L., "Some Remarks on Integral Moment Methods for Laminar Boundary Layers with Applications to Separation and Reattachment", AD 275557, California Institute of Technology, December, 1961.

The present project phase is divided into four separate areas representing the effective moment of inertia for oscillations about different axes. These areas are:

1. The Effective Moment of Inertia of a Filled Cylindrical Tank Oscillating about a Yaw-Pitch Axis through the Center of Mass.

2. The Effective Moment of Inertia of a Filled Cylindrical Tank Oscillating about a Yaw-Pitch Axis Displaced from the Center of Mass.

3. The Effective Moment of Inertia of a Filled Cylindrical Tank Oscillating about a Roll Axis through the Center of Mass.

4. The Effective Moment of Inertia of a Filled Cylindrical Tank Oscillating about a Displaced Roll Axis.

These areas will be discussed separately in the following sections.

The major emphasis has been placed on the moment of inertia of completely filled tanks. Even though most fuel tanks are usually in the partially filled state, a study of filled tanks is beneficial for several reasons. First, this study will reveal the internal behavior of liquid as it rotates about a given axis. This will give a better insight into the correlation between the moment of inertia theory for liquids and solids of the same shape. Secondly, in a partially filled container the moment of inertia of the non-sloshing liquid has to be known. This is particularly important, since the moment of inertia of a liquid may deviate strongly from that of the solidified liquid. This is accomplished by considering the non-sloshing part of the liquid as a completely filled tank, while the sloshing part of the liquid is considered as an extra degree-of-freedom of the complete dynamic system.

2.3.2.2.2 Moment of Inertia About a Yaw-Pitch Axis

The moment of inertia of an incompressible and non-viscous liquid in a completely filled cylindrical container with a flat bottom and top is to be determined for small rotational oscillations about an axis through the center of mass of liquid and perpendicular to the longitudinal axis of the tank as shown in Figure 127. This can be achieved by solving the Laplace Equation

$$\nabla^2 \Phi = 0 \tag{161}$$

FIGURE 127

COORDINATE SYSTEM FOR PITCH EXCITATIONS ABOUT AN AXIS THROUGH THE CENTER OF MASS OF THE LIQUID

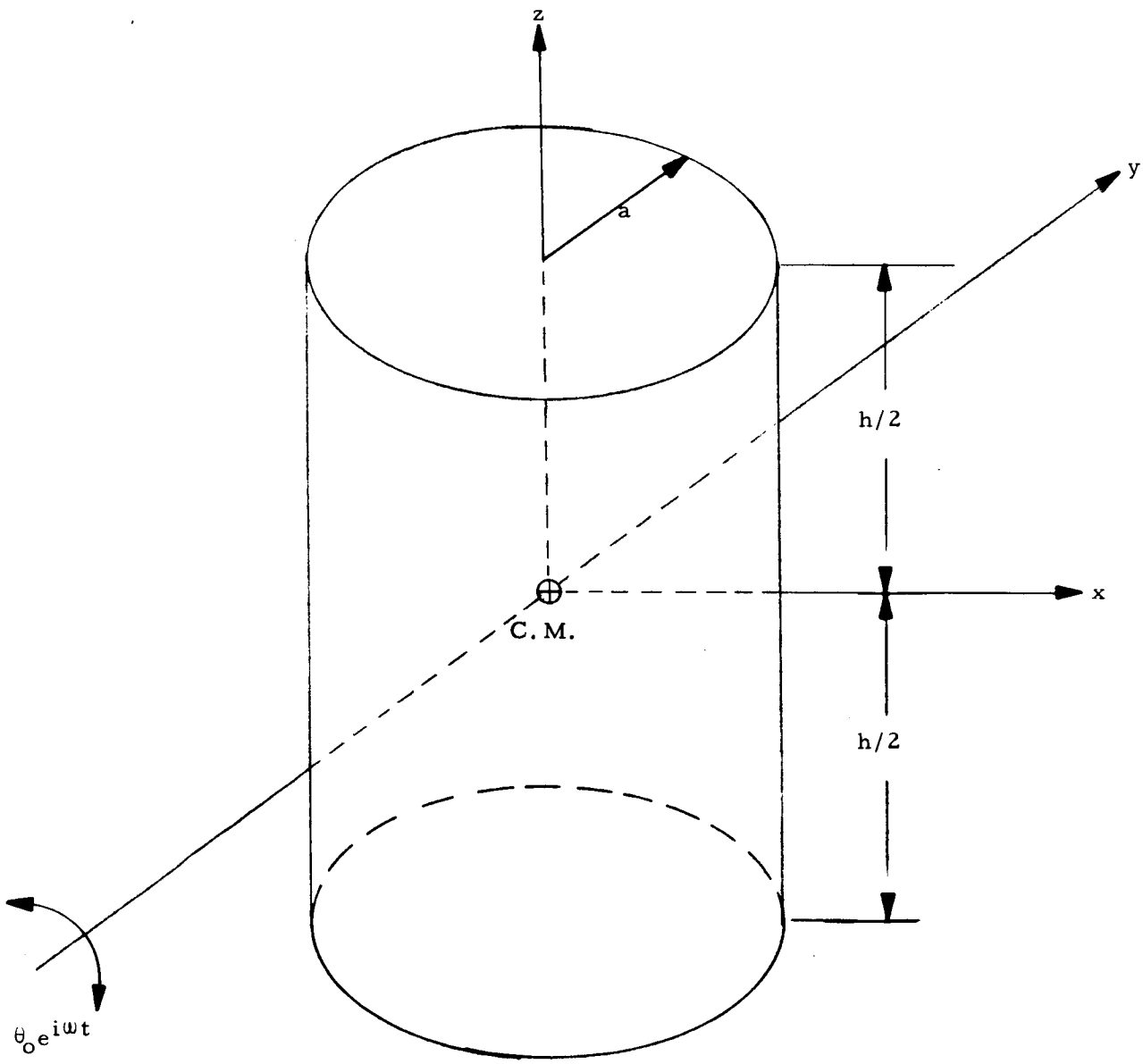

with boundary (linearized) conditions

$$\partial \Phi / \partial r = -i\omega\theta_o e^{i\omega t} z \cos\varphi \qquad \text{at} \quad r = a \tag{162}$$

$$\partial \Phi / \partial z = i\omega\theta_o e^{i\omega t} r \cos\varphi . \qquad \text{at} \quad z = \pm\frac{h}{2} \tag{163}$$

The derivation of the Laplace Equation and boundary conditions is given in Appendix C8. The coordinate system has been chosen to have its origin in the center of mass of the liquid. The oscillations are about the y-axis and exhibit an amplitude θ_o . The value Φ represents the velocity potential and ω is the circular forcing frequency.

The solution of Equation 161 satisfying the boundary conditions 162 and 163 is given by the expression

$$\Phi(r, \varphi, z, t) = i\omega\theta_o e^{i\omega t} a^2 \cos\varphi \left\{ -rz/a^2 + 4 \cdot \sum_{n=1}^{\infty} \frac{J_1(\epsilon_n r/a) \sinh(\epsilon_n z/a)}{\epsilon_n(\epsilon_n^2 - 1) J_1(\epsilon_n) \cosh(\epsilon_n h/2a)} \right\} \tag{164}$$

where $J_1(\epsilon_n \frac{r}{a})$ is the Bessel function of the first kind and first order, and ϵ_n are the roots of its first derivative ($J_1'(\epsilon_n) = 0$). The derivation of Equation 164 is given in Appendix C9.

The pressure distribution is derived from the unsteady Bernoulli Equation which is:

$$P = -\rho \left\{ \partial\Phi/\partial t + (1/2)\left[(\partial\Phi/\partial x)^2 + (\partial\Phi/\partial y)^2 + (\partial\Phi/\partial z)^2\right] - \Omega - F(t) \right\} . \tag{165}$$

The velocities $\partial\Phi/\partial x$, $\partial\Phi/\partial y$, and $\partial\Phi/\partial z$ are small and their squares can be neglected. $F(t)$ can be included in the potential function Φ and can be set equal to zero in Equation 165. Ω is the external force potential and depends on the tank orientation. Therefore, the linearized pressure distributions are:

$$P_{wall} = -\rho(\partial\Phi/\partial t)_{r=a} + \rho g(h/2 - z + a\theta_o\left[1 - \cos\varphi\right]) \tag{166}$$

$$P_{bottom} = -\rho(\partial\Phi/\partial t)_{z=-h/2} + \rho g(h + \theta_o\left[a - r\cos\varphi\right]) \tag{167}$$

$$P_{top} = -\rho(\partial\Phi/\partial t)_{z=h/2} + \rho g\theta_o\left[a - r\cos\varphi\right] \tag{168}$$

$$P_{wall} = -\rho\omega^2\theta_o e^{i\omega t}a^2\cos\varphi\left\{z/a - 4\sum_{n=1}^{\infty}\frac{\sin h(\epsilon_n z/a)}{\epsilon_n(\epsilon_n^2-1)\cosh(\epsilon_n h/2a)}\right\}$$

$$+ \rho g(h/2 - z - a\theta_o\cos\varphi + a\theta_o) \tag{169}$$

$$P_{bottom} = -\rho\omega^2\theta_o e^{i\omega t}a^2\cos\varphi\left\{(-hr/2a^2) + 4\sum_{n=1}^{\infty}\right.$$

$$\left.\frac{J_1(\epsilon_n r/a)\tanh(\epsilon_n h/2a)}{\epsilon_n(\epsilon_n^2 - 1)J_1(\epsilon_n)}\right\} + \rho g(h - \theta_o r\cos\varphi + a\theta_o) \tag{170}$$

$$P_{top} = -\rho\omega^2\theta_o e^{i\omega t}a^2\cos\varphi\left\{hr/2a^2 - 4\sum_{n=1}^{\infty}\right.$$

$$\left.\frac{J_1(\epsilon_n r/a)\tanh(\epsilon_n h/2a)}{\epsilon_n(\epsilon_n^2-1)J_1(\epsilon_n)}\right\} + \rho g(a\theta_o - r\theta_o\cos\varphi). \tag{171}$$

The moment of the liquid about the origin is then obtained from

$$\overset{\curvearrowright}{M}_y = \int_0^{2\pi} \int_{-h/2}^{h/2} P_{wall}\, a\, z \cos\varphi\, dz\, d\varphi +$$

$$\int_0^{2\pi} \int_0^{a} (P_{bottom} - P_{top}) r^2 \cos\varphi\, dr\, d\varphi \tag{172}$$

and yields

$$\overset{\curvearrowright}{M}_y = -ma^2\omega^2\theta_o e^{i\omega t}\left\{h^2/12a^2 - 1/4 + 4\sum_{n=1}^{\infty} \frac{\frac{2\tanh(\epsilon_n h/2a)}{\epsilon_n h/2a} - 1}{\epsilon_n^2(\epsilon_n^2 - 1)}\right\}. \tag{173}$$

From this, the effective moment of inertia of the liquid in the container can be obtained with

$$\overset{\curvearrowright}{M}_y = I_{eff}\ddot{\theta} = -\omega^2\theta I_{eff} \tag{174}$$

and is finally given by the expression

$$I_{eff} = ma^2\left[h^2/12a^2 - 1/4 + 4\sum_{n=1}^{\infty} \frac{\frac{2\tanh(\epsilon_n h/2a)}{(\epsilon_n h/2a)} - 1}{\epsilon_n^2(\epsilon_n^2 - 1)}\right]. \tag{175}$$

For a solid circular cylinder of the same magnitude as the liquid volume the moment of inertia about the y-axis is:

$$I_{solid} = ma^2\left[h^2/12a^2 + 1/4\right]. \tag{176}$$

Therefore, the ratio of the effective moment of inertia of the liquid to that of the solidified body yields:

$$I_{eff}/I_{solid} = \left\{ 1 - \frac{1/2 + 4 \sum_{n=1}^{\infty} \frac{1 - \frac{2\tanh(\epsilon_n h/2a)}{(\epsilon_n h/2a)}}{\epsilon_n^2(\epsilon_n^2 - 1)}}{h^2/12a^2 + 1/4} \right\} . \tag{177}$$

The result of this equation for various aspect ratios is shown in Table 42. The zeros of the first derivative of the Bessel functions are given in Table 43. A graph showing I_{eff}/I_{solid} versus the aspect ratio is shown by the solid line in Figure 128. As h/a approaches zero or infinity, the moment of inertia ratio approaches unity.

$$\lim_{\substack{h \to o \\ h \to \infty}} \left\{ \frac{I_{eff}}{I_{solid}} \right\} = 1 \tag{178}$$

This means that in shallow and very long containers most of the liquid participates in the rotational motion. It furthermore can be seen that the moment of inertia of the liquid can be quite small since not all of the liquid takes part in motion. Some of it is almost completely at rest. As the aspect ratio h/a of the container increases from the shallow tank to a long container, the moment of inertia ratio decreases from unity at h/a = 0 to a minimum of 0.16 at about h/a = 1.72 and then increases again to unity as h/a approaches infinity.

These are the results for ideal liquid. It may be mentioned that for a real liquid the internal friction causes more of the liquid to follow the tank motion. This means that not only a small amount of damping is present, but also that the effective moment of the liquid is somewhat larger than indicated in Figure 128.

The experimental data are exhibited by the x's shown in Figure 128. This data was obtained from tanks with two feet diameters using ordinary tap water. The results of the analytical expression and experimental data gives very good agreement. The experimental points are a little higher than the analytical curve, as discussed previously, because the liquid is viscous. A higher viscosity liquid would cause the experimental points to be even higher. The frequency of oscillation did not affect the moment of inertia of the water, for the frequency range covered, but extremely low frequencies would cause the moment of inertia to be higher.

TABLE 42

RESULTS OF I_{eff}/I_{solid} FOR VARIOUS ASPECT RATIOS

h/a	I_{eff}/I_{solid}	h/a	I_{eff}/I_{solid}
.4	.84046	2.6	.27136
.6	.64824	3.0	.35617
.8	.50176	4.0	.53828
1.0	.34886	5.0	.66344
1.2	.24463	6.0	.74758
1.4	.18072	7.0	.80478
1.6	.15686	8.0	.85220
1.8	.14762	9.0	.87606
2.0	.16365	10.0	.89606
2.2	.19347		

TABLE 43

ZEROS ϵ_n OF THE FIRST DERIVATIVE OF THE BESSEL-FUNCTION OF FIRST ORDER AND FIRST KIND

$J_1(\epsilon_n) = 0.$

n	ϵ_n	n	ϵ_n	n	ϵ_n
1	1.84119	12	36.89000	23	71.45677
2	5.33144	13	40.03341	24	74.60000
3	8.53631	14	43.17665	25	77.74383
4	11.70600	15	46.31957	26	80.88514
5	14.86359	16	49.46238	27	84.02718
6	18.01553	17	52.60507	28	87.16914
7	21.16440	18	55.74758	29	90.31228
8	24.31145	19	58.89000	30	93.45301
9	27.45751	20	62.03234	31	96.59499
10	30.60194	21	65.17465	32	99.73675
11	33.74397	22	68.31682		

FIGURE 128

RATIO OF THE MOMENT OF INERTIA OF LIQUID TO SOLID
VERSUS
ASPECT RATIO FOR A COMPLETELY FILLED CYLINDRICAL TANK

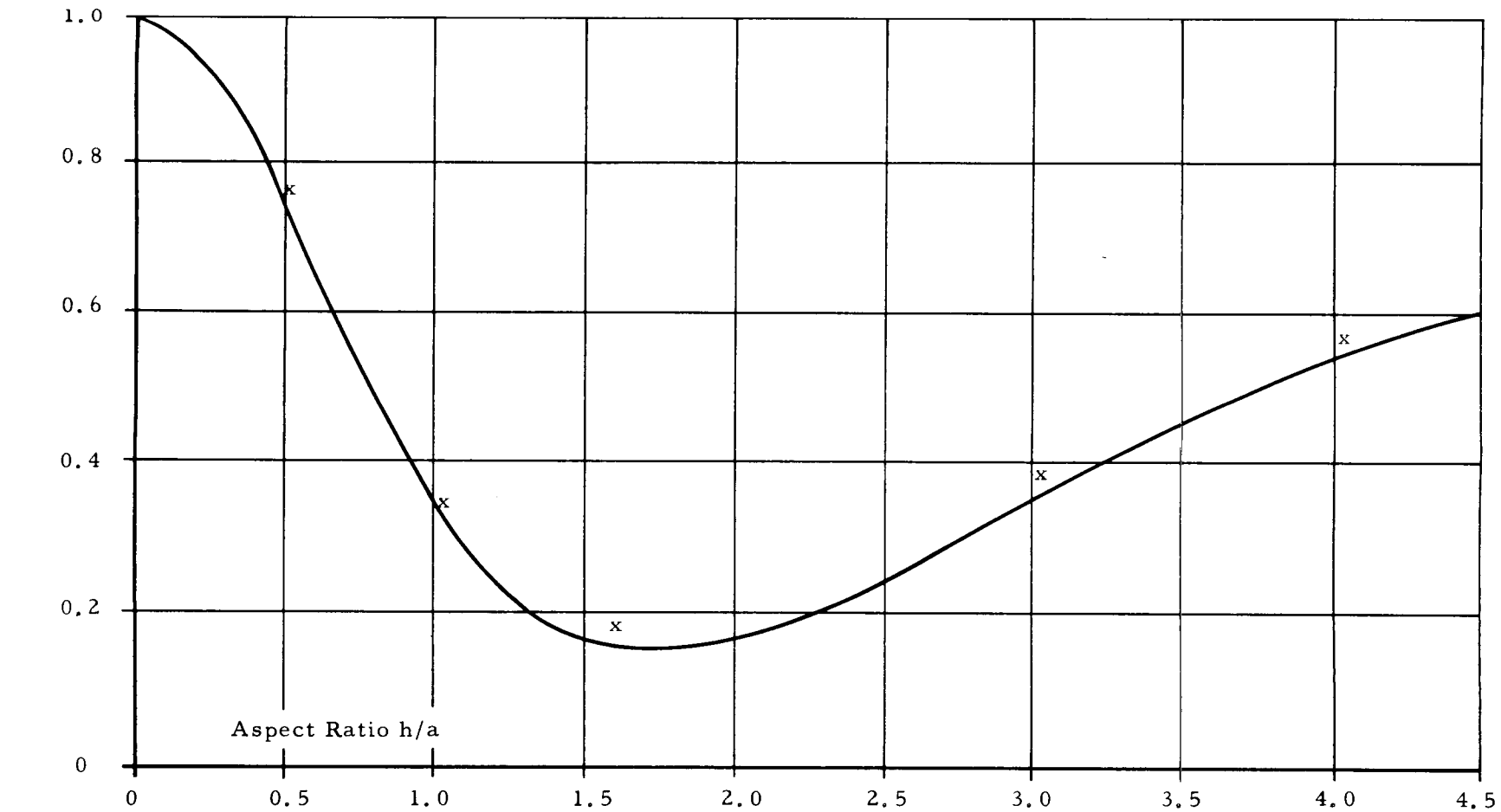

2. 3. 2. 2. 3 Moment of Inertia About A Displaced Yaw-Pitch Axis

The moment of inertia of a liquid in a completely filled container oscillating about an axis perpendicular to the longitudinal tank axis, but not passing through the center of mass, as shown in Figure 129, can be obtained by solving the Laplace Equation:

$$\nabla^2 \Phi = 0 \tag{179}$$

with the boundary conditions:

$$\partial \Phi / \partial r = -i\omega \theta_o e^{i\omega t} z \cos \varphi \qquad \text{at } r = a \tag{180}$$

$$\partial \Phi / \partial z = i\omega \theta_o e^{i\omega t} r \cos \varphi . \qquad \text{at } z = (\lambda - 1)h \text{ and } \lambda h \tag{181}$$

The coordinate system has been chosen such that the y-axis represents the axis of rotation about which the excitation takes place.

The solution of Equation 179 with the boundary conditions Equations 180 and 181 is given by the expression:

$$\Phi(r, \varphi, z, t) = i\omega\theta_o e^{i\omega t} a^2 \cos \varphi \left\{ -rz/a^2 + 4 \sum_{n=1}^{\infty} \frac{J_1(\epsilon_n r/a)\ F(z)}{\epsilon_n(\epsilon_n^2 - 1)\ J_1(\epsilon_n) \sinh(\epsilon_n h/a)} \right\} \tag{182}$$

where:

$$F(z) = \left[\cosh(\epsilon_n/\lambda - 1)ha - \cosh(\epsilon_n \lambda h/a)\right] \cosh(\epsilon_n z/a) + \left[\sinh(\epsilon_n \lambda h/a) - \sinh(\epsilon_n/(\lambda - 1)ha)\right] \sinh(\epsilon_n z/a) . \tag{183}$$

The solution of this equation is similar to the one in the previous section. For $\lambda = 1/2$ it can be seen that the Equation 182 presents the same result

FIGURE 129

COORDINATE SYSTEM FOR PITCH-EXCITATION
ABOUT ARBITRARY AXIS

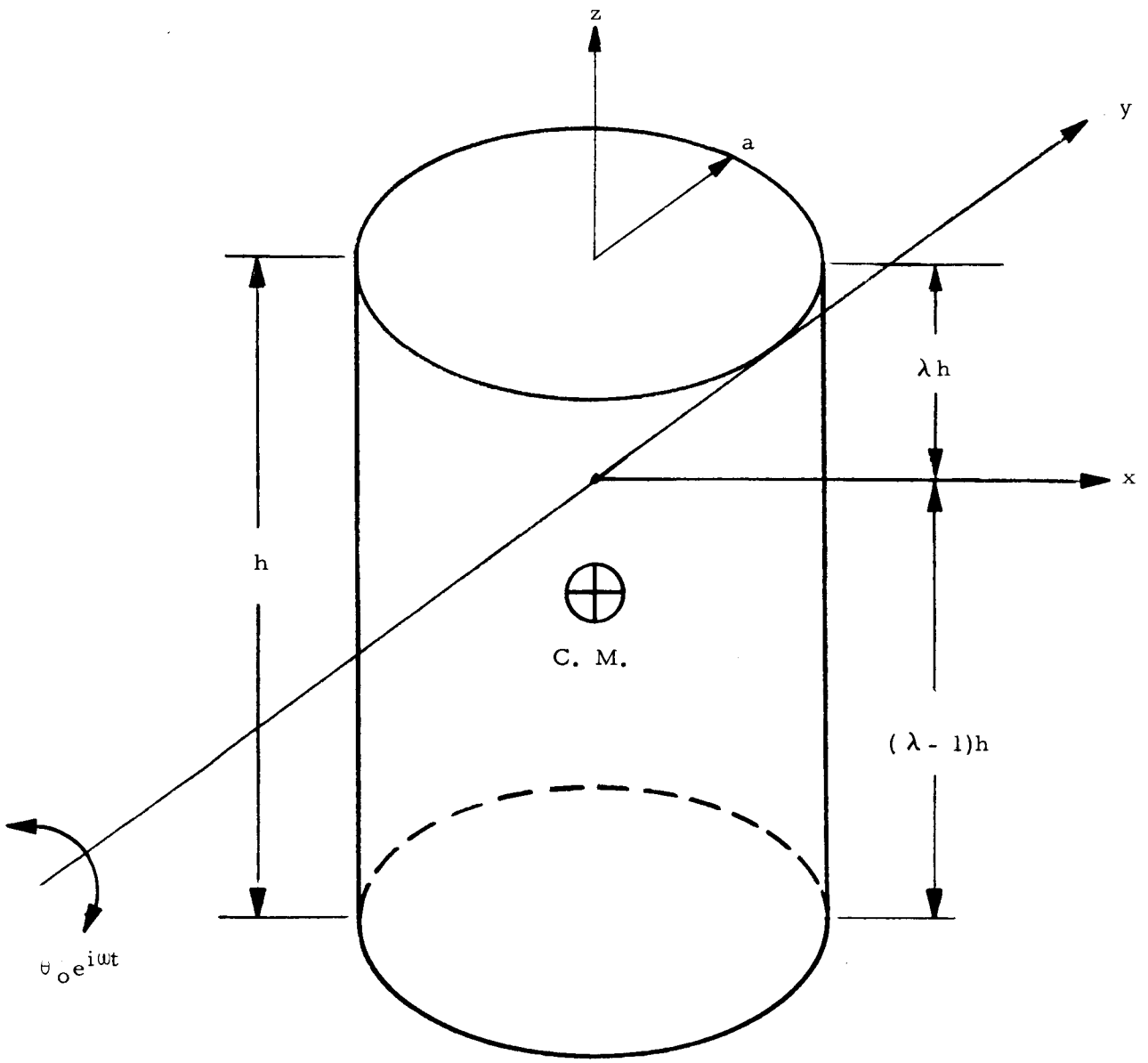

of Equation 164 the velocity potential of the previous case.

The pressure distribution in the container is given by:

$$P_{wall} = -\rho(\partial\Phi/\partial t)_{r=a} + \rho g(\lambda h - z + a\theta_o\left[1 - \cos\varphi\right]) \tag{184}$$

$$P_{bottom} = -\rho(\partial\Phi/\partial t)_{z=(\lambda-1)h} + \rho g\left[(\lambda - 1)h + \theta_o(a - r\cos\varphi)\right] \tag{185}$$

$$P_{top} = -\rho(\partial\Phi/\partial t)_{z=\lambda h} + \rho g\theta_o\left[a - r\cos\varphi\right] \tag{186}$$

and yields at the container wall, bottom, and top, the expressions:

$$P_{wall} = -\rho\omega^2\theta_o e^{i\omega t}a^2\cos\varphi\left\{+ z/a - 4\sum_{n=1}^{\infty}\frac{F(z)}{\epsilon_n(\epsilon_n^2 - 1)\sinh(\epsilon_n h/a)}\right\}$$

$$+ \rho g(\lambda h - z + a\theta_o\left[1 - \cos\varphi\right]) \tag{187}$$

$$P_{bottom} = -\rho\omega^2\theta_o e^{i\omega t}a^2\cos\varphi\left\{r(\lambda - 1)h/a^2 + 4\sum_{n=1}^{\infty}\right. \tag{188}$$

$$\left.\frac{J_1(\epsilon_n r/a)\cdot F(\lambda - 1)h}{\epsilon_n(\epsilon_n^2 - 1)J_1(\epsilon_n)\sinh(\epsilon_n h/a)}\right\} + \rho g\left[(\lambda - 1)h + \theta_o(a - r\cos\varphi)\right]$$

$$P_{top} = -\rho\omega^2\theta_o e^{i\omega t}a^2\cos\varphi\left\{r\lambda h/a^2 + 4\sum_{n=1}^{\infty}\frac{J_1(\epsilon_n r/a)\cdot F(\lambda h)}{\epsilon_n(\epsilon_n^2 - 1)J_1(\epsilon_n)\sin(\epsilon_n h/a)}\right\}$$

$$+ \rho g\theta_o\left[a - r\cos\varphi\right]. \tag{189}$$

The moment of the liquid about the y-axis can be determined from:

$$\overset{\curvearrowright}{M_y} = \int_0^{2\pi}\int_{(\lambda-1)h}^{\lambda h} aP_{wall}z\cos\varphi\, d\varphi\, dz + \int_0^{2\pi}\int_0^{a}(P_{bottom} - P_{top})\cdot$$

$$r^2\cos\varphi\, d\varphi\, dr \tag{190}$$

which yields:

$$\overset{\curvearrowright}{M}_y = - ma^2\omega^2\theta_o e^{i\omega t}\left[(h^2/3a^2)\left[\lambda^3 - (\lambda - 1)^3\right] - 1/4 + 4 \sum_{n=1}^{\infty} \frac{\dfrac{2\tanh(\epsilon_n h/2a)}{(\epsilon_n h/2a)} - 1}{\epsilon_n^2(\epsilon_n^2 - 1)}\right] - (mg(1-2\lambda)\, h\theta_o e^{i\omega t})\,/2\,, \tag{191}$$

The last term is the static moment which appears because the axis does not pass through the center of mass. This term has no effect upon the moment of inertia of the liquid; therefore, one obtains from Equation 191:

$$-\omega^2\theta I_{eff} = -ma^2\omega^2\theta_o e^{i\omega t}\left[(h^2/3a^2)\left[\lambda^3 - (\lambda-1)^3\right] - 1/4 + 4 \sum_{n=1}^{\infty} \frac{\dfrac{2\tanh(\epsilon_n h/2a)}{\epsilon_n h/2a} - 1}{\epsilon_n^2(\epsilon_n^2 - 1)}\right]. \tag{192}$$

Only the first term in Equation 192 differs from Equation 173 and Equation 192 equals 173 for $\lambda = 1/2$.

The effective moment of inertia of the liquid about the axis of rotation is is therefore:

$$I_{eff} = ma^2\left[(h^2/3a^2) + (h^2/a^2)\lambda(\lambda - 1) - 1/4 + 4 \sum_{n=1}^{\infty} \frac{\dfrac{2\tanh(\epsilon_n h/2a)}{(\epsilon_n h/2a)} - 1}{\epsilon_n^2(\epsilon_n^2 - 1)}\right]. \tag{193}$$

For a solid circular cylinder occupying the same volume as the liquid, the moment of inertia about the y-axis can be obtained with the transfer theorem which yields

$$I_{solid} = I_{cm} + mx^2 \tag{194}$$

where:

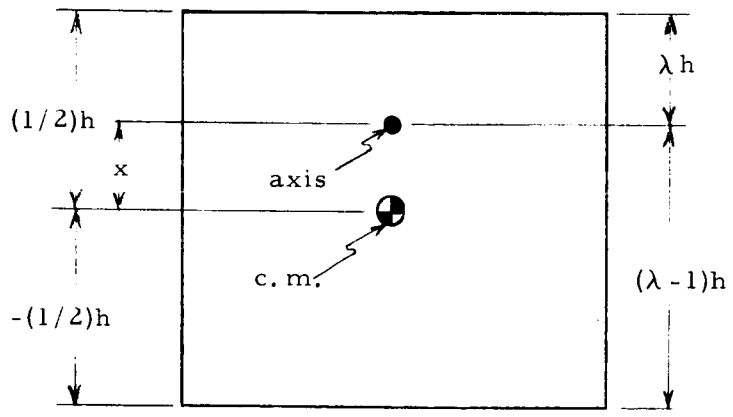

$$x + \lambda h = h/2$$

$$x = (h/2)(1-2\lambda)$$

$$x^2 = (h^2/4)(1-2\lambda)^2.$$

It is therefore:

$$I_{solid} = I_{cm} + (mh^2 (1-2\lambda)^2)/4 \tag{195}$$

or:

$$I_{solid} = ma^2 \left\{1/4 + (h/a)^2 \left[1/3 + \lambda(\lambda - 1)\right]\right\} \tag{196}$$

where:

$$I_{cm} = m\left[a^2/4 + h^2/12\right] \tag{197}$$

the moment of inertia of a rigid cylinder about its center of mass has been used. Therefore, the ratio of effective moment of inertia of the liquid to that of the solidified liquid is given by the expression:

$$I_{eff}/I_{solid} = \left\{1 - \frac{1/2 + 4 \sum_{n=1}^{\infty} \frac{1 - \frac{2\tanh(\epsilon_n h/2a)}{\epsilon_n h/2a}}{\epsilon_n^2(\epsilon_n^2 - 1)}}{1/4 + (h/a)^2\left[1/3 + \lambda(\lambda - 1)\right]}\right\}. \tag{198}$$

From this we can conclude that the Transfer Theorem is valid for the liquid as can be seen from the expression:

$$I_{eff} = (mh^2(1-2\lambda)^2)/4 + I_{eff}\ c.m. \tag{199}$$

$$I_{eff} = (mh^2(1-2\lambda)^2)/4 + ma^2\left[h^2/12a^2 - 1/4 + 4 \sum_{n=1}^{\infty} \frac{\frac{2\tanh(\epsilon_n h)}{(\epsilon_n h/2a)} - 1}{\epsilon_n^2(\epsilon_n^2 - 1)}\right] \tag{200}$$

$$I_{eff} = ma^2\left[(h/a)^2(1/3 + \lambda(\lambda - 1)) - 1/4 + 4 \sum_{n=1}^{\infty} \frac{\frac{2\tanh(\epsilon_n h/2a)}{\epsilon_n h/2a} - 1}{\epsilon_n^2(\epsilon_n^2 - 1)}\right] \tag{201}$$

indicating that Equation 201 is identical to 193. This means that for an oscillation about any axis perpendicular to the longitudinal axis, the moment of inertia of the liquid in the container can be determined by adding the effective moment of inertia of the liquid about its center of mass to the product of the mass times the square of the distance between the parallel axis of oscillation and that through the center of mass.

Calculations I_{eff}/I_{solid} at various aspect ratios and axis displacements are shown in Table 44. This data is also presented in plotted form in Figure 130.

From the analytical results of this investigation, it can be seen that the influence of the effective moment of inertia of the liquid about an axis through the center of mass is diminishing steadily with increasing λ, i.e., increasing distance of the rotational axis and the center of

TABLE 44

RESULTS OF I_{eff}/I_{solid} FOR VARIOUS ASPECT RATIOS AND AXIS DISPLACEMENTS

I_{eff}/I_{solid} For Different Axis Displacements, ν

$\frac{h}{a}$	ν=.5	ν=.6	ν=.7	ν=.8	ν=.9	ν=1.0	ν=2.0	ν=5.0
.4	.8405	.8414	.8442	.8487	.8546	.8615	.9326	.9880
.6	.6482	.6516	.6611	.6759	.6946	.7156	.8877	.9826
.8	.5018	.5121	.5405	.5813	.6275	.6738	.9133	.9886
1.0	.3489	.3678	.4186	.4873	.5600	.6283	.9159	.9912
1.2	.2446	.2729	.3456	.4406	.5345	.6172	.9226	.9905
1.4	.1807	.2178	.3114	.4258	.5342	.6251	.9298	.9916
1.6	.1569	.2010	.3095	.4369	.5525	.6459	.9372	.9925
1.8	.1476	.1976	.3177	.4539	.5732	.6764	.9432	.9933
2.0	.1637	.2173	.3437	.4829	.6013	.6920	.9491	.9940
2.2	.1935	.2491	.3778	.5161	.6309	.7172	.9544	.9947
2.6	.2714	.3273	.4532	.5832	.6873	.7633	.9630	.9957
3.0	.3562	.4093	.5266	.6443	.7361	.8019	.9697	.9965
4.0	.5383	.5807	.6712	.7582	.8236	.8691	.9805	.9978
5.0	.6634	.6960	.7644	.8286	.8760	.9085	.9866	.9985

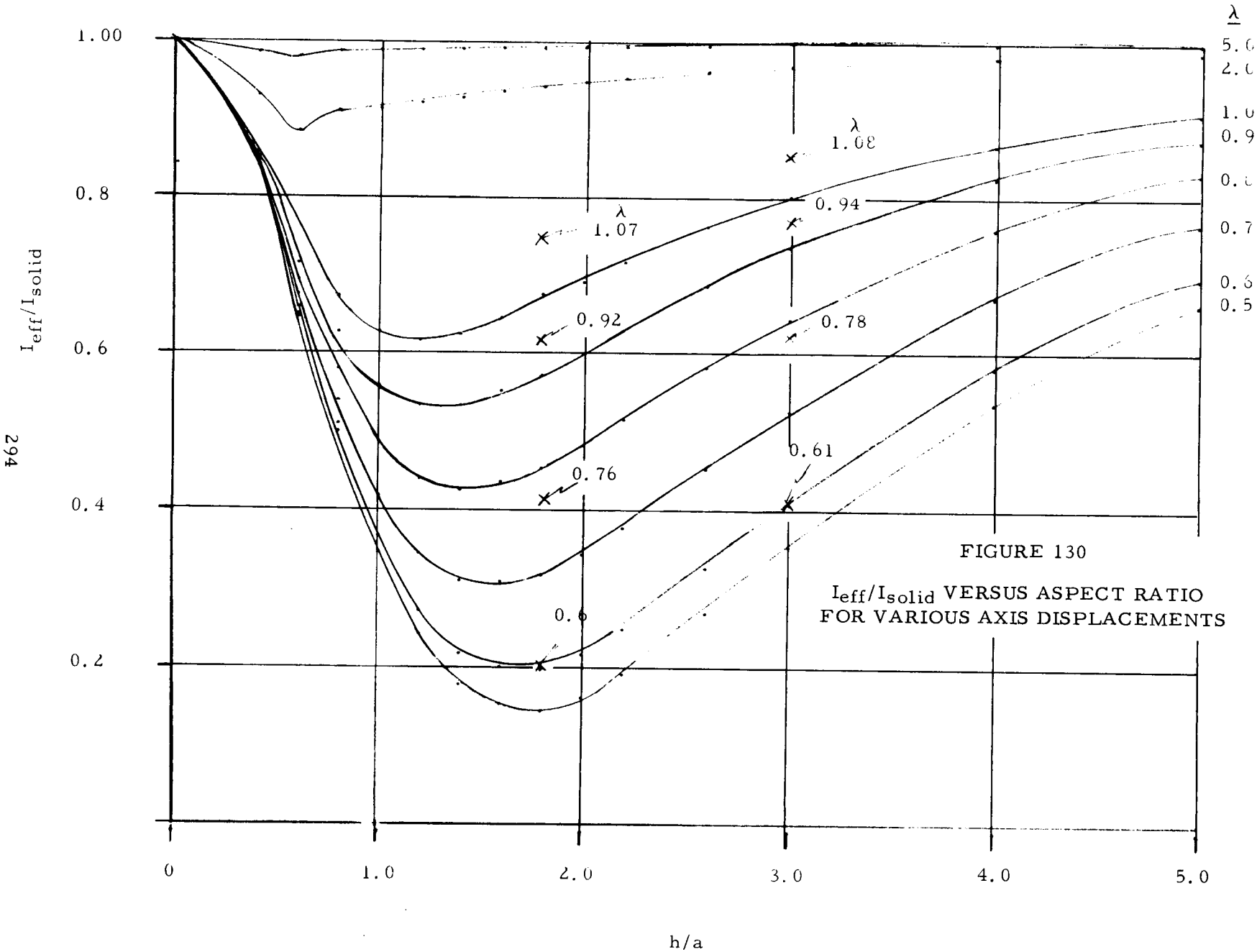

FIGURE 130

I_{eff}/I_{solid} VERSUS ASPECT RATIO FOR VARIOUS AXIS DISPLACEMENTS

mass. For $\lambda \to \infty$, Equation 198 shows that I_{eff}/I_{solid} approaches unity. As indicated in Figure 130, the minimum amount of inertia ratio shifts with increasing λ to smaller liquid height ratios of h/a and exhibits smaller deviations from unity.

The experimental data are represented by x/s in Figure 130, where the value of λ is shown by each respective point. By interpolating between the solid lines, we see that the experimental results agree very well with the analytical solution. The experimental points may be a little high which is caused by the viscosity of the liquid; also, experimental errors cause some variations.

2.3.2.2.4 Moment of Inertia about a Roll Axis

A circular cylindrical container which is completely filled with liquid performs roll oscillations about its longitudinal axis. Due to friction in the liquid and at the tank wall, part of the liquid participates in the motion of the container. The purpose of the following section is to find the effective moment of inertia and effective damping of the liquid in the container. Due to the difficulties in satisfying the boundary conditions, the problem is treated in two parts. In the first part, the cylindrical wall influence is investigated alone. This is performed by treating an infinitely long tank and solving the Navier-Stokes Equation with the corresponding boundary conditions. The second part of the problem investigates the effect of the container top and bottom. In this case, the influence of the cylinder walls is neglected. The superposition of wall, bottom, and top results should represent a good approximation.

In both cases the Navier-Stokes Equation has to be solved. With the velocity vector in cylindrical polar coordinates.

$$\vec{v} = \mu_r \vec{e}_r + \mu_\varphi \vec{e}_\varphi + w\vec{k} \tag{202}$$

the Navier-Stokes Equation for incompressible liquids

$$\partial\vec{v}/\partial t + (1/2)\text{grad}\,\vec{v}^2 - \left[\vec{v} \times \text{curl}\vec{v}\right] + (1/\rho)\text{grad}\ p = \vec{g} + \nu\nabla^2\vec{v} \tag{203}$$

can be written in component form as

$$\partial\mu/\partial t + \mu_r\partial\mu_r/\partial r + (\mu\varphi/r)(\partial\mu_r/\partial\varphi) - \mu_\varphi{}^2/r + w\,\partial\mu_r/\partial z + (1/\rho)(\partial p/\partial r) =$$

$$\nu\left[\partial^2\mu_r/\partial r^2 + (1/r)(\partial\mu_r/\partial r) - \mu_r/r^2 + (1/r^2)(\partial^2\mu_r/\partial\varphi^2) - (2/r^2)(\partial\mu_\varphi/\partial\varphi) + \partial^2\mu_r/\partial z^2\right] \tag{204}$$

$$\partial\mu_\varphi/\partial t + \mu_r\partial\mu_\varphi/\partial r + (\mu_\varphi/r)(\partial\mu_\varphi/\partial\varphi) + \mu_r\mu_\varphi/r + w\partial\mu_\varphi/\partial z + (1/\rho r)(\partial p/\partial_\varphi) =$$

$$\nu\left[\partial^2\mu_\varphi/\partial r^2 + (1/r)(\partial\mu_\varphi/\partial r) - \mu_\varphi/r^2 + (1/r^2)(\partial^2\mu/\partial\varphi^2) + \right.$$

$$\left.(2/r^2)(\partial\mu_r/\partial\varphi) + \partial^2\mu_\varphi/\partial z^2\right] \tag{205}$$

$$\partial w/\partial t + \mu_r\partial w/\partial r + (\mu_\varphi/r)(\partial w/\partial\varphi) + w\partial w/\partial z + (1/\rho)(\partial p/\partial z) = g +$$

$$\nu\left[\partial^2 w/\partial r^2 + (1/r)(\partial w/\partial r) + (1/r^2)(\partial^2 w/\partial\varphi^2) + \partial^2 w/\partial z^2\right]. \tag{206}$$

ρ is the mass density and ν is the kinematic viscosity. The vector $\vec{g}$ represents the acceleration due to external forces. Since the liquid is incompressible the continuity equation reads div $\vec{v} = o$

or

$$\partial\mu_r/\partial r + (1/r)(\partial\mu_\varphi/\partial\varphi) + \mu_r/r + \partial w/\partial z = 0\,. \tag{207}$$

For the determination of the torque that is exerted on the liquid by the motion of the walls the stress components have to be determined. The normal stress components are given by

$$\sigma_r = -p + 2\eta\partial\mu_r/\partial r \tag{208}$$

$$\sigma_\varphi = -p + 2\eta\left[(1/r)(\partial\mu_\varphi/\partial\varphi) + \mu_r/r\right] \tag{209}$$

$$\sigma_z = -p + 2\eta\partial w/\partial z \tag{210}$$

while the shear stresses are represented by the expressions

$$\tau_{r\varphi} = \eta\left[r\partial(\mu_\varphi/r)/\partial r + (1/r)(\partial\mu_r/\partial\varphi)\right] \tag{211}$$

$$\tau_{\varphi z} = \eta\left[\partial\mu_{\varphi}/\partial z + (1/r)(\partial w/\partial\varphi)\right] \tag{212}$$

$$\tau_{rz} = \eta\left[\partial\mu_{r}/\partial z + \partial w/\partial r\right] \tag{213}$$

where η is the dynamic viscosity of the liquid.

Treating an infinitely long circular cylindrical container, Figure 131, roll oscillating with $\theta(t) = \theta_o e^{i\omega t}$ about its longitudinal axis reveals that due to symmetry $\partial/\partial\varphi \equiv 0$ and $\partial/\partial z \equiv 0$. It furthermore can be seen that only the angular velocity component is not vanishing, i.e. $\mu_r = w = 0$. With these observations the Navier-Stokes Equation, which originally represented three non-linear partial differential equations, yields a linear differential equation of the form

$$\partial\mu_{\varphi}/\partial t = \nu\left[\partial^2\mu_{\varphi}/\partial r^2 + (1/r)(\partial\mu_{\varphi}/\partial r) - \mu_{\varphi}/r^2\right] \tag{214}$$

while the continuity Equation 207 is identically satisfied. The boundary conditions are given by:

$$\mu_{\varphi} = ai\omega\theta_o e^{i\omega t} \qquad \text{at } r = a \tag{215}$$

$$\mu_{\varphi} = 0 . \qquad \text{at } r = 0 \tag{216}$$

This means that the liquid particle at the wall performs the same motion as the wall, while along the center axis (axis of rotation) the particles are at rest. With:

$$\mu_{\varphi} = U(r)e^{i\omega t} \tag{217}$$

Equation 214 transforms into:

$$d^2U/dr^2 + (1/r)(dU/dr) - (1/r^2 + i\omega/\nu)U = 0 \tag{218}$$

which represents nothing but a Bessel differential equation, the solution of which is given by:

FIGURE 131

INFINITELY LONG ROLL OSCILLATING CYLINDER

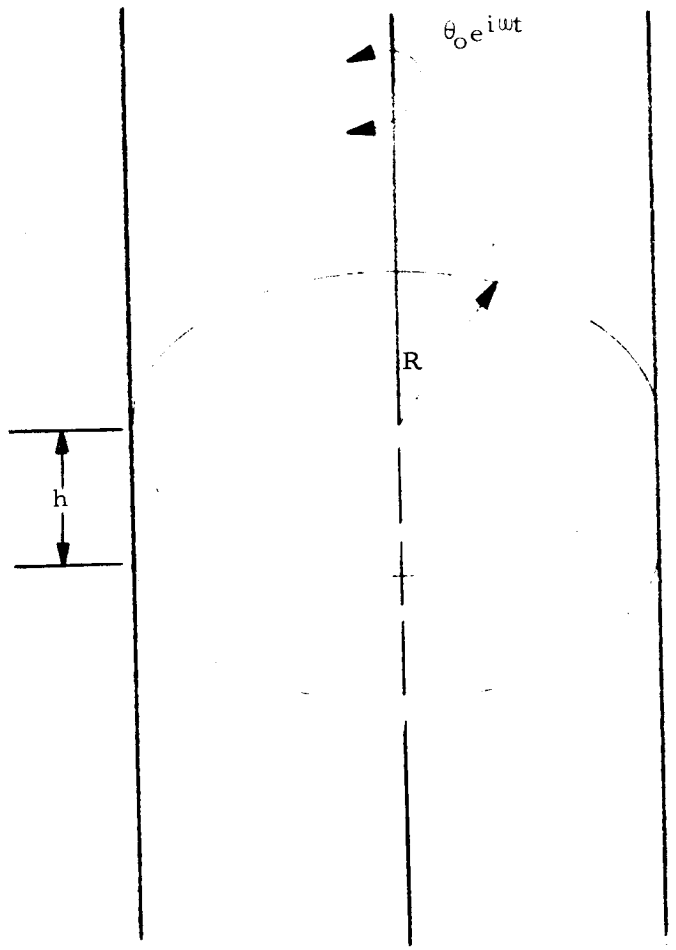

$$U(r) = AI_1(\lambda r) + BK_1(\lambda r) \tag{219}$$

where $\lambda = \sqrt{i\omega/\nu}$. The boundary conditions Equations 215 and 216 are with Equation 217 given by:

$$U = ai\omega\theta_o \qquad \text{at } r = a \tag{220}$$

and

$$U = 0. \qquad \text{at } r = 0 \tag{221}$$

Since the modified Bessel function K, exhibits at $r = 0$ a singularity, the integration constant B must vanish. It is

$$I_1(r\sqrt{i\omega/\nu}) = ber_1(r\sqrt{\omega/\nu}) + ibei_1(r\sqrt{\omega/\nu}) \tag{222}$$

and the solution of Equation 218 is therefore, with $\gamma = \sqrt{\omega/\nu}$

$$U(r) = A\left\{ber_1(r\sqrt{\omega/\nu}) + ibei_1(r\sqrt{\omega/\nu})\right\} \tag{223}$$

where A is an integration constant and yields with Equations 220 and 221

$$A = \frac{ai\omega\theta_o\left[bei_1(\gamma a) + ibei_1(\gamma a)\right]}{\left[ber_1^2(\gamma a) + bei_1^2(\gamma a)\right]} . \tag{224}$$

Thus the velocity distribution μ_φ in angular direction yields

$$\mu_\varphi(r) = \frac{a\omega\theta_o\sqrt{\alpha^2 + \beta^2}\; e^{i\left[\omega t + \arctan(\beta/\alpha)\right]}}{\left[ber_1^2(\gamma a) + bei_1^2(\gamma a)\right]} \tag{225}$$

where:

$$\alpha = ber_1(\gamma r)bei_1(\gamma a) - bei_1(\gamma r)\, ber_1(\gamma a) \tag{226}$$

$$\beta = ber_1(\gamma r)\, ber_1(\gamma a) + bei_1(\gamma r)\, bei_1(\gamma a). \tag{227}$$

The ber and bei functions are the modified Kelvin functions and can be represented by the series expansions:

$$\mathrm{ber}_1 x = \sum_{n=0}^{\infty} \frac{(-1)^n x^{2n+1}}{2^{2n+1} n!(n+1)!} \cos\left[3\pi(2n+1)/4\right] \tag{228}$$

$$\mathrm{bei}_1 x = \sum_{n=1}^{\infty} \frac{(-1)^n x^{2n+1}}{2^{2n+1} n!(n+1)!} \sin\left[3\pi(2n+1)/4\right]. \tag{229}$$

The shear stress at the container wall is given by:

$$(\tau_{r\varphi})_{r=a} = \eta\left\{r\partial(\mu_\varphi/r)/\partial r\right\}_{r=a} = \eta\left[\partial\mu_\varphi/\partial r - i\omega\theta_o e^{i\omega t}\right] \tag{230}$$

and yields

$$(\tau_{r\varphi})_{r=a} = \frac{(\eta a\omega\theta_o\gamma e^{i\omega t})}{\left[\mathrm{ber}_1^2(\gamma a) + \mathrm{bei}_1^2(\gamma a)\right]}\left[\chi + i\delta\right] - \eta i\omega\theta_o e^{i\omega t} \tag{231}$$

where

$$\chi = \mathrm{ber}_1'(\gamma a)\mathrm{bei}_1(\gamma a) - \mathrm{bei}_1'(\gamma a)\mathrm{ber}_1(\gamma a) \tag{232}$$

$$\delta = \mathrm{ber}_1'(\gamma a)\mathrm{ber}_1(\gamma a) + \mathrm{bei}_1'(\gamma a)\mathrm{bei}_1(\gamma a) \tag{233}$$

The forcing torque T_o on the liquid of height h is then:

$$T_o = \int_0^h \int_0^{2\pi} (\tau_{r\varphi})_{r=a} a^2 d\varphi\, dz \tag{234}$$

which yields

$$T_o = 2\pi h a^2 \eta\omega\left\{\frac{a\sqrt{\omega/\nu}(\chi + i\delta)}{\mathrm{ber}_1^2(a\sqrt{\omega/\nu}) + \mathrm{bei}_1^2(a\sqrt{\omega/\nu})} - 1\right\}\theta_o e^{i\omega t}. \tag{235}$$

The equation of the vibrational motion of the liquid is represented by

$$I_{eff}\ddot{\theta} + C_{eff}\dot{\theta} = T_o \tag{236}$$

where I_{eff} is the effective moment of the liquid and C_{eff} its effective damping. It can be seen that no restoring force is present, i. e. the liquid system has no natural frequency and the liquid will not exhibit a magnification function for the angular displacement. The equation thus serves for the determination of the effective moment of inertia and damping of the liquid in the container. With $\theta = \theta_o e^{i\omega t}$ Equation 236 assumes an algebraic form which by separation of real and imaginary part yield the desired expressions of the effective moment of inertia of the liquid

$$I_{eff} = \frac{2\pi a^3 \sqrt{\omega/\nu}\left[bei_1'(a\sqrt{\omega/\nu})ber_1(a\sqrt{\omega/\nu}) - ber_1(a\sqrt{\omega/\nu})bei_1(a\sqrt{\omega/\nu})\right]}{\sqrt{\omega}\left[ber_1^2(a\sqrt{\omega/\nu}) + bei_1^2 a\sqrt{\omega/\nu})\right]} \tag{237}$$

and the effective damping coefficient

$$C_{eff} = \frac{2\pi a^3 h\eta(\sqrt{\omega/\nu})\left[ber_1'(a\sqrt{\omega/\nu})ber_1(a\sqrt{\omega/\nu}) + bei_1'(a\sqrt{\omega/\nu})bei_1(a\sqrt{\omega/\nu})\right]}{\sqrt{\omega}\left[ber_1^2(a\sqrt{\omega/\nu}) + bei_1^2(a\sqrt{\omega/\nu})\right]} . \tag{238}$$

It can be seen that for decreasing frequency $\omega \to 0$ the effective moment of the liquid approaches the value of the " solidified" liquid.

$$\lim_{\omega \to o} I_{eff} = I_{solid} = \frac{ma^2}{2}$$

The effective damping coefficient approaches zero

$$\lim_{\omega \to o} C_{eff} = 0 .$$

It may be advantageous to represent the effective moment of inertia of the liquid as a part of the liquid that can be considered solidified. This means that the liquid of height h is represented as liquid of height h_{eff} being considered solidified. This effective height is given by

$$h_{eff} = (4h/a)\sqrt{\nu/\omega}\,\frac{\left[\mathrm{bei}_1'(a\sqrt{\omega/\nu})\,\mathrm{ber}_1(a\sqrt{\omega/\nu}) - \mathrm{ber}_1'(a\sqrt{\omega/\nu})\,\mathrm{bei}_1(a\sqrt{\omega/\nu})\right]}{\left[\mathrm{ber}_1^2(a\sqrt{\omega/\nu}) + \mathrm{bei}_1^2(a\sqrt{\omega/\nu})\right]}. \tag{239}$$

It is as the effective moment of inertia of the liquid depending upon the container radius a the kinematic viscosity ν, and the exciting frequency ω. If $a\sqrt{\omega/\nu} < 1$ the effective height can be approximated by:

$$(h_{eff}/h) \approx 1 - a^4\omega^2/128\nu^2 . \tag{240}$$

The effective moment of inertia is approximately

$$I_{eff} = ma^2(1 - a^4\omega^2/128\nu^2)/2 \quad \text{or} \quad I_{eff}/I_{solid} = 1 - a^4\omega^2/128\nu^2 . \tag{241}$$

The effective damping coefficient can be approximated for small ω and a, or large ν (as long as $a\sqrt{\omega/\nu} < 1$)

$$C_{eff} = \pi a^6 h\omega^2\eta/48\nu^2 = ma^4\omega^2/48\nu . \tag{242}$$

It can be seen that the effective moment decreased rapidly for increasing forcing frequency ω and that it decreases less rapidly for a more viscous liquid. Since the magnitude of the value $\sqrt{\omega/\nu} \approx 10^3[1/m]$ for the propellants used in space flight, the argument of the modified Kelvin functions is large, indicating that the asymptotic expansion for these functions may be applied. It is the asymptotic expansion of:

$$\mathrm{ber}_1 x \approx e^{x/\sqrt{2}}/\sqrt{2\pi x}\Big[(1 - 3/8x\sqrt{2})\cos(x/\sqrt{2} + 3\pi/8) - 1/8x\sqrt{2} \cdot \sin(x/\sqrt{2} + 3\pi/8)\Big] \tag{243}$$

$$\mathrm{bei}_1 x \approx e^{x/\sqrt{2}}/\sqrt{2\pi x}\Big[1/x8\sqrt{2}\cos(x/\sqrt{2} + 3\pi/8) + (1 - 3/8x\sqrt{2}) \cdot \sin(x/\sqrt{2} + 3\pi/8)\Big] \tag{244}$$

$$\mathrm{ber}_1 x \approx e^{x/\sqrt{2}}/\sqrt{2\pi x}\Big[(1 - 7/8x\sqrt{2})\cos(x/\sqrt{2} + 5\pi/8) - 7/8x\sqrt{2} \cdot \sin(x/\sqrt{2} + 5\pi/8)\Big] \tag{245}$$

$$\mathrm{bei}_1 x \approx e^{x/\sqrt{2}}/\sqrt{2\pi x}\Big[7/8x\sqrt{2}\cos(x\sqrt{2} + 5\pi/8) + (1 - 7/8x\sqrt{2}) \cdot \sin(x/\sqrt{2} + 5\pi/8)\Big]. \tag{246}$$

Introducing these values into the Equation 237, it yields the effective moment of inertia of the liquid in the most important tank diameter, frequency and viscosity range. It is

$$I_{eff}/I_{solid} = 2\sqrt{2}\left\{\frac{1 - \sqrt{2\nu}/4a\sqrt{\omega}}{a\sqrt{\omega/\nu} + 5\sqrt{\nu}/64a\sqrt{\omega} - 3\sqrt{2/8}}\right\} \tag{247}$$

or

$$I_{eff}/I_{solid} = (2\sqrt{2}/a)\sqrt{\nu/\omega} \qquad \text{for small } \sqrt{\nu/\omega}. \tag{248}$$

From this we conclude that for propellants used in space flight, the moment of inertia ratio is indirectly proportional to the container diameter proportional to the square root of the kinematic viscosity, and indirectly proportional to the square root of the forcing frequency.

The results of Equation 247 are shown in Table 45 and in plotted form in Figure 132. The curves show that the I_{eff}/I_{solid} ratio is extremely small for water at all frequencies except those at extremely low frequencies which are not normally encountered during space flight. Because these ratios are so small, the moment of inertia about the roll axis of a cylindrical tank can be assumed zero. The ratio of I_{eff}/I_{solid} for higher viscosity liquids is much larger as would be expected, but these viscosities, however, are not encountered in space flight.

The experimental data are again shown as x's in Figure 132. A tank with a 3.75 inch radius was used with oil and water as the liquid. The test results are in good agreement with the analytical solution. The deviation of the two is attributed to experimental error and the difference in the experimental and theoretical viscosities.

From previous results, Reference 3, it can be seen that the contribution to the moment of inertia of the liquid, due to the container top and bottom motion, is negligible. At extremely small forcing frequencies, approximately 10^{-6} radians/seconds, the inertia added by the top and bottom is still one order of magnitude smaller than those of the wall.

2.3.2.2.5 Moment of Inertia About A Displaced Roll Axis

Since the transfer theorem was applicable for the moment of inertia about a displaced yaw-pitch axis, it should be applicable for a displaced roll axis. With this assumption we have

$$I_{eff} = I_{eff\ c.m.} + m(\kappa R)^2 \tag{249}$$

where κ is the ratio of the displacement to the radius of the tank as shown in Figure 133. Equation 249 can be rewritten as

$$I_{eff} = (I_{eff\ c.m.}/I_{solid\ c.m.})I_{solid\ c.m.} + m\kappa^2 R^2 \tag{250}$$

because the ratio of $I_{eff\ c.m.}$ to $I_{solid\ c.m.}$ has already been obtained. For a solid, the moment of inertia is

TABLE 45

ANALYTICAL RESULTS FOR I_{eff}/I_{solid} FOR THE ROD AXIS OSCILLATIONS

		$I_{eff}/I_{solid} \approx (2\sqrt{2}/a)(\sqrt{\nu/\omega})$			
		ν_{water} = 23.2 $\times 10^{-4}$(in^2/sec)		ν_{oil} = 1.28 in^2/sec	
T	ω	a = 3.75"	a = 11.88"	a = 3.75"	a = 11.88"
12.52	0.5	.051	.016	.826*	.381
6.28	1.0	.032	.011	.653*	.269
3.14	2.0	.026	.008	.626*	.190
2.09	3.0	.021	.007	.423*	.156
1.26	5.0	.016	.005	.390*	.120
0.63	10.0	.011	.003	.270	.085
0.42	15.0	.009	.003	.220	.069
0.31	20.0	.008	.003	.191	.060
0.25	25.0	.007	.002	.171	.054
0.21	30.0	.007	.002	.156	.049
0.10	60.0	.005	.002	.110	.035
0.07	90.0	.004	.001	.090	.028

* Equation 3.24 must be used to calculate these values because $\sqrt{\nu/\omega}$ is too large.

TABLE 46

ANALYTICAL RESULTS FOR I_{eff}/I_{solid} FOR THE DISPLACED ROLL AXES

	I_{eff}/I_{solid} For Water	
λ	a = 3.75" ω = 15.0	a = 11.88 ω = 5.0
0.25	0.12	0.12
0.50	0.34	0.34
0.75	0.53	0.53
1.00	0.67	0.67
1.50	0.82	0.82
2.00	0.89	0.89
3.00	0.95	0.95
5.00	0.98	0.98

FIGURE 132

ANALYTICAL RESULTS FOR I_{eff}/I_{solid}
VERSUS
ROLL AXIS OSCILLATION FREQUENCIES

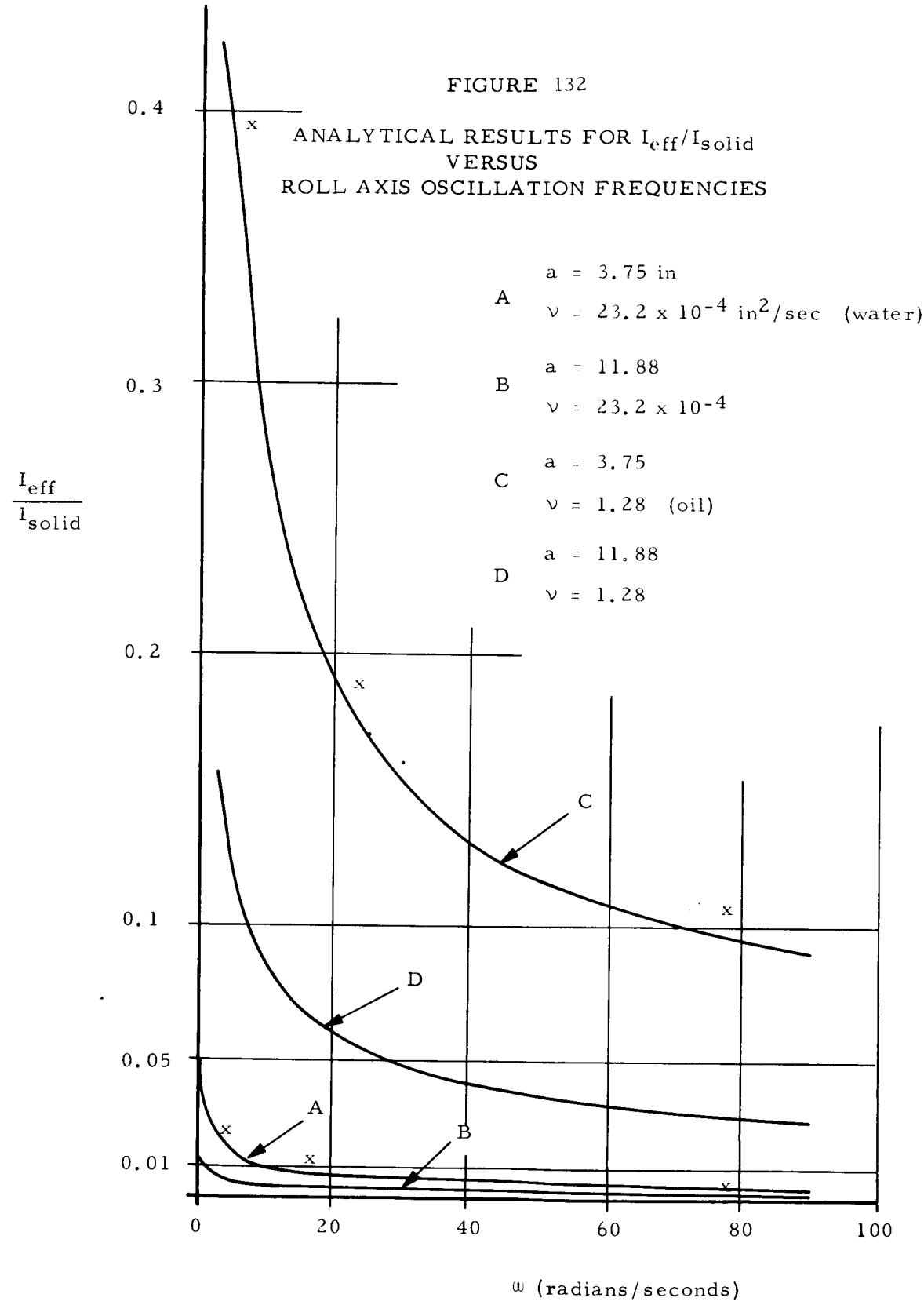

FIGURE 133

CYLINDER OSCILLATING ABOUT A DISPLACED AXIS

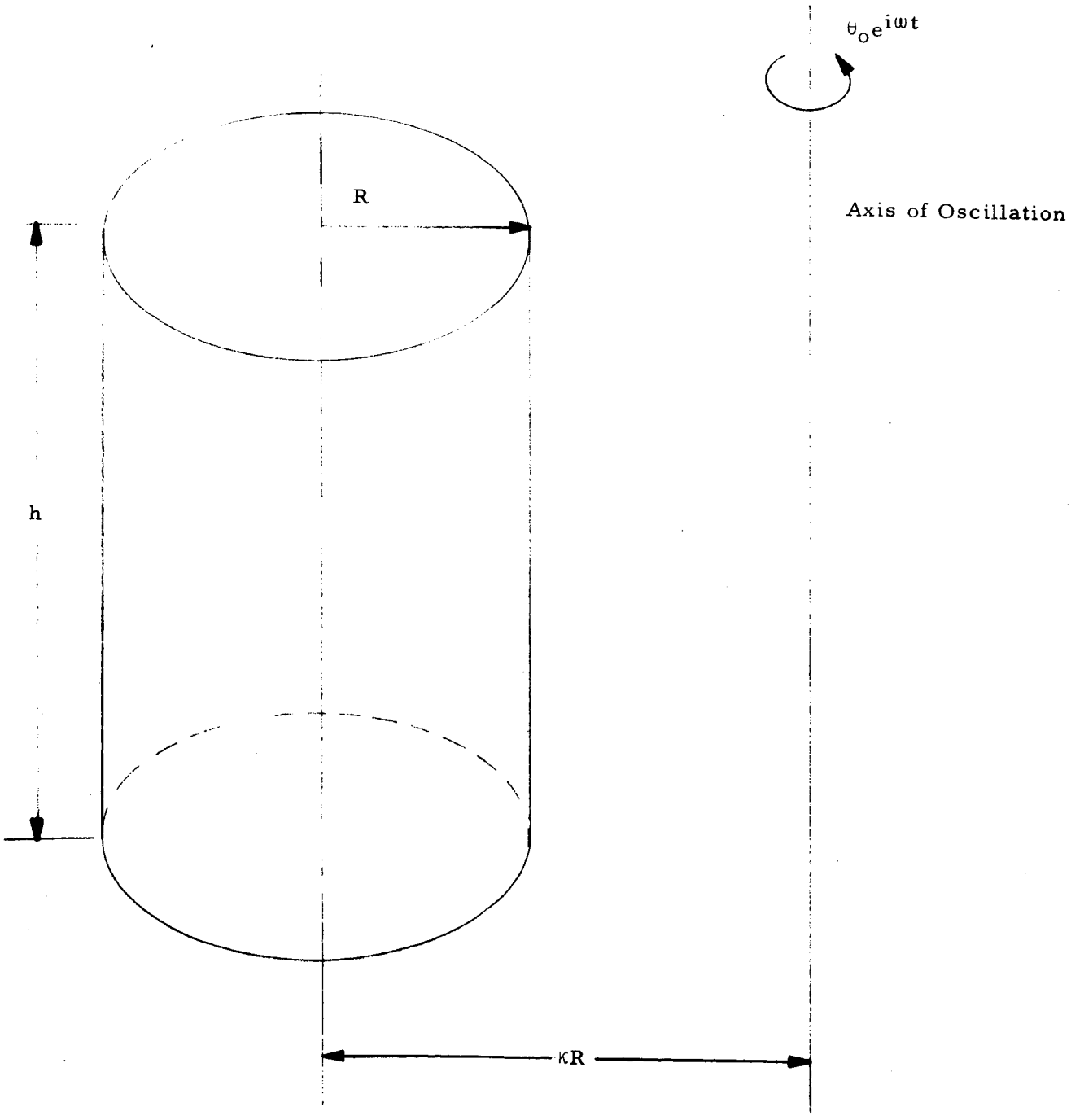

$$I_{solid} = I_{solid\ c.m.} + m\kappa^2 R \tag{251}$$

or

$$I_{solid} = mR^2(1/2 + \kappa^2) . \tag{252}$$

The ratio of the effective moment of inertia to that of the solid one is then

$$I_{eff}/I_{solid} = \frac{mR^2((I_{eff\ c.m.}/2\ I_{solid\ c.m.}) + \kappa^2)}{mR^2(1/2 + \kappa^2)} \tag{253}$$

or

$$I_{eff}/I_{solid} = \frac{(1/2)(I_{eff\ c.m.}/I_{solid\ c.m.}) + \kappa^2}{1/2 + \kappa^2} . \tag{254}$$

For $\kappa = 0$ i.e. the location of the roll axis is passing through the center of mass, we obtain the expression of Equation 247. With increasing κ, i.e. increasing distance of the roll axis to the axis of symmetry of the container, the moment of inertia ratio approaches the value unity, which means, that the effective moment of inertia approaches that of the value of the solidified liquid.

The results of the analytical expression, Equation 254 is shown in Table 46 and Figure 134. The x's in Figure 134 show the experimental data points which are in good agreement with those of the analytical results.

2.3.2.2.6 Conclusions

A set of equations have been derived and verified experimentally with very good agreement. It is thus possible to accurately determine the moment of inertia of a filled cylindrical tank as it oscillates about various axes. The equation for the yaw-pitch axis oscillating about the center of mass is

$$I_{eff}/I_{solid} = \left\{1 - \frac{1/2 + 4 \sum_{n=1}^{\infty} \frac{1 - \frac{2\tanh(\varepsilon_n h/a)}{\varepsilon_n h/2a}}{\varepsilon_n^2(\varepsilon_n^2 - 1)}}{h^2/12a^2 + 1/4}\right\} . \tag{255}$$

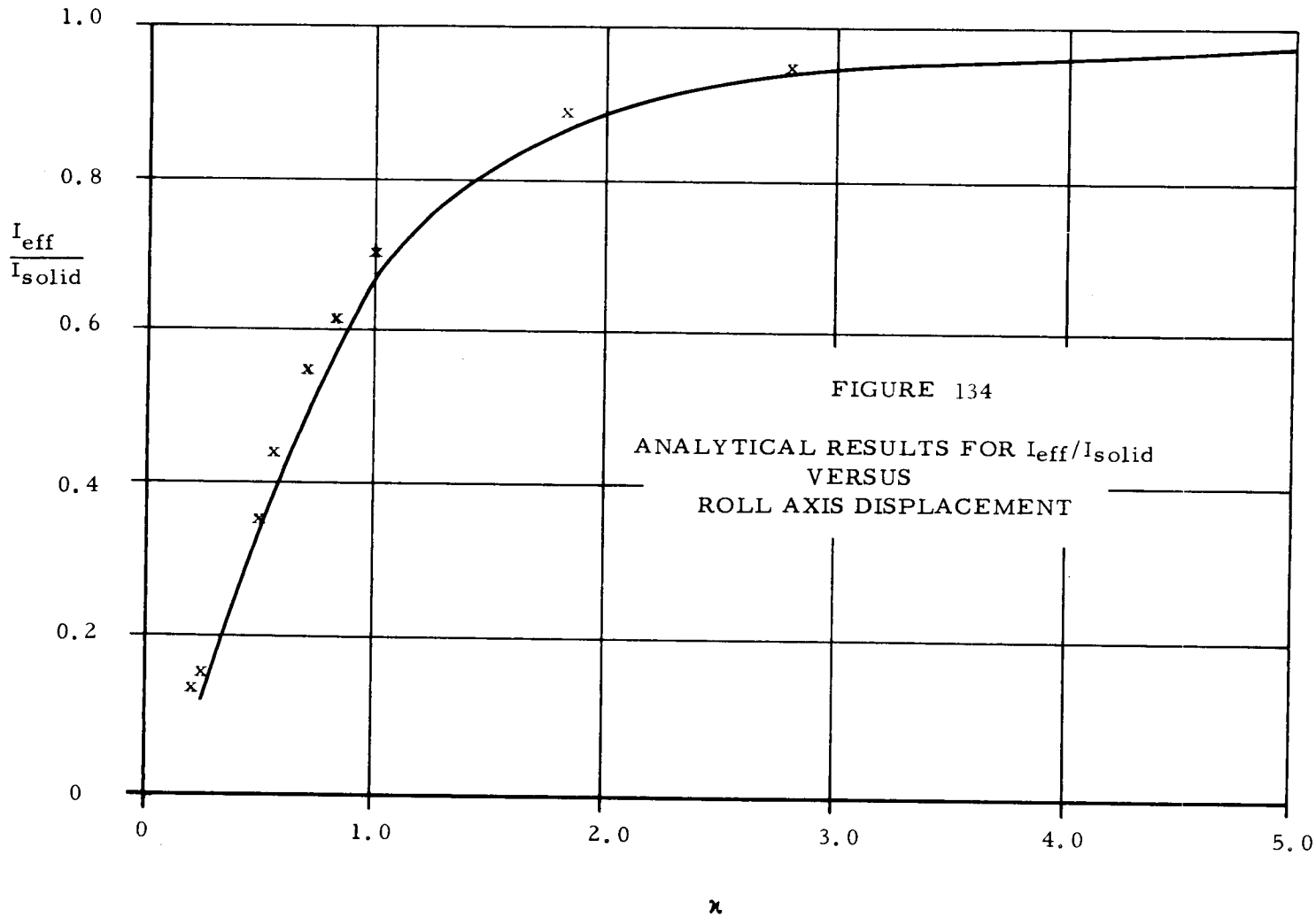

FIGURE 134

ANALYTICAL RESULTS FOR I_{eff}/I_{solid}
VERSUS
ROLL AXIS DISPLACEMENT

The only variable considered is the aspect ratio, h/a. The zeros of the first derivative of the Bessel function, ϵ_n are given in Table 43; therefore, I_{eff}/I_{solid} can be determined easily. This solution is for an ideal liquid, that is, nonviscous, but the viscosity of liquid fuel is small enough so that this equation will yield a result accurate enough for space flight purposes. The equation for oscillation about a displaced yaw-pitch axis obeys the Theorem of Steiner, or the Transfer Theorem, and is

$$I_{eff}/I_{solid} = \left\{ 1 - \frac{1/2 + 4 \sum_{n=1}^{\infty} \dfrac{1 - \dfrac{2 \tanh(\epsilon_n h/2a)}{\epsilon_n h/2a}}{\epsilon_n^2(\epsilon_n^2 - 1)}}{1/4 + (h/a)^2 \left[1/3 + \lambda(\lambda + 1) \right]} \right\} . \tag{256}$$

The symbols in this equation are the same as before and λ is the ratio of the axis displacement from the container top to the tank height.

The equation for the roll axis about the center of mass is

$$I_{eff}/I_{solid} = 2\sqrt{2} \left\{ \frac{1 - \sqrt{2\nu/4a\sqrt{\omega}}}{a\sqrt{\omega}/\nu + 5\sqrt{\nu/64a\sqrt{\omega}} - 3\sqrt{2/8}} \right\} \approx (2\sqrt{2}/a)\sqrt{\nu/\omega} \tag{257}$$

where the variables are the angular frequency ω, kinematic viscosity ν, and the tank radius. This is valid for small ν/ω. Since most fuels have low viscosities and the tank walls are relatively smooth, the moment of inertia about the roll axis can be assumed zero without producing any error. The displaced roll axis also obeys the Transfer Theorem and is

$$I_{eff}/I_{solid} = \frac{(1/2)(I_{eff\ c.m.}/I_{solid\ c.m.}) + \kappa^2}{1/2 + \kappa^2} \approx \frac{1}{1 + 1/2\kappa^2} \tag{258}$$

where I_{eff}/I_{solid} c.m. is the results obtained for roll axis about its center of mass and κ is the ratio of the axis displacement to the tank radius. For all practical purposes, I_{eff} c.m. $/I_{solid}$ c.m. can be assumed zero. With increasing distance of the tank and oscillation axis, this ratio quickly approaches unity.

These four equations accurately describe the moment of inertia of a filled cylindrical tank and are useful in determining the moment of inertia of a tank configuration which contains a cylinder.

LIST OF SYMBOLS

SYMBOL	DEFINITION
Φ, ψ, ξ	Velocity potential functions
ω	Circular forced frequency
t	Time
i	Imaginary unit
r, φ, z	Cylindrical coordinates
a	Tank radius
h	Tank height
θ_o	Maximum amplitude of small angular displacement
J_1	Bessel function of first order and first kind
ϵ_n	Zeros of the first derivative of the Bessel function of first order and first kind $J_1'(\epsilon_n) = 0$.
P	Pressure
ρ	Density
$x, y, z,$	Cartisian coordinates
Ω	External force potential
$\vec{i}, \vec{j}, \vec{k}$	Unit vectors
g	Acceleration of external forces
M_y	Liquid moment around center of mass of undisturbed liquid (clockwise positive)
m	Liquid mass

LIST OF SYMBOLS (CONT'D)

SYMBOLS	DEFINITION
λ	Ratio of axis displacement from the container top to tank height, for yaw-pitch oscillation
v	Velocity vector
$V = \{\mu_r, \mu_\varphi, w\}$	Velocity vector of liquid particles
e_r, e_φ, k	Unity vectors
η	Dynamic viscosity
$\nu = \eta/\rho$	Kinematic viscosity
$\sigma_r, \sigma_\varphi, \sigma_z$	Normal stress
$\tau_{r\varphi}, \tau_{\varphi z}, \tau_{rz}$	Shear stresses
T_o	Forcing torque
κ	Ratio of axis displacement to tank radius for roll oscillations

REFERENCES

1. Bauer, H. F., "Fluid Oscillations in a Circular Cylindrical Tank," Army Ballistic Missle Agency, Report No. DA-TR-1-58, (April 1958).

2. Bauer, H. F.. "The Moment of Inertia of a Liquid in a Circular Cylindrical Tank," Army Ballistic Missle Agency, Report No. DA-TR-5-58, (April 1958).

3. Bauer, H. F., "The Effective Moment of Inertia in Roll of Propellant and Roll Damping," Army Ballistic Missle Agency, Report No. DA-TM-67-59, (May 1959).

4. Lamb, H., Hydrodynamics, Dover Publication, sixth edition, New York, (1945).

5. Rouse, H., Advanced Mechanics of Fluids, Prentice-Hall, Inc., Englewood, New Jersey, (1959).

2.3.2.3 Investigate Analytical Method of Describing the Moment of Inertia of Liquid Filled Tanks with Baffles

2.3.2.3.1 Introduction

In order to decrease the adverse effect of propellant sloshing upon the stability of a space vehicle, the damping of the propellant has to be increased in some way. This is universally performed by introducing annular ring baffles into the propellant container, thus changing the flow pattern of the liquid decisively at the location of the maximum longitudinal flow velocity. For the design of the control system and for load considerations, relatively accurate knowledge of the moment of inertia of the liquid propellant has to be known. This is obviously hampered by the presence of the slosh baffles. If one would consider the propellant as rigid, then the control system may be overdesigned and one might have to omit certain critical ascent phases. If the liquid were considered ideal and the smooth container wall value would be used for the effective moment of inertia, then the control system may be underdesigned and the space vehicle would in some cases not be able to fulfill its mission. The deviations of the effective moment of inertia of the liquid propellant due to the presence of slosh baffles is therefore of some importance and shall be treated here by an approximate analytical method.

2.3.2.3.2 Determination of Approximate Pressure Distribution Across the Ring Baffle

The pressure and velocity distribution in a circular cylindrical container with smooth tank walls can be determined for non-viscous liquid with the help of potential theory, Reference 1. The introduction of baffles in order to reduce the influence of propellant sloshing upon the stability of a space vehicle changes the flow pattern and the pressure distribution in the immediate vicinity of the slosh baffles, decisively. A simple approximation shall now describe the influence of a baffle, with the help of a disturbance potential.

In a circular cylindrical container, a horizontal annular baffle of width w, is attached at the container wall as shown in Figure 135. The width w of the baffle is considered to be small compared to the container radius a, i.e. $w/a << 1$. This expresses the fact that for all practical uses the velocity distribution that would be present without the baffle can be considered constant over the width of the baffle. We furthermore assume that the flow around the baffle can be considered as a two-dimensional flow. The disturbance potential created by the slosh baffle can therefore be approximated by the flow around a flat plate.

The pattern of a flow around a flat plate can be seen in Figure 136. Noting with ϕ^* the disturbance potential created by the existence of the slosh baffle, then the total potential of the flow yields, Reference 2,

FIGURE 135

POTENTIAL FLOW ABOUT BAFFLE
AND ELLIPTIC COORDINATES

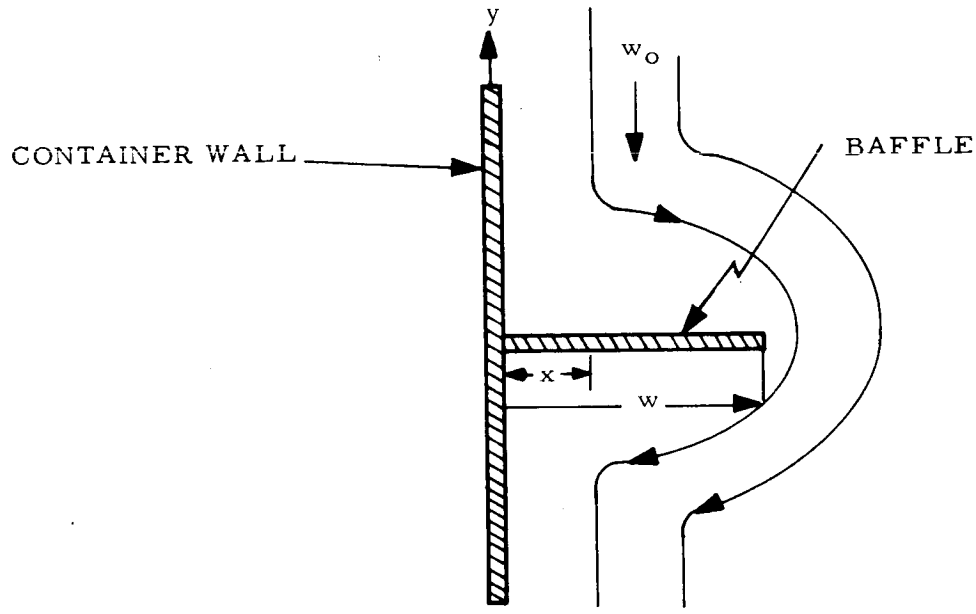

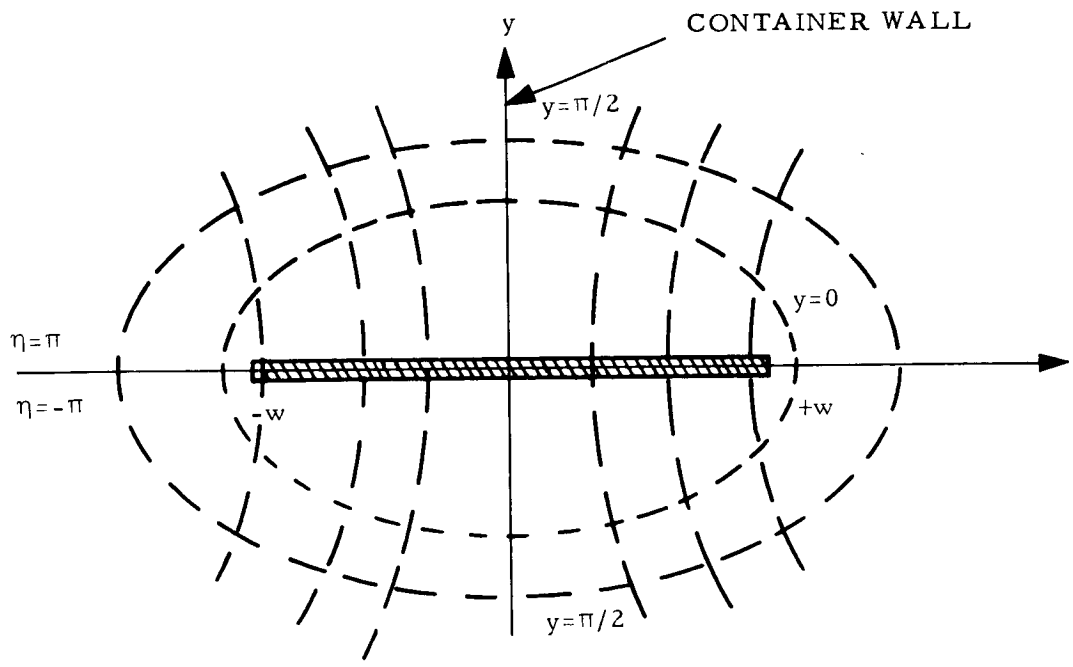

$$\Phi = \varphi + \phi^* \tag{259}$$

where φ is the potential of the liquid motion in a container with smooth tank walls.

By adding the image of the slosh baffle to the whole configuration, the tank wall becomes a stream line and one is able to solve the flow problem by the application of complex functions. The stationary flow around a flat plate can be obtained from the complex stream function.

$$\Psi = \Phi + i\psi = iw_o w \sinh \zeta \tag{260}$$

where W_o is the flow velocity at infinity, i.e. here the velocity of the liquid at the location of the baffle for smooth wall, $\zeta = \xi + i\eta$ and $z = w \cosh \zeta = x = iy$. It is $0 \leq \xi \leq \infty$ and $-\pi \leq \eta \leq +\pi$. The potential function is

$$\psi = w_o w \sin \xi \sin \zeta \tag{261}$$

and the stream function is

$$\psi = w_o w \sinh \xi \cos \eta \tag{262}$$

At the container wall ($\eta = \pm\pi/2$) and the slosh baffle ($\xi = 0$) which represents a streamline, the stream function (ψ) is $\psi = 0$. It is

$$\begin{aligned} x &= w \cosh \xi \cos \eta \\ y &= w \sinh \xi \sin \eta \end{aligned} \tag{263}$$

Subtracting the potential function of the parallel stream from the total potential yields the disturbance potential

$$\phi^* = w_o[y - w \cosh \xi \sin \eta] = w_o w e^{-\xi} \sin \eta \tag{264}$$

The disturbance velocity v* is then given with

$$\phi^*_\xi = -w_o w e^{-\xi} \sin \eta \tag{265}$$

$$\phi^*_\eta = w_o w e^{-\xi} \cos \eta \tag{266}$$

by the expression

$$v^* = \frac{W_o e^{-\xi}}{\sinh^2 \xi + \sin^2 \eta} \tag{267}$$

This disturbance velocity v*, caused by the baffle, is at the container wall $\eta = \pm \pi/2$ given by

$$v^*_{wall} = \frac{W_o e^{-\xi}}{\cosh \xi} \tag{268}$$

and at the baffle it is

$$v^*_{baffle} = \frac{W_o}{\sin \eta} \tag{269}$$

The nonstationary Bernoulli equation is

$$\frac{v^{*2}}{2} + \frac{p^*}{\rho} - \frac{\partial \phi^*}{\partial t} = 0 \tag{270}$$

Here the static pressure term gz has been omitted since we are only interested in the pressure difference across the slosh baffle. The nonstationary force can now be obtained with the following values.

$$\frac{\partial \phi^*}{\partial y} = \frac{\partial \phi^*}{\partial \xi} \frac{\partial \xi}{\partial y} + \frac{\partial \phi^*}{\partial \eta} \frac{\partial \eta}{\partial y} \tag{271}$$

$$\frac{\partial \phi^*}{\partial \xi} = -w_o w e^{-\xi} \sin \eta \tag{272}$$

$$\frac{\partial \phi^*}{\partial \eta} = w_o w e^{-\xi} \cos \eta \tag{273}$$

$$\frac{\partial \xi}{\partial y} = -\frac{\partial x/\partial \eta}{F(x, y)}; \quad \frac{\partial \eta}{\partial y} = \frac{\partial x/\partial \xi}{F(x, y)} \tag{274}$$

where $F(x, y)$ is the functional determinants and is represented by the expression

$$F(x, y) = \begin{vmatrix} \frac{\partial x}{\partial \xi} & \frac{\partial y}{\partial \xi} \\ \frac{\partial x}{\partial \eta} & \frac{\partial y}{\partial \eta} \end{vmatrix} = w^2 \{\sinh^2 \xi \cos^2 \eta + \cosh^2 \xi \sin^2 \eta\} \tag{275}$$

Finally

$$\xi_y = \frac{1}{w} \frac{\cosh \xi \sin \eta}{\{\sinh^2 \xi \cos^2 \eta + \cosh^2 \xi \sin^2 \eta\}} \tag{276}$$

$$\eta_y = \frac{1}{w} \frac{\sinh \xi \cos \eta}{\{\sinh^2 \xi \cos^2 \eta + \cosh^2 \xi \sin^2 \eta\}} \tag{77}$$

$$\frac{\partial \phi^*}{\partial y} = -w_o e^{-\xi} \frac{[\cosh \xi \sin^2 \eta - \sinh \xi \cos^2 \eta]}{[\sinh^2 \xi \cos^2 \eta + \cosh^2 \xi \sin^2 \eta]} \tag{278}$$

This is

$$\frac{\partial \phi^*}{\partial t} = \dot{w}_o w e^{-\xi} \sin \eta + w_o^2 e^{-\xi} \frac{[\cosh \xi \sin^2 \eta - \sinh \xi \cos^2 \eta]}{[\sinh^2 \xi \cos^2 \eta + \cosh^2 \xi \sin^2 \eta]} \tag{279}$$

At the container wall $\zeta = \pm \pi/2$ are obtained, therefore

$$\left(\frac{\partial \phi^*}{\partial t}\right)_{wall} = \pm w_o w e^{-\xi} + w_o^2 \frac{e^{-\xi}}{\cosh \xi} \tag{280}$$

with which the pressure disturbance by the presence of the slosh baffle is given by

$$p^*_{wall} = \pm \rho \dot{w}_o w e^{-\xi} + \rho w_o^2 \left[\frac{e^{-\xi}}{\cosh \xi} \quad \frac{e^{-2\xi}}{2 \cosh^2 \xi}\right] \tag{281}$$

The upper sign in this equation belongs to the pressure above the slosh baffle, while the lower sign belongs to the pressure below the baffle neglecting terms of higher order the pressure disturbance at the wall yields

$$p^*_{wall} = \pm \rho \dot{w}_o w e^{-\xi} \tag{282}$$

where $\dot{w}_o$ is the acceleration of the wall at the location of the baffle (for smooth wall). It can be seen that the disturbance pressure is larger at the baffle ($\xi = 0$) and decays exponentially as the distance from the baffle increases. The pressure disturbance, furthermore, is proportional to the liquid density, the acceleration (for smooth wall) of the liquid at the location of the baffle and to the width w of the baffle. It may be noted, however, that the width w has to satisfy the conditions $w/a << 1$. The pressure distribution at the slosh baffle ($\xi = 0$) yield, with Equations 267, 270, and 279, the expression

$$p^* = \rho \dot{w}_o w \sin \eta + \rho w_o^2 \left[1 - \frac{1}{2 \sin^2 \eta}\right] \tag{283}$$

At the upper side of the baffle it is $\eta \geq 0$, while at the lower side $\eta \leq 0$. Therefore, the pressure difference across the baffles yields the value

$$p = 2\rho \dot{w}_o w \sin \eta \tag{284}$$

which is with $z = w \cosh \zeta$ giving for $\zeta = i\eta$ in the expression $x = w \cosh \eta$, the expression

$$p = 2\rho \dot{w}_o w \sqrt{1 - (x/w)^2} \tag{285}$$

The pressure difference is of parabolic form across the baffle. It is zero at the edge of the baffle, and exhibits its maximum value at the root of the slosh baffle. Again it is proportional to the liquid density, the acceleration of the liquid at the baffle (for smooth wall) and the width w of the baffle.

For a circular cylindrical container, as shown in Reference 1, the velocity distribution is given by

$$w_o = 2i\Omega x_o e^{i\Omega t} \cos\varphi \sum_{n=1}^{\infty} \frac{\epsilon_n \sinh\{(\epsilon_n/a)(z+h)\} J_1(\epsilon_n r/a)\eta_n^2}{(\epsilon_n^2 - 1)\cosh(\epsilon_n h/a) J_1(\epsilon_n)(1 - \eta_n^2)} \tag{286}$$

Therefore, the pressure difference at this slosh baffle yields

$$\left|p\right| = 4\rho\Omega^2 x_o \cos\varphi\, w \quad 1 - (x/w)^2 \left| \sum_{n=1}^{\infty} \frac{\epsilon_n \sinh\left[\epsilon_n/a(z+h)\right] J_1(\epsilon_n r/a)\eta_n^2}{(\epsilon_n^2 - 1)\cosh(\epsilon_n h/a) J_1(\epsilon_n)(1 - \eta_n^2)} \right. \tag{287}$$

where J_1 is the Bessel function of first kind and first order, ϵ_n are the roots of the first derivative thereof, $J_1'(\epsilon_n) = 0$, and $\eta_n = \Omega/\omega_n$ is the frequency ratio of the forcing frequency of the natural frequency of the liquid. It may be noted here, that the velocity w_o in z—direction is due to harmonic excitation in x—direction of a liquid with a free fluid surface. Expressing this result with the aid of the free fluid surface elevation (Reference 1)

$$\zeta = \frac{\Omega^2 x_o e^{i\Omega t}}{g/a} \cos\varphi \frac{r}{a} + 2 \sum_{n=1}^{\infty} \frac{J_1(\epsilon_n r/a)}{(\epsilon_n^2 - 1) J_1(\epsilon_n)} \frac{\eta_n^2}{(1 - \eta_n^2)} \tag{288}$$

which, because of

$$\frac{r}{a} = 2 \sum_{n=1}^{\infty} \frac{J_1(\epsilon_n r/a)}{(\epsilon_n^2 - 1) J_1(\epsilon_n)} \tag{289}$$

and

$$\omega_n^2 = \frac{g}{a}\epsilon_n \tanh(\epsilon_n h/a) \tag{290}$$

can be written in the form

$$\zeta = 2x_o e^{i\Omega t}\cos\varphi \sum_{n=1}^{\infty} \frac{J_1(\epsilon_n r/a)\epsilon_n \tanh(\epsilon_n h/a)\eta_n^2}{(\epsilon_n^2 - 1)J_1(\epsilon_n)(1 - \eta_n^2)} \equiv \zeta_w \cos\varphi\, e^{i\Omega t} \tag{291}$$

The pressure difference is therefore with the consideration of the first sloshing mode only (n = 1), given by

$$p = 2\rho\Omega^2\zeta_w w \cos\varphi\sqrt{1 - (x/w)^2}\, e^{\epsilon_1 z/a} e^{i\Omega t} \tag{292}$$

where z is the depth at which the baffle is located below the undisturbed free fluid surface. ζ_w is the liquid elevation at the wall at $\varphi = 0$. For the location $z = -d$ of the baffle below the undisturbed free fluid surface, the pressure on the baffle yields, as shown in Figure 136,

$$p = 2\rho\Omega^2 w\zeta_w\sqrt{1 - (x/w)^2}\, e^{-\epsilon_1 d/a} e^{i\Omega t}\cos\varphi \tag{293}$$

For a completely filled container performing pitch and oscillations about its center of mass, the velocity potential yields (Reference 3)

$$\phi(r, \varphi, z, t) = -i\Omega\theta_o e^{i\Omega t} a^2 \cos\varphi \left[\frac{zr}{a^2} - 4\sum_{n=1}^{\infty} \frac{J_1(\epsilon_n r/a)\sinh(\epsilon_n z/a)}{\epsilon_n(\epsilon_n^2 - 1)J_1(\epsilon_n)\cosh(\frac{\epsilon_n}{2}\frac{h}{a})}\right] \tag{294}$$

and the velocity distribution in z–direction is represented by

FIGURE 136

PRESSURE DISTRIBUTION AT THE BAFFLE
FOR VARIOUS BAFFLES

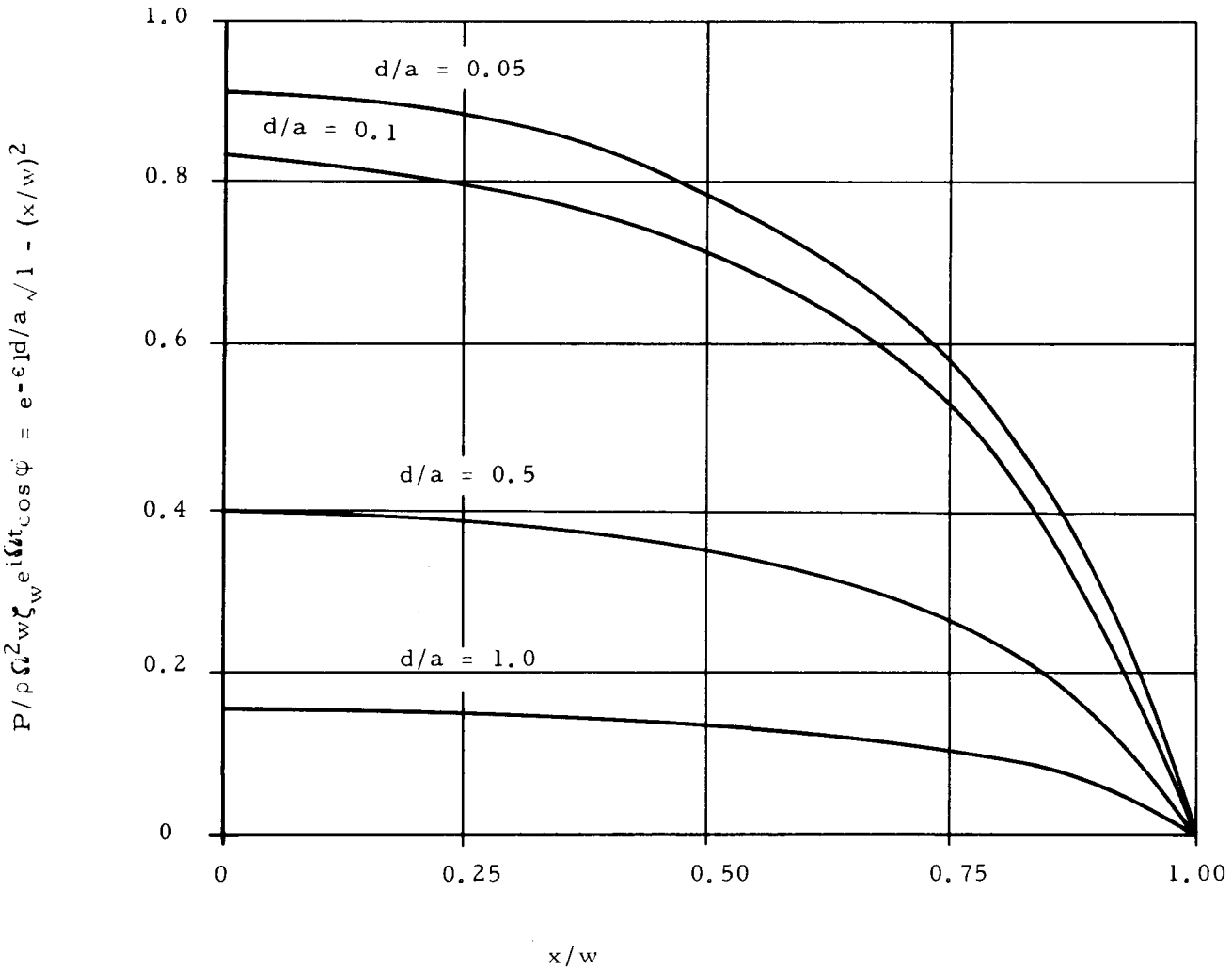

$$w_o = \frac{\partial \phi}{\partial z} = -i\Omega\theta_o e^{i\Omega t} a \cos\varphi \left[\frac{r}{a} - 4 \sum_{n=1}^{\infty} \frac{J_1(\epsilon_n r/a)\cosh(\epsilon_n z/a)}{(\epsilon_n^2 - 1)J_1(\epsilon_n)\cosh(\frac{\epsilon_n}{2}\frac{h}{a})} \right] \tag{295}$$

The acceleration (for smooth wall) is given by

$$\dot{w}_o = 2\Omega^2\theta_o e^{i\Omega t} a \cos\varphi \sum_{n=1}^{\infty} \frac{J_1(\epsilon_n r/a)}{(\epsilon_n^2 - 1)J_1(\epsilon_n)} \left[1 - 2 \frac{\cosh(\epsilon_n z/a)}{\cosh(\frac{\epsilon_n}{2}\frac{h}{a})} \right] \tag{296}$$

For r = a it is

$$\dot{w}_o = 2\Omega^2\theta_o e^{i\Omega t} a \cos\varphi \sum_{n=1}^{\infty} \frac{\left[1 - 2 \frac{\cosh(\epsilon_n z/a)}{\cosh(\frac{\epsilon_n}{2}\frac{h}{a})} \right]}{(\epsilon_n^2 - 1)} \tag{297}$$

which is for various z/a—values given in Figure 137. For very large containers (i.e. h/a >> 1) the acceleration is given at z = 0 by

$$\dot{w}_o = \Omega^2\theta_o e^{i\Omega t} a \cos\varphi \tag{298}$$

where

$$\sum_{n=1}^{\infty} \frac{1}{(\epsilon_n^2 - 1)} = \frac{1}{2} \tag{299}$$

has been applied.

FIGURE 137

DISTRIBUTION OF LONGITUDINAL ACCELERATION
$\dot{w}_o$ IN COMPLETELY FILLED CONTAINERS

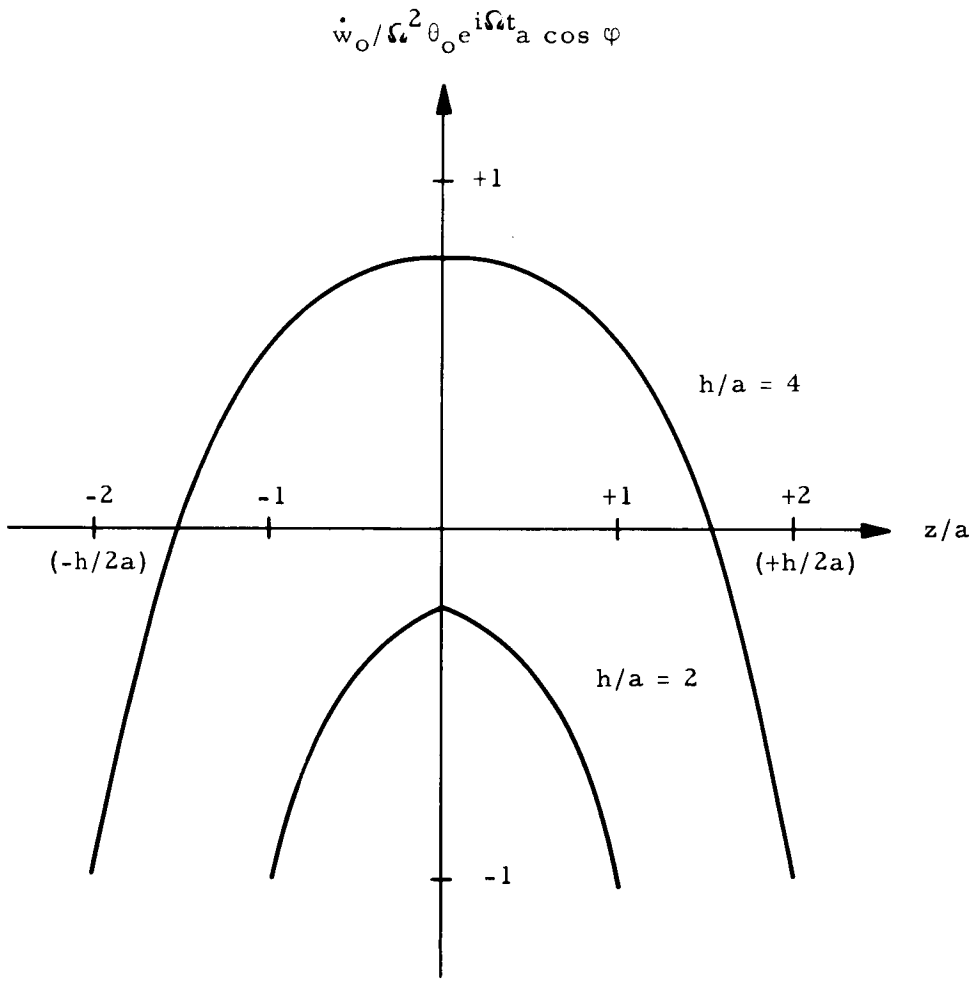

The pressure difference across the baffle is therefore of parabolic shape

$$p = 4\rho w \Omega^2 \theta_o e^{i\Omega t} a \cos\varphi \sqrt{1 - (x/w)^2} \tag{300}$$

It is zero at the edge of the baffle and exhibits its maximum value at the container wall. From this we conclude that the pressure difference is proportional to the liquid density, the excitation amplitude of the container, the width w, the diameter of the container, and the square of the circular forcing frequency, as well as the cos φ, as shown in Figure 138.

2.3.2.3.3 Influence of Slosh Baffles Upon the Effective Moment of Inertia

The moment of inertia of the liquid in a completely filled circular cylindrical container with smooth walls has been obtained previously (Reference 3) for various orientations of the axis of oscillation. For an axis of excitation, perpendicular to the longitudinal axis of the container through the center of mass, the effective moment of inertia of the liquid is given by the expression

$$I_{eff} = ma^2 \left[\frac{1}{12}\left(\frac{h}{a}\right)^2 + \frac{1}{4} - 4 \sum_{n=1}^{\infty} \frac{2 - \dfrac{2\tanh\left(\frac{\epsilon_n}{2}\frac{h}{a}\right)}{\frac{\epsilon_n}{2}\frac{h}{a}}}{\epsilon_n^2(\epsilon_n^2 - 1)} \right] \tag{301}$$

It has been shown that this effective moment of inertia of the liquid agrees very well with the experimental results.

With the universally used ring baffles in the containers, an estimate of the effective moment of inertia of the liquid in a completely filled container has to be determined. As the baffle moves through the liquid, it will carry along a part of the liquid. To determine the effective mass that is carried along by the baffle, one needs the pressure distribution at the baffle. The total force obtained through integration of the pressure distribution yields by division with the known acceleration of the baffle the effective liquid mass attached to the baffle. It is with Equation 285

$$dF = 2\rho \dot{w}_o w \sqrt{1 - (x/w)^2}\, dA \tag{302}$$

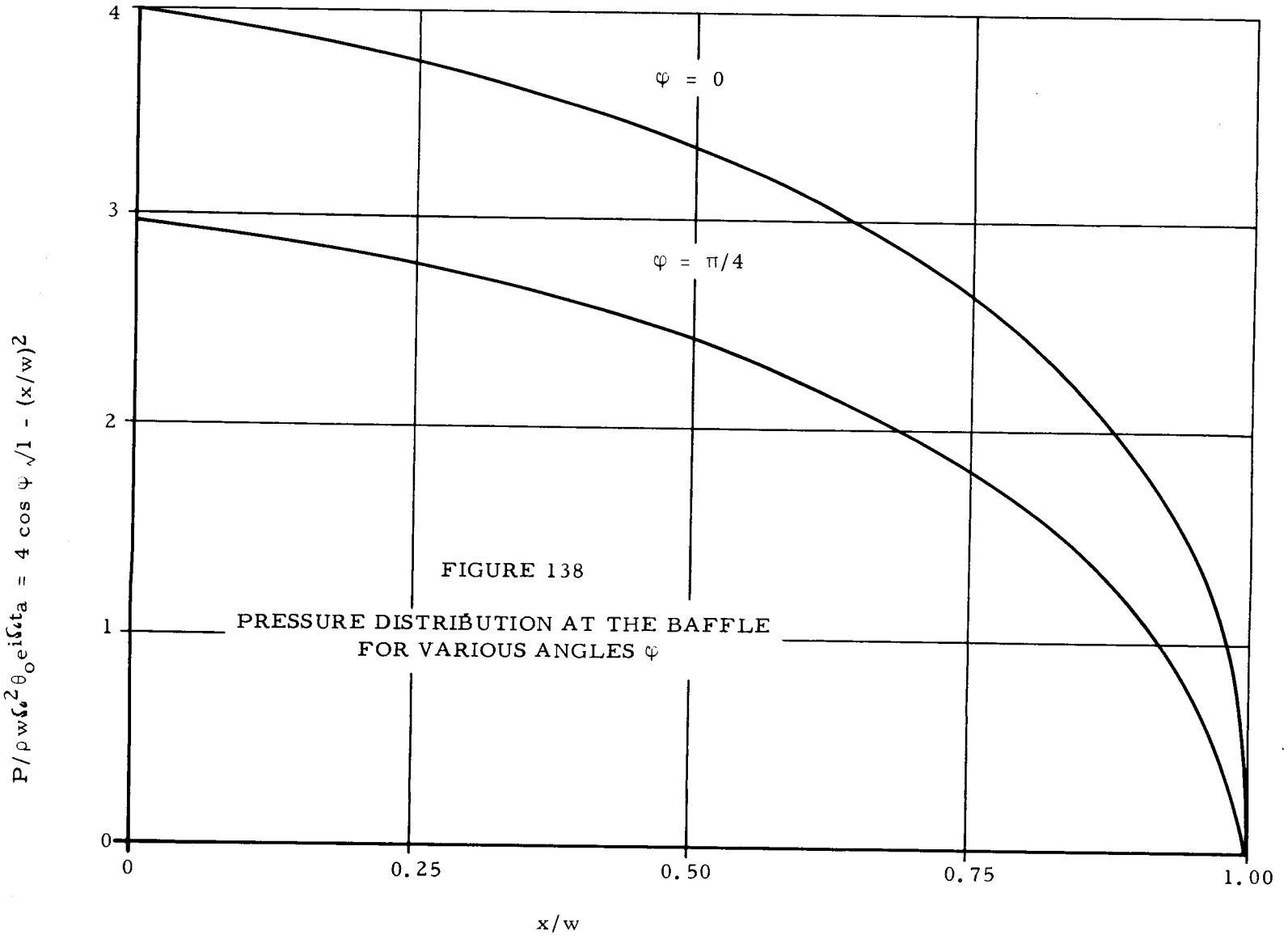

FIGURE 138

PRESSURE DISTRIBUTION AT THE BAFFLE FOR VARIOUS ANGLES φ

the force on the area element $dA = 1 \cdot dx$. The effective mass with respect to the circumferential strip of unit width is therefore

$$\mu_{eff} = 2\rho w \int_0^w \sqrt{1 - (x/w)^2}\, dx = \frac{\pi}{2} \rho w^2 \tag{303}$$

It can be seen that the effective mass is proportional to the liquid density and the square of the baffle width. Expressing the effective mass of the liquid carried along with the baffle by its height h_{eff} over the baffle area, one obtains

$$h_{eff} = \frac{\pi}{2} w \tag{304}$$

From this we can conclude that for damping baffles of distance $D \geq h_{eff}$, the effective mass carried along by the slosh baffle is obtained by Equation 292. For a distance between baffles $D \leq h_{eff}$ the mass carried along by the baffle can be obtained by considering all of the liquid trapped between baffles.

The moment of inertia increase due to a slosh baffle at a distance $\ell = \sqrt{\delta^2 + a^2 \cos^2\varphi}$ from the rotational axis, which is chosen here to be perpendicular to the longitudinal axis of the container is therefore (See Figure 139)

$$I_{baffle} \approx \frac{\pi}{2} \rho w^2 a^3 \int_0^{2\pi} \left[\cos^2\varphi + \frac{\delta^2}{a^2}\right] = \frac{\pi^2}{2} \rho a^3 w^2 \left[1 + \frac{2\delta^2}{a^2}\right] \tag{305}$$

where δ is the distance of the baffle plane to the center of mass plane. For a slosh baffle in the plane of the rotational axis, the moment of inertia increase is then with $\ell = a(\delta = 0)$

$$I_{baffle} = \frac{\pi^2}{2} \rho a^3 w^2 \tag{306}$$

With this the ratio of the increase of the moment of inertia of the liquid due to a baffle located in the plane of the rotational axis to the moment of inertia of the rigid body yields

$$\frac{I_{baffle}}{I_{rigid}} = \frac{\pi^2 \rho a^3 w^2}{2ma^2[(1/12)(h/a)^2 + 1/4]} = \frac{\pi (w/a)^2}{2(h/a)[(1/12)(h/a) + 1/4]} \tag{307}$$

For a container of which the total cylindrical part is provided with closely spaced baffles, i.e. for which the baffle distance $D \leq (\pi/2)w$, the effective moment of inertia of the liquid can be approximately obtained of the following two parts: the first part is the moment of inertia of the annular circular cylinder of innner radius $b = a - w$ and outer radius a, while the second part is the effective moment of inertia of the cylindrical part of radius b. The liquid between the baffles has been considered as trapped and has a moment of inertia

$$I^*_{baffle} = m^* a^2 [(1/12)(h/a)^2 + (1 + k^2)/4] \tag{308}$$

where $k = 1 - w/a$ is the diameter ratio and m^* represents the mass of the trapped liquid, and is

$$m^* = \pi \rho h w (2a - w) \tag{309}$$

The effective moment of inertia of the liquid in a container with close baffle spacing ($D \leq (\pi/2)w$) is therefore given by the expression

$$I_{eff} = \rho \pi h (a - w)^2 \frac{h^2}{12} - \frac{(a - w)^2}{4} + 4 \sum_{n=1}^{\infty} (a - w)^2 \frac{2\tanh\left(\frac{\epsilon_n h}{2(a - w)}\right)}{\frac{\epsilon_n}{2} \frac{h}{(a - w)}} - 1$$

$$+ \rho \pi h w (2a - w) \frac{h^2}{12} - \frac{2a^2 - w^2}{4} \tag{310}$$

For a baffle with decreasing width $w \to 0$ the above expression approaches the value of the effective moment of inertia of a smooth walled container with ideal liquid, while for $w = a$ the moment of inertia of the rigid body is obtained.

The conclusion of these results can now be summerized as follows:
1) For a container with closely spaced ($D \leq (\pi/2)w$) baffles, the ratio of moment of inertia of the liquid and rigid body is given by

$$\frac{I_{eff}}{I_{rigid}} = \left(\frac{I_{eff}}{I_{rigid}}\right)_{\substack{\text{smooth wall}\\ r=b}} \left(\frac{I_{rigid\ r=b}}{I_{rigid\ r=a}}\right) + \frac{I^{*}_{baffles}}{I_{rigid\ r=a}} \tag{311}$$

The first term contains as its first factor the effective moment of inertia of the ideal fluid in a container of radius $b = a - w$ and smooth walls, and it has as its second factor the ratio of the moments of inertia of the cylindrical rigid body of radius b and that of radius a. The second term represents the moment of inertia ratio of the trapped liquid between the baffles.

2) The approximate effective moment of inertia ratio of N baffles of distance ℓ_n from the axis of rotation and of width w_n yields the expression (for $D_n \geq (\pi/2)w_n$)

$$\frac{I_{eff}}{I_{rigid}} = \left(\frac{I_{eff}}{I_{rigid}}\right)_{\text{smooth wall}} + \sum_{n=1}^{N} \frac{I_n}{I_{rigid}} \tag{312}$$

which yields with $\ell_n = c(w = w_n)$ and Equation 297

$$\frac{I_{eff}}{I_{rigid}} = \left(\frac{I_{eff}}{I_{rigid}}\right)_{\text{smooth wall}} + \sum_{n=1}^{N} \frac{\pi(w_n/a)^2(\ell_n/a)^2}{2(h/a)[(1/12)(h/a)^2 + 1/4]} \tag{313}$$

this is with $\ell_n^2 = a^2 + D_n^2$ the expression

$$\frac{I_{eff}}{I_{rigid}} = \left(\frac{I_{eff}}{I_{rigid}}\right)_{\text{smooth wall}} + \frac{\pi \sum_{n=1}^{N} (w_n/a)^2[0.1 + (D_n^2/a^2)]}{2(h/a)[(1/12)(h/a)^2 + 1/4)]} \tag{314}$$

which yields for equidistant baffles of equal $w_n = w$, and $D_n = nD$

$$\frac{I_{eff}}{I_{rigid}} = \left(\frac{I_{eff}}{I_{rigid}}\right)_{\text{smooth wall}} + \frac{N\pi(w/a)^2[1 + n^2(D^2/a^2)]}{2(h/a)[(1/12)(h/a)^2 + 1/4]} \tag{315}$$

To determine the accuracy of the given approximations the analytical results will be composed with the experimental results performed at the Mass Metrology Laboratory of SPACO, INC. and also with results of Southwest Research Institute (Reference 4). The circular cylindrical container was of the height ratio $h/a = 2.0$, as shown in Figure 139, and the sloshing baffles of width $w = 0.155a$ at a distance of $D = 0.4a$. This distance is obviously larger than $(\pi/2)w$. Therefore, the method of the completely trapped liquid would only give an upper limit for the moment of inertia. The moment of inertia was measured for no baffles, one, three, and five baffles. The ratio of the increase of moment of inertia due to one baffle in the plane of the mass center (plane of the axis of rotation to the moment of inertia of the solidified liquid), is in this case

$$\left(\frac{I_s}{I_{rigid}}\right)_{\ell=a} = 0.033 \tag{316}$$

Adding this expression to the value of the moment of inertia ratio of the container with smooth wall ($I_{eff}/I_{rigid} = 0.21$) yields the value

$$\frac{I_{eff}^{(1)}}{I_{rigid}} = 0.243 \tag{317}$$

for the moment of inertia ratio of the liquid in a container with one baffle. This value agrees quite well with the experimental results of 0.28 — 0.31. For a container with three baffles it is

$$\frac{I_{eff}^{(3)}}{I_{rigid}} = \left(\frac{I_{eff}}{I_{rigid}}\right) + \left(\frac{I_s}{I_{rigid}}\right)_1 + 2\left(\frac{I_s}{I_{rigid}}\right)_2 = 0.332 \tag{318}$$

This value again is smaller than the experimentally obtained values of 0.34 — 0.50. If one would consider the liquid between the baffles as rigid, its mass would be m^{**} and its moment of inertia I_D^{**}. It is

$$m^{**} = 2\pi\rho Dw(2a - w) \tag{319}$$

$$I_D^{**} = m^{**}a^2[(1/3)(D/a)^2 + (1+k^2)/4] \tag{320}$$

FIGURE 139. CONTAINER GEOMETRY WITH BAFFLES (Reference 4)

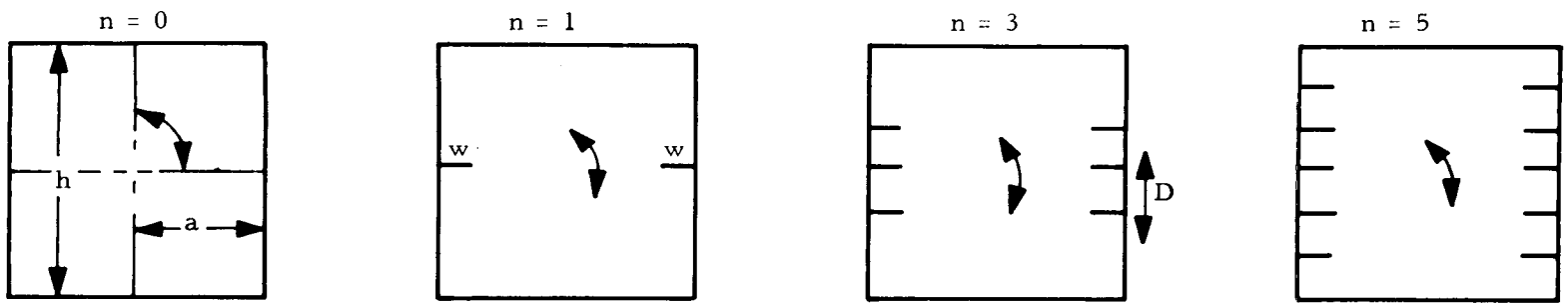

Therefore, it is the ratio of the moment of inertia of this part

$$\frac{I_D^{**}}{I_{rigid}} = \frac{2(D/a)(w/a)[2 - (w/a)][(1/3)(D/a)^2 + (1+k^2)/4]}{(h/a)[(1/12)(h/a)^2 + 1/4]} \approx 0.097 \tag{321}$$

and that of the total system

$$\frac{I_{eff}^{(3)}}{I_{rigid}} = \left(\frac{I_{eff}}{I_{rigid}}\right)_{\text{smooth wall}} + \frac{I_D^{**}}{I_{rigid}} + \left(\frac{I_s}{I_{rigid}}\right)_2 \approx 0.346 \tag{322}$$

A container with five baffles yields for the ratio of the moment of inertia the expression

$$\frac{I_{eff}^{(5)}}{I_{rigid}} = \left(\frac{I_{eff}}{I_{rigid}}\right)_{\text{smooth wall}} + \left(\frac{I_s}{I_{rigid}}\right)_1 + 2\left(\frac{I_s}{I_{rigid}}\right)_2 + 2\left(\frac{I_s}{I_{rigid}}\right)_3 \approx 0.483 \tag{323}$$

This value again is smaller than the experimental result of 0.51 — 0.70. If one would consider the liquid completely trapped between the slosh baffles, one obtains

$$\frac{I_D^{**}}{I_{rigid}} = \frac{(w/a)[(1/12)(h/a)^2 + (1+k^2)/4][2 - (w/a)]}{(1/12)(h/a)^2 + 1/4} \approx 0.38 \tag{324}$$

For the ratio of the effective moment of inertia of the liquid to that of the solidified liquid, one obtains the expression

$$\frac{I_{eff}^{(5)}}{I_{rigid}} = \left(\frac{I_{eff}}{I_{rigid}}\right)_{r=b} \cdot \left(\frac{I_{rigid\ r=b}}{I_{rigid\ r=a}}\right) + \frac{I_b^*}{I_{rigid}} = 0.51 \tag{325}$$

The following table exhibits the results of the approximate theory and the experimental values as reported in Reference 4.

	n=0	n=1	n=3	n=5
Theory	0.17	0.243	0.33-0.34	0.48-0.51
Experimental	0.17-0.19	0.28-0.31	0.34-0.50	0.51-0.70

The results obtained by the Mass Metrology Laboratory at SPACO, INC. are shown below and are described in detail in Section 2.3.1.5.

	n=0	n=1	n=3	n=5	n=7
Theory	0.17	0.224	0.252	0.279	0.309
Experimental	0.18	0.20	0.24	0.255	0.27

From these results it can be seen that a good agreement of theory and experiment exists.

REFERENCES

1. Bauer, H. F., "Fluid Oscillations in the Container of a Space Vehicle and Their Influence Upon Stability," NASA-TR-R-187, (1964).

2. Bauer, H. F., "Approximate Effect of Ring Stiffness on the Pressure Distribution in an Oscillating Cylindrical Tank Partially Filled with a Liquid," Army Ballistic Missle Agency, Report No. DA-M-114, Huntsville, Alabama, (September 1957).

3. Bauer, H. F., "The Moment of Inertia of a Liquid in a Circular Cylindrical Tank," Army Ballistic Missle Agency, Report No. DA-TR-S-58, (April 1958).

4. Dodge, F. T. and Dana, D. D., "Moment of Inertia and Damping of Liquids in Baffled Cylindrical Tanks," Journal of Spacecraft and Rockets, Volume 3, No. 1, pp. 153-155, (January 1966).

2.4 CENTER OF GRAVITY

The primary objective of the center of gravity program was to develop the capability of locating the C. G. of an object as accurately as was practical. Because of the fact that the accurate determination of the moment of inertia and the product of inertia of an object is dependent on the accurate location of the center of gravity of the object, this sub-program is a very important part of the mass properties determination program.

The center of gravity program has been chiefly concerned with locating the C. G. of test objects, although several "Drop Packages" were balanced for the Propulsion Division of Propulsion & Vehicle Engineering Laboratory.

2.4.1 Equipment

A description of the equipment associated with the center of gravity program is presented in the following paragraphs.

2.4.1.1 Spherical Segment Air Bearing Table

This system consists essentially of an object support platform attached to a spherical segment air bearing. The air bearing provides a very low friction pivot point over which the center of gravity of the test object is located. If the center of gravity of the test object is not located directly over the pivot point, the moment causes the system to rotate until the center of gravity is located over the pivot point. This rotation can be detected by levels placed on the x and y axes of the object support platform. In operation the platform is initially levelled and then the test object is positioned on the platform so that the platform again reaches a level condition. When this occurs the center of gravity of the test object is directly over the pivot point. Figure 140 shows the spherical segment air bearing table and identifies its component parts.

2.4.1.1.1 Test Object Support Surface

Two support surfaces are used. One is a 24 inch diameter x 1/2 inch thick hard-anodized aluminum plate, which is lapped to a flatness of 0.0005 inch and the other a 24 inch diameter x 1 inch thick surface composed of two 1/16 inch thick hard-anodized aluminum sheets bonded to each side of a honeycomb core and lapped to 0.0005 inch flatness. The aluminum support surface is for use with heavy test objects. This aluminum support surface is used to prevent objects having feet, pads, or other small supports from rupturing the honeycomb core. A light-weight support surface is needed to increase the sensitivity of the system when small or light objects are to be tested.

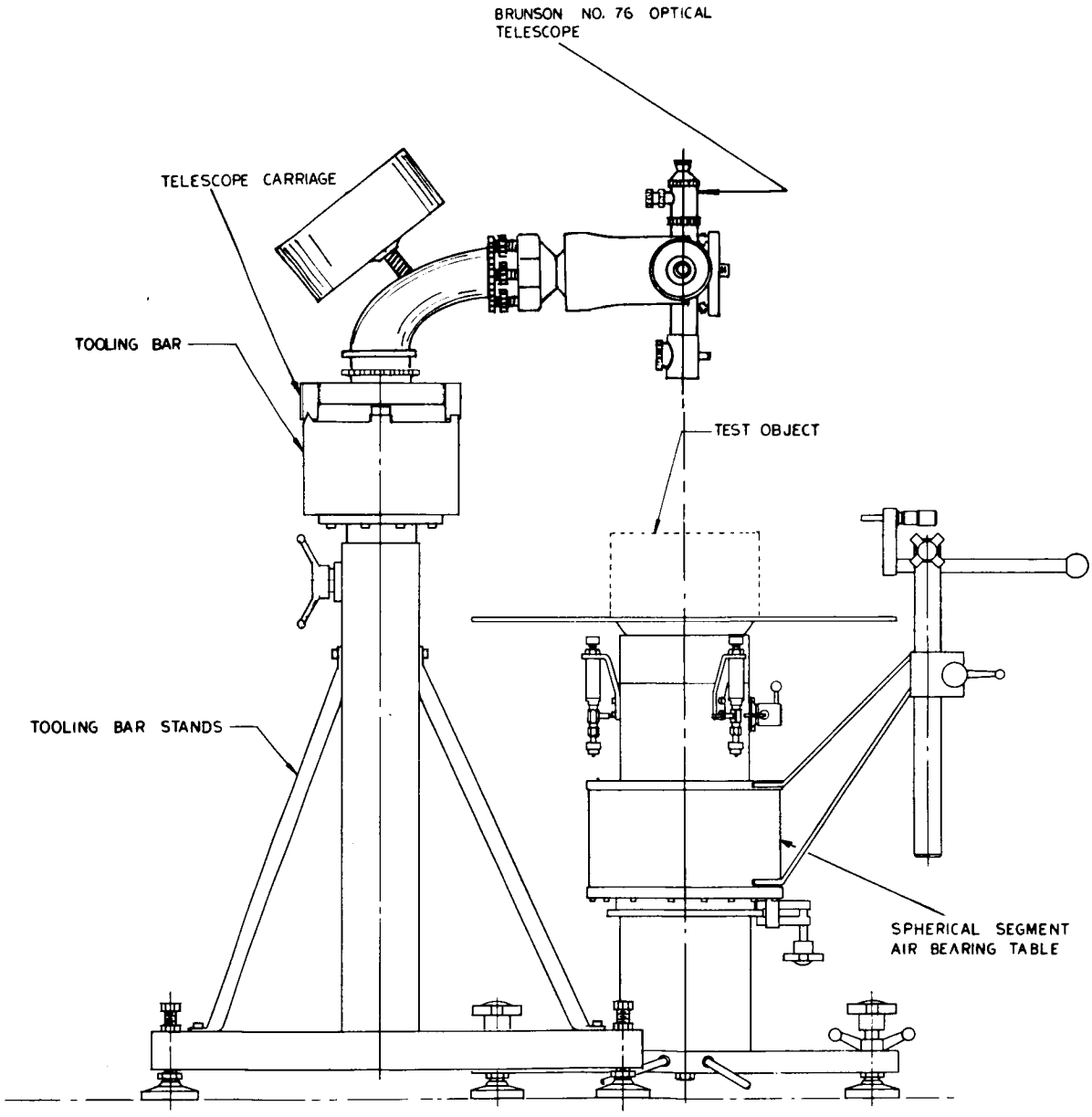

FIGURE 140

CENTER OF GRAVITY LOCATING SYSTEM USING A SPHERICAL SEGMENT AIR BEARING AND OPTICAL TELESCOPE

These object support surfaces fasten to the spherical segments of hard-anodized aluminum by means of four 1/4 diameter flat head stainless steel screws.

2.4.1.1.2 Spherical-Segment Air Bearing

The air bearing consists of a segment of a 5 inch nominal radius, hard-anodized, aluminum cup. The cup is fastened into a stainless steel air chamber. The cup and ball are lapped to a roundness of 4 millionths of an inch.

The air for operation of the bearing is filtered to 7 microns and supplied to the air chamber of the bearing through 1/8 inch O. D. nylon tubing. The air then passes through a series of very small holes in the cup and forces the ball to ride on a layer of air with no metal contact. A 1/4 diameter hole in the center of the cup allows air to enter a sealed air chamber below the bearing.

This chamber of air dampens vibrations of the ball caused by air flow.

A teflon ring around the edge of the cup prevents contact between the ball and cup when the air supply is off.

2.4.1.1.3 Stabilizing Air Cylinders

Three air cylinders are mounted, 120° apart, below the object support surface. These cylinders have a 1/2 inch diameter bore and a 1 inch stroke and are used to stabilize the object support surface while a test object is being repositioned. Each cylinder has an individual needle valve used to control the rate of plunger travel. It is necessary that the three cylinders make contact with the support surface at approximately the same time. This is necessary to prevent tipping of the support surface and causing unwanted movements of the test object.

An improved stabilization system was designed but was not built because it was decided that the "Bytrex" unit was the superior system and would be used for locating the center of gravity.

2.4.1.1.4 Air Cylinder Control Valve

The air cylinder control valve is used to control air flow to the three air cylinders. This three-way valve has ports for air input, air extraction and system bleeding.

2.4.1.1.5 Support and Leveling Stand

The object support surface is held 28 inches above the floor by this support stand and a floor area of 5 sq. ft. is needed for proper operation of the equipment.

The stand consist of a 7.25 inch O.D. aluminum tube welded to a three legged base. The base is 1.25 inch thick steel, machined such that three arms protrude 8 inches from an 8 inch diameter center section. The three arms are 120° apart and each contains a leveling pad. Attached to the steel tube is a bearing-supported rotating arm, referred to as the test object positioner.

2.4.1.1.6 Test Object Positioner

The test object positioner consists of a micrometer, mounted on a 3/4 inch diameter shaft that is movable in a horizontal direction. The horizontal shft is held by an adjustable, 1.50 inch diameter, vertical shaft. A rotating arm supports the vertical shaft. This arm extends approximately 16 inches from the center of the stand and is mounted to 7.25 diameter aluminum tube. The arm is mounted on a ball bearing and rotates freely through 360° and may be locked in any position. A micrometer positioner is used to obtain very small movements of the test objects in order to secure a level condition of the support surface.

2.4.1.2 Moment Detection System (Bytrex)

This system consists of a 250 inch pound capacity and a 25 inch pound capacity moment detection unit and an instrumentation and power supply unit. These items were manufactured by the Bytrex Corporation, Newton, Mass. The moment detector produces an electrical signal directly proportional to any unbalanced moment about its center. It has two perpendicular axes of sensitivity and resolves unbalanced moment into two components. The instrumentation and power supply unit amplifies the electrical signal to a level high enough to drive a read out device. The related equipment furnished by the Mass Metrology Laboratory includes two test object support plates and a support and leveling stand that incorporates four overload protection arms and provides for the rotation of the object support plate and indexing at 90° intervals.

Figure 141 shows the "Bytrex" system and identifies its component parts. The following paragraphs present brief descriptions of the component parts of the system:

2.4.1.2.1 Test Object Support Surface

The test object support surface is an 18 inch square, 1/2-inch thick, hard anodized aluminum plate. It is inscribed with perpendicular positioning lines which run from +x to -x and from +y to -y .

2.4.1.2.2 Support and Leveling Stand

A stand to support and level the moment detector was added to the

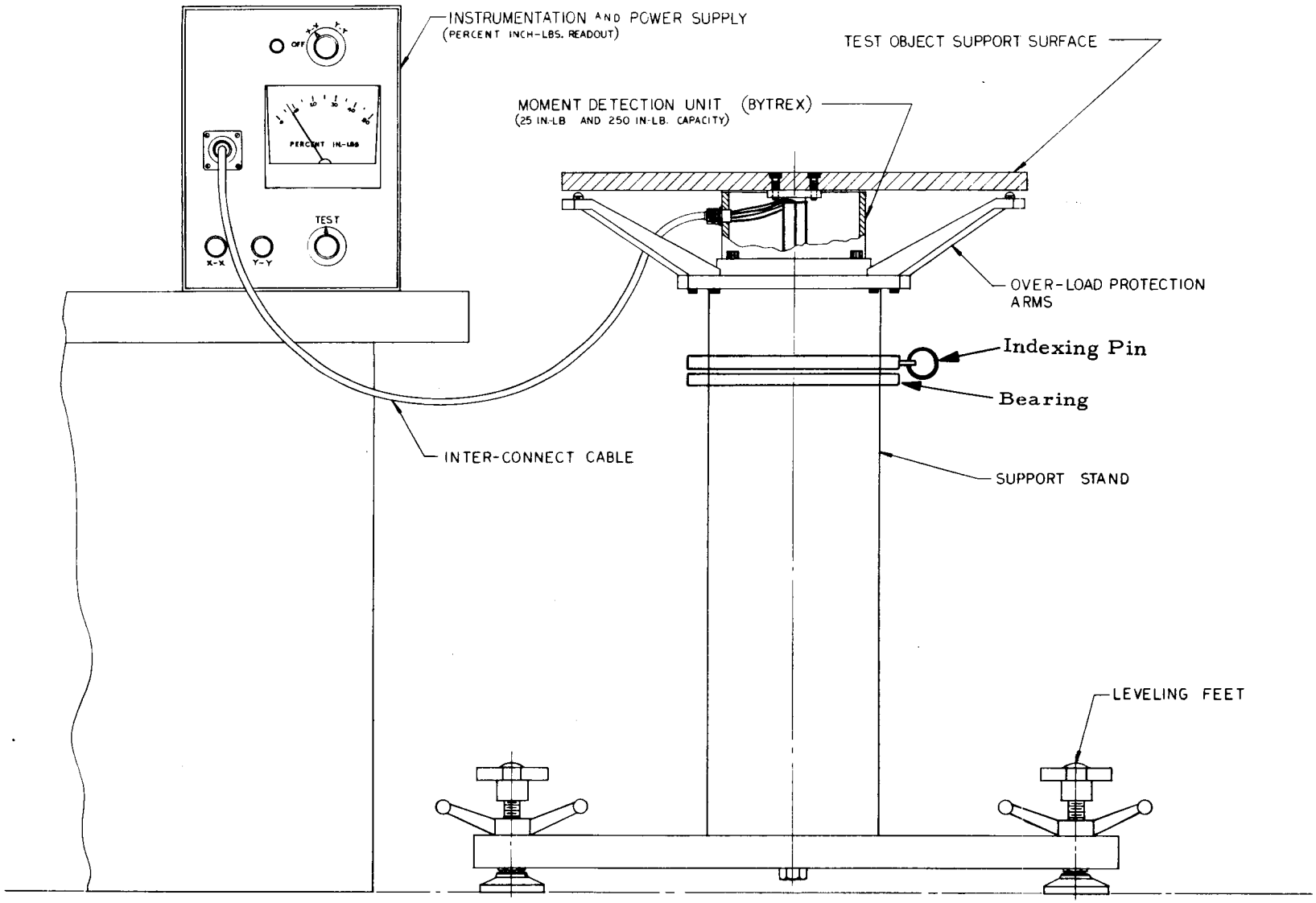

FIGURE 141

MOMENT DETECTION SYSTEM FOR CENTER OF GRAVITY DETERMINATION

TED WILLIAMS

system. The moment detector must be leveled before reliable results can be obtained. The support surface is positioned at a convenient height for testing large and heavy test specimens. The support stand was modified to allow the object support surface to be rotated and indexed at 90° intervals. This feature allows the C. G. of an object to be located relative to two axes without moving the object relative to the support surface.

2.4.1.2.3 Overload Protection Supports

Four protection supports protect the moment detector against overload damage. These support arms are designed to take-over when an object weighing more than 250 in.-lb is placed on the test object support surface.

2.4.1.2.4 Moment Detector Unit

The moment detector consists essentially of a vertical bending element bolted to two horizontal plates. The bending element has eight bonded wire strain gages cemented to it to sense bending strains. These gages are mounted into two separate Wheatstone Bridges, each composed of four gages mounted two and two on opposite sides of the neutral bending axis. These gages change their electrical resistances proportional to strain, and electrically unbalance the Wheatstone bridge. When voltage is applied across two corners of the Wheatstone bridge, an output voltage directly proportional to bridge unbalance appears across the output connections.

The object support surface, fastened to the top of the bending element, is machined and positioned so that its edges are precisely located with respect to the centerline of the moment detector. The bottom plate is drilled so that the detector may be bolted down. A rugged cylindrical cover encircles the bending element.

These detectors can withstand a vertical load ten times their moment rating. The accuracy of the unbalance moment reading is not affected by the vertical load.

2.4.1.2.5 Instrumentation and Power Supply Unit

This unit operates on four flashlight batteries which give about 100 hours of service. Its basic components are an oscillator which supplies voltage to the strain gage bridge, a detector, an amplifier, and a meter. Feedback circuits are used to achieve maximum stability. The principal operating controls of the unbalance indicator are an operation selector switch; an add-to reading switch, which is used to increase the range of the meter and select proper polarity; a meter adjust control, which is used to set the amplifier gain; two zero sets, one each for the x-x and y-y axis to bring the meter to zero with no applied unbalance; and two span controls, one each

for the x-x and y-y axis used to set the calibration of the system.

The indicator and moment detector are connected by a 20 foot cable with connectors at each end.

The indicator reads in percent of in. -lb of full range of the detector. For example, an 80 percent reading with the 25 in. -lb detector indicates an unbalance of 20 in. -lb about the center line of the detector.

The above description of the Instrumentation and Power Supply Unit is true for the unit as it existed in June of 1965. See papagraph 2. 4. 2. 3. 3 for modifications.

2. 4. 1. 3 Advanced Center of Gravity Locator

Due to the fact that the accurate determination of the product of inertia and the moment of inertia of an object is dependent on the center of gravity location it was deemed necessary to obtain a system with which the center of gravity could be located more accurately than with the air bearing table or the moment detection (Bytrex) system.

Several C. G. determining systems were investigated and evaluated. The system selected consisted of a test object support surface supported at three points-one at the center and two others on 90° axes intersecting at the center support. The center support is a flexural pivot utilizing a universal flexure. The supports at the axes each utilize a load cell which measures the force required to balance the test object. The C. G. location relative to the pivot point can easily be calculated by the equation:

$$\ell = \frac{\ell R}{w} \tag{326}$$

where

x = Distance from pivot point to C. G.
ℓ = Distance from pivot point to load cell reaction point
R = Indicated load on load cell
W = Weight of test object.

These quantities can all be measured except "X".

Almost all the weight of the test object is carried by the flexure at the center. The load cells only have a capacity of 25 pounds, therefore an

overload protection device must be built into the system to prevent damage to the load cells by inadvertantly placing a heavy object on the edge of the object support platform.

By reducing the capacity of the load cells the error in C. G. location is reduced because the error in load indication is given as a percent of capacity. A smaller capacity load cell is also more sensitive than a larger capacity load cell.

The center of gravity locator was designed to handle loads up to 1,000 pounds.

Figure 142 shows the center of gravity locator and identifies its components parts.

After the C. G. locator was designed it was decided that the present capabilities of C. G. location using the "Bytrex" unit were sufficient for present needs. Therefore, the center of gravity locator was not built.

2.4.1.4 Optical System

The optical equipment consists basically of a 10 ft. tooling bar extrusion mounted on two mobile tooling bar stands, a master index bar, a scale and vernier, a telescope carriage, a telescopic transit square, a micrometer reticle and a collimotion mirror. (See Figure 140)

In general the procedure for locating the C. G. of a test object using the optical system in conjunction with the C. G. locating systems mentioned above is as follows: (These procedures are for the null-balance method.)

1. Level the C. G locating device with the line of sight through the line of sight through the telescope aligned with the pivot point of the C. G. locating device.

2. Place test object on the object support platform so that the object is balanced over the pivot point. The line of sight through the telescope is now coincident with the center of gravity of the test object.

3. Rotate the object support surface 90 degrees and locate the C. G. on another plane.

Test have proven that the error in linear measurements made with the optical system is less than .001 inch.

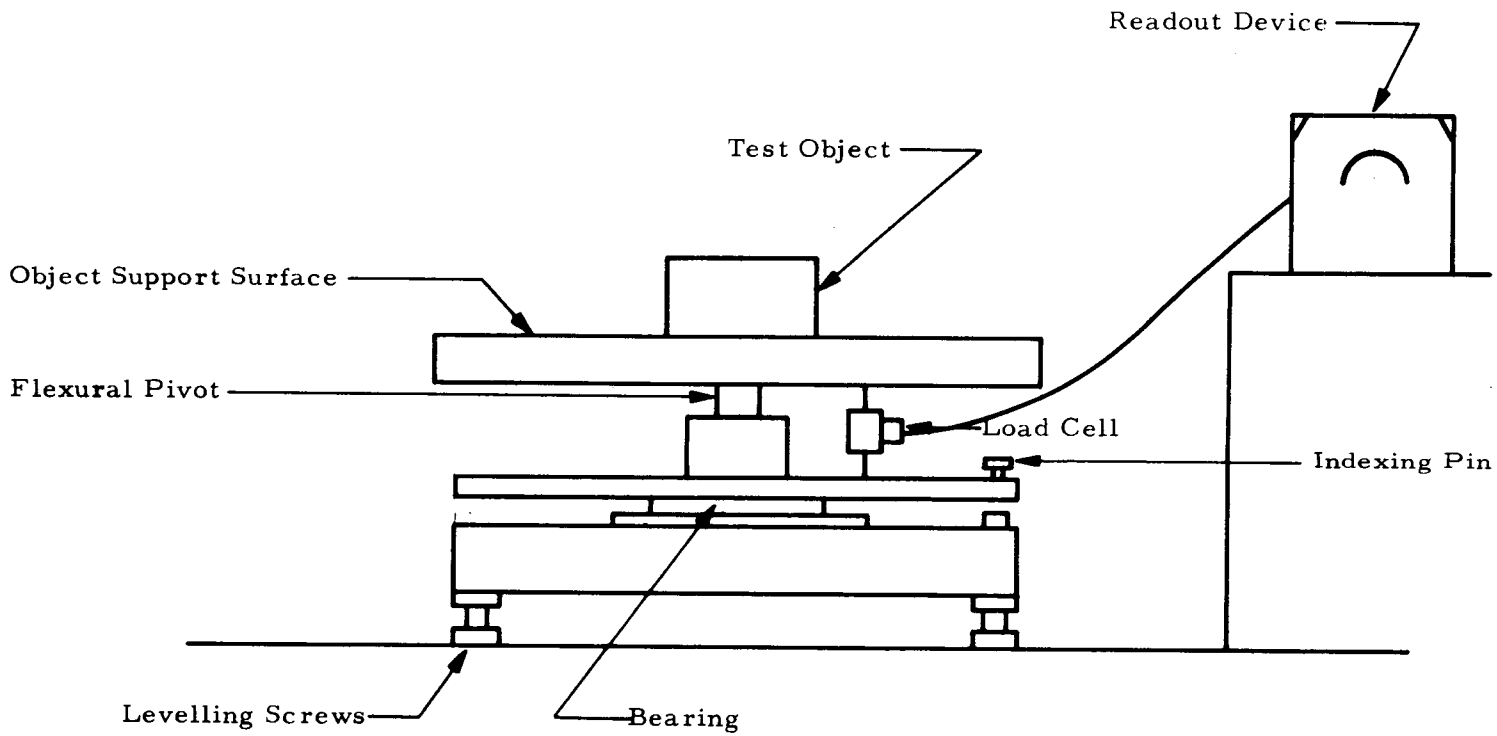

FIGURE 142

PRECISION CENTER OF GRAVITY LOCATOR

2.4.1.4.1 Modification

The optical system was modified to provide for the line of sight through the telescope to be positioned vertically. This feature was necessary to allow the telescope to be aligned perpendicular to the plane formed by the "X" and "Y" axes on the object support surface of the C. Gl locator.

The modification consisted of installing a 90° elbow between the telescope mount and the tooling bar. To counteract the moment induced by the cantilevered telescope and elbow a counterweight was installed.

2.4.1.5 C.G. Marking System

An error analysis of the C. G. locator system indicates that the largest single source of error is in the physical location of the C. G. on the object.

The center of gravity of an object can be located very precisely relative to the pivot point of the object support platform, but in order for this accuracy to be meaningful there must be some means of accurately locating a reference point, can be determined.

This section presents a discussion of three methods by which the center of gravity of an object can be located and recorded on the objece. The discussion is written around the advanced C. G. locator which was designed by the Spaco Mass Metrology Laboratory but could easily be adapted to the other C. G. locating systems.

2.4.1.5.1 Method I

One system which has been considered for use in marking the C. G. location on an object entails the use of a precision grid which would be attached to the object whose C. G. is to be located.

By attaching the grid, which contains a set of perpendicular axes, to the object approximately over its center of gravity and by observing the grid through the telescope, which has been previously aligned with the platform pivot point, the center of gravity can be located as follows:

1. The C. G. location, relative to the origin formed by the reticle crosshairs, can be calculated using the loads acting on the load cells at a known distance from the pivot point.

2. The location of the reticle origin, relative to the origin on the grid, can be read directly by counting lines between the two origins.

3. The C. G. location relative to the grid origin can be obtained by the algebraic addition of the two sets of coordinates obtained above.

This system was abandoned for the following reasons:

1. The inability to economically obtain a precision grid.

2. In order to obtain the accuracy approaching that which can be attained by the use of Method III, a grid of 1000 lines per inch would be required. The magnification factor for the telescope now in use in the laboratory is too small to permit the direct reading of distance between two given points on a grid of 1000 lines per inch.

3. Error would be induced if the grid is not perpendicular to the line of sight.

4. It would be extremely difficult to get perfect angular alignment between the axes of the reticle and the axes on the grid.

Two unsuccessful attempts to make a grid are shown in Figures 143 and 144.

2.4.1.5.2 Method II

Another method which has been considered consists of projecting the image of the reticle crosshairs onto an adhesive backed, photo-sensitive material after it has been attached to the object whose center of gravity is to be located. This is an ideal system for which no real equipment is readily available. Another disadvantage is the fact that the equipment would probably have to be used in a darkened room.

It was decided that the cost of developing a system of this type was not justified since an accurate system is already available--a system with which laboratory personnel are already familiar. This system is discussed under Method III.

2.4.1.5.3 Method III

The following described method appears to be the most practical of all methods which were investigated.

The C. G. locator will be placed under the telescope and leveled and balanced. The telescope will then be aligned with the platform pivot point on the C. G. locator. The object whose C. G. is to be located will then be placed on the C. G. locator and shifted until the loads on the load cells are zero. This indicates that the C. G. of the object is directly over the platform pivot point

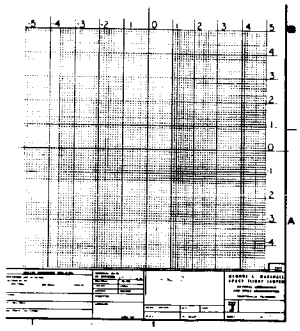

FIGURE 143. REDUCED GRID PATTERN

The original of this grid is 10 inches square with 10 lines per inch drawn on Mylar. It is obvious that this could not be reduced to obtain a grid of 1000 lines per inch with the equipment available in the Spaco Photo Laboratory.

FIGURE 144. RONCHI RULING GRID PATTERN

This grid was made by photographing a stack of two Ronchi rulings arranged so that the lines formed a grid. The photograph was then enlarged so that detail retention could be checked. Actual size of the Ronchi rulings is 1 inch square with 300 lines per inch.

and in line with the telescope. A small square of adhesive backed foil on which has been scribed a set of perpendicular axes will then be attached to the object approximately in line with the line of sight through the telescope. The axes on th foil target will be used as a reference point from which the center of gravity will be located.

Because of the virtual impossibility of consistently attaching the target in line with the telescope reticle, the center of gravity displacement relative to the reference axes will be measured by use of the micrometer reticle on the telescope or by using the vernier scale on the tooling bar. Tests have shown that the error in linear measurement using these devices is less than .001 inch.

After the measurements have been made from the pivot point to the reference axes the C. G. location relative to the reference axes will be scribed on the target in the form of X and Y coordinates.

This system seems to be the most promising of all the systems which were investigated and will be used in the Mass Metrology Laboratory until a better system is found.

2.4.2 Test and Evaluations

This section deals primarily with tests performed with the systems associated with the center of gravity program and the evaluation of the tests and of the equipment itself.

2.4.2.1 Test Studies - Existing Equipment

A test was made to determine the effect of sight point elevation on the accuracy at linear measurements made with the optical system. The results are summarized in Table 47 and Figure 145 is a plot of the data in Table 47. They clearly show a trend of relationship. In an attempt to determine the cause, calculations were made of the system center of gravity elvation with various test objects in position on the air bearing table. Figure 146 is a plot of the results of this study. The curve shows no significant trend, indicating that the system C. G. elevation is not a contributing factor.

The optical system was then realigned to place the axis of the telescope more nearly perpendicular to the plane of the leveled air bearing table. A new test was then run to measure the shift in center of rotation with sight point elevation. The results of this test are shown in Table 48. The largest shift measured was 0.0007 inch, which is within the normal measurement tolerance of the optical equipment. From this investigation it is concluded that the center of rotation of the air bearing table is stable with various loads and C. G. elevations and any apparent change is due to misalignment of the optical telescope.

TABLE 47

Spherical Segment Air Bearing
Test Data

Test Object	Change in Center of Rotation of Air Bearing (Inches)	Sight Point Elevation (inches)
Teflon Target	Set Up Position	.310
Brass Block	- .0007	1.500
Brass Block	- .00012	3.000
Triangular Solid	+ .00017	4.130
Brass Block	- .0002	5.000
Brass Cylinder	+ .00005	5.250
Avg. Shift	- .00016	

TABLE 48

SIGHT POINT EVALUATION TEST DATA

Test No.	Test Object	Sight Point Elevation (Inches)	Test Object Weight (lbs)	Telescope Setting
1	None	0	0	3.039
1	Teflon Target	.341	.02	3.035
2	Alum. Block	1.500	2.25	3.0265
2	Alum. Block	3.000	2.25	3.021
2	Alum. Block	5.000	2.25	3.0145
3	Brass Block	1.500	6.81	3.0265
3	Brass Block	3.000	6.81	3.021
3	Brass Block	5.000	6.81	3.0145
4	Small Brass Cyl.	5.25	9.68	3.014
4	Large Brass Cyl.	5.25	24.20	3.014

FIGURE 145

TELESCOPE SETTING FOR CENTER OF
ROTATION OF AIR BEARING
VERSUS
SIGHT POINT ELEVATION

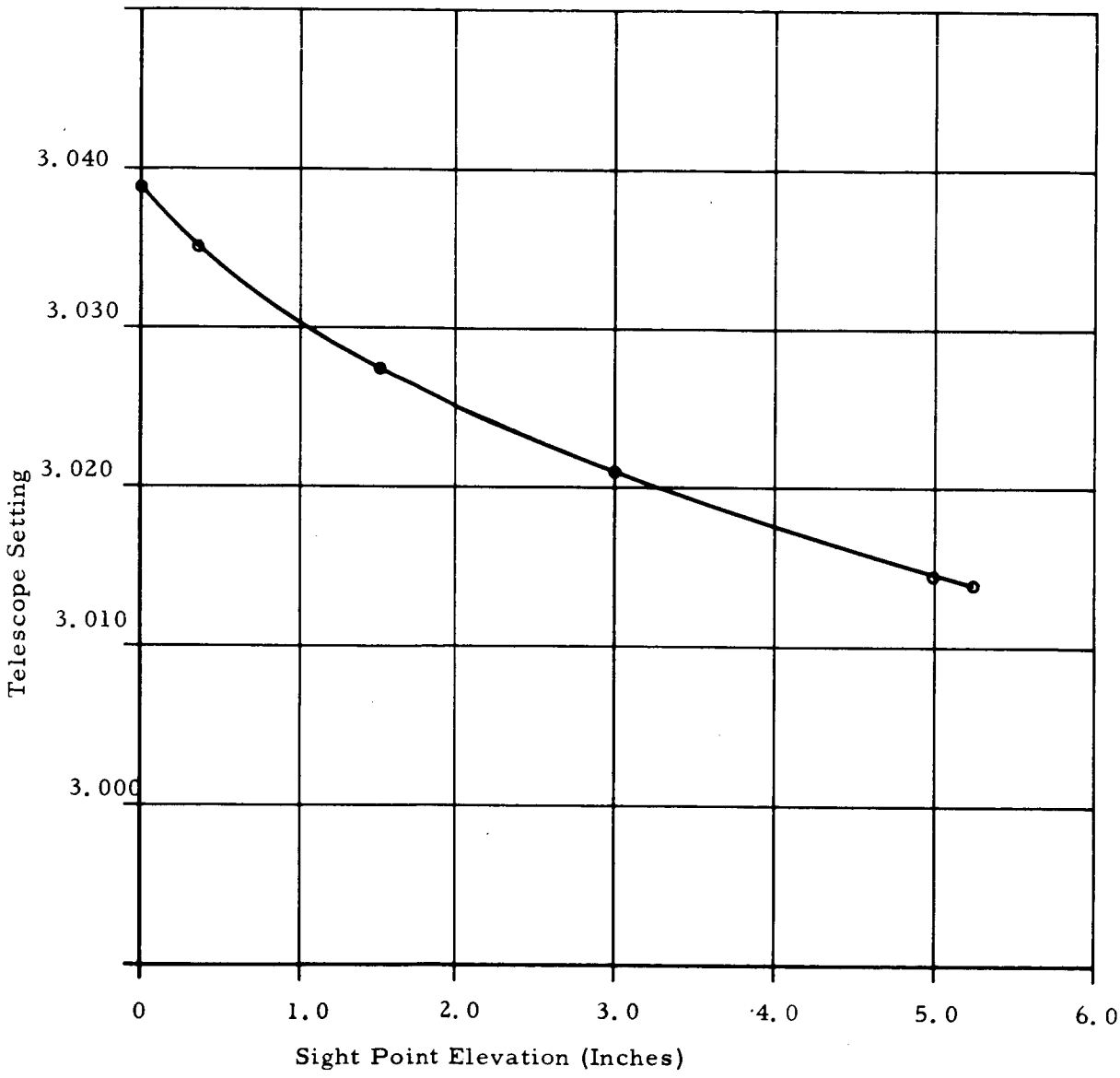

FIGURE 146

SYSTEM C.G. BELOW CENTER OF
OSCILLATION OF AIR BEARING
VERSUS
APPARENT CHANGE IN CENTER OF ROTATION

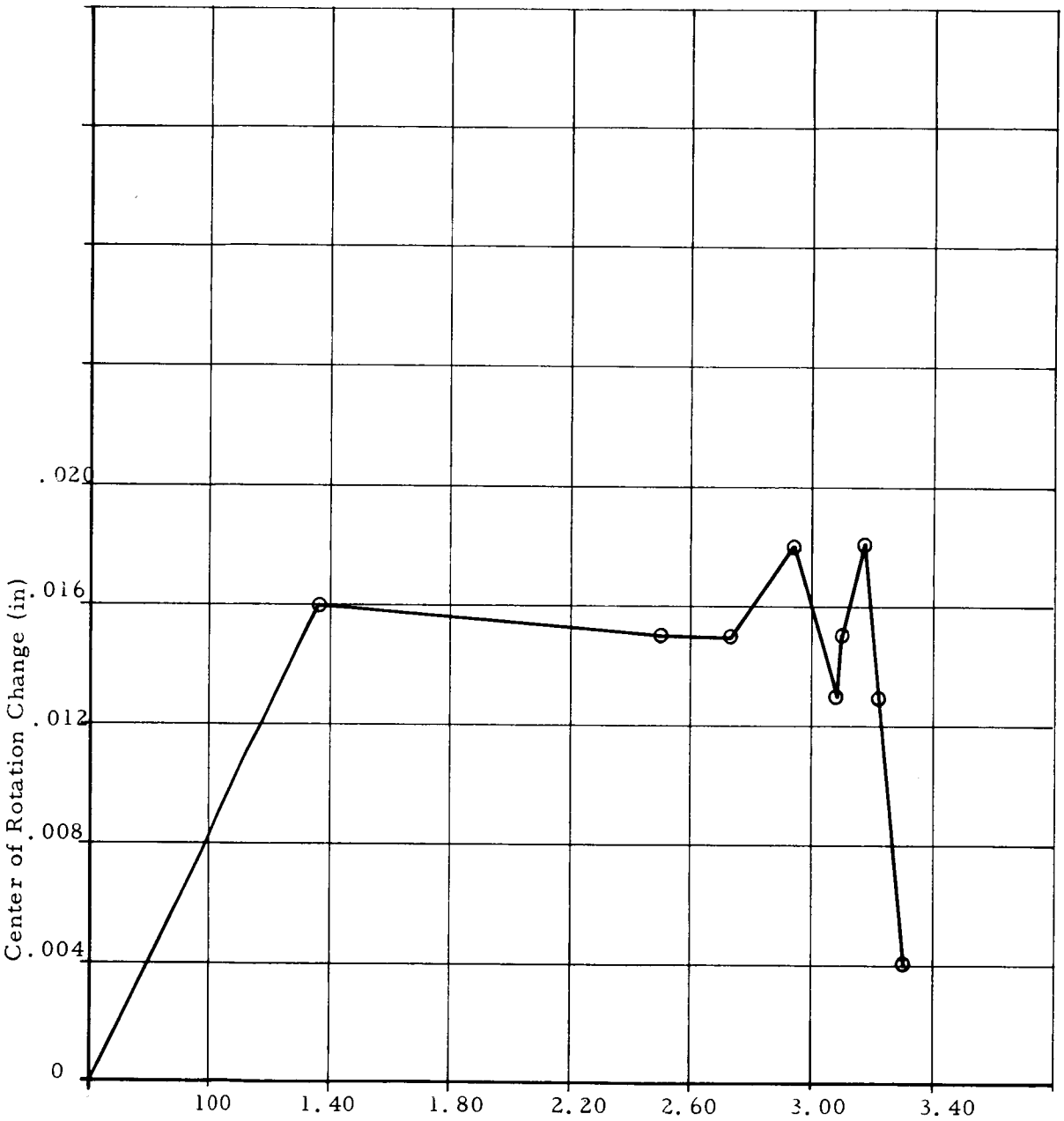

System C.G. Below Center of Oscillation

2.4.2.2 Comparison of "Null Balance" Method and "Unbalance" Method of C. G. Location Using the Bytrex Unit

Two sets of tests were completed. One set of tests was made using the "null balance" method wherein the test specimen is repositioned on the moment detecting table until the readout device indicates zero moment. This locates the C. G. of the specimen over the center of bending of the moment detection unit. This center of bending was predetermined as was the approximate C. G. of the test specimens. Measurements were then made with the optical equipment to determine the accuracy of this method.

The second set of tests was made by placing the test specimen at a random location on the moment detecting table. The amount of moment was read and divided by the specimen weight, yielding the distance between the center of bending of the table and the center of gravity of the specimen. This was also checked with the optical equipment.

The results of these tests are shown in Tables 49 and 50. It is evident from this data that the "null-balance" method yielded the best results over the un-balance method. There are several reasons that this should be the case. One reason is that the test object deflects the support surface of the moment detection unit when it is placed at any point other than the center of the unit. This deflection causes the line of action of gravity to vary from the geometric center of the test object. Because the C. G. is measured with the optical equipment, as if it were acting through this geometric center, this introduces some error. (See Figure 147) Dimension "x" is the actual moment arm of the induced moment detected by the "Bytrex" unit where dimension "y" is the moment arm measured with the optical equipment.

An additional error is introduced when the telescope carriage is moved along the tooling bar to make the moment across measurement. The additional error is not involved with the "null-balance" method because only the optical micrometer is used for measurements. A third source of error is in reading the instrumentation dial. When the needle is between graduation lines it becomes a matter of guess as to the percentage of the distance the needle is between the lines. With the "null-balance" method the instrument needle is positioned directly over the zero line of the scale. One disadvantage of the "null-balance" method is that the "Bytrex" system is not as accurate when used on the low range side. However, the errors involved in the moment detection method apparently override this error.

2.4.2.3 Systems Evaluation and Comparison Tests

Several evaluation and comparison tests were performed with the air bearing table and the "Bytrex" Unit. Some of the more conclusive tests are discussed in the following paragraphs:

TABLE 49

"BYTREX" TEST BY THE UNBALANCE MOMENT METHOD USING THE BYTREX INSTRUMENTATION UNIT FOR % UNBALANCE READINGS

Test Specimen	Specimen Weight (lbs.)	Instrument Reading (% Unbalance) Axis x-x	Instrument Reading (% Unbalance) Axis y-y	Telescope Reading (Ins.) Axis x-x	Telescope Reading (Ins.) Axis y-y	Actual C.G. Location of Specimen from "Bytrex" Center Axis x-x	Actual C.G. Location of Specimen from "Bytrex" Center Axis y-y	Error (Ins.) Axis x-x	Error (Ins.) Axis y-y	Test Set No.
Alum. Block	2.25	44.5	59	5.094	6.445	4.944	6.555	.150	.110	
Brass Block	6.81	94	97.5	3.473	3.549	3.451	3.579	.022	.030	
S. Brass Cyl.	9.68	89.5	84.5	2.121	2.367	2.311	2.182	.190	.185	1
L. Brass Cyl.	24.20	64	99	.640	1.064	.661	1.023	.021	.041	Avg. Error .094
Alum. Block	2.25	44	59.5	5.086	6.450	4.889	6.611	.195	.161	
Brass Block	6.81	94	97.5	3.496	3.574	3.451	3.579	.045	.005	
S. Brass Cyl.	9.68	89.5	84.5	2.111	2.391	2.311	2.182	.200	.209	2
L. Brass Cyl.	24.20	64	99	.645	1.041	.661	1.023	.016	.018	Avg. Error .106
Alum Block	2.25	44.5	59	5.130	6.444	4.944	6.555	.186	.111	
Brass Block	6.81	94	97.5	3.495	3.549	3.451	3.579	.044	.030	
S. Brass Cyl.	9.68	89.5	84.5	2.120	2.371	2.311	2.182	.191	.189	3
L. Brass Cyl.	24.20	64	99	.645	1.066	.661	1.023	.016	.043	Avg. Error .10
								Total Avg. Error		.100
	Max. Repeatability Error									
Alum. Block	2.25	0.5	0.5	.044	.006	.055	.056	.045	.051	
Brass Block	6.81	0	0	.023	.025	0	0	.023	.025	
S. Brass Cyl.	9.68	0	0	.010	.024	0	0	.010	.024	
L. Brass Cyl.	24.20	0	0	.005	.025	0	0	.005	.025	
								Avg. Repeatability		.026

TABLE 50

"BYTREX" TEST BY THE NULL-BALANCE METHOD USING THE BYTREX INSTRUMENTATION UNIT AT ZERO READING

Test Specimen	Specimen Weight (lbs.)	Instrument Reading (% Unbalance) Axis y-y	Instrument Reading (% Unbalance) Axis x-x	Optical Telescope Reading (Ins.) Axis y-y	Optical Telescope Reading (Ins.) Axis x-x	Test Set Number
Alum. Block	2.25	0	0	.019	.020	
Brass Block	6.81	0	0	.016	.010	
S. Brass Cyl.	9.68	0	0	.016	.016	1
L. Brass Cyl.	24.20	0	0	.007	.006	
Triangle # 7	43.98	0	0	.007	.004	
						Avg. Error .012
Alum. Block	2.25	0	0	.015	.035	
Brass Block	6.81	0	0	.014	.0005	
S. Brass Cyl.	9.68	0	0	.006	.005	2
L. Brass Cyl.	24.20	0	0	.004	.007	
Triangle # 7	43.98	0	0	.014	.004	
						Avg. Error .010
						Total Avg. Error .011
Repeatability Error Between Set 1 & 2						
Alum. Block	2.25	0	0	.004	.015	
Brass Block	6.81	0	0	.002	.0095	
S. Brass Cyl.	9.68	0	0	.010	.011	
L. Brass Cyl.	24.20	0	0	.003	.001	
Triangle # 7	43.98	0	0	.007	0	
					Avg. Repeatability	.006

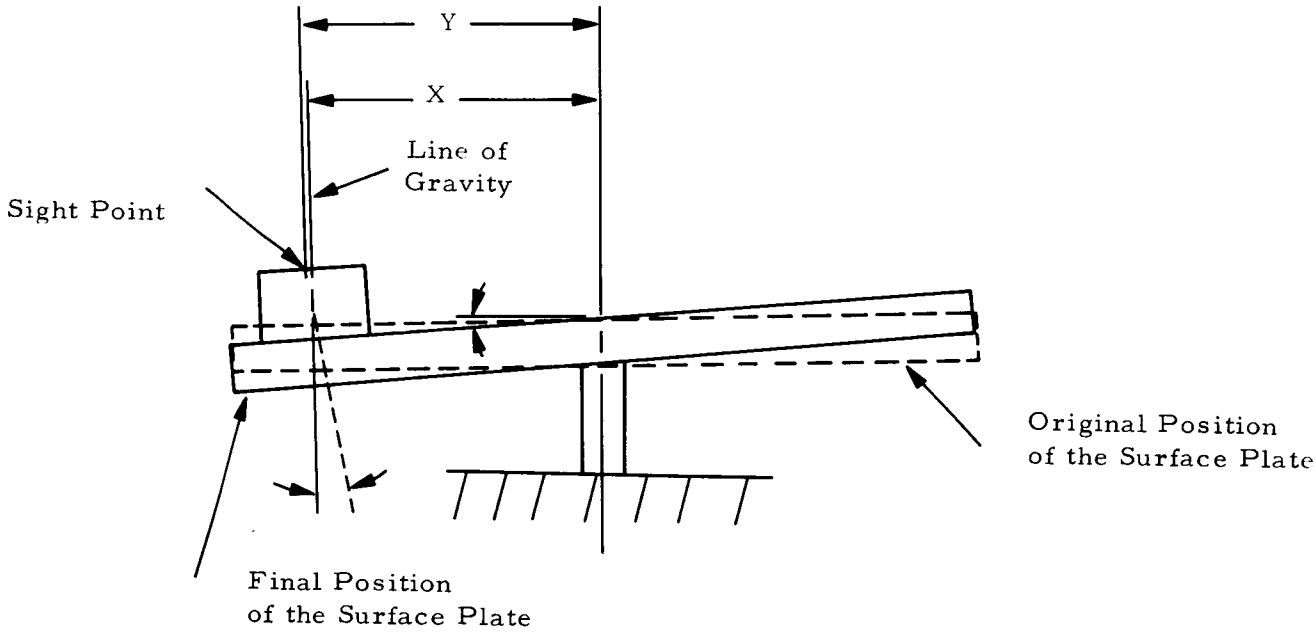

FIGURE 147

EFFECT OF TABLE TILT ON C.G. LOCATION ACCURACY

2.4.2.3.1 Spherical Segment Air Bearing Table

The triangular laboratory standards were weighed and their dimensions were obtained. From this data the center of gravity of each triangle was determined by using standard formulae. The calculated locations were scribed on pressure sensitive foil patches applied to the standards, and the location checked with the spherical air bearing center of gravity locator. The difference between the calculated center of gravity and the measured center of gravity is shown in Table 51. The rotation in Table 51 can best be explained by examining Figures 148 through 151.

Figure 148 shows the triangle alignment for position 1-R. The X, Y, Z coordinate system is the triangle body fixed axis system. The Z axis is the axis along which the optical scope must be moved in the X direction to measure the difference between the measured and calculated centers of gravity. These letters stand for red and black respectively, which is a characteristic of the scope. Under position 1-R in Table 51 the scope had to be moved 0.022 inches in the red direction to determine the difference in the measured and calculated centers of gravity. Position 1-B is obtained by rotating the table top 180° as shown in Figure 149. The data here is obtained in the same manner as before except the scope was moved in the black direction instead of the red. This is a check to assure that the center of gravity of the object is located on the center axis of the table. The object was rotated 180° twice more to obtain good repeatable data as seen for triangle number 1 in positions 1-R and 1-B. Position 2 is obtained by initially rotating the object 90° from position 1 and measuring R and B as before. These positions are shown in Figures 150 and 151. This later test checks the center of gravity measurements in a body fixed Y direction. The average difference between the respective readings 180° apart was only 0.00058 inches, which indicates extremely good stability.

However, evaluation tests which will be discussed in the following paragraphs prove that the "Bytrex" unit with modifications, is better than the spherical segment air bearing table for locating the center of gravity

2.4.2.3.2 "Bytrex" Moment Detection System

2.4.2.3.2.1 System Evaluation Tests

Similar tests as described in section 2.4.2.3.1 were performed using the Bytrex unit. The test results are shown in Table 52 where the same rotation as described before has been used. The average difference between respective readings 180° apart was 0.0016 inches which was not as good as that obtained from the air bearing table.

2.4.2.3.3 Modified Bytrex Unit Evaluation

TABLE 51
ACCURACY TEST - AIR BEARING G.G. LOCATOR

Triangle Number	Position 1 R	Position 1 B	Position 2 R	Position 2 B
1	.022 in.	.0225 in.	.0115 in.	.0115 in.
	.022	.0225	.011	.0115
2	.030	.029	.008	.008
	.030	.0295	.008	.008
3	.068	.065	.006	.006
	.067	.065	.006	.006
4	.0675	.068	.000	.003
	.067	.068	.000	.003
5	.026	.025	.011	.010
	.0255	.025	.010	.010
6	.016	.017	.004	.006
	.016	.017	.004	.0055

TABLE 52
ACCURACY TEST - BYTREX C.G. LOCATOR

Triangle Number	Position 1 R	Position 1 B	Position 2 R	Position 2 B
	.0215	.0215	.012	.0125
1	.0215	.022	.012	.0115
	.021	.0215	.012	.0115
	.030	.029	.0085	.0075
2	.0305	.0295	.0085	.0075
	.0305	.0295	.0085	.0075
	.0665	.065	.007	.006
3	.067	.066	.007	.006
	.067	.0655	.007	.006
	.0675	.0675	.0015	.0015
4	.0675	.0675	.001	.0015
	.0675	.068	.0015	.0015
	.0255	.024	.011	.011
5	.025	.0245	.011	.0115
	.025	.024	.011	.011
	.018	.018	.0040	.0045
6	.018	.018	.0040	.004
	.0185	.018	.0045	.004

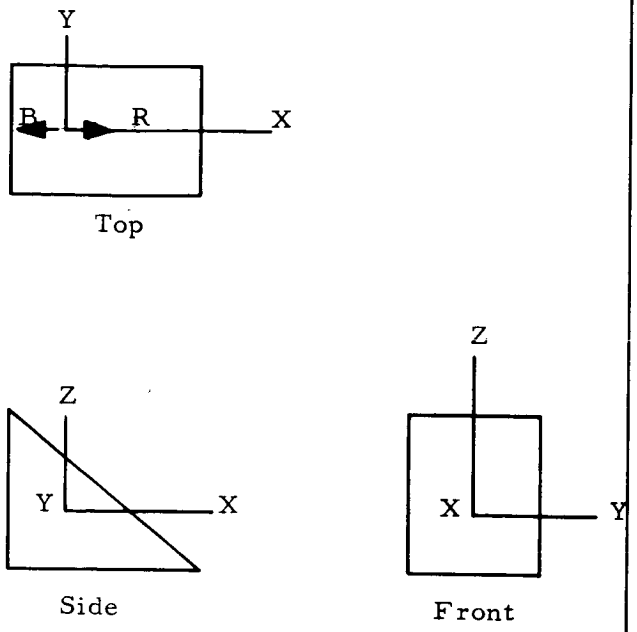

FIGURE 148
TRIANGLE STANDARD AXES
POSITION 1-R

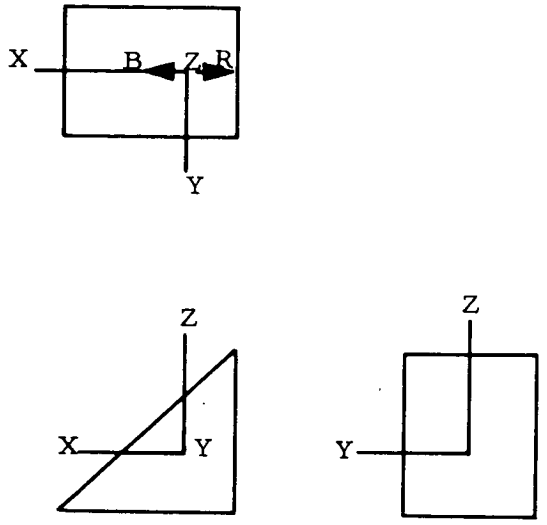

FIGURE 149
TRIANGLE STANDARD AXES
POSITION 1-B

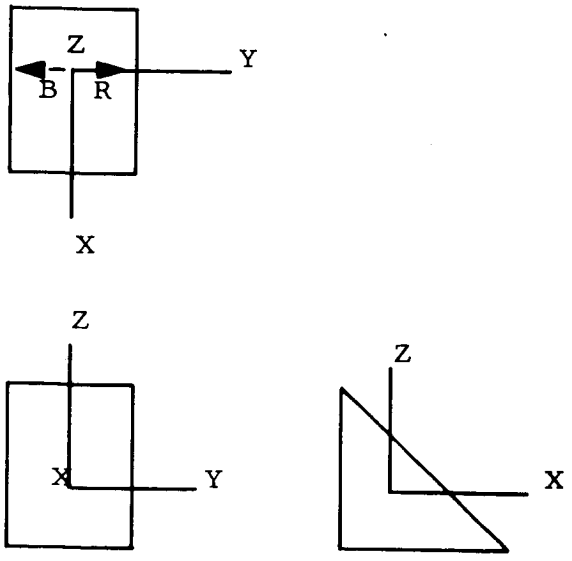

FIGURE 150
TRIANGLE STANDARD AXES
POSITION 2-R

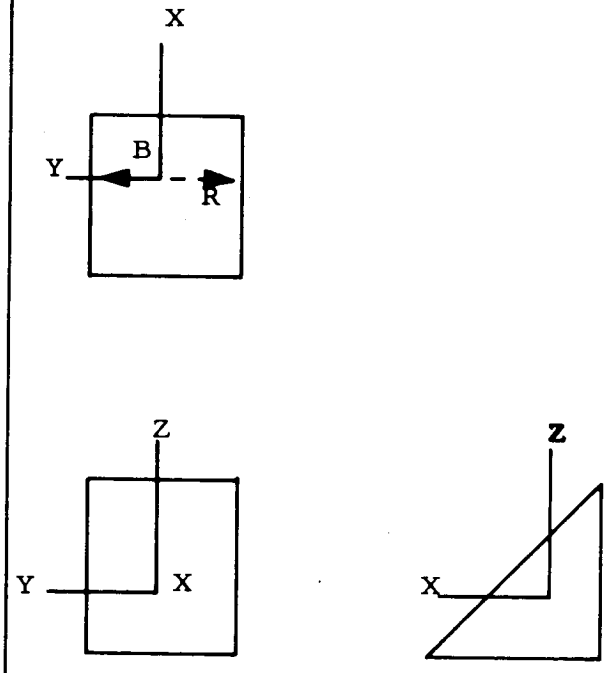

FIGURE 151
TRIANGLE STANDARD AXES
POSITION 2-B

2.4.2.3.3.1 Introduction

Previous experience with the Bytrex center of gravity locator has shown that the normal error to be expected in C. G. location is about 0.01 inch when using the machine in the manner intended by the manufacturer. A study of the device indicated that the limiting factor was readability of the meter rather than some inherent limitation in the transducers or circuitry. Therefore, it was deemed worthwhile to attempt improvement of the readout resolution and accuracy of the Bytrex device.

2.4.2.3.3.2 Equipment Modification

The basic Bytrex unit consists of a table supported on a rectangular flexure column with strain gages attached on all 4 sides of the column. The strain gage bridges are supplied with an alternating voltage from an oscillator in the instrument, and the output from the gages is amplified and detected, and displayed on a 200 microamp D' Arsonval meter. Moments applied to table from off-center C. G. locations result in flexing of the column and a proportional output from the strain gages. The rectangular column allows independent measurement of moments along two perpendicular axes.

The meter is calibrated in units of zero to 50 percent of the rated moment of the detector head. Detector heads can be interchanged for different load ranges. In this experiment, a 25 in-lb. detector was used so that full scale of the meter represented 12.5 in-lb. With a meter of this type, the best resolution that can be expected is on the order of 0.5% of full scale, which would be equivalent to a moment of 0.0625 in-lb. Because of the likelihood of a zero error in the meter of another 0.5, the best accuracy to be expected near the zero end is about 0.1%, or 0.125 in-lb. moment. This would allow location of the center of gravity of a ten pound weight to within $\pm$ .0125 inch, which is typical of experimental results with the equipment.

The voltage across the meter at full scale is about 0.2 volts, so that the sensitivity is 0.2/12.5 or 0.016 volts/in-lb. A laboratory digital voltmeter with a resolution of 10 microvolts was connected across the meter to produce a theoretical resolution of .00001/.016 or 0.000625 inch-lb. moment, a factor of 200 better than with the meter. It was then found that drift in the power supply batteries prevented utilization of the full potential resolution. A regulated power supply was connected across the batteries, and the unit checked again. The stability was then adequate to permit using the full resolution of the DVM. With this set-up, it is theoretically possible to locate the C. G. of a one pound object to within $\pm$ .001 inch.

2.4.2.3.3.3 Evaluation Tests

The modified Bytrex machine was tested for sensitivity on a comparative

basis with the spherical segment air bearing C. G. locator. The purpose of this test was both to see how much the Bytrex unit had been improved and to see if it could be used for future high precision work rather than the air bearing. The air bearing table is subject to varying sensitivity depending on the configuration of the test object, and requires the use of counterweights to cover a practical range of sizes.

The test consisted of determining the least amount of moment required to produce a detectable indication on each device. The procedures used for the test are shown in Appendicies D1 and D2. Small weights were placed on the table until an indication was obtained, and the weight and distance from the center were recorded.

2. 4. 2. 3. 3. 4 Test Results

The results of the comparison test are shown in Tables 53 and 54. Table 53 shows the results of the Bytrex test, and Table 54 shows that of the air bearing test. The columns labeled C. G. resolution in inches are obtained by dividing the least detectable moment by the weight on the table at the time. Where > is indicated no moment was detected with the specified weight at the edge of the table.

It can be seen by comparing Tables 53 and 54 that the Modified Bytrex system is somewhat more sensitive than the air bearing table, regardless of the weight on the table. In both devices an increase in weight on the table caused a reduction in sensitivity. No explanation is offered for this phenomenon on the Bytrex unit. On the air bearing it is conceivable that the increase in viscous friction of the air bearing caused by the weight more than offset the increase in sensitivity caused by elevation of the C. G.

It should be noted here that the sensitivities shown are barely detectable under ideal conditions by a trained observer, and are not typical of what could be achieved in everyday use. The general relationship in accuracy between the two will probably remain the same, however.

2. 4. 2. 3. 3. 5 Conclusions

From the above data it is concluded that the modified Bytrex C. G. locator is on the order of 30 to 50 percent more sensitive than the spherical segment air bearing system.

2. 4. 2. 3. 3. 6 Recommendations

It is recommended that the modified Bytrex C. G. locator be used in the future for all work because of its greater convenience and sensitivity.

TABLE 53
RESULTS OF MODIFIED BYTREX C.G.
LOCATOR SENSITIVITY TEST
(25 inch-pound detector)

Load Weight lb.	Sensitivity Weight, mg.	Distance from Center, inches	Moment in-lb. x 10^{-6}	C.G. Resolution inches x 10^{-6}
0	5	6.5	72	∞
0	10	5.5	121	∞
0	50	5.0	550	∞
0	500	0.5	550	∞
6.8	5	>8.0	>88	>12.9
6.8	10	>8.0	>176	>25.9
6.8	50	>8.0	>880	>129.0
6.8	500	0.5	550	80.9
24.2	20	>8.5	>374	>15.4
24.2	50	8.0	880	36.3
24.2	100	3.0	660	27.2
24.2	200	2.5	1100	45.4
Average			560	47.4

TABLE 54
RESULTS OF SPHERICAL SEGMENT AIR BEARING
C.G. LOCATOR SENSITIVITY TEST

Load Weight lb.	Sensitivity Weight, mg.	Distance from Center, in.	Moment in-lb x 10^{-6}	C.G. Resolution inches x 10^{-6}
0	5	11.0	121	∞
0	10	11.0	242	∞
0	50	6.0	660	∞
0	500	1.5	1650	∞
6.8	5	>11.0	>121	>17.8
6.8	10	>11.0	>242	>35.6
6.8	50	>11.0	>1210	>177.9
6.8	500	1.0	1100	161.7
24.2	20	>11.0	>484	>20.0
24.2	50	7.5	825	34.1
24.2	100	3.5	770	31.8
24.2	200	3.0	1320	54.5
Average			835	70.5

2.5 LABORATORY WEIGHING SYSTEM

2.5.1 Introduction

In the past, objects requiring precision weighing have been sent out to other laboratories. This procedure usually results in a time lag of several weeks. In order to alleviate this problem, it was desirable to provide an in-house precision weighing system with a capacity of 1,000 pounds.

After evaluating several weighing systems it was decided that a compound beam balance would best meet the needs of the Mass Metrology Laboratory. Because of the fact that the price and delivery time for a balance purchased from a supplier was not compatible with the prevailing budget and schedule, it was decided to design and manufacture the balance at Spaco. This section presents a discussion of the beam balance.

2.5.2 System Description

The laboratory weighing system is a compound beam balance mounted on flexural pivots. (See Figure 152.) There is a 10 to 1 ratio between the distance from the fulcrum to the light weight pan and the distance from the fulcrum to the heavy weight pan. These distances are established by weight comparisons of standards rather than by linear measurements. The arrangement of the pivot lines allow the pivot points to form a parallelogram as the system oscillates. Therefore, a vertical line through the pivot points at either end of the balance remains vertical as the system pivots about the fulcrum. The amplitude of the oscillation is limited by a hold-down fixture near the end of the lower beam.

The Spaco manufactured components of the laboratory weighing system are fabricated from 6061-T6 aluminum black anodized except for the counterweights and centerpoise assembly which are chrome plated steel, and the flexures which are steel.

2.5.3 Design Considerations

Following are some of the more pertinent design considerations concerning the laboratory weighing system:

2.5.3.1 Centerpoise

The centerpoise is essentially an inverted pendulum mounted on the upper beam directly over the fulcrum pivots. The function of the centerpoise is to increase the sensitivity of the system by counteracting the bending spring constant of the flexures. The sensitivity of the system can be improved either

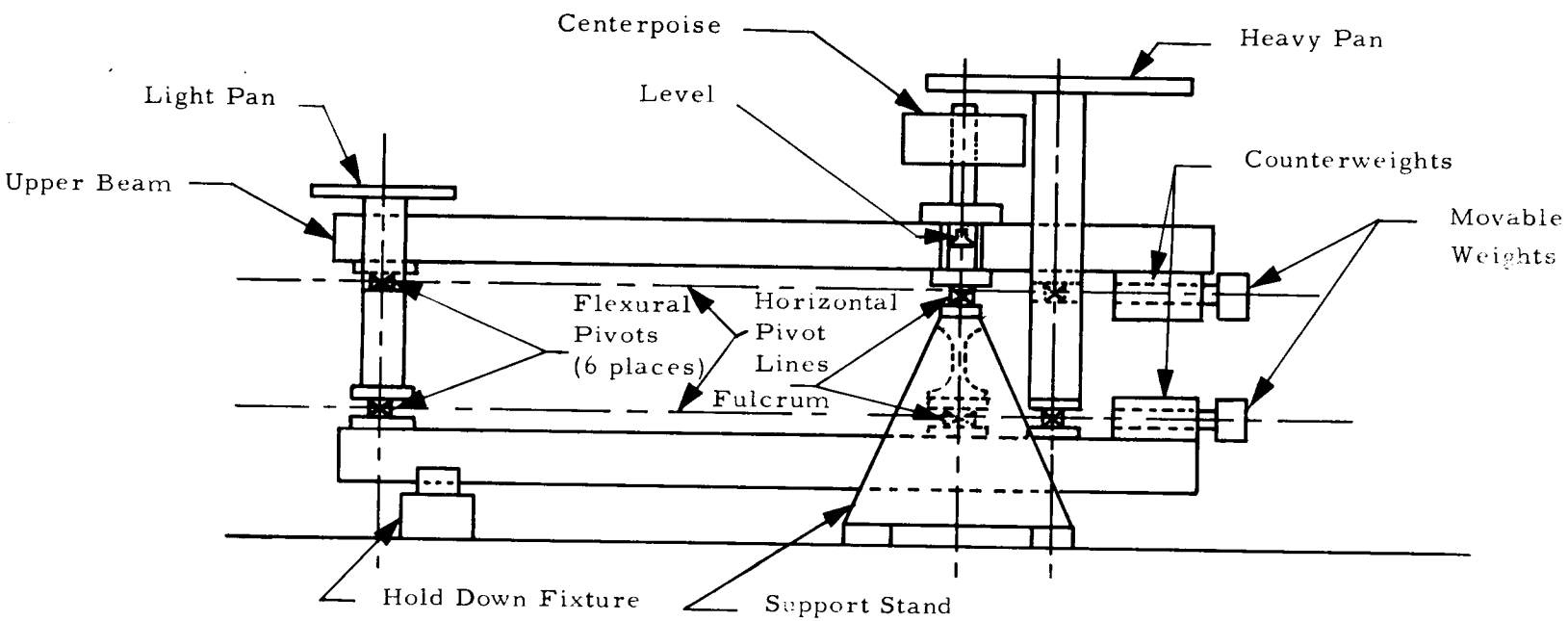

FIGURE 152

LABORATORY WEIGHING SYSTEM

by increasing the weight of the centerpoise or by increasing the distance from the centerpoise to the main fulcrum pivot point. The maximum sensitivity is obtained when the system is balanced according to the equation:

$$Wh \sin \theta = K\theta \tag{327}$$

where:

h = The vertical distance from the main fulcrum pivot point to the center of mass of the centerpoise assembly.
W= The weight of the centerpoise assembly.
θ = The oscillation angle from the "at rest" position.
K = The combined bending spring constants of all the flexures.

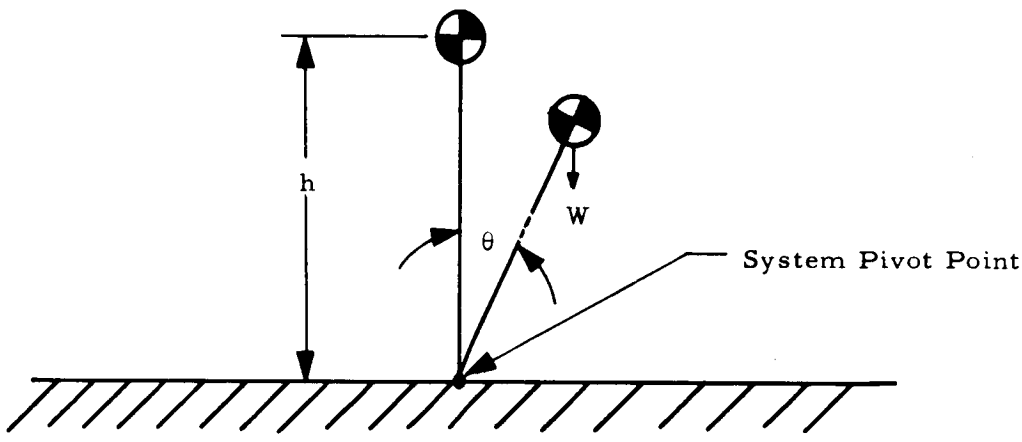

Figure 153. Effect of Centerpoise Weight on Balance Stability.

Obviously, when the term on the left side of the equation is greater than the term on the right side the system is unstable and will come to rest only when the system is restrained by some external force, in this case the hold-down fixture. During calibration the height of the centerpoise is adjusted so that the system is just barely stable and will return to the unloaded, level condition when the weights in the weight pans balance each other. A model 394-T coincidence level purchased from the Brunson Instrument Co., Kansas City, Mo. is used to indicate the level or balanced condition of the system. The level is accurate within two seconds of arc. If, during the weighing of an

unknown the centerpoise, which weighs approximately 66 lbs, is allowed to come to rest with a two second deviation from the unloaded, level condition the indicated error is .0024 lbs which would be 24 parts per million for a 100 pound object. It's obvious that for precise weight determination it is very important that the level indicator be very sensitive.

2.5.3.2 Counterweights

The function of the counterweights is simply to balance the system in the unloaded condition. The weights required for the counterweights are determined by summing the moments about the fulcrum pivots. An adjustable weight is provided on each counterweight for minute adjustment.

2.5.3.3 Flexural Pivots

In order to eliminate the many variables associated with knife edges and bearings it was decided that flexures should be used for pivot points. The use of flexures eliminates such variables as slop, wear and friction. If the bending spring constant is counteracted by a centerpoise as was described in the preceeding paragraph, the only consideration involved with the use of flexures as pivots is alignment. If the bending element of the flexure is not perpendicular to the pivot line (See Figure 152) the effective spring constant is increased. Because the accuracy of the system decreases with an increase in the spring constant it is very important that the bending elements be aligned with each other and are perpendicular to the pivot lines.

After evaluating flexures from several sources it was decided that Ormond, Incorporated of California produced the most efficient flexures, therefore they were purchased from this source.

The Laboratory optical system was used to align the flexures at assembly.

2.5.4 Calibration

After the balance was assembled, it was calibrated as described below. It was desirable to calibrate the balance with weights up to 1000 pounds, but 400 pounds was the upper limit of the calibration range due to the limited laboratory weights.

1. The weighing system was balanced in the unloaded condition by means of the movable weights in the counterweights.

2. The centerpoise height was adjusted for optimum sensitivity.

3. The system was balanced again.

4. A 10 pound laboratory weight was placed on the light weight pan and two 50 pound weights were placed on the heavy weight pan.

5. By noting the direction of rotation of the system, the heavy end was determined and the flexure mounting pads were shifted accordingly.

6. The weights were removed from the weight pans and the system was rebalanced in the unloaded condition.

7. Steps 4, 5, and 6 were repeated (several times) until perfect balance of the system was obtained--both in the unloaded condition and with 10 to 1 weight ratio. This balanced condition indicates that the 10 to 1 length ratio between the moment arms of the two weights pans has been attained.

2.6 GENERAL PROJECTS

2.6.1 Low Gravity Test Packages

2.6.1.1 Introduction

A current project being conducted by MSFC-Propulsion & Vechicle Engineering Laboratory utilizes a drop package to study the behavior of liquids in a partially filled container under low gravity conditions. One of the requirements of the project is that the package remain level within two degrees during the drop time of about four seconds. Package tilts somewhat greater than this have been experienced in previous tests. For these tests the packages were balanced so that the center of mass falls on the the thrust axis. No attempt was made to correct for mass shifts due to the loss of compressed gas, motion picture film movement, and liquid tank movements during the drop.

This report describes a study by the Mass Metrology Laboratory to determine the effects of these shifting masses on the attitude of the falling drop package. The Mass Metrology Laboratory is operated by SPACO, INC. for the Propulsion & Vehicle Engineering Laboratory of MSFC.

2.6.1.2 Procedure

A drop package of the latest design was obtained for approximately two weeks, during which time the necessary physical measurements were made for this investigation. Three effects were to be studied specifically. First, during the drop the acceleration is controlled by discharging compressed nitrogen through a thrust nozzle on the vertical axis of the package. The bottle of nitrogen is mounted near the outside of the package, so that as the mass of the gas reduces, a moment about a horizontal axis is generated, which tends to cause rotation of the package. The second variable is the movement of the film in the motion picture camera which photographs the liquid tank during the drop. The third effect is the movement of the liquid tank itself, which is done in steps of 0.1 inch to introduce transient lateral accelerations to the tank.

The method used to measure the effects of these movements was to place the package in a static balance initially, and measure the unbalance moment resulting when the mass shift occurred. The device used for measuring the moments was a modified Bytrex center of gravity locator. This consists basically of a table supported by a rectangular column. Strain gages are bonded to the four vertical sides of the column to detect bending produced by tilting the table. Figure 154 shows the device. A voltage output from an amplifier driven by the strain gages is monitored on a digital voltmeter. This voltage is proportional to moment about a given axis. The instrument is designed so that moment can be resolved into two perpendicular components.

The procedure used to measure the moments was as follows: The C. G. locator was set up, energized, and allowed to stabilize for about four hours.

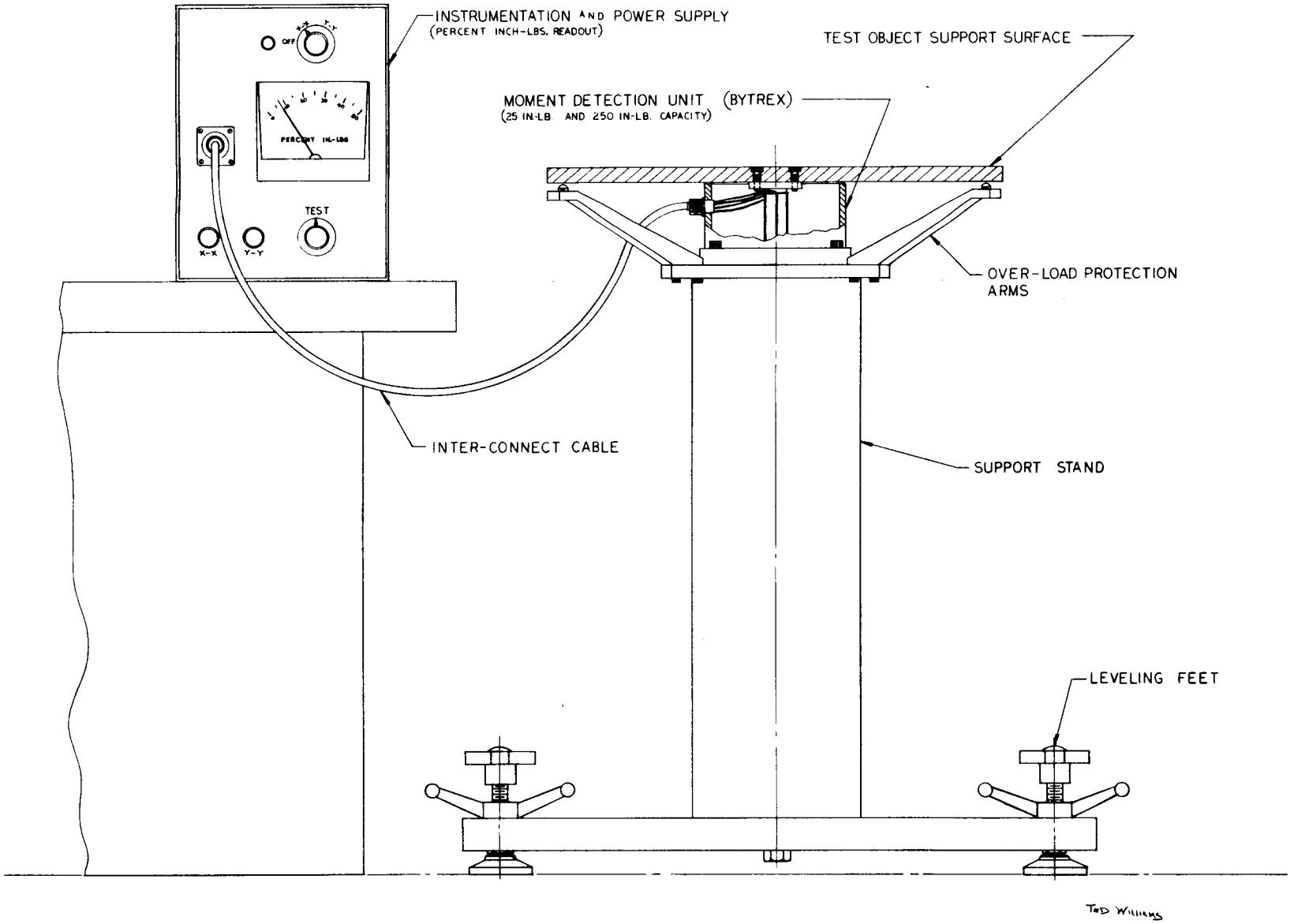

FIGURE 154
MOMENT DETECTION SYSTEM FOR CENTER OF GRAVITY DETERMINATION

The indicator was zeroed in both the x and y axes with the support table empty. The C. G. locator was calibrated by placing standard weights at known distances from the vertical axis and recording the output voltage. The drop package was then placed on the table and the nozzle centerline positioned over the vertical axis of the table. Weights were then placed in appropriate positions on the package to locate its center of gravity on the thrust axis. Each of the mass variables was then introduced in increments and the resulting unbalance voltage recorded in both horizontal axes. The bottle was discharged in 500 psi increments from its initial pressure of 2800 psi, down to 1000 psi. The camera was operated for ten second intervals, and the moment recorded at the end of each interval. The liquid tank was shifted in increments of 0.1 inch, up to a total of 1 inch. Two complete runs were made of each test, and the results averaged.

The data recorded was converted into torque about the x and y axes, as a function of time and acceleration, so that angular acceleration could be calculated.

After completion of the moment tests, the drop package was mounted on the air bearing table and the moment of inertia was measured about the same pair of axes. The procedure used here is given below:

The center of gravity of the package along the z axis was found with the Bytrex C. G. locator. The z axis is the thrust nozzle axis. The package was then mounted on the large air bearing table with the C. G. on the oscillation axis of the table. The moment of inertia was determined by measuring the period time of the torsional pendulum, such as done many times previously. Figure 155 shows the package mounted on the air bearing table

With the torque and corresponding moment of inertia about the horizontal axis, it was then possible to calculate the package tilt as a function of time, using conventional methods. The angular acceleration of the drop package is given by:

$$\alpha = \frac{T}{I} \tag{327}$$

where: α = Angular acceleration - radians/sec^2

T = Torque - inch-lb.

I = Moment of Inertia - inch-lb-sec^2

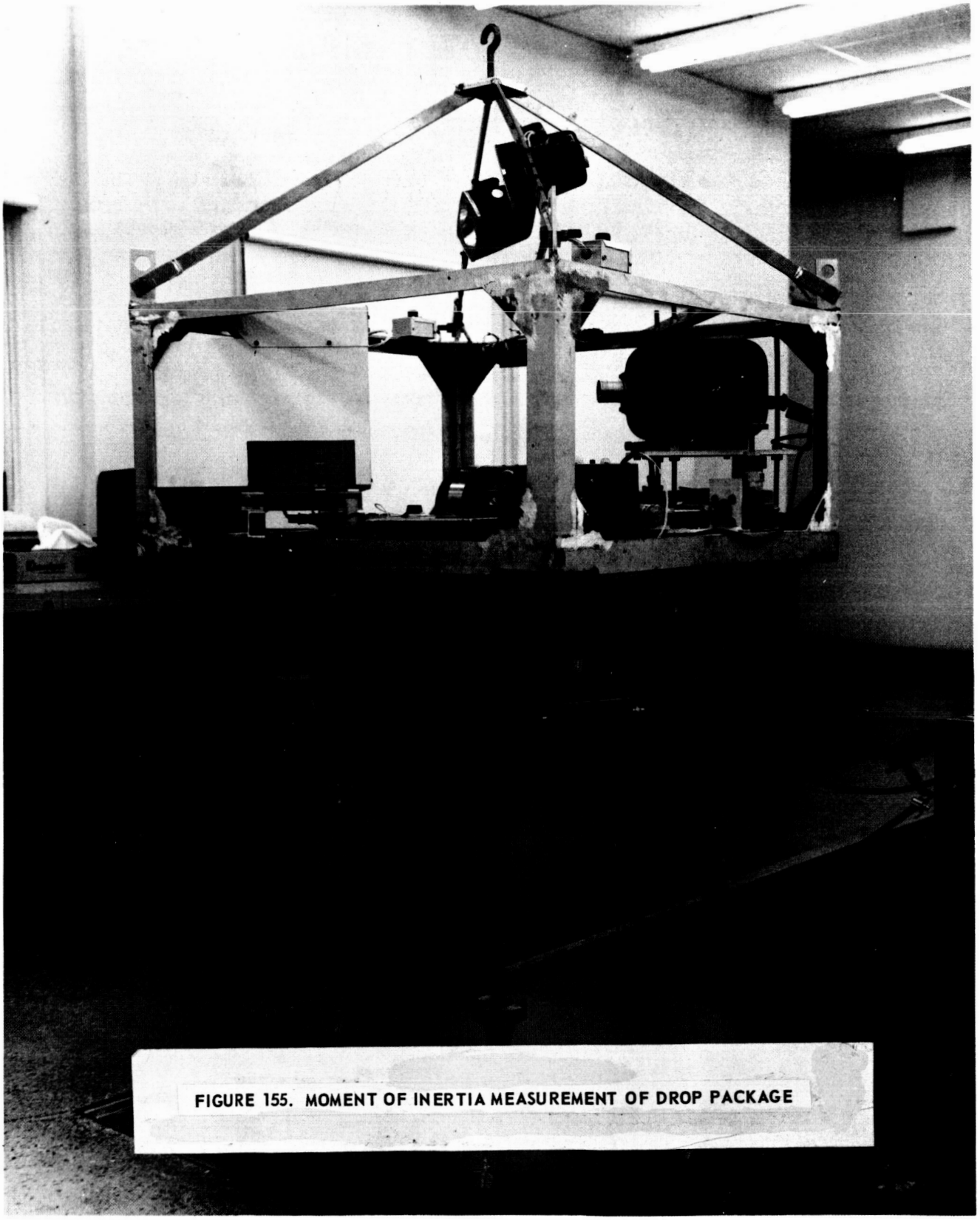

FIGURE 155. MOMENT OF INERTIA MEASUREMENT OF DROP PACKAGE

However, T is a function of time and the linear acceleration of the package, thus

$$T = f(t, a)$$

$$t = \text{time, seconds} \tag{328}$$

$$a = \text{acceleration, G.}$$

To calculate the change in angle of the package, the following is used, assuming the initial angle zero and angular velocity are zero

$$\theta = \frac{1}{2}\alpha t^2 \tag{329}$$

where: θ = angle of bottom of package with horizontal-radians.

The torque shown as a function of time will be linear in the case of the nitrogen bottle and the camera, since they are displacing mass at a constant rate. Also, the linear acceleration produced by the thrust nozzle can be considered

$$T = Kt \tag{330}$$

where: K = appropriate constant - $\frac{\text{in-lb}}{\text{G-sec}}$

Therefore, the angular shift is given by:

$$\theta = \frac{Kt^3 a}{2I} \tag{331}$$

The G is inserted in the denominator of Equation 330 to indicate that the tilt angle calculated must be multiplied by the linear acceleration of the package to get the actual angle. Since the moment measurements from the tests are based on a field of one G acceleration, it is convenient to use it as a unit in the equations rather than more conventional units. Had (a) been used in in/sec^2, for example, K would then be in lb-sec, and the calculated would be multiplied by acceleration in in/sec^2 units.

For the case of the shifting tank, the torque is not a continuous function of time, and the only practical method of calculating package tilt is to assume a typical program sequence during the drop and calculate the tilt in steps. This is the method used in this analysis.

2.6.1.3 Results

The moment of inertia measurement results are given in Table 55.

TABLE 55

MOMENT OF INERTIA MEASUREMENT OF DROP PACKAGE

$$I_x = 100.076 \text{ in-lb-sec}^2$$

$$I_y = 88.197 \text{ in-lb-sec}^2$$

$$I_z = 139.016 \text{ in-lb-sec}^2$$

The axes are as shown in Figure 156. This coordinate system was used throughout the test. The results of the moment measurement test of the discharging gas bottle are given in Table 56. In order to obtain a time function of moment, a constant pressure loss rate of 100 psi per sec and a constant linear acceleration of .032G. Calculations of the package tilt at different times are given in Table 57. The maximum tilt will occur in the X axis, and will be about one degree at the end of the drop from the gas bottle discharge alone.

The results of the moment measurement test of the motion picture camera are shown in Table 58. The moments are considerably less than from the gas bottle because the film moves only a very short distance in the camera. The data has been converted to units of in-lb/G-sec, as before. In Table 59 are calculations of the package tilt resulting from this movement, assuming an acceleration of .032G. An attempt was also make to detect the dynamic effects of the film transfer, but the magnitude was such that they were marked by other factors such as random air disturbances and instrumentation noise.

The results of the tank shift test are given in Tables 60 and 61. Table 60 is for a liquid level 0.3" above the tank parting line, and Table 61 is for a level 1.85" above the line. As can be seen by comparing Tables 60 and 61, the moment for a given tank displacement is in a few cases greater for the 0.3" liquid level than the 1.85" level. This is attributed to normal measurement errors, such as air movements, zero drift, and instrumentation noise.

FIGURE 156

DROP PACKAGE COORDINATE ORIENTATION

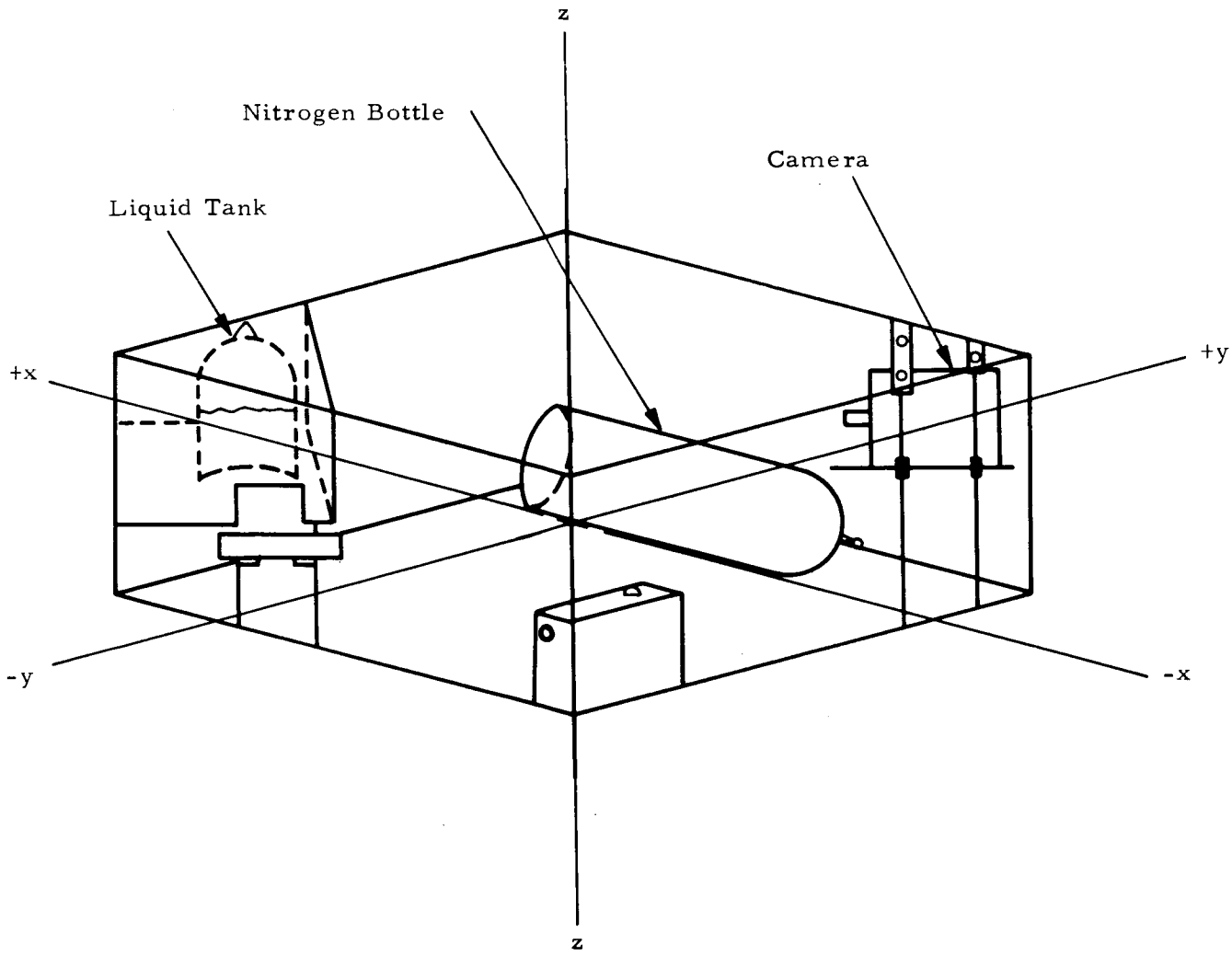

TABLE 56

EFFECT OF GAS BOTTLE DISCHARGE
ON UNBALANCE MOMENT ABOUT X AND Y AXES

Pressure in Bottle psi	y axis Moment-inch-lb/G Run #1	y axis Moment-inch-lb/G Run #2	y axis Moment-inch-lb/G Avg.	y axis Moment Change $\frac{\text{in-lb}}{\text{G-psi}} \times 10^{-3}$	y axis Moment Change $\frac{\text{in-lb}}{\text{G-sec*}}$	x axis Moment-inch-lb/G Run #1	x axis Moment-inch-lb/G Run #2	x axis Moment-inch-lb/G Avg.	x axis Moment Change $\frac{\text{in-lb}}{\text{G-psi}} \times 10^{-3}$	x axis Moment Change $\frac{\text{in-lb}}{\text{G-sec}}$
2800	0	0	0	-----	------	0	0	0	-----	-----
2500	- 1.96	- 2.63	- 2.30	-7.67	-0.767	- 4.69	- 5.40	- 5.05	-16.8	-1.68
2000	- 6.48	- 7.50	- 6.99	-9.38	-0.938	-13.77	-15.52	-14.64	-19.2	-1.92
1500	-10.72	-12.80	-11.76	-9.55	-0.955	-24.13	-25.90	-25.01	-20.7	-2.07
1000	-15.45	-17.70	-16.57	-9.62	-0.962	-35.48	-35.95	-35.72	-21.4	-2.14
average				-9.05	-0.905				-19.5	-1.95

*Assuming pressure loss rate of 100 psi per second.

TABLE 57

DROP PACKAGE TILT CAUSED
BY GAS BOTTLE DISCHARGE

Time After Drop-Seconds	Tilt Angle — Degrees From Initial Angle	
	x axis	y axis
0	0	0
0.5	- .0022	- .0012
1.0	- .0179	- .0094
1.5	- .0603	- .0317
2.0	- .143	- .0752
2.5	- .279	- .147
3.0	- .482	- .254
3.5	- .766	- .403
4.0	-1.14	- .602
4.5	-1.63	- .857
5.0	-2.23	-1.176

$$\theta_x = \frac{1}{2}\alpha t^2 = \frac{1}{2}\left[\frac{1.95 \cdot t \cdot .032}{100.076}\right] t^2 \cdot \frac{180}{\pi} \text{ degrees} = .01786t^3$$

$$\theta_y = \frac{1}{2}\left[\frac{.905 \cdot t \cdot .032}{88.197}\right] t^2 \cdot \frac{180}{\pi} \text{ degrees} = .009406t^3$$

TABLE 58

EFFECT OF MOTION PICTURE CAMERA
OPERATION ON UNBALANCE MOMENT

Time-Seconds	y axis Moment-in-lbs./G			K Moment Change in-lb/G-sec	x axis Moment-in-lbs./G			K Moment Change in-lb/G-sec
	Run #1	Run #2	M_i Avg.		Run #1	Run #2	M_i Avg.	
0	0	0	0	-------	0	0	0	------
10	-.0572	-.0817	-.0694	-.00694	-.125	-.125	-.125	-.0125
20	-.123	-.163	-.143	-.00736	-.227	-.251	-.239	-.0114
30	-.221	-.253	-.237	-.00941	-.344	-.368	-.356	-.0117
40	-.319	-.343	-.331	-.00940	-.446	-.525	-.485	-.0129
50		-.441	-.441	-.01104		-.642	-.642	-.0157
average				-.00883				-.0146

TABLE 59

DROP PACKAGE TILT CAUSED BY
OPERATION OF MOTION PICTURE CAMERA

Time after Drop-sec	Tilt Angle-Degrees x 10^{-3}							
	Camera Started at Drop		Camera Operated 10 seconds before drop		Camera Operated 20 seconds before drop		Camera Operated 30 seconds before drop	
	x axis	y axis	x axis	y axis	x axis	y axis	x axis	y axis
0	0	0	0	0	0	0	0	0
0.5	- .0167	- .0115	- .3006	- .1893	- .5603	- .3811	- .8286	- .6280
1.0	- .1337	- .0917	- 1.2596	- .7934	- 2.2937	- 1.5628	- 3.3682	- 2.5612
1.5	- .4514	- .3097	- 2.963	- 1.8665	- 5.2784	- 3.6025	- 7.6991	- 5.8727
2.0	- 1.0700	- .7342	- 5.496	- 4.0395	- 9.5927	- 6.5574	-13.9017	-10.6361
2.5	- 2.0900	- 1.434	- 8.9457	- 5.6355	-15.3149	-10.4851	-22.0564	-16.9246
3.0	- 3.6110	- 2.4780	-13.3970	- 8.4398	-22.5235	-15.4428	-32.2435	-24.8115
3.5	- 5.7340	- 3.9350	-18.9362	-11.9293	-31.2966	-21.4879	-44.5435	-34.3703
4.0	- 8.5590	- 5.8688	-25.6490	-16.1583	-41.7126	-28.6778	-58.1793	-45.6744
4.5	-12.1872	- 8.3561	-33.6214	-21.1807	-53.8499	-37.0700	-75.8035	-58.7969
5.0	-16.7177	-11.4625	-42.9392	-27.0507	-71.2218	-46.7217	-94.9243	-73.8114

$$\theta = \frac{1}{2}\alpha t^2 = \frac{180t^2a}{2\pi}\left[\frac{M_i + Kt}{1}\right]$$

where: M_i = initial moment $\frac{\text{in-lb}}{G}$

K = moment per time $\frac{\text{in-lb}}{\text{G-sec}}$

a = linear acceleration
= .032G

TABLE 60

EFFECT OF LIQUID TANK RELOCATION ON UNBALANCE MOMENT
LIQUID LEVEL .3" ABOVE PARTING LINE

Tank Location inches from center line	y axis Moment/G Run #1	y axis Moment/G Run #2	y axis Moment/G Avg.	x axis Moment/G Run #1	x axis Moment/G Run #2	x axis Moment/G Avg.
0	0	0	0	0	0	0
0.1	- .908	- 1.162	- 1.035	- 1.100	- 1.310	- 1.205
0.2	- 1.931	- 2.046	- 1.988	- 2.208	- 2.309	- 2.258
0.3	- 2.946	- 3.044	- 2.995	- 3.307	- 3.354	- 3.331
0.4	- 3.944	- 4.009	- 3.977	- 4.337	- 4.485	- 4.411
0.5	- 4.844	- 4.951	- 4.888	- 5.437	- 5.530	- 5.484
0.6	- 5.876	- 5.982	- 5.929	- 6.615	- 6.646	- 6.630
0.7	- 7.038	- 6.890	- 6.964	- 7.644	- 7.722	- 7.683
0.8	- 7.921	- 7.921	- 7.921	- 8.736	- 8.783	- 8.760
0.9	- 8.838	- 8.920	- 8.879	- 9.813	- 9.891	- 9.852
1.0	-10.622	-10.622	-10.622	-10.694	-10.694	-10.694

TABLE 61

EFFECT OF LIQUID TANK RELOCATION ON UNBALANCE MOMENT
LIQUID LEVEL 1.85" ABOVE PARTING LINE

Tank Location inches from center line	y axis Moment-in-lb/G Run #1	Run #2	M_i Avg.	x axis Moment-in-lb/G Run #1	Run#2	M_i Avg.
0	0	0	0	0	0	0
0.1	- .743	- .823	- .783	- 1.048	- 1.032	- 1.040
0.2	- 1.805	- 1.893	- 1.849	- 2.218	- 2.226	- 2.222
0.3	- 2.835	- 2.979	- 2.907	- 3.347	- 3.388	- 3.367
0.4	- 3.946	- 4.058	- 4.002	- 4.517	- 4.565	- 4.541
0.5	- 5.152	- 5.112	- 5.132	- 5.808	- 5.719	- 5.764
0.6	- 6.182	- 6.142	- 6.162	- 6.962	- 6.881	- 6.921
0.7	- 7.220	- 7.205	- 7.212	- 8.115	- 7.977	- 8.046
0.8	- 8.323	- 8.315	- 8.319	- 9.318	- 9.261	- 9.289
0.9	- 9.401	- 9.401	- 9.401	-10.496	-10.414	-10.455
1.0	-10.375	-10.375	-10.375	-11.625	-11.625	-11.625

Typical zero drift for the equipment after warm up is $\pm$ 0.04% of full scale, which is about $\pm$ 0. 05 in-lb moment for the unit used. In Tables 62 through 67 are calculations of the rotation of the package under different sets of tests conditions. The assumption was made that the package was balanced with the tank in the zero position and the drop thus begins with an initial angular acceleration, depending on the amount of displacement. When the solenoid is energized, the tank will return to the balanced position, reducing the acceleration to zero and causing the angular velocity to remain constant for the remainder of the drop. Tables 62 and 63 assumes the shift occurs one second after the drop, Tables 64 and 65 for 2 seconds, etc. Tilt for the package with a lequid level 0. 3" above the parting line was not calculated, since it can be seen from Tables 60 and 61 that the difference is quite small. The X-axis tilt angles tabulated in Tables 57, 59, 63, 65, and 67 are plotted against time in Figure 157.

For all of the angular displacement calculations, the simplifying assumption was made that the tilt angle remains small. Therefore, some small error can be expected at large angles, but it is of no consequence in view of this investigation. Also, the fact that the moment of inertia of the package does not remain constant results in an additional error, which is also insignificant.

2. 6. 1. 4 Conclusions

The test results show that the rotation caused by the various mass movements are, at worst barely acceptable. The camera film transfer proved to be an insignificant factor, but the effect from the bottle discharge and tank impulse was considerably greater. The only condition which could cause the package tilt to exceed two degrees during the drop is maintaining the tank in its fully displaced position of one inch from balance for three seconds after drop. Under these conditions the gas bottle mass loss and liquid tank offset would each contribute slightly over one degree rotation at the end of four seconds. The use of a smaller tank offset distance and/or a shorter time before impulse would reduce the package tilt. Likewise, an increase or decrease in the normal .032G package acceleration would cause a proportionate change in the tilt from all causes.

It appears that, except for extreme sets of conditions, the drop package tilt can be kept within the two degree maximum. Tilt can be minimized by shifting the liquid tank as quickly after drop as possible, and by avoiding any changes to the package after it has been balanced.

TABLE 62

DROP PACKAGE TILT CAUSED BY SHIFT OF LIQUID
TANK ONE SECOND AFTER DROP
LIQUID LEVEL 1.85" ABOVE PARTING LINE

Tilt Angle — degrees for given shift distance

x axis

Time After Drop Seconds	0.1 inch	0.2 inch	0.3 inch	0.4 inch	0.5 inch	0.6 inch	0.7 inch	0.8 inch	0.9 inch	1.0 inch
0	0	0	0	0	0	0	0	0	0	0
0.5	-.00238	-.00509	-.00771	-.01039	-.01319	-.01584	-.01842	-.02127	-.02394	-.02662
1.0	-.00953	-.02035	-.03084	-.04159	-.05276	-.06339	-.07370	-.08509	-.09577	-.10649
1.5	-.01429	-.03053	-.04626	-.06239	-.07914	-.09509	-.11055	-.12764	-.14366	-.15973
2.0	-.01905	-.04071	-.06168	-.08319	-.10553	-.12679	-.14741	-.17018	-.19154	-.21298
2.5	-.02382	-.05088	-.07711	-.10399	-.13191	-.15849	-.18426	-.21273	-.23943	-.26622
3.0	-.02858	-.06106	-.09253	-.12479	-.15829	-.19019	-.22111	-.25527	-.28731	-.31947
3.5	-.03334	-.07124	-.10795	-.14559	-.18467	-.22189	-.25796	-.29781	-.33520	-.37271
4.0	-.03811	-.08142	-.12337	-.16638	-.21105	-.25359	-.29481	-.34036	-.38309	-.42596
4.5	-.04287	-.09159	-.13879	-.18718	-.23743	-.28529	-.33167	-.38291	-.43097	-.47920
5.0	-.04763	-.10177	-.15421	-.20798	-.26381	-.31699	-.36850	-.42545	-.47886	-.53245

$$\theta = \frac{1}{2}\left[\frac{M_i a}{I}\right] t_1^{\,2} + \omega t_2$$

$$= \frac{90 M_i a t_1}{I\pi}\,(t_1 + t_2)$$

where: M_i = initial unbalance moment, $\frac{\text{in-lb}}{G}$

a = linear acceleration = .032G

t_1 = time from drop to tank shift-seconds

t_2 = remainder of time

ω = angular velocity at end of t_1, $= t_1 \left[\frac{M_i a}{I}\right]$

TABLE 63

DROP PACKAGE TILT CAUSED BY SHIFT OF LIQUID
TANK ONE SECOND AFTER DROP
LIQUID LEVEL 1.85" ABOVE PARTING LINE

Tilt Angle — degrees for given shift distance

Time After Drop Seconds	y axis 0.1 inch	0.2 inch	0.3 inch	0.4 inch	0.5 inch	0.6 inch	0.7 inch	0.8 inch	0.9 inch	1.0 inch
0	-. 0	0	0	0	0	0	0	0	0	0
0.5	-.00203	-.00470	-.00755	-.01039	-.01333	-.01600	-.01873	-.02160	-.02441	-.02694
1.0	-.00813	-.01921	-.03021	-.04158	-.05332	-.16402	-.07493	-.08643	-.09767	-.10779
1.5	-.01219	-.02881	-.04531	-.06237	-.07998	-.09603	-.11239	-.12964	-.14650	-.16168
2.0	-.01626	-.03842	-.06042	-.08316	-.10664	-.12804	-.14986	-.17286	-.19534	-.21558
2.5	-.02032	-.04802	-.07552	-.10395	-.13330	-.16005	-.18732	-.21607	-.24417	-.26947
3.0	-.02439	-.05763	-.09063	-.12474	-.15996	-.19206	-.22479	-.25929	-.29301	-.32337
3.5	-.02845	-.06723	-.10573	-.14553	-.18662	-.22407	-.26225	-.30250	-.34184	-.37726
4.0	-.03252	-.07684	-.12084	-.16632	-.21328	-.25608	-.29972	-.34572	-.39068	-.43116
4.5	-.03658	-.08644	-.13594	-.18711	-.23994	-.28809	-.33718	-.38893	-.43951	-.48505
5.0	-.04065	-.09605	-.15105	-.20790	-.26660	-.32010	-.37465	-.43215	-.48835	-.53895

$$\theta = \frac{1}{2}\left[\frac{M_i a}{I}\right] t_1^{\,2} + \omega t_2$$

$$= \frac{90 M_i a t_1}{I\pi}\,(t_1 + t_2)$$

where:

M_i = initial unbalance moment, $\frac{\text{in-lb}}{G}$

a = linear acceleration = .032G

t_1 = time from drop to tank shift-seconds

t_2 = remainder of time

ω = angular velocity at end of t_1, $= t_1 \left[\frac{M_i a}{I}\right]$

TABLE 64

DROP PACKAGE TILT CAUSED BY SHIFT OF LIQUID
TANK TWO SECONDS AFTER DROP
LIQUID LEVEL = 1.85" ABOVE PARTING LINE
ACCELERATION = .032G

Tilt Angle — degrees for given shift distance

x axis

Time After Drop Seconds	0.1 inch	0.2 inch	0.3 inch	0.4 inch	0.5 inch	0.6 inch	0.7 inch	0.8 inch	0.9 inch	1.0 inch
0	0	0	0	0	0	0	0	0	0	0
0.5	-.00238	-.00508	-.00771	-.01039	-.01319	-.01584	-.01842	-.02127	-.02394	- .02662
1.0	-.00952	-.02035	-.03084	-.04159	-.05279	-.06339	-.07370	-.08508	-.09576	- .10648
1.5	-.02142	-.04578	-.06939	-.09357	-.11877	-.14262	-.16582	-.19143	-.21546	- .23958
2.0	-.03808	-.08140	-.12336	-.16636	-.21116	-.25356	-.29480	-.34032	-.38304	- .42592
2.5	-.04760	-.10175	-.15420	-.20795	-.26395	-.31695	-.36850	-.42540	-.47880	- .53240
3.0	-.05712	-.12210	-.18504	-.24954	-.31674	-.38034	-.44220	-.51048	-.57456	- .63888
3.5	-.06664	-.14245	-.21588	-.29113	-.36953	-.44373	-.51590	-.59556	-.67032	- .74536
4.0	-.07616	-.16280	-.24672	-.33272	-.42232	-.50712	-.58960	-.68064	-.76608	- .85184
4.5	-.08568	-.18315	-.27756	-.37431	-.47511	-.57051	-.66330	-.76572	-.86184	- .95832
5.0	-.09520	-.20350	-.30840	-.41590	-.52790	-.63390	-.73700	-.85080	-.95760	-1.06480

TABLE 65

DROP PACKAGE TILT CAUSED BY SHIFT OF LIQUID
TANK TWO SECONDS AFTER DROP
LIQUID LEVEL = 1.85" ABOVE PARTING LINE
ACCELERATION = .032G

Tilt Angle — degrees for given shift distance

y axis

Time After Drop Seconds	0.1 inch	0.2 inch	0.3 inch	0.4 inch	0.5 inch	0.6 inch	0.7 inch	0.8 inch	0.9 inch	1.0 inch
0	0	0	0	0	0	0	0	0	0	0
0.5	-.00203	-.00470	-.00755	-.01039	-.01333	-.01600	-.01873	-.02160	-.02441	-.02694
1.0	-.00813	-.01921	-.03020	-.04158	-.05332	-.06402	-.07493	-.08643	-.09767	-.10779
1.5	-.01829	-.04322	-.06795	-.09355	-.11997	-.14404	-.16791	-.19446	-.21975	-.24252
2.0	-.03252	-.07684	-.12080	-.16632	-.21328	-.25608	-.29852	-.34572	-.39068	-.43116
2.5	-.04065	-.09605	-.15100	-.20790	-.26660	-.32010	-.37315	-.43215	-.48835	-.53895
3.0	-.04878	-.11526	-.18120	-.24948	-.31992	-.38412	-.44778	-.51858	-.58602	-.64674
3.5	-.05691	-.13447	-.21140	-.29106	-.37324	-.44814	-.52241	-.60501	-.68369	-.75453
4.0	-.06504	-.15368	-.24160	-.33264	-.42656	-.51216	-.59704	-.69144	-.78136	-.86232
4.5	-.07317	-.17289	-.27180	-.37422	-.47988	-.57618	-.67167	-.77787	-.87903	-.97011
5.0	-.08130	-.19210	-.30200	-.41580	-.53320	-.64020	-.74930	-.86430	-.97670	-1.07790

TABLE 66

DROP PACKAGE TILT CAUSED BY SHIFT OF LIQUID
TANK THREE SECONDS AFTER DROP
LIQUID LEVEL = 1.85" ABOVE PARTING LINE
ACCELERATION = .032G

Tilt Angle — degrees for given shift distance

x axis

Time After Drop Seconds	0.1 inch	0.2 inch	0.3 inch	0.4 inch	0.5 inch	0.6 inch	0.7 inch	0.8 inch	0.9 inch	1.0 inch
0	0	0	0	0	0	0	0	0	0	0
0.5	-.00238	-.00508	-.00771	-.01039	-.01319	-.01584	-.01842	-.02127	-.02394	-.02662
1.0	-.00952	-.02035	-.03084	-.04159	-.05279	-.06339	-.07370	-.08508	-.09576	-.10648
1.5	-.02142	-.04578	-.06939	-.09357	-.11877	-.14262	-.16582	-.19143	-.21546	-.23958
2.0	-.03808	-.08140	-.12336	-.16636	-.21116	-.25356	-.29480	-.34032	-.38304	-.42592
2.5	-.05950	-.12718	-.19275	-.25993	-.32993	-.39618	-.46062	-.53175	-.59850	-.66550
3.0	-.08568	-.18315	-.27756	-.37431	-.47511	-.57051	-.66330	-.76572	-.86184	-.95832
3.5	-.09996	-.21367	-.32382	-.43669	-.55429	-.66559	-.77385	-.89334	-1.00548	-1.11804
4.0	-.11424	-.24420	-.37008	-.49908	-.63348	-.76068	-.88440	-1.02096	-1.14912	-1.27776
4.5	-.12852	-.27472	-.41634	-.56146	-.71266	-.85576	-.99495	-1.14858	-1.29276	-1.43748
5.0	-.14280	-.30525	-.46260	-.62385	-.79185	-.95085	-1.10550	-1.27620	-1.43640	-1.59720

TABLE 67

DROP PACKAGE TILT CAUSED BY SHIFT OF LIQUID
TANK THREE SECONDS AFTER DROP
LIQUID LEVEL = 1.85" ABOVE PARTING LINE
ACCELERATION = .032G

Tilt Angle — degrees for given shift distance

y axis

Time After Drop Seconds	0.1 inch	0.2 inch	0.3 inch	0.4 inch	0.5 inch	0.6 inch	0.7 inch	0.8 inch	0.9 inch	1.0 inch
0	0	0	0	0	0	0	0	0	0	0
0.5	-.00203	-.00470	-.00755	-.01039	-.01333	-.01600	-.01873	-.02160	-.02441	-.02694
1.0	-.00813	-.01921	-.03020	-.04158	-.05332	-.06402	-.07493	-.08643	-.09767	-.10779
1.5	-.01829	-.04322	-.06795	-.09355	-.11997	-.14404	-.16791	-.19446	-.21975	-.24252
2.0	-.03252	-.07684	-.12080	-.16632	-.21328	-.25608	-.29852	-.34572	-.39068	-.43116
2.5	-.05081	-.12006	-.18875	-.25987	-.33325	-.40012	-.46839	-.54018	-.61043	-.67368
3.0	-.07317	-.17289	-.27180	-.37422	-.47988	-.57618	-.67437	-.77787	-.87903	-.97011
3.5	-.08536	-.20170	-.31710	-.43659	-.55986	-.67221	-.78676	-.90751	-1.02553	-1.13179
4.0	-.09756	-.23052	-.36240	-.49896	-.63984	-.76824	-.89916	-1.03716	-1.17204	-1.29348
4.5	-.10975	-.25933	-.40770	-.56133	-.71982	-.86427	-1.01155	-1.16680	-1.31854	-1.45516
5.0	-.12195	-.28815	-.45300	-.62370	-.79980	-.96030	-1.12395	-1.29645	-1.46505	-1.61685

FIGURE 157

PACKAGE TILT CAUSED BY VARIOUS MASS MOVEMENTS

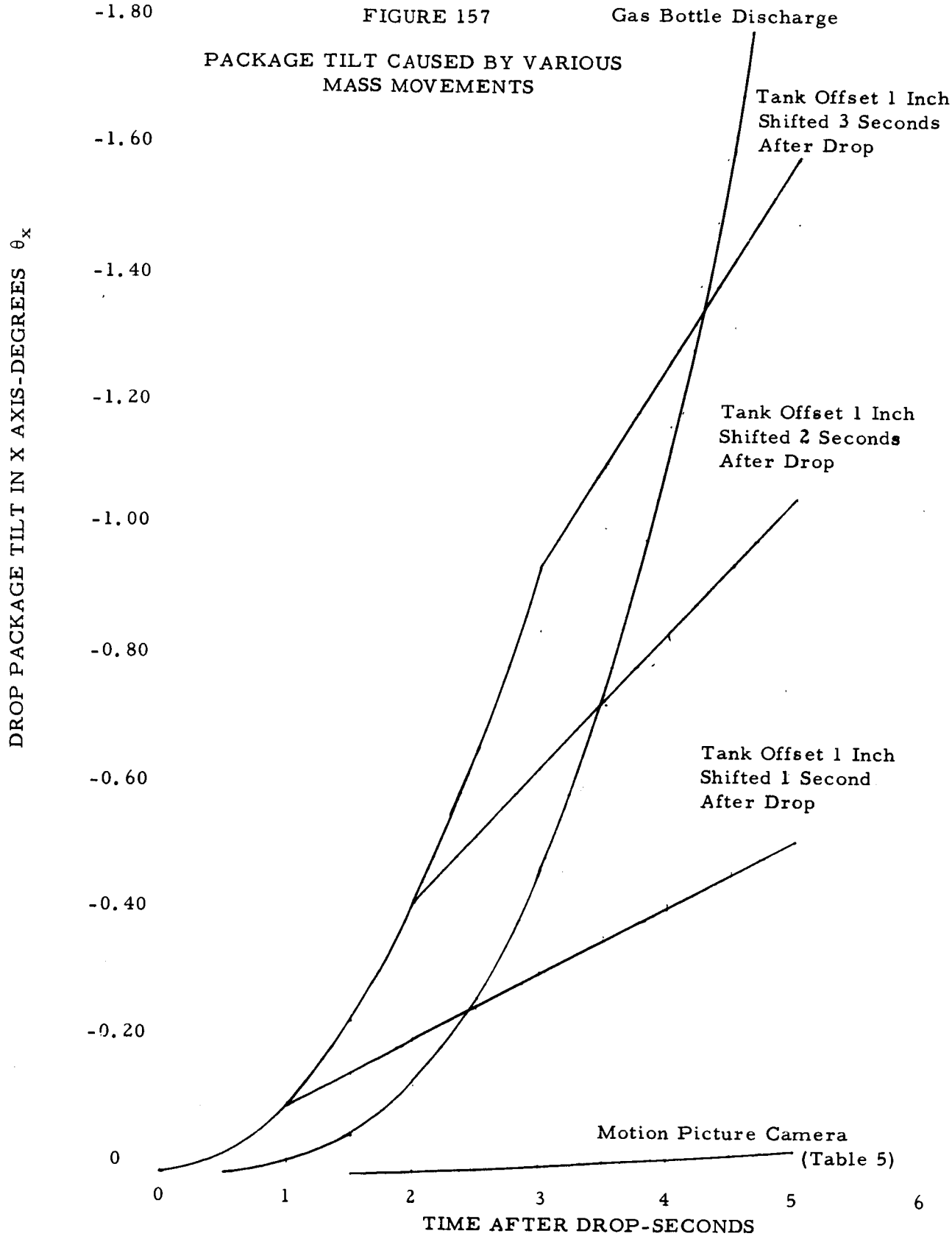

III Program Management

3.1 June, 1965 to December, 1965

Management of the contract effort was built on a system of individual responsibility for discrete technical projects. At the time of extension of the contract in June, 1965, a program plan and schedule was developed which would accomplish the desired goal. The effort was divided into five major areas, with one engineer responsible for the progress of each. These major areas were: Moment of Inertia, Product of Inertia, Mass Properties of Liquids, Center of Gravity, and General Laboratory Improvements. Each of these areas was divided into between two and five projects, which were in turn divided into several sub-projects. Each sub-project was assigned a time schedule for completion. Figure 158 is a span chart of the schedule, showing the major areas and projects. Figures 159 thru 162 are span charts of each of the projects showing the breakdown of the sub-projects. Each sub-project was also assigned a number, which was used to identify corresponding technical reports and project plans.

To assure objective activity in the work, a project plan was written for each project, which summerized the needs, goals and schedules. An example of one of these Project Plans is included as Figure 163. Copies of all of the Project Plans are in Appendix E.

Except where inappropriate, each sub-project was completed and summarized with a separate technical report.

3.2 December, 1965 to June, 1966

At the mid-point of the second contract year, (December, 1965) all completed and remaining projects were reviewed to ascertain their value in the light of six months additional experience. As a result of this review, the Project Plans and schedules were revised to reflect what was, in the opinion of the Contractor and Contracting Officer's Representative, the most desirable approach. Projects which were no longer important to the effort were dropped, and some new ones were added. A new set of Project Plans and span charts was prepared. The revised charts are included as Figures 164 thru 169.

SPACO, INC.
MASS METROLOGY LABORATORY
PROGRAM SCHEDULE 1965-1966
CONTRACT NAS8-11314

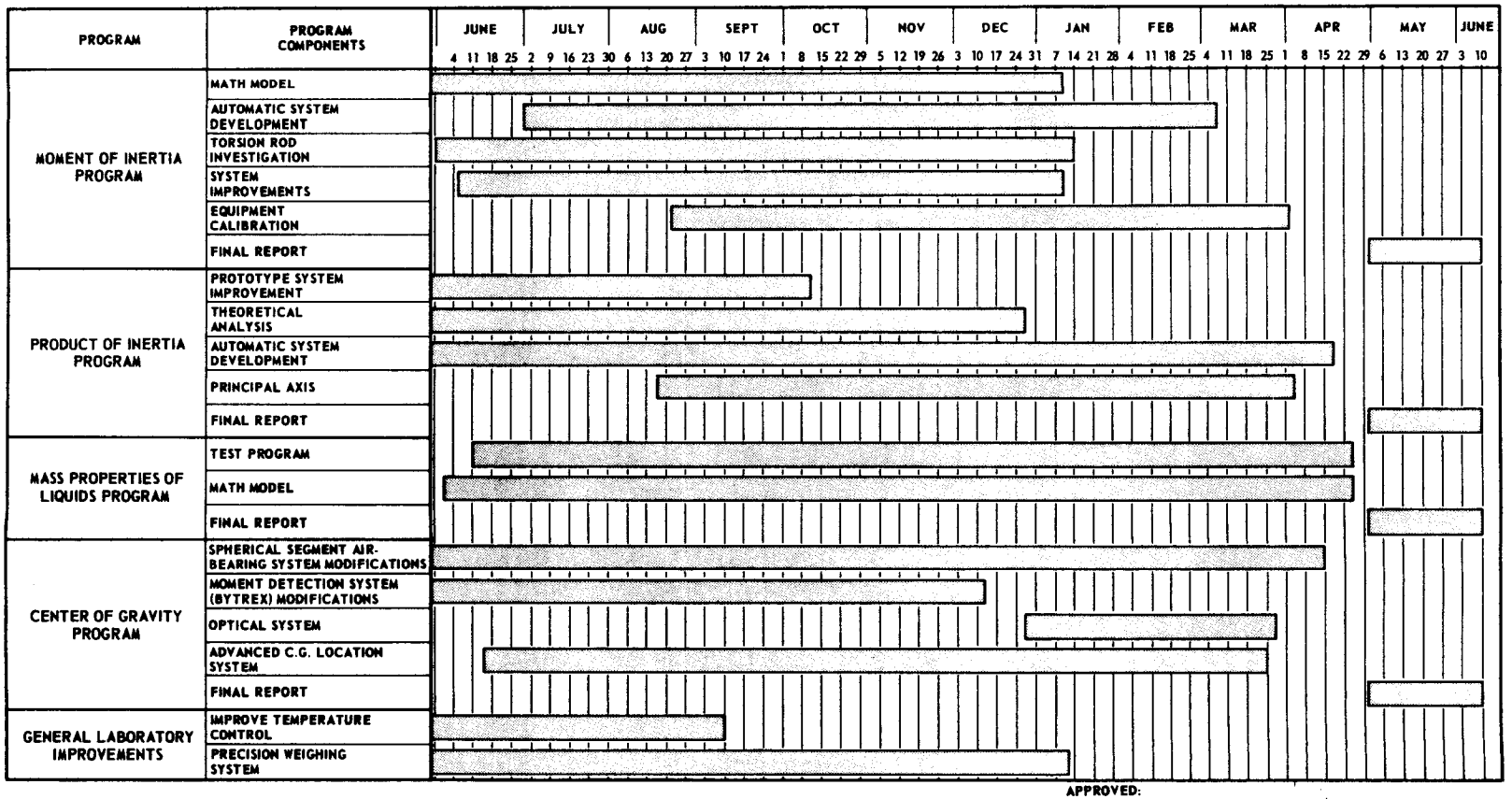

APPROVED:

DIRECTOR, MASS METROLOGY LABORATORY, SPACO

ENGINEERING MANAGER, SPACO

MSFC CONTRACTING OFFICER REPRESENTATIVE

FIGURE 158
PROGRAM SCHEDULE

SPACO, INC.
MASS METROLOGY LABORATORY
PROGRAM SCHEDULE 1965-1966

MOMENT OF INERTIA PROGRAM

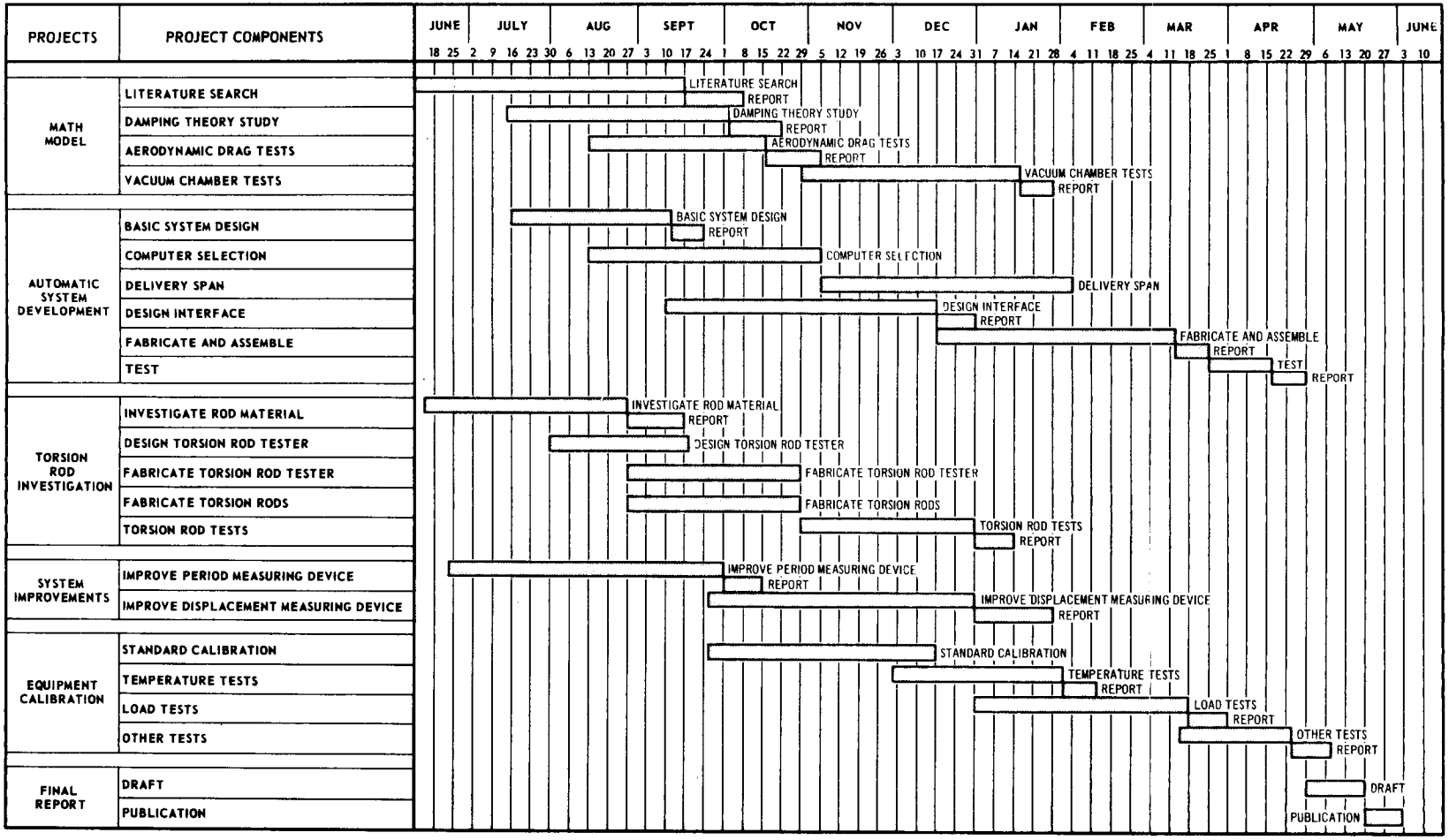

FIGURE 159
MOMENT OF INERTIA PROGRAM SCHEDULE

SPACO, INC.
MASS METROLOGY LABORATORY
PROGRAM SCHEDULE 1965-1966

PRODUCT OF INERTIA PROGRAM

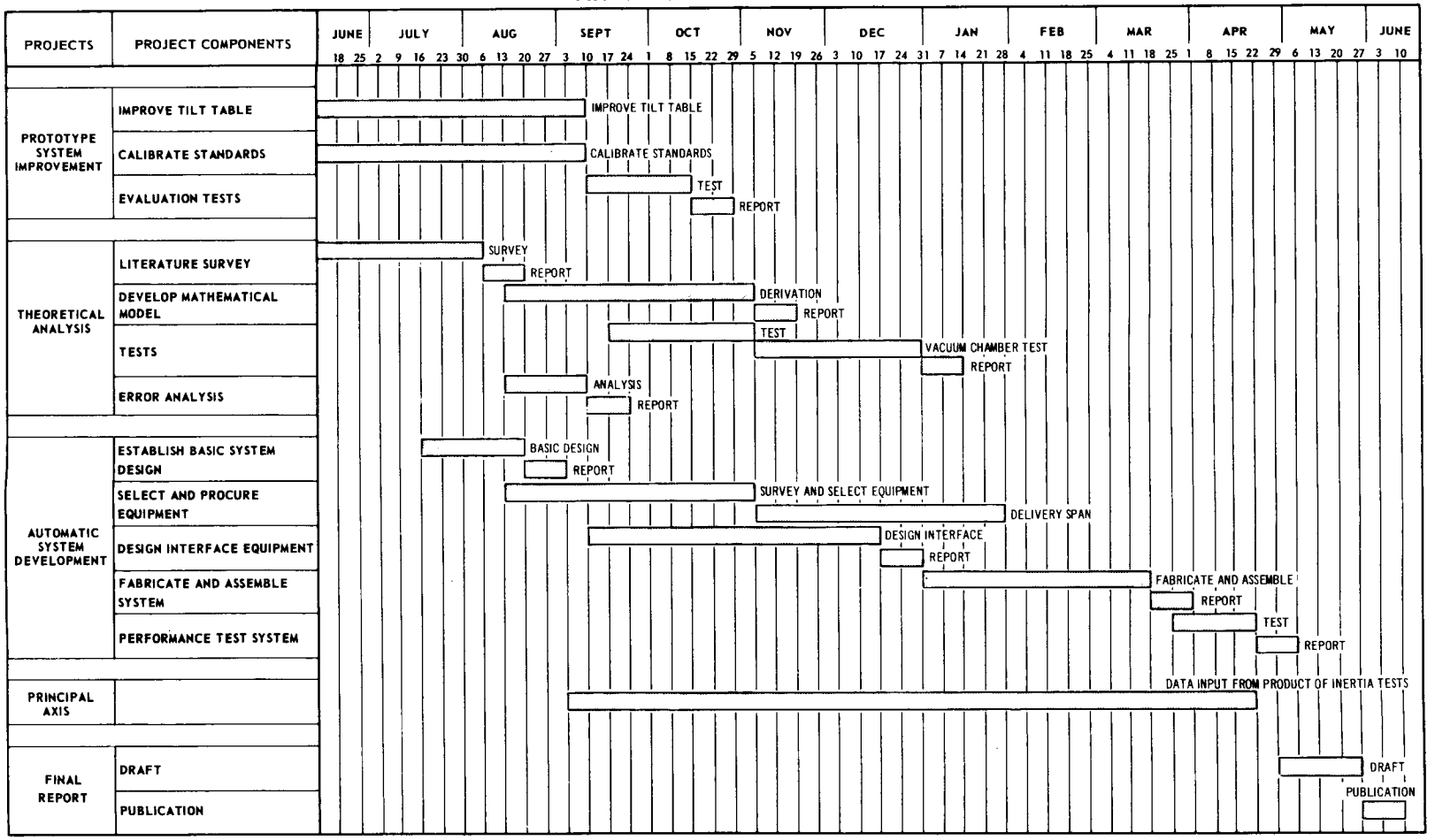

FIGURE 160
MOMENT OF INERTIA PROGRAM SCHEDULE

SPACO, INC.
MASS METROLOGY LABORATORY
PROGRAM SCHEDULE 1965-1966

CENTER OF GRAVITY PROGRAM

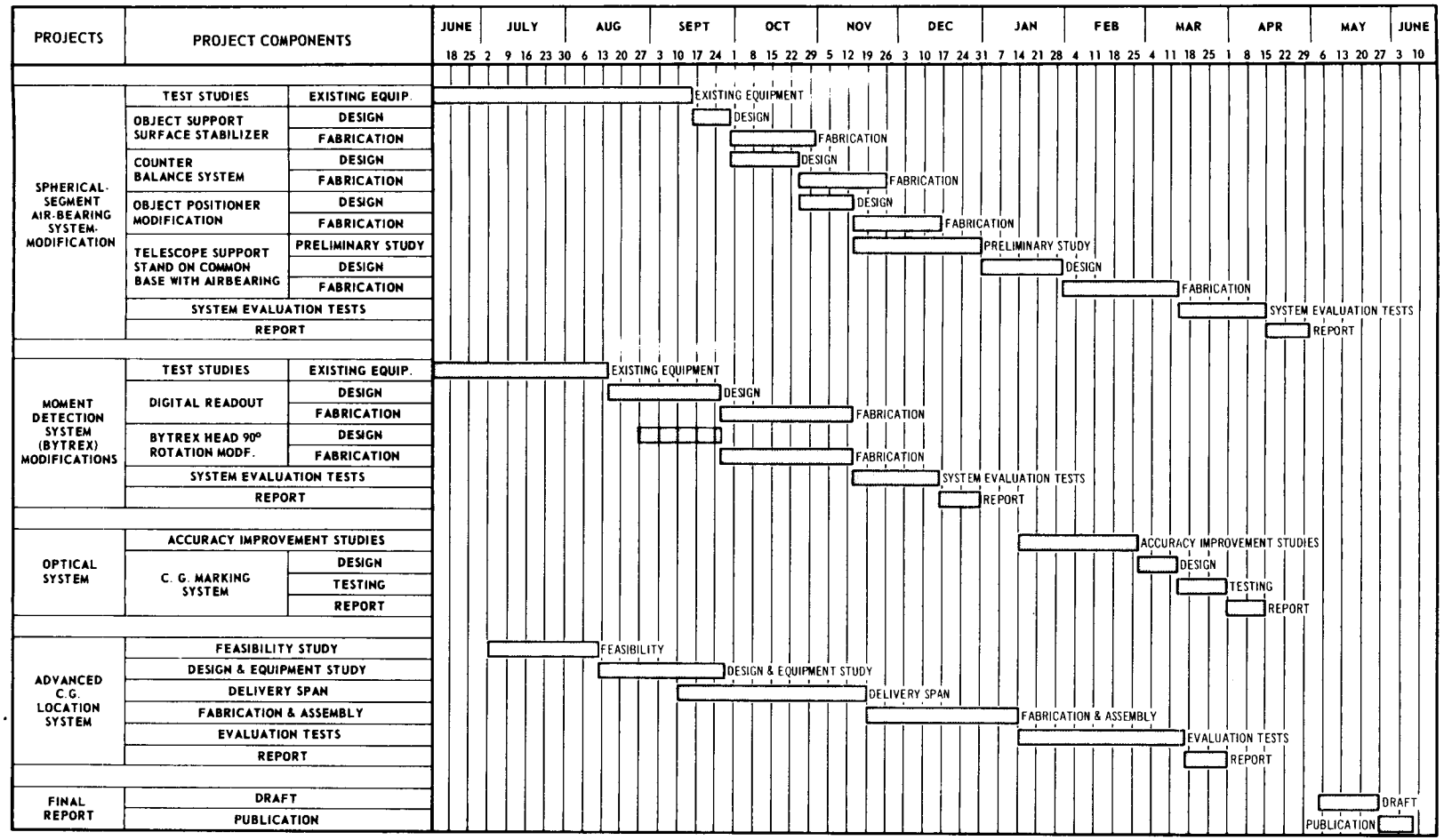

FIGURE 161
MOMENT OF INERTIA PROGRAM SCHEDULE

SPACO, INC.
MASS METROLOGY LABORATORY
PROGRAM SCHEDULE 1965-1966

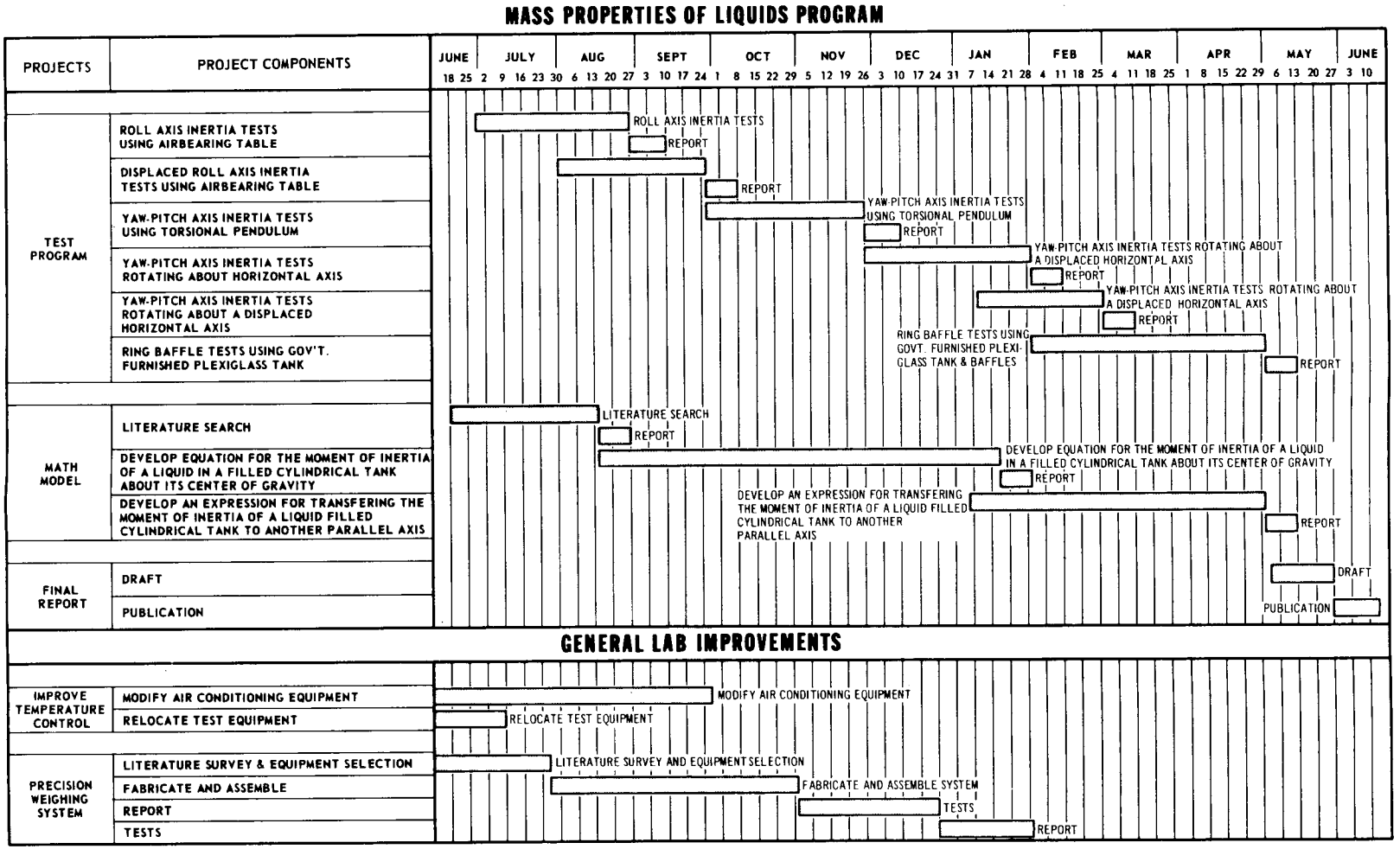

FIGURE 162
MOMENT OF INERTIA PROGRAM SCHEDULE

FIGURE 163

Mass Metrology Laboratory

PROJECT PLAN

Program: Moment of Inertia Number: 1.5

Project: Equipment Calibration Date: July 6, 1965

Scheduled Completion Date: May 15, 1966 Approved: [illegible]

Assigned Personnel:

Responsible: M. S. Phillips

Support: F. A. Pauli

BACKGROUND: The moment of inertia equipment will presently yield accuracies in the order of one tenth of one percent. With minor modifications and calibrations, for temperature and load, the accuracy should increase to one-hundredth of one per cent.

OBJECTIVE: The objective of this project is to compensate for all variables that might effect the accuracy of the moment of inertia determination. If possible an empirical equation will be derived that will correct the moment of inertia for any set of known conditions.

WORK PLAN:

1.5.1 Standard Calibration - The dumbbell standards will be recalibrated to obtain their exact moments of inertia and the accuracy of this value will be determined.

1.5.2 Temperature Tests - Test will be performed at various temperatures to obtain a correction factor which will compensate for the effect of temperature changes on the airbearing table.

1.5.3 Load Tests - The effect of different loads on the air bearing table will be investigated in this test program. The optimum air pressure to use for a certain weight will be determined and a compensation factor for correcting any errors caused by loading will be determined.

1.5.4 Other Tests - Any other tests will be performed that might be needed for calibrating the equipment.

REPORTS: 1.5.2 - Temperature Test - Due - February 15, 1966
1.5.3 - Load Test - Due - April 1, 1966
1.5.4 - Other Tests - Due - May 10, 1966

FIGURE 164

MASS METROLOGY LABORATORY
OVERALL PROGRAM

Program	Program Component	
Moment of Inertia Program 1.0	Math Model	1.1
	System Improvements	1.2
	Torsion Rod Investigation	1.3
	System Analysis	1.4
	Final Report	1.5
Product of Inertia Program 2.0	Prototype System Improvements	2.1
	System Analysis	2.2
	Principal Axis	2.3
	Final Report	2.5
Mass Properties of Liquids Program 3.0	Test Program	3.1
	Math Model	3.2
	Final Report	3.3
Center of Gravity Program 4.0	C.G. Marking System	4.1
	Advanced C.G. Location System	4.2
	Final Report	4.3
Mass Determination Program 5.0	Measurement Laboratory Weighing Syster	5.1
	Advanced Weighing Systems	5.2

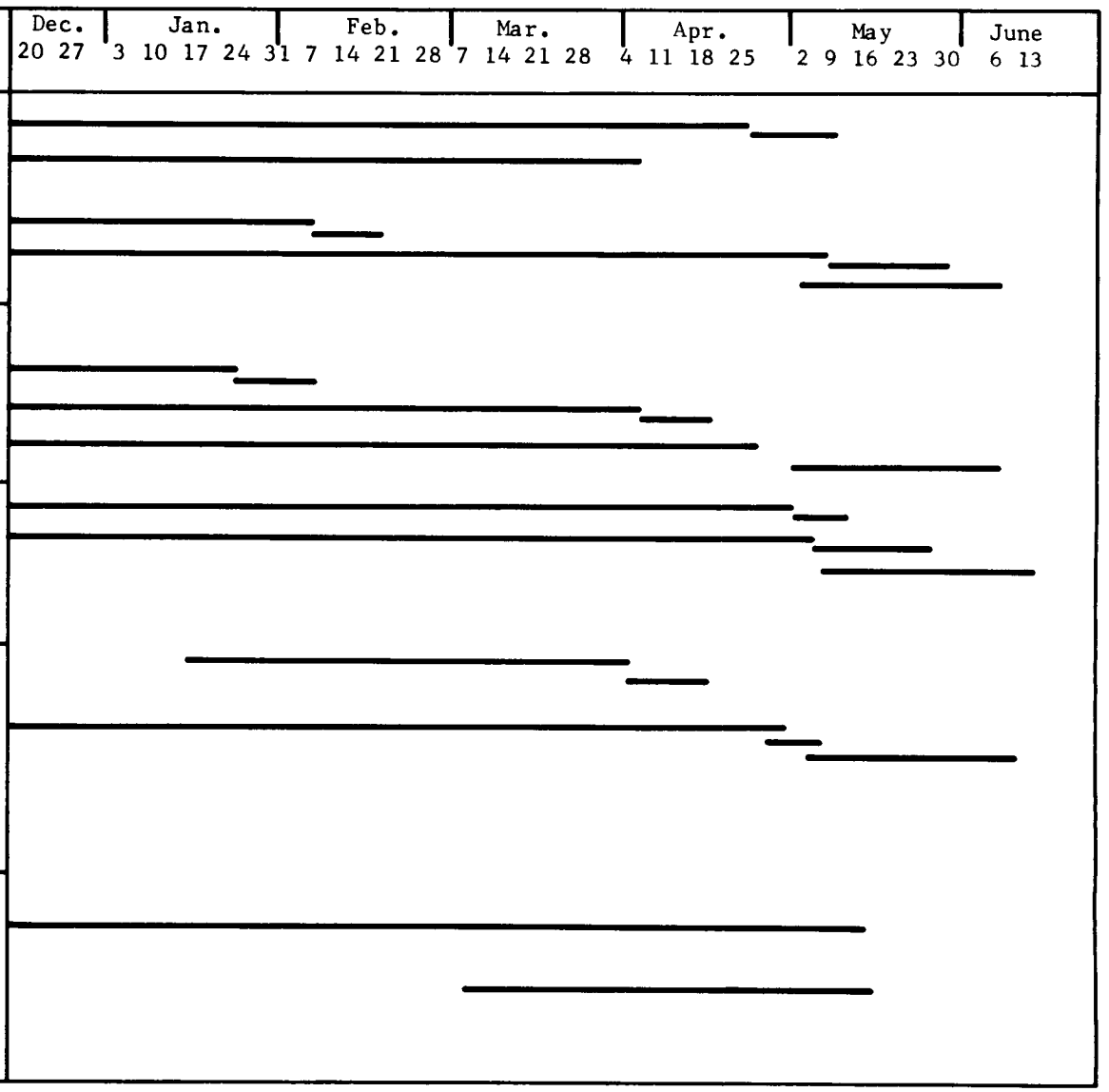

FIGURE 165

MOMENT OF INERTIA PROGRAM 1.0

Project	Project Component	
Math Model 1.1	Literature Search	1.1.1
	Aerodynamic Drag Tests	1.1.2
	Vacuum Chamber Tests	1.1.3
	Damping Theory Study	1.1.4
System Improvements 1.2	Improve Period Measuring Device	1.2.1
	Improve Displacement Measuring Device	1.2.2
	Air Bearing Table Improvements	1.2.3
Torsion Rod Investigation 1.3	Investigate Rod Material	1.3.1
	Design Torsion Rod Tester	1.3.2
	Fabricate Torsion Rod Tester	1.3.3
	Torsion Rod Tests	1.3.4
System Analysis	Evaluate Analysis Methods	1.4.1
	Program IBM 360	1.4.2
	Install Card Punch	1.4.3
	Perform Tests & Analyze Results	1.4.4
Final Report	Draft	
	Publication	

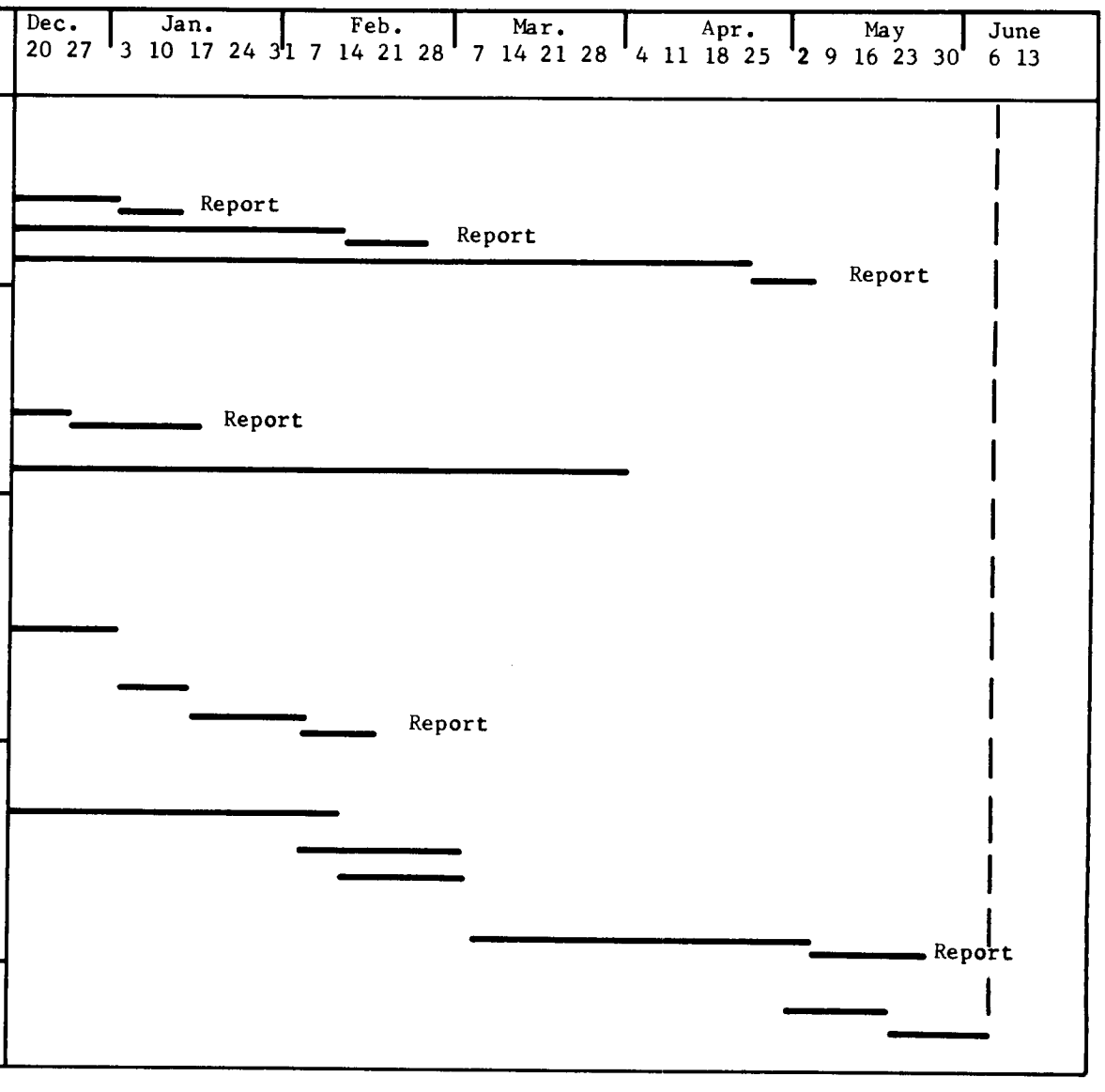

FIGURE 166

PRODUCT OF INERTIA PROGRAM 2.0

Project	Project Component	
System Improvements 2.1	Improve Tilt Table	2.1.1
	Calibrate Standards	2.1.2
	Evaluation Tests	2.1.3
System Analysis 2.2	Evaluate Analysis Methods	2.2.1
	Error Analysis	2.2.2
	Program IBM 360	2.2.3
	Develop Mathematical Model	2.2.4
	Perform Tests and Analyze Results	2.2.5
Principal Axis 2.3	Revise Computer Program for IBM 360	2.3.1
Final Report	Draft	
	Publication	

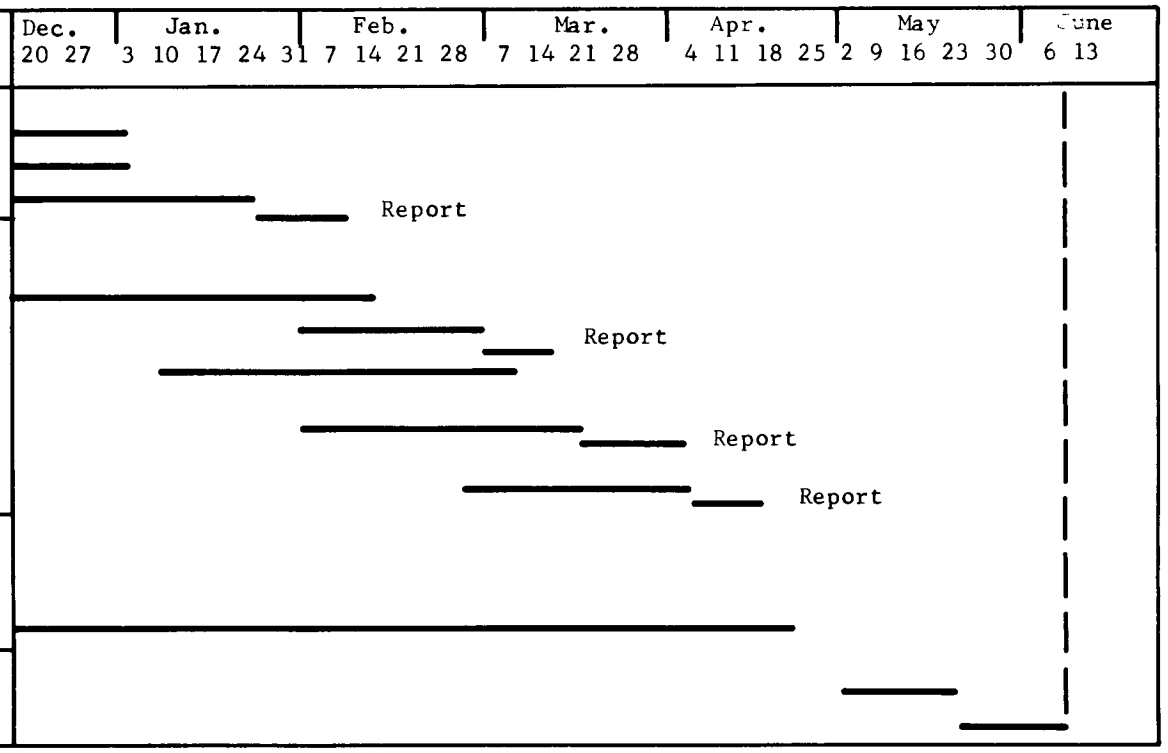

MASS PROPERTIES OF LIQUIDS PROGRAM 3.0

Project	Project Component
Test Program 3.1	Roll Axis Inertia Tests Using Air Bearing Table 3.1.1 Displaced Roll Axis Inertia Tests Using Air Bearing Table 3.1.2 Yaw-Pitch Axis Inertia Tests 3.1.3 Yaw-Pitch Axis Inertia Tests Rotating about a Displaced Horizontal Axis 3.1.4 Ring Baffle Tests Using Gov't. Furnished Plexiglass Tank 3.1.5
Math Model 3.2	Literature Search 3.2.1 Develop Equation for the Moment Inertia of a Liquid in a Filled Cylindrical Tank about its Center of Gravity and Displaced Axes 3.2.2 Investigate Analytical Method of Describing the Moment of Inertia of Liquid Filled Tanks with Baffles 3.2.3
Final Report	Draft Publication

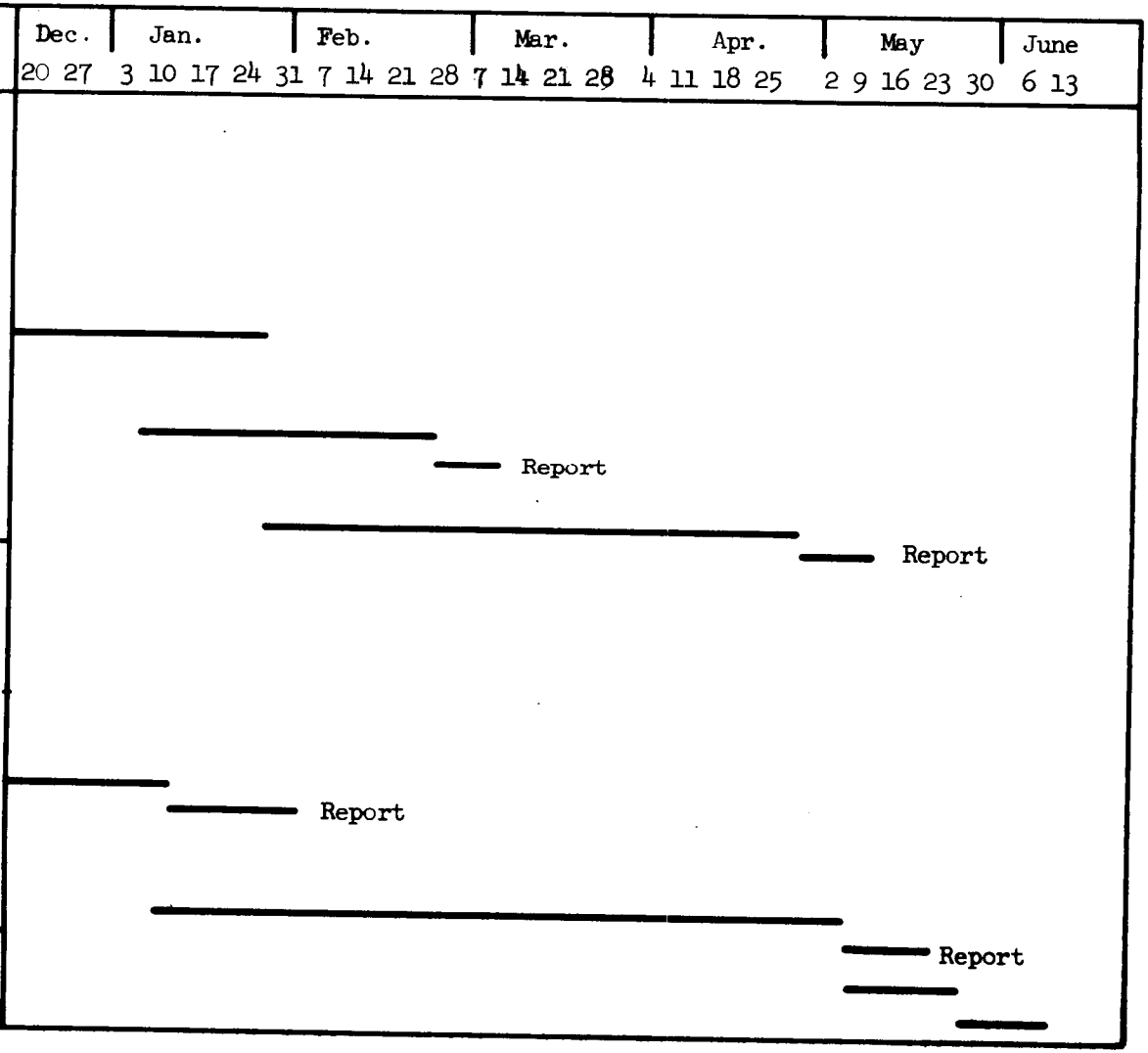

Fig. 167

CENTER OF GRAVITY PROGRAM 4.0

Project	Project Component	
C.G. Marking System 4.1	Preliminary Design	4.1.1
	Detail Design and Fabrication	4.1.2
	Evaluation Test	4.1.3
	Report	4.1.4
Advanced C.G. Location System 4.2	Feasibility Study	4.2.1
	Design and Equipment Selection	4.2.2
	Fabrication and Assembly	4.2.3
	Evaluation Tests	4.2.4
	Report	4.2.5
Final Report 4.3	Draft	4.3.1
	Pubilcation	4.3.2

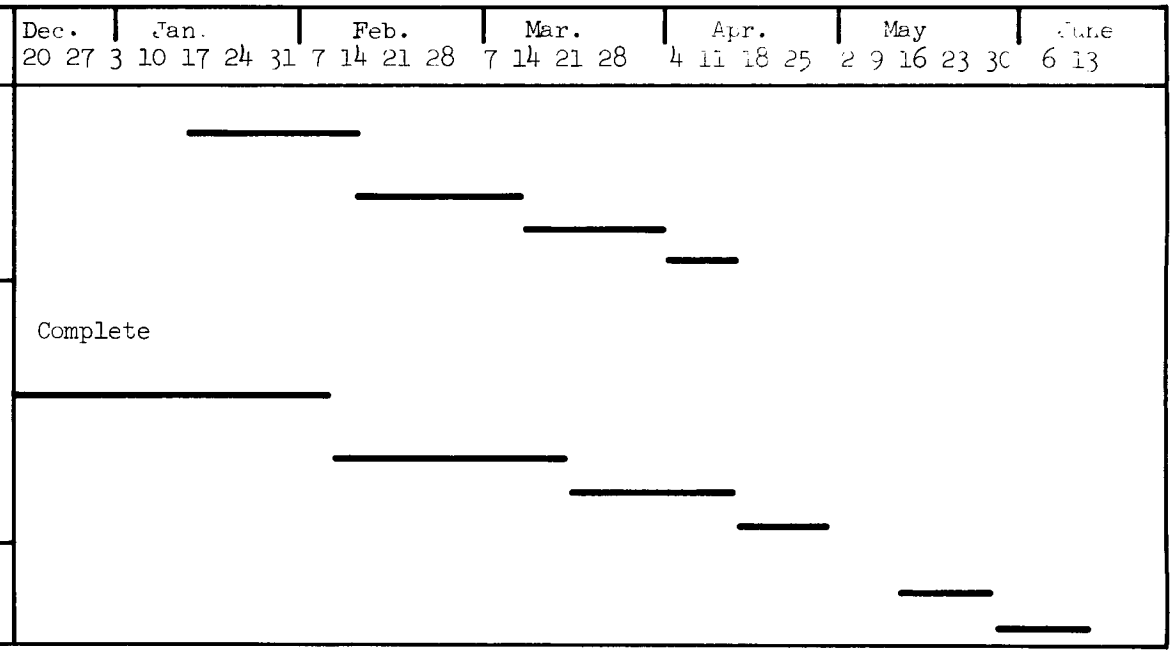

Fig 168

MASS MEASUREMENT PROGRAM 5.0

Projects	Projects Components	Dec. 20	27	Jan. 3	10	17	24	31	Feb. 7	14	21	28	Mar. 7	14	21	28	Apr. 4	11	18	25	May 2	9	16	23	30	June 6	13
5.1 Laboratory Weighing Sys System	Equipment Selection 5.1.1																										
	Fabricate & Assemble 5.1.2																										
	Tests 5.1.3																										
5.2 Advanced Weighing Systems	Investigate Commercial High Precision Weighing Systems 5.2.1																										
	Report 5.2.2																										

Fig. 169

APPENDIX

Appendix A — Moment of Inertia
Appendix B — Product of Inertia
Appendix C — Mass Properties of Liquids
Appendix D — Center of Gravity
Appendix E — Program Management

Appendix A

Moment of Inertia

APPENDIX A1

TEST PROCEDURE

1.1.3 Aerodynamic Drag Tests

1.1.3.1 Purpose

To study the effect of aerodynamic drag on the torsional pendulum air bearing table.

1.1.3.2 Equipment

(1) 24 inch air bearing table.
(2) Photocell timing device.
(3) Hewlett-Packard 524D frequency counter.
(4) Hewlett-Packard 560A digital recorder.
(5) Radian scale, light and mirror arrangement.
(6) Torsion Rod Number 120.
(7) 100 pound cylindrical weights.
(8) Special cylindrical drag adapter.
(9) Drag plates for cylinder drag adapter.

1.1.3.3 Set-Up

(1) Turn on electronic equipment for warm up.
(2) Level the air bearing table on the iso-pad.
(3) Firmly mount the wand for triggering the photocell device to the air bearing table top.
(4) Set air pressure at 30 psi.
(5) Mount _____ 100 pound weights on table as shown.

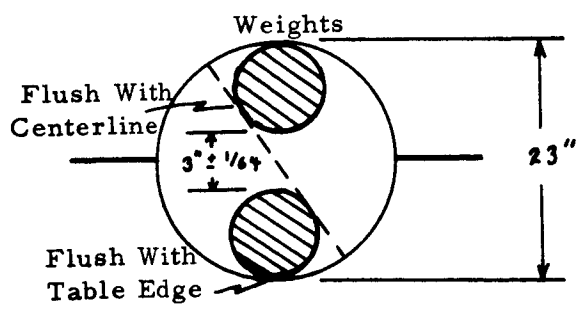

(6) Place special drag adapter over weights and fasten to table top.

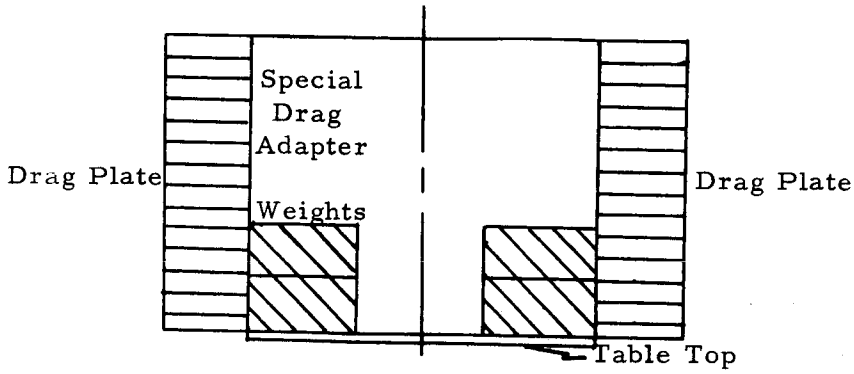

(7) Mount drag plates _____ to special drag adapter as shown.

(8) Insert rod number 120 into the table.

(9) Place radian scale 140 inches from the center of the table.

(10) With the rod aligned, the table level and the specimen mounted, zero the wand and photocell device and zero the light source on the radian scale.

1.1.3.4 Test Procedure

(1) After the test equipment has been arranged as outlined in the test set up, testing is ready to begin.

(2) Gradually displace the table top, increasing its maximum amplitude until it reaches .05 radians. Then release the table top and let the maximum amplitude decay to .035 radians. At 0.035 radians start recording data. Record data until the oscillations stop.

1.1.3.5 Test Data

(1) Test Number -
(2) Date -
(3) Personnel -
(4) Temperature -
(5) Humidity -
(6) Number of 100 pound weights -
(7) Total Cycles -
(8) Automatic period tape readout -
(9) Maximum displacement readings for every 20th cycle -

(10) Weights - Right: Left:

1.1.3.6 Number of Test

(1) Run each test _____ times.
(2) Record the period every 20th cycle for a 10 period average to the nearest .00001 second.
(3) Record the maximum displacement for every 20th cycle to the nearest .001 radian.

1.1.3.7 Special Work

(1) Plot the period versus total number of cycles for every period recorded and connect a smooth curve through the points. Average the period between .001 and .002 radians.

Test No. Average

$T_{.002 - .001} =$

(2) Plot the $\log_{10}$ of the maximum displacements versus the total number of cycles for every 20th cycle and connect a smooth curve through the points.

(3) Calculate $I = KT^2/4\pi^2$

Test No. Average

$I_{.002 - .001} =$

Written by: _____

Approved by: _____

Date: _____

APPENDIX A2

TEST PROCEDURE

1.1.3 Aerodynamic Drag Tests

1.1.3.1 Purpose

To determine the effects of aerodynamic drag on the torsional pendulum air bearing table.

1.1.3.2 Equipment

(1) 24 inch air bearing table.
(2) Photocell timing device.
(3) Radian scale, light, and mirror arrangement.
(4) Displacement detector.
(5) Two Hewlett-Packard 524D frequency counters.
(6) Two Hewlett-Packard 560A digital recorders.
(7) One Accurate Instrument Co. Model 51553 counter.
(8) Torsion Rods, Dumbbell C, Drag Plates.

1.1.3.3 Set-Up

(1) Turn on electronic equipment for warm-up.
(2) Level air bearing table on iso-pad.
(3) Set air pressure at 30 psi.
(4) Mount _____ on air bearing table with drag plates _____.
(5) Insert rod number 120 into the table.
(6) Zero the wand and grating for triggering the photocells for both the period and displacement devices.
(7) Place radian scale 140 inches from table center and align light and mirror on scale.
(8) Connect the Accurate Instrument counter for recording the total number of cycles.
(9) Use the Hewlett-Packard frequency counter and digital recorder for recording the displacements.
(10) Use the Hewlett-Packard counter and digital recorder for recording the period every _____ cycle.

1.1.3.4 Test Procedure

(1) After the test procedure has been arranged as outline in the test set-up, testing is ready to begin.

(2) Displace the table top until its maximum displacement reaches at least ____ radians. When the maximum displacement decays to ____ radians, start recording the number of cycles, the displacements, and the periods until the amplitude decays to ____ .

1.1.3.5 Test Data

(1) Date -
(2) Personnel -
(3) Dumbbell -
(4) Test Number -
(5) Temperature -
(6) Humidity -
(7) Number of Cycles -
(8) Include tape or data of displacement measurements.
(9) Include tape of period measurements.

1.1.3.6 Number of Tests

(1) Repeat each test _____ times.

1.1.3.7 Special Work

(1) Plot θ vs N, where θ is the maximum displacement and N is the number of cycles.
(2) Plot Lnθ vs N.
(3) Plot T vs N where T is the period of oscillation.
(4) Perform any other works described below.

Written by: _____

Approved by: _____

Date: _____

APPENDIX A3

TEST PROCEDURE

1.0 Moment of Inertia

1.1 Math Model

1.1.4 Vacuum Chamber Test

To determine the effect of aerodynamic drag on the period decay of an oscillating object.

1.1.4.2 Equipment

(1) Vacuum chamber
(2) Overhead fixture for mounting the torsion rod.
(3) Torsion rod
(4) Dumbbell C with bearing adapter.
(5) Drag plates C and D with adapters for dumbbell C.
(6) Solenoid operated striker and bearing device.
(7) Photocell timing device
(8) Photocell - grating displacement device.
(9) Two counters and digital printers.

1.1.4.3 Test Set-Up

(1) Mount torsion rod to overhead beam.
(2) Use the torsion rod adapter to secure dumbbell C to the torsion rod.
(3) Mount the prescribed drag plates to the dumbbell.
(4) Secure the wand and grating to the dumbbell for recording time and displacement, respectively.
(5) Align the timing and displacement devices so that a zero reading is obtained when the dumbbell is in a static condition.
(6) Place the bearing device so that the bearing is on center line with the rod, and is aligned with the bearing adapter on the dumbbell.

1.1.4.4 Test Procedure

(1) With the equipment arranged as stated in the set-up procedure, the testing is ready to begin.
(2) Turn on electronic equipment for warm-up.

(3) Evacuate the vacuum chamber to the prescribed vacuum.
(4) On the control panel, engage the "Pivot Hold" and "Pivot Pull-In" switches, and immediately release the "Pivot Pull-In" switch. Keep the "Pivot Hold" switch on.
(5) On the control panel engage the "Striker" switch, and observe the read out on the H. P. 524 Counter.
(6) Disengage the "Pivot Hold" switch on the control panel, observing both the T. V. monitor and the read out on the 524 Counter to insure that the dumbbell is swinging about the vertical axis of rotation with minor random motion.
(7) When the read out on the 524 Counter reaches _____ , turn on the two 560A Counters and the 1452 and 524 Digital Printers.
(8) Stop the test at _____ on the counter.
(9) Record a 10 period average every 11 cycles and displacement every other cycle.

1.1.4.5 Test Data

(1) Date -
(2) Personnel -
(3) Temperature -
(4) Humidity -
(5) Vacuum -
(6) Torsion Rod -
(7) Drag Plate -
(8) Include print outs of period and displacement measurements.

Written By: _____

Approved By: _____

Date: _____

APPENDIX A4

TEST PROCEDURE

1.2.2 Measurement of Displacement Transducer Accuracy

1.2.2.1 Purpose

The purpose of this test is to determine the accuracy of the Displacement Transducer in measuring small angles.

1.2.2.2 Equipment

(1) Large Torsional Pendulum.
(2) Displacement measuring system.
(3) The Period measuring system.
(4) The Tuckerman Autocollimator.
(5) A small plane optical mirror for the collimator.
(6) Miscellaneous hardware as needed.

1.2.2.3 Set-Up

(1) Set up the large torsional pendulum system for peak displacement measurements using the new displacement transducer.
(2) Set up the Tuckerman autocollimator (with a small plane mirror attached to the edge of the table) to measure the angular displacement of the pendulum. This is to be used for a reference.

1.2.2.4 Test Procedure

(1) Check the zero of the displacement and period transducers and the autocollimator. Start the unloaded pendulum oscillating at a peak amplitude slightly above .012 radian as measured with the autocollimator.

(2) Start the displacement printer and mark the value printed out when the peak displacement decays to .012 radian as measured with the autocollimator.

(3) Run the test 3 times at the .012 radian level.

(4) Then run the test 3 times at the .006 radian level.

Written by: [illegible]

Approved by: [illegible]

Date: 1-13-66

APPENDIX A5

TEST PROCEDURE

1.3.4 Torsion Rod Tests

1.3.4.1 Purpose

To evaluate the linearity of the stress-strain relationship in torsion for solid cylindrical rods of various materials.

1.3.4.2 Equipment

(1) 23-inch air bearing table.
(2) Small pulley air bearing.
(3) Davidson auto-collimator.
(4) Standard weights with mounting trays.
(5) Nylon cord.
(6) Torsion rods.

1.3.4.3 Set-Up

(1) Level the air bearing table on the iso-pad.
(2) Set air pressure at 30 psi.
(3) Insert rod into table and align.
(4) Mount pulley air bearing to the bottom of the table and connect its air supply through a regulator set at 20 psi.
(5) Attach the nylon cord to the table top and extend it partially around the top and over the pulley air bearing to the first tray, tie, and then take back over the pulley to the second tray and tie again. The nylon cord must be tangent and parallel to the top in Figure 1.
(6) Zero the two trays by adding weight to one of them as shown in Figure 1.
(7) Zero the Davidson auto-collimator by aligning it with a first surface mirror on the table top.
(8) The standard weights can be added and taken off of the trays for displacing table top.

1.3.4.4 Test Procedure

(1) After the test procedure has been arranged as outlined in the test set-up, testing is ready to begin.
(2) As standard weights are added and taken off, the displacement is recorded for each weight in the test data section.

1.3.4.5 Test Data

(1) Date -
(2) Personnel -

(3) Rod -
(4) Test Number -
(5) Temperature -
(6) Humidity -

Mass	Weights Added								Aug.
		diff.		diff.		diff.		diff.	

Mass	Weights Removed								Aug.
		diff.		diff.		diff.		diff.	

1.3.4.6 Special Work

Written By: [illegible]

Approved By: [illegible]

Date: 2-15-60

APPENDIX A6

Test Procedure

1.0 Moment of Inertia

1.3 Torsion Rod Investigation

1.3.5 Torsion Rod Tests

1.3.5.1 Purpose:

To determine the spring constants of the rods to be used in the air bearing table.

1.3.5.2 Equipment:

(1) 24 inch air bearing table.
(2) Photocell timing device.
(3) Hewlett-Packard 524 D frequency counter.
(4) Hewlett-Packard 560 A digital recorder.
(5) Radian scale, light and mirror arrangement.
(6) Torsion rods.
(7) Dumbbell Standards.

1.3.5.3 Set Up:

(1) Turn on electronic equipment for warm-up.
(2) Level air bearing table on iso-pad.
(3) Firmly mount the wand for triggering the photocell device to the air bearing table top.
(4) Set air pressure at 30 psi.
(5) Mount dumbbell_____ to the table top.
(6) Insert rod number_____ into the table.
(7) Place the radian scale 140 inches from the center of the table.
(8) With the rod aligned, the table level and the dumbbell mounted, zero the wand, and photocell device and zero the light source on the radian scale.

1.3.5.4 Test Procedure:

(1) After the test equipment has been arranged as outlined in the test set up, testing is ready to begin.

(4) Repeat each test 3 times.

1.3.4.5 Test Data

(1) Date -
(2) Personnel -
(3) Test Number -
(4) Temperature -
(5) Humidity -
(6) Total Number of Cycles -
(7) Include tape of displacement measurements.
(8) Include tape of 10-period average measurements.

1.3.4.7 Special Work

(1) Plot period vs number of cycles.
(2) Perform any other work described below.

Written by: M. L. Phillips

Approved by: C. W. Hall

Date: Mar. 21, 1966

APPENDIX A7

Test Procedure

1.0 Moment of Inertia

1.3 Torsion Rod Investigation

1.3.5 Torsion Rod Tests

1.3.5.1 Purpose:

To determine the spring constants of the rods to be used in the air bearing table.

1.3.5.2 Equipment:

(1) 24 inch air bearing table.
(2) Photocell timing device.
(3) Hewlett-Packard 524 D frequency counter.
(4) Hewlett-Packard 560 A digital recorder.
(5) Radian scale, light and mirror arrangement.
(6) Torsion rods.
(7) Dumbbell Standards.

1.3.5.3 Set Up:

(1) Turn on electronic equipment for warm-up.
(2) Level air bearing table on iso-pad.
(3) Firmly mount the wand for triggering the photocell device to the air bearing table top.
(4) Set air pressure at 30 psi.
(5) Mount dumbbell _____ to the table top.
(6) Insert rod number _____ into the table.
(7) Place the radian scale 140 inches from the center of the table.
(8) With the rod aligned, the table level and the dumbbell mounted, zero the wand, and photocell device and zero the light source on the radian scale.

1.3.5.4 Test Procedure:

(1) After the test equipment has been arranged as outlined in the test set up, testing is ready to begin.

(2) Gradually displace the table top, increasing its maximum amplitude until it reaches .003 radians. Then release the table top and let the maximum amplitude decay to .002 radians. At .002 radians start recording the period and number of cycles from a maximum displacement of .002 to .001 radians.

1.3.5.5 Test Data:

(1) Test Number -
(2) Date -
(3) Personnel -
(4) Temperature -
(5) Humidity -
(6) Dumbbell -
(7) Every other period between the maximum displacement of .002 and .001 radians -
(8) Total Number of cycles between the maximum displacement of .002 and .001 radians -

1.3.5.6 Number of Tests:

(1) Run each test 10 times.
(2) Record the periods to the nearest .000,001 second (microsecond).

1.3.5.7 Special Work:

(1) Determine the average period between the maximum displacement of .002 and .001 radians by averaging each indiviual period.

(2) Record the following data:

Average Period	Deviation from Average
_____	_____
_____	_____
_____	_____
_____	_____
_____	_____
_____	_____
_____	_____
_____	_____
_____	_____
_____	_____
Average	
_____	_____

(3) Determine the standard deviation from $s = \sqrt{\frac{\sum (\bar{x} - x)^2}{N - 1}}$ and record _____.

(4) Record any other information described below.

Written by: M. S. Phillips Approved By: C. W. Phillips

APPENDIX A8

Investigation of the Effect of Earth Rotation On the Moment of Inertia Measurement System

All factors that affect the determination of moments of inertia when using the air bearing table must be considered in order to obtain maximum accuracy. The earth's rotation is one of these factors that must be analyzed. Three forces caused by the earth's rotation must be considered in determining the moment of inertia of an object by using the air bearing table. These forces are:

1. Centrifugal
2. Coriolis
3. Gyroscopic

Each force will be examined separately and its effect upon the air bearing table will be analyzed.

The centrifugal force is produced by the earth's rotation and is mathematically expressed by

$$F_c = m\bar{\omega} \times (\bar{\omega} \times \bar{r}) \qquad (1)$$

where:

m = mass of object
$\bar{\omega}$ = angular velocity of earth
$\bar{r}$ = radius of earth.

The direction of this force is normal to $\bar{\omega}$ and points outward from the earth. Figure 1 shows the direction of the centrifugal force with respect to the gravitational force and the air bearing table. The component of the centrifugal force which has the same direction as the gravitational force, $F_c \cos \theta$, is the dominant force. It can be considered the only force contributed by the centrifugal acceleration. Since this force has the same direction as the force of gravity but an opposite direction, it can be considered as part of the gravitational force. The maximum centrifugal acceleration is 3.38 cm/sec^2 which is only 0.3% of the gravitational acceleration. Since the air bearing table is aligned and adjusted for the weight of the object, the centrifugal force is considered as part of the gravitational force and has no effect on the system performance.

The Coriolis force is a force which is produced by a motion with respect to a moving reference system. It is mathematically expressed as

$$F_{co} = 2m\,(\bar{\omega} \times \bar{v}) \qquad (2)$$

where:

m = mass of object
$\bar{\omega}$ = angular velocity of earth
$\bar{v}$ = velocity of the object relative to earth.

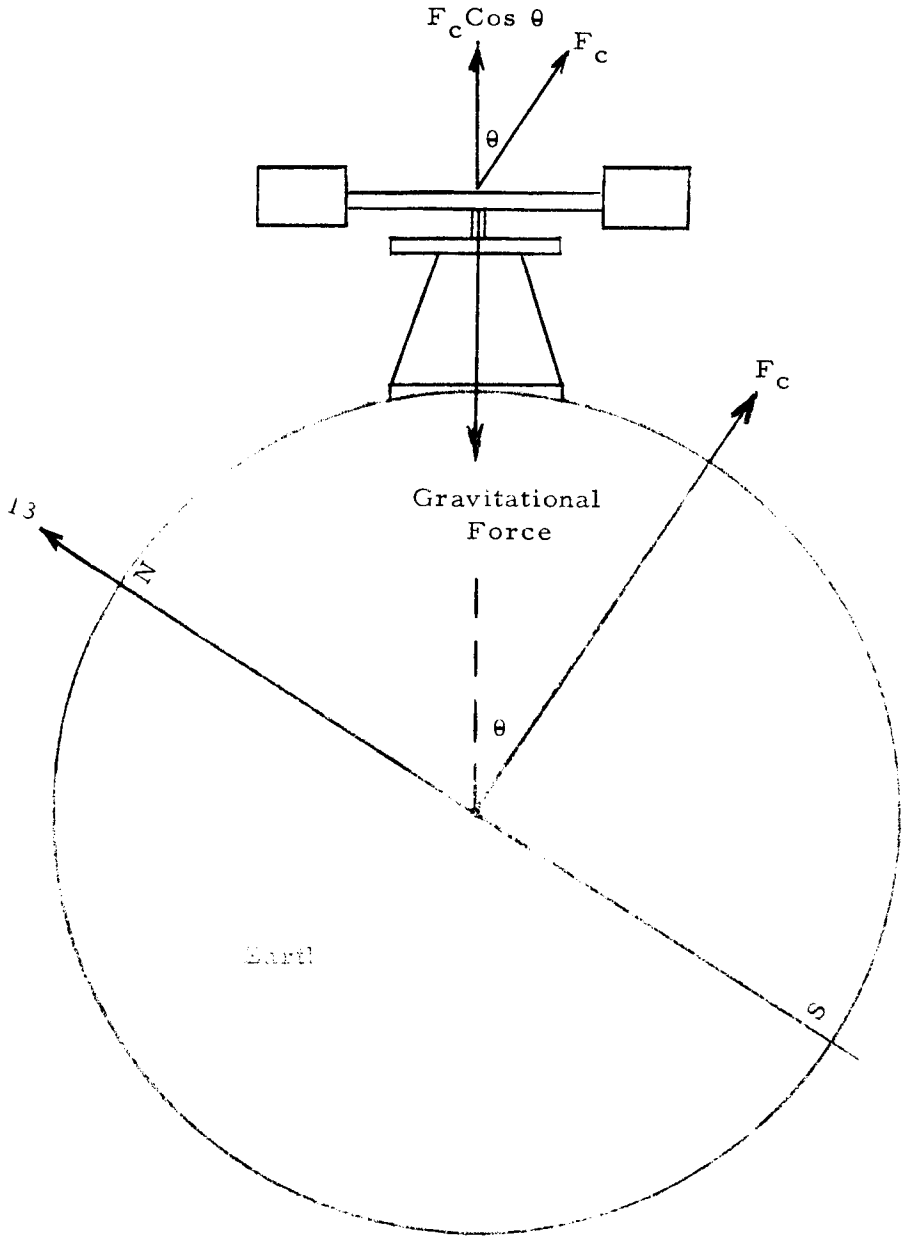

FIGURE 1

There is a Coriolis force in the air bearing torsional pendulum because the object rotates within the moving reference frame of the earth. The direction of the force is perpendicular to the velocity of the object. Since the object rotates about its center of gravity there will be two Coriolis forces opposing each other. Figure 2 is an example of the velocities and forces present. In Figure 2 the Coriolis forces are directed outward for clockwise motion and inward for counterclockwise motion. The magnitude of the force is always less than 1.5×10^{-4} mv, where mv is the momentum of the object. For a 200 pound dumbbell with an angular velocity of 0.1 radian per second the force is approximately 7×10^{-6} pounds. The force produced by the torque of the same oscillating dumbbell is approximately 700 pounds force. Therefore, the Coriolis force is a factor of 10^{-8} smaller than the oscillating force. This force is extremely small; however, it will not enter into the system because the forces cancel each other as shown in Figure 2.

The last force to consider is that caused by gyroscopic effects. The air bearing torsional pendulum acts as gyroscope because the table top rotates on a rotating earth. The object on the table top acts as the rotor of a gyroscope and the earth produces the precession. The torques produced by this motion can be computed from the law of gyroscopics. This law is

$$T = I\omega_s\omega_p \tag{3}$$

where:

T = torque
I = moment of inertia of object
ω_s = spin velocity of table top
ω_p = precession velocity of earth

Figure 3 shows the factors stated in Equation 3 and their direction. The torque vector has a direction perpendicular to the axis of rotation. Using Equation 3, the magnitude of this torque for a 200 pound dumbbell is approximately 6.9×10^{-4} inch-pounds. Several tests were performed to determine the effect of this gyroscopic torque on the air bearing table. First a dynamic test was performed to measure the vertical deflection of the ends of the dumbbells that was produced by gyroscopic forces. A dial indicator with a sensitivity of .0001 of an inch was mounted on the air bearing table as shown in Figure 4. The air bearing table

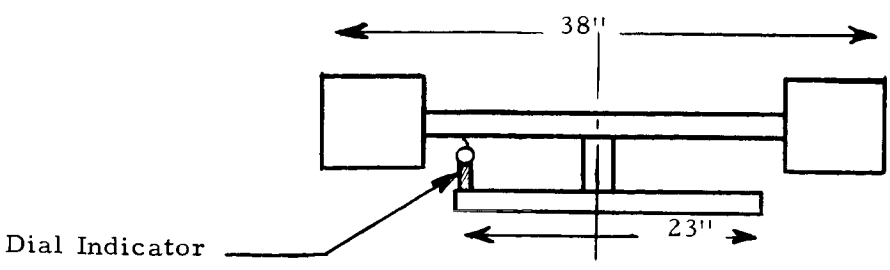

FIGURE 4

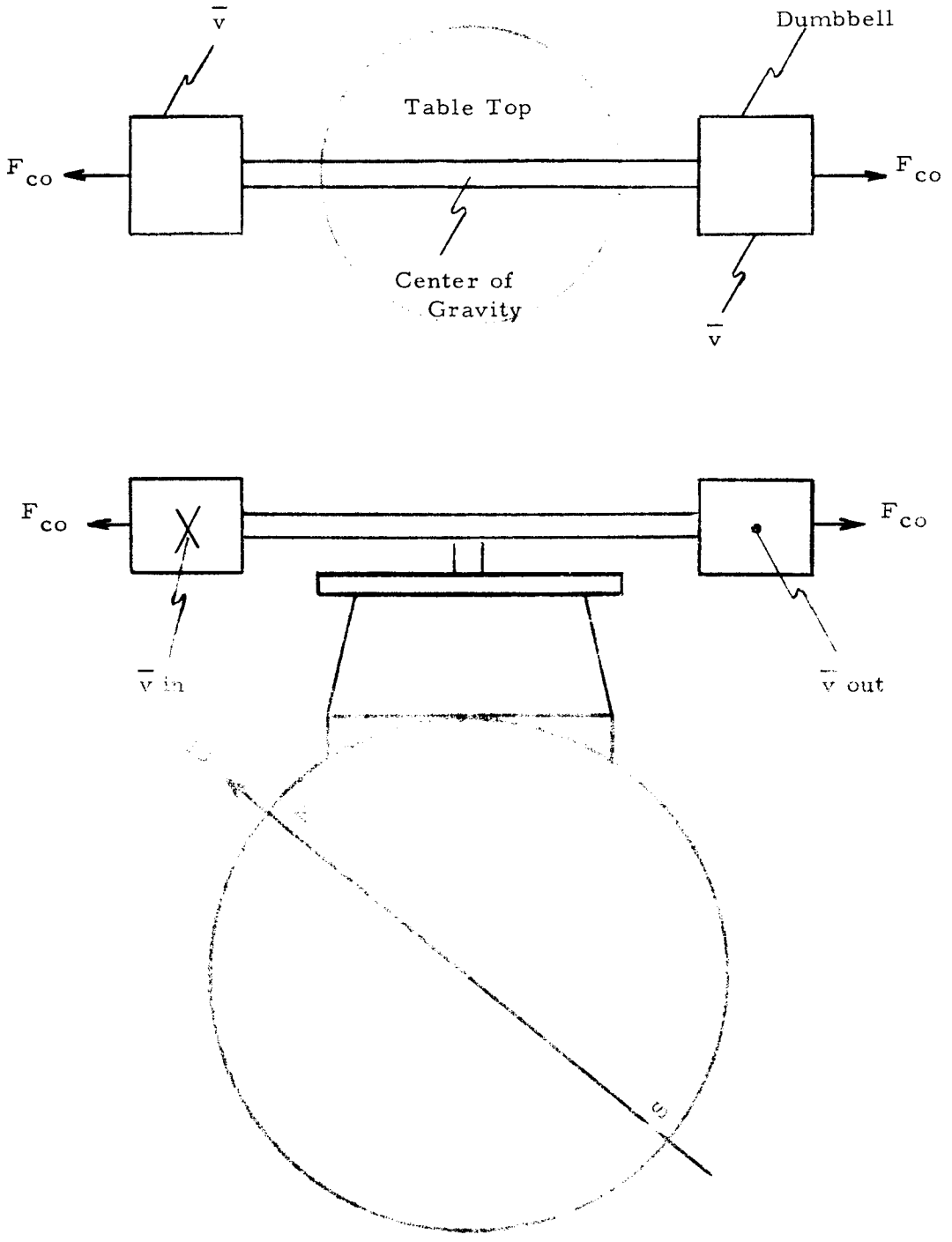
$\bar{v}$
Dumbbell
Table Top
F_{co}
F_{co}
Center of Gravity
$\bar{v}$
F_{co}
F_{co}
$\bar{v}$ in
$\bar{v}$ out

FIGURE 2

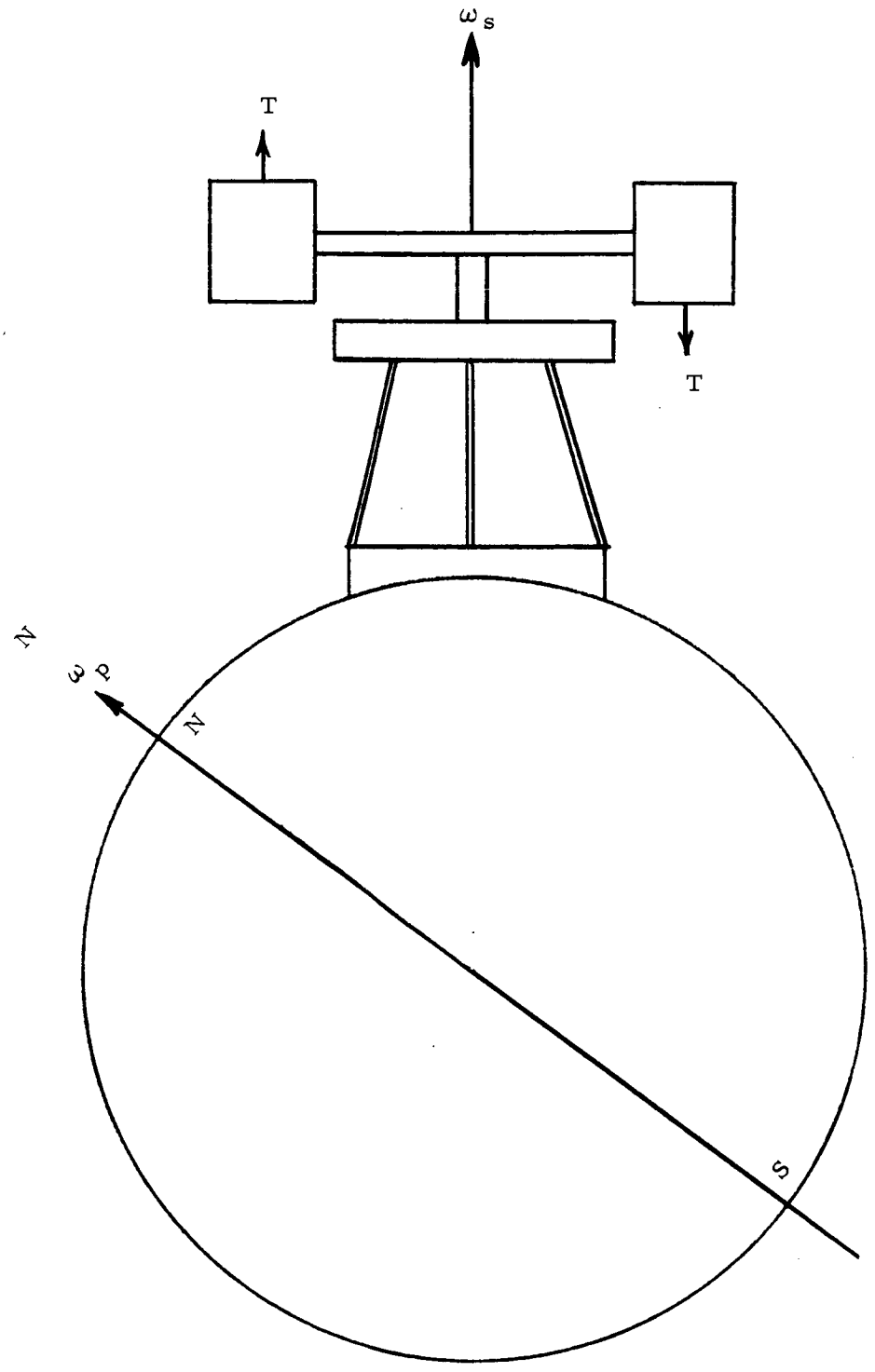

FIGURE 3

was rotated to .05 radians and released. As the table oscillated the dial indicator was observed. There was no deflection of the dial indicator needle; therefore, the deflection had to be less than .0001 of an inch.

In order to determine the specific torque, a static test was performed. The same set up as shown in Figure 4 was used except weights were added to the end of the dumbbell. Table 1 shows the results of these tests. By extrapolating the

TABLE 1

Torque	Weight	Deflection
19 in-lb.	1 lb.	.0004
38	2	.0008
95	5	.0018
190	10	.0034
475	25	.0122

data in Table 1, the deflection necessary to produce one inch-pound of torque is 2×10^{-5} inches. Therefore, the deflection produced by the gyroscopic forces on the 200 pound dumbbell is approximately 14×10^{-9} inches. This deflection is at least an order of 10^{-10} inches smaller than any other length measurement considered. Since this deflection is so small the gyroscopic forces upon the air bearing table can be neglected.

In summary, none of the three forces caused by the earth's rotation affect the system performance. Other forces which may affect the system will be analyzed later.

APPENDIX A9

Report of Calibration for

Moment of

Inertia Standards

HEADQUARTERS
U. S. ARMY MISSILE SUPPORT COMMAND
U. S. ARMY MISSILE COMMAND
REDSTONE ARSENAL, ALABAMA 35809

IN REPLY
REFER TO SMIDW-OLPP

Army Missile Command Calibration Center
Physical Standards Laboratory

Report of Calibration
For

Moment of Inertia Standards

A - 75 Lbs Nominal
B - 110 Lbs Nominal
C - 180 Lbs Nominal
D - 200 Lbs Nominal
E - 300 Lbs Nominal

Submitted By

SPACO
Huntsville, Alabama

Moment of Inertia Standards were intercompared with standard masses to determine their mass. The weighing system involved using a load cell as a transducer, feeding a signal into a precision readout. The weighing scheme was evolved at the National Bureau of Standards, and in these tests, involved intercomparing the unknown mass with two nearly identical standard masses. Thus each test run produced two estimates of the difference between the unknown and a standard, together with an estimate of the difference between the two standards, whose true difference was known to an accuracy well beyond that obtainable in the tests. These data were analyzed statistically to determine the errors involved in the weighings, and the final estimate of the mass of the unknown was a mean of a number of repeated tests, the quantity of which was sufficient to reduce the uncertainty to a satisfactory level. The design of the test was such that systematic errors are negligible, leaving only random errors to consider.

Test No 65-461
Page 1 of 5

KEEP FREEDOM IN YOUR FUTURE WITH U.S. SAVINGS BONDS

The results of these tests are as follows:

No	Nominal Size	True Mass Lb	Uncertainty (3 σ) Lb	Uncertainty (3 σ) % of Mass	No of Tests
A	75	74.981 6	.001 2	.002	15
B	110	112.874 5	.001 3	.001	10
C	180	182.821	.004	.002	34
D	200	198.750	.003	.002	17
E	300	290.966	.006	.002	12

Purpose and Procedure

The inertia standards were intercompared with mass standards to determine their mass with the highest degree of accuracy attainable at the Calibration Center.

To gain this end, a weighing scheme, evolved by the National Bureau of Standards and called the 3:1 cycle, was invoked. For a completely rigorous treatment of this scheme the reader is referred to the report by Lt. Perry Fisher*, but the essence of the scheme is described below.

The scheme involves use of the following items: two mass standards, differing from one another by some small amount, 0.1 pound, for example; a transducer-readout system capable of adequate resolution and sufficiently stable to operate with a slow, linear drift over say, an hour's time; a lifting system, free of vibration when holding the load; a timer and a small "sensitivity weight", of about 0.02% of the transducer capacity; and of course, the unknown mass.

* Theory and Technique Employed in the Calibration of Large Metric Masses at the George C. Marshall Space Flight Center, 25 January - 16 March 1965

If one were so fortunate as to have an ideal system, completely stable and impervious to drift, repeated weighings of the same mass would produce an identical readout. If, now, the sensitivity weight were added to this mass, we would get an increment in our readout which would be attributable to the increment in mass, and the ratio of these increments would be an indication of the sensitivity of our system for small increments in this range of mass. If we selected our two standard masses in such a manner that one was a trifle less than our unknown, and the other a trifle more, but with the total spread preferably less than the value of the sensitivity weight, we could operate entirely in this very small range of mass difference, with the result that even with a thoroughly non-linear system (in terms of linear increase of readout for a linear increase in mass from zero to capacity) we could feel safe in assuming that this small operating range is essentially linear.

Unfortunately, any real system has drift, due mainly to thermal effects in this case. The best we can do is to set up our procedure* in such a manner that each successive weighing occurs at the end of an identical history, and also that each set of inter-relating data is obtained over a short period of time, so that long-term non-linear effects are minimized. In addition, if the resulting data can be analyzed in such a fashion that the drift increments associated with each reading tend to cancel one another out, the problem of drift becomes at least a manageable one.

The 3:1 scheme involves three independent sets of readings for each test. In the present case they involve the following comparisons:

1. First standard with the specimen.
2. Second standard with the specimen.
3. First standard with the second standard.

* See appendix for a step-by-step summary of procedure.

Thus each test gives two estimates of the difference between the unknown and a standard, plus an estimate of the difference between the two standards. The value of the first two estimates is obvious, while that of the mass inter-comparisons yields a test result which can be compared with a known value.

An additional virtue of this weighing scheme is its freedom from systematic errors; those inherent in the system, such as offset meter zero, are reflected in all readings and are without moment due to our interest in differences of reading only. Drift has already been dealt with above, and the cumulative test results on the standard-versus-standard evaluation confirm the assumption that systematic errors are indeed trivial.

If systematic errors are slight, we are faced with the problem of reducing the random error in our final mean value of mass to a satisfactory value. N.B.S. has set up a series of analytical relationships (whose justification can be explored fully in Lt. Fisher's report) which yield least squares evaluations whose estimated variance is but 2/3 that of the raw data. They also provide a means of estimating the variance for the crude data in each test cycle. In accordance with classical statistics, the estimate of the mean value of the mass increases in precision with the number of trials, and by this rather brute-force method an increase in accuracy can be gained at the expense of time. For a halving of the estimated error, for example, four times the number of trials is required, a process which soon becomes economically unfeasible. In the tests thus far performed, a tolerable estimate of variance was achieved before the time expenditure became excruciating.

Unfortunately, the random errors suffered are essentially inherent in the weighing system with its attendant procedural crudities. If the same system is used for the evaluation of progressively smaller specimens, the absolute value of random error should remain the same. These errors, in terms of a percent-of-the-mass-involved, will then loom progressively larger with each progressively smaller mass. Inasmuch as the only solution (barring refinement of the system) is to increase the number of trials, this limitation ~~will~~ becomes increasingly serious with the smaller masses.

The data gleaned suggest that the estimate of variance computed is indeed realistic. As mentioned above, the cumulative estimate of the difference between the two standards is one which can be compared to a known value. The estimates thus far come within about half the estimated standard deviation ($\frac{1}{2}\sigma$) computed for the estimated value of mass. In addition, the cumulative estimated mean derived from each of the two unknown-versus-standard determinations comes within $\frac{1}{2}\sigma$ of the final estimate of the unknown mass.

The three larger masses were weighed using a BLH 500 lb capacity load cell, while the weighing of the two smaller masses were successfully weighed when a 200 lb capacity load cell was discovered which had the necessary stability. This discovery, coupled with some very useful recommendations on the part of Lt. Fisher, brought the program out of a serious impasse.

DAVID J. SHERK
In Charge of Test

ROY L. CAMERON
Chief, Physical Measurements Branch

APPENDIX

Step-by-step procedure of mass evaluation, 3:1 method.

A. Preliminary

1. Weigh unknown mass, using system as a weighing instrument to obtain first approximation of mass value.

2. Select standard masses such that one combination is slightly less than this value, and another slightly more. (Usually the second standard is the same basic masses as the first, with a small mass added.)

3. "Exercise" the system: raise the standard for the prescribed length of time and then let it rest for the prescribed length; repeat until the readout shows a tolerably small drift. (The time up - time down cycle may have to be altered to give satisfactorily small drift.)

B. Weighing

a. First Comparison

1. Raise the first standard and record the reading (Item "A" on test data sheet) following the prescribed time cycle. Then lower, and change to the specimen mass.

2. Raise the specimen mass, and record its reading (Item "B") then lower according to the time cycle.

3. Place the sensitivity weight on the platform with the specimen, and raise again, taking its reading (Item "C").

4. Lower, replace with the first standard and also the sensitivity weight. Then raise and take its reading (Item "D").

b. Data

We get four readings I_1, I_2, I_3, I_4 such that

Standard (S_1) yields I_1 (Item "A")

Specimen (X) yields I_2 (Item "B")

X + sensitivity weight yields I_3 (Item "C")

S_1 + sensitivity weight yields I_4 (Item "D")

with these data one can get an estimate of the difference between the standard and specimen (S_1 - X) by:

$$S_1 - X = \text{Sens Wt} \times \frac{\text{average difference between readings of } S_1 \text{ and X}}{\text{difference between readings due to sens wt}}$$

$$= \frac{1}{2}\left[W\left(\frac{I_1 - I_2}{I_3 - I_2}\right) + W\left(\frac{I_4 - I_3}{I_3 - I_2}\right)\right]$$

which reduces to

$$S_1 - X = W\left[\frac{(I_1 - I_2) + (I_4 - I_3)}{2\,(I_3 - I_2)}\right];$$ (listed as "a_1" on data sheet)

Note that, for any constant drift through this cycle (usually comprising 20 minutes), the error due to drift becomes zero if $I_1 - I_2 = I_3 - I_2$, or $I_4 - I_3 = I_3 - I_2$, since the first and second terms of the first expression become equal, but the drift component will be opposite in sign. Thus the ideal weight selection is that the sensitivity weight be equal to the difference between standard and specimen.

c. Second Comparison

Here weighing standard$_1$ (S_1) yields I_1

standard$_2$ (S_2) yields I_2

S_2 + Sens Wt yields I_3

S_1 + Sens Wt yields I_4, all of which are treated in a similar manner to give (S_1 - S_2). Listed as "a_2".

d. Third Comparison

Finally, weighing specimen (X) yields I_1

S_2 yields I_2

S_2 + Sens Wt yields I_3

X + Sens Wt yields I_4, which give a result of (X - S_2). Listed as "a_3".

C. Data Reduction, Using Least Squares Technique

The derivation of the relationship for the least squares result is involved, and is delineated in Lt. Fisher's report; suffice that it involves all three of the comparisons yielded above, and tends to add values in such a manner that the redundant value (considering that S_1, S_2 and X are evaluated completely by any two values) is used as a device for estimating the error in the system. Similarly, the estimated standard deviation for the test is the result of a derivation in Lt. Fisher's report.

The Data Reduction Work Sheet was laid out for a weighing scheme which involves only one standard and two unknowns; here it was used for one unknown and two standards, using standard number two for "X_2". The fifty pound masses usually do not weigh exactly fifty pounds and care must be taken to identify them and take their departures from nominal into consideration in the final mass calculation. The smaller masses are accurate well beyond the resolution of the system. In these tests S_2 was made by adding or removing a small weight from S_1. The result is that $S_1 - S_2$ should approximate the value of this small weight, and the sum of a_1 and a_3 should also approach this value. Significant departures from this value in the final least-squares estimate demonstrate the existence of large errors in this particular run, and are a valid reason for rejecting the results. A mean value for, say, a dozen runs which departs considerably from the true value suggests some systematic error in the procedure. This situation manifested itself during the weighing of Mass C, resulting in a mean estimate of $S_1 - S_2$ which was 0.003 lb in error. This error was well beyond that which would have arisen due to pure chance, and as a result the entire set of runs was rejected and a smaller sensitivity weight with closer-to-unknown standards was set up. The resulting cumulative estimate of $S_1 - S_2$was found to be well inside the bounds of random error.

The formulas for deriving the least-squares estimates were derived at NBS, which derivation is shown in Lt. Fisher's report. In essence, $S_1 - X$, $S_1 - S_2$, and $X - S_2$ are adjusted in such a manner that the errors in each estimate are at a minimum and the three estimates are consistent with each other. The relationships resulting in the estimate of standard deviation are also NBS derived, and Lt. Fisher's report may be consulted for this as well.

The final computations involve, first, finding a mean value for $S_1 - X$, $S_1 - S_2$ and $X - S_2$. The mean value of $S_1 - S_2$ should compare very closely (within, say, 0.0005% of total mass) with the known true value of $S_1 - S_2$. In the example shown, it is in error by about 70 millionths of a pound in 112 pounds. This encouraging result, plus an estimate of uncertainty

for the mean of but 0.0013 lb, are two realistic results which indicate that the test series was "under control", and that the resulting estimate of mass may be proclaimed with some confidence.

All the different masses comprising S_1 are added, giving a total true mass of 112.8799 lb. The mean of $S_1 - X$ was computed to be .005402 lb, which when subtracted from S_1 gives an estimated value of this mass of 112.8745 lb. The sum of $S_1 - X$ and $X - S_2$ should agree very well with $S_1 - S_2$ in each run; this is a means of checking computations. The "True Mass Correction" was not entered on each run; instead it was added at the final computation. Not only is there less chance of error, but the physical picture of what is being done is readily grasped.

Note that "3 σ" is computed, which is the uncertainty of the final value for the mass. Statistically, "3 σ" is an estimate of error which has but one chance in about 250 of being less than the actual error in the estimate.

TEMPERATURE — °C	HUMIDITY — %	PRESSURE — mm	TEST NO. 3 SET 2
OBSERVER D JS	BALANCE L.C.	DATE 6-22-65	SHEET 1 of 2 SERIES

S * = S_1 = 50, 50, 10, 2, .5, .2 lb + 2, ½, ¼, ⅛ oz	A	32.6	(1) A-B 0.7	$a_1 = \frac{(1)+(3)}{2(2)}(w) = \frac{.7+.5}{2 \times 6.6} \times .02$
X_1 = D # 2	B	31.9	(2) C-B 6.6	$a_1 =$ .00182 lb
$X_1 + w$ = X_1 + 0.02 lb	C	38.5	(3) D-C 0.5	
S + w = S_1 + w	D	39.0		
S = S_1	A	34.5	(1) A-B 3.7	$a_2 = \frac{(1)+(3)}{2(2)}(w) = \frac{3.7+2.9}{2 \times 5.1} \times .02$
$X_2 = S_2$ = S without ¼ oz	B	30.8	(2) C-B 5.1	$a_2 =$ .01296 lb
$X_2 + w$	C	35.9	(3) D-C 2.9	
S + w = S_1 + w	D	38.8		

* In this case, the standard "S" consisted of 50 lb. wt. #5, 50 lb. wt. #8, and 10, 2, 0.5 and 0.2 lb. wts. out of a set, plus a 2, ½, ¼ and 1/8 oz. wts. from a set.

Since, in this series, X_2 is another standard rather than an unknown, it has been designated as "S_2" for clarity, and S becomes "S_1". The weighing scheme remains the same and the chief advantage of another standard is that it furnishes us with a very useful check, as will be seen in the final calculations.

XERO COPY XERO COPY XERO COPY

TEMPERATURE	HUMIDITY	PRESSURE	TEST NO. 3	SET 2
OBSERVER	BALANCE L.C.	DATE	SHEET 2 of 2	SERIES

X_1	A	33.3	(1) A-B 4.3	$a_3 = \frac{(1)+(3)}{2(2)}(w)$ $= \frac{4.3 + 3.2}{2 \times 5.3} \times 02$ $a_3 = .01415$ lb
$X_2 = S_2$	B	29.0	(2) C-B 5.3	
$X_2 + w = S_2 + w$	C	36.3	(3) D-C 3.2	
$X_1 + w$	D	39.5		

DATA REDUCTION WORK SHEET

Set 2 Test No 3 Date 6-22-65

S = $50_5 + 50_8 + 10 + 2 + .5 + .2$ lb $+ 2 + \frac{1}{2} + \frac{1}{4} + \frac{1}{8}$ oz = _____ kg lb

X_1 = D # 2 _____ kg

X_2 = Switchout $\frac{1}{4}$ oz = "S_2" _____ kg

T.M. Corr. of S = K — _____ kg

From Data:

			X_1		X_2 = "S_2"		
$(S-X_1) = (S_1 - X_1)$	a_1	.00182 kg lb	$-2a_1$	-.364 kg lb	$-a_1$	-.182 kg lb	
$(S-X_2) = (S_1 - S_2)$	a_2	.01296 kg	$-a_2$	-.1296 kg	$-2a_2$	-.2592 kg	
$(X_1-X_2) = (X_1 - S_2)$	a_3	.01415 kg	sum	-.1660 kg	sum	-.2774 kg	
			$+a_3$	+.1415 kg	$-a_3$	-.1415 kg	
			Sum X_1	-.245 kg	Sum X_2	-.4189 kg	
Least Squares $(S-X_1) \rightarrow$ $=(S_1 - X_1)$			Sum X_1 / 3	-.00082 kg	Sum X_2 / 3	-.01396 kg	Least sq. $(S-X_2)$ $=(S_1-S_2)$
			+ K	— kg *	+ K	— kg *	
			sum	— kg *	sum	— kg *	

T.M. Corr. of X_1 ( ) — _____ kg *

T.M. Corr. of X_2 ( ) — _____ kg *

Std. Deviation (σ):

a_1	.00182 kg lb	σ = 0.577A =	.00174 kg lb		
$+a_3$	.1415 kg	3σ =	.0052 kg		
sum	.1597 kg	σ^2 =	3.02 $\times 10^{-6}$ kg^2		
$-a_2$	-.1296 kg				
sum	.00301 kg				
A= |sum|	.00301 kg				

* The original form was set up for this work to be done on each run. However, since the same correction is to be made each time, in practice the correction was made to the final average value, thus eliminating extra calculation with its chance for arithmetic error.

a_1 .00182
$-a_2$ -.1296
Σ -.1114
$-2a_3$ -.2830
3 | -.03944
-.01315 Lb

Least Sq. $(X_1 - X_2)$ $= (X_1 - S_2)$

FORM SV 3. 10 MA XERO COPY (ONE-TIME) XERO COPY XERO COPY

Computations of Estimate of Mass of Dumbbell No. 2, and Uncertainty

Sheet 1

Run No.	$S_1 - X$	$X - S_2$	$S_1 - S_2$	σ^2
1	.00489	.00476	.00960	$.01 \times 10^{-6}$
2	630	1093	1723	6.88
3	82	1315	1396	3.02
4	563	933	1497	.56
5	523	1084	1606	0
6	459	678	1136	0
7	172	1468	1640	6.73
8	1157	1034	2193	1.30
9	608	1234	1856	.78
10	719	967	1686	.03
	.05402	.10282	.15693	19.31×10^{-6}

Computation of Actual Mass of S_1:

Σ Small Lb. wts: $10 + 2 + .5 + .2$
$= 12.7000$

Σ Small oz wts: $2 + \frac{1}{2} + \frac{1}{4} + \frac{1}{8} = 2\frac{7}{8}$ oz
$= .17976$ Lb

Summing all wts:

$50_5 =$ 50.0001
$50_3 =$ 50.0001
12.7000
.1797
112.8799 Lb. = True Mass S_1

$S_1 - X$ $-.0054$
112.8745 = True Mass of X

ave Value of $S_1 - X = \frac{.05402}{10} = .005402$ Lb
ave Value of $X - S_2 = \frac{.10282}{10} = .010282$
check: estimate of $S_1 - S_2 = \varepsilon = .015684$
True est. of $S_1 - S_2 = .015625$
error $= .000069$ Lb

$S_1 - S_2 = \frac{.15693}{10} = .015693$
True $S_1 - S_2 = .015625$
$.000068$ Lb

Good agreement – hence computations appear OK

(From the above we may confidently estimate it to be .0054 Lb less than S_1

XERO COPY

Sheet 2

$\Sigma\sigma^2 = 19.31 \times 10^{-6}$ Lb

est. σ of mean value $= \sqrt{\frac{2}{3}\,\frac{\Sigma\sigma^2}{N(N-1)}}$

$$= \sqrt{\frac{2}{3} \times \frac{19.31 \times 10^{-6}}{10 \times 9}}$$

$\therefore \hat{\sigma} = 3.8 \times 10^{-4} = .00038$ Lb

Uncertainty = Systematic error $+ 3\hat{\sigma}$

The close agreement of the estimate of $S_1 - S_2$ with the actual value (70 millionths Lb error in 112 Lb) suggests that the systematic error is negligible.

$\therefore U \approx 3\hat{\sigma} = 3 \times .00038 = .0012$ Lb.

APPENDIX A10

Dumbbell Moment of Inertia Standard Calculation - An IBM 1620 computer program has been prepared for calculating the moment of inertia of the five dumbbell standards. The program is also capable of performing an analysis on the misalignment of the center of gravity of the dumbbell. (Figure 1.)

Figure 2 shows the dumbbell configuration and the terminology used for the dimensions. The computer program is shown below. No attempt will be made to explain the mechanics since an understanding of Fortran II programing would be essential.

The input data for each dumbbell, the center of gravity variations, the moment of inertia and the percentage error for the center of gravity misalignment is shown in Figures 3 through 7. The true moment of inertia for each dumbbell corresponds to the zero center of gravity location. The percentage error should be multiplied by 100 to obtain the true percentage. It is obvious upon examining the maximum errors for all the dumbbells that the mislocation of the dumbbell's center of gravity is insignificant. The maximum variation of 0.11 inches represents a gross error in aligning the dumbbell. Since the center of gravity can easily be located within 0.01 of an inch on the air bearing table the error can be assumed to be zero. The computer program is also capable of performing a diagnostic test on the program, that is, it will print out every bit of data it calculates. This could be useful in performing a detailed error analysis on the dumbbells.

The data on the dumbbells which includes the weights obtained from the Army Calibration Center, minus the new holes and the moments of inertia obtained from these calculations are listed below in Table 1.

TABLE 1

Dumbbell	A	B	C	D	E
Weight	74.963	112.856	182.802	198.731	290.947
Moment of Inertia	27.504	60.934	92.516	124.108	188.059

A computer program written in Fortran IV is shown in Figure 8 for future use in an IBM 360 system.

MAIN DUMBBELL MOI DETERMINATION

FIGURE 1

```
      DIMENSION WORD(18), COM(60)
      COMMON COM
C     BEGIN INPUT DATA STORAGE ASSIGNMENTS
      EQUIVALENCE
     1(COM   (   1),    DA),(COM   (   2),    DB),(COM   (   3),    DC),
     2(COM   (   4),    HA),(COM   (   5),    HB),(COM   (   6),    HC),
     3(COM   (   7),    TM),(COM   (   8),   XRA),(COM   (   9),   XRB),
     4(COM   (  10),  XR1A),(COM   (  11),  XR1B),(COM   (  12),  XR2A)
      EQUIVALENCE
     1(COM   (  13),  XR2B),(COM   (  14),    H1),(COM   (  15),    H2),
     2(COM   (  16),    D1),(COM   (  17),    D2),(COM   (  18),   VAR),
     3(COM   (  19),    CH),(COM   (  20),    XN),(COM   (  21),  ZERO)
C
C     BEGIN INTERNAL STORAGE ASSIGNMENTS
      EQUIVALENCE
     1(COM   (  25),    VA),(COM   (  26),    VB),(COM   (  27),   VH1),
     2(COM   (  28),   VH2),(COM   (  29),   VCT),(COM   (  30),    VC),
     3(COM   (  31),    VT),(COM   (  32),     P),(COM   (  33),    AM),
     4(COM   (  34),    BM),(COM   (  35),   H1M),(COM   (  36),   H2M)
      EQUIVALENCE
     1(COM   (  37),   CMT),(COM   (  38),    AI),(COM   (  39),    BI),
     2(COM   (  40),  H1IA),(COM   (  41),  H1IB),(COM   (  42),  H2IA),
     3(COM   (  43),  H2IB),(COM   (  44),   HIS),(COM   (  45),    CI),
     4(COM   (  46),    TI),(COM   (  47),    RA),(COM   (  48),    RB)
      EQUIVALENCE
     1(COM   (  49),   R1A),(COM   (  50),   R1B),(COM   (  51),   R2A),
     2(COM   (  52),   R2B)
C
      TYPE 100
  100 FORMAT(//38HTO CHANGE CG LOCATION TURN SWITCH 1 ON/61HFOR INTERNAL
     1 STORAGE ASSIGNMENTS TURN SWITCH 3 ON PRESS START)
      PAUSE
C
C     CLEAR INPUT DATA AND INTERNAL STORAGE ASSIGNMENTS
      CALL CLEAR1(COM,0.0,1,24,1)
   22 CALL CLEAR1(COM,0.0,25,60,1)
C
C     READ     INPUT DATA
      READ 1,(WORD(K),K=1,18)
    1 FORMAT (18A4)
      CALL DECRD(COM)
C
C     BEGIN DUMBBLL MOI DETERMINATION COMPUTATION
      N    = XN
      J    = ZERO
      I    = 0
      GO TO 40
   45 VAR  = VAR+CH
      J    =J+1
      ZERO = J
   40 IF(SENSE SWITCH 1)15,20
   15 I    = I+1
      GO TO 30
   20 I    = 1
      N    = 0
   30 RA   = XRA-VAR
      R1A  = XR1A-VAR
      R2A  = XR2A-VAR
      RB   = XRB+VAR
      R1B  = XR1B+VAR
```

(Continued)

```
      R2B   = XR2B+VAR
      PI    =3.14159
      VA    =(PI*DA**2*HA)/4.
      VB    =(PI*DB**2*HB)/4.
      VH1   =(PI*D1**2*H1)/4.
      VH2   =(PI*D2**2*H2)/4.
      VCT   =(PI*DC**2*HC)/4.
      VC   =VCT-2.*(VH1+VH2)
      VT    =VA+VB+VC
      P     =TM/VT
      AM    =P*VA
      BM    =P*VB
      H1M   =P*VH1
      H2M   =P*VH2
      CMT   =P*VCT
      AI   =AM*(DA**2/16.+HA**2/12.)
      BI   =BM*(DB**2/16.+HB**2/12.)
      H1IA =   (H1M*D1**2/8.+H1M*R1A**2)
      H1IB =   (H1M*D1**2/8.+H1M*R1B**2)
      H2IA =   (H2M*D2**2/8.+H2M*R2A**2)
      H2IB =   (H2M*D2**2/8.+H2M*R2B**2)
      HIS  =H1IA+H1IB+H2IA+H2IB
      CI   =CMT*(DC**2/16.+HC**2/12.)-HIS
      TI    =AI+BI+CI+AM*RA**2+BM*RB**2
C
C     PAGE HEADING PRINT OUT
      IF(J)6,6,7
    6 CAL  = TI
      PUNCH 1,(WORD(K),K=1,18)
    7 ERROR   =(CAL-TI)/CAL
C
C     PRINT OUT INTERNAL STORAGE ASSIGNMENTS
      IF(J)23,23,24
   24 IF(SENSE SWITCH 3 )23,115
   23 CALL NOZERO(COM,25,60)
  115 IF(J)150,150,225
  150 IF(SENSE SWITCH 3)80,90
   80 TYPE 1,(WORD(K),K=1,18)
      TYPE 200
   90 PUNCH 1,(WORD(K),K=1,18)
C
C     PRINT OUT INPUT DATA
      PUNCH 5,(COM(L),L=1,20)
    5 FORMAT(6X,2HDA,10X,2HDB,10X,2HDC,10X,2HHA,10X,2HHB/5F12.5//6X,2HHC
     1,10X,2HTM,10X,2HRA,10X,2HRB,10X,3HR1A/5F12.5//6X,3HR1B,9X,3HRA2,
     29X,3HR2B,9X,2HH1,10X,2HH2/5F12.5//6X,2HD1,10X,2HD2,6X,9HVARIATION,
     33X,9HCG CHANGE,4X,6HNUMBER/5F12.5//)
C
C     PRINT OUT OUTPUT NAMES
      PUNCH 200
  200 FORMAT(///5X, 13HCG VARIATIONS, 3X, 17HMOMENT OF INERTIA,3X,13HPER
     1CENT ERROR/)
C
C     PRINT OUT DATA
  225 IF(SENSE SWITCH 3)250,275
  250 TYPE 300, VAR, TI,ERROR
  275 PUNCH 300,VAR,TI,ERROR
  300 FORMAT(3X,F12.4,7X,F12.6,4X,F12.6/)
      IF (I-N)45,45,50
```

(Continued)

```
 50 CONTINUE
    TYPE 400
400 FORMAT(////12HEND OF CASE.//43H1F MORE DATA, TURN SWITCH 2 ON. PRE
   1SS START/)
    PAUSE
    IF(SENSE SWITCH 2)22,500
500 CONTINUE
    STOP
    END
```

FIGURE 2

DUMBBELL CONFIGURATION

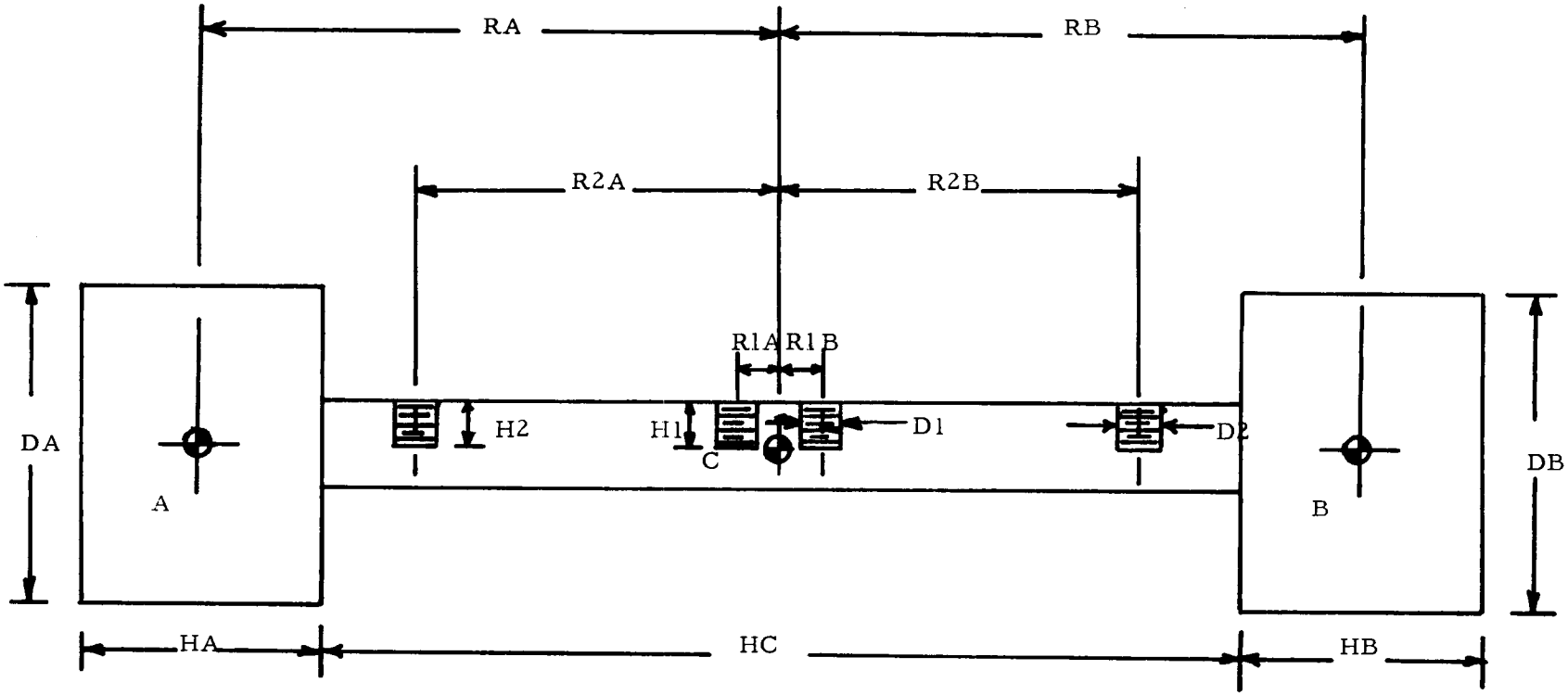

FIGURE 3

DUMBBELL CONFIGURATION (A)

DA	DB	DC	HA	HB
5.93810	5.93810	.98130	4.50010	4.50030
HC	TM	RA	RB	R1A
19.50290	.19440	12.00160	12.00150	.50000
R1B	RA2	R2B	H1	H2
.50000	8.25000	8.25000	.56000	.56000
D1	D2	VARIATION	CG CHANGE	NUMBER
.21700	.27600	0.00000	.00100	10.00000

CG VARIATIONS	MOMENT OF INERTIA	PERCENT ERROR
0.0000	27.503508	0.000000
.0010	27.503508	0.000000
.0020	27.503509	0.000000
.0030	27.503510	0.000000
.0040	27.503512	0.000000
.0050	27.503513	0.000000
.0060	27.503514	0.000000
.0070	27.503517	0.000000
.0080	27.503521	0.000000
.0090	27.503523	0.000000
.0100	27.503527	0.000000
.0200	27.503583	-.000002
.0300	27.503676	-.000006
.0400	27.503805	-.000010
.0500	27.503971	-.000016
.0600	27.504174	-.000024
.0700	27.504413	-.000032
.0800	27.504690	-.000042
.0900	27.505002	-.000054
.1000	27.505351	-.000067
.1100	27.505738	-.000081

FIGURE 4

DUMBBELL CONFIGURATION (B)

DA	DB	DC	HA	HB
6.37600	6.37530	1.94660	5.00020	5.00000
HC	TM	RA	RB	R1A
26.00000	.29270	15.50000	15.50000	.50000
R1B	RA2	R2B	H1	H2
.50000	9.87500	9.87500	.56000	.56000
D1	D2	VARIATION	CG CHANGE	NUMBER
.21700	.27600	0.00000	.00100	10.00000

CG VARIATIONS	MOMENT OF INERTIA	PERCENT ERROR
0.0000	60.934121	0.000000
.0010	60.934120	0.000000
.0020	60.934119	0.000000
.0030	60.934118	0.000000
.0040	60.934120	0.000000
.0050	60.934121	0.000000
.0060	60.934123	0.000000
.0070	60.934124	0.000000
.0080	60.934128	0.000000
.0090	60.934132	0.000000
.0100	60.934135	0.000000
.0200	60.934197	-.000001
.0300	60.934305	-.000003
.0400	60.934460	-.000005
.0500	60.934662	-.000008
.0600	60.934912	-.000012
.0700	60.935209	-.000017
.0800	60.935553	-.000023
.0900	60.935945	-.000029
.1000	60.936382	-.000037
.1100	60.936867	-.000045

FIGURE 5

DUMBBELL CONFIGURATION (C)

DA	DB	DC	HA	HB
6.62680	6.62670	1.94910	8.44200	8.44200
HC	TM	RA	RB	R1A
20.05780	.47400	14.24990	14.24990	.50000
R1B	RA2	R2B	H1	H2
.50000	8.25000	8.25000	.56000	.56000
D1	D2	VARIATION	CG CHANGE	NUMBER
.21700	.27600	0.00000	.00100	10.00000

CG VARIATIONS	MOMENT OF INERTIA	PERCENT ERROR
0.0000	92.516441	0.000000
.0010	92.516441	0.000000
.0020	92.516441	0.000000
.0030	92.516440	0.000000
.0040	92.516444	0.000000
.0050	92.516448	0.000000
.0060	92.516452	0.000000
.0070	92.516459	0.000000
.0080	92.516466	0.000000
.0090	92.516472	0.000000
.0100	92.516480	0.000000
.0100	92.516480	0.000000
.0200	92.516607	-.000001
.0300	92.516820	-.000004
.0400	92.517119	-.000007
.0500	92.517506	-.000011
.0600	92.517975	-.000016
.0700	92.518531	-.000022
.0800	92.519174	-.000029
.0900	92.519903	-.000037
.1000	92.520720	-.000046
.1100	92.521619	-.000055

FIGURE 6

DUMBBELL CONFIGURATION (D)

DA	DB	DC	HA	HB
10.00120	10.00120	1.98500	3.87490	3.87530
HC	IM	RA	RB	R1A
28.26960	.51530	16.07220	16.07200	.50000
R1B	RA2	R2B	H1	H2
.50000	9.87500	9.87500	.56000	.56000
D1	D2	VARIATION	CG CHANGE	NUMBER
.21700	.27600	0.00000	.00100	10.00000

CG VARIATIONS	MOMENT OF INERTIA	PERCENT ERROR
0.0000	124.107570	0.000000
.0010	124.107570	0.000000
.0020	124.107570	0.000000
.0030	124.107580	0.000000
.0040	124.107580	0.000000
.0050	124.107590	0.000000
.0060	124.107590	0.000000
.0070	124.107600	0.000000
.0080	124.107610	0.000000
.0090	124.107620	0.000000
.0100	124.107620	0.000000
.0200	124.107770	-.000001
.0300	124.108000	-.000003
.0400	124.108320	-.000006
.0500	124.108730	-.000009
.0600	124.109230	-.000013
.0700	124.109820	-.000018
.0800	124.110510	-.000023
.0900	124.111280	-.000029
.1000	124.112140	-.000036
.1100	124.113100	-.000044

FIGURE 7

DUMBBELL CONFIGURATION (E)

DA	DB	DC	HA	HB
9.99820	9.99730	1.95380	5.99400	5.99360
HC	TM	RA	RB	R1A
26.00510	.75440	15.99940	15.99960	.50000
R1B	RA2	R2B	H1	H2
.50000	9.87500	9.87500	.56000	.56000
D1	D2	VARIATION	CG CHANGE	NUMBER
.21700	.27600	0.00000	.00100	10.00000

CG VARIATIONS	MOMENT OF INERTIA	PERCENT ERROR
0.0000	188.058990	0.000000
.0010	188.058990	0.000000
.0020	188.058990	0.000000
.0030	188.058990	0.000000
.0040	188.058990	0.000000
.0050	188.059000	0.000000
.0060	188.059000	0.000000
.0070	188.059010	0.000000
.0080	188.059010	0.000000
.0090	188.059020	0.000000
.0100	188.059040	0.000000
.0200	188.059220	-.000001
.0300	188.059540	-.000002
.0400	188.060000	-.000005
.0500	188.060600	-.000008
.0600	188.061340	-.000012
.0700	188.062220	-.000017
.0800	188.063240	-.000022
.0900	188.064400	-.000028
.1000	188.065700	-.000035
.1100	188.067130	-.000043

FIGURE 8

MOI PROGRAM

```
C MAIN DUMBBELL MOI DETERMINATION IN FORTRAN IV        FEB. 4, 1966   JHJ
C
C
C  COM 1 TO 17 ARE THE DUMBBELL DIMENTIONS
C  COM 18, VAR IS THE DISPLACEMENT OF THE DUMBBELL CG FROM
C          THE TABLE ROTATION AXIS
C  COM 19, CH IS THE AMOUNT TO CHANGE THE CG WITH EACH RUN
C  COM 20, XN IS THE NUMBER OF RUNS
C  COM 21, ZERO  DATA TO ZERO SHOULD BE 0.0
C  COM 22, XMODE  0.0 DATA WILL PRINT ONLY OUT PUT DATA
C          XMODDE 1.0 DATA WILL PRINT OUT PUT DATA AND INTERNAL STORAGE
C          ONE TIME FOR FIRST CASE
C          XMODDE 2.0 DATA WILL PRINT OUT PUT DATA AND INTERNAL STORAGE
C          FOR EACH CASE
C
      DIMENSION WORD(12), COM(60)
C     BEGIN INPUT DATA STORAGE ASSIGNMENTS
      COMMON COM
      EQUIVALENCE
     1(COM   (   1),    DA),(COM   (   2),    DB),(COM   (   3),    DC),
     2(COM   (   4),    HA),(COM   (   5),    HB),(COM   (   6),    HC),
     3(COM   (   7),    TM),(COM   (   8),   XRA),(COM   (   9),   XRB),
     4(COM   (  10),  XR1A),(COM   (  11),  XR1B),(COM   (  12),  XR2A),
     5(COM   (  13),  XR2B),(COM   (  14),    H1),(COM   (  15),    H2),
     6(COM   (  16),    D1),(COM   (  17),    D2),(COM   (  18),   VAR),
     7(COM   (  19),    CH),(COM   (  20),    XN),(COM   (  21),  ZERO),
     8(COM   (  22), XMODE)
C
C     BEGIN INTERNAL STORAGE ASSIGNMENTS
      EQUIVALENCE
     1(COM   (  25),    VA),(COM   (  26),    VB),(COM   (  27),   VH1),
     2(COM   (  28),   VH2),(COM   (  29),   VCT),(COM   (  30),    VC),
     3(COM   (  31),    VT),(COM   (  32),     P),(COM   (  33),    AM),
     4(COM   (  34),    BM),(COM   (  35),   H1M),(COM   (  36),   H2M),
     5(COM   (  37),   CMT),(COM   (  38),    AI),(COM   (  39),    BI),
     6(COM   (  40),  H1IA),(COM   (  41),  H1IB),(COM   (  42),  H2IA),
     7(COM   (  43),  H2IB),(COM   (  44),   HIC),(COM   (  45),    CI),
     8(COM   (  46),    TI),(COM   (  47),    RA),(COM   (  48),    RB),
     9(COM   (  49),   R1A),(COM   (  50),   R1B),(COM   (  51),   R2A),
      EQUIVALENCE
     1(COM   (  52),   R2B)
C
C     CLEAR INPUT DATA AND INTERNAL STORAGE ASSIGNMENTS
      CALL CLEAR1(COM,0.0,1,24,1)
   22 CALL CLEAR1(COM,0.0,25,60,1)
C
C     READ      INPUT DATA
      READ(5, 1)  (WORD(K), K = 1, 12)
    1 FORMAT (12A6)
      CALL DECRD(COM)
C
```

MOI PROGRAM CONTINUED

```
C     BEGIN DUMBBLL MOI DETERMINATION COMPUTATION
      N     = XN
      J     = ZERO
      I     = 0
      M     = XMODE
      GO TO 40
   45 VAR   = VAR+CH
      J     =J+1
      ZERO  = J
   40 I     = I + 1
      RA    = XRA-VAR
      R1A   = XR1A-VAR
      R2A   = XR2A-VAR
      RB    = XRB+VAR
      R1B   = XR1B+VAR
      R2B   = XR2B+VAR
      PI    =3.14159
      VA    =(PI*DA**2*HA)/4.
      VB    =(PI*DB**2*HB)/4.
      VH1   =(PI*D1**2*H1)/4.
      VH2   =(PI*D2**2*H2)/4.
      VCT   =(PI*DC**2*HC)/4.
      VC   =VCT-2.*(VH1+VH2)
      VT    =VA+VB+VC
      P     =TM/VT
      AM    =P*VA
      BM    =P*VB
      H1M   =P*VH1
      H2M   =P*VH2
      CMT   =P*VCT
      AI   =AM*(DA**2/16.+HA**2/12.)
      BI   =BM*(DB**2/16.+HB**2/12.)
      H1IA =   (H1M*D1**2/8.+H1M*R1A**2)
      H1IB =   (H1M*D1**2/8.+H1M*R1B**2)
      H2IA =   (H2M*D2**2/8.+H2M*R2A**2)
      H2IB =   (H2M*D2**2/8.+H2M*R2B**2)
      HIS   =H1IA+H1IB+H2IA+H2IB
      CI   =CMT*(DC**2/16.+HC**2/12.)-HIS
      TI    =AI+BI+CI+AM*RA**2+BM*RB**2
C
      IF(J) 23, 23, 24
   23 CAL   = TI
C
```

MOI PROGRAM

```
C  DECIMAL DUMP ROTINE IN FORTRAN IV                FEB. 7 1966    JHJ
C
      SUBROUTINE NOZERO(DATA, IFIRST, LAST)                                  +
      DIMENSION DATA(4)
      KOUNT      = 0
      DO 10 JSUB = IFIRST, LAST
      IF( DATA(JSUB))20, 80, 20
   20 KOUNT      = KOUNT + 1
      GO TO (30, 40, 50, 60) , KOUNT
   30 J1         = JSUB
      GO TO 80
   40 J2         = JSUB
      GO TO 80
   50 J3         = JSUB
      GO TO 80
   60 J4         = JSUB
      KOUNT      = 0
      WRITE(6, 102) J1,DATA(J1), J2,DATA(J2), J3,DATA(J3), J4,DATA(J4)
  102 FORMAT(4(I4, F16.8))
   80 IEND       = JSUB - LAST
      IF( IEND) 10, 110, 120
  110 IF( KOUNT) 120, 10, 170
  170 GO TO (130, 140, 150), KOUNT
  130 WRITE (6, 131)J1, DATA(J1)
  131 FORMAT (I4, E16.8)
      GO TO 10
  140 WRITE (6, 141) J1, DATA(J1), J2, DATA(J2)
  141 FORMAT(2(I4, F16.8))
      GO TO 10
  150 WRITE (6, 151) J1, DATA(J1), J2, DATA(J2), J3, DATA(J3)
  151 FORMAT(3(I4, F16.8))
   10 CONTINUE
      GO TO 200
  120 WRITE (6, 121) KOUNT , IEND
  121 FORMAT(8H KOUNT =, I4, 5X, 6HIEND =, I4)
  200 CONTINUE
      RETURN
      END


C  CLEAR1 IN FORTRAN IV                          FEB. 8 1966   JHJ          00001
C                                                                              2
C     ARRAY CLEARING ROUTINE                                                   3
      SUBROUTINE CLEAR1(A,B,LOC1,LOC2,K)                                       4
      DIMENSION A(1)                                                           5
      DO 10 I = LOC1,LOC2,K                                                    6
   10 A(I)          = B                                                        7
      RETURN                                                                   8
      END                                                                      9
```

MOI PROGRAM

```
C  RELATIVE READ ROUTINE FOR DECIMAL DATA IN FORTRAN IV  FEB. 4, 1966JHJ
C
      SUBROUTINE DECRD(B)
      DIMENSION   A(5), B(5), ND(5)
C
    5 READ (5, 10) LOC, (ND(I), I=1, 5), (A(J), J=1, 5)
   10 FORMAT(I6,I2,4I1, 5F12.8)
      IF(LOC)21,20,23
   20 WRITE(6, 30) (A(I), I=1,5)
   30 FORMAT(1H1 56H THE LOCATIONS FOR THE FOLLOWING DATA WAS NOT SPECIF
     1YED.'/ 10X,4F12.8/ 33H FIX THE CARD AND THEN REPROGRAM.)
      GO TO 55
   21 IF(LOC + 9999)22,55,22
   22 LC          = 1
      LOC         = - LOC
      GO TO 40
   23 LC          = 2
   40 DO 50 I = 1, 5
      IF(ND(I))50,45,50
   45 J           = LOC - 1 + I
      B(J)        = A(I)
   50 CONTINUE
      GO TO (60, 5), LC
   55 WRITE(6, 56)
   56 FORMAT(13H JOB COMPLETE)
      CALL EXIT
   60 CONTINUE
      RETURN
      END
```

APPENDIX A11

TEST PROCEDURE

1.4 System Analysis

1.4.1 Evaluation Tests

1.4.1.1 Purpose

To analyse the air bearing torsional pendulum system to determine the accuracy to which moments of inertia can be obtained.

1.4.1.2 Equipment

(1) 24-inch air bearing table
(2) Photocell timing device
(3) Displacement detector
(4) Two Hewlett-Packard 524D frequency counters
(5) One Hewlett-Packard 560A digital recorders
(6) Torsion rod
(7) Dumbbell standard

1.4.1.3 Set-Up

(1) Turn on electronic equipment for warm-up.
(2) Level air bearing table on iso-pad.
(3) Set air pressure at 30 psi.
(4) Mount dumbbell C on the table top.
(5) Insert rod number 124 into the table.
(6) Zero the wand and grating for triggering the photocells for both the period and displacement devices.
(7) Use one Hewlett-Packard frequency counter for recording the displacements.
(8) Use the other Hewlett-Packard counter and the digital recorder for recording the periods.

1.4.1.4 Test Procedure

(1) After the test procedure has been arranged as outlined in the test set-up, testing is ready to begin.

(2) Manually displace the table top to a displacement slightly greater than the starting displacement given in the Test Data section.

(3) When the maximum displacement decays to the starting

displacement, start the time counter. Obtain the data called for in the data sheet below.

1.4.1.5 Test Data

(1) Date -
(2) Personnel -
(3) Dumbbell - C
(4) Torsion Rod - 124
(5) Starting Displacement - 0.001 radians
(6) Number of Cycles - 500
(7) Sampling Frequency - 10 period averages every 20 cycles
(8) Test No. Temp. Humidity Time

(9) Include Period Print-out Tape

Written By: M. L. Phillips

Approved By: C. Phillips

Date: Mar 29 1966

APPENDIX A12

STATISTICAL ANALYSIS

A statistical analysis computer program was written to define and provide basic statistical properties of sample data, so that a more sophisticated analysis may be performed at the discretion of the user. The statistical computer program, with its subroutines, is shown in Table 1. The actual operation and input data requirements are explained in the comment section of the program. The main program consist of four subroutines DECRD, FREQ, STAT, and POPUL. Figure 1 is the functional flow chart of the main program.

Subroutine DECRD is used to read in the data points to be analyzed. Figure 2 is the functional flow chart for DECRD.

Subroutine FREQ is used for computing the frequency distributions of the population sample. This subroutine also uses subroutine SMOOTH to apply the least squares polynomial approximation principal to a set of four data points to obtain a polynomial equation of the second degree which best fits these points. FREQ then compares the next data point to see if the relative error (A-B/A+B) between its computed value and actual data is greater than the preset limit. The limit is part of the input data. This test and correction prevents an error of large magnitude from greatly biasing the output conclusions. After all the data points have been smoothed, subroutine FREQ arranges the data in ascending order. The choice of printing out the Y input data, the Y ascending order, and the Y deviation (Y-Y) is a function of the input data.

The program automatically divides the data into a number of classes based on Sturges rule $m = 1 + 3.3 \log_{10} N$. (See Table 2.) Sturges rule seems to suggest too many classes when the number of cases are small and too few classes when the number of cases are large. The actual choice of the number of classes will depend on the nature of the data studied, and on the units in which they are stated. To facilitate the study of special data, an alternate mode is included in the program. When the number of classes, considering the magnitude of each class and its base number, is inserted with input data, (see Table 3), the program automatically follows the above input guide lines. The number of cases in each class is then counted and control returns to the main program. Figure 3 is the functional flow chart for FREQ and Figure 4 is the functional flow chart for SMOOTH.

Subroutine STAT produces a general knowledge of the measures of central tendencies in ungrouped data. There is no limit to the number of ways in which one could select a value as representative of a group of data. STAT computes the methods that are in most common use among statisticians:

Arithmetic mean Y	=	$\Sigma(Y)/N$	(9)
Geometric mean Y_g	=	$e(\Sigma(\mathrm{Log}(Y))/N)$	(10)
Harmonic mean Y_h	=	$N/\Sigma(1/Y)$	(11)
Quadratic mean Y_q	=	$\Sigma(Y^2)/N$	(12)
Sigma (σ) S1	=	$\Sigma((Y - Y)^2)/N - 1$	(13)
Sigma (σ^2) S2	=	$N\Sigma(Y^2) - (\Sigma(Y))^2)/N(N - 1)$	(14)

The program also provides the numerical values of the various sums computed. The median and mode may be determined from the array of the ascending values of Y and a frequency distribution table. The median is the value of Y at $(N + 1)/2$ and the mode is the value of Y occurring most frequently.

The arithmetic mean is the most widely used and most commonly understood of all the averages. The arithmetic mean is usually stable in sampling, running more uniform from sample to sample than any of the other averages. When there is a marked skewness in a distribution so that the arithmetic mean, the median, and the mode differ widely in value, it should be considered a possiblility that the arithmetic mean is not truly representative or a typical value, and that the median or mode should be used in preference to it.

The geometric mean is used in cases involving average rate of increase or decrease, or cases involving the computation of index number. Its value is not greatly influenced by extreme items as are the values of the quadratic, arithmetic, and harmonic means.

The harmonic mean is used in certain cases of finding the average of rates. Every rate is stated as a variable number of units of something per constant number of unit of something else. The harmonic mean is rigidly defined and its value depends on the value of each item in the distribution. The results can be used for further mathematical computation. The program is such that it will skip a zero number, not entering it into the computations.

In certain theoretical probability problems it is important to use the squares of numbers, rather than the numbers themselves. In such cases the quadratic mean is natural.

The population parameters corresponding to S and S^2 are the population standard deviation and variance respectively. Figure 5 is the functional flow chart for STAT.

Subroutine POPUL computes the population percentage of the whole population within the interval of the first, second, and third sigma values (1S, 2S, and 3S); Figure 6 is the functional flow chart for POPUL. The statistical computer program typical output format is shown in Tables 2 through 4.

STATISTICAL ANALYSIS PROGRM

```
C     STATISTICAL ANALYSIS PROGRAM    MARCH 23, 1966      JHJ
C
C     WORD = ALPHAMERIC FIELD FOR PAGE HEADING COL1 TO 72 ON FIRST DATA CARD
C     XN   = NUMBER OF DATA POINTS INPUT DATA SHOULD IN COL1 TO 12 OF
C            SECOND DATA CARD
C     YLIMIT = A-B/A+B THE MAXIMUM PERMISSIBLE RELATIVE Y DATA DEVIATION
C              INPUT DATA SHOULD BE IN COL 13 TO 24 OF SECOND DATA CARD
C     XKXM = NUMBER OF CLASS INTERVALS IF EXTERNAL MODE CONTROL IS USED
C              INPUT DATA SHOULD BE IN COL 25 TO 36 OF SECOND DATA CARD
C     CLASS= THE AMOUNT TO INCREMENT EACH INTERVAL
C              IMPUT DATA SHOULD BE IN COL 37 TO 48 OF SECOND DATA CARD
C     BASE = THE LEAST Y VALUE TO BEGAIN INCREMENTING EACH INTERVAL
C              IMPUT DATA SHOULD BE IN COL 49 TO 60 OF SECOND DATA CARD
C     XMODE = FOR PRINT OUT OF X,Y,Y ASCENDING AND Y DEVIATION PUT
C            ANY NUMBER IN COL 61 TO 72 OF SECOND DATA CARD
C     Y    = VALUES OF Y TO BE READ IN BY SUBROUTINE DECRD
C
C
      DIMENSION WORD(18),A(225),X(225),Y(225),YSUM(20),ASTEP(20),D(225)
    1 READ 10, (WORD(K),K=1,18)
   10 FORMAT(18A4)
      READ 5, XN,YLIMIT,XKXM,CLASS,BASE,XMODE
    5 FORMAT (6F12.6)
      CALL DECRD(Y)
      N    = XN
      KXM  = XKXM
      DO 16 I=1,N
   16 X(I) = I
      CALL FREQ(Y,X,A,YSUM,N,YLIMIT,ASTEP,KXM,CLASS,BASE)
      CALL  STAT (A,D,N,S1,S2,YS,YS2,YG,YH,YQ,YB,YD,YD2,YL,YR)
      CALL POPUL(A,N,YB,S1,S1P,S2P,S3P)
      IF(XMODE)19,14,19
   19 PUNCH 15, (WORD(K),K=1,18)
   15 FORMAT(//18A4//)
      PUNCH 20
   20 FORMAT(13X16H X-Y DATA POINTS10X,11HY-DEVIATION3X,12H Y-ASCENDING
     1/11X,2H X14X,2H Y13X,3H YD12X,3H YA/)
      ICOUNT=0
      DO 30 I=1,N
      PUNCH 40,   I ,Y(I),D(I),A(I)
   40 FORMAT(9X,I4,6X,3F16.8)
      ICOUNT=ICOUNT+1
      IF(ICOUNT-50) 30,45,45
   45 ICOUNT=0
      PUNCH 46, (WORD(K),K=1,18)
   46 FORMAT(//1H118A4/5X,  10H CONTINUED/)
      PUNCH 20
   30 CONTINUE
   14 PUNCH 15, (WORD(K),K=1,18)
      PUNCH 50
   50 FORMAT(///19X,16H CLASS INTERVALS,22X,9H OBSERVED/
     1 16X,5H FROM,12X,3H TO,21X,10H FREQUENCY)
```

TABLE 1 - a.

STATISTICAL ANALYSIS PROGRAM CONTINUED

```
      PUNCH 55,(ASTEP(J),ASTEP(J+1),YSUM(J),J=1,KXM)
   55 FORMAT (12X,2F16.8,10X,F9.1)
      PUNCH 60, N,YB,YQ,YG,YH
   60 FORMAT(//6X,5H DATA6X,11H ARITHMETIC4X,9HQUADRATIC5X,9HGEOMETRIC
     16X,8HHARMONIC/5X,7H POINTS9X,4HMEAN9X,4HMEAN10X,4HMEAN
     211X,4HMEAN//7X,I4,3X,4F14.7//)
      PUNCH 70, S1,S2,S1P,S2P,S3P
   70 FORMAT(6X,9H STANDARD5X,9H VARIANCE5X,8H PERCENT6X,8H PERCENT6X,
     18H PERCENT/4X,13H DEVIATION S16X,3H S26X,14H 1S POPULATION
     228H 2S POPULATION 3S POPULATION//2X,5F14.6//)
      PUNCH 80, YS,YS2,YR,YL,YD,YD2
   80 FORMAT(7X,9H SUM OF Y11X,17H SUM OF Y SQUARES5X,21H SUM OF Y RECIP
     1ROCALS//2(E19.8,5X),E19.8//5X13HSUM OF LOG(Y)8X15HSUM OF Y - YBAR
     24X,25H SUM OF (Y - YBAR)SQUARES //2(E19.8,5X),E19.8//)
      GO TO 1
      END
```

```
C     RELATIVE READ ROUTINE FOR DECIMAL DATA
      SUBROUTINE DECRD(B)
      DIMENSION   A(5), B(5), ND(5)
C
    5 READ 10, LOC, (ND(I), I = 1, 5), (A(J), J = 1, 5)
   10 FORMAT(I6,I2,4I1, 5F12.8)
      IF(LOC)21,20,23
   20 PRINT 30,(A(I), I = 1, 5)
   30 FORMAT(1H0,10X,58HYOU FORGOT TO SPECIFY THE LOCATIONS FOR THE FOLL00000001
     1OWING DATA//11X, 5F12.8//11X,  6HSTUPID//11X,60HIF YOU KNOW HOW TO00000002
     2 FIX THE CARD, FIX IT AND THEN PRESS START/11X, 47HIF YOU DON-T KN00000003
     3OW HOW, THEN DON-T WASTE MY TIME)
      PAUSE
      GO TO 5
   21 IF(LOC + 9999)22,55,22
   22 LC          = 1
      LOC         = - LOC
      GO TO 40
   23 LC          = 2
   40 DO 50 I = 1, 5
      IF(ND(I))50,45,50
   45 J           = LOC - 1 + I
      B(J)        = A(I)
   50 CONTINUE
      GO TO (60, 5), LC
   55 PRINT 56
   56 FORMAT( 12HJOB COMPLETE)
      STOP
   60 CONTINUE
      RETURN
      END
```

TABLE 1 - b.

STATISTICAL ANALYSIS PROGRM

```
      SUBROUTINE FREQ(Y,X,A,YSUM,N,YLIMIT,ASTEP,KXM,CLASS,BASE)
C
C     FOR COMPUTING FREQUENCY DISTRIBUTION FORTRAN II  9-10-66  JHJ
C
C     Y     = ARRAY FOR Y DATA
C     X     = ARRAY FOR X DATA
C     A     = ARRAY FOR REARRANGED Y DATA
C     YSUM  = ARRAY FREQUENCY DISTRIBUTION VALUES
C     N     = NUMBER OF DATA POINTS
C     ASTEP = ARRAY FOR THE CLASS INTERVALS
C     KXM   = NUMBER OF CLASS INTERVALS
C     CLAS  = THE AMOUNT TO INCREMENT EACH INTERVAL
C
      DIMENSIONY(1),A(1),SUB(4),C(3),TY(4),TX(4),YSUM(20),X(1),
     1 ASTEP(1)
C
C     TESTING DATA POINTS FOR RANDOM ERRORS OUT SIDE ANY PRESENT LIMIT.
C     CORRECTION IS WITH A LEAST SQUARES CURVE FITTING ROUTINE
C     USING A QUADRATIC EQUATION Y= C1+C2*X+C3*X**2
      I     =0
      IX    =0
      KX    = 0
   50 DO 90 J=1,4
      I     =I+1
      TY(J) = Y(I)
      TX(J) = X(I)
      IF(IX) 65,65,90
   65 IF(N-I-1)80,80,90
   80 IF(J-3) 70,70,75
   70 I     = I-4
   75 IX    = J
   90 CONTINUE
      CALL SMOOTH(TX,TY,4,2,C)
      K     =1
   85 K     =K+1
      YTEST = C(1)+C(2)*X(K)+C(3)*X(K)**2
      TEST = (YTEST-Y(K))/(YTEST+Y(K))
      IF (ABSF(TEST)-YLIMIT)102,102,105
  105 Y(K) = YTEST
  102 IF(K-N)101,120,120
  101 GO TO 50
  120 CONTINUE
C
```

TABLE 1 - c.

STATISTICAL ANALYSIS PROGRAM CONTINUED

```
C     ARRANGING Y TERMS IN ASCENDING ORDER IN ARRAY A
      DO 275 I=1,N
  275 A(I)=ABSF(Y(I))
      DO 350 I=1,N
      DO 350 J=I,N
      IF (A(I)-A(J))350,350,355
  355 TEMP = A(I)
      A(I) = A(J)
      A(J) = TEMP
  350 CONTINUE
C
C     TESTING IF EXTERNIAL CLASS INTERVIAL MODE DESIRED
C     IF NOT CLASS INTERVIAL COMPUTED BY CLASS = 3.3*LOG (N)+1
      IF(KXM)415,415,420
  415 YDIF = A(N)-A(1)
      XNUM = N
      KXM  = 0.43429488*LOGF(XNUM)*3.3+1.5
      XM   = KXM
      CLASS= YDIF/XM
  425 ASTEP(1)= A(1)
      GO TO 426
  420 ASTEP(1) = BASE
  426 KXMP1= KXM+1
      DO 427 I=2,KXMP1
      ASTEP(I)= ASTEP(I-1)+CLASS
  427 CONTINUE
      I=0
      XN    =0.0
      DO 435 J=1,KXM
  435 YSUM(J)=0.
      DO 450 J=2,KXMP1
      JM1=J-1
  444 I     = I+1
      IF(ASTEP(J)-A(I))440,445,445
  445 XN    =XN+1.
      YSUM(JM1)=XN
      IF (I-N) 444,450,450
  440 XN    =0.0
      XN    = XN +1.
      YSUM(J)=XN
  450 CONTINUE
      RETURN
      END
```

```
      SUBROUTINE SMOOTH(X, Y, NODP, M, C )
C
C     LEAST SQUARES TECHNIQUE FOR SMOOTHING DATA POINTS   FORTRAN II SHO
C
C     THIS SUBROUTINE APPLIES THE LEAST SQUARES POLYNOMIAL APPROXIMATION
C     PRINCIPAL TO A SET OF N DATA POINTS TO OBTAIN A POLYNOMIAL OF
C     DEGREE M WHICH BEST FITS THESE POINTS.
C
C     THE POLYNOMTAL EQUATION IS OF THE FOLLOWING FORM----
C     Y = C(1) + C(2)*X + C(3)*X**2---- + C(M+1)*X**M

     NODP  THE ACTUAL NUMBER OF X-Y DATA PAIRS
C     M     THE DEGREE OF THE POLYNOMIAL  MAXIMUM OF 10
C     N     THE NUMBER OF EQUATIONS (=M + 1)
C     X,Y   ARRAYS FOR THE DATA PAIRS
C           ARRAY FOR THE SUMS, WHICH BECOME THE COEFICIENTS OF THE
C           UNKNOWNS IN THE SIMULTANEOUS EQUATIONS
C     B     ARRAY FOR CONSTANT TERMS IN THE SIMULTANEOUS EQUATIONS
C     C     ARRAY FOR THE UNKNOWNS, WHICH BECOME THE COEFICIENTS IN
C           THE POLYNOMIAL
C     P     ARRAY FOR THE POWERS OF THE  X(I), FROM 1 TO 2M
C
C
      DIMENSION X(1), Y(1), A(11, 11), C(11), P(20), B(11)
      IF(NODP - M + 1)5, 5, 6
    5 TYPE 30
   30 FORMAT( 44H1INSUFFICIENT DATA POINTS FOR THE POLYNOMIAL )
      STOP
C
C     FORMING THE POWERS OF X
    6 MX2 = M * 2
      N     = M +1
      DO 10 J = 1, MX2
   10 P(J) = 0.0
      DO 20 J= 1, N
   20 B(J) = 0.0
      DO 11 I = 1, NODP
      T     = Y(I)
      B(1) = B(1) + T
      DO 25 K = 2,N
      T     = X(I) *T
   25 B(K) = B(K) + T
      TEMP = 1.
      DO 11 J = 1, MX2
      TEMP = TEMP * X(I)
   11 P(J) = P(J) + TEMP
C
C     ARRANGING POWERS OF X IN ARRAY A
      A(1, 1) = NODP
      DO 12 I = 1, N
      DO 12 J = 1, N
      K     = I+J-2
      IF(K)13,12,13
   13 A(I,J)= P(K)
```

TABLE 1 - d.

```
   12 CONTINUE
C
      DO 300 K=1, M
      KP1 = K+1
      L   = K
      DO 400 I = KP1, N
      IF(ABSF(A(I,K))-ABSF(A(L,K))) 400,400,401
  401 L = I
  400 CONTINUE
      IF(L - K) 500, 500, 405
  405 DO 410 J = K, N
      TEMP = A(K, J)
      A(K, J) = A(L, J)
  410 A(L, J) = TEMP
      TEMP = B(K)
      B(K) = B(L)
      B(L) = TEMP
C
C ELIMINATE COLUMN K BELOW ROW K FOR FINAL TRIANGULAL SET OF EQUATIONS
  500 DO 300 I= KP1, N
      FACTOR = A(I, K) / A(K, K)
      A(I, K) = 0.0
      DO  301 J= KP1, N
  301 A(I, J) = A(I, J) - FACTOR * A(K, J)
  300 B(I) = B(I) - FACTOR * B(K)
C
C     ELIMINATION COMPLETE BEGIN BACK SUBSTITUTION FOR ANSWERS
      C(N) = B(N) / A(N, N)
      I = M
  710 IP1 = I + 1
      SUM = 0.0
      DO 700 J = IP1, N
  700 SUM = SUM + A(I, J) * C(J)
      C(I) = (B(I) - SUM) / A(I, I)
      I = I - 1
      IF(I) 800, 800, 710
  800 CONTINUE
      PROD = 1.
      DO 3 I = 1, N
    3 PROD = PROD * A(I, I)
      IF(PROD) 7,4,7
    4 TYPE 31
   31 FORMAT( 16H1SINGULAR MATRIX )
      STOP
    7 CONTINUE
      RETURN
      END
```

STATISTICAL ANALYSIS PROGRM

```
      SUBROUTINE STAT(Y,D,N,S1,S2,YS,YS2,YG,YH,YQ,YB,YD,YD2,YL,YR)
      DIMENSION Y(1),D(1)
      DP    = N
      DPM1  = N-1
      YS    = 0.0
      YS2   = 0.0
      YR    = 0.0
      YL    = 0.0
      YD    = 0.0
      YD2   = 0.0
      DO 11, J=1,N
      YS    = YS +Y(J)
      YS2   = YS2 + Y(J)**2
      YL    = YL +  LOGF(Y(J))
      IF(Y(J))13,11,13
   13 YR= YR + 1./Y(J)
   11 CONTINUE
      YB    = YS/DP
      S2    = (DP*YS2-YS**2)/(DP*DPM1)
      DO 12  I=1,N
      D(I)  = Y(I)-YB
      YD    = YD + ABSF(D(I))
      YD2   = YD2 + D(I)**2
   12 CONTINUE
      S1    = SQRTF(YD2/DPM1)
      YG    = EXPF(YL/DP)
      YQ    = SQRTF(YS2/DP)
      YH    = DP/YR
      RETURN
      END
```

TABLE 1 - e.

STATISTICAL ANALYSIS PROGRM

```
      SUBROUTINE POPUL(Y,N,YB,S1,S1P,S2P,S3P)
      DIMENSION Y(1)
      XN    = N
      S1C   = 0.0
      S2C   = 0.0
      S3C   = 0.0
      YBPS1 = ABSF(YB)+S1
      YBP2S = YBPS1+S1
      YBP3S = YBP2S+S1
      DO 10 J = 1,N
      IF(YBPS1-ABSF(Y(J)))13,12,12
   12 S1C   = S1C + 1.
      GO TO 17
   13 IF(YBP2S-ABSF(Y(J)))15,17,17
   17 S2C   = S2C + 1.
      GO TO 18
   15 IF(YBP3S-ABSF(Y(J)))10,18,18
   18 S3C   = S3C + 1.
   10 CONTINUE
      S1P   = 100.*S1C/XN
      S2P   = 100.*S2C/XN
      S3P   = 100.*S3C/XN
      RETURN
      END
```

TABLE 1 - f.

FREQUENCY DISTRIBUTION Y=(10./X)*SIN(X)+5. AUTO

X-Y DATA POINTS X	Y	Y-DEVIATION YD	Y-ASCENDING YA
1.00000000	14.59334100	-2.43743870	2.83080230
2.00000000	14.73545800	-2.40785930	2.86938170
3.00000000	14.20310900	-2.28224630	2.99499470
4.00000000	13.41470000	-2.16924720	3.10799380
5.00000000	12.41198500	-1.97619220	3.30104880
6.00000000	11.24733300	-1.70923050	3.56801050
7.00000000	9.98052560	-1.56004150	3.71719950
8.00000000	8.67493350	-1.19048520	4.08675580
9.00000000	7.39383850	-1.15150680	4.12573420
10.00000000	6.19638620	-1.14778380	4.12945720
11.00000000	5.13413110	-1.07827920	4.19896180
12.00000000	4.24840860	-1.03850370	4.23873730
13.00000000	3.56801050	-1.02883240	4.24840860
14.00000000	3.10799380	-1.02256700	4.25467400
15.00000000	2.86938170	-.86497410	4.41226690
16.00000000	2.83980230	-.85683400	4.42040700
17.00000000	2.99499470	-.83474150	4.44249950
18.00000000	3.30104880	-.82701850	4.45022250
19.00000000	3.71719950	-.82126210	4.45597890
20.00000000	4.19896180	-.76443320	4.51280780
21.00000000	4.70137300	-.74612770	4.53111330
22.00000000	5.18210810	-.72195670	4.57528430
23.00000000	5.60425350	-.68555960	4.59168140
24.00000000	5.93855220	-.68034870	4.59689230
25.00000000	6.16498160	-.65620900	4.62103200
26.00000000	6.27357840	-.65365740	4.62358360
27.00000000	6.26448260	-.64885040	4.62839060
28.00000000	6.14723220	-.63355090	4.64369010
29.00000000	5.93939650	-.62169430	4.65554670
30.00000000	5.66467860	-.61960430	4.65763670
31.00000000	5.35065750	-.61246970	4.66477130
32.00000000	5.02635680	-.59623460	4.68100640
33.00000000	4.71983450	-.57586800	4.70137300
34.00000000	4.45597890	-.55740650	4.71983450
35.00000000	4.25467400	-.55683600	4.72040500
36.00000000	4.12945720	-.55413820	4.72310280
37.00000000	4.08675580	-.55138430	4.72585670
38.00000000	4.12573420	-.55087840	4.72636260
39.00000000	4.23873730	-.54188940	4.73535160
40.00000000	4.41226690	-.54165070	4.73559030
41.00000000	4.62839060	-.53030540	4.74693560
42.00000000	4.86644830	-.51341790	4.76382310
43.00000000	5.10490710	-.51307440	4.76416660
44.00000000	5.32320540	-.50639370	4.77084730
45.00000000	5.50343590	-.50513360	4.77210740
46.00000000	5.63173660	-.50333940	4.77390160
47.00000000	5.69928590	-.50175430	4.77548670
48.00000000	5.70283560	-.49102490	4.78621610
49.00000000	5.64475520	-.48257690	4.79466410
50.00000000	6.52976000	-.47988360	4.79735740

TABLE 2.

1 FREQUENCY DISTRIBUTION Y=(10./X)*SIN(X)+5. AUTO
CONTINUED

X-Y DATA POINTS X	Y	Y-DEVIATION YD	Y-ASCENDING YA
51.00000000	5.87927600	-.47494620	4.80229480
52.00000000	5.19683000	-.47312310	4.80411790
53.00000000	5.00507200	-.47188430	4.80535670
54.00000000	4.82005950	-.47067690	4.80656410
55.00000000	4.65763670	-.45901460	4.81822640
56.00000000	4.53111330	-.45718050	4.82006050
57.00000000	4.45022250	-.45304380	4.82419720
58.00000000	4.42040700	-.45117020	4.82607080
59.00000000	4.44249950	-.44944980	4.82779120
60.00000000	4.51280780	-.44877140	4.82846960
61.00000000	4.62358360	-.44746350	4.82977750
62.00000000	4.76382310	-.44702270	4.83021830
63.00000000	4.92032140	-.44404090	4.83320010
64.00000000	5.07888270	-.43121650	4.84602450
65.00000000	5.22557790	-.42484580	4.85239520
66.00000000	5.34794060	-.42339920	4.85384180
67.00000000	5.43600200	-.42287090	4.85437010
68.00000000	5.48307940	-.41354790	4.86369310
69.00000000	5.48625840	-.41079270	4.86644830
70.00000000	5.44653610	-.40815390	4.86908710
71.00000000	5.36862280	-.40757570	4.86966530
72.00000000	5.26042750	-.40172460	4.87551640
73.00000000	5.13228230	-.39531680	4.88192420
74.00000000	4.99597670	-.38910810	4.88813290
75.00000000	4.86369310	-.38531340	4.89192760
76.00000000	4.74693560	-.38142330	4.89581770
77.00000000	4.65554670	-.37346580	4.90377520
78.00000000	4.59689230	-.36280350	4.91443750
79.00000000	4.57528430	-.36258430	4.91465670
80.00000000	4.59168140	-.35691960	4.92032140
81.00000000	4.64369010	-.35456840	4.92267260
82.00000000	4.72585670	-.34886420	4.92837680
83.00000000	4.83021830	-.34841050	4.92883050
84.00000000	4.94705930	-.33803210	4.93920890
85.00000000	5.06580230	-.33018170	4.94705930
86.00000000	5.17595330	-.31419530	4.96304570
87.00000000	5.26801720	-.30355730	4.97368370
88.00000000	5.33430570	-.29596630	4.98127470
89.00000000	5.36956890	-.29555520	4.98168580
90.00000000	5.37139960	-.29458510	4.98265590
91.00000000	5.34038110	-.29335040	4.98389060
92.00000000	5.27996940	-.29173010	4.98551090
93.00000000	5.19612840	-.29027590	4.98696510
94.00000000	5.09675200	-.28951490	4.98772610
95.00000000	4.99093170	-.28630930	4.99093170
96.00000000	4.88813290	-.28585130	4.99138970
97.00000000	4.79735740	-.28126430	4.99597670
98.00000000	4.72636260	-.27724100	5.00000000
99.00000000	4.68100640	-.27216900	5.00507200
100.00000000	4.66477130	-.26545710	5.01178390

1 FREQUENCY DISTRIBUTION Y=(10./X)*SIN(X)+5. AUTO
CONTINUED

X-Y DATA POINTS X	Y	Y-DEVIATION YD	Y-ASCENDING YA
101.00000000	4.62103200	-.25088420	5.02635680
102.00000000	4.72040520	-.23859470	5.03864630
103.00000000	4.78621610	-.23345680	5.04378420
104.00000000	4.86966530	-.23122640	5.04601460
105.00000000	4.96304570	-.22990120	5.04733980
106.00000000	5.05792260	-.22837520	5.04886580
107.00000000	5.14588980	-.22459210	5.05264890
108.00000000	5.21930720	-.21931840	5.05792260
109.00000000	5.27196010	-.21852510	5.05871590
110.00000000	5.29957860	-.21143870	5.06580230
111.00000000	5.30037850	-.20298960	5.07425140
112.00000000	5.27419440	-.19835830	5.07888270
113.00000000	5.22439810	-.19770460	5.07953640
114.00000000	5.15561250	-.18550330	5.09173770
115.00000000	5.07425140	-.18544100	5.09180000
116.00000000	4.98772610	-.18048900	5.09675200
117.00000000	4.90377520	-.17696040	5.10028060
118.00000000	4.82977750	-.17233390	5.10490710
119.00000000	4.77210740	-.17009080	5.10715020
120.00000000	4.73559030	-.16603090	5.11121010
121.00000000	4.72310280	-.15660670	5.12063430
122.00000000	4.73535160	-.15153300	5.12570800
123.00000000	4.77084730	-.14951400	5.12772700
124.00000000	4.82607080	-.14620290	5.13103810
125.00000000	4.89581770	-.14495870	5.13228230
126.00000000	4.97368370	-.14310990	5.13413110
127.00000000	5.05264890	-.13992790	5.13731310
128.00000000	5.12570800	-.13223660	5.14500440
129.00000000	5.18648680	-.13135120	5.14588980
130.00000000	5.22979630	-.12162850	5.15561250
131.00000000	5.25207160	-.11895560	5.15828540
132.00000000	5.25166240	-.11875420	5.15848680
133.00000000	5.22894890	-.11438910	5.16285190
134.00000000	5.18627820	-.10850220	5.16873880
135.00000000	5.12772700	-.10622880	5.17101220
136.00000000	5.05871590	-.10605610	5.17118490
137.00000000	4.98551090	-.10128770	5.17595330
138.00000000	4.91465670	-.10091220	5.17632880
139.00000000	4.85239520	-.09513290	5.18210810
140.00000000	4.80411790	-.09096280	5.18627820
141.00000000	4.77390160	-.09075420	5.18648680
142.00000000	4.76416660	-.08750500	5.18973600
143.00000000	4.77548670	-.08561080	5.19163020
144.00000000	4.80656410	-.08120010	5.19604090
145.00000000	4.85437010	-.08111260	5.19612840
146.00000000	4.91443750	-.08041100	5.19683000
147.00000000	4.98127470	-.07788470	5.19935630
148.00000000	5.04886580	-.06077960	5.21646140
149.00000000	5.11121010	-.05955290	5.21768810
150.00000000	5.16285190	-.05793380	5.21930720

1 FREQUENCY DISTRIBUTION Y=(10./X)*SIN(X)+5. AUTO
CONTINUED

X-Y DATA POINTS X	Y	Y-DEVIATION YD	Y-ASCENDING YA
151.00000000	5.19935630	-.05284290	5.22439810
152.00000000	5.21768810	-.05166310	5.22557790
153.00000000	5.21646140	-.04822210	5.22894890
154.00000000	5.19604090	-.04744470	5.22979630
155.00000000	5.15848680	-.02557860	5.25166240
156.00000000	5.10715020	-.02516940	5.25207160
157.00000000	5.04733980	-.01681350	5.26042750
158.00000000	4.98389060	-.00922380	5.26801720
159.00000000	4.92267260	-.00528090	5.27196010
160.00000000	4.86908710	-.00304660	5.27419440
161.00000000	4.82779120	.00272840	5.27996940
162.00000000	4.80229480	.02233760	5.29957860
163.00000000	4.79466410	.02313750	5.30037850
164.00000000	4.80535670	.04596440	5.32320540
165.00000000	4.83320910	.05706470	5.33430570
166.00000000	4.87551640	.06314010	5.34038110
167.00000000	4.92837630	.07069960	5.34794060
168.00000000	4.98696510	.07341650	5.35065750
169.00000000	5.04601460	.09138180	5.36862280
170.00000000	5.10028060	.09232790	5.36956890
171.00000000	5.14500440	.09415860	5.37139960
172.00000000	5.17632880	.15876100	5.43600200
173.00000000	5.19163020	.16929510	5.44653610
174.00000000	5.18973600	.20583840	5.48307940
175.00000000	5.17101220	.20901740	5.48625840
176.00000000	5.13731310	.22619490	5.50343590
177.00000000	5.09180000	.32701250	5.60425350
178.00000000	5.03864630	.35449560	5.63173660
179.00000000	4.98265590	.36751420	5.64475520
180.00000000	4.92883050	.38743760	5.66467860
181.00000000	4.88192420	.42204490	5.69928590
182.00000000	4.84602450	.42559460	5.70283560
183.00000000	4.82419720	.60203500	5.87927600
184.00000000	4.81822640	.66131120	5.93855220
185.00000000	4.82846960	.66215550	5.93939650
186.00000000	4.85384180	.86999120	6.14723220
187.00000000	4.89192760	.88774060	6.16498160
188.00000000	4.93920890	.91914520	6.19638620
189.00000000	4.99138970	.99724160	6.26448260
190.00000000	5.04378420	.99633740	6.27357840
191.00000000	5.09173770	1.25251900	6.52976000
192.00000000	5.13103810	2.11664750	7.39388850
193.00000000	5.15828540	3.39774250	8.67498350
194.00000000	5.17118490	4.70328560	9.98052660
195.00000000	5.16873880	5.97009400	11.24733500
196.00000000	5.00000000	7.13474400	12.41198500
197.00000000	5.12063430	8.13746800	13.41470900
198.00000000	5.07953640	8.92586800	14.20310900
199.00000000	5.01178390	9.31610000	14.59334100
200.00000000	4.98168580	9.45821700	14.73545800

CLASS INTERVALS FROM	TO	OBSERVED FREQUENCY
2.17803260	2.83980230	1.00000000
2.83980230	3.50067200	4.00000000
3.50067200	4.16154170	5.00000000
4.16154170	4.82241140	46.00000000
4.82241140	5.48328110	118.00000000
5.48328110	6.14415080	11.00000000
6.14415080	6.80502050	6.00000000
6.80502050	7.46589020	1.00000000
7.46589020	8.12675990	1.00000000
8.12675990	8.78762960	1.00000000
8.78762960	9.44849930	1.00000000
9.44849930	10.10936900	1.00000000
10.10936900	10.77023800	1.00000000
10.77023800	11.43110700	1.00000000
11.43110700	12.09197600	1.00000000
12.09197600	12.75284500	2.00000000
12.75284500	13.41371400	3.00000000
13.41371400	14.07458300	4.00000000

DATA POINTS	ARITHMETIC MEAN	QUADRATIC MEAN	GEOMETRIC MEAN	HARMONIC MEAN
200	5.2772410	5.5168213	5.1291948	5.0285545

STANDARD DEVIATION S1	VARIANCE S2	PERCENT 1S POPULATION	PERCENT 2S POPULATION	PERCENT 3S POPULATION
1.612149	2.599040	95.500000	96.000000	97.000000

SUM OF Y	SUM OF Y SQUARES	SUM OF Y RECIPROCALS
.10554482E+04	.60870636E+04	.39772861E+02

SUM OF LOG(Y)	SUM OF Y - YBAR	SUM OF (Y - YBAR)SQUARES
.32698975E+03	.14177528E+03	.51720609E+03

TABLE 3.

FREQUENCY DISTRIBUTION Y=(10./X)*SIN(X)+5.

CLASS INTERVALS FROM	TO	OBSERVED FREQUENCY
2.00000000	3.00000000	3.00000000
3.00000000	4.00000000	4.00000000
4.00000000	5.00000000	91.00000000
5.00000000	6.00000000	87.00000000
6.00000000	7.00000000	6.00000000
7.00000000	8.00000000	1.00000000
8.00000000	9.00000000	1.00000000
9.00000000	10.00000000	1.00000000
10.00000000	11.00000000	1.00000000
11.00000000	12.00000000	1.00000000
12.00000000	13.00000000	1.00000000
13.00000000	14.00000000	1.00000000
14.00000000	15.00000000	2.00000000

DATA POINTS	ARITHMETIC MEAN	QUADRATIC MEAN	GEOMETRIC MEAN	HARMONIC MEAN
200	5.2772410	5.5168213	5.1291948	5.0285545

STANDARD DEVIATION S1	VARIANCE S2	PERCENT 1S POPULATION	PERCENT 2S POPULATION	PERCENT 3S POPULATION
1.612149	2.599040	95.500000	96.000000	97.000000

SUM OF Y	SUM OF Y SQUARES	SUM OF Y RECIPROCALS
.10554482E+04	.60870636E+04	.39772861E+02

SUM OF LOG(Y)	SUM OF Y - YBAR	SUM OF (Y - YBAR)SQUARES
.32698975E+03	.14177528E+03	.51720609E+03

TABLE 4.

FIGURE 1

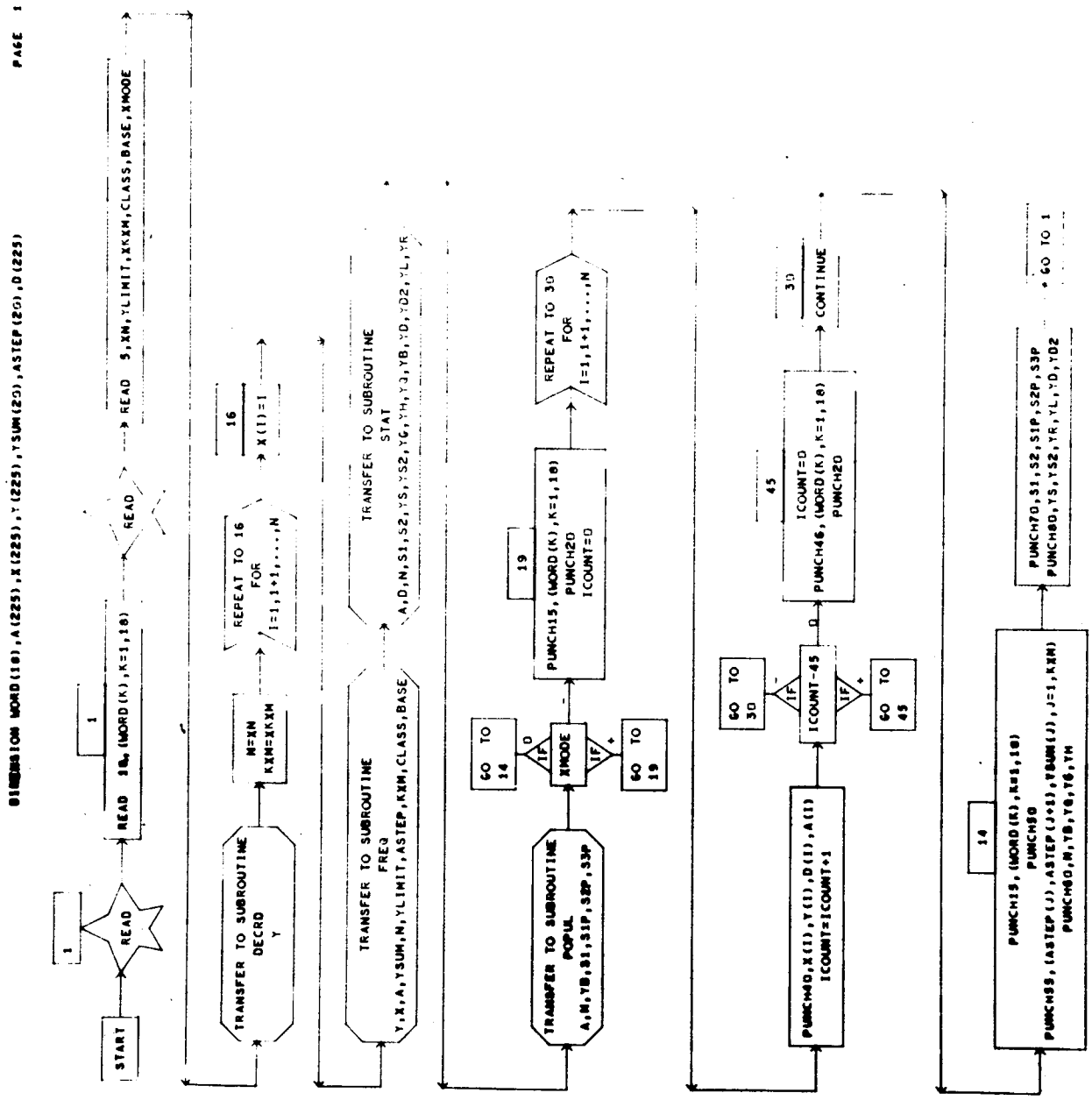
DIMENSION WORD(10),A(225),X(225),Y(225),YSUM(20),ASTEP(20),D(225)
PAGE 1
START
READ
1
READ 10, (WORD(K),K=1,10)
READ
READ 5,XN,YLIMIT,KXM,CLASS,BASE,XMODE
TRANSFER TO SUBROUTINE
DECRD
Y
M=XN
KXM=KXM
REPEAT TO 16
FOR
I=1,1+1,...,N
16
X(I)=I
TRANSFER TO SUBROUTINE
FREQ
Y,X,A,YSUM,N,YLIMIT,ASTEP,KXM,CLASS,BASE
TRANSFER TO SUBROUTINE
STAT
A,D,N,S1,S2,YS,YS2,YG,YH,YQ,YB,YD,YD2,YL,YR
TRANSFER TO SUBROUTINE
POPUL
A,M,YB,S1,S1P,S2P,S3P
XMODE
60 TO
14
60 TO
19
19
PUNCH15, (WORD(K),K=1,10)
PUNCH20
ICOUNT=0
REPEAT TO 30
FOR
I=1,1+1,...,N
PUNCH40,X(I),Y(I),D(I),A(I)
ICOUNT=ICOUNT+1
ICOUNT-45
60 TO
30
60 TO
45
45
ICOUNT=0
PUNCH46, (WORD(K),K=1,10)
PUNCH20
30
CONTINUE
14
PUNCH15, (WORD(K),K=1,10)
PUNCH50
PUNCH55, (ASTEP(J),ASTEP(J+1),YSUM(J),J=1,KXM)
PUNCH60,M,YB,YG,YG,YM
PUNCH70,S1,S2,S1P,S2P,S3P
PUNCH80,YS,YS2,YR,YL,YD,YD2
GO TO 1

FIGURE 2

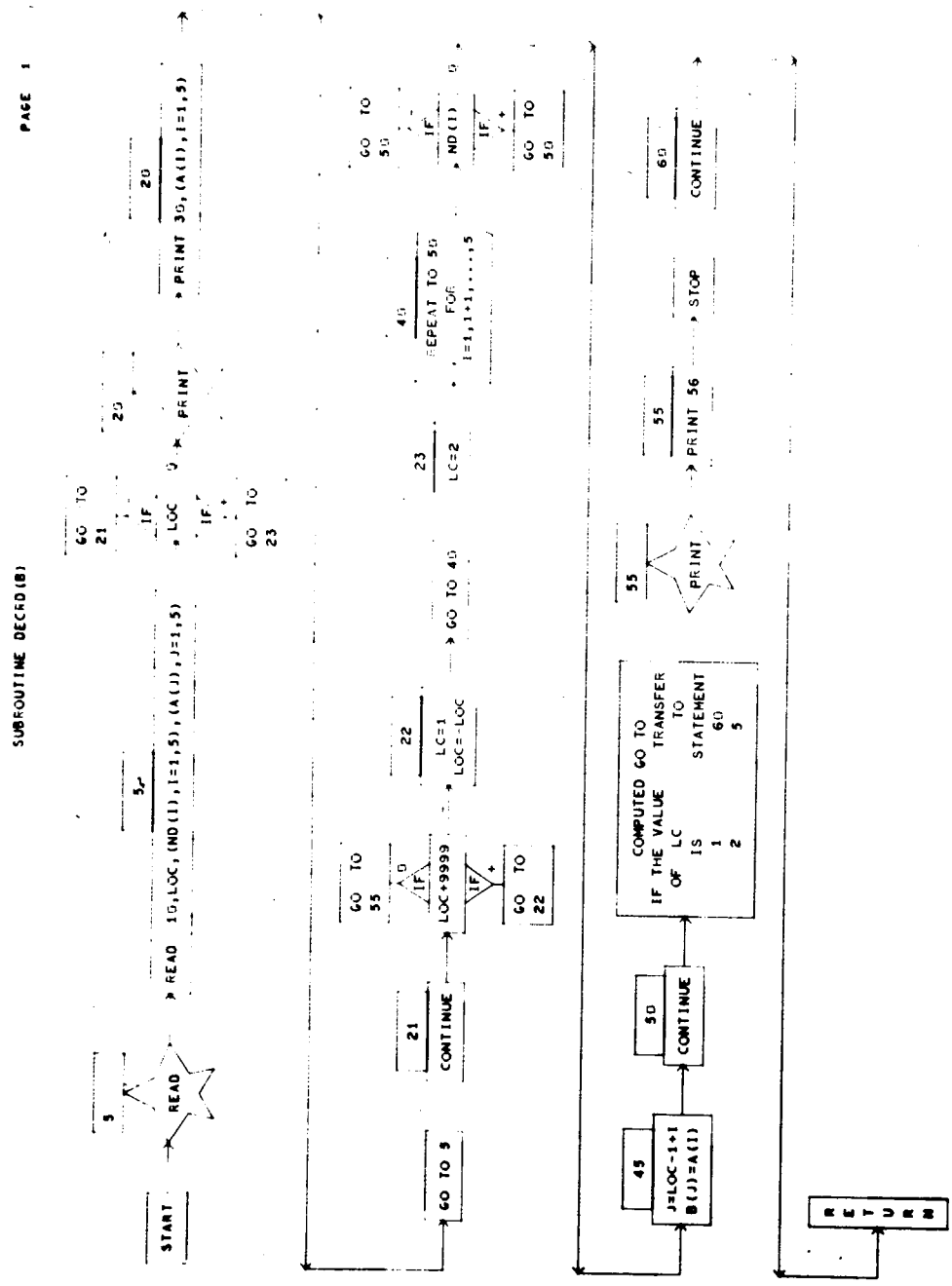
SUBROUTINE DECRD(B)
PAGE 1
START
5
READ
READ 10,LOC,(ND(I),I=1,5),(A(J),J=1,5)
GO TO 21
IF
LOC
IF
GO TO 23
20
PRINT
PRINT 30,(A(I),I=1,5)
GO TO 5
21
CONTINUE
GO TO 55
IF
LOC+9999
IF
GO TO 22
22
LC=1
LOC=-LOC
GO TO 40
23
LC=2
40
REPEAT TO 50
FOR
I=1,1+1,...,5
GO TO 50
IF
ND(I)
IF
GO TO 50
45
J=LOC-1+I
B(J)=A(I)
50
CONTINUE
COMPUTED GO TO
IF THE VALUE OF LC IS 1 2
TRANSFER TO STATEMENT 60 5
55
PRINT
55
PRINT 56
STOP
60
CONTINUE
RETURN

FIGURE 3

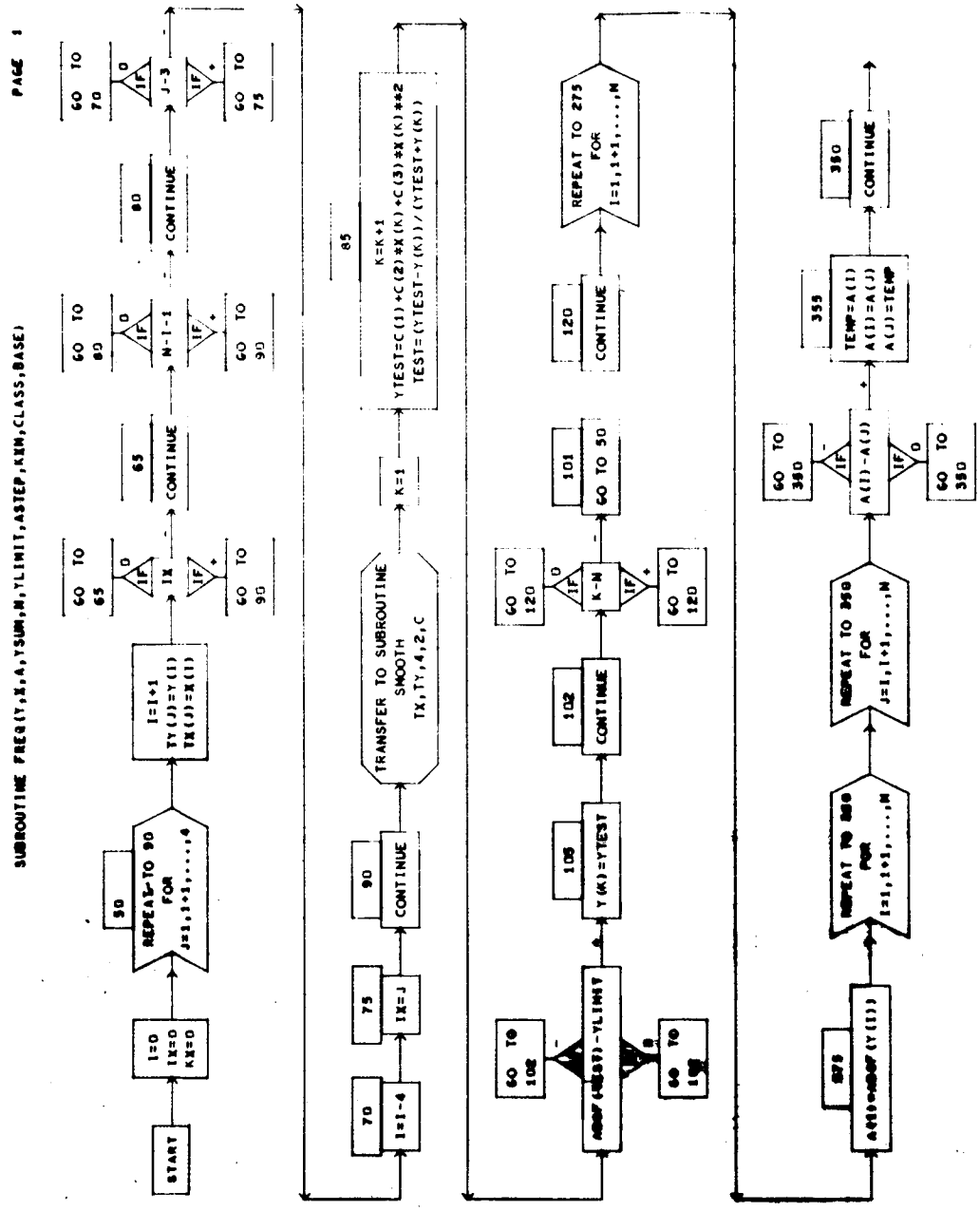
SUBROUTINE FREQ(Y,X,A,YSUM,N,YLIMIT,ASTEP,KEN,CLASS,BASE)
PAGE 1
START
I=0
IX=0
KK=0
50
REPEAT TO 90
FOR
J=1,1+1,...,4
I=I+1
TY(J)=Y(I)
TX(J)=X(I)
60 TO 65
IF
IX
60 TO 90
65
CONTINUE
60 TO 80
IF
N-I-1
60 TO 90
80
CONTINUE
60 TO 70
IF
J-3
60 TO 75
70
I=I-4
75
IX=J
90
CONTINUE
TRANSFER TO SUBROUTINE
SMOOTH
TX,TY,4,2,C
K=1
85
K=K+1
YTEST=C(1)+C(2)*X(K)+C(3)*X(K)**2
TEST=(YTEST-Y(K))/(YTEST+Y(K))
60 TO 102
ABSF(TEST)-YLIMIT
60 TO 105
105
Y(K)=YTEST
102
CONTINUE
K-N
60 TO 120
60 TO 120
101
60 TO 50
120
CONTINUE
REPEAT TO 275
FOR
I=1,1+1,...,N
275
REPEAT TO 350
FOR
I=1,1+1,...,N
A(I)-A(J)
60 TO 350
60 TO 350
355
TEMP=A(I)
A(I)=A(J)
A(J)=TEMP
350
CONTINUE

FIGURE 3 - a.

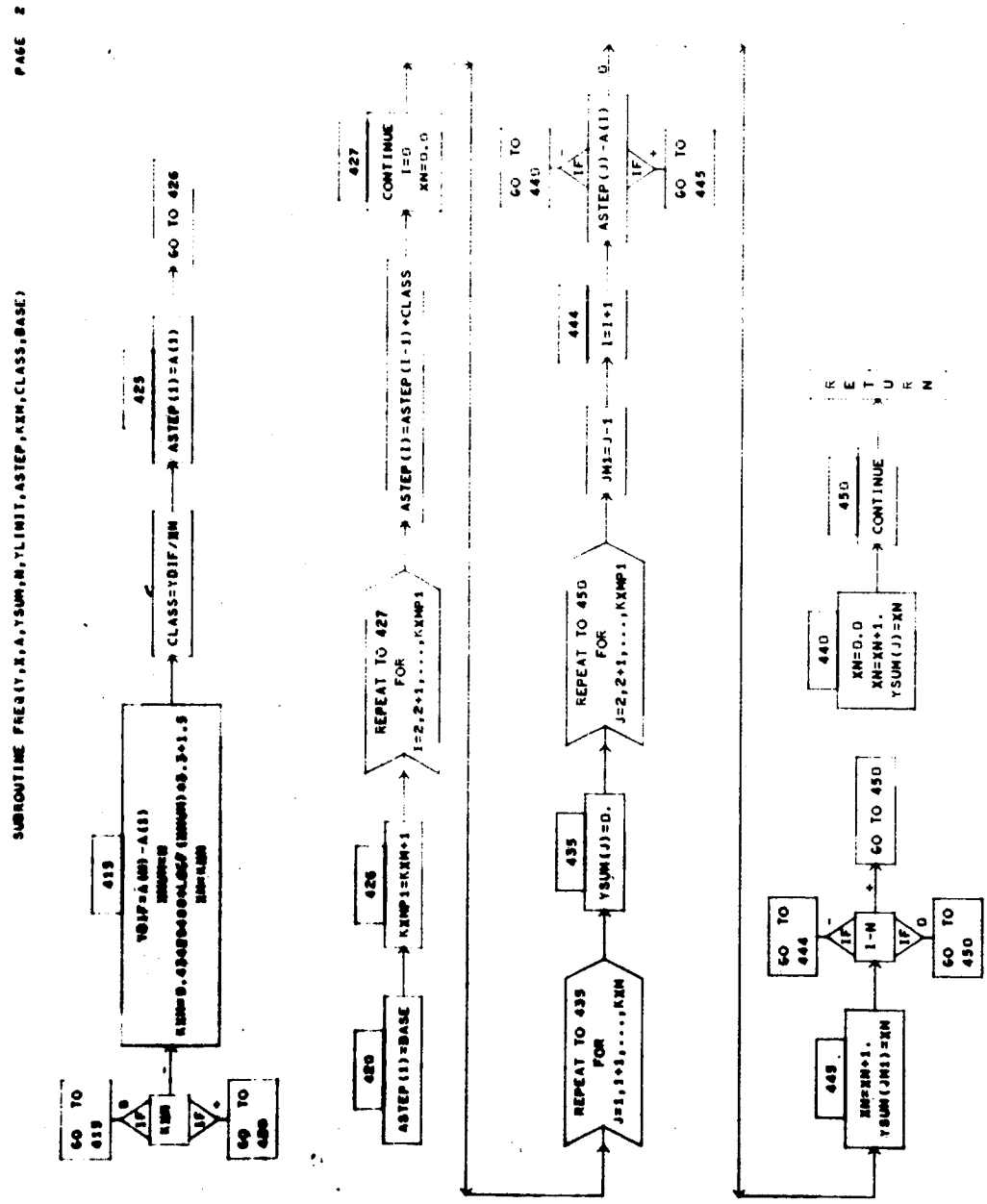
SUBROUTINE FREQ(Y,X,A,YSUM,N,YLIMIT,ASTEP,KXM,CLASS,BASE)
PAGE 2
GO TO 415
GO TO 420
415
CLASS=YDIF/XN
425
ASTEP(1)=A(1)
GO TO 426
420
ASTEP(1)=BASE
426
KXMP1=KXM+1
REPEAT TO 427
FOR
I=2,2+1,...,KXMP1
ASTEP(I)=ASTEP(I-1)+CLASS
427
CONTINUE
I=0
XN=0.0
REPEAT TO 435
FOR
J=1,1+1,...,KXM
435
YSUM(J)=0.
REPEAT TO 450
FOR
J=2,2+1,...,KXMP1
JM1=J-1
444
I=I+1
GO TO 440
ASTEP(J)-A(I)
GO TO 445
449
XN=XN+1.
YSUM(JM1)=XN
GO TO 444
I-N
GO TO 450
GO TO 450
440
XN=0.0
XN=XN+1.
YSUM(J)=XN
450
CONTINUE
RETURN

FIGURE 4

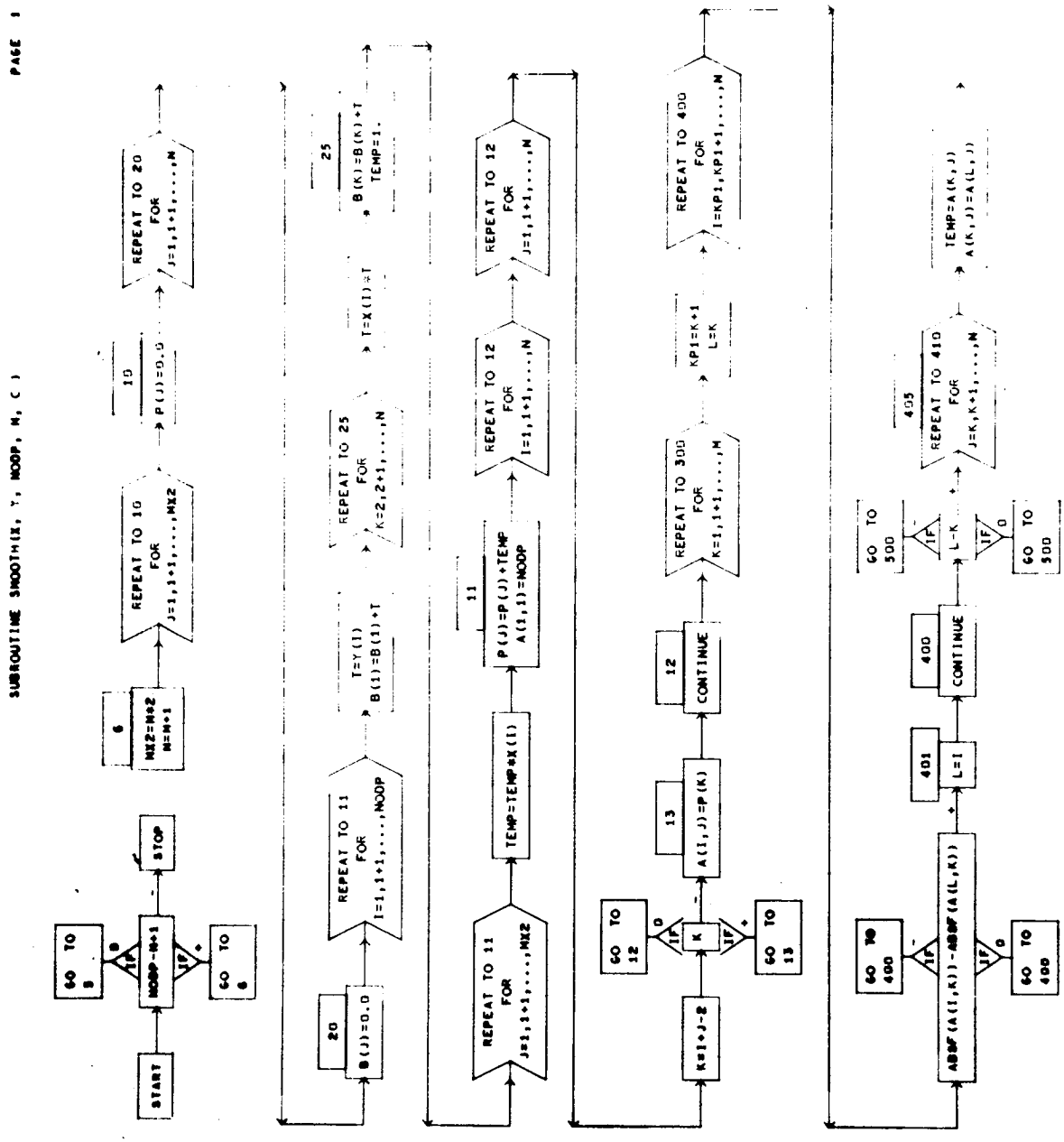
SUBROUTINE SMOOTH(X, Y, NODP, M, C)
PAGE 1
START
NODP-M+1
IF
GO TO 5
GO TO 6
STOP
6
MX2=M*2
M=M+1
REPEAT TO 10
FOR
J=1,1+1,...,MX2
10
P(J)=0.0
REPEAT TO 20
FOR
J=1,1+1,...,N
20
B(J)=0.0
REPEAT TO 11
FOR
I=1,1+1,...,NODP
T=Y(I)
B(1)=B(1)+T
REPEAT TO 25
FOR
K=2,2+1,...,N
T=X(I)*T
25
B(K)=B(K)+T
TEMP=1.
REPEAT TO 11
FOR
J=1,1+1,...,MX2
TEMP=TEMP*X(I)
11
P(J)=P(J)+TEMP
A(1,1)=NODP
REPEAT TO 12
FOR
I=1,1+1,...,N
REPEAT TO 12
FOR
J=1,1+1,...,N
K=I+J-2
K
GO TO 12
GO TO 13
13
A(I,J)=P(K)
12
CONTINUE
REPEAT TO 300
FOR
K=1,1+1,...,M
KP1=K+1
L=K
REPEAT TO 400
FOR
I=KP1,KP1+1,...,N
ABSF(A(I,K))-ABSF(A(L,K))
GO TO 400
401
L=I
400
CONTINUE
L-K
GO TO 500
405
REPEAT TO 410
FOR
J=K,K+1,...,N
TEMP=A(K,J)
A(K,J)=A(L,J)

FIGURE 4 - a.

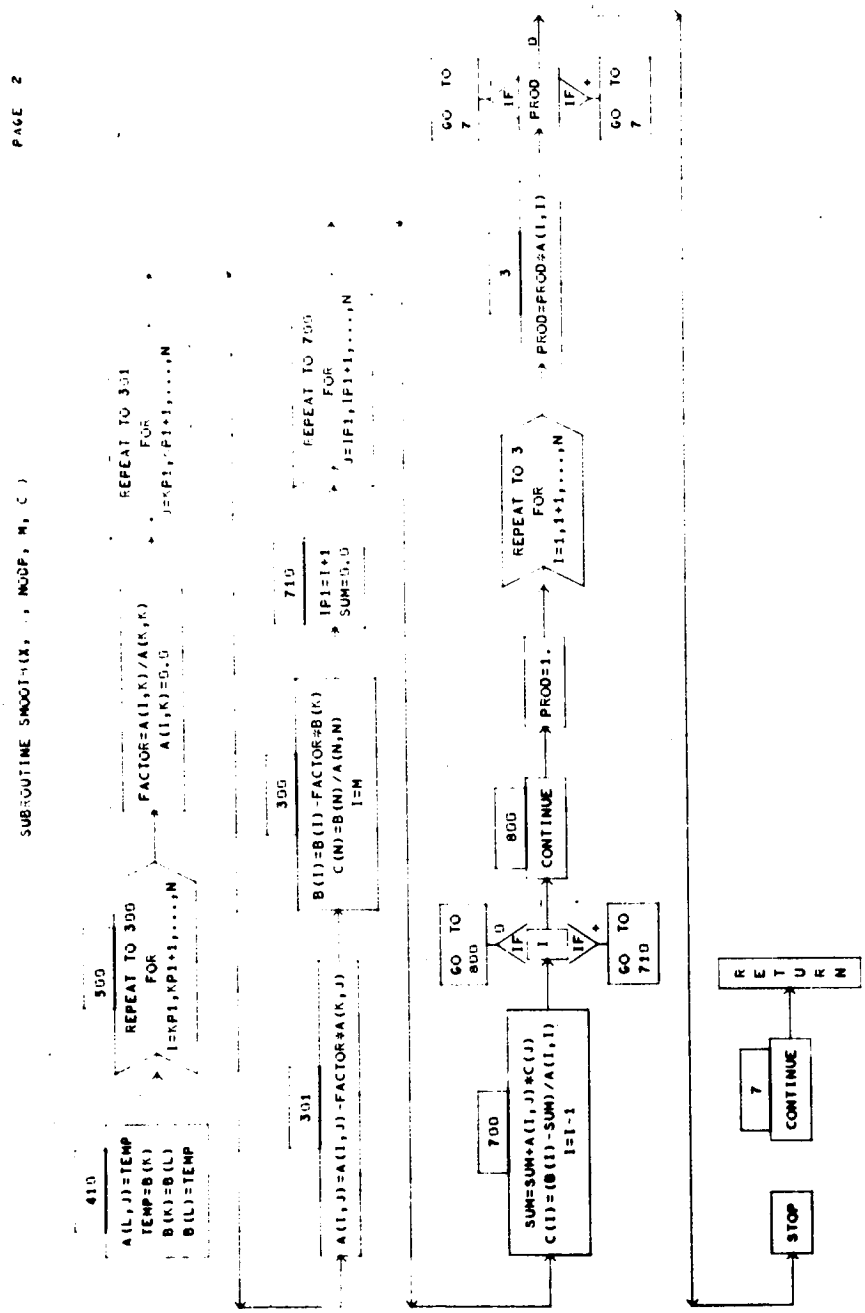
PAGE 2
410
A(L,J)=TEMP
TEMP=B(K)
B(K)=B(L)
B(L)=TEMP
300
REPEAT TO 300
FOR
I=KP1,KP1+1,...,N
FACTOR=A(I,K)/A(K,K)
A(I,K)=0.0
REPEAT TO 301
FOR
J=KP1,KP1+1,...,N
301
A(I,J)=A(I,J)-FACTOR*A(K,J)
300
B(I)=B(I)-FACTOR*B(K)
C(N)=B(N)/A(N,N)
I=M
710
IP1=I+1
SUM=0.0
REPEAT TO 700
FOR
J=IP1,IP1+1,...,N
700
SUM=SUM+A(I,J)*C(J)
C(I)=(B(I)-SUM)/A(I,I)
I=I-1
GO TO 800
IF
I
IF
GO TO 710
800
CONTINUE
PROD=1.
REPEAT TO 3
FOR
I=1,1+1,...,N
3
PROD=PROD*A(I,I)
GO TO 7
IF
PROD
IF
GO TO 7
STOP
7
CONTINUE
RETURN

FIGURE 5

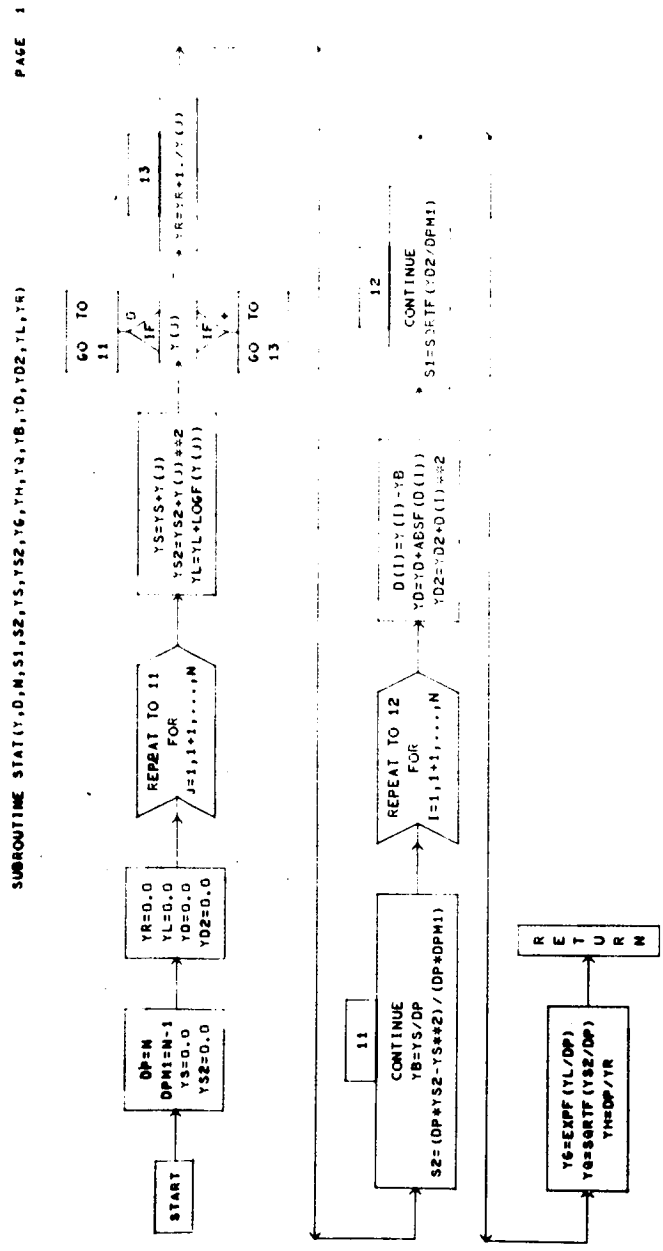
SUBROUTINE STAT(Y,D,N,S1,S2,YS,YS2,YG,YH,YQ,YB,YD,YD2,YL,YR)
PAGE 1
START
DP=N
DPM1=N-1
YS=0.0
YS2=0.0
YR=0.0
YL=0.0
YD=0.0
YD2=0.0
REPEAT TO 11
FOR
J=1,1+1,...,N
YS=YS+Y(J)
YS2=YS2+Y(J)**2
YL=YL+LOGF(Y(J))
GO TO
11
IF
Y(J)
IF
GO TO
13
13
YR=YR+1./Y(J)
11
CONTINUE
YB=YS/DP
S2=(DP*YS2-YS**2)/(DP*DPM1)
REPEAT TO 12
FOR
I=1,1+1,...,N
D(I)=Y(I)-YB
YD=YD+ABSF(D(I))
YD2=YD2+D(I)**2
12
CONTINUE
S1=SQRTF(YD2/DPM1)
YG=EXPF(YL/DP)
YQ=SQRTF(YS2/DP)
YH=DP/YR
RETURN

FIGURE 6

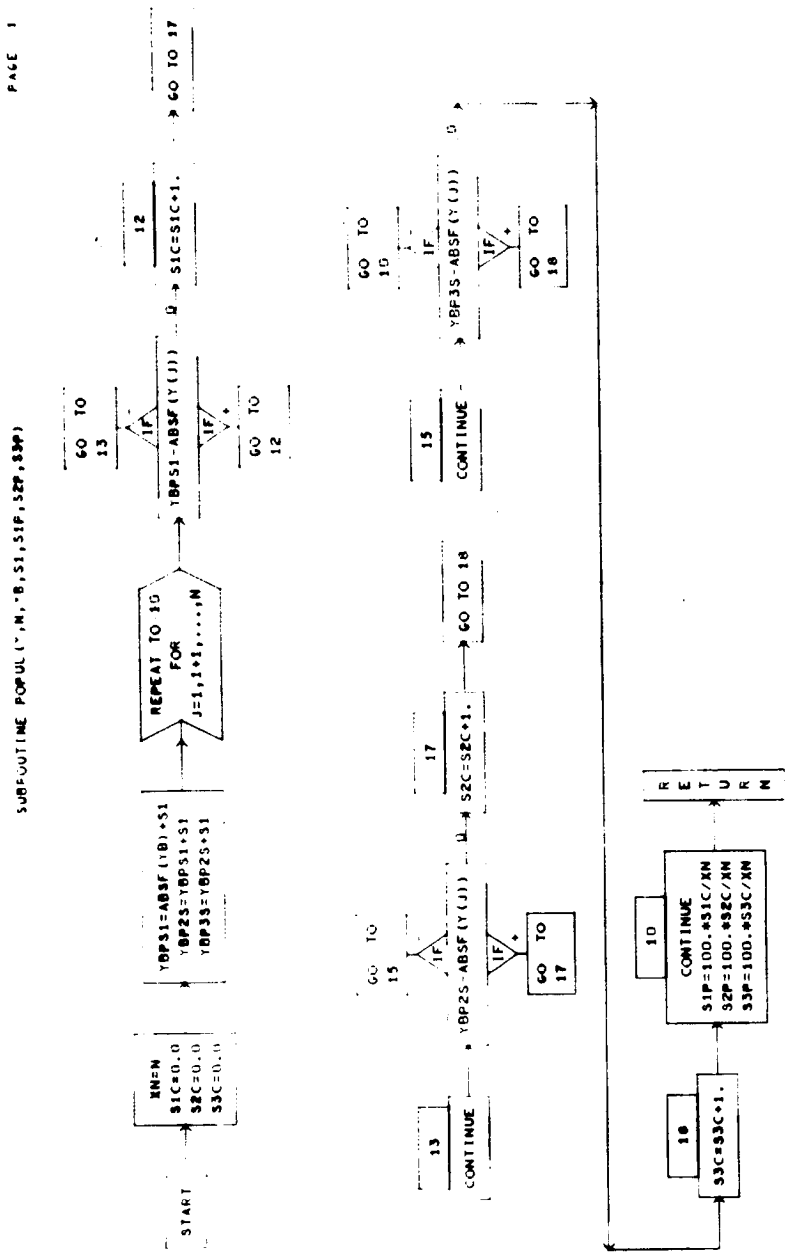
PAGE 1
SUBROUTINE POPUL(Y,N,YB,S1,S1F,S2P,S3P)
START
XN=N
S1C=0.0
S2C=0.0
S3C=0.0
YBP1=ABSF(YB)+S1
YBP2=YBP1+S1
YBP3=YBP2+S1
REPEAT TO 15
FOR
J=1,1+1,...,N
YBP1-ABSF(Y(J))
IF
GO TO 13
GO TO 12
12
S1C=S1C+1.
GO TO 17
13
CONTINUE
YBP2-ABSF(Y(J))
GO TO 15
GO TO 17
17
S2C=S2C+1.
GO TO 18
15
CONTINUE
YBP3-ABSF(Y(J))
GO TO 19
GO TO 18
18
S3C=S3C+1.
10
CONTINUE
S1P=100.*S1C/XN
S2P=100.*S2C/XN
S3P=100.*S3C/XN
RETURN

APPENDIX A13

ANALYSIS OF TEST 1873 DUMBBELL C ROD 124 TEMPERATURE 72 F MARCH 31, 1966

X	X-Y DATA POINTS Y	Y-DEVIATION YD	Y-ASCENDING YA
1	1.23000600	-.00004860	1.22990300
2	1.22993300	-.00004760	1.22990400
3	1.22997200	-.00002660	1.22992500
4	1.22998700	-.00002560	1.22992600
5	1.22997300	-.00002460	1.22992700
6	1.22995700	-.00002060	1.22993100
7	1.22996800	-.00001560	1.22993600
8	1.22997100	-.00000760	1.22994400
9	1.22997300	-.00000660	1.22994500
10	1.22994800	-.00000660	1.22994500
11	1.22995500	-.00000560	1.22994600
12	1.22994500	-.00000560	1.22994600
13	1.22994600	-.00000360	1.22994800
14	1.22993100	-.00000260	1.22995100
15	1.22996500	.00000340	1.22995500
16	1.22995100	.00000540	1.22995700
17	1.22994600	.00001340	1.22996500
18	1.22993600	.00001540	1.22996800
19	1.22990400	.00001840	1.22997000
20	1.22994400	.00001940	1.22997100
21	1.22994500	.00002140	1.22997300
22	1.22993600	.00002740	1.22997900
23	1.22993500	.00003140	1.22998300
24	1.22993700	.00003540	1.22998700
25	1.22990300	.00005440	1.23000600

ANALYSIS OF TEST 1873 DUMBBELL C ROD 124 TEMPERATURE 72 F MARCH 31, 1966

CLASS INTERVALS FROM	TO	OBSERVED FREQUENCY
1.22989450	1.22990300	1.0
1.22990300	1.22991150	1.0
1.22991150	1.22992000	1.0
1.22992000	1.22992850	2.0
1.22992850	1.22993700	2.0
1.22993700	1.22994550	3.0
1.22994550	1.22995400	4.0
1.22995400	1.22996250	2.0
1.22996250	1.22997100	4.0
1.22997100	1.22997950	2.0
1.22997950	1.22998800	2.0
1.22998800	1.22999650	2.0

DATA POINTS	ARITHMETIC MEAN	QUADRATIC MEAN	GEOMETRIC MEAN	HARMONIC MEAN
25	1.2299516	1.2299515	1.2299515	1.2299520

STANDARD DEVIATION S1	VARIANCE S2	PERCENT 1S POPULATION	PERCENT 2S POPULATION	PERCENT 3S POPULATION
.000025	0.000000	84.000000	96.000000	100.000000

SUM OF Y	SUM OF Y SQUARES	SUM OF Y RECIPROCALS
.30748791E+02	.37819518E+02	.20325995E+02
SUM OF LOG(Y)	SUM OF Y - YBAR	SUM OF (Y - YBAR)SQUARES
.51743702E+01	.49180000E-03	.15095800E-07

Appendix B

Product of Inertia

APPENDIX B1

TEST PROCEDURE

2.1.3 Final Technical Report

2.1.3.1 Purpose

To determine the repeatability, linearity, and alignment of the load system.

2.1.3.2 Equipment

(1) Modified Model 712 rate table.

(2) Load cell amplifying circuitry.

(3) Hewlett-Packard 3460A Digital Volt Meter.

(4) Standard weights (0.48 lb., 5.0 lbs., 9.69 lbs.)

2.1.3.3 Set-Up

(1) Turn on electronic equipment for warm up (1.5 hours).

(2) Monitor amplified load cell output signal with DVM.

(3) Zero surface plate—using zeroing potentiometer on the amplifier adjust until DVM reads 0.000.

(4) Calibrate surface plate—Place a known weight a known distance from the center of the table top (on a line that is perpendicular to axis formed by the two 3,000 lb. flexures which are located on the center line) and adjust the amplifier gain potentiometer to give a previously calculated output on the DVM.

Example: 0.1 x Distance x Weight = DVM reading.
0.1 x 9 ins. x 9.69 lbs. = 8.721 in-lb (read on DVM)

2.1.3.4 Test Procedure

(1) After the test procedure has been arranged as outlined in the test set-up, testing is ready to begin.

(2) Two random charts are utilized, one to determine the order of the various grid positions and the other to determine the weights to be used.

(3) Using the random charts select the first weight and place it on the first specified grid position.

(4) Record all the different grid positions for a single weight on one grid sheet before proceeding to the next prescribed weight. (Record sign of $\pm$ reading)

(5) Each weight will be cycled through each of the 45 grid positions, two different times in the order called out in the random chart.

Written By: _____

Approved By: _____

Date: _____

RANDOM CHART

Random Sample (6 points)

Weights: 0.5 lbs., 5.0 lbs., 10.0 lbs.

Repeat each weight 2 times.

1	10 lbs.	4	0.5 lbs.
2	0.5	5	5
3	5	6	10

Random Sample (45 points) P. 340 Mathematical Statistics

1	15(-3, +3)	24	24(+3, 0)
2	1(-6, +9)	25	7(-6, +6)
3	40(+9, -6)	26	13(-9, +3)
4	16(0, +3)	27	8(-3, +6)
5	20(-9, 0)	28	9(0, +6)
6	22(-3, 0)	29	19(+9, +3)
7	28(-6, -3)	30	23(0, 0)
8	26(+9, 0)	31	41(-6, -9)
9	36(-3, -6)	32	3(0, +9)
10	17(+3, +3)	33	38(+3, -6)
11	34(-9, -6)	34	6(-9, +6)
12	10(+3, +6)	35	18(+6, +3)
13	33(+9, =3)	36	42(-3, -9)
14	11(+6, +6)	37	25(+6, 0)
15	4(+3, +9)	38	31(+3. -3)
16	5(+6, +9)	39	21(-6, 0)
17	12(+9, +6)	40	44(+3, -9)
18	14(-6, +3)	41	39(+6, -6)
19	35(-6, -6)	42	43(0, -9)
20	45(+6, -9)	43	27(-9, -3)
21	29(-3, -3)	44	30(0, -3)
22	2(-3, +9)	45	37(0, -6)
23	32(+6, -3)		

APPENDIX B2

```
C     PROGRAM FOR DETERMINING MASS PROPERTIES OF TRIANGLE STANDARDS
C
      DIMENSION WORD(18)
C
C     READ      INPUT DATA
C
   13 READ 1,(WORD(K),K=1,18)
    1 FORMAT (18A4)
      READ 100,A,B,C,D,E,W
  100 FORMAT(6F10.4)
      G     = 385.684
      XMT   = W /G
      XMAS  = XMT*12.
      XN    = (A**3*(2.*B+C)) - (3.*A**2*C*D ) + (D**2*(C-B)*(3.*A-D))
      XD    = (3.*A**2*(B+C)) + 3.*D**2*(C-B) - 6.*A*C*D
      YN    = B**3*(2.*A+D) - 3.*B**2*C*D + C**2*(D-A)*(3.*B-C)
      YD    = 3.*B**2*(A+D) + 3.*C**2*(D-A) - 6.*B*C*D
      X     = A-XN/XD
      Y     = B-YN/YD
      Z     = E/2.
      R     = C*(D-A)/(C-B)
      Q     = D*(C-B)/(D-A)
      DIV   = A*B+A*C+B*D-C*D
      XMS   = XMT*Q*D/DIV
      XMV   = XMT*C*R/DIV
      XMO   = XMT+XMS+XMV
      AIXX  = XMO/36.*(2.*(B+Q)**2+3.*E**2) + XMO*((B+Q)/3.-Y)**2-XMS/36.
     1        *(2.*Q**2+3.*E**2)-XMS*(B+Q/3.-Y)**2-XMV/36.*(2.*C**2+3.
     2        *E**2)-XMV*(Y-C/3.)**2
      AIYY  = XMO/36.*(2.*(A+R)**2+3.*E**2)+XMO*((A+R)/3.-X)**2-XMS/36.
     1        *(2.*D**2+3.*E**2)-XMS*(X-D/3.)**2-XMV/36.*(2.*R**2
     2        +3.*E**2)-XMV*(A+R/3.-X)**2
      AIZZ  = XMO/18.*((A+R)**2+(B+Q)**2)+XMO*((B+Q)/3.-Y)**2
     1        +((A+R)/3.-X)**2 -XMS*((D**2+Q**2)/18.+(X-D/3.)**2
     2        +(B+Q/3.-Y)**2)-XMV*((R**2-C**2)/18.+(A+R/3.-X)**2
     3        +(Y-C/3.)**2)
      XA    = A-D
      YA    = B-C
      XBA   = -(2.*XA)/3.-X+A
      YBA   = -(2.*YA)/3.-Y+B
      XBB   = X-0.5*D
      YBB   = 0.5*(B+C)-Y
      XBC   = 0.5*A-X
      YBC   = Y-0.5*C
      AA    = 0.5*YA*XA
      AB    = D*YA
      AC    = A*C
      AT    = AA+AB+AC
      P     = XMT/AT
      XMA   = AA*P
      XMB   = AB*P
      XMC   = AC*P
      AIXZ  = XA*YA*XMA/36.-XBA*YBA*XMA+XBB*YBB*XMB+XBC*YBC*XMC
      AIYZ  = AIXZ
      AIXY  = 0.
```

```
C     PRINT OUT DATA
      PUNCH 105
  105 FORMAT(1H1//16X,38H MASS PROPERTIES OF TRIANGLE STANDARDS/)
      PUNCH 1,(WORD(K),K=1,18)
      PUNCH 101,A,B,C,D,E
  101 FORMAT(///26X20H TRIANGLE DIMENSIONS// 8X,2H A,12X,2H B,12X,2H C,
     1 12X,2H D,12X,2H E/6X,7H INCHES,7X,7H INCHES,7X,7H INCHES,7X,7H IN
     2CHES,7X,7H INCHES//2X,5F14.6//)
      PUNCH 102,W,XMAS,X,Y,Z
  102 FORMAT(9X16H WEIGHT AND MASS23X15H CENTER OF MASS//5X7H WEIGHT
     111X5H MASS17X2H X8X2H Y8X2H Z/5X7H POUNDS9X10H   SLUGS  12X
     27H INCHES3X7H INCHES3X7H INCHES//F13.4,4X,F13.4,11X,3F10.4)
      CALL PAIXS(AIXX,AIYY,AIZZ,AIXY,AIXZ,AIYZ)
      GO TO 13
      END
```

APPENDIX B3

```
**PAIXS
      SUBROUTINE PAIXS (AIXX,AIYY,AIZZ,AIXY,AIXZ,AIYZ)
C     PRINCIPAL AXIS AND DIRECTION COSINE PROGRAM FORTRANII 4-15-66 JHJ
C
C     ROUTINE FOR CALCULATING MOMENTS OF INERTIA ABOUT PRINCIPAL AXIS
C     AND TO SOLVE FOR DIRECTION COSINES.
C
C     THIS PROGRAM REQUIRES TWO FUNCTION SUBROUTINES ACOS(X) + ACOSD(X)
C
C     IXX, IYY, IZZ, ARE MOMENTS OF INERTIA AND IXY, IXZ, IYZ, ARE
C     PRODUCTS OF INERTIA ABOUT A REFERENCE AXIS THROUGH THE C.G.
C
      DIMENSION RT(3), X(3), Y(3), Z(3),WORD(12),AX(3),AY(3),AZ(3)
C
C     SOLVE CUBIC EQUATION FORM X**3+P*X**2+Q*X+R=0
C
C     CALCULATE COEFFICIENT (P) MAKE NEGATIVE
      P     = -(AIXX + AIYY + AIZZ)
C
C     CALCULATE COEFFICIENT (Q)
      Q     = AIXX*AIYY + AIXX*AIZZ + AIYY*AIZZ - AIXY**2-AIXZ**2-AIYZ**2
C
C     CALCULATE CONSTANT TERM (R)
      R     = -AIXX*AIYY*AIZZ+ 2.*AIXY*AIXZ*AIYZ+ AIYY*AIXZ**2+
     1AIXX*AIYZ**2+AIZZ*AIXY**2
C
      A     = (3.*Q - P**2)/3.
      B     = (2.*P**3 - Q*P*9. + 27.*R)/27.
      CONS  = -A**3/27.
      BETA  = -B*.5/SQRTF(CONS)
      BETA  = ACOS(BETA)
      ANGL1= BETA/3.
      ANGL2= ANGL1 + 2.0944
      ANGL3= ANGL1 + 4.1888
      CONS  = -A/3.
      TSQC  =2.*SQRTF(CONS)
      XONE  = TSQC*COSF(ANGL1)
      XTWO  = TSQC*COSF(ANGL2)
      XTHRE = TSQC*COSF(ANGL3)
      PD3   = P/3.
      RT(1)= XONE - PD3
      RT(2)= XTWO - PD3
      RT(3)= XTHRE- PD3
      DO 400 I = 1, 3
      CONS  = AIYZ*(AIXX-RT(I))+AIXY*AIXZ
      DONS  = CONS/(AIXZ*(AIYY-RT(I))+AIXY*AIYZ)
      CONS  = CONS/(AIXY*(AIZZ-RT(I))+AIXZ*AIYZ)
      X(I)  =1./SQRTF(1.+DONS**2+CONS**2)
      Y(I)  = DONS*X(I)
      Z(I)  = CONS*X(I)
      AX(I)= ACOSD(X(I))
      AY(I)= ACOSD(Y(I))
      AZ(I)= ACOSD(Z(I))
      CONS  = RT(I)*.29841E-04
```

```
      OUTPUT PRINT OUT
      GO TO (500,510,510), I
  500 PUNCH 502 , AIXX, AIYY, AIZZ, AIXY, AIYZ, AIXZ
  502 FORMAT(///15X,39H INERTIA COEFFICIENTS WITH RESPECT TO C///
     13X,28H -----MOMENTS OF INERTIA----8X,28H ----PRODUCTS OF INERTIA--
     2--//3X,4H IXX8X,4H IYY8X,4H IZZ8X,4H IXY8X,4H IXZ8X,4H IYZ/6E12.6)
      PUNCH 503
  503 FORMAT(/
     1///29X,15H PRINCIPAL AXIS///7X,18H MOMENT OF INERTIA6X,16H DIRECTI
     2ON ANGLE4X,17H DIRECTION COSINE//6X,7H LB-IN25X,10H KG-M-SEC2
     33X,2H X5X,2H Y5X2H Z5X,2H X5X,2H Y5X,2H Z/)
  510 PUNCH 511, I, RT(I), CONS, AX(I), AY(I), AZ(I),X(I), Y(I), Z(I)
  511 FORMAT(3H RT11, 2E13.6    ,3E7.2,3E7.4/)
  400 CONTINUE
      RETURN
      END
```

1

APPENDIX B4

MASS PROPERTIES OF TRIANGLE STANDARDS

STANDARD NO. 534338

TRIANGLE DIMENSIONS

A INCHES	B INCHES	C INCHES	D INCHES	E INCHES
5.716300	3.254600	.128600	.142300	3.363000

WEIGHT AND MASS

WEIGHT POUNDS	MASS SLUGS
8.6250	.2683

CENTER OF MASS

X INCHES	Y INCHES	Z INCHES
1.9772	1.1118	1.6815

INERTIA COEFFICIENTS WITH RESPECT TO 0

--MOMENTS OF INERTIA----			----PRODUCTS OF INERTIA----		
IXX	IYY	IZZ	IXY	IXZ	IYZ
.034819	.064553	.057240	0.000000	.012150	.012150

PRINCIPAL AXIS

	MOMENT OF INERTIA		DIRECTION ANGLE			DIRECTION COSINE		
	LB-IN2	KG-M-SEC2	X	Y	Z	X	Y	Z
RT1	.075019	.000002	78.84	41.98	129.81	.1935	.7433	-.6402
RT2	.028758	0.000000	27.78	81.38	63.80	.8847	.1498	.4413
RT3	.052835	.000001	64.91	130.68	128.95	.4240	-.6519	-.6286

1

MASS PROPERTIES OF TRIANGLE STANDARDS

STANDARD NO. 738578

TRIANGLE DIMENSIONS

A INCHES	B INCHES	C INCHES	D INCHES	E INCHES
7.389600	5.913600	.140000	.125000	7.558000

WEIGHT AND MASS		CENTER OF MASS		
WEIGHT POUNDS	MASS SLUGS	X INCHES	Y INCHES	Z INCHES
44.3250	1.3791	2.5199	2.0043	3.7790

INERTIA COEFFICIENTS WITH RESPECT TO 0

--MOMENTS OF INERTIA----			----PRODUCTS OF INERTIA----		
IXX	IYY	IZZ	IXY	IXZ	IYZ
.777383	.911137	.594368	0.000000	.144439	.144439

PRINCIPAL AXIS

	MOMENT OF INERTIA		DIRECTION ANGLE			DIRECTION COSINE		
	LB-IN2	KG-M-SEC2	X	Y	Z	X	Y	Z
RT1	.983572	.000029	72.56	31.47	115.32	.2996	.8528	-.4276
RT2	.476894	.000014	65.48	73.31	30.30	.4149	.2871	.8633
RT3	.822424	.000024	30.78	115.85	105.53	.8590	-.4361	-.2678

1

MASS PROPERTIES OF TRIANGLE STANDARDS

STANDARD NO. 1112514

TRIANGLE DIMENSIONS

A INCHES	B INCHES	C INCHES	D INCHES	E INCHES
11.642000	5.261600	.154600	.148300	5.301000

WEIGHT AND MASS

WEIGHT POUNDS	MASS SLUGS
43.6700	1.3587

CENTER OF MASS

X INCHES	Y INCHES	Z INCHES
3.9907	1.7767	2.6505

INERTIA COEFFICIENTS WITH RESPECT TO 0

--MOMENTS OF INERTIA----			----PRODUCTS OF INERTIA----		
IXX	IYY	IZZ	IXY	IXZ	IYZ
.443362	1.164323	1.077424	0.000000	.199586	.199586

PRINCIPAL AXIS

	MOMENT OF INERTIA		DIRECTION ANGLE			DIRECTION COSINE		
	LB-IN2	KG-M-SEC2	X	Y	Z	X	Y	Z
RT1	1.343717	.000040	81.57	42.63	131.39	.1465	.7356	-.6612
RT2	.381596	.000011	17.71	85.68	72.85	.9525	.0751	.2948
RT3	.959801	.000028	74.53	132.31	133.61	.2665	-.6731	-.6897

1

MASS PROPERTIES OF TRIANGLE STANDARDS

STANDARD NO. 4581414

TRIANGLE DIMENSIONS

A INCHES	B INCHES	C INCHES	D INCHES	E INCHES
14.259500	4.635000	.125300	.101000	4.751500

WEIGHT AND MASS		CENTER OF MASS		
WEIGHT POUNDS	MASS SLUGS	X INCHES	Y INCHES	Z INCHES
42.0970	1.3097	4.8776	1.5566	2.3757

INERTIA COEFFICIENTS WITH RESPECT TO 0

--MOMENTS OF INERTIA----			----PRODUCTS OF INERTIA----		
IXX	IYY	IZZ	IXY	IXZ	IYZ
.337308	1.501057	1.427701	0.000000	.206292	.206292

PRINCIPAL AXIS

	MOMENT OF INERTIA		DIRECTION ANGLE			DIRECTION COSINE		
	LB-IN2	KG-M-SEC2	X	Y	Z	X	Y	Z
RT1	1.687490	.000050	84.15	42.43	131.83	.1019	.7380	-.6669
RT2	.298404	.000008	10.83	88.17	79.32	.9821	.0317	.1852
RT3	1.280180	.000038	80.91	132.37	136.19	.1578	-.6740	-.7216

1

MASS PROPERTIES OF TRIANGLE STANDARDS

STANDARD NO. 600834

TRIANGLE DIMENSIONS

A INCHES	B INCHES	C INCHES	D INCHES	E INCHES
8.710600	6.012300	.117300	.115000	6.157000

WEIGHT AND MASS		CENTER OF MASS		
WEIGHT POUNDS	MASS SLUGS	X INCHES	Y INCHES	Z INCHES
43.1280	1.3418	2.9588	2.0304	3.0785

INERTIA COEFFICIENTS WITH RESPECT TO 0

--MOMENTS OF INERTIA----			----PRODUCTS OF INERTIA----		
IXX	IYY	IZZ	IXY	IXZ	IYZ
.583402	.842007	.718908	0.000000	.167433	.167433

PRINCIPAL AXIS

	MOMENT OF INERTIA		DIRECTION ANGLE			DIRECTION COSINE		
	LB-IN2	KG-M-SEC2	X	Y	Z	X	Y	Z
RT1	.984907	.000029	74.85	42.75	128.80	.2613	.7342	-.6266
RT2	.445279	.000013	41.84	74.96	52.07	.7449	.2593	.6145
RT3	.714132	.000021	52.13	128.86	118.63	.6137	-.6274	-.4792

1

MASS PROPERTIES OF TRIANGLE STANDARDS

STANDARD NO. 4141738

TRIANGLE DIMENSIONS

A INCHES	B INCHES	C INCHES	D INCHES	E INCHES
17.351800	4.298900	.127300	.140700	4.301700

WEIGHT AND MASS / CENTER OF MASS

WEIGHT POUNDS	MASS SLUGS	X INCHES	Y INCHES	Z INCHES
42.4250	1.3199	5.9493	1.4453	2.1508

INERTIA COEFFICIENTS WITH RESPECT TO 0

--MOMENTS OF INERTIA----			----PRODUCTS OF INERTIA----		
IXX	IYY	IZZ	IXY	IXZ	IYZ
.284222	2.111489	2.056546	0.000000	.235246	.235246

PRINCIPAL AXIS

	MOMENT OF INERTIA		DIRECTION ANGLE			DIRECTION COSINE		
	LB-IN2	KG-M-SEC2	X	Y	Z	X	Y	Z
RT1	2.333182	.000069	85.49	43.48	133.13	.0784	.7255	-.6837
RT2	.253021	.000007	7.61	89.04	82.44	.9911	.0166	.1314
RT3	1.866064	.000055	83.87	133.47	135.87	.1067	-.6880	-.7177

1

MASS PROPERTIES OF TRIANGLE STANDARDS

STANDARD NO. 578514

TRIANGLE DIMENSIONS

A INCHES	B INCHES	C INCHES	D INCHES	E INCHES
5.848000	5.221800	.125500	.135000	5.321800

WEIGHT AND MASS

WEIGHT POUNDS	MASS SLUGS
22.2120	.6910

CENTER OF MASS

X INCHES	Y INCHES	Z INCHES
1.9950	1.7799	2.6609

INERTIA COEFFICIENTS WITH RESPECT TO 0

--MOMENTS OF INERTIA----			----PRODUCTS OF INERTIA----		
IXX	IYY	IZZ	IXY	IXZ	IYZ
.226880	.250197	.205233	0.000000	.050820	.050820

PRINCIPAL AXIS

	MOMENT OF INERTIA		DIRECTION ANGLE			DIRECTION COSINE		
	LB-IN2	KG-M-SEC2	X	Y	Z	X	Y	Z
RT1	.297093	.000008	63.85	48.72	127.50	.4406	.6597	-.6087
RT2	.147529	.000004	60.14	67.37	38.98	.4978	.3847	.7772
RT3	.237689	.000007	41.66	130.20	99.14	.7470	-.6455	-.1588

APPENDIX B5

TEST PROCEDURE

2.2.1 Dynamic Tests

2.2.1.1 Purpose

The purpose of this test procedure is to establish a method of performing dynamic tests on the product of inertia machine.

2.2.1.2 Equipment

(1) Modified Model 712 rate table with its speed controls and speed calibrator.
(2) Load cell amplifying circuitry (narrow band, D. C.) and power supply.
(3) Hewlett-Packard model 3460 A digital volt meter.
(4) C. M. C. model 226 A electronic counter.
(5) Representative triangular standard test blocks.

2.2.1.3 Set-Up

(1) Turn on electronic equipment for warm up (1.5 hours).
(2) With the table unloaded, zero the D. V. M. with the amplifier zeroing control.
(3) Check to see that the rotational axis is vertical by operating the rate table at a slow speed and observing that the D. V. M. reading is steady.
(4) Stop the machine. Re-zero the D. V. M., as in step 2, and place a test weight, e. g. 5 lbs., on the tilt table a known distance from the flexured axis. (The 9 inch grid line may be used for this purpose.) Adjust the amplifier gain to get the desired scale factor. (A scale factor of 10 in-lbs per volt is a desirable value when using the operational amplifiers of the E. A. I. model TR-48 analog computer for the load cell amplifier).

Example: Scale Factor = Torque ÷ D. V. M. reading.
= 9 inch x 5 lb ÷ 4.5 volts.
= 10 in-lb per volt.

(5) Remove the calibrating weight and place a test block on the tilt table in the desired position, being careful to keep

shock loads to a minimum. Slide the test block perpendicular to the tilt axis in the direction that reduces the D.V.M. reading. A plastic hammer may be used to tap the block gently as the reading approaches zero. It will be necessary to tap the tilt table gently over the tilt axis with the plastic hammer to reduce static friction as zero is approached.

(6) When zero output has been achieved, tighten the holding clamp screws to secure the test block. Only enough pressure should be used to secure the blocks as the tightening operation will stress the tilt table and upset the zero.

(7) Return the D.V.M. output to zero as in step 2. The machine is now ready to operate.

2.2.1.4 Test Procedure

(1) After the set-up procedure has been completed, the test can be run. Adjust the rate table to the speed value required to give the desired revolution period as read on the electronic counter (the counter is set to the period mode).

(2) Record the period and the corresponding load cell output voltage on a data sheet.

(3) Repeat steps 1 and 2 up to the desired speed, but not above the maximum safe speed.

NOTE: It has been found that the machine can be operated up to a tilt table torque of 35 in-lbs provided the clamping screws are moderately tight.

(4) The following approximate formula may be used to compute the product of inertia:

$$\text{Product of Inertia} = \frac{\text{Scale factor x Volts x Period in Seconds}}{4\pi^2}$$

Written By: M. K. Lewis

Approved By: C. W. Allgier

Date: 4-26-66

DATA SHEET

PRODUCT OF INERTIA TEST NUMBER: _____.

Test Block Number: _____. Torque Scale Factor: _____in-lbs per Volt.

Give the test block dimensions in relation to the tilt table as shown in Figure 1.

1 _____ Inches.
2 _____ Inches.
3 _____ Inches.
4 _____ Inches.

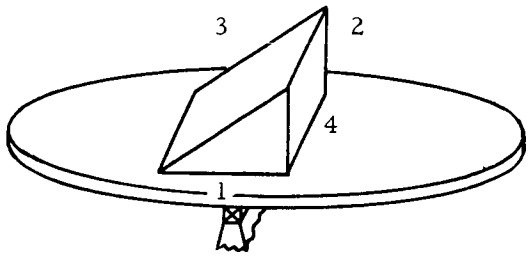

FIGURE 1

Load cell is in TENSION COMPRESSION when table is turning (Scratch out one).

SPEED Degrees per Second	PERIOD OF REVOLUTION Seconds	TORQUE INDICATION Volts	PRODUCT OF INERTIA in-lbs-sec^2

APPENDIX B6

PRINCIPAL AXIS PROGRAM

```
C     PRINCIPAL AXIS AND DIRECTION COSINE PROGRAM FORTRAN IV 2-15-66 JHJ
C
C     ROUTINE FOR CALCULATING MOMENTS OF INERTIA ABOUT PRINCIPAL AXIS
C     AND TO SOLVE FOR DIRECTION COSINES.
C
C     THIS PROGRAM REQUIRES TWO FUNCTION SUBROUTINES ACOS(X) + ACOSD(X)
C
C     IXX, IYY, IZZ, ARE MOMENTS OF INERTIA AND IXY, IXZ, IYZ, ARE
C     PRODUCTS OF INERTIA ABOUT A REFERENCE AXIS THROUGH THE C.G.
C
C     THE FIRST DATA CARD IS A ALPHAMERIC FIELD FOR PAGE HEADING IN COL 1 TO 72
C
C     THE SECOND DATA CARD HAS
C     IXX IN COL 1  TO 12
C     IYY IN COL 13 TO 24
C     IZZ IN COL 25 TO 36
C     IXY IN COL 37 TO 48
C     IXZ IN COL 49 TO 60
C     IYZ IN COL 61 TO 72
C     ANY NUMBER IN COL 73 TO 80 IS USED TO TERMINATE PROGRAM
C
      DIMENSION RT(3), X(3), Y(3), Z(3),WORD(12),AX(3),AY(3),AZ(3)
C
   50 READ(5, 100)(WORD(K), K = 1, 12)
  100 FORMAT (12A6)
      READ(5, 110) AIXX, AIYY, AIZZ, AIXY, AIXZ, AIYZ, XIND
  110 FORMAT(6F12.5,F8.4)
C
C     SOLVE CUBIC EQUATION FORM X**3+P*X**2+Q*X+R=0
C
C     CALCULATE COEFFICIENT (P) MAKE NEGATIVE
      P     = -(AIXX + AIYY + AIZZ)
C
C     CALCULATE COEFFICIENT (Q)
      Q     = AIXX*AIYY + AIXX*AIZZ + AIYY*AIZZ - AIXY**2-AIXZ**2-AIYZ**2
C
C     CALCULATE CONSTANT TERM (R)
      R     = (-AIXX*AIYY*AIZZ+2.*AIXY*AIXZ*AIYZ+AIYY*AIXZ**2
     1+AIXX*AIYZ**2+AIZZ*AIXY**2)
     1+AIZZ*AIXY**2)
C
      A     = (3.*Q - P**2)/3.
      B     = (2.*P**3 - Q*P*9. + 27.*R)/27.
      CONS  = -A**3/27.
      BETA  = -B*.5/SQRT(CONS)
      BETA  = ACOS(BETA)
      ANGL1= BETA/3.
      ANGL2= ANGL1 + 2.0944
      ANGL3= ANGL1 + 4.1888
      CONS  = -A/3.
      TSQC  = 2.*SQRT(CONS)
      XONE  = TSQC*COS(ANGL1)
      XTWO  = TSQC*COS(ANGL2)
      XTHRE= TSQC*COS(ANGL3)
      PD3   = P/3.
```

PRINCIPAL AXIS PROGRAM CONTINUED

```
      RT(1)= XONE - PD3
      RT(2)= XTWO - PD3
      RT(3)= XTHR - PD3
      DO 400 I = 1, 3
      CONS = AIYZ*(AIXX-RT(I))+AXY*AIXZ
      DONS = CONS/(AIXZ*(AIYY-RT(I))+AIXY*AIYZ)
      CONS = CONS/(AIXY*(AIZZ-RT(I))+AIXZ*AIYZ)
      X(I) = 1./SQRT(1.+ DONS**2 + CONS**2)
      Y(I) = DONS*X(I)
      Z(I) = CONS*X(I)
      AX(I)= ACOSD(X(I))
      AY(I)= ACOSD(Y(I))
      AZ(I)= ACOSD(Z(I))
      CONS = RT(I)*.29841E-04
C
C     OUTPUT PRINT OUT
      GO TO (500, 510, 510) I
C     PAGE HEADING
  500 WRITE(6, 501) (WORD(K),K = 1, 12)
  501 FORMAT(1H1 12A6)
C     PRINT INPUT DATA
      WRITE(6, 502) AIXX, AIYY, AIZZ, AIXY, AIXZ, AIYZ
  502 FORMAT(///15X,40H INERTIA COEFFICIENTS WITH RESPECT TO O///
     13X,28H -----MOMENTS OF INERTIA----8X,28H ----PRODUCTS OF INERTIA--
     2--//3X,4H IXX8X,4H IYY8X,4H IZZ8X,4H IXY8X,4H IXZ8X,4H IYZ/6F12.6/
     3///29X,15H PRINCIPAL AXIS///7X,18H MOMENT OF INERTIA6X,16H DIRECTI
     4ON ANGLE4X,17H DIRECTION COSINE//6X,7H LB-IN25X,10H KG-M-SEC2
     53X,2H X5X,2H Y5X,2H Z5X,2H X5X,2H Y5X,2H Z/)
  510 WRITE(6, 511)I ,RT(I),CONS,AX(I),AY(I),AZ(I),X(I),Y(I),Z(I)
  511 FORMAT(3H PAI1, 2F13.6    ,3F7.2,3F7.4/)
  400 CONTINUE
      IF(XIND)55, 50,55
   55 CALL EXIT
      END
```

PRINCIPAL AXIS PROGRAM

```
C     SUBPROGRAM FOR DETERMINING THE ARC COS          FORTRAN IV  3-15-66  JHJ
      FUNCTION ACOS(X)
      IF (ABSF(X)-1.)10, 15, 20
   20 TYPE 12, X
   12 FORMAT( 43HARC COS  VALUE GREATER THAN ABS OF ONE.  X=, F12.8)
      GO TO 60
   15 IF(X-1.) 35, 40, 22
   22 TYPE 14
   14 FORMAT (32HFUNCTION ROUTINE ERROR RECOMPILE)
      GO TO 60
   40 ACOS        = 0.0
      GO TO 50
   35 ACOS        = 3.141593
      GO TO 50
   10 IF(X) 25, 30 ,25
   30 ACOS        = 3.141593/2.
      GO TO 50
   25 Y           =SQRTF(1.-(X**2))
      ACOS        =ATANF(Y/X)
      IF(ACOS)26,50,50
   26 ACOS = 3.14159265 + ACOS
   50 CONTINUE
      RETURN
   60 CONTINUE
      STOP
      END
```

```
C     SUBPROGRAM FOR CHANGING ARC COS FROM RADIANS TO DEGREES
      FUNCTION ACOSD(X)
      ACOSD        = ACOS(X) * 57.295779
      RETURN
      END
```

APPENDIX B7

Product of Inertia Literature Survey

A literature survey was conducted in order to obtain all available information on methods determining products of inertia and locating the principal axes. This survey included a thorough search of the Redstone Scientific Information Center and the Defense Documentation Center for articles pertaining to the product of inertia. Also the publications of the American Institute of Astronautics and Aeronautics and the Society of Aeronautical Weight Engineers were surveyed for pertinent information. The metrology division of the National Bureau of Standards was contacted to obtain any information they had available on mass characteristics and methods of measuring these quantities.

The results of the literature survey has not produced very much new information on methods of determining products of inertia and locating principal axes. The theoretical approach to the problem is covered in much detail in texts on classical mechanics and dynamics. References 1 through 4 explain the basic definitions and principles associated with the product of inertia and principal axes. References 5 and 6 cover the detailed theory and derivations of important formula which relate the products of inertia, the principal moments of inertia and the principal axes to each other. Chapter 4 of Reference 5 describes the principle behind the rate table product of inertia machine which is presently being used in the laboratory.

Reference 7 is a paper which explains an experimental method of determining products of inertia. The basic instrument for this determination is a bifilar pendulum which is used to find the product of inertia of a missile control fin. The product of inertia is determined by adding counterweights to the control fin to induce turning torques. These turning torques counteract the inbalance of the control fin; thereby, dynamically balancing the fin. The product of inertia of the test body can readily be obtained from the mass and geometry of the counterweights. This system does not have a high degree of accuracy but it is a fairly simple test procedure.

References 8 through 10 are papers and reports that give a theoretical approach for determining the principal axes and principal moments of inertia for a specific problem. The product of inertia must already be known for these determinations.

The National Bureau of Standards does not do any work pertaining to product of inertia, moment of inertia or principal axes on a continual basis. If the need arises they may do some special work on the subject, otherwise their information is limited.

From the literature survey conducted, it is apparent that the literature available on product of inertia determination is limited. This limited supply of information probably results from the fact that accuracies in determining principal axes and principal moments of inertia do not require the knowledge of the products of inertia at this time. As space missions become more involved and accurate rendezvous become very critical, the determination of products of inertia will be very important.

REFERENCES

1. Goldstein, Herbert, Classical Mechanics, Addison-Wesley Publishing Company, Inc., Reading Massachusetts, 1959.

2. McCuskey, S. W., An Introduction to Advanced Dynamics, Addison-Wesley Publishing Company, Inc., Reading,Massachusetts, 1959.

3. Seely, Fred B. and Smith, James 9., Advanced Mechanics of Materials, John Wiley and Sons, Inc., New York, 1932.

4. Yeh, Hausan and Abrams, Joel I., Mechanics of Solids and Fluids, Volume 1, Particles and Rigid Body Mechanics, McGraw-Hill Book Co., Inc., New York, 1960

5. Arnold, Ronald N. and Maunder, Leonard, Gyrodynamics and Its Engineering Applications, Academic Press, New York, 1961.

6. Huddleston, John W., Introduction to Engineering Mechanics, Addison-Wesley Publishing Company, Inc., Reading, Massachusetts, 1961.

7. Codr, J. J. and Harris, E. C., "A Simplified Technique for Measurement of Product of Inertia", Engineering Paper Number 1564, Douglas Missile and Space Division, S.A.W.E., Technical Paper Number 369, Presented to the Twenty Second National Conference of the Society of Aeronautical Weight Engineers, St. Louis, Missouri, April 29, 1963.

8. Carpenter, John E., "Inertial Principal Axes as an Eigenvalue Problem"

9. Holmstrom, J. S., "Effect of Dynamic Inbalance on the Motion of a Spinning Vehicle in Free Flight", Chrysler Report Number SAE-TN-12-62, Chrysler Corporation Missile Division, Prepared for the Air Force Ballistic Systems Division, U.S.A.F., Inglewood, California, Air Force Technical Note Number BSD-TDR-62-80, April, 1962.

10. Ehlers, Janet G. and Cowgill, Glenn R., "Fortran Program for Computing the Principal Moments of Inertia of a Rigid Molecule", N.A.S.A Technical Note, N.A.S.A T.N. D-2085, Lewis Research Center, Cleveland, Ohio, February, 1964.

Appendix C

Mass Properties of Liquids

APPENDIX C1

Test Procedure

3.0 Mass Properties of Liquids

3.1 Test Program

3.1.1 Roll Axis Inertia Tests Using the Air Bearing Table

3.1.1.1 Purpose:

To determine the moment of inertia of a cylindrical liquid container about its roll axis.

3.1.1.2 Equipment:

(1) 24 inch Air Bearing Table
(2) Photocell Timing Device
(3) Hewlett-Packard 524D Frequency Counter
(4) Hewlett-Packard 560A Digital Recorder
(5) Radian Scale, Light and Mirror Arrangement
(6) Torsion Rods
(7) Cylindrical Tanks

3.1.1.3 Set-Up:

(1) Turn on electronic equipment for warm up.
(2) Level air bearing table on iso-pad.
(3) Firmly mount the wand for triggering the photocell device to the air bearing table top.
(4) Set air pressure at ____psi.
(5) Do / do not fill cylinder_____with water.
(6) Place cylinder_____on the air bearing table such that the center of the tank is over the center of the table. Use two faced tape if greater adhesion is necessary to keep the tank from slipping.
(7) Insert rod number 120 in the table.
(8) Place the radian scale 140 inches from the center of the table.
(9) With the rod aligned, the table level and the tank mounted, zero the wand and photocell device and zero the light source on the radian scale.

3.1.1.4 Test Procedure:

(1) After the test equipment has been arranged as outlined in the test set up, testing is ready to begin.
(2) Gradually displace the table top, increasing its maximum amplitude until it reaches .006 radians. Then

release the table top and let the maximum amplitude decay to .004 radians. At .004 radians start recording the time and number of cycles from a maximum displacement of .004 to .003 radians. Run each test 5 times to determine the repeatability.

3.1.1.5 Test Data:

(1) Date -

(2) Personnel -

(3) Cylindrical Tank Number -

(4) Test Numbers -

(5) Temperature -

(6) Humidity -

(7) Total time between the maximum displacement of .004 and .003 radians to the nearest 10 microsecond (.000,010) -

(8) Total number of cycles between the maximum displacement of .004 and .003 radians -

3.1.1.6 Special Work:

(1) Determine the average period between the maximum displacement of .004 and .003 radians for each test by dividing the total time by the total number of cycles between .004 and .003 radians.

(2) Record the average periods and compute their average.

_____

_____

_____

_____

_____

_____ Average

(3) Determine the moment of inertia of the tank system by squaring the average period then multiply by the rod constant and divide by $4\pi^2$. Record the moment of inertia_____.

(4) Perform any other work described below.

Written by:_____

Approved by:_____

Date:_____

APPENDIX C2

TEST PROCEDURE

3.0 Mass Properties of Liquids

3.1 Test Program

3.1.2 Displaced Roll Axis Inertia Tests Using the Air Bearing Table

3.1.2.1 Purpose

To determine the effect of translating the axis of rotation of a cylindrical tank on its roll moment of inertia.

3.1.2.2 Equipment

(1) 24-inch air bearing and 45-inch extension ring
(2) Photocell timing device
(3) Displacement detector
(4) Two Hewlett-Packard 524D frequency counters
(5) Two Hewlett-Packard 560A digital recorders
(6) One Accurate Instrument Co. Model 51553 counter
(7) Torsion rods
(8) Cylindrical tanks

3.1.2.3 Set - Up

(1) Turn on electronic equipment for warm-up.
(2) Do, do not, place extension ring on air bearing table and secure with pin.
(3) Level air bearing table on iso-pad.
(4) Set air pressure at _____ psi.
(5) Do, do not, fill cylinder _____ with water.
(6) Place cylinder _____ on the air bearing table such that the edge of the tank is _____ inches from the center of the table. Use two faced tape if greater adhesion is necessary to keep the tank from slipping.
(7) Insert rod number _____ in the table.
(8) With the rod aligned, the table level and the tank mounted, zero the wand and grating for triggering the photocells for both the period and displacement devices.
(9) Connect the Accurate Instrument counter for recording the total number of cycles.

(10) Use the Hewlett-Packard frequency counter and digital recorder for recording the displacements.

(11) Use the Hewlett-Packard counter and digital recorder for recording 10 period averages every 20th cycle.

3.1.2.4 Test Procedure

(1) After the test equipment has been arranged as outlined in the test set-up, testing is ready to begin.

(2) Displace the table top until its maximum amplitude reaches .020 radians. Then release the table top and let the maximum amplitude decay to .015 radians. At .015 radians start recording the period, displacement, and number of cycles from a maximum displacement of .015 until the oscillation ceases.

3.1.2.5 Test Data

(1) Date -
(2) Personnel -
(3) Cylindrical Tank -
(4) Test Number -
(5) Temperature -
(6) Humidity -
(7) Number of Cycles -
(8) Include tape of displacement measurements.
(9) Include tape of 10 period average measurements.

3.1.2.6 Number of Tests

(1) Repeat each test _____ times.

3.1.2.7 Special Work

(1) Record the average periods for a displacement of _____ radians and compute their average.

(2) Determine the moment of inertia of the tank system by using

$$I = KT^2/4\pi^2 \qquad (1)$$

Record the moment of inertia _____.

(3) Perform any other work described below.

Written By: _____

Approved By: _____

Date: _____

APPENDIX C3

TEST PROCEDURE

3.1.3 Yaw-Pitch Axis Inertia Tests Using a Torsional Pendulum

3.1.3.1 Purpose

To determine the moment of inertia of a filled cylindrical tank about its yaw-pitch axis.

3.1.3.2 Equipment

(1) Overhead "I" beam with leveling plates.
(2) Photocell timing device.
(3) Hewlett-Packard 524D frequency counter.
(4) Hewlett-Packard 560A digital recorder.
(5) Radian scale, light, and mirror arrangement.
(6) Torsion rods.
(7) Cylindrical Tanks.

3.1.3.3 Set Up

(1) Turn on electronic equipment for warm-up.
(2) Level leveling plates on "I" beam.
(3) Mount rod number _____ to the leveling plates.
(4) Do, do not, fill tank _____ with water.
(5) Attach tank _____ to rod so that the center of the tank is on the vertical axis of the rod.
(6) Place the teflon bearing against the rod with minimum of pressure.
(7) Place the wand on the tank and align the photocell and light.
(8) Place radian scale at 140 inches.
(9) With the rod aligned and tank mounted, zero the wand, photocell device, and the light source.

3.1.3.4 Test Procedure

(1) With the test set up as described above, the testing is ready to begin.
(2) Gradually displace the tank, increasing its amplitude until it reaches .05 radians, then release the tank and let it decay to .03 radians. At .03 radians, release the bearing and start recording data. Record data for the first 50 cycles. Run each test 3 times to determine the repeatability.

3.1.3.5 Data

(1) Test Numbers - _____, _____, _____.
(2) Date -
(3) Personnel -
(4) Temperature -
(5) Humidity -
(6) Torsion Rod Number and Rod Constant - _____, K = _____.
(7) Tank Number -
(8) Average the period for the first 50 cycles to the nearest 10 microsecond (.000010) - _____, _____, _____.

3.1.3.6 Special Work

(1) Record the average periods and compute their average.

_____
_____
_____
_____ Average

(2) Determine the moment of inertia of the tank system by multiplying the average period squared by the rod constant and dividing by $4\pi^2$. Record the moment of inertia _____.
(3) Perform any other work described below.

Written By: _____

Approved By: _____

Date: _____

APPENDIX C4

TEST PROCEDURE

3.1.3 Yaw-Pitch Axis Test Rotating about a Horizontal Axis

3.1.3.1 Purpose

To determine the moment of inertia of a filled cylindrical tank as it oscillates about its yaw-pitch axis.

3.1.3.2 Equipment

(1) Government furnished aluminum tanks and stand.
(2) Photocell timing device.
(3) Radian Scale.
(4) Hewlett-Packard 524D counter.
(5) Hewlett-Packard 560A automatic readout.
(6) Tank Number _____.
(7) Torsion Rod Number _____.

3.1.3.3 Set Up

(1) Turn on electronic equipment for warm-up.
(2) Align tank on its center of gravity.
(3) Install rod, align rod vertically and horizontally before clamping outside bracket.
(4) With the rod aligned, position the tank such that the three zero marks on the side of the tank and frame are in line, then fasten the outside bracket.
(5) Zero the photocell, light source, and radian scale.

3.1.3.4 Test Procedure

(1) With the tank set up as described above, the testing is ready to begin.
(2) Gradually displace the tank, increasing the displacement until it reaches .05 radians, then release the tank and let it decay to .03 radians. At .03 radians start recording data. Record data for 50 cycles.
(3) Repeat each test 3 times.
(4) Before each test tighten all bolts to prevent any slipage.
(5) Perform this procedure for tank empty and full.

3.1.3.5 Test Data

(1) Date -
(2) Personnel -
(3) Temperature -
(4) Humidity -
(5) Rod Number -
(6) Tank Number -
(7) Test Number -
(8) Number of Cycles -
(9) Period Readout Sheet -

Empty	Full

3.1.3.6 Special Work

(1) Obtain the period for each test by averaging the period for 50 cycles. Average this period for all similar tests and record.

T_{empty} = _____ sec.

T_{full} = _____ sec.

(2) Calculate the moment of inertia of the system empty and full by using:

$$I = KT^2/4\pi^2$$

where K = _____ in-lb.
and T is given above.

I_{empty} = _____ in-lb-sec^2

I_{full} = _____ in-lb-sec^2

$I_{water} = I_{full} - I_{empty}$ = _____ in-lb-sec^2

Written By: _____

Approved By: _____

Date: _____

APPENDIX C5

TEST PROCEDURE

3.1.4 Yaw-Pitch Axis Inertia Tests Rotating about a Displaced Axis

3.1.4.1 Purpose

To determine the moment of inertia of a filled cylindrical tank as it oscillates about different displaced yaw-pitch axes.

3.1.4.2 Equipment

(1) Government furnished aluminum tanks and stand.
(2) Photocell timing device.
(3) Radian Scale.
(4) Hewlett-Packard 524D counter.
(5) Hewlett-Packard 560A automatic readout.
(6) Tank Number _____.
(7) Torsion Rod Number _____.

3.1.4.3 Set Up

(1) Turn on electronic equipment for warm-up.
(2) Align tank on specified displacement in the stand.
(3) Install rod, align rod vertically and horizontally before clamping outside bracket.
(4) With rod aligned, position the tank such that the three zero marks on the side of the tank and frame are in line, then fasten the outside bracket.
(5) Zero the photocell, light source, and radian scale.

3.1.4.4 Test Procedure

(1) With the tank set up as described above, the testing is ready to begin.
(2) Gradually displace the tank, increasing the displacement until it reaches .05 radians, then release the tank and let it decay to .03 radians. At .03 radians start recording data. Record data for 50 cycles.
(3) Repeat each test 3 times.
(4) Before each test tighten all bolts to prevent any slipage.
(5) Perform this procedure for tank empty and full.

3.1.4.5 Test Data

(1) Date -
(2) Personnel -
(3) Temperature -
(4) Humidity -
(5) Rod Number - _____
(6) Tank Number - _____
(7) Empty Test Number - _____
(8) Number of Cycles - _____

Displacement

	L_1 =	L_2 =	L_3 =	L_4 =	L_5 =

(9) Include period readout sheets.
(10) Full Test Number - _____
(11) Number of Cycles - _____
(12) Include period readout sheets.

3.1.4.6 Special Work

(1) Obtain the period for each test by averaging the period for 50 cycles. Average this period for all similar tests and records.

	L_1	L_2	L_3	L_4	L_5
T (full) =					
T (empty) =					

(2) Calculate the moment of inertia of the system by using

$$I = (WL + K)\, T^2/4\pi^2$$

where:

W = _____ lbs.
K = _____ in-lbs.

and L and T are given above. Calculate I empty and full and determine I_{water} by using

$$I_{water} = I_{full} - I_{empty}$$

and fill in the chart below.

	L_1	L_2	L_3	L_4	L_5
I_{water}					

Written By: _____

Approved By: _____

Date: _____

APPENDIX C6

TEST PROCEDURE

3.1.5 Ring Baffle Tests Using the Government Furnished Plexiglass Tank

3.1.5.1 Purpose

To determine the moment of inertia of a filled cylindrical tank with ring baffles as it oscillates about its yaw-pitch axis.

3.1.5.2 Equipment

(1) Government furnished plexiglass tank, baffles and stand.
(2) Photo-cell timing device.
(3) Hewlett-Packard 524D counter.
(4) Hewlett-Packard 560A automatic readout
(5) Torsion rod No. _____.
(6) Baffles —

3.1.5.3 Set-Up

(1) Turn on electronic equipment for warm-up.
(2) Align tank with baffles on its center of gravity.
(3) Install rod, align rod vertically and horizontally before clamping outside bracket.
(4) With rod aligned, position the tank such that the three zero marks on the side of the tank and frame are in line, then fasten the outside bracket.
(5) Zero the photo-cell and light source.

3.1.5.4 Test Procedure

(1) With the tank set up as described above, the testing is ready to begin.
(2) Gradually displace the tank, increasing the displacement until it reaches .03 radians, then release the tank and let it decay to .02 radians. At .02 radians start recording data. Record data until the displacement ceases.
(3) Record the period every other cycle and obtain an average for the first 50 cycles.
(4) Repeat each test three times.
(5) Before each test tighten all bolts to prevent any slipage.

3.1.5.5 Test Data

(1) Date -
(2) Personnel -

		Empty	Full
(3)	Temperature -		
(4)	Humidity -		
(5)	Baffles -		
(6)	Period Printout -		
(7)	Rod Number and K		
(8)	Test Number -		
(9)	Period -		
(10)	Average Period -		
(11)	Rod Number and K		
(12)	Test Number -		
(13)	Period -		
(14)	Average Period -		
(15)	Rod Number and K		
(16)	Test Number -		
(17)	Period -		
(18)	Average Period -		
(19)	Rod Number and K		
(20)	Test Number -		
(21)	Period -		
(22)	Average Period -		

3.1.5.6 Special Work

(1) Calculate the moment of inertia of the systems by using $I = KT^2/4\pi^2$.

Rod	I_{empty}	I_{full}	I_{water}

(2) Calculate I_{water}/I_{solid} = _____.

I_{solid} =

Written By: M. S. Phillips

Approved By: _____

Date: _____

APPENDIX C7

TEST PROCEDURE

3.1.5 Baffle Tests Using the Air Bearing Table

3.1.5.1 Purpose

To determine the moment of inertia of a liquid filled cylindrical container with various baffle arrangements as it oscillates about yaw-pitch axis.

3.1.5.2 Equipment

(1) 24 inch air bearing table
(2) Photocell timing and displacement devices
(3) Two Hewlett-Packard 524D counters
(4) Two Hewlett-Packard 560A digital recorders
(5) Torsion rods
(6) Cylindrical tank with baffles and spacers

3.1.5.3 Set-Up

(1) Turn on electronic equipment for warm-up.
(2) Level air bearing table on iso-pad.
(3) Set air pressure at 30 psi.
(4) Place ____ baffles, with ____ spacers into tank.
(5) Place the tank on the air bearing table such that the center of mass of the liquid is over the center of the table, using the special brackets.
(6) Insert rod number ____ in the table.
(7) With the rod aligned, the table level and the tank mounted, zero the wand and photocell device and zero the light source on the radian scale.
(8)

3.1.5.4 Test Procedure

(1) After the test equipment has been arranged as outlined in the test set-up, testing is ready to begin.
(2) Gradually displace the table top, increasing its maximum amplitude until it reaches ____ radians. Then release the table top and let the maximum amplitude decay to ____ radians. At ____ radians start recording the time and number of cycles from a maximum displacement of ____ to ____ radians. Run each test ____ times to determine the repeatability.

3.1.1.5 Test Data

(1) Test Numbers -
(2) Date -
(3) Personnel -
(4) Temperature -
(5) Humidity -
(6) Baffles and Spacers -
(7) 10 period average print out every 20 cycles.

3.1.1.6 Special Work

(1) Determine the average period for ____ cycles starting at a maximum displacement of ____ radians.
(2) Record the average periods and compute their average.

T_{empty}		T_{full}	
_____		_____	
_____		_____	
_____		_____	
_____	Average	_____	Average

(3) Calculate

$$I_e = KT_e^2/4\pi^2 =$$

$$I_f = KT_f^2/4\pi^2 =$$

$$I_w = I_f - I_e =$$

(4) Perform any other work describe below.

Written By: M. S. Phillips

Approved By: _____

Date: _____

REFERENCES

1. Abramson, H. N. and Ransleben, G. E., "Some Comparisons of Sloshing Behavior in Cylindrical Tanks with Flat and Conical Bottoms," SWRI Project 43-768-2, Report No. 4, May, 1959.
2. Phillips, M. S., "A Precision System for Determining Mass Moments of Inertia," Presented to the Apollo Application Program of the Society of Engineering Science in Huntsville, Alabama, January, 1966.
3. Dodge, F. T. and Kana, D. D. , "Moment of Inertia and Damping of Liquids in Baffled Cylindrical Tanks," SWRI Project 02-1072, Report No. 11, June, 1965.

APPENDIX C8

In order to understand the basic foundation of the theoretical approach a brief review of basic hydrodynamics is undertaken. The equations of motion of a liquid can be obtained by using the equations of Euler. From these the velocity, the pressure, and the density at all points of space occupied by the liquid for all instants are obtained. The velocity components u, v, w, at the locations x, y, z parallel to the co-ordinate axis at time t, are shown below.

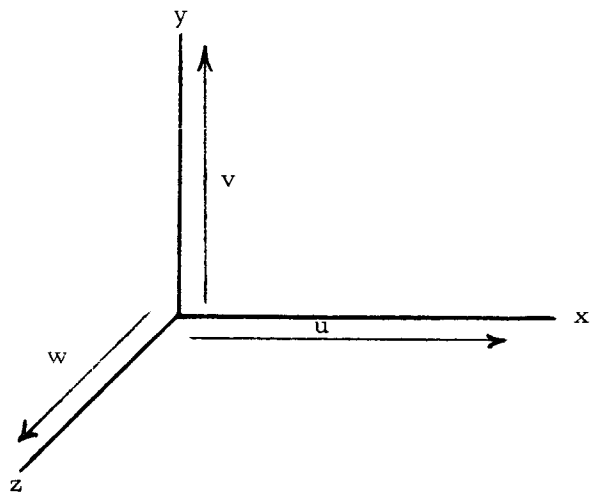

Their derivatives

$$\frac{\partial u}{\partial x}, \frac{\partial v}{\partial x}, \frac{\partial w}{\partial x}, \frac{\partial u}{\partial y}, \frac{\partial v}{\partial y}, \frac{\partial w}{\partial y}, \frac{\partial u}{\partial z}, \frac{\partial v}{\partial z}, \frac{\partial w}{\partial z} \tag{1}$$

are assumed everywhere to be finite. Let p be the pressure, ρ the density and X, Y, Z, the components of the external forces per unit mass at point x, y, z, and at time t. The equations of motion are derived by examining a volume element of liquid as shown below.

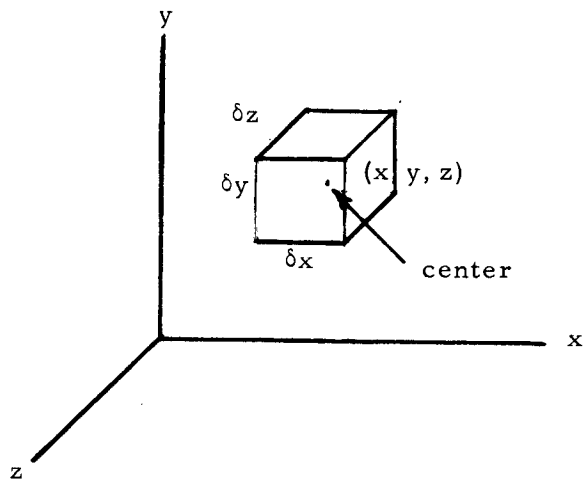

The rate at which the x-component of the momentum is increasing in the x direction is given by

$$\rho \ \delta x \, \delta y \ \delta z \ \frac{du}{dt} \ . \tag{2}$$

The external force in the x direction is given by $\rho X \delta x \, \delta y \delta z$. The pressure on the $\delta y \ \delta z$ faces are

$$(p - 1/2 \frac{\partial p}{\partial x} \cdot \frac{\delta x}{2}) \ \delta y \ \delta z \tag{3}$$

and

$$(p + 1/2 \frac{\partial p}{\partial x} \cdot \frac{\delta x}{2}) \ \delta y \ \delta z \tag{4}$$

respectively from the origin outward. Therefore, the resultant pressure is their difference.

$$- \frac{\partial p}{\partial x} \ \delta x \ \delta y \ \delta z \ . \tag{5}$$

The equation of motion for the x direction is obtained by summing all the forces,

$$\rho\,\delta x\,\delta y\,\delta z\,\frac{du}{dt} = \rho\delta x\,\delta y\delta z\,X - \frac{\partial p}{\partial x}\,\delta x\,\delta y\,\delta z\,. \tag{6}$$

Substitute

$$\frac{du}{dt} = \frac{\partial u}{\partial t} + u\frac{\partial u}{\partial x} + v\frac{\partial u}{\partial y} + w\frac{\partial u}{\partial z} \tag{7}$$

the total differential of u(x, y, z, t) in the above equation now becomes

$$\frac{\partial u}{\partial t} + u\frac{\partial u}{\partial x} + v\frac{\partial u}{\partial y} + w\frac{\partial u}{\partial z} = X - \frac{1}{\rho}\frac{\partial p}{\partial x}\,. \tag{8}$$

Likewise for the y and z directions:

$$\frac{\partial v}{\partial t} + u\frac{\partial v}{\partial x} + v\frac{\partial v}{\partial y} + w\frac{\partial v}{\partial z} = Y - \frac{1}{\rho}\frac{\partial p}{\partial y} \tag{9}$$

$$\frac{\partial w}{\partial t} + u\frac{\partial w}{\partial x} + v\frac{\partial w}{\partial y} + w\frac{\partial w}{\partial z} = Z - \frac{1}{\rho}\frac{\partial p}{\partial z}\,. \tag{10}$$

The equations along with the conservation of mass must be satisfied for any liquid system. The conditions that must be satisfied for the conservation of mass can be described by considering an element of liquid as shown.

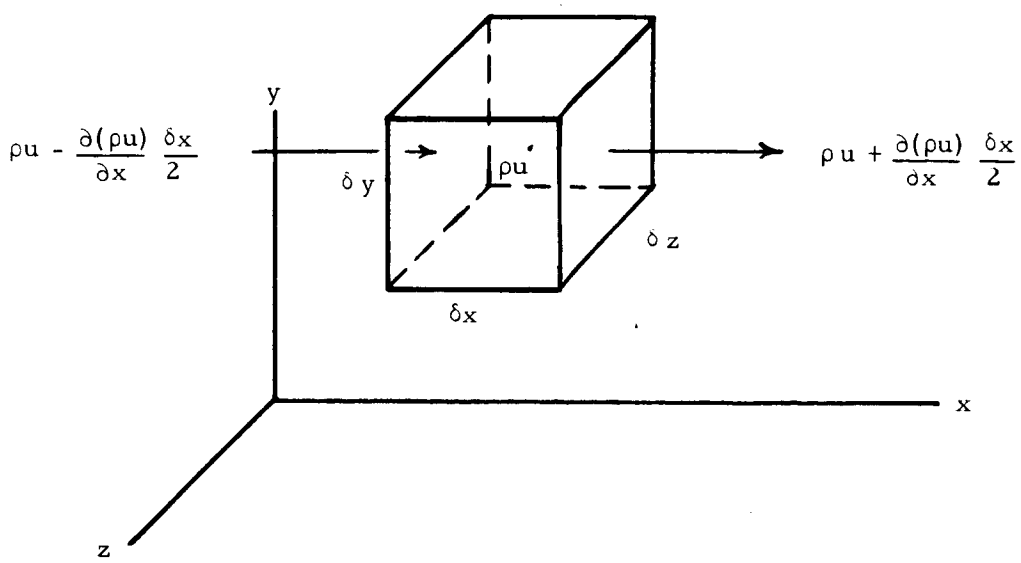

If the change in velocity with distance is considered, the rate of mass flux across the face $\delta y\ \delta z$ is

$$\left(\rho u - \frac{\partial(\rho u)}{\partial x}\ \frac{\delta x}{2}\right)\ \delta y\ \delta z \tag{11}$$

and

$$\left(\rho u + \frac{\partial(\rho u)}{\partial x}\ \frac{\delta x}{2}\right)\ \delta y\ \delta z \tag{12}$$

as shown. The net rate of influx of mass into the element is their difference

$$-\ \frac{\partial(\rho u)}{\partial x}\ \delta x\ \delta y\ \delta z\ . \tag{13}$$

Likewise, for the other two faces

$$-\ \frac{\partial(\rho v)}{\partial y}\ \delta x\ \delta y\ \delta z \tag{14}$$

$$-\ \frac{\partial(\rho w)}{\partial y}\ \delta x\ \delta y\ \delta z\ . \tag{15}$$

The sum of these three must equal the total change of mass

$$-\left[\frac{\partial(\rho u)}{\partial x} - \frac{\partial(\rho v)}{\partial y} + \frac{\partial(\rho w)}{\partial z}\right]\delta x\ \delta y\ \delta z = \frac{\partial(\rho\ \delta x\ \delta y\ \delta z)}{\partial t} \tag{16}$$

or

$$\frac{\partial(\rho u)}{\partial x} + \frac{\partial(\rho v)}{\partial y} + \frac{\partial(\rho w)}{\partial z} = -\ \frac{\partial \rho}{\partial t}\ . \tag{17}$$

This is the equation of continuity. For a homogenous incompressible fluid the density is independent of time and space; therefore, the above equation reduces to

$$\frac{\partial u}{\partial x} + \frac{\partial v}{\partial y} + \frac{\partial w}{\partial z} = 0 \ . \tag{18}$$

For an incompressible, non-viscous, irrotational, homogenous liquid, i.e. a perfect liquid, a function called the velocity potential can be used. This velocity potential Φ is analogous to potentials such as that of gravitational attraction and electrostatic, forces, and satisfies the relations

$$u = \frac{\partial \Phi}{\partial x} \tag{19}$$

$$v = \frac{\partial \Phi}{\partial y} \tag{20}$$

$$w = \frac{\partial \Phi}{\partial z} \ . \tag{21}$$

The continuity equation now becomes

$$\frac{\partial^2 \Phi}{\partial x^2} + \frac{\partial^2 \Phi}{\partial y^2} + \frac{\partial^2 \Phi}{\partial z^2} = 0 \ . \tag{22}$$

This equation is also called the Laplacian and is represented by

$$\nabla^2 \Phi = 0 \ . \tag{23}$$

These equations describing the velocity potential also yield

$$\frac{\partial v}{\partial z} = \frac{\partial w}{\partial y} \tag{24}$$

$$\frac{\partial w}{\partial x} = \frac{\partial u}{\partial z} \tag{25}$$

$$\frac{\partial u}{\partial y} = \frac{\partial v}{\partial x} \tag{25}$$

which can be substituted in the three previous equations of motion to give

$$\frac{\partial^2 \Phi}{\partial x \partial t} + u \frac{\partial u}{\partial x} + v \frac{\partial v}{\partial x} + w \frac{\partial w}{\partial x} = X - \frac{1}{\rho} \frac{\partial p}{\rho x} \tag{27}$$

$$\frac{\partial^2 \Phi}{\partial y \partial t} + u \frac{\partial u}{\partial y} + v \frac{\partial v}{\partial y} + w \frac{\partial w}{\partial y} = Y - \frac{1}{\rho} \frac{\partial p}{\partial y} \tag{28}$$

$$\frac{\partial^2 \Phi}{\partial z \partial t} + u \frac{\partial u}{\partial z} + v \frac{\partial v}{\partial z} + w \frac{\partial w}{\partial z} = Z - \frac{1}{\rho} \frac{\partial p}{\partial z} \ . \tag{29}$$

In most cases the external forces X, Y, Z have a potential

$$X = - \frac{\partial \Omega}{\partial x} \tag{30}$$

$$Y = - \frac{\partial \Omega}{\partial y} \tag{31}$$

$$Z = - \frac{\partial \Omega}{\partial z} \ . \tag{32}$$

Using this assumption and integrating the previous equations with respect to x, y, z respectively gives

$$\frac{\partial \Phi}{\partial t} + \frac{u^2}{2} + \frac{v^2}{2} + \frac{w^2}{2} = -\Omega - \frac{p}{\rho} + F_1(t) \tag{33}$$

$$\frac{\partial \Phi}{\partial t} + \frac{u^2}{2} + \frac{v^2}{2} + \frac{w^2}{2} = -\Omega - \frac{p}{\rho} + F_2(t) \tag{34}$$

$$\frac{\partial \Phi}{\partial t} + \frac{u^2}{2} + \frac{v^2}{2} + \frac{w^2}{2} = -\Omega - \frac{p}{\rho} + F_3(t) \ . \tag{35}$$

Since F_1, F_2, and F_3 are arbitrary constants of integration, let $F_1 = F_2 = F_3 = F$; therefore, the three equations above reduce to

$$\frac{\partial \Phi}{\partial t} + \frac{u^2}{2} + \frac{v^2}{2} + \frac{w^2}{2} = -\Omega - \frac{p}{\rho} + F(t) \tag{36}$$

which is Bernoulli's Equation. Bernoulli's Equation along with the continuity Equation, the kinematic free surface condition and the boundary condition, are the basic equations necessary for solving the hydrodynamic problem at hand.

The Laplacian can now be applied to a cylindrical tank performing the rotational motion. Since the tank is a cylinder, the best coordinate system to use is the cylindrical coordinate system. The Laplacian in cylindrical coordinates is

$$\frac{\partial^2 \Phi}{\partial r^2} + \frac{1}{r}\frac{\partial \Phi}{\partial r} + \frac{1}{r^2}\frac{\partial^2 \Phi}{\partial \theta^2} + \frac{\partial^2 \Phi}{\partial z^2} = 0 \tag{37}$$

where

$$x = r \cos \theta \tag{38}$$

and

$$y = r \sin \theta \tag{39}$$

have been used.

To find the velocity potential Φ for the specific system, the Laplacian must satisfy the specific boundary condition dictated by the system. Since the liquid cannot penetrate the wall or the bottom, the liquid velocity component normal to the tank surface must equal the velocity of the tank surface normal to itself. As the tank rotates about the center of gravity of the liquid the following conditions must be satisfied.

$$\frac{\partial \Phi}{\partial r} = - i \omega \theta_o e^{i\omega t} z \cos \varphi \qquad \text{for } r = a \tag{40}$$

and

$$\frac{\partial \Phi}{\partial z} = i \omega \theta_o e^{i\omega t} r \cos \varphi \, . \qquad \text{for } z = \pm h/2 \tag{41}$$

APPENDIX C9

For the solution of the Laplace equation

$$\nabla^2 \Phi = 0 \tag{1}$$

with boundary conditions

$$\partial\Phi/\partial r = -i\omega\theta_o e^{i\omega t} z \cos\varphi \qquad \text{at } r = a \tag{2}$$

and

$$\partial\Phi/\partial z = i\omega\theta_o e^{i\omega t} r \cos\varphi \qquad \text{at } z = \pm h/2 \tag{3}$$

the velocity potential $\Phi = \Phi(r, \varphi, z, t)$ can be transformed into a time independent potential $\psi(r, \varphi, z)$ by using

$$\Phi = \psi e^{i\omega t} \tag{4}$$

which fulfills the Laplace Equation

$$\nabla^2 \psi = 0$$

and has the boundary conditions

$$\partial\psi/\partial r = -i\omega\theta_o z \cos\varphi \qquad \text{at } r = a \tag{5}$$

and

$$\partial\psi/\partial z = i\omega\theta_o r \cos\varphi . \qquad \text{at } z = \pm h/2 \tag{6}$$

In order to make the first boundary condition homogenous, we introduce the transformation

$$\xi = \psi + i\omega\theta_o zr \cos\varphi \tag{7}$$

and we obtain a new set of equations

$$\nabla^2\xi = 0 \tag{8}$$

$$\partial\xi/\partial r = 0 \qquad \text{at } r = a \tag{9}$$

$$\partial\xi/\partial z = 2i\omega\theta_o r \cos\varphi . \qquad \text{at } z = \pm h/2 \tag{10}$$

Equation 8 is derived from

$$\nabla^2\xi = \nabla^2\psi + \nabla^2(i\omega\theta_o zr \cos\varphi) \tag{11}$$

and since

$$\nabla^2\psi = 0 \tag{12}$$

with

$$\nabla^2 = \partial^2/\partial r^2 + (1/r)(\partial/\partial r) + (1/r^2)(\partial^2/\partial\varphi^2) + \partial^2/\partial z^2 \tag{13}$$

it is then

$$\nabla^2(i\omega\theta_o zr \cos\varphi) = i\omega\theta_o(z/r)\cos\varphi - i\omega\theta_o(z/r)\cos\varphi \tag{14}$$

therefore

$$\nabla^2\xi = 0 . \tag{15}$$

Likewise Equation 9 comes from

$$\partial\xi/\partial r = \partial\psi/\partial r + i\omega\theta_o z \cos\varphi \tag{16}$$

and since

$$\partial\psi/\partial r = -i\omega\theta_o z \cos\varphi \tag{17}$$

the radial boundary condition becomes

$$\partial \xi / \partial r = 0 . \tag{18}$$

Also, Equation 10 becomes

$$\partial \xi / \partial z = i\omega\theta_o r \cos \varphi + i\omega\theta_o r \cos \varphi \tag{19}$$

therefore,

$$\partial \xi / \partial z = 2i\omega\theta_o r \cos \varphi . \tag{20}$$

Now Equation 8 with boundary conditions Equations 9 and 10 must be solved.

Using the method of the separation of variables

$$\xi(r, \varphi, z) = F(r, \varphi) Z(z) \tag{21}$$

and introducing this into the Laplace Equation yields

$$\partial^2 \left[F(r, \varphi) Z(z)\right] / \partial r^2 + (1/r) \partial \left[F(r, \varphi) Z(z)\right] / \partial r +$$

$$(1/r^2) \partial^2 \left[F(r, \varphi) Z(z)\right] / \partial \varphi^2 + \partial^2 \left[F(r, \varphi) Z(z)\right] / \partial z^2 = 0 \tag{22}$$

$$Z \partial^2 F / \partial r^2 + (Z/r) \partial F / \partial r + (Z/r^2) \partial^2 F / \partial \varphi^2 + F \partial^2 Z / \partial z^2 = 0 \tag{23}$$

or

$$(1/F)(\partial^2 F / \partial r^2) + (1/Fr)(\partial F / \partial r) + (1/Fr^2)(\partial^2 F / \partial \varphi^2) =$$

$$-(1/Z)(\partial^2 Z / \partial z^2) . \tag{24}$$

The left hand side is a function of r and φ while the right hand side is a

function of z, this can only happen if both are a constant $\pm\lambda^2$. The minus sign is chosen, because the following Bessel functions are real and the relation in z is a hyperbolic one. Finally, we have to solve two differential equations

$$\partial^2 Z/\partial z - \lambda^2 Z = 0 \tag{25}$$

and

$$r^2(\partial^2 F/\partial r^2) + r(\partial F/\partial r) + \partial^2 F/\partial\varphi^2 + \lambda^2 r^2 F = 0 . \tag{26}$$

The general solution for Equation (25) is

$$Z(z) = A\cosh(\lambda z) + B\sinh(\lambda z) \tag{27}$$

where A and B are arbitrary. Equation 26 is solved by using the separation of variables technique used previously. Now

$$F(r, \varphi) = R(r)\ G(\varphi) \tag{28}$$

and Equation 26 becomes

$$r^2\partial^2\left[R(r)\ G(\varphi)\right]/\partial r^2 + r\partial\left[R(r)\ G(\varphi)\right]/\partial r + \partial^2\left[R(r)\ G(\varphi)\right]/\partial\varphi^2 + \lambda^2 r^2\left[R(r)\ G(\varphi)\right] = 0 \tag{29}$$

$$r^2 G(\partial^2 R/\partial r^2) + rG(\partial R/\partial r) + \lambda^2 r^2 RG = -R(\partial^2 G/\partial\varphi^2) . \tag{30}$$

The left of Equation 30 is a function of r and the right is a function of φ; therefore, we set each side equal to $\pm\nu^2$ as stated before.

$$(r^2/R)(\partial^2 R/\partial r^2) + (r/R)(\partial R/\partial r) + \lambda^2 r^2 = \pm\nu^2 \tag{31}$$

and

$$-(\partial^2 G/\partial\varphi^2)(1/G) = \pm\nu^2 . \tag{32}$$

The plus sign is used since the solution in the y-direction must be periodic. Using

$$\lambda r = \xi \tag{33}$$

Equation 31 can be transformed into

$$(\lambda^2 r^2)(\partial^2 R/\partial\xi^2) + (\lambda r/R)(\partial R/\partial\xi) + \lambda^2 r^2 = +\nu^2 \tag{34}$$

and

$$\xi^2 \partial^2 R/\partial\xi + \xi\partial R/\partial\xi + (\xi^2 - \nu^2)R = 0 . \tag{35}$$

Equation 35 has the same form as the Bessel differential equation

$$x^2\partial^2 y/\partial x^2 + x\partial y/\partial x + (x^2 - n^2)y = 0 \tag{36}$$

which has a solution

$$y = C_1 J_n(x) + C_2 Y_n(x) \tag{37}$$

C_1 and C_2 are aribtrary constants and $J_n(x)$ is the Bessel function of order n of the first kind and $Y_n(x)$ is the Bessel function of order n of the second kind. Therefore, the solution of Equation 35 is

$$R(\xi) = C_1 J_\nu(\xi) + C_2 Y_\nu(\xi) \tag{38}$$

or

$$R(\lambda r) = C_1 J_\nu(\lambda r) + C_2 Y_\nu(\lambda r) . \tag{39}$$

Since Y_ν (becomes infinity at $r = 0$), F must be identically zero and Equation 39 becomes

$$R(\lambda r) = C_1 J_\nu(\lambda r). \tag{40}$$

The solution of Equation 32 yields

$$G = C\sin(\nu\varphi) + D\cos(\nu\varphi) \tag{41}$$

Finally, the solution of Equation 8 becomes

$$\xi(r, \varphi, z) = \left[A\cosh(\lambda z) + B\sinh(\lambda z)\right]\left[C\sin(\nu\varphi) + D\cos(\nu\varphi)\right]J_\nu(\lambda r) \tag{42}$$

or

$$\xi_n(r, \varphi, z) = \left[A_n\cosh(\lambda_n z) + B_n\sinh(\lambda_n z)\right]\left[C_n\sin(\nu\varphi) + D_n\cos(\nu\varphi)\right] \cdot J_\nu(\lambda_n r). \tag{43}$$

Equation 43 must now be satisfied by boundary conditions

$$\partial \xi_n / \partial r = 0 \qquad \text{at } r = a \tag{44}$$

and

$$\partial \xi_n / \partial z = 2i\omega\theta_o r \cos\varphi . \qquad \text{at } z = \pm h/2 \tag{45}$$

Equation 43 with boundary condition, Equation 44 yields

$$(\partial J_\nu / \partial r)(a\lambda_n) = 0 \tag{46}$$

which will be fulfilled for

$$a\lambda_n = \epsilon_n^{(\nu)} \tag{47}$$

where $\epsilon_n^{(\nu)}$ are the zeroes of J_ν'.

Equations 43 and 45 yield

$$\partial \xi / \partial z = \sum_{n=1}^{\infty} \left[(\epsilon_n/a)A_n \sinh(\epsilon_n h/2a) + (\epsilon_n/a)B_n \cosh(\epsilon_n h/2a)\right]\left[C_n \sin(\nu\varphi) + D_n \cos(\nu\varphi)\right] \cdot J_\nu(r\epsilon_n/a) = 4i\omega\theta_o a \sum_{n=1}^{\infty} J_\nu(\epsilon_n r/a)/(\epsilon_n^2 - 1)J_\nu(\epsilon_n) \cos\varphi \tag{48}$$

and

$$\sum_{n=1}^{\infty} \left[-(\epsilon_n/a)A_n \sinh(\epsilon_n h/2a) + (\epsilon_n/a)B_n \cosh(\epsilon_n h/2a)\right]\left[C_n \sin(\nu\varphi) + D_n \cos(\nu\varphi)\right] J_\nu(r\epsilon_n/a) = 4i\omega\theta_o a \sum_{n=1}^{\infty} (J_\nu(\epsilon_n r/a)/(\epsilon_n^2 - 1)J_\nu(\epsilon_n)) \cos\varphi \tag{49}$$

from which we can immediately conclude that $C_n = 0$, $\nu = 1$, and $\epsilon_n^{(1)} = \epsilon_n$. Taking $D_n = 1$, we obtain two linear equations for A_n and B_n, and by solving these equations we obtain for the integration constants A_n and B_n

$$A_n = 0 \tag{50}$$

$$B_n = \frac{4i\omega\theta_o a^2}{\epsilon_n(\epsilon_n^2-1)J_1(\epsilon_n)\cosh(\epsilon_n h/2a)} . \tag{51}$$

Introducing this into ξ, we finally obtain

$$\xi(r,\varphi,z) = i\omega\theta_o e^{i\omega t} a^2 \cos\varphi \sum_{n=1}^{\infty} \frac{J_1(\epsilon_n r/a)}{\epsilon_n(\epsilon_n^2-1)J_1(\epsilon_n)} \cdot \frac{\sinh(\epsilon_n z/a)}{\cosh(\epsilon_n h/2a)} \tag{52}$$

by applying Equations 7 and 4, Equation 52 becomes

$$\Phi(r,\varphi,z,t,) = -i\omega\theta_o e^{i\omega t} a^2 \cos\varphi \left[zr/a^2 - 4 \sum_{n=1}^{\infty} \frac{J_1(\epsilon_n r/a)}{\epsilon_n(\epsilon_n^2-1)J_1(\epsilon_n)} \cdot \frac{\sinh(\epsilon_n z/a)}{\cosh(\epsilon_n h/2a)} \right] . \tag{53}$$

Appendix D

Center of Gravity

APPENDIX D1

TEST PROCEDURE

4.0 Center of Gravity Program

4.1 Spherical Segment Air Bearing System Modification

4.1.6 System Evaluation Tests

4.1.6.1 Purpose

To determine the sensitivity of the spherical segment air bearing center of gravity locator with different loads.

4.1.6.2 Equipment

(1) Spherical segment air bearing system
(2) Laboratory weights, 6.8 lb. and 24.2 lb.
(3) Laboratory sensitivity weights, 5 mg to 500 mg.
(4) Reference inclinometer

4.1.6.3 Procedure

(1) Allow empty air bearing table to stabilize and check reading of levels against inclinometer. Adjust if necessary.
(2) Place 5 mg weight near the center of the table and note if levels indicate movement. Continue moving weight outward until an indication is obtained. Record the distance from the center.
(3) Repeat operation no. 2 with the 10, 50, and 500 mg weights, and record the minimum detectable distance for each.
(4) Place the 6.8 lb. weight on the table and position it until a level indication is obtained.
(5) Repeat steps 2 and 3 with the 6.8 lb. weight in place.
(6) Repeat step 4 with the 24.2 lb. weight.
(7) Repeat steps 2 and 3 with the 24.2 lb. weight in place.

APPENDIX D2

TEST PROCEDURE

4.0 Center of Gravity Program

4.2 Moment Detection System (Bytrex) Modifications

4.2.4 System Evaluation Tests

4.2.4.1 Purpose

To determine the sensitivity of the modified Bytrex center of gravity locator with different loads.

4.2.4.2 Equipment

(1) Bytrex C.G. locator with 25 inch-pound detector head
(2) Hewlett-Packard Model 3460A digital voltmeter
(3) Trygon Model 40-700 regulated power supply
(4) Laboratory weights, 6.8 lb. and 24.2 lb.
(5) Laboratory sensitivity weights, 5mg to 500mg

4.2.4.3 Procedure

(1) Connect power supply across Bytrex power supply batteries and set for 6.0 volts.
(2) Connect digital voltmeter across Bytrex meter terminals.
(3) Turn on equipment for 2 hour warm-up.
(4) Zero voltmeter reading with table empty.
(5) Place 5 mg weight near the center of the table and note if the meter indication changes. Continue moving weight outward until an indication is obtained. Record the distance from the center.
(6) Repeat no. 5 with the 10, 50, and 500 mg weights and record the minimum detectable distance for each.
(7) Place the 6.8 lb. weight on the table and position it until the DVM indicates zero moment.
(8) Repeat steps 5 and 6 with the 6.8 lb. weight in place.
(9) Repeat step 7 with the 24.2 lb. weight.
(10) Repeat steps 5 and 6 with the 24.2 lb. weight in place.

Appendix E

Program Management

APPENDIX E1

Mass Metrology Laboratory

PROJECT PLAN

Program: Moment of Inertia

Number - 1.1

Project: Math Model

Date: July 2, 1965

Scheduled Completion Date: 10-1-65

Approved: [illegible]

Assigned Personnel:

Responsible: M. S. Phillips

Support: F. A. Pauli

BACKGROUND: In order to obtain the moment of inertia of an object by using the torsional air bearing table, the equation of motion of the system must be known. This equation for a damped oscillating system, with viscous damping proportional to velocity, has been known for quite some time. The solution of this equation has been derived and is also understood very well. The equation approximates the torsional air bearing table for a certain degree of accuracy but it is not adequate for the accuracy desired. Therefore, a theoretical and experimental study will be performed to determine the exact equation and its solution. With this exact solution greater accuracies can be obtained.

OBJECTIVE: The objective of this project is to obtain an exact mathematical expression for the torsional air bearing table system. With this exact expression, only the system experimental errors will have to be considered in order to improve the system accuracy.

WORK PLANS:

1.1.1 Literature Search - A thorough search of the Redstone Scientific Information Center, the Defense Documentation Center and any other available library sources, will be performed to obtain any information on moment of inertia determination methods. Also private companies, government agencies and any one else that might have any knowledge about moment of inertia determination, will be contacted.

1.1.2 Damping Theory Study - A theoretical study to determine the exact damping term to use in the equation of motion of the air bearing table system will be performed. The equation

$$I\ddot{\theta} + f(\dot{\theta}) + K\theta = 0$$

will be used where $f(\dot{\theta})$ is the damping term which must be determined.

1.1.3 Aerodynamic Drag Tests - Necessary testing will be performed to verify the theoretical solutions derived in Section 1.1.2. These tests will consist mainly of drag plate tests on the air bearing table.

1.1.4 Vacuum Chamber Test - Similar drag test to those in Section 1.1.3 will be performed in a vacuum chamber. A special torsional system will have to be designed and fabricated for use in the vacuum chamber. These tests will also be used to verify the theoretical results of section 1.1.2.

REPORTS:

1.1.1 - Literature Search - Due October 8, 1965
1.1.2 - Damping Theory Study - Due October 22, 1965
1.1.3 - Aerodynamic Drag Tests - Due November 5, 1965
1.1.4 - Vacuum Chamber Tests - Due January 28, 1966

APPENDIX E2

Mass Metrology Laboratory

PROJECT PLAN

Program: Moment of Inertia

Number: 1.2

Project: Automatic System Development

Date: 7/12/65

Scheduled Completion Date: 4/29/66

Approved: C. D. Phillips

Assigned Personnel:

Responsible: M. K. Lewis

Support: M. S. Phillips
T. B. Shelton
F. A. Pauli

BACKGROUND: In the past, the period of oscillation of a gas bearing supported torsional pendulum has been measured by an electronic counter and printed out automatically by a numerical printer. The moment of inertia was then manually calculated from the period. To permit rapid measurement of a number of objects with high precision, it is desirable to eliminate the manual data recording and calculation.

OBJECTIVE: Fully automate the Moment of Inertia measurement system, and provide automatic printout of the moment of inertia.

WORK PLAN:

1.2.1 Basic System Design - A study will be made to determine the optimum system. The system design will then be made and will include a position detector, one or more electronic counters, an electronic computer, interface equipment, and printout equipment (which may be included with the computer). Necessary power supplies, interconnecting cables, and equipment housing will be included in the design. In so far as feasible, the design will incorporate equipment already on hand. If any modifications to the existing torsion pendulum are necessary, they will be covered in the design.

1.2.2 Computer Selection - An electronic computer will be selected to fulfill the design requirements. Since other systems in the lab will share this computer, their design requirements must be part of the selection criteria. Complexity of the interface equipment and cost must also be considered.

1.2.3 Delivery Span - All equipment must be on hand by 2/4/66.

1.2.4 Design Interface - The interface equipment design will be based on the choice of computer and electronic counters. Basically the equipment will consist of code translators. The design will include a clock pulse generator if needed. A power supply also will be included. This equipment will be purchased if commerically available. Otherwise, it will have to be designed.

1.2.5 Fabricate and Assemble - Experiments with the improved period measuring device should indicate whether modifications to the torsion pendulum structure are necessary. Any interface equipment not purchased must be fabricated.

Assembly will primarily consist of mounting the equipment in the housings and installing interconnecting cables.

1.2.6 Test - The system will be tested by actual operation using various torsion rods and weights. The tests will be performed in random order to minimize setup variables.

REPORTS:

1.2.1 Basic System Design - Due 9/24/65

1.2.4 Design Interface - Due 12/31/65

1.2.5 Fabricate and Assemble - Due 3/25/66

1.2.6 Test - Due 4/29/66

APPENDIX E3

Mass Metrology Laboratory

PROJECT PLAN

Program: Moment of Inertia

Number: 1.3

Project: Torsion Rod Investigation

Date: July 2, 1965

Scheduled Completion Date: 1/15/66

Approved: [illegible]

Assigned Personnel:

Responsible: M. S. Phillips

Support: T. A. Williams
M. K. Lewis
T. B. Shelton

BACKGROUND: In the past torsion rods generally have been made of some type of steel. Also, some types of ceramic materials have been used for small precision torsional applications. Since the use of torsion rods is limited, there is very little information on which materials make the best torsion rods. Therefore, a torsion rod investigation project will be conducted to find the best material to be used.

OBJECTIVE: The objective of this project is to obtain sufficient information from the material investigation that will allow the best material for use as torsion rods to be selected. The foremost characteristic of the rod is that it must have a very linear stress-strain relationship and have very little mechanical hysteresis.

WORK PLAN:

1.3.1 Investigate Rod Material - A thorough search of available literature will be conducted. Also, a search of material information furnished by vendors on torsional properties of materials will be accomplished.

1.3.2 Design Torsion Rod Tester - A system will be designed to test torsion rods statically. The 24" air bearing table can be used as the basic instrument in this system. The 24" air bearing table will also be used as the dynamic rod tester without any modifications.

1.3.3 Fabricate Torsion Rod Tester - The torsion rod testing system will be fabricated to meet the design outlined by Section 1.3.2.

1.3.4 Fabricate Torsion Rods - Torsion rods made out of the various materials decided upon in Section 1.3.1 will be fabricated to fit the torsion rod tester.

1.3.5 Torsion Rod Tests - A test program will be designed that will determine the torsional characteristics of all the rods fabricated in Section 1.3.4. From these tests the best torsion rod material will be selected.

REPORTS:

1.3.1 Investigate Rod Material - Due - Septermber 17, 1965
1.3.2 Torsion Rod Tests - Due - January 14, 1966

APPENDIX E4

Mass Metrology Laboratory

PROJECT PLAN

Program: Moment of Inertia

Number: 1.4

Project: System Improvements

Date: 7/2/65

Scheduled Completion Date: 1-28-66

Approved: [illegible]

Assigned Personnel:

Responsible: M. K. Lewis

Support: M. S. Phillips
T. A. Williams
T. B. Shelton

BACKGROUND: The accuracy of the decaying oscillation method used in determining moment of inertia has thus far been the inability to make accurate measurements at low amplitudes of oscillation. Measurements of both period and amplitude have been made although period measurement has received the most development.

OBJECTIVE: Improve the accuracy of period and amplitude measurements as required to fulfill the accuracy requirements of the automatic system.

WORK PLAN:

1.4.1 Improve Period Measuring Device - It appears, at the present, that the photoelectric transducer holds the most promise for accurate period measurements. This device will be examined closely to determine the best way to utilize it. A system will then be built based on this investigation.

1.4.2 Improve Displacement Measuring Device - The present method of projecting a reflected light beam onto a radian sector scale for measuring displacement is both subjective and cumbersome. Other ways of making this measurement will be studied. A system will then be built based on the most promising method.

REPORTS: 1.4.1 Improve Period Measuring Device - Due 10/15/65

1.4.2 Improve Displacement Measuring Device - Due 1/28/66

APPENDIX E5

Mass Metrology Laboratory

PROJECT PLAN

Program: Moment of Inertia Number: 1.5

Project: Equipment Calibration Date: July 6, 1965

Scheduled Completion Date: May 15, 1966 Approved: [illegible]

Assigned Personnel:

Responsible: M. S. Phillips

Support: F. A. Pauli

BACKGROUND: The moment of inertia equipment will presently yield accuracies in the order of one tenth of one percent. With minor modifications and calibrations, for temperature and load, the accuracy should increase to one-hundredth of one per cent.

OBJECTIVE: The objective of this project is to compensate for all variables that might effect the accuracy of the moment of inertia determination. If possible an empirical equation will be derived that will correct the moment of inertia for any set of known conditions.

WORK PLAN:

1.5.1 Standard Calibration - The dumbbell standards will be recalibrated to obtain their exact moments of inertia and the accuracy of this value will be determined.

1.5.2 Temperature Tests - Test will be performed at various temperatures to obtain a correction factor which will compensate for the effect of temperature changes on the airbearing table.

1.5.3 Load Tests - The effect of different loads on the air bearing table will be investigated in this test program. The optimum air pressure to use for a certain weight will be determined and a compensation factor for correcting any errors caused by loading will be determined.

1.5.4 Other Tests - Any other tests will be performed that might be needed for calibrating the equipment.

REPORTS: 1.5.2 - Temperature Test - Due - February 15, 1966
1.5.3 - Load Test - Due - April 1, 1966
1.5.4 - Other Tests - Due - May 10, 1966

APPENDIX E6

Mass Metrology Laboratory

PROJECT PLAN

Program: Product of Inertia

Number: 2.1

Project: Prototype System Improvement

Date: 6/30/65

Scheduled Completion Date: 10/29/65

Approved: Wm Phillips

Assigned Personnel:

Responsible: M. K. Lewis

Support: T. A. Williams
T. B. Shelton

BACKGROUND: Tests run on the prototype machine show that the accuracy attained was $\pm$ 3.5%. It is desirable to improve this accuracy before attempting to automate the system.

OBJECTIVE: Improve the accuracy of the prototype as much as possible, and make modifications as required to improve the overall performance of the system.

WORK PLAN:

2.1.1 Improve Tilt Table - The tilt table will be redesigned to provide flexure mounts for the load cell(s). A more rigid work surface will be provided if necessary. A work holdown and positioning device will be included in the design.

2.1.2 Calibrate Standards - The product of inertia standards (triangular blocks) will be returned to the vendor for regrinding and chrome plating. After they are received, they will be measured and weighed. Their products of inertia will then be computed.

2.1.3 Evaluation Tests - The product of inertia standards will be used to evaluate the revised performance of the machine. The product of inertia of each standard will be measured using the machine. (The force and speed will be read with a DVM and counter respectively.) The measured values will be compared with the computed values to determine the machine performance.

REPORTS: 2.1.3 Evaluation Test - Due 10-29-65

APPENDIX E7

Mass Metrology Laboratory

PROJECT PLAN

Program: Product of Inertia

Number: 2.2

Project: Theoretical Analysis

Date: 6/30/65

Scheduled Completion Date: 1/14/66

Approved: M. S. Phillips

Assigned Personnel:

Responsible: M. S. Phillips

Support: M. K. Lewis

BACKGROUND: The need for the precise determination of the products of inertia of a mass is basically to help obtain the principal axes. If the principal axes are known then the object can be oriented so that it is dynamically balanced. The method of determining products of inertia is a classical problem and has been investigated vigorously.

OBJECTIVE: The object of this project is to perform a thorough study of the theoretical approach to determining products of inertia.

WORK PLAN:

2.2.1 Literature Survey - A survey of all available literature will be conducted to find the latest work done on determining products of inertia.

2.2.2 Develop Mathematical Model - A theoretical study will be conducted to determine the best mathematical model to use for obtaining the product of inertia, by using the rate table.

2.2.3 Vacuum Chamber Tests - Test using the rate table in a vacuum chamber will be performed to determine the effect of aerodynamic lift on the product of inertia determination.

2.2.4 Error Analysis - An error analysis of the product of inertia machine will be conducted to determine the accuracy of the machine.

REPORTS:
2.2.1 Due 8/20/65
2.2.2 Due 11/19/65
2.2.3 Due 1/14/66
2.2.4 Due 9/24/65

APPENDIX E8

Mass Metrology Laboratory

PROJECT PLAN

Program: Product of Inertia Number: 2.3

Project: Automatic System Development Date: 6/30/65

Scheduled Completion Date: 5/6/66 Approved: [illegible]

Assigned Personnel:

Responsible: M. K. Lewis

Support: M. S. Phillips
T. B. Shelton

BACKGROUND: The ultimate accuracy of the prototype machine is limited by the analog computer whose accuracy is ± 1%. Further improvement will necessitate conversion to a digital system. It is also desirable to have an automatic computation and printout feature to increase operating speed and minimize human errors.

OBJECTIVE: Develop a complete digitized product of inertia measurement system which will provide a real-time printed result without further calculation.

WORK PLAN: 2.3.1 Establish Basic System Design - The desired system end results are accuracy and operating ease. These factors will govern the design of the system.

Strain gage load cells are used in the prototype for measuring the unbalanced force. Since strain gages require expensive measuring equipment, a literature survey will be made to determine whether some other device is more appropriate. If strain gauges are used, a power supply will be included for them. Tests will be run to determine whether a DVM or counter is more accurate for measuring the angular velocity of the rate table.

A digital computer will be used to compute the product of inertia using the angular velocity and unbalanced force signals as inputs. These input signals - previously digitized by the measuring equipment - will go to the computer through interface equipment. The interface design will depend on the choice of computer and measuring instruments. When the design is finalized, a system block diagram will be made.

2.3.2 Select and Procure Equipment - The available equipment will be surveyed to determine which most nearly satisfies the basic system design requirements. Equipment on hand will be included in the survey.

Various usable equipment combinations will be investigated from the standpoints of accuracy, cost, and versatility to determine that combination which is most desirable. The interface equipment complexity and procurement lead time will also be governing factors.

After the equipment is selected, housing and mating connectors will be bought.

2.3.3 Design Interface Equipment - The design of the interface equipment will depend on the choice of computer and digitizing instruments. The equipment will primarily consist of code translators. A clock pulse generator will be incorporated into the design if needed. A power supply will also be included. The literature will be surveyed to see if this equipment is available. If not, it will have to be designed.

2.3.4 Fabricate and Assemble System - Fabrication will consist primarily of mounting the equipment in the housings and making and installing interconnecting cables. Some modifications to the rate table may be required, e.g. the height may need to be reduced. Tests with the prototype should indicate whether the load cell mounting system needs further modification.

2.3.5 Performance Test System - Performance testing will consist of operating each of the test standards at various angular velocities. The measured products of inertia will be tabulated and compared with the computed values to obtain the system accuracy. Several tests will be made and the results averaged to reduce random errors.

REPORTS:
- 2.3.1 Establish Basic System Design - Due 9-3-65
- 2.3.3 Design Interface Equipment - Due 12-31-65
- 2.3.4 Fabricate and Assemble System - Due 4-1-66
- 2.3.5 Performance Test System - Due 5-6-66

APPENDIX E9

Mass Metrology Laboratory

PROJECT PLAN

Program: Product of Inertia

Number: 2.4

Project: Principal Axis

Date: 6/30/65

Scheduled Completion Date: 4/22/66

Approved: M. S. Phillips

Assigned Personnel:

Responsible: M. S. Phillips

BACKGROUND: The principal axes of an object must be known before it can be dynamically balanced. In order to obtain the principal axes of an object, its moments and products of inertia must be known about a given point. The process of obtaining the principal axes from moments and products of inertia has been programed for the IBM 1620 computer and is operational.

OBJECTIVE: The object of this project is to have a computer program that will take the moments and products of inertia about a given point from the present laboratory equipment and calculate the principal axes about that point.

WORK PLAN: 2.4.1 Data Input from Product and Moment of Inertia Test - The data obtained from the product of inertia machine along with the data obtained from the moment of inertia machine will be used in the computer program to determine the principal axes.

APPENDIX E10

Mass Metrology Laboratory

PROJECT PLAN

Program: Mass Properties of Liquids Number: 3.1

Project: Test Program Date: July 2, 1965

Scheduled Completion Date: May 15, 1966 Approved: [illegible]

Assigned Personnel:

Responsible: M. S. Phillips

Support: F. A. Pauli

BACKGROUND: In the past there has been much experimental work done in the field of liquid characteristics in dynamic fuel tanks. This work has been accomplished in order to better predict the aerodynamic behavior of a launch vehicle which has liquid contained in fuel tanks. The knowledge of the moment of inertia of such a launch vehicle is very critical if the trajectory and planned missions are to be met. In operational launch vehicles to date these problems have effectively been eliminated or compensated for, but for future launch vehicles and missions the present knowledge may not be sufficient. Therefore, a further study of the moment of inertia of a filled liquid tank will be pursued.

OBJECTIVE: The objective of this project is to perform tests to determine the moment of inertia of a liquid filled cylindrical tank about its roll and yaw-pitch axis. Also, some testing to determine the effects of baffles on determining the moment of inertia of a filled tank will be performed.

WORK PLAN:

3.1.1 Roll Axis Inertia Tests Using the Air Bearing Table - The government furnished aluminum cylindrical tanks will be used on the 24 inch air bearing table to determine the moment of inertia of the liquid container about its roll axis.

3.1.2 Displaced Roll Axis Inertia Tests Using the Air Bearing Table - The same tanks and air bearing table as described in Section 3.1.1 will be used to determine the effect of translating the axis of rotation of the cylinder on its roll moment of inertia.

3.1.3 Yaw-Pitch Axis Inertia Tests Using a Torsional Pendulum - The same tanks will be used on the torsional pendulum to determine the moment of inertia of a filled cylindrical tank about its yaw-pitch axis.

3.1.4 Yaw-Pitch Axis Inertia Tests Rotating About a Horizontal Axis- The same tanks will be rotated about their yaw-pitch axis oriented in a horizontal

plane instead of a vertical plane as stated in Section 3.1.3. The testing will be performed using the government furnished stand and special adapters for mounting the cylindrical tanks vertically.

3.1.5 Yaw-Pitch Axis Inertia Tests Rotating About a Displaced Horizontal Axis - The same tests performed in Section 3.1.4 will be carried out again with the exception that the center of gravity will be translated. These test will be accomplished by using the special adapter described in Section 3.1.4 which will allow the center of gravity to be displaced.

3.1.6 Ring Baffle Tests Using Government Furnished Plexiglass Tank and Baffles - The effect of ring baffles on determing the liquid moment of inertia of the government furnished plexiglass tank will be investigated.

REPORTS:
3.1.1 - Due- September 10, 1965
3.1.2 - Due- October 8, 1965
3.1.3 - Due- December 10, 1965
3.1.4 - Due- February 11, 1966
3.1.5 - Due- March 11, 1966
3.1.6 - Due- May 13, 1966

APPENDIX E11

Mass Metrology Laboratory

PROJECT PLAN

Program: Mass Properties of Liquids

Number: 3.2

Project: Math Model

Date: July 2, 1965

Scheduled Completion Date: May 15, 1966

Approved: [illegible]

Assigned Personnel:

Responsible: M. S. Phillips

BACKGROUND: Math models for the moment of inertia of liquid filled tanks have been derived. These models are obtained by using potential theory and specific boundary conditions. This method of derivation is very complicated but presently it yields the most accurate theoretical results.

OBJECTIVE: The objective of this program is to derive a mathematical expression either theoretical or empirical that will accurately give the moment of inertia of a liquid filled tank. The model will be relatively simple, so that it can be used in general applications, and as accurate as possible.

WORK PLAN:

3.2.1 Literature Search - A thorough search of the Redstone Scientifice Information Center, the Defense Documentation Center and any other available library source, will be performed to obtain information on the moment of inertia of liquid systems.

3.2.2 Develop an Equation for the Moment of Inertia of a Liquid Filled Cylindrical Tank About Its Center of Gravity - Theoretical studies will be conducted to obtain a mathematical model for the moment of inertia of a filled tank about its center of gravity. Also emperical relations will be investigated.

3.2.3 Develop a Mathematical Expression for Transferring the Moment of Inertia of a Liquid Filled Cylindrical Tank to Another Parallel Axis - Studies similar to those in Section 3.2.2 will be conducted.

REPORTS: 3.2.1- Due - August 27, 1965
3.2.2- Due - February 1, 1966
3.2.3- Due - May 13, 1966

APPENDIX E12

Mass Metrology Laboratory

PROJECT PLAN

Program: Center of Gravity

Number: 4.1

Project: Spherical Segment Air Bearing

Date: June 30, 1965

Scheduled Completion Date: 5-1-66

Approved: C Wm Phillips

Assigned Personnel:

Responsible: T. A. Williams

Support: K. Comer

BACKGROUND: A center of gravity locator employing a spherical segment air lubricated bearing was developed during the first year effort of this contract.

The accuracy obtained with this system thus far has not been up to the original expectation. Testing of the unit has been limited, and the sources of error have not yet been detected. Other modifications to the system are necessary to improve the ease of operation and the consistency of results.

OBJECTIVE: To achieve the maximum possible accuracy and ease of operation of the spherical air bearing C. G. locator, consistent with available time and funds.

WORK PLAN:

4.1.1 Test Studies: Additional testing of the existing system is to be conducted in order to determine the performance characteristics and to investigate areas that improvements might be made.

4.1.2 Object Support Surface Stabilizer: A new system for stabilizing the object support surface is to be designed and built.

4.1.3 Counter Balance System: The present system of varying the stability of the inverted pendulum is not satisfactory for the desired precision. A new system will be designed which will be easier to operate and will suffice for a larger range of object sizes.

4.1.4 Object Positioner Modification: The object positioner will likely be modified to supply clearance for the addition of the object support surface stabilizer. A longer horizontal shaft, with a teflon tip, is needed also.

4.1.5 Telescope and Air Bearing Support Stand: The air bearing table and optical measuring equipment will be combined into one system, mounted on a common base.

4.1.6 System Evaluation Tests: Testing of the system will be done in order to evaluate the modifications and determine the system's accuracy.

4.1.7 Report: A report will be prepared by May 1, 1966.

APPENDIX E13

Mass Metrology Laboratory

PROJECT PLAN

Program: Center of Gravity

Number: 4.2

Project: Moment Detection Modification

Date: July 1, 1965

Scheduled Completion Date: January 1, 1966

Approved: C Wm Phillips

Assigned Personnel:

Responsible: T. A. Williams

Support: T. B. Shelton

BACKGROUND: The Moment Detection System is made up of purchased items incorporated with equipment that was designed by the Mass Metrology Laboratory.

The purchased equipment consists of a 25 in-lb and a 250 in-lb Moment Detection Unit and an Instrumentation and Power Supply Unit.

These items were manufactured by the Bytrex Corporation, Newton, Massachusetts. The moment detector produces an electrical signal directly proportional to any unbalance moment about its center. It has two perpendicular axes of sensitivity and resolves unbalance moments into two components. The portable instrumentation and power supply unit amplify the electrical signals to a level high enough to drive a meter movement.

The related equipment furnished by the Mass Metrology Lab includes two test object support surfaces and a support and leveling stand that incorporates four overload protection arms.

Modification to this equipment is necessary to facilitate its use with the optical measuring system and to improve the accuracy with which the unbalance moment can be read.

OBJECTIVE: To improve the accuracy and ease of operation of this test equipment for the location of the centers of gravity of system components for space vehicles, and other objects related to the space program.

WORK PLAN:

4.2.1 Test Studies: Testing is to be performed in order to determine the areas where the accuracy of the equipment can be improved.

4.2.2 Digital Readout: A digital voltmeter is to be installed to replace the graduated scale readout of the instrumentation unit.

4.2.3 Bytrex Head 90° Rotation Modification: The support stand is to be modified to allow rotation of the moment detector head thru 360° at 90° intervals. This modification allows the use of the optical measuring equipment for locating the C.G. of objects in two planes without having to reposition the test object.

4.2.4 System Evaluation Tests: Tests will be made to determine the performance characteristics of the system and to checkout the function of the above modifications.

4.2.5 Report: Due December 31, 1965.

APPENDIX E14

Mass Metrology Laboratory

PROJECT PLAN

Program: Center of Gravity

Number: 4.3

Project: Optical System

Date: 7/1/65

Scheduled Completion Date: 4/15/66

Approved: Wm Phillips

Assigned Personnel:

Responsible: T. A. Williams

Support: K. Comer

BACKGROUND: Due to the need for a precision measuring system that could measure from any reference point on a particular test object, the following equipment was purchased, modified, and installed by the Mass Metrology Laboratory.

(1) #200-10-AM tooling bar assembly with vertical adjusting stands.

(2) #76 telescopic transit square with an optical micrometer.

(3) #185 stellite mirror

It has been proved that this equipment is capable of measurements to within $\pm$ .001 inch. However, in actual practice, this accuracy is difficult to achieve because of other error contributing factors. A major source of error is the lack of a well defined point, on the test objects, from which to measure. Other errors may be introduced by improper alignment and collimination of the equipment.

OBJECTIVE: To improve the ease of operation and accuracy of the equipment. This improvement is desired in order to permit consistant achievement of the full capabilities of the optical system.

WORK PLAN:

4.3.1 (a) Run tests to determine the amount and type of errors in the system.

(b) Analyze test data

(c) Make necessary adjustments or equipment modifications.

4.3.2 (a) Conduct a study of various marking methods.

(b) Design and build or purchase the most promising method.

(c) Install and test the selected system.

REPORT: Due 4/15/66

APPENDIX E15

Mass Metrology Laboratory

PROJECT PLAN

Program: Center of Gravity

Number: 4.4

Project: Advanced C.G. System

Date: 7/1/65

Scheduled Completion Date: 5/1/66

Approved: [illegible]

Assigned Personnel:

Responsible: T.A. Williams

Support: M. K. Lewis
T. B. Shelton
M. S. Phillips

BACKGROUND: To this point, in the Center of Gravity Program, work has been confined to the development of the existing spherical air bearing and moment detection (Bytrex) systems.

The air bearing table has proved difficult to operate, the accuracy obtained to date is not entirely satisfactory, and capacity of the system is limited.

The moment detection system is also limited in capacity and accuracy. The accuracy of this system is limited by the creep and hysteresis of the bending element in the moment detector heads and by inherent errors in the associated electronics.

Work should continue on these systems because they can be used for testing objects within their capacity and their accuracy potential has not yet been fully realized.

OBJECTIVE: To develop a center of gravity system that has a large range of capacity and will yield an accuracy of $\pm$ .001 inch or better.

WORK PLAN:

4.4.1 Feasibility Study: Mathematical and theoretical system analysis due by August 15, 1965.

4.4.2 Design & Equipment Study: An investigation into the use of flexures and load cells or any other electro-mechanical components, for measuring the weight and unbalance moment of test objects, is to be made. If these components prove capable of yielding the desired accuracy, then a system will be designed and built using a combination of the most suitable components .

A typical system being considered utilizes three load cells, one mounted in the center of two supporting plates and two mounted at the edges of the plates. Each load cell has universal flexures attached to each end to provide for load alignment through the load axis of the cells. (See Fig. 1) Construction of the system is such that it has a negative spring constant, thereby eliminating energy losses in the flexures.

4.4.3 Delivery Span: Purchased equipment due January 15, 1966.

4.4.4 Fabrication and Assembly: Due to be completed by March 15, 1966.

4.4.5 Evaluation Tests: Thorough testing of the system is to be performed to establish the performance characteristics and accuracies obtainable throughout the capacity range of the equipment.

4.4.6 Report: Due April 1, 1965

APPENDIX E16

Mass Metrology Laboratory

PROJECT PLAN

Program: General Laboratory Improvements Number: 5.1

Project: Improvement of Temperature Control Date: 6/30/65

Scheduled Completion Date: 9/29/65 Approved: [illegible]

Assigned Personnel:

Responsible: T. B. Shelton

Support: C. W. Phillips

BACKGROUND: The accuracy of measurements of moment of inertia is known to be influenced by the temperature in the laboratory area. A temperature constant to within $\pm$ 1°F is necessary for successful laboratory experiments. The present equipment is incapable of maintaining this requirement during the summer months.

OBJECTIVE: To improve the temperature control in the laboratory to permit maintenance of a $\pm$ 1°F tolerance at all times.

WORK PLAN:

5.1.1 Modify Air Conditioning Equipment:

1. The laboratory will be surveyed by an air conditioning contractor to determine two or three possible methods of modifying the system. Price estimates will be obtained for each method.

2. The desired method will be selected based on anticipated performance and cost.

3. The necessary modifications will be made and completed by 9/29/65.

5.1.2 Relocate Test Equipment: The test equipment now located in the experiment room will be moved and installed in the control room. All subsequent tests will be run with all personnel in the control room. New instrumentation cables will be fabricated as required.

APPENDIX E17

Mass Metrology Laboratory

PROJECT PLAN

Program: General Laboratory Improvements

Number: 5.2

Project: Precision Weighing System

Date: 6/30/65

Scheduled Completion Date: 1/28/66

Approved: [illegible]

Assigned Personnel:

Responsible: M. K. Lewis

Support: M. S. Phillips
T. A. Williams
T. B. Shelton

BACKGROUND: In the past, objects requiring precision weighing have been sent to the Army Calibration Lab. This procedure usually results in a time lag of many weeks. In order to alleviate this problem, it is desirable to provide an in-house precision weighing system. The need for a 1,000 lb capacity is anticipated.

OBJECTIVE: Provide a precision weighing system with a 1,000 lb capability. The precision should be as high as practical.

WORK PLAN:

5.2.1 Literature Survey and Equipment Selection - A literature survey will be made to determine the system most suited to our needs and budget. If such a system cannot be purchased directly, a design will be made and equipment selected. Provisions for alignment and calibration will be included in the design, as will handling equipment. If a balancing system is chosen, additional weights, to supplement those on hand, will be selected. Any power supplies and metering equipment needed will also be chosen. The metering equipment will include range changing and readout functions. Interconnecting cables will also be specified.

5.2.2 Fabricate and Assemble - The system will be fabricated and assembled in accordance with the design. Then it will be aligned and calibrated.

5.2.3 Tests - Selected weights throughout the systems range will be used in testing. The tests will be conducted in random order and the results averaged, if necessary, to improve accuracy. Any recalibration needed will be done at this time. A correction curve or table will be made if needed.

REPORTS: Tests - Due 1/28/66